



PB99-142531

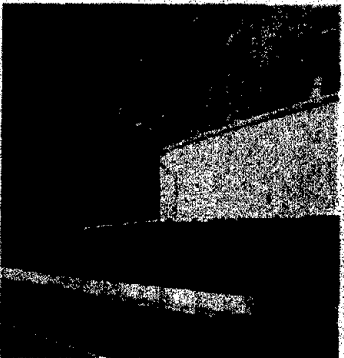
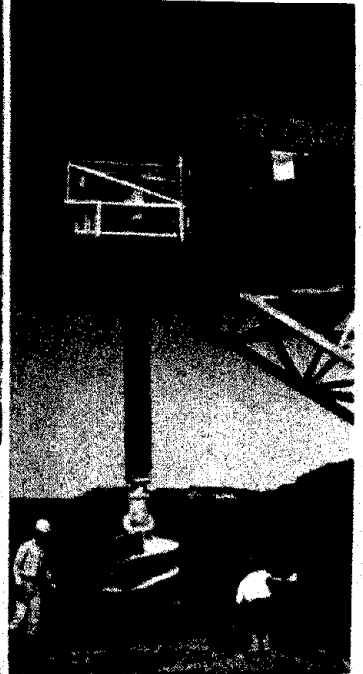
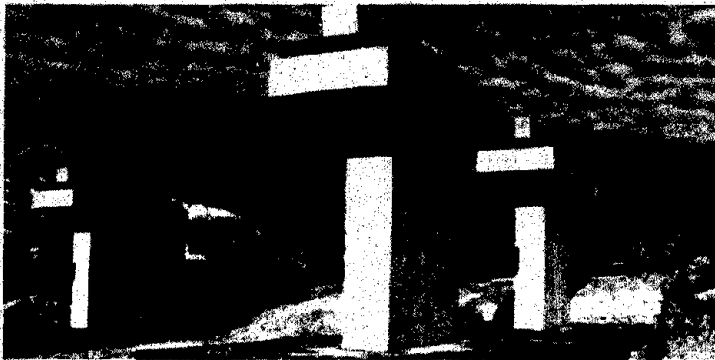
TRAINING COURSE IN GEOTECHNICAL AND FOUNDATION ENGINEERING

NHI COURSE NO. 13239 - MODULE 9

PUBLICATION NO. FHWA HI-99-012
DECEMBER 1998

GEOTECHNICAL EARTHQUAKE ENGINEERING

REFERENCE MANUAL



U.S. Department of Transportation
Federal Highway Administration

REPRODUCED BY: **NTIS**
U.S. Department of Commerce
National Technical Information Service
Springfield, Virginia 22161




National Highway Institute

PROTECTED UNDER INTERNATIONAL COPYRIGHT
ALL RIGHTS RESERVED.
NATIONAL TECHNICAL INFORMATION SERVICE
U.S. DEPARTMENT OF COMMERCE

Reproduced from
best available copy.



Technical Report Documentation Page

1. Report No. FHWA-HI-99-012		 PB99-142531	3. Recipient's Catalog No.	
4. Title and Subtitle GEOTECHNICAL EARTHQUAKE ENGINEERING REFERENCE MANUAL		5. Report Date December 1998		
		6. Performing Organization Code		
7. Author(s) Principal Investigator: George Munfakh* Authors: Edward Kavazanjian, Jr.▲, Neven Matasović▲, Tarik Hadj-Hamou▲, and Jaw-Nan (Joe) Wang*		8. Performing Organization Report No.		
9. Performing Organization Name and Address * Parsons Brinckerhoff Quade & Douglas, Inc. One Penn Plaza, New York, NY 10119 In association with: ▲ GeoSyntec Consultants 2100 Main St., Suite 150, Huntington Beach, CA 92648		10. Work Unit No. (TRAIS)		
		11. Contract or Grant No. DTFH61-94-C-00104		
12. Sponsoring Agency Name and Address Federal Highway Administration National Highway Institute 901 North Stuart Street, Suite 300 Arlington, Virginia 22203		13. Type of Report and Period Covered		
		14. Sponsoring Agency Code		
15. Supplementary Notes FHWA Technical Consultants - J.A. DiMaggio, A. Munoz and P. Osborn FHWA Contracting Officer - J. Mowery III; COTR - L. Jones, National Highway Institute				
16. Abstract This manual has been written to provide training on how to apply principles of geotechnical earthquake engineering to planning, design, and retrofit of highway facilities. Geotechnical earthquake engineering topics discussed in Part I of this manual include: <ul style="list-style-type: none"> • deterministic and probabilistic seismic hazard assessment; • evaluation of design ground motions; • seismic site response analyses; • evaluation of liquefaction potential and seismic settlements; • seismic slope stability and deformation analyses; and • seismic design of foundations and retaining structures. The manual provides detailed information on basic principles and analyses, with reference to where detailed information on these analyses can be obtained. Design examples illustrating these principles and analyses are provided in Part II of this manual.				
17. Key Words Geotechnical earthquake engineering, soil dynamics, engineering seismology, engineering geology, liquefaction, slopes, foundations, retaining walls		18. Distribution Statement No restrictions.		
19. Security Classif. (of this report) UNCLASSIFIED	20. Security Classif. (of this page) UNCLASSIFIED	21. No. of Pages 392	22. Price	

PREFACE

This module is the ninth in a series of eleven modules that constitute a comprehensive training course in geotechnical and foundation engineering. Sponsored by the National Highway Institute (NHI) of the Federal Highway Administration (FHWA), the training course is given at different locations in the U.S. The intended audience is civil engineers and engineering geologists involved with the design and construction of transportation facilities.

This manual adopted much of the information from the following FHWA publications:

Geotechnical Engineering Circular No. 3

“Design Guidance: Geotechnical Earthquake Engineering for Highways, Volume I-Design Principles; Volume II- Design Examples.”

Publication No.: FHWA-SA-97-076 and FHWA-SA-97-077

May 1997.

The subjects that have been added, expanded and/or revised in this manual are as follows:

- The results of the latest study by USGS on seismic hazard calculations have been included in this manual (Chapter 3).
- The site classification guidelines used on the site response analyses have been updated to be consistent with the latest recommendation by NEHRP (Chapter 4).
- The latest developments in liquefaction evaluation and the recommendations from the NCEER workshop on the subject have been incorporated (Chapter 8).
- Chapter 9 has been significantly expanded to include complete design guidance for deep foundations and retaining walls.
- The manuscript has been completely reformatted to be compatible with those of the remaining 10 modules; and
- The manual has been extensively cross-referenced to other modules where more detailed information on a given subject may be available.

This manual has been written to provide information on how to apply principles of geotechnical earthquake engineering to planning, design, and retrofit of highway facilities. Geotechnical earthquake engineering topics discussed in this manual include:

- deterministic and probabilistic seismic hazard assessment;
- evaluation of design ground motions;
- seismic site response analyses;
- evaluation of liquefaction potential and seismic settlements;
- seismic slope stability and deformation analyses; and
- seismic design of foundations and retaining structures.

This manual is divided into two parts. Part I of the manual provides detailed information on basic principles and analyses, with reference to where detailed information on these analyses can be obtained. Part II presents design examples illustrating the principles and analyses described in Part I.

This manual has been prepared using up-to-date information. However, earthquake engineering is a rapidly evolving field. Codes and standards are updated at regular intervals and analytical procedures are

revised and improved frequently. Furthermore, almost every major earthquake leads to modification, qualification, extension, and/or improvement of some of the methods and techniques presented herein. Therefore, the geotechnical professional using this document is encouraged to consult the technical literature for recent advances in geotechnical earthquake engineering relevant to his/her project prior to completing his/her design.

Finally, this manual is developed to be used as a living document. After attending the training session, it is intended that the participant will use it as a manual of practice in everyday work. Throughout the manual, attention is given to ensure the compatibility of its content with those of the participants manuals prepared for the other training modules. Special efforts are made to ensure that the included material is practical in nature and represents the latest developments in the field.

ACKNOWLEDGMENTS

Permission by the FHWA to adapt the original manuscript prepared by GeoSyntec Consultants for Geotechnical Circular No. 3 is gratefully acknowledged. Provision of the original electronic files for the circular by GeoSyntec Consultants is also acknowledged. Furthermore, the authors appreciate Jerry DiMaggio, Andy Muñoz and Peter Osborn of FHWA for their thorough reviews and recommendations. The authors would also like to acknowledge the assistance of Dr. Ke Fan, Jeremy Hung, and a number of other professionals from Parsons Brinckerhoff Quade & Douglas, Inc., in the preparation of this manual.

NOTICE

The information in this document has been funded wholly or in part by the US Department of Transportation, Federal Highway Administration (FHWA), under Contract No. DTFH 61-94-C-00104 to Parsons Brinckerhoff Quade & Douglas, Inc. The document has been subjected to peer and administrative review by FHWA, and it has been approved for publication as a FHWA document.

In this document, certain products have been identified by trade name. Also, photographs of these products have been included in the document for illustration purposes. Other products which are not identified in this document may be equally viable to those identified. The mention of any trade name or photograph of a particular product does not constitute endorsement or recommendation for use by either the authors or FHWA.

CONVERSION FACTORS

Approximate Conversions to SI Units			Approximate Conversions from SI Units		
When you know	Multiply by	To find	When you know	Multiply by	To find
(a) Length					
inch	25.4	millimeter	millimeter	0.039	inch
foot	0.305	meter	meter	3.28	foot
yard	0.914	meter	meter	1.09	yard
mile	1.61	kilometer	kilometer	0.621	mile
(b) Area					
square inches	645.2	square millimeters	square millimeters	0.0016	square inches
square feet	0.093	square meters	square meters	10.764	square feet
acres	0.405	hectares	hectares	2.47	acres
square miles	2.59	square kilometers	square kilometers	0.386	square miles
(c) Volume					
fluid ounces	29.57	milliliters	milliliters	0.034	fluid ounces
gallons	3.785	liters	liters	0.264	gallons
cubic feet	0.028	cubic meters	cubic meters	35.32	cubic feet
cubic yards	0.765	cubic meters	cubic meters	1.308	cubic yards
(d) Mass					
ounces	28.35	grams	grams	0.035	ounces
pounds	0.454	kilograms	kilograms	2.205	pounds
short tons (2000 lb)	0.907	megagrams (tonne)	megagrams (tonne)	1.102	short tons (2000 lb)
(e) Force					
pound	4.448	Newton	Newton	0.2248	pound
(f) Pressure, Stress, Modulus of Elasticity					
pounds per square foot	47.88	Pascals	Pascals	0.021	pounds per square foot
pounds per square inch	6.895	kiloPascals	kiloPascals	0.145	pounds per square inch
(g) Density					
pounds per cubic foot	16.019	kilograms per cubic meter	kilograms per cubic meter	0.0624	pounds per cubic foot
(h) Temperature					
Fahrenheit temperature(°F)	5/9(°F- 32)	Celsius temperature(°C)	Celsius temperature(°C)	9/5(°C)+ 32	Fahrenheit temperature(°F)

Notes: 1) The primary metric (SI) units used in civil engineering are meter (m), kilogram (kg), second(s), newton (N) and pascal (Pa=N/m²).

2) In a "soft" conversion, an English measurement is mathematically converted to its exact metric equivalent.

3) In a "hard" conversion, a new rounded metric number is created that is convenient to work with and remember.

MODULE 9

TABLE OF CONTENTS

PART I- DESIGN PRINCIPLES

	Page
LIST OF FIGURES	viii
LIST OF TABLES	xii
LIST OF SYMBOLS	xiii
1.0 Introduction	1-1
1.1 Introduction	1-1
1.2 Sources of Damage in Earthquakes	1-2
1.2.1 General	1-2
1.2.2 Direct Damage	1-2
Classification of Direct Damage	1-2
Primary Damage	1-2
Secondary Damage	1-3
1.2.3 Indirect Damage	1-5
1.3 Earthquake-Induced Damage to Highway Facilities	1-6
1.3.1 Overview	1-6
1.3.2 Historical Damage to Highway Facilities	1-6
1.4 Organization of the Document	1-8
2.0 Earthquake Fundamentals	2-1
2.1 Introduction	2-1
2.2 Basic Concepts	2-1
2.2.1 General	2-1
2.2.2 Plate Tectonics	2-1
2.2.3 Fault Movements	2-3
2.3 Definitions	2-6
2.3.1 Introduction	2-6
2.3.2 Type of Faults	2-6
Strike Slip Faults	2-6
Dip Slip Faults	2-6
Other Special Cases	2-6
2.3.3 Earthquake Magnitude	2-7
2.3.4 Hypocenter and Epicenter	2-8
2.3.5 Zone of Energy Release	2-8
2.3.6 Site-to-Source Distance	2-9
2.3.7 Peak Ground Motions	2-9
2.3.8 Response Spectrum	2-12
2.3.9 Attenuation Relationships	2-14
2.3.10 Intensity Scales	2-14

3.0	Seismic Hazard Analysis	3-1
3.1	General	3-1
3.2	Seismic Source Characterization	3-1
3.2.1	Overview	3-1
3.2.2	Methods for Seismic Source Characterization	3-2
3.2.3	Defining the Potential for Fault Movement	3-4
3.2.4	Seismic Source Characterization in the Eastern and Central States	3-5
3.3	The Determination of the Intensity of Design Ground Motions	3-6
3.3.1	Introduction	3-6
3.3.2	Published Codes and Standards	3-6
3.3.3	The Deterministic Approach	3-14
3.3.4	The Probabilistic Approach	3-15
4.0	Ground Motion Characterization	4-1
4.1	Basic Ground Motion Characteristics	4-1
4.2	Peak Values	4-1
4.2.1	Evaluation of Peak Parameters	4-1
4.2.2	Attenuation of Peak Values	4-2
4.2.3	Selection of Attenuation Relationships	4-4
4.2.4	Selection of Attenuation Relationship Input Parameters	4-8
4.2.5	Distribution of Output Ground Motion Parameter Values	4-8
4.3	Frequency Content	4-9
4.4	Energy Content	4-11
4.5	Duration	4-13
4.6	Influence of Local Site Conditions	4-16
4.6.1	Local Site Effect	4-16
4.6.2	Codes and Standards	4-18
4.6.3	Energy and Duration	4-24
4.6.4	Resonant Site Frequency	4-24
4.7	Selection of Representative Time Histories	4-26
5.0	Site Characterization	5-1
5.1	Introduction	5-1
5.2	Subsurface Profile Development	5-1
5.2.1	General	5-1
5.2.2	Water Level	5-1
5.2.3	Soil Stratigraphy	5-2
5.2.4	Depth to Bedrock	5-3
5.3	Required Soil Parameters	5-3
5.3.1	General	5-3
5.3.2	Relative Density	5-3
5.3.3	Shear Wave Velocity	5-4
5.3.4	Cyclic Stress-Strain Behavior	5-5
5.3.5	Peak and Residual Shear Strength	5-7
5.4	Evaluation of Soil Properties	5-8
5.4.1	General	5-8
5.4.2	In Situ Testing for Soil Profiling	5-9
	Standard Penetration Testing (SPT)	5-9
	Cone Penetration Testing (CPT)	5-14

5.4.3	Soil Density	5-15
5.4.4	Shear Wave Velocity	5-15
	General	5-15
	Geophysical Surveys	5-15
	Compressional Wave Velocity	5-22
5.4.5	Evaluation of Cyclic Stress-Strain Parameters	5-22
	Laboratory Testing	5-22
	Use of Empirical Correlations	5-23
5.4.6	Peak and Residual Shear Strength	5-26
6.0	Seismic Site Response Analysis	6-1
6.1	General	6-1
6.2	Site-Specific Site Response Analysis	6-1
6.3	Simplified Seismic Site Response Analyses	6-1
6.4	Equivalent-Linear One-Dimensional Site Response Analyses	6-6
6.5	Advanced One- and Two-Dimensional Site Response Analyses	6-9
	6.5.1 General	6-9
	6.5.2 One-Dimensional Non-Linear Response Analyses	6-9
	6.5.3 Two-Dimensional Site Response Analyses	6-10
7.0	Seismic Slope Stability	7-1
7.1	Background	7-1
7.2	Seismic Coefficient-Factor of Safety Analyses	7-3
	7.2.1 General	7-3
	7.2.2 Selection of the Seismic Coefficient	7-4
7.3	Permanent Seismic Deformation Analyses	7-6
	7.3.1 Newmark Sliding Block Analysis	7-6
7.4	Unified Methodology for Seismic Stability and Deformation Analysis	7-11
7.5	Additional Considerations	7-13
8.0	Liquefaction and Seismic Settlement	8-1
8.1	Introduction	8-1
8-2	Factors Affecting Liquefaction Susceptibility	8-1
8-3	Evaluation of Liquefaction Potential	8-5
	8.3.1 Introduction	8-5
	8.3.2 Simplified Procedure	8-5
	8.3.3 Variations on the Simplified Procedure	8-12
8-4	Post-Liquefaction Deformation and Stability	8-12
8-5	Seismic Settlement Evaluation	8-17
8-6	Liquefaction Mitigation	8-20
9.0	Seismic Design of Foundations and Retaining Walls	9-1
9.1	Introduction	9-1
	9.1.1 Seismic Response of Foundation Systems	9-1
	9.1.2 Seismic Performance of Retaining Walls	9-3
9.2	Design of Shallow Foundations	9-3
	9.2.1 General	9-3
	9.2.2 Pseudo-Static Analyses	9-5
	General	9-5
	Load Evaluation for Pseudo-Static Bearing Capacity Analysis	9-5

	The General Bearing Capacity Equation	9-6
	Bearing Capacity from Penetration Tests	9-9
	Sliding Resistance of Shallow Foundations	9-10
	Factors of Safety	9-12
9.2.3	Equivalent Foundation Stiffness	9-12
	General	9-12
	Stiffness Matrix of a Circular Surface Footing	9-13
	Damping	9-14
	Rectangular Footings	9-14
	Embedment Effects	9-16
	Implementation of Dynamic Response Analyses	9-16
9.3	Design of Deep Foundations	9-18
9.3.1	General	9-18
9.3.2	Seismic Vulnerability of Deep Foundations	9-20
9.3.3	General Design Procedure	9-20
9.3.4	Seismic Response of Pile Foundations	9-22
9.3.5	Method of Analysis	9-23
	Group Effects	9-28
9.3.6	Equivalent Foundation Stiffness	9-30
	Equivalent Cantilever Method	9-30
	Foundation Stiffness Matrix Method	9-31
9.3.7	Other Design Issues	9-33
	Foundation Design Forces	9-33
	Soil Strength	9-43
	Pile Uplift Capacity	9-43
	Liquefaction	9-44
	Ground Displacement Loading	9-44
9.4	Retaining Structures	9-45
9.4.1	General	9-45
9.4.2	Gravity Type Retaining Walls	9-46
	Dynamic Earth Pressure Approach	9-46
	Permissible Displacement Approach	9-49
9.4.3	Mechanically Stabilized Earth (MSE) Walls	9-51
	External Seismic Stability	9-52
	Internal Seismic Stability	9-54
9.4.4	Soil-Nailed Walls	9-55
9.4.5	Anchored Walls	9-57
9.4.6	Stiffness of Abutment Walls	9-59
10.0	References	10-1

PART II- DESIGN EXAMPLES

	Page
LIST OF FIGURES	ii
LIST OF TABLES	iv
1.0 Introduction	1-1
2.0 Seismic Analysis of a Shallow Bridge Foundation	2-1
2.1 Introduction	2-1
2.1.1 Description of the Project	2-1
2.1.2 Source Materials Required	2-1
2.2 Site Geology	2-1
2.3 Geotechnical Exploration	2-1
2.4 Design of Shallow Foundation	2-4
2.5 Seismic Settlement and Liquefaction Potential	2-7
2.6 Calculations	2-7
2.7 Summary and Conclusions	2-7
2.8 Detailed Calculations - Example 1 - Seismic Analysis of a Shallow Bridge Foundation	2-7
3.0 Seismic Design of a Deep Foundation System	3-1
3.1 Introduction	3-1
3.1.1 Description of the Project	3-1
3.1.2 Source Materials Required	3-1
3.2 Geotechnical Exploration	3-1
3.3 Design of Pile Foundations	3-5
3.4 Detailed Calculations - Example 2 - Seismic Design of a Deep Foundation System .	3-8
3.5 Summary and Conclusion	3-18
4.0 Site Response Analysis	4-1
4.1 Introduction	4-1
4.1.1 Description of the Project	4-1
4.1.2 Source Materials Required	4-1
4.2 Site Conditions	4-1
4.2.1 Subsurface Profile	4-1
4.2.2 Dynamic Soil Properties	4-2
4.2.3 Fundamental Period	4-5
4.3 Seismic Hazard Analysis	4-6
4.3.1 Introduction	4-6
4.3.2 Response Spectra	4-6
4.3.3 Magnitude Distribution	4-6
4.3.4 Selection of Time Histories	4-8
4.4 Seismic Response Analysis	4-9
4.4.1 Method of Analysis	4-9
4.4.2 Results of the Analysis	4-9
5.0 Slope Stability Analysis	5-1

5.1	Introduction	5-1
	5.1.1 Description of the Project	5-1
	5.1.2 Source Materials Required	5-1
5.2	Site Geology	5-1
5.3	Geotechnical Exploration	5-3
	5.3.1 General	5-3
	5.3.2 Geotechnical Properties	5-3
5.4	Deterministic Seismic Hazard Analysis	5-3
5.5	Slope Stability Analysis	5-6
	5.5.1 Design Criteria	5-6
	5.5.2 Stability Analyses	5-6
5.6	Results	5-6
5.7	Remedial Solution	5-12
5.8	Summary and Conclusions	5-12
6.0	Liquefaction Potential Analysis	
6.1	Introduction	6-1
	6.1.1 Description of the Project	6-1
	6.1.2 Source Materials Required	6-1
6.2	Geological Setting	6-1
	6.2.1 Regional Setting	6-1
	6.2.2 Local Geology	6-1
6.3	Seismic Design Criteria	6-3
6.4	Probabilistic Seismic Hazard Analysis	6-3
6.5	Geotechnical Information	6-6
6.6	Design of the Embankment	6-6
	6.6.1 Design Considerations	6-6
	6.6.2 Seismic Slope Stability	6-12
	6.6.3 Liquefaction Potential	6-12
	6.6.4 Evaluation of the Consequences of Liquefaction	6-15
6.7	Site Response Analyses	6-18
6.8	Detailed Calculations - Example 5 - Liquefaction Potential Analysis	6-18
6.9	Summary and Conclusions	6-42
7.0	References	7-1

PART I

DESIGN PRINCIPLES

LIST OF FIGURES

<u>No.</u>	<u>Caption</u>	<u>Page</u>
1-1	Areas Impacted by Major Historical Earthquakes in the United States	1-1
1-2	Tilting of Buildings Due to Soil Liquefaction During the Niigata (Japan) Earthquake of 1964	1-4
1-3	Slumping of the Lower San Fernando Dam in the 1971 San Fernando Earthquake	1-4
1-4	Secondary Earthquake Damage Caused by Fire	1-5
1-5	Collapse of Hanshin Expressway During the 1995 Kobe (Hyogo-ken Nabu, Japan) Earthquake	1-7
2-1	Major Tectonic Plates and Their Approximate Direction of Movement	2-2
2-2	Cross-section Through Tectonic Plates in Southern Alaska	2-2
2-3	Thrust Faulting Without Surface Rupture	2-4
2-4	Types of Fault Movement	2-7
2-5	Comparison of Earthquake Magnitude Scale	2-8
2-6	Definition of Basic Fault Geometry	2-9
2-7	Various Distance Measures Used in Earthquake Engineering	2-10
2-8	Acceleration, Velocity, and Displacement Time Histories	2-11
2-9	Schematic Representation of Acceleration Response Spectra	2-12
2-10	Tripartite Representation of Acceleration, Velocity, and Displacement Response Spectra	2-13
3-1	Seismic Stations in the Central United States.	3-3
3-2	Epicenters of Earthquakes in the Southeastern United States from July 1977 through June 1985 (Sibol et al., 1985): Magnitude of 3 or Greater	3-3
3-3	Effective Peak Acceleration Levels (In Decimal Fractions of Gravity) with a 10% Probability of Being Exceeded During a 50-year Period	3-7
3-4	Map and Table for UBC Seismic Zone Factor, Z	3-8
3-5	Peak Horizontal Ground Acceleration in Bedrock with a 10 Percent Probability of Exceedance in 50 Years	3-10
3-6	Seismic Source Zones in the Central United States	3-12
3-7	Seismic Source Zones in the Central and Eastern United States	3-13
3-8	Probabilistic seismic Hazard Analysis Data	3-16
3-9	Cumulative Frequency-magnitude Plot of Instrumental Seismicity; San Andreas Fault South-central Segment Data	3-17
3-10	Magnitude-distance Distribution for a Specified Peak Ground Acceleration	3-18
4-1	Comparison of Attenuation Relationships by Various Investigators	4-5
4-2	Comparison of Attenuation Relationship for Eastern and Central United States to Attenuation Relationship for Western United States	4-7
4-3	Abrahamson and Silva (1997) Attenuation Relationship	4-7
4-4	Comparison of Smoothed Acceleration Response Spectra for Various Earthquake Magnitudes	4-10
4-5	Comparison of Smoothed Acceleration Response Spectra by Various Investigators	4-10
4-6	Real Spectra vs. Smoothed Spectra	4-11

4-7	Attenuation of the Root Mean Square Acceleration	4-12
4-8	Arias Intensity Attenuation Relationship (Kayen and Mitchell, 1997)	4-13
4-9	Accelerogram Recorded During the 1989 Loma Prieta Earthquake	4-14
4-10	Bolt (1973) Duration of Strong Shaking	4-15
4-11	Trifunac and Brady (1975) Duration of Strong Shaking	4-15
4-12	Duration Versus Earthquake Magnitude for the Western United States	4-16
4-13	Soil Conditions and Characteristics of Recorded Ground Motions, Daly City (San Francisco) M_w 5.3 Earthquake of 1957	4-17
4-14	Comparison of Soil and Rock Site Acceleration Response Spectra for M_w 8 Event at 5 km	4-18
4-15	PGA Attenuation in 1985 Mexico City Earthquake (Krinitzsky, 1986)	4-19
4-16	Spectral Amplification in 1985 Mexico City Earthquake (Romo and Seed, 1986)	4-19
4-17	Normalized 1994 Uniform Building Code Response Spectra	4-20
4-18	1997 Uniform Building Code Response Spectra	4-21
4-19	Fundamental Frequency of Trapezoidal Dam/Embankment	4-25
5-1	Stresses Induced in a Soil Element by Vertically Propagating Shear Wave	5-6
5-2	Hysteretic Stress-Strain Response of Soil Subjected to Cyclic Loading	5-7
5-3	Shear Modulus Reduction and Equivalent Viscous Damping Ratio Curves	5-8
5-4	SPT-Relative Density Correlation	5-10
5-5	Correction Factor for the Effective Overburden Pressure, C_N	5-14
5-6	Soil Classification System Based on the CPT	5-16
5-7	CPT-Soil Behavior - SPT Correlation Chart	5-17
5-8	Schematic Sketch of Cross Hole Survey	5-18
5-9	Schematic Sketch of Down Hole Survey	5-19
5-10	Schematic Sketch of Seismic Cone Penetration Testing (SCPT).	5-19
5-11	Schematic of SASW Testing	5-21
5-12	Shear Modulus Reduction Curves for Sands	5-27
5-13	Shear Modulus Reduction Curves for Sands	5-28
5-14	Shear Modulus Reduction and Damping Ratio as a Function of Shear Strain and Soil Plasticity Index	5-28
5-15	Relationship Between Corrected "Clean Sand" Blow Count $(N_1)_{60-cs}$ and Undrained Residual Strength (S_u) from Case Studies	5-30
6-1	Refraction of Near Surface S-Waves	6-2
6-2	Relationship Between PHGA on Rock and on Other Local Site Conditions	6-3
6-3	Relationship Between PHGA on Rock and on Soft Soil Sites	6-4
6-4	Comparisons of Peak Base and Crest Accelerations Recorded at Earth Dams	6-4
6-5	Variation of Peak Average Acceleration Ratio with Depth of Sliding Mass	6-6
6-6	1-Dimensional Column for SHAKE Analysis (Schnabel et al., 1972)	6-8
6-7	1-Dimensional Analysis for 2-Dimensional Response (Vrymoed and Calzascia, 1978)	6-9
7-1	Composite Shear Strength Envelope	7-2
7-2	Pseudo-Static Limit Equilibrium Analysis for Seismic Loads	7-4
7-3	Influence of Vertical Seismic Coefficient on Horizontal Yield Acceleration	7-5
7-4	Permanent Seismic Deformation Chart	7-6
7-5	Basic Elements of Newmark Deformation Analysis	7-7

7-6	Newmark Analysis Using Peak and Residual Shear Strengths (Matasovic, Kavazanjian, and Giroud, 1998)	7-9
7-7	Comparison of Results from Newmark Analysis Using Peak and Residual Shear Strengths (Matasovic, Kavazanjian, and Giroud, 1998)	7-10
7-8	Inter-Relationship of Yield Acceleration and Peak Average Acceleration	7-10
7-9	Permanent Displacement Versus Normalized Yield Acceleration for Embankments	7-13
8-1	Grain Size Distribution Curves of Potentially Liquefiable Soils	8-4
8-2	Stress Reduction Factor, R_d	8-6
8-3	Relationship Between Stress Ratio Causing Liquefaction and $(N_1)_{60}$ Values for Sands for $M_w=7.5$ Earthquakes	8-8
8-4	Curve for Estimation of Magnitude Correction Factor, k_m	8-9
8-5	Curves for Estimation of Correction Factor k_c	8-9
8-6	Curves for Estimation of Correction Factor, k_u	8-10
8-7	Effects of Gravel Content on Liquefaction Resistance of Gravelly Soils	8-11
8-8	Relationship between Cyclic Stress Ratio Causing Liquefaction and CPT Tip Resistance, q_{c1N} for Sands for $M = 7.5$	8-13
8-9	Relationship Between Cyclic Stress Ratio Causing Liquefaction and Shear Wave Velocity Values, V_{s1} , for Sands for $M= 7.5$ Earthquakes	8-14
8-10	Curves for Estimation of Post-Liquefaction Volumetric Strain Using SPT Data and Cyclic Stress Ratio for $M_w 7.5$ Earthquakes	8-15
8-11	Plot for Determination of Earthquake-Induced Shear Strain in Sand Deposits . . .	8-18
8-12	Relationship Between Volumetric Strain, Cyclic Strain and Penetration Resistance for Unsaturated Sands	8-19
8-13	Post-Earthquake Settlements at Two Port Sites due to the 1995 Kobe Earthquake.	8-21
9-1	Superstructure Loads Resolved Into Components at Footing	9-2
9-2	Principle of Superposition of Loads on Footing	9-2
9-3	Degrees of Freedom of a Footing and Corresponding Stiffness Matrix	9-4
9-4	Coupled Rocking and Sliding	9-4
9-5	Evaluation of Overturning Moment	9-8
9-6	Calculation of Equivalent Radius Rectangular Footing	9-16
9-7	Shape Factor α for Rectangular Footings	9-17
9-8	Embedment Factors for Footings with $D/R < 0.5$	9-17
9-9	Embedment Factors for Footings with $D/R > 0.5$	9-18
9-10	Commonly Used Deep Foundations for Highway Bridges	9-19
9-11	Potential Failure Modes for Pile Foundations	9-21
9-12	Three-Dimensional Soil Pile Interaction	9-23
9-13	Soil-Pile Characterization in Laterally Loaded Pile/Pile Group Analyses.	9-24
9-14	Typical p-y Curve for Soft Clay.	9-27
9-15	Graphical Presentation of Laterally Loaded Pile Analysis.	9-27
9-16	p-Multiplier for Group Effects.	9-30
9-17	Methods for Representing Deep Foundation Stiffness	9-31
9-18	Equivalent Cantilever Method- Equal Deflection Assumption.	9-32
9-19	Coefficient of Variation of Subgrade Modulus for Sand.	9-34
9-20	Coefficient of Variation of Subgrade Modulus for Clay.	9-35
9-21	Lateral Stiffness of Free-Headed Piles	9-36

9-22	Lateral Stiffness of Fixed Head Piles.	9-37
9-23	Rotational Stiffness at Pile Head.	9-38
9-24	Cross-Coupling Stiffness at Pile-Head.	9-39
9-25	Embedment Effects on Lateral Stiffness of Fixed Head Piles.	9-40
9-26	Embedment Effects on Rotational Stiffness.	9-41
9-27	Embedment Effect on Cross-Coupling Stiffness	9-42
9-28	Dynamic Active Forces Behind a Gravity Wall in the Mononobe-Okabe Theory	9-47
9-29	Effect of Seismic Coefficients and Friction Angles on Seismic Active Pressure Coefficient	9-48
9-30	Range of Normalized Displacements Using Newmark Sliding Block Model, and Various Equations Approximating the Upper Envelope	9-50
9-31	Seismic External Stability of MSE Wall	9-53
9-32	Seismic Internal Stability of MSE Wall	9-56
9-33	Design Value of the Lateral Earth Pressure Coefficient, K, for Various Types of Soil Reinforcement Systems	9-56
9-34	Seismic Effects on Anchored Bulkheads	9-58

LIST OF TABLES

<u>No.</u>	<u>Caption</u>	<u>Page</u>
2-1	Modified Mercalli Intensity Scale	2-15
4-1	Attenuation Relationships for the Western United States	4-3
4-2	Attenuation Relationship for Subduction Zone Earthquakes	4-6
4-3	1997 UBC Classification (NEHRP)	4-21
4-4	Seismic Coefficient C_a	4-22
4-5	Seismic Coefficient C_v	4-22
4-6	Seismic Source Type	4-22
4-7	Near-Source Factor N_a	4-23
4-8	Near-Source Factor N_v	4-23
5-1	Relative Density of Sandy Soil	5-4
5-2	Recommended Standardized SPT Equipment	5-12
5-3	Corrected Factors for Non-Standardized SPT Procedure	5-13
5-4	Typical Values of Initial Shear Modulus	5-24
5-5	Correlations for Estimating Initial Shear Modulus	5-25
8-1	Susceptibility of Sedimentary Deposits to Liquefaction During Strong Shaking	8-2
8-2	Influence of Earthquake Magnitude on Volumetric Strain Ratio for Dry Sands	8-19
8-3	Improvement Techniques for Liquefiable Soil Foundation Condition	8-22
8-3	Improvement Techniques for Liquefiable Soil Foundation Condition	8-23
8-3	Improvement Techniques for Liquefiable Soil Foundation Condition	8-24
8-3	Improvement Techniques for Liquefiable Soil Foundation Condition	8-25
9-1	Inclination Factors for Bearing Capacity of Shallow Foundations	9-11
9-2	Equivalent Damping Ratios for Rigid Circular Footings	9-15
9-3	Typical Values of K_s and ϵ_{50}	9-26
9-4	Summary of Centrifuge Model Tests in Sand Results (3 x 3 Group, Free and Fixed Head, Plumb)	9-29
9-5	Recommended "p-Multiplier" Values for Pile Group Design	9-29

SYMBOLS

A	normalizing constant for G_{\max} calculation (Section 5.4.5) and/or maximum acceleration of earthquake record (Section 9.4)
A_m	maximum wall acceleration
a_n	dam/embankment fundamental frequency coefficient
a_{\max}	peak average acceleration, peak acceleration at the top of the embankment
$a(t)$	acceleration time history
B	foundation width (footing width) and/or width of the abutment wall
B'	effective width of footing
c	cohesion and/or viscous damping coefficient
C_{60}	product of correction factors for use in calculating N_{60}
C_N	correction factor for use in calculating $(N_1)_{60}$
C_{HT}	SPT correction factor for nonstandard hammer type
C_{HW}	SPT correction factor for nonstandard hammer weight/height of fall
C_{SS}	SPT correction factor for nonstandard sample setup
C_{RL}	SPT correction factor for change in rod length
C_{BD}	SPT correction factor for nonstandard borehole diameter
CSR_{EQ}	critical stress ratio induced by earthquake
CSR_L	corrected critical stress ratio resisting liquefaction
C_a	seismic coefficient (UBC)
C_v	seismic coefficient (UBC)
C_{w1}, C_{w2}	correction factors that depend on depth of the groundwater table
d_R	residual displacement of wall
D	pile diameter and/or damping ratio
D_{50}	mean grain size
$D_{50_{15}}$	average mean grain size in granular layer included in H_{15}
D_b	bracketed duration of strong ground motion
D_f	depth to the base of the footing from ground surface
D_r	relative density
D_s	significant duration of strong shaking
D_w	depth of the groundwater level
e	eccentricity of the resultant force and/or void ratio
E	Young's modulus of a pile
e_f	efficiency factor for stiffness of p-y curve due to group effects
e_{\max}	maximum void ratio
E_{\max}	small strain (initial) Young's modulus
e_{\min}	minimum void ratio
e_o	in situ void ratio
E_s	Young's modulus
f_e	fundamental frequency
f_o	resonant frequency
f_s	cone penetration test sleeve resistance
F_{15}	average fines content for granular layers included in H_{15}
F_{VE}	SPT energy correction factor using F2 method

SYMBOLS (continued)

FS_L	factor of safety against liquefaction
G	dynamic (secant) shear modulus
G_{max}	small strain (initial) shear modulus
H	height of the wall and/or resultant horizontal seismic load and/or soil layer thickness
H_{15}	cumulative thickness of saturated granular layers with corrected blow counts, $(N_1)_{60}$, less than or equal to 15
H_E	combined energy correction factor
i	slope of the surface of the backfill
I	moment of inertia of a pile
I_A	Arias intensity
i_c, i_γ, i_q	load inclination factors
k	SDOF system spring constant and/or power factor for small strain shear modulus calculation
K	stiffness matrix
K_{ECF}	stiffness matrix of equivalent circular footing
k_α	correction factor for the initial driving static shear stress
K_δ	stiffness coefficient relating force and displacement
K_θ	stiffness coefficient relating moment and rotation
k_σ	correction factor for stress levels larger than 96 kPa
K_{11}, K_{22}	stiffness coefficient for horizontal rotation
K_2	factor for G_{max} calculation
K_{33}	stiffness coefficient for vertical translation
K_{44}, K_{55}	stiffness coefficient for rocking rotation
K_{66}	stiffness coefficient for torsional rotation
K_{ae}	seismic active earth pressure coefficient
K_{pe}	seismic passive earth passive coefficient
k_h	horizontal seismic coefficient
K_i	initial slope of soil modulus in laterally loaded pile analysis
K_{ij}	coefficient of stiffness matrix
k_M	correction factor for earth quake magnitudes other than M_w 7.5
k_{max}	peak horizontal average acceleration
K_o	coefficient of lateral earth pressure at rest
k_s	seismic coefficient
K_s	translational stiffness
k_v	vertical seismic coefficient
K_{vg}	vertical ground acceleration
KW_s	pseudo-static inertia force
k_y	yield acceleration
L	foundation length
L_{ei}	effective resistant length of reinforcement for MSE wall
m	mass
m_b	(short period) body wave magnitude

SYMBOLS (continued)

m_B	(long period) body wave magnitude
M_{JMS}	Japan Meteorological Agency Magnitude
M_L	Local (Richter) Magnitude
M_S	Surface Wave Magnitude
M_W	Moment Magnitude
n	effective strain factor and/or correction factor
N	uncorrected Standard Penetration Test (SPT) blow count and/or yield acceleration
N^*	average blow count adjusted for submergence effects
N_{60}	standardized SPT blow count
$(N_1)_{60}$	normalized standard SPT blow count
$(N_1)_{60-cs}$	normalized standard "clean sand" SPT blow count
N_a	Near-Source Factor (UBC)
N_{corr}	correction factor for fines
N_c, N_γ, N_q	bearing capacity factors
N_v	Near-Source Factor (UBC)
OCR	overconsolidation ratio
P_a	atmospheric pressure
P_{ae}	seismic active earth force or thrust
P_{ir}	horizontal inertial force of reinforced soil mass for MSE wall
P_{is}	horizontal inertial force of retained backfill for MSE wall
P_{pe}	seismic passive earth force or thrust
P_u	ultimate soil resistance along pile
P_I	horizontal inertial force due to the weight of active backfill zone for MSE wall
P_{IR}	horizontal inertial force for MSE wall
PI	Plasticity Index
q_c	Cone Penetration Test (CPT) point resistance
q_{c1}, q_{c1N}	normalized Cone Penetration Test (CPT) point resistance
q, q_s	uniform surcharge load applied at ground surface
q_{ult}	ultimate bearing capacity (ultimate bearing pressure)
r_d	stress reduction factor
r_o	equivalent radius for rectangular footing
R_E	epicentral distance
R_H	hypocentral distance
R_I	load inclination factor
R_{JB}	Joyner and Boore distance
R_R	rupture distance
R_S	seismogenic distance
S	center to center spacing of piles in a pile group and/or ground slope (in percent)
S_a	spectral acceleration
S_c, S_γ, S_q	foundation shape factors
S_d	spectral displacement

SYMBOLS (continued)

S_r	residual shear strength
S_{su}	steady-state shear strength
S_v	spectral velocity
s_v	vertical spacing between reinforcements for MSE wall
t_f	duration of strong ground shaking
T_o	fundamental period
T, T_i	period
T_{max}	maximum static load of reinforcement for MSE wall
T_{md}	dynamic incremental force in reinforcement for MSE wall
T_{total}	maximum total tensile force in reinforcement for MSE wall
u_{max}	maximum permanent displacement
V	resultant vertical seismic load and/or peak velocity of the earthquake record
V_p	compression wave velocity
V_s	shear wave velocity
V_{si}	normalized shear wave velocity
$(V_s)_{avg}$	average shear wave velocity
W	weight of the potential failure mass, or ratio of the height of the free face to the distance from the base of the free face to the point in question
W_s	weight of the sliding wedge
W_w	weight of the wall
Z	seismic zone factor, as used in UBC (1994)
$(\tau_{max})_d$	peak shear stress of a soil column
$(\tau_{max})_r$	peak shear stress of a rigid body
α	inclination of resultant force and/or foundation shape correction factor
α_{ae}	active failure surface inclination angle behind wall
α_{pe}	passive failure surface inclination angle in front of wall
β	backfill slope angle and/or foundation embedment factor
γ	unit weight
γ_c	cyclic shear strain
$\gamma_{d max}$	maximum dry density
$\gamma_{d min}$	minimum dry density
$\gamma_{eff} (G_{eff}/G_{max})$	hypothetical effective shear strain factor
γ_{eff}	effective shear strain
γ_f	unit weight of backfill zone
γ_{max}	maximum unit weight; maximum shear strain
γ_{min}	minimum unit weight
γ_o	in situ unit weight
γ_r	unit weight of reinforced zone
γ_t	total unit weight
δ	angle of friction of the wall/backfill interface or unit horizontal deflection of a pile head
Δ_L	liquefaction-induced lateral displacement
ϵ_c	volumetric strain due to compaction

SYMBOLS (continued)

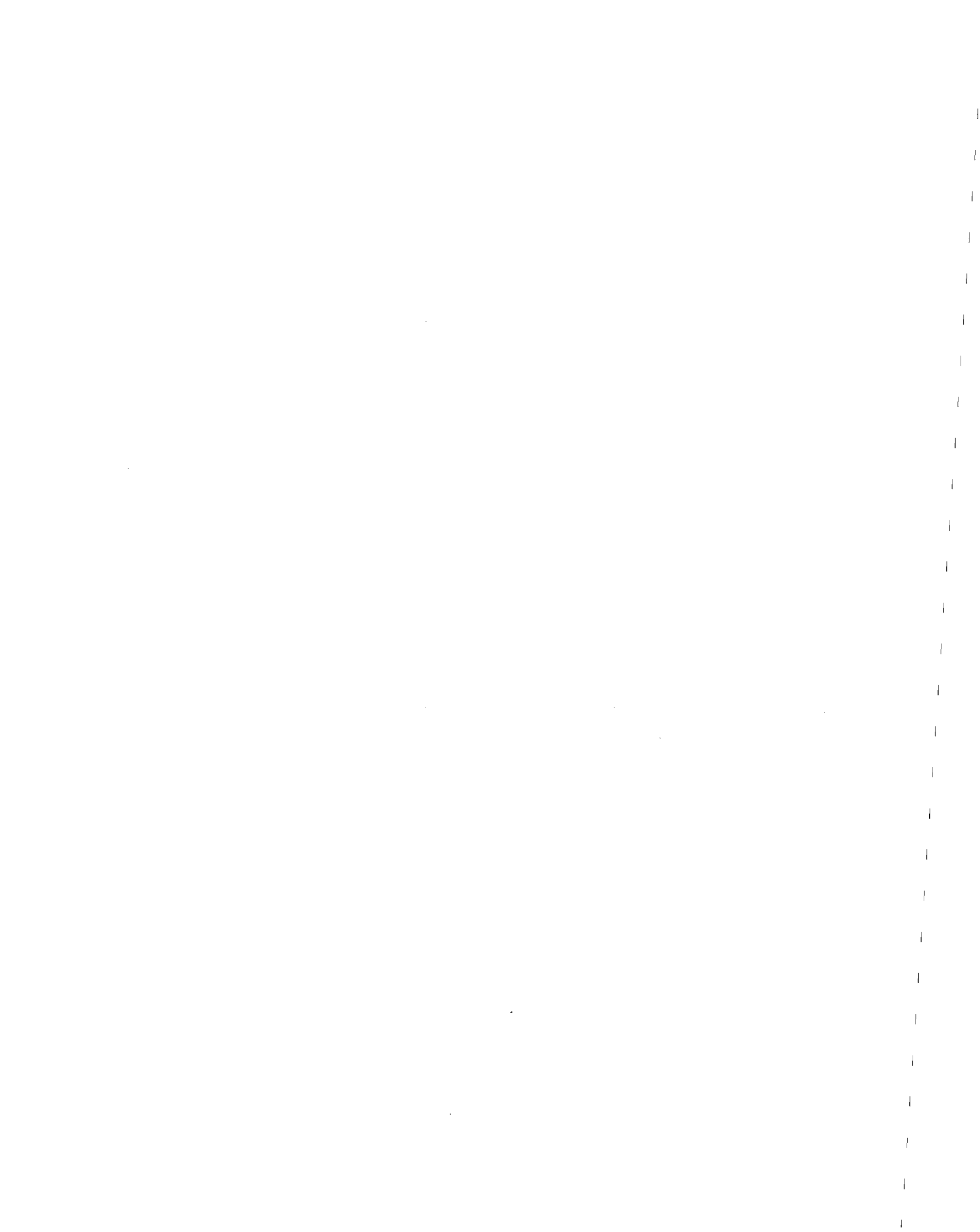
ε_v	post-liquefaction volumetric strain
ε_{50}	strain at 50% maximum principal stress
ν	Poisson's ratio
ρ	mass density
σ_h	horizontal total stress
σ_m	mean normal total stress
σ'_m	mean normal effective stress or confining pressure
σ_o	vertical total stress
σ'_o	vertical effective stress
σ_v	vertical total stress
σ'_v	vertical effective stress
τ_{ho}	initial static shear stress on a horizontal plane
τ_{max}	maximum earthquake-induced shear stress at depth
ϕ	angle of internal friction
ϕ_b	angle of internal friction between the base of the wall and the foundation soil
ω_o	circular natural frequency
λ	equivalent viscous dumping ratio
θ	unit rotation of a pile head (Section 9.3), or angle of backface of the wall with the vertical (Section 9.4)
ψ	equivalent angle based on seismic coefficients k_h and k_v

ABBREVIATIONS AND ACRONYMS

AASHTO	American Association of State Highway and Transportation Officials
ASCE	American Society of Civil Engineers
ASTM	American Society for Testing and Materials
ATC	Applied Technology Council
BPT	Becker Penetration Test
CALTRANS	California Department of Transportation
CSSASW	Controlled Source Spectral Analysis of Surface Waves
CDMG	California Division of Mines and Geology
CPT	Cone Penetration Test
CSR	Critical Stress Ratio
CyDSS	Cyclic Direct Simple Shear (Test)
EERC	Earthquake Engineering Research Center
EERI	Earthquake Engineering Research Institute
EPA	Effective Peak Acceleration
EPRI	Electric Power Research Institute
FEMA	Federal Emergency Management Agency
FHWA	Federal Highway Administration
FSAR	Final Safety Analysis Report
GEC	Geotechnical Engineering Circular
HBA	Hypothetical Bedrock Outcrop
IDOT	Illinois Department of Transportation
JSSMFE	Japanese Society for Soil Mechanics and Foundation Engineering
MCE	Maximum Credible Earthquake
MFZ	Mendocino Fracture Zone
MHA	Maximum Horizontal Acceleration
MM	Modified Mercalli (Intensity Scale)
MPE	Maximum Probable Earthquake
MSE	Mechanically Stabilized Earth
NAPP	National Aerial Photographic Program
NAVFAC	Naval Facilities Engineering Command
NCEER	National Center for Earthquake Engineering Research
NCHRP	National Cooperative Highway Research Program
NEHRP	National Earthquake Hazards Reduction Program
NGDC	National Geophysical Data Center
NHI	National Highway Institute
NISEE	National Information Service for Earthquake Engineering
NRC	National Research Council
NTIS	National Technical Information Service
NYSDOT	New York State Department of Transportation
PGA	Peak Ground Acceleration
PGD	Peak Ground Displacement
PGV	Peak Ground Velocity

ABBREVIATIONS AND ACRONYMS (continued)

PHGA	Peak Horizontal Ground Acceleration
PHGD	Peak Horizontal Ground Displacement
PHGV	Peak Horizontal Ground Velocity
PI	Plasticity Index
PSAR	Preliminary Safety Analysis Report
PVGA	Peak Vertical Ground Acceleration
RMS	Root Mean Square
RMSA	Root Mean Square of Acceleration
SASW	Spectral Analysis of Surface Waves
SDOF	Single Degree of Freedom (System)
SPT	Standard Penetration Test
SSA	Seismological Society of America
SSI	Soil-Structure-Interaction
UBC	Unified Building Code
USEPA	United States Environmental Protection Agency
USGS	United States Geological Survey



CHAPTER 1.0 INTRODUCTION

1.1 INTRODUCTION

In the United States, design of constructed facilities to resist the effects of earthquakes is often considered a problem restricted to California or the western United States. However, historical records show that damaging earthquakes can, and do, also occur over broad areas of the eastern and central United States. Some of these historical eastern and central United States earthquakes have been truly major events, with intensities equal to or greater than that of the 1906 San Francisco earthquake, impacting areas far larger than the impact areas of major earthquakes that have occurred in the western United States in historical times (Figure 1-1).

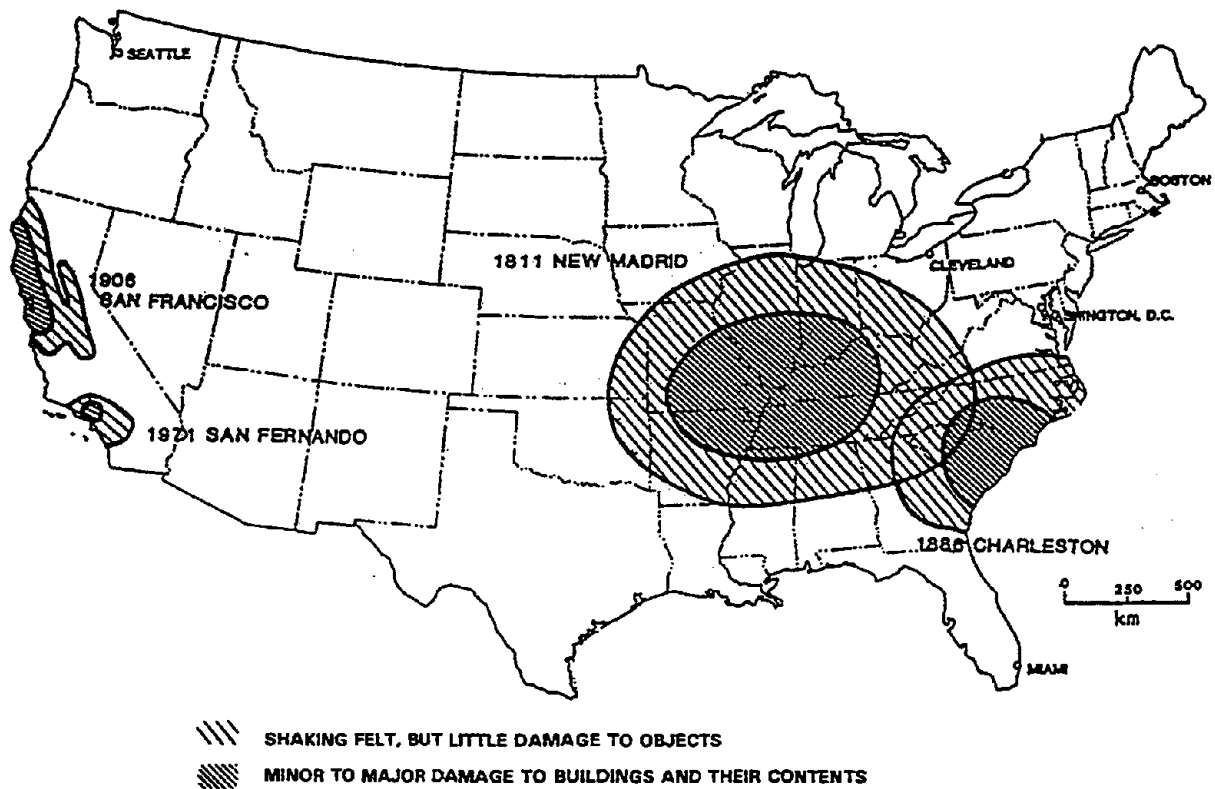


Figure 1-1: Areas Impacted by Major Historical Earthquakes in the United States. (After Nuttli, 1974, reprinted by permission of ASCE)

The areas over which damaging earthquakes may reasonably be expected to occur cover more than 40 percent of the continental United States (e.g., see the seismic risk maps in Chapter 3 of this document). Until recently, highway facilities in many of these areas have not been designed for seismic loading. Seismic design concepts are therefore relatively new to highway engineers in these regions. Furthermore, the state-of-practice in earthquake engineering has evolved rapidly in the past 25 years, as lessons learned from new earthquakes are incorporated into practice.

The objective of this document is to provide general guidance to geotechnical engineers on the seismic design of highway facilities. This document is intended to supplement existing FHWA guidance documents on seismic design of bridges and other highway facilities. Therefore, detailed information on geotechnical aspects of seismic design is provided herein while other aspects are addressed by reference and only briefly addressed herein. Furthermore, it is assumed that the geotechnical engineer using this document is familiar with the static design of highway facilities. Accordingly, this document only focuses on those aspects of geotechnical investigation, analysis, and design that relate to seismic design.

The practice of earthquake engineering continues to evolve rapidly. For instance, the coefficients for some of the acceleration attenuation relationships described in Chapter 4 are updated on a yearly basis. A design engineer using this document should check the technical literature on geotechnical earthquake engineering for enhancements or modifications of the methods presented herein and for new developments in the field to be completely up to date.

1.2 SOURCES OF DAMAGE IN EARTHQUAKES

1.2.1 General

Damage resulting from earthquakes may be directly attributable to the effects of the earthquake or may be an indirect result of direct earthquake damage. Likewise, direct damage from earthquakes may result from both the primary impacts from the earthquake (i.e., ground shaking and fault displacement) or from secondary impacts, like landslides and soil liquefaction, generated by the primary impacts.

1.2.2 Direct Damage

Classification of Direct Damage

Damage that is directly linked to the effects of the earthquake is referred to as *direct damage*. Direct damage can be separated into two broad classes: *primary damage* due to strong shaking and fault rupture and *secondary damage* due to the effects of strong shaking and fault rupture.

Primary Damage

Primary damage is damage that is a direct result of strong shaking or fault rupture. Primary damage attributable to strong shaking and fault rupture includes partial or total collapse of a structure. The magnitude of the damage due to strong shaking will depend on both the intensity of the motion and the frequency (or frequency content) of the motion. These factors, in turn, may depend upon the earthquake magnitude and source mechanism (e.g., strike-slip or thrust faulting), the location of the site with respect to the point of energy release of the earthquake (e.g., distance, azimuth), and the response characteristics of both the foundation for the impacted structure and the structure itself (e.g., natural period). Damage due to fault rupture depends upon the amplitude, spatial distribution (e.g., concentrated along a single strand or diffused across a zone), and direction (e.g., vertical or lateral) of the fault displacement.

The relationship of the natural frequency of a structure (earthen or man-made) to the predominant frequency of the strong shaking generated at the site by the earthquake is an important factor influencing the damage potential of the ground motions. The predominant frequency of the strong shaking at the site is, in turn, influenced not only by the earthquake source mechanism, but also by travel path of the seismic waves from the source to the site and by the local geology and topography at the site. A notable example

is the seismic response of the Mexico City sedimentary basin to distant earthquakes and associated structural damage to buildings. Both in the 1957 and 1985 earthquakes, only certain buildings in selected areas of the city were damaged whereas other areas remained unaffected.

Damage linked to vertical and horizontal fault displacement is most often associated with linear systems such as water lines, gas mains, roadways, and railways. Many of these linear systems provide essential services to the community and are therefore referred to as *lifelines*. Fault rupture will also impact structures that are constructed directly above the fault.

Secondary Damage

In addition to direct damage to constructed facilities and natural slopes caused by the inertial forces due to ground shaking and permanent ground displacement due to faulting, structures may also experience secondary damage as a consequence of direct damage induced by earthquake ground motions. For instance, the strong shaking may cause a landslide that damages a bridge or viaduct. In some soils (e.g., saturated sands), strong shaking may cause a loss of soil strength or stiffness in level ground that results in settlement or lateral spreading of foundations and failure of earthen structures. Secondary damage due to earthquake ground motions is an important consideration for highway systems. Examples of secondary damage to highway facilities include:

- *Damage due to landslides:* There are numerous documented cases of landslides generated by earthquake ground motions. Ground movement associated with a landslide can cause structural damage to the superstructure or foundation of a highway facility, block roadways, and generate other types of secondary impacts (e.g., seiches in reservoirs, rupture to pipelines).
- *Liquefaction:* Strong ground shaking can cause a loss of strength in saturated cohesionless soils. This loss of strength is referred to as *liquefaction*. Liquefaction of saturated sands during earthquakes was first identified as a major source of secondary damage after the 1964 Niigata and Alaska earthquakes. Since that time, a considerable amount of research has been performed to understand and mitigate liquefaction problems. Soil liquefaction is discussed in detail in Chapter 8 of this document. The consequences of liquefaction may include bearing capacity failure, lateral spreading, and slope instability.
- Bearing capacity failure: When the soil supporting a structure liquefies and loses strength, the bearing capacity of the soil drops to almost zero. As a consequence of this loss of bearing capacity, large foundation deformations can occur. Bearing capacity failure may result in the structure settling and rotating (tilting) as in Niigata in 1964 (see Figure 1-2). Seismically-induced bearing capacity failure can also occur without liquefaction of the underlying soil.
- Lateral spreading: Lateral spreading is the lateral displacement of large surficial blocks of soil as a result of liquefaction in a subsurface layer. Liquefaction of a layer or seam of soil in even gently sloping ground can often result in lateral spreading. Movements may be triggered by the inertial forces generated by the earthquakes and continue in response to gravitational loads. Lateral spreading has been observed on slopes as gentle as 5 degrees.
- Slope instability: Liquefaction of even thin seams of soil can induce an overall stability failure in a slope or embankment. These slope failures can occur during or after the earthquake. The slumping of the Los Angeles (Lower San Fernando) Dam in the 1971 San Fernando earthquake is perhaps the best known example of a liquefaction-induced slope failure (see Figure 1-3).

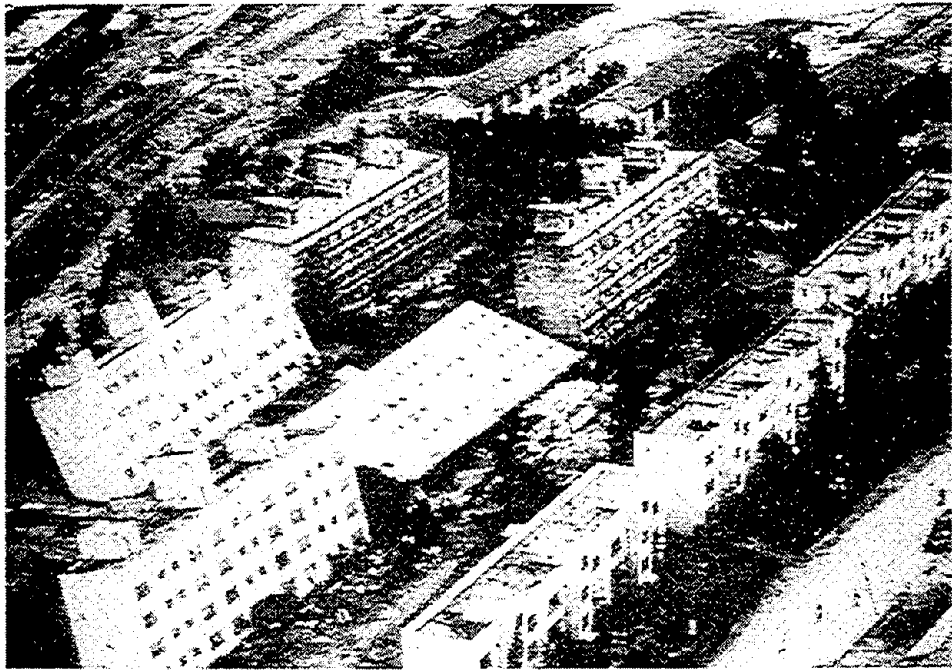


Figure 1-2: Tilting of Buildings Due to Soil Liquefaction During the Niigata (Japan) Earthquake of 1964.



Figure 1-3: Slumping of the Lower San Fernando Dam in the 1971 San Fernando Earthquake.

- *Fire and explosion:* Fire or explosions have historically been a major source of damage following earthquakes. Rupture of gas and electric lines is often the cause of dramatic explosions and fires. In many cases, the right-of-way for oil and gas pipelines is located along highway alignments. During the 1994 Northridge earthquake, fire following rupture of a gas line in a street provided some of the most graphic images of the earthquake (see Figure 1-4).
- *Other sources of secondary damage:* Other sources of secondary damage from earthquakes include chemical spills, sewer damage, and loss of potable water supplies. Secondary damage to underground sewer and water supply pipelines often may not be evident immediately following the earthquake.

1.2.3 Indirect Damage

Indirect damage refers to the socio-economic impact of an earthquake. Indirect damage may include loss of business or essential services and environmental impacts.

- *Loss of services:* An important effect of earthquakes that is not easily quantifiable is cost in terms of loss of business and disruption of services. Many businesses cannot operate after an earthquake, and many other businesses may be impaired by increased travel and delivery times due to earthquake damage. The indirect impacts of earthquakes can last months and even years after the event. Loss of essential services such as transportation facilities and power and water systems are major contributors to indirect damage.
- *Environmental impact:* The indirect environmental side effects of an earthquake can include increased consumption of fossil fuels, resulting in air pollution and health impacts due to disruption of waste disposal services. Increased travel time and traffic congestion can significantly increase air emissions following a seismic event. Closure of waste disposal facilities and disruption of waste collection both contribute to post-earthquake environmental impacts.



Figure 1-4: Secondary Earthquake Damage Caused by Fire.

1.3 EARTHQUAKE-INDUCED DAMAGE TO HIGHWAY FACILITIES

1.3.1 Overview

Recent earthquakes in the United States and abroad have provided a vivid reminder of the potential for damage to highway facilities in earthquakes and the impact of that damage on the community. Damage in the 1989 Loma Prieta (Santa Cruz Mountains) and 1994 Northridge earthquakes in the United States and the 1995 Kobe (Hyogo-Ken Nabu) earthquake in Japan have illustrated the potential for not only direct damage, including loss of life and destruction of highway structures, but also indirect damage due to loss of service of portions of highway systems. Economic loss due to closure of the Bay Bridge following the Loma Prieta earthquake is a good example of the potential magnitude of indirect damage. Economic losses associated with closure of the bridge include the costs associated with increased travel time and air pollution due to necessary detours. Furthermore, in many cases, business trips to San Francisco were simply deferred or canceled, resulting in loss of business. Travel and tourism also suffered. Estimates of the cost of these indirect losses exceed \$10 billion. Thus, the estimated indirect costs are greater than the estimated \$6.5 billion cost of repairing the direct damage from the earthquake. Disruption of highway systems also contributed to delays in emergency response and recovery activities, possibly increasing direct damage, including loss of life and fire-related damage.

1.3.2 Historical Damage to Highway Facilities

The historical record of damage to highway facilities in major earthquakes does not begin until the 1933 Long Beach earthquake since there were few major highway facilities prior to that time. However, the accounts of the impact of the 1906 San Francisco earthquake include reports of minor damage to railway tunnels from strong shaking (primarily at the tunnel portal) and numerous reports and pictures of damage to local thoroughfares induced by local ground failures that are now known to have been caused by liquefaction (see, e.g., Youd and Hoose, 1976). Furthermore, in earthquakes throughout history, there have been reports of landslides and mass soil movements blocking travel routes and disrupting commerce.

At the time of the 1933 Long Beach earthquake, the Los Angeles freeway network had yet to be developed. Furthermore, the earthquake struck south of Los Angeles in, at the time, relatively sparsely populated Orange County. However, damage accounts from the earthquake include reports of disruption to the Pacific Coast Highway, the main thoroughfare between Long Beach and the coastal areas of Orange County, due to lateral spreading of the ground. The lateral spreading is now recognized as attributable to liquefaction.

The first reports of major damage to structural elements of highway facilities due to earthquakes were from the 1964 Niigata and Alaska earthquakes. Numerous bridges were destroyed in both of these earthquakes by soil movements attributable to liquefaction (see, e.g., Ross, *et al.*, 1969). In fact, it was only after study of the damage induced by these earthquakes that liquefaction was recognized as an important phenomenon in earthquakes.

The 1971 San Fernando earthquake was the first event in which major damage to highway facilities were not attributed to liquefaction or landslides. Damage to highway facilities in the San Fernando event included toppling of highway overpasses and structural damage to bridge piers and retaining walls. Following the San Fernando event, the engineering profession undertook a comprehensive reassessment of procedures and practices for seismic design of highway facilities.

Significant damage to transportation systems was one of the major characteristics of the 1989 Loma Prieta earthquake. The collapse of a more than 1.5-km long section of elevated roadway on Interstate 880 (the Cypress Street Viaduct) along with the loss of a 15-m long span of the upper deck of the Bay Bridge linking San Francisco to Oakland resulted in both loss of life and major disruption to the transportation system. At both locations, amplification of the ground motions from the relatively distant earthquake by local soil conditions (i.e., soft to medium-stiff clay soils) significantly affected the seismic loads on the structure, contributing to its collapse. Of the 1,500 highway bridges in the felt area of the Loma Prieta earthquake, 10 were closed due to structural damage, 10 required shoring to remain in service, and 73 experienced lesser damage (EERI, 1989). In addition to this structural damage, a series of landslides disrupted State Route 17, the only direct high capacity roadway between the Santa Cruz and the San Jose areas.

It is estimated that approximately 10 percent of the 20,000 km of state highway in California experienced ground acceleration greater than 0.25 g during the 1994 Northridge earthquake (CDMG, 1995). The most significant damage to highway facilities occurred at the State Route 14-Interstate 5 interchange, constructed between 1971 to 1974. This interchange was under construction during the 1971 San Fernando earthquake and was designed to pre-San Fernando earthquake standards. In addition to bridge failure and damage, there was also extensive non-structural damage to highway systems in the Northridge event. Highway damage included excessive settlement of bridge approaches, soil settlement under pavement, and landslides.

The collapse of the Hanshin expressway due to strong shaking during the 1995 Kobe earthquake in Japan provided another graphic example of damage to highway structures during earthquakes (see Figure 1-5).

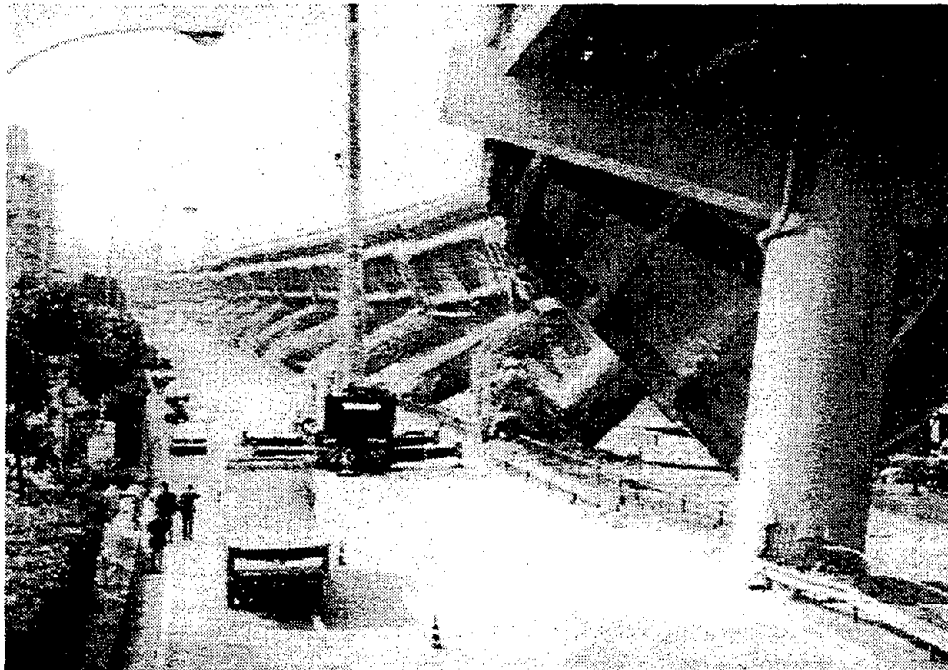


Figure 1-5: Collapse of Hanshin Expressway During the 1995 Kobe (Hyogo-ken Nabu, Japan) Earthquake.

This expressway was constructed before modern seismic details for columns were incorporated into practice (EERI, 1995). In this earthquake, some bridges in Kobe also experienced significant damage due to soil liquefaction.

Experience from the Loma Prieta, Northridge, and Kobe earthquakes indicates that bridges and other structural highway facilities designed in accordance with current codes will, in general, perform well when subjected to strong ground motions. However, damage from these earthquakes also illustrates the fragility of structures not designed in compliance with current codes. The damage to highway facilities in these events emphasizes the continuing importance of consideration of effects of strong shaking, soil liquefaction, landslides, and local soil amplification.

1.4 ORGANIZATION OF THE DOCUMENT

Part I

General background information on the sources, types, and effects of earthquakes, including the definition of key terms used in earthquake engineering, is provided in Chapter 2. Chapter 3 of this document discusses seismic source characterization and provides information on readily available geological, seismological, and geophysical data. Chapter 4 describes the characterization of earthquake ground motions for use in engineering analysis. Details of geotechnical site characterization for seismic analyses are presented in Chapter 5. Seismic site response analyses are addressed in Chapter 6, and methods for evaluating the seismic stability of slopes and embankments based upon the results of a seismic site response analysis are presented in Chapter 7. Techniques for evaluating the liquefaction and seismic settlement potential of a site are discussed in Chapter 8. Basic elements of the seismic design of retaining walls, spread footings, and piles are presented in Chapter 9. References cited in the document are listed in Chapter 10.

Part II

Examples illustrating the application of the methods discussed in Part I are presented in Part II - "Design Examples", immediately following the Part I document.

CHAPTER 2.0 EARTHQUAKE FUNDAMENTALS

2.1 INTRODUCTION

Earthquakes are produced by abrupt relative movements on fractures or fracture zones in the earth's crust. These fractures or fracture zones are termed *earthquake faults*. The mechanism of fault movement is elastic rebound from the sudden release of built-up strain energy in the crust. The built-up strain energy accumulates in the earth's crust through the relative movement of large, essentially intact pieces of the earth's crust called *tectonic plates*. This relief of strain energy, commonly called *fault rupture*, takes place along the *rupture zone*. When fault rupture occurs, the strained rock rebounds elastically. This rebound produces vibrations that pass through the earth crust and along the earth's surface, generating the ground motions that are the source of most damage attributable to earthquakes. If the fault along which the rupture occurs propagates upward to the ground surface and the surface is uncovered by sediments, the relative movement may manifest itself as *surface rupture*. Surface ruptures are also a source of earthquake damage to constructed facilities.

2.2 BASIC CONCEPTS

2.2.1 General

Faults are ubiquitous in the earth's crust. They exist both at the contacts of the tectonic plates and within the plates themselves. In some areas of the western United States, it is practically impossible to perform a site investigation and not encounter a fault. However, not all faults are *seismogenic* (i.e., not all faults produce earthquakes). Faults that are known to produce earthquakes are termed *active faults*. Faults that at one time produced earthquakes but no longer do are termed *inactive faults*. Faults for which the potential for producing earthquakes is uncertain are termed *potentially active faults*. When a fault is encountered in an area known or suspected to be a source of earthquakes, a careful analysis and understanding of the fault is needed to evaluate its potential for generating earthquakes.

2.2.2 Plate Tectonics

Plate tectonics theory has established that the earth's crust is a mosaic of tectonic plates. These plates may pull apart from each other, override one another, and slide past each other. The motions of the tectonic plates are driven by convection currents in the molten rock in the earth's upper mantle. These convection currents are generated by heat sources within the earth. Plates grow in size at spreading zones, where the convection currents send plumes of material from the upper mantle to the earth's surface. Plates are consumed at subduction zones, where the relatively rigid plate is drawn downwards back into and consumed by the mantle.

The major tectonic plates of the earth's crust are shown in Figure 2-1 (modified from Park, 1983). There are also numerous smaller, minor plates not shown on this figure. The motions of these plates are related to the activation of faults, the generation of earthquakes, and the presence of volcanism. Most earthquakes occur on or near plate boundaries, in the so-called *Benioff zone*, the inclined contact zone between two tectonic plates that dips from near the surface to deep under the earth's crust, as illustrated in Figure 2-2 (modified after Gere and Shah, 1984). Earthquakes also occur in the interior of the plates, although with a much lower frequency than at plate boundaries.

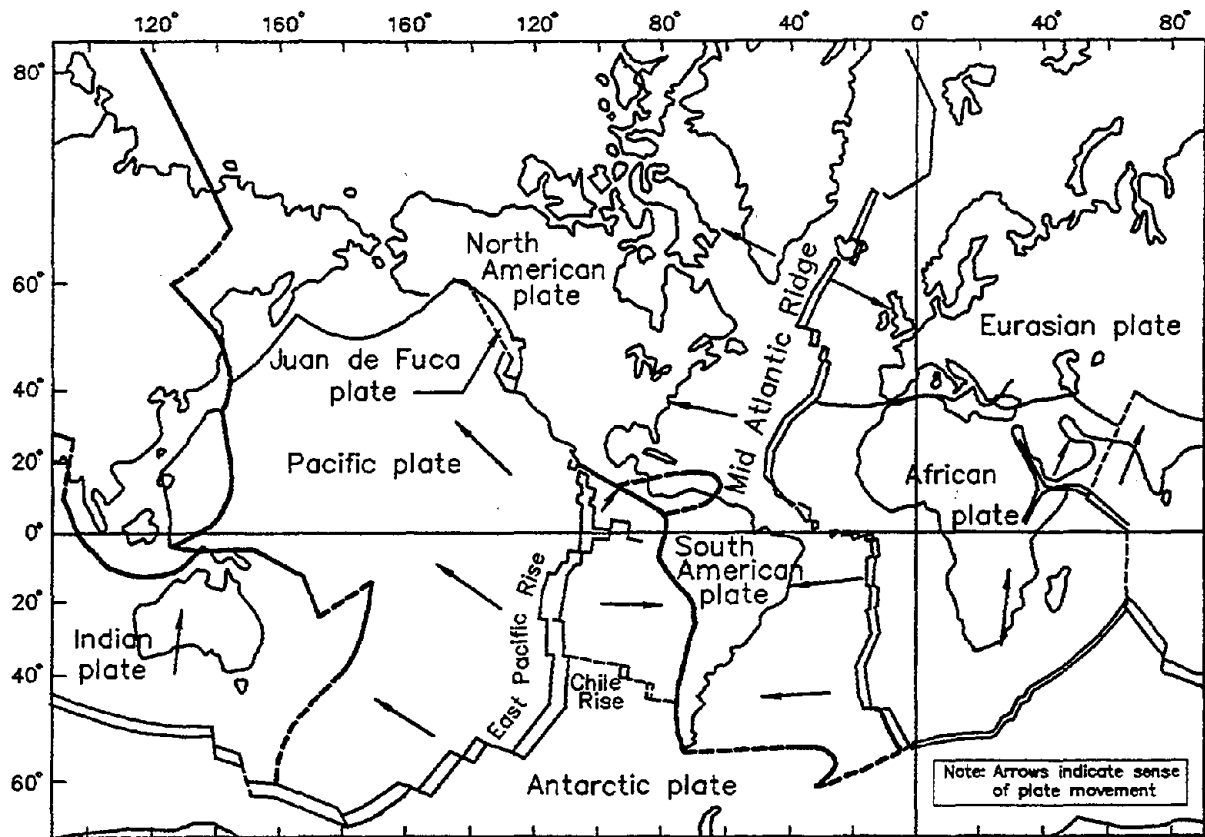


Figure 2-1: Major Tectonic Plates and Their Approximate Direction of Movement. (Modified from Park, 1983, Foundations of Structural Geology, Chapman and Hall)

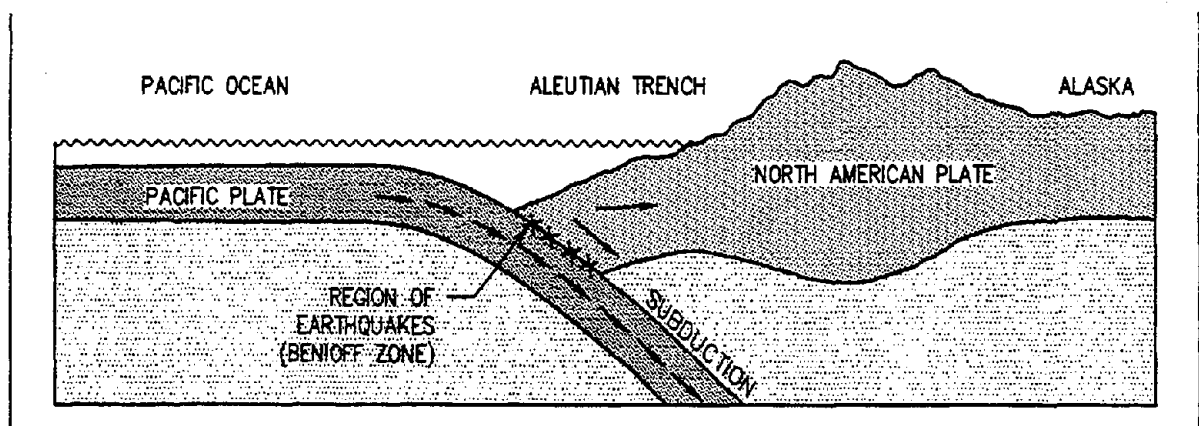


Figure 2-2: Cross-Section Through Tectonic Plates in Southern Alaska. (After Gere and Shah, 1984)

For the continental United States, the principal tectonic plate boundary is along the western coast of the continent, where the North American Plate and the Pacific Plate are in contact (see Figure 2-1). In California, the boundary between these plates is a transform fault wherein the relative movement is generally one of lateral slippage of one plate past the other. Elsewhere along the west coast (e.g., off the coast of Oregon, Washington, and Alaska), the plate boundary is a *subduction zone* wherein one plate dives (subducts) beneath the other plate (as illustrated in Figure 2-2). In the western interior of the United States, adjacent to the western edge of the American Plate, there may be subplates that have formed as a result of subcrustal flow. Earthquake sources in Utah and Montana may be attributable to such subplate sources. Earthquake source areas in the central and eastern United States and along the Saint Lawrence Valley are within the American Plate and are considered to be intraplate source zones. The mechanisms generating earthquakes in these intraplate zones are poorly understood, but may be related to relief of locked-in stresses from ancient tectonic movements, crustal rebound from the ice ages, re-adjustment of stress in the interior of the plate due to boundary loads, sediment load such as the Mississippi River basin, or other unrecognized mechanisms. Earthquakes in Hawaii are believed to be associated with an isolated plume of molten rock from the mantle referred to as a hot spot.

The intensity and impact of earthquakes may be as great or greater in the plate interiors as they are at the active plate boundaries. The differences between plate boundary and intraplate earthquakes is in their geographic spread and the frequency of occurrence. Earthquake activity is much greater along the plate boundaries than in the plate interior. However, ground motions from intraplate earthquakes tend to attenuate, or dissipate, much more slowly than those from plate boundary events. Plate boundary faults are relatively longer than those in the plate interior and tend to be associated with a smaller *stress drop* (the stress drop is the sudden reduction of stress across the fault plane during rupture), longer duration of shaking, and a more frequent rate of earthquake occurrence.

In a subduction zone, such as that along the coast of Oregon and Washington, there are faults that are both shallow and located within the over-riding crust (< 19 km focal depth) and deep within the subducting plate (> 20 km focal depth). The subduction zone that now exists off the Washington and Oregon coast has been gradually migrating eastward for millions of years. A southern extension of it was consumed beneath California during the collision of the North American and Pacific plates ten to twenty million years ago. In the plate interior, faults may vary from shallow to deep. In California, the plate boundary is generally of the transform type, wherein the plates slide laterally past each other, and faults are relatively shallow (< 20 km).

2.2.3 Fault Movements

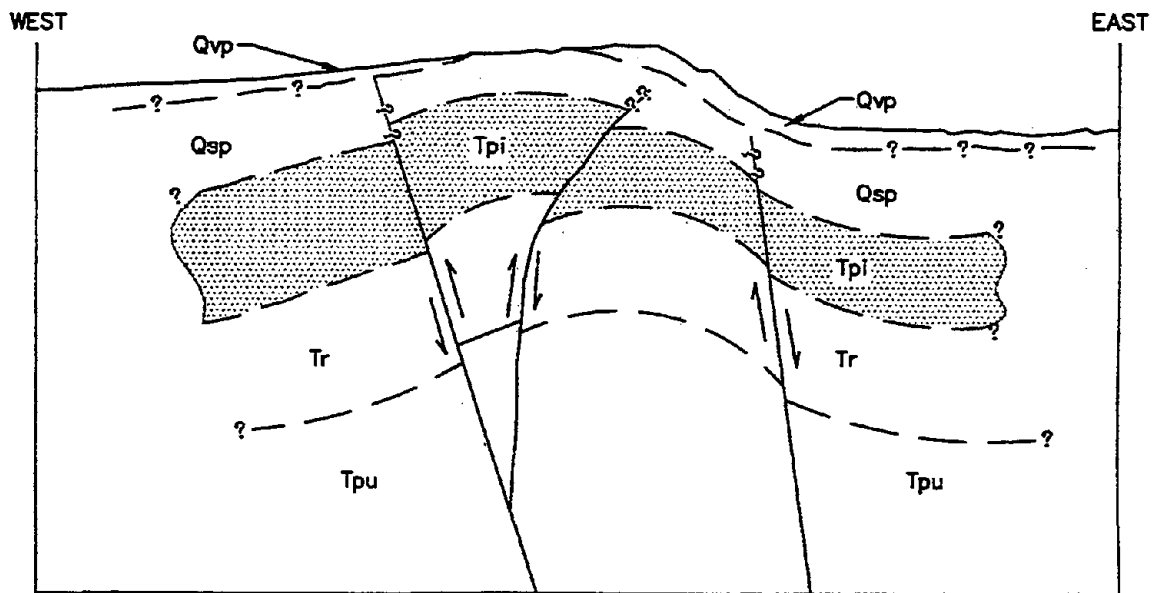
Faults are created when the stresses within geologic materials exceed the ability of those materials to withstand the stresses. Most faults that exist today are the result of tectonic activity that occurred in earlier geological times. These faults are usually inactive, but faults related to past tectonism can be reactivated by present-day tectonism.

Not all faults along which relative movement is occurring are a source of earthquakes. Some faults may be surfaces along which relative movement is occurring at a slow, relatively continuous rate, with an insufficient stress drop to cause an earthquake. Such movement is called *fault creep*. Fault creep may occur along a shallow fault, where the low overburden stress results in a relatively rapid dissipation of stresses. Alternatively, a creeping fault may be at depth in soft and/or ductile materials that deform plastically. Also, there may be a lack of frictional resistance or asperities (non-uniformities) along the fault plane, allowing steady creep and associated release of the strain energy along the fault. Fault creep may also prevail where phenomena such as magma intrusion or growing salt domes activate small shallow faults

in soft sediments, where faults are generated by extraction of fluids (e.g., oil or water in southern California) which causes ground settlement and thus activates faults near the surface, where movements are associated with steady creep in response to adjustments of tectonically activated faults, and where faults are generated by gravity slides that take place in thick, unconsolidated sediments.

Active faults that extend into crystalline basement rocks are generally capable of building up the strain energy needed to produce, upon rupture, earthquakes strong enough to affect highway facilities. Fault ruptures may propagate from the crystalline basement rocks to the ground surface and produce ground rupture. However, in some instances, fault rupture may be confined to the subsurface with no breakage of the ground surface due to fault movement. Subsurface faulting without primary fault rupture at the ground surface is characteristic of almost all earthquakes in the central and eastern United States. In addition, several of the most recent significant earthquakes in the Pacific Coast plate boundary areas are due to rupture of thrust faults that do not break the ground surface, termed *blind thrust* faults. Figure 2-3 illustrates the fault in which rupture does not propagate to the ground surface. Strong shaking associated with fault rupture may also generate secondary ground breakage such as graben structures, ridge-top shattering, landslides, and liquefaction. While this secondary ground breakage may sometimes be interpreted as faulting, it is generally not considered to represent a surface manifestation of the fault.

- LEGEND
- Qvp - PALOS VERDES SAND
 - Qsp - SAN PEDRO FORMATION
 - Tpi - PICO FORMATION
 - Tr - REPETTO FORMATION
 - Tpu - PUENTE FORMATION



SECTION ORIENTED E-W THROUGH SITE, VIEWING NORTH

Figure 2-3: Thrust Faulting Without Surface Rupture

Whether or not a fault has the potential to produce earthquakes is usually judged by the recency of previous fault movements. If a fault has propagated to the ground surface, evidence of faulting is usually found in geomorphic features associated with fault rupture (e.g., relative displacement of geologically young sediments). For faults that do not propagate to the ground surface, geomorphic evidence of previous earthquakes may be more subdued and more difficult to evaluate (e.g., near surface folding in sediments or evidence of liquefaction or slumping generated by the earthquakes). If a fault has undergone relative displacement in relatively recent geologic time (within the time frame of the current tectonic setting), it is reasonable to assume that this fault has the potential to move again. If the fault moved in the distant geologic past, during the time of a different tectonic stress regime, and if the fault has not moved in recent (Holocene) time (generally the past 11,000 years), it may be considered inactive.

Geomorphic evidence of fault movement cannot always be dated. In practice, if a fault displaces the base of unconsolidated alluvium, glacial deposits, or surficial soils, then the fault is likely to be active. Also, if there is micro-seismic activity associated with the fault, the fault may be judged as active and capable of generating earthquakes. Microearthquakes occurring within basement rocks at depths of 7 to 20 km may be indicative of the potential for large earthquakes. Microearthquakes occurring at depths of 1 to 3 km are not necessarily indicative of the potential for large, damaging earthquake events. In the absence of geomorphic, tectonic, or historical evidence of large damaging earthquakes, shallow microtremors may simply indicate a potential for small or moderate seismic events. Shallow microearthquakes of magnitude 3 or less may also sometimes be associated with mining or other non-seismogenic mechanisms. If there is no geomorphic evidence of recent seismic activity and there is no microseismic activity in the area, then the fault may be inactive and not capable of generating earthquakes.

The maximum potential size of an earthquake on a capable (active or potentially active) fault is generally related to the size of the fault (i.e., a small fault produces small earthquakes and a large fault produces large earthquakes). Faults contain asperities (non-uniformities) and are subject to certain frictional and geometric restraints that allow them to move only when certain levels of accumulated stress are achieved. Thus, each fault tends to produce earthquakes within a range of magnitudes that are characteristic for that particular fault.

A long fault, like the San Andreas fault in California or the Wasatch fault in Utah, will generally not move along its entire length at any one time. Such faults typically move in portions, one segment at a time. An immobile (or "locked") segment, a segment which has remained stationary while the adjacent segments of the fault have moved, is a strong candidate for the next episode of movement. The lengths of fault segments may be interpreted from geomorphic evidence of prior movements or from fault geometry and kinematic constraints (e.g., abrupt changes in the orientation of the fault).

Short, disconnected faults aligned en-echelon in sediments at the ground surface may well be continuous at depth, with their surface expression modified by the near surface geologic structure. Thus, the observed length of a group of such faults is often shorter than their true length. However, these groups of faults may also move in distinct segments. The lengths of these groups of short fault segments may be identified by the continuity of the geomorphic evidence.

A variety of correlations between the size (magnitude) of an earthquake, the length or area of a fault plane, and the amount of displacement along the fault are available (Bonilla, *et al.*, 1984; de Polo and Slemmons, 1990; Hanks and Kanamori, 1979; Wesnousky, 1986; Woodward-Clyde Consultants, 1979; Wyss, 1979). However, evaluation of fault segmentation and magnitude potential is a complex task that is best left to qualified geologists and seismologists and should not be attempted by unqualified geotechnical engineers.

Finally, even in the best of circumstances, with a thorough understanding of local geology, geomorphology, and seismicity, one cannot assume that all active faults have been found. Engineering evaluations should be made in such a way that the potential for earthquakes from unknown faults is considered. For this purpose, *floating* or *random* earthquakes that can occur anywhere within a known earthquake zone are often used in engineering practice.

2.3 DEFINITIONS

2.3.1 Introduction

A variety of different terms are used to describe earthquakes and their influence on the ground and on engineering structures. A summary of terms commonly used in earthquake engineering and that will be frequently used in this document is provided below.

2.3.2 Type of Faults

Faults may be broadly classified according to their mode, or style of relative movement. The principal modes of relative displacement are illustrated in Figure 2-4 and are described subsequently.

Strike Slip Faults

Faults along which relative movement is essentially horizontal (i.e., the opposite sides of the fault slide past each other laterally), are called strike slip faults. Strike slip faults are often essentially linear (or planar) features. Strike slip faults that are not fairly linear may produce complex surface features. The San Andreas fault is a strike slip fault that is essentially a north-south linear feature over most of its length. Strike slip faults may sometimes be aligned in en-echelon fashion wherein individual sub-parallel segments are aligned along a linear trend. En-echelon strike slip faulting is sometimes accompanied by step over zones where fault displacement is transferred from adjacent strike slip faults. Ground rupture patterns within these zones may be particularly complex.

Dip Slip Faults

Faults in which the deformation is perpendicular to the fault plane may occur due to either *normal* (extensional) or *reverse* (compressional) motion. These faults are sometimes referred to as *dip slip* faults. Reverse faults are also referred to as *thrust faults*. Dip slip faults may produce multiple fractures within rather wide and irregular fault zones. Some dip slip fault zones may contain broad deformational features such as pressure ridges and sags rather than clearly defined fault scarps or shear zones (Hart, 1980).

Other Special Cases

Faults that show both strike slip and dip slip displacement may be referred to as *oblique slip faults*. In some cases, due to changes in fault alignment, the type of a given fault may be mixed. A good example of this is in the vicinity of the so-called "big-bend" in the alignment of the San Andreas fault in California, where the fault, generally north-south trending, bends into a generally east-west alignment. In the vicinity of the big-bend, the generally strike slip lateral movement along the plate boundary is transferred into thrusting and compression, generating deformation perpendicular to the east-west trending fault plane.

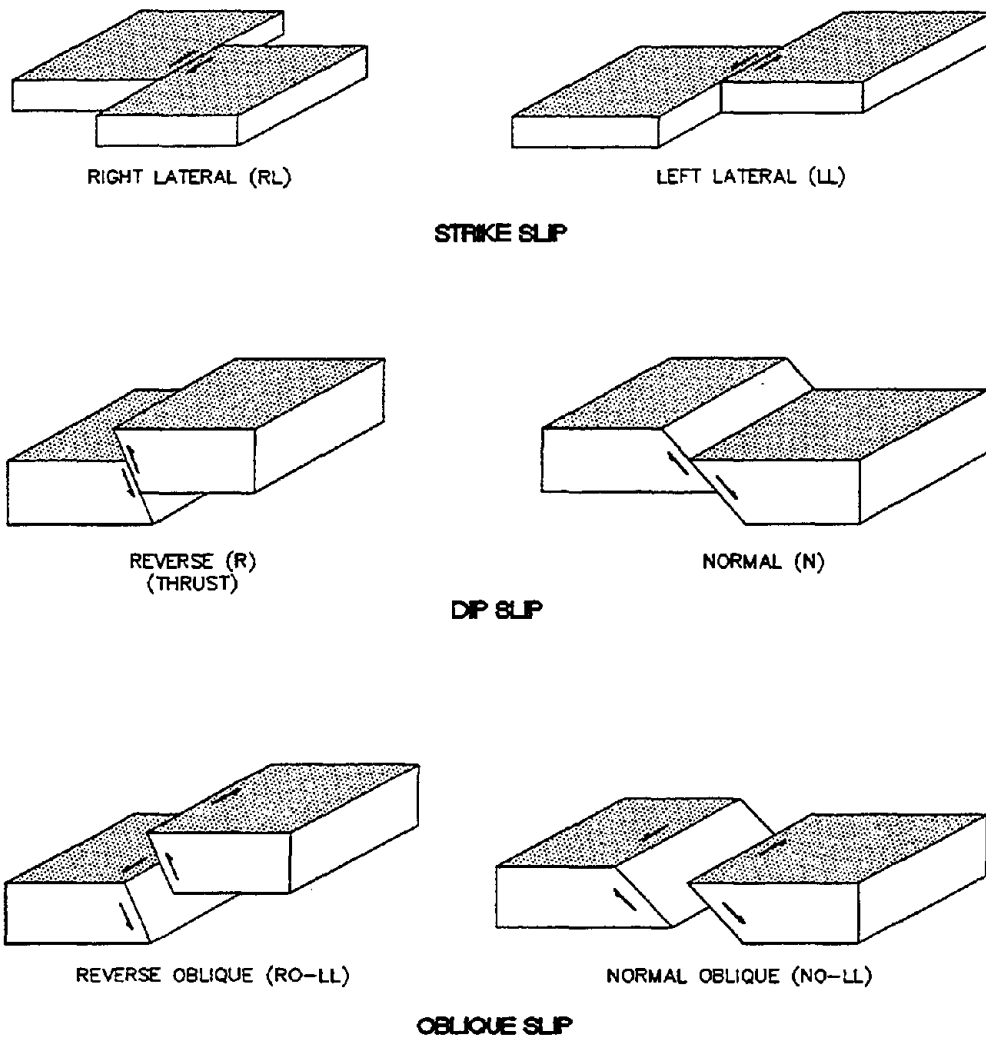


Figure 2-4: Types of Fault Movement.

2.3.3 Earthquake Magnitude

Earthquake magnitude, M , is a measure of the energy released by an earthquake. A variety of different earthquake magnitude scales exist. The differences among these scales is attributable to the earthquake characteristic used to quantify the energy content. Characteristics used to quantify earthquake energy content include the local intensity of ground motions, the body waves generated by the earthquake, and the surface waves generated by the earthquake. In the eastern United States, earthquake magnitude is commonly measured as a (short period) *body wave magnitude*, m_b . However, the (long period) body wave magnitude, m_B , scale is also sometimes used in the central and eastern United States. In California, earthquake magnitude is often measured as a *local (Richter) magnitude*, M_L , or *surface wave magnitude*, M_s . The *Japan Meteorological Agency Magnitude* (M_{JMA}) scale is commonly used in Japan.

Due to limitations in the ability of some recording instruments to measure values above a certain amplitude, some of these magnitude scales tend to reach an asymptotic upper limit. To correct this, the *moment*

magnitude, M_w , scale was developed by seismologists (Hanks and Kanamori, 1979). The moment magnitude of an earthquake is a measure of the kinetic energy released by the earthquake. M_w is proportional to the *seismic moment*, defined as a product of the material rigidity, fault rupture area, and the average dislocation of the rupture surface. Moment magnitude has been proposed as a unifying, consistent magnitude measure of earthquake energy content. For this reason, moment magnitude is consistently used in this document to describe earthquake magnitude unless it is otherwise noted. Figure 2-5 (Heaton, *et al.*, 1986) provides a comparison of the various other magnitude scales with the moment magnitude scale. Note that in the magnitude range of 0 to 6, moment magnitude M_w is approximately equal to the local (Richter) magnitude M_L , while in the magnitude range of 6 to 7.5, moment magnitude M_w is approximately equal to the surface wave magnitude M_s .

2.3.4 Hypocenter and Epicenter

The *hypocenter* (focus) of an earthquake is the point from which the seismic waves first emanate. Conceptually, it may be considered as the point on a fault plane where the slip responsible for an earthquake was initiated. The *epicenter* is a point on the ground surface directly above the hypocenter. Figure 2-6 shows the relationship between the hypocenter, epicenter, fault plane, and rupture zone of an earthquake. Figure 2-6 also shows the definition of the *strike* and *dip angles* of the fault plane.

2.3.5 Zone of Energy Release

The *zone of energy release*, sometimes referred to as the *zone of seismogenic rupture*, is the area on the fault plane from which the seismic waves that generate strong ground motions emanate. The zone of energy release is generally the portion of the rupture zone that is within crystalline rock. Therefore, even if the fault plane ruptures to the ground surface, the zone of energy release may not extend to the ground surface.

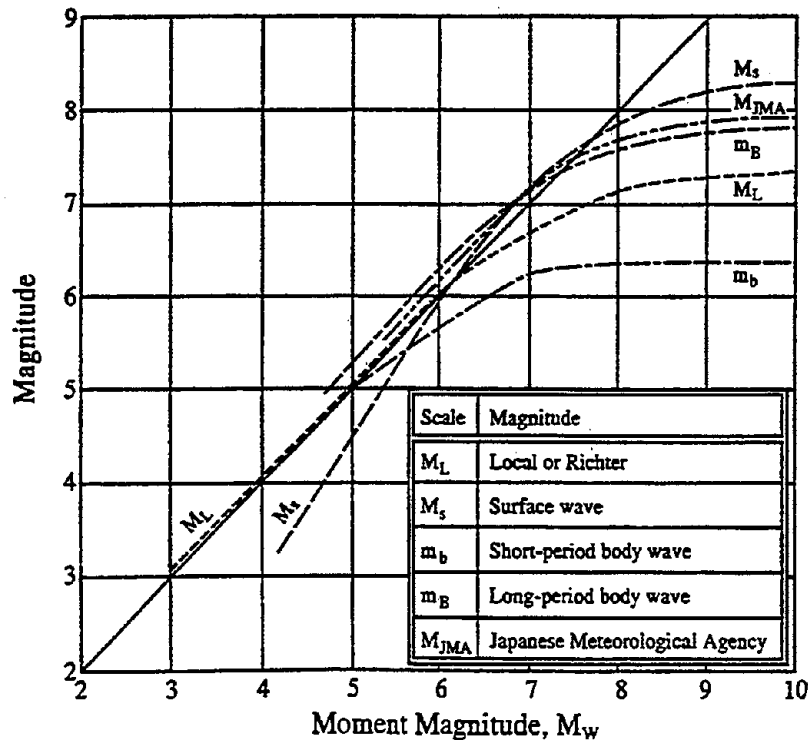


Figure 2-5: Comparison of Earthquake Magnitude Scales. (Heaton, *et al.*, 1986)

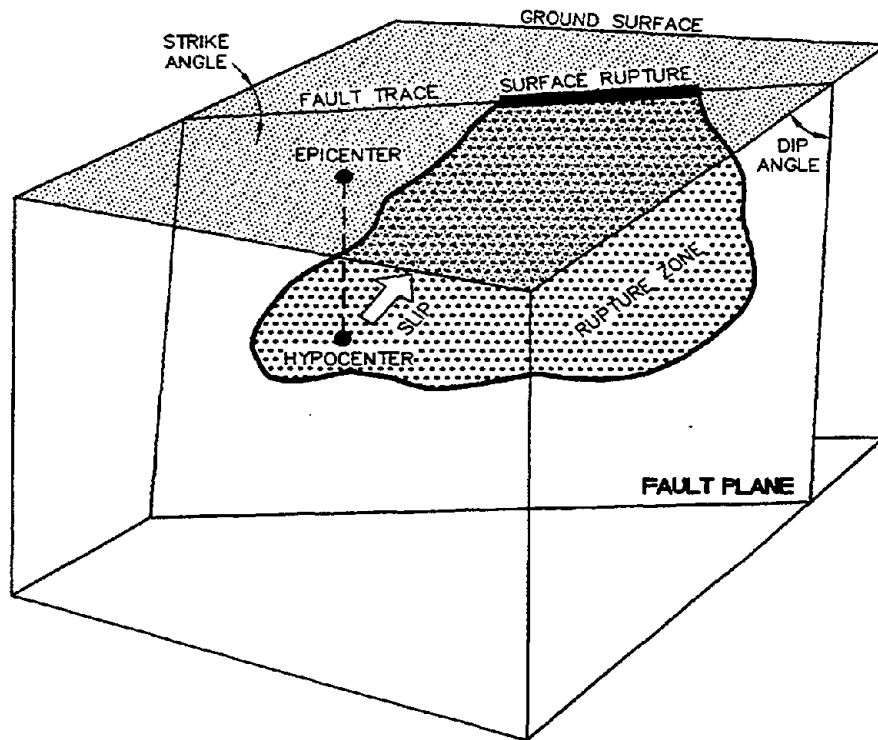


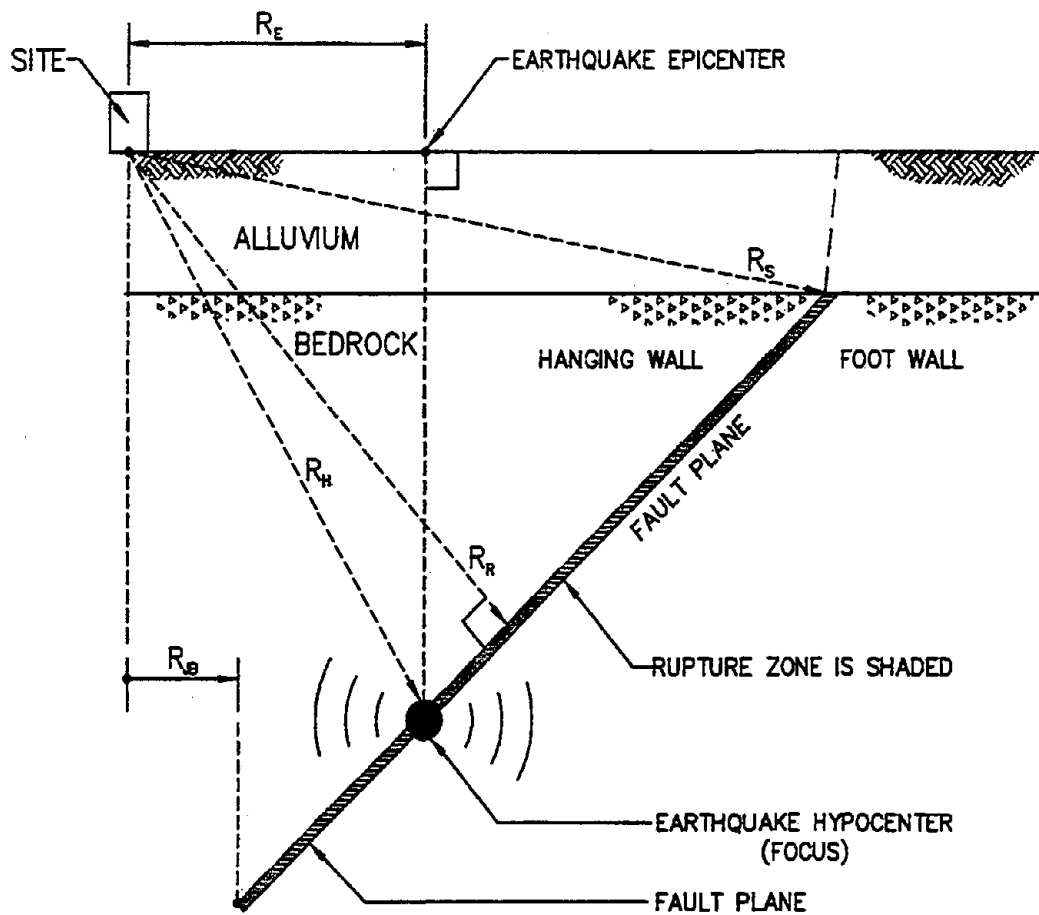
Figure 2-6: Definition of Basic Fault Geometry.

2.3.6 Site-to-Source Distance

Figure 2-7 provides definitions of various *site-to-source distances* commonly used to estimate earthquake-induced ground motions. In the eastern United States, epicentral distance, R_E , is commonly used. In the western United States, the rupture distance, R_R , the seismogenic distance, R_S , the hypocentral distance, R_H , and, the so-called Joyner and Boore distance, R_{JB} , are commonly used. It should be noted that if the site is located within the vertical projection of the fault plane, then R_{JB} is equal to zero.

2.3.7 Peak Ground Motions

The intensity of earthquake-induced ground motion is often described by the peak value of the acceleration time history, the *peak ground acceleration (PGA)*. *Peak ground velocity (PGV)* and/or *peak ground displacement (PGD)* are also sometimes used as indices of earthquake damage potential. Peak ground motions are generally specified for the motions in the horizontal plane, as the horizontal ground motions generated by an earthquake tend to be the motions that cause the greatest damage. Figure 2-8 illustrates the acceleration, velocity, and displacement time histories from the horizontal component of an earthquake. The corresponding *peak horizontal ground acceleration (PHGA)*, *peak horizontal ground velocity (PHGV)*, and *peak horizontal ground displacement (PHGD)* values are indicated on Figure 2-8 by solid dots. Both horizontal and vertical components of PGA, PGV, and PGD are commonly referred to as *ground motion parameters*.



- R_E = EPICENTRAL DISTANCE
- R_r = CLOSEST DISTANCE TO THE FAULT PLANE (RUPTURE DISTANCE)
- R_S = SEISMOGENIC DISTANCE
- R_H = HYPOCENTRAL DISTANCE
- R_B = CLOSEST HORIZONTAL DISTANCE TO THE VERTICAL PROJECTION OF THE FAULT PLANE (JOYNER AND BOORE DISTANCE)

Figure 2-7: Various Distance Measures Used in Earthquake Engineering.

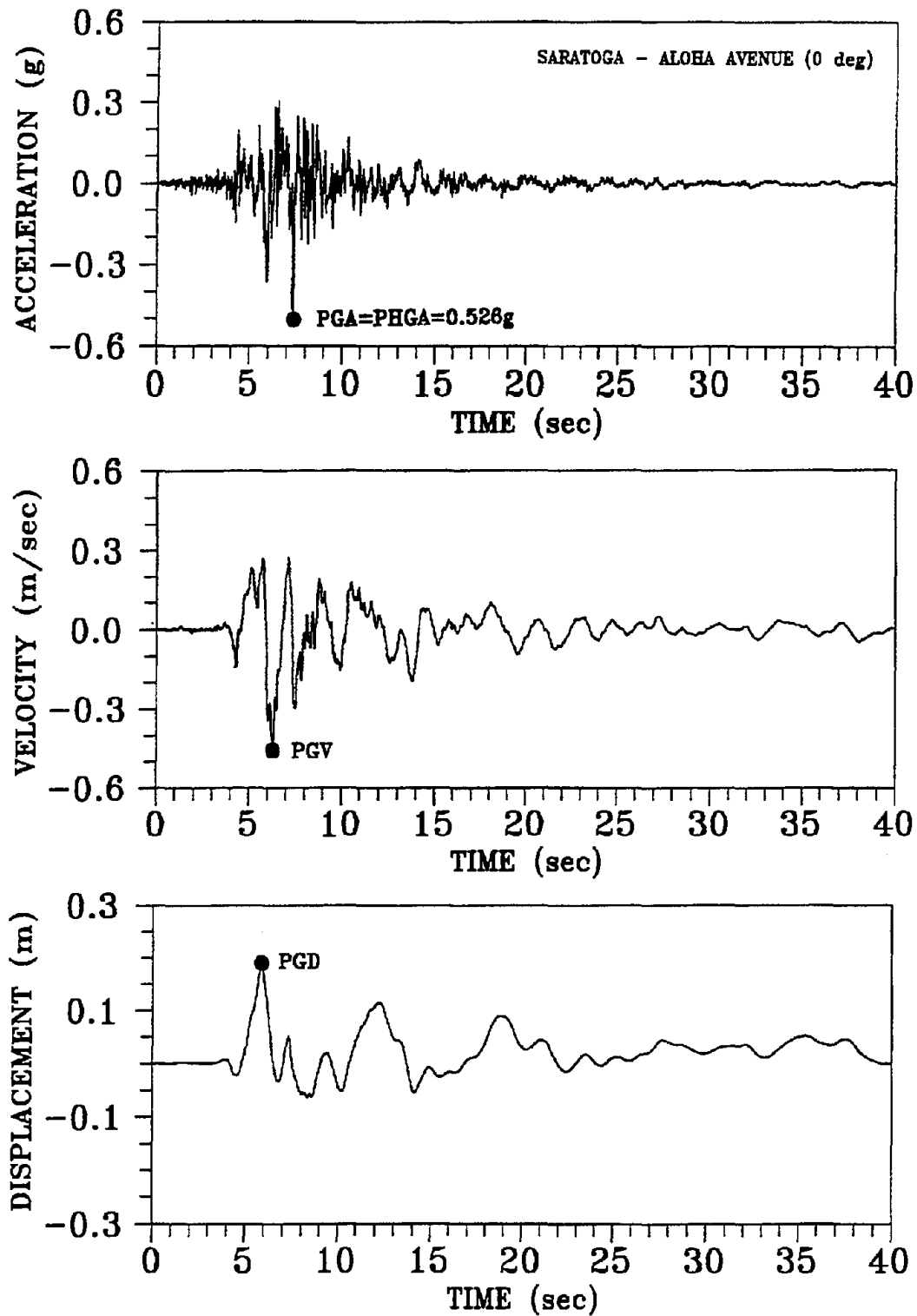


Figure 2-8: Acceleration, Velocity, and Displacement Time Histories.

2.3.8 Response Spectrum

The *response spectrum* of an earthquake record is a plot of the maximum (acceleration, velocity or displacement) response of a series of linear single degree-of-freedom (SDOF) systems with the same damping, c , and mass, m , but variable stiffness, k_i , to the specified ground motion (accelerogram). Development of an acceleration response spectrum is illustrated on Figure 2-9.

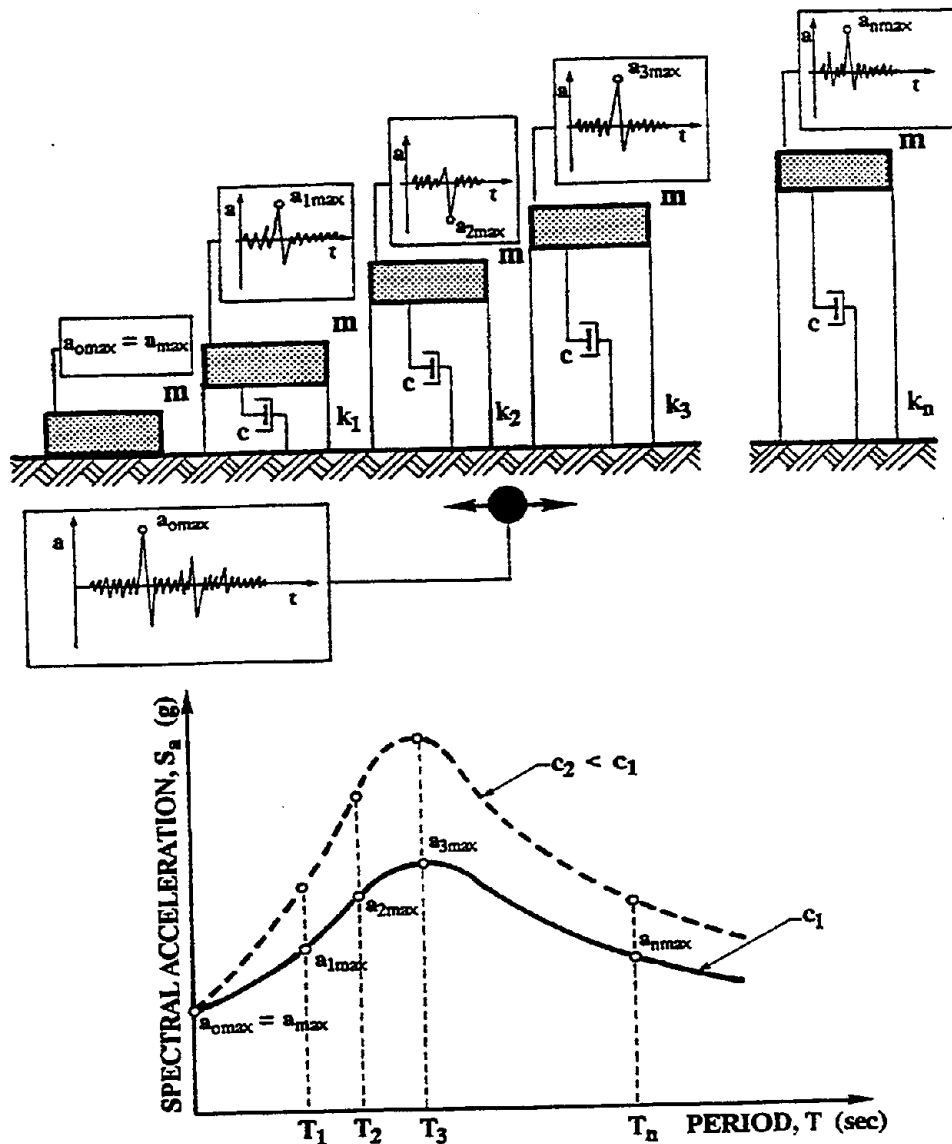


Figure 2-9: Schematic Representation of Acceleration Response Spectra. (Reproduced from Matasović, 1993)

The undamped fundamental period, T_o , of each SDOF system used to develop the response spectrum is calculated as:

$$T_o = 2\pi \sqrt{\frac{m}{k_i}} \quad (2-1)$$

The damping of the SDOF system is represented by the *viscous damping coefficient*, c , commonly referred to as the *spectral damping*. In geotechnical earthquake engineering, spectral damping is commonly assumed to be equal to 5%.

Response spectra are commonly calculated by commercial computer programs (e.g., Nigam and Jennings, 1968; Idriss, *et al.*, 1992). The *spectral accelerations*, S_a , *spectral velocities*, S_v , and *spectral displacements*, S_d , can be presented in several graphical forms. The most common presentation is a plot of the spectral values as a function of T_i , as illustrated on Figure 2-9.

In structural and retaining wall design, where spectral velocities or displacements may govern the design, presentation of the response spectrum as a tripartite spectral plot is common. An example of such a tripartite plot is shown on Figure 2-10. A tripartite plot simultaneously displays S_a , S_v , and S_d values for the selected spectral damping. For a given fundamental period, T_o , (or fundamental frequency $f_o = 1/T_o$), S_a , S_v , and S_d are read from appropriate ordinates. For example, as indicated on Figure 2-10, for $T_o = 0.7$ s ($f_o = 1.4$ Hz), $S_a = 0.19$ g, $S_v = 0.25$ m/s, and $S_d = 0.03$ m.

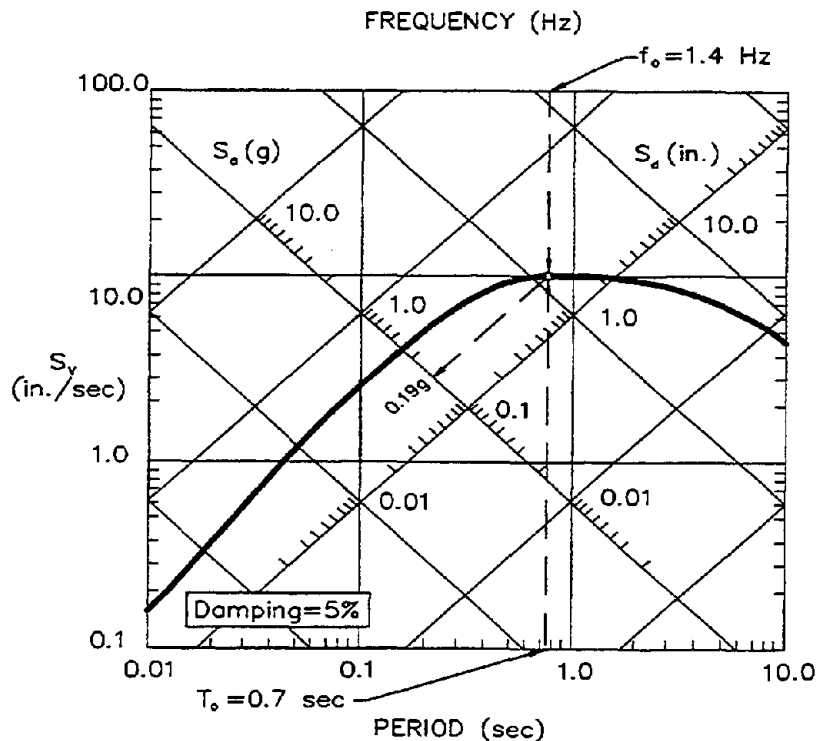


Figure 2-10: Tripartite Representation of Acceleration, Velocity, and Displacement Response Spectra.

2.3.9 Attenuation Relationships

An *attenuation relationship* describes the relationship between earthquake magnitude, site-to-source distance, and the peak or spectral value of a ground motion parameter (e.g., PHGA, PHGV, PHGD, S_a , S_v , or S_d). Acceleration attenuation relationships (for both peak and spectral values) are most common. Attenuation relationships are usually developed by statistical analysis of ground motion parameters observed in previous earthquakes. The variability in the ground motion parameters for a given magnitude and distance is generally characterized by the standard deviation of the statistical data. This variability is usually assumed to be log-normally distributed (i.e., the logarithm of the parameter value is normally distributed).

Numerous attenuation relationships can be found in the technical literature. Commonly used attenuation relationships are described in Chapter 4. Figure 2-7 identifies the distance measures associated with the most common attenuation relationships used in engineering practice.

2.3.10 Intensity Scales

The local strength, or intensity, of earthquake ground motions depend on a variety of factors, including earthquake magnitude, site-to-source distance, the travel path of the seismic waves, the type of faulting, the direction of fault propagation, and local site conditions. Several different intensity scales exist, including the Rossi-Forel scale and the Modified Mercalli Intensity scale. The modified Mercalli Intensity scale is the most commonly used measure of intensity of earthquake ground motions and is presented in Table 2-1.

TABLE 2-1
MODIFIED MERCALLI INTENSITY SCALE
1956 VERSION (Bott, 1988)

Intensity Value	Description
I.	Not felt. Marginal and long-period effects of large earthquakes.
II.	Felt by persons at rest, on upper floors, or favorably placed.
III.	Felt indoors. Hanging objects swing. Vibration-like passing of light trucks. Duration estimated. May not be recognized as an earthquake.
IV.	Hanging objects swing. Vibration-like passing of heavy trucks; or sensation of a jolt like a heavy ball striking the walls. Standing cars rock. Windows, dishes, doors rattle. Glasses clink. Crockery clashes. In the upper range of IV, wooden walls and frames creak.
V.	Felt outdoors; direction estimated. Sleepers awakened. Liquids disturbed, some spilled. Small unstable objects displaced or upset. Doors swing, close, open. Shutters, pictures move. Pendulum clocks stop, start, change rate.
VI.	Felt by all. Many frightened and run outdoors. Persons walk unsteadily. Windows, dishes, glassware broken. Knickknacks, books, etc., off shelves. Pictures off walls. Furniture moved or overturned. Weak plaster and masonry D cracked. Small bells ring (church, school). Trees, bushes shaken visibly, or heard to rustle.
VII.	Difficult to stand. Noticed by drivers. Hanging objects quiver. Furniture broken. Damage to masonry D, including cracks. Weak chimneys broken at roof line. Fall of plaster, loose bricks, stones, tiles, cornices, also unbraced parapets and architectural ornaments. Some cracks in masonry C. Waves on ponds, water turbid with mud. Small slides and caving in along sand or gravel banks. Large bells ring. Concrete irrigation ditches damaged.
VIII.	Steering of cars affected. Damage to masonry C; partial collapse. Some damage to masonry B; none to masonry A. Fall of stucco and some masonry walls. Twisting, fall of chimneys, factory stacks, monuments, towers, elevated tanks. Frame houses moved on foundations if not bolted down; loose panel walls thrown out. Decayed piling broken off. Branches broken from trees. Changes in flow or temperature of springs and wells. Cracks in wet ground and on steep slopes.
IX.	General panic. Masonry D destroyed; masonry C heavily damaged, sometimes with complete collapse; masonry B seriously damaged. General damage to foundations. Frame structures, if not bolted, shifted off foundations. Frames cracked. Serious damage to reservoirs. Underground pipes broken. Conspicuous cracks in ground. In alluviated areas, sand and mud ejected, earthquake foundations, sand craters.
X.	Most masonry and frame structures destroyed with their foundations. Some well-built wooden structures and bridges destroyed. Serious damage to dams, dikes, embankments. Large landslides. Water thrown on banks of canals, rivers, lakes, etc. Sand and mud shifted horizontally on beaches and flat land. Rails bent slightly.
XI.	Rails bent greatly. Underground pipelines completely out of service.
XI.	Damage nearly total. Large rock masses displaced. Lines of sight and level distorted. Objects thrown into the air.

Notes: Masonry A, B, C, D. To avoid ambiguity of language, the quality of masonry, brick, or otherwise, is specified by the following lettering:

Masonry A: *Good workmanship, mortar, and design; reinforced, especially laterally, and bound together by using steel, concrete, etc.; designed to resist lateral forces.*

Masonry B: *Good workmanship and mortar; reinforced, but not designed in detail to resist lateral forces.*

Masonry C: *Ordinary workmanship and mortar; no extreme weaknesses like failing to tie in at corners, but neither reinforced nor designed against horizontal forces.*

Masonry D: *Weak materials, such as adobe; poor mortar; low standards of workmanship; weak horizontally.*

CHAPTER 3.0 SEISMIC HAZARD ANALYSIS

3.1 GENERAL

The process by which design ground motion parameters are established for a seismic analysis is termed the *seismic hazard analysis*. Seismic hazard analyses generally involve the following steps:

- identification of the seismic sources capable of strong ground motions at the project site;
- evaluation of the seismic potential for each capable source; and
- evaluation of the intensity of the design ground motions at the project site.

Identification of seismic sources includes establishing the type of fault and its geographic location, depth, size, and orientation. Seismic source identification may also include specification of a random seismic source to accommodate earthquakes not associated with any known fault. Evaluation of the seismic potential of an identified source involves evaluation of the earthquake magnitude (or range of magnitudes, see section 3.3.3) that the source can generate and, often times, the expected rate of occurrence of events of these magnitudes.

Identification of capable seismic sources together with evaluation of the seismic potential of each capable source may be referred to as *seismic source characterization*. Once the seismic sources are characterized, the intensity of ground motions at the project site from these sources must be characterized. There are three general ways by which the intensity of ground motions at a project site are assessed in practice. They are, in order of complexity: (1) use of local building codes and standards; (2) deterministic seismic hazard evaluation; and (3) probabilistic seismic hazard evaluation. Which particular approach is adopted may depend on the importance and complexity of the project and may be dictated by regulatory agencies.

3.2 SEISMIC SOURCE CHARACTERIZATION

3.2.1 Overview

The importance of seismic source characterization cannot be overemphasized. Seismic source characterization forms the basis for the evaluation of potential ground motions for design analysis. Even if the intensity of the design ground motion is obtained from a building code or published map, seismic source characterization is still required for most geotechnical analyses to establish an earthquake magnitude for use in design.

Seismic source characterization is best done as part of a comprehensive geologic and seismologic evaluation that includes review of pertinent literature, aerial photograph interpretation, geologic field reconnaissance, geologic mapping, and micro-seismicity evaluations.

General information on regional seismic sources can usually be obtained from published information. Site specific studies may be required to characterize local seismic sources. Geophysical surveys, geologic mapping, and trenching are often useful for locating local faults and characterizing their seismic potential. However, such investigations may only identify those faults along which rupture has propagated to the ground surface. Buried faults without surface expression must also be considered in the characterization

of seismic sources. A *micro-seismicity study* (study of instrumentally-recorded earthquakes that are generally not felt and do not cause damage to structures) using data from local or regional seismic monitoring networks may be useful in evaluating the potential for buried faults in the project vicinity.

3.2.2 Methods for Seismic Source Characterization

Seismic sources are generally characterized on a fault-specific basis by geometry (location, length, dip angle, depth, and distance to the site), seismic potential (earthquake magnitude, activity, recurrence), and style of faulting (strike slip, dip slip, or oblique slip). In regions where the observed seismicity cannot be correlated with specific faults, broad area sources may be appropriate.

An investigation to identify the seismic sources that may impact a given site typically includes both a review of available data and field geologic reconnaissance. Available data may include pertinent technical publications, university theses and research reports, maps, aerial photographs, and interviews with experts familiar with the region under study. Pertinent technical publications include maps prepared by the California Division of Mines and Geology (CDMG) identifying young faults in the western states (e.g., Jennings, 1994), publications of the Seismological Society of America (e.g., SSA, 1988), and regional reports from seismological networks and state geological surveys. A detailed summary of available sources of engineering geologic information is presented by Trautmann and Kulhawy (1983).

Studies performed for siting of nuclear power plants and for high and low level radioactive waste disposal facilities can be a useful source of information on regional seismicity and geology. All applications for construction permits for nuclear generating stations are required to contain documentation on regional geology, including known faults and observed seismicity, within a 320 kilometer radius of the site. This information can be found in the Preliminary Safety Analysis Report (PSAR) and the Final Safety Analysis Report (FSAR) for the project. These reports are available through the National Technical Information Service (NTIS) for all existing and many proposed nuclear generating stations. However, as many of these reports are more than 20 years old, more recent sources of information on regional seismicity and tectonics should be consulted. More recent information may be available from siting studies performed for low level radioactive waste repositories, regional landfills, and other important or critical facilities.

Existing seismic networks often provide very detailed information about recent earthquakes within seismic impact regions. Figure 3-1 shows the location of seismic monitoring stations in the Central United States. Information provided by the existing seismic networks typically includes the magnitude and epicentral location of all detected events and is commonly available in plotted map form. A detailed evaluation of each detected event may also be available. The presence of micro-seismic activity can also be used to infer the location of a subsurface seismic source. For instance, Figure 3-2 presents seismicity information in the Southeastern United States from 1977 through 1985. The clusters of seismic events shown in Figure 3-2 are good indicators of the locations of the significant seismic sources in this area. Information from most of the established seismic networks in the United States can be obtained for a nominal cost from the National Geophysical Data Center which is located in Boulder City, Colorado.

Interpretation of aerial photographs can be particularly useful in identifying and locating potentially active faults. Sources of such photographs are discussed by Trautmann and Kulhawy (1983). Evidence of active faults may be indicated in aerial photographs by geomorphic features such as fault scarps, triangular facets, fault scarples, fault rifts, fault slice ridges, shutter ridges, and fault saddles (Cluff, *et al.*, 1972). Additional evidence can be provided by ground features such as open fissures, offsets in such features as fence lines, landscape features, mole tracks, and furrows, rejuvenated streams, folding or warping of young deposits, groundwater barriers in recent alluvium, and fault paths on young surfaces. Usually a

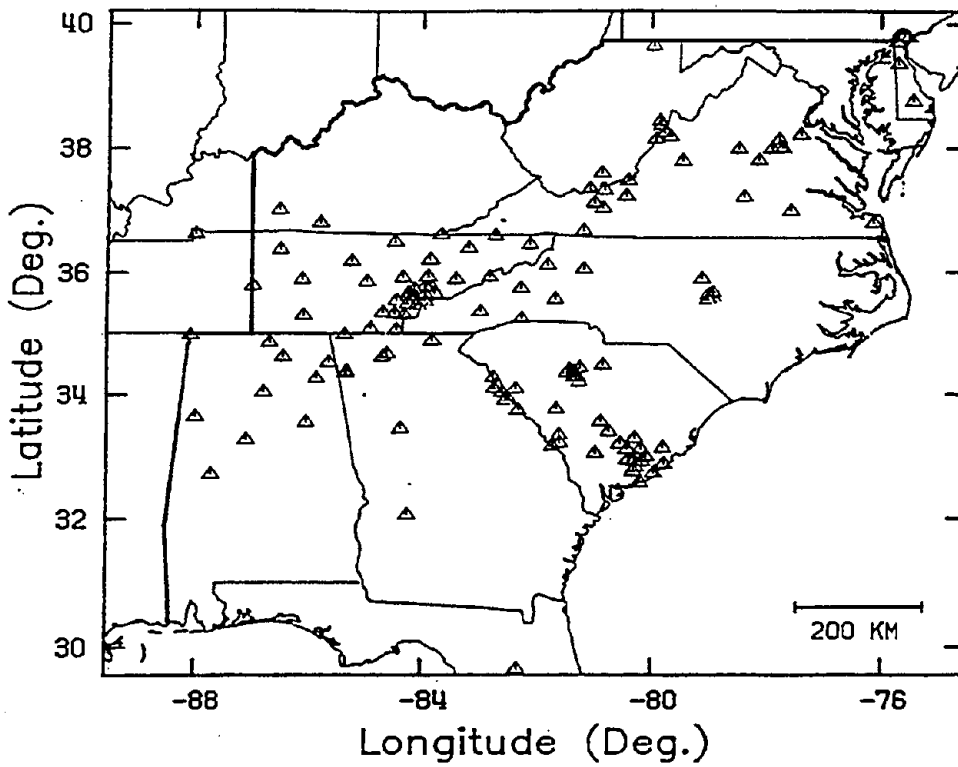


Figure 3-1: Seismic Stations in the Central United States

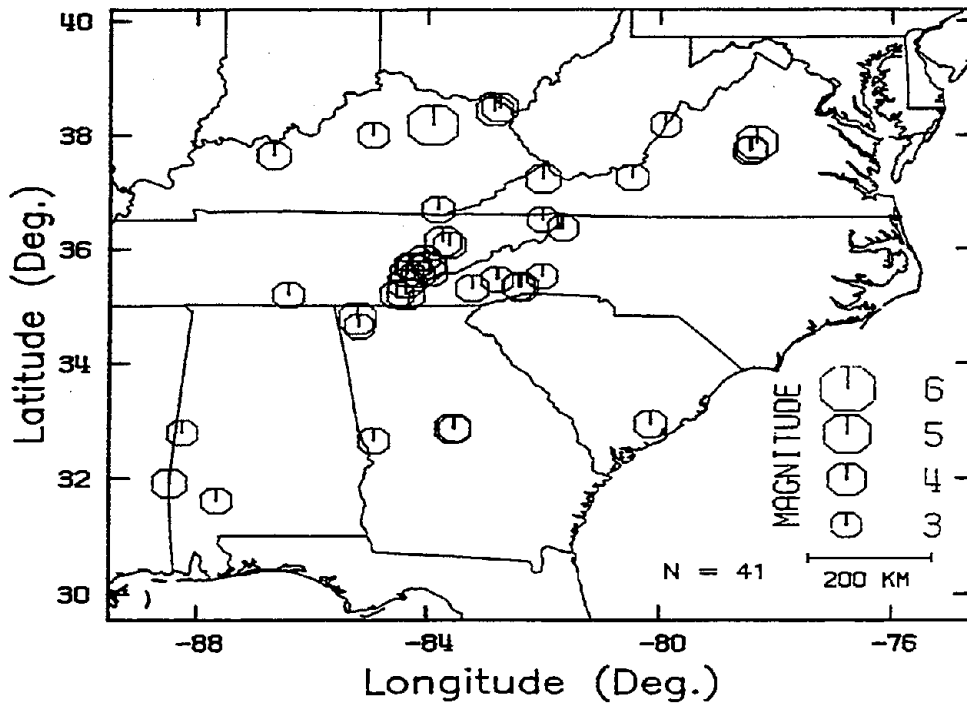


Figure 3-2: Epicenters of Earthquakes in the Southeastern United States from July 1977 through June 1985 (Sibol et al., 1985); Magnitude of 3 or Greater

combination of such features is generated by recent fault movement at the ground surface. Note that many of the fault movement indicators require the presence of undisturbed surface soils at the site. Regions that have limited surface soils due to geologic mechanisms or man's activities can provide a significant challenge in evaluating the recency of movement on existing faults.

Seismic source identification almost always includes preliminary field reconnaissance. Preliminary field reconnaissance should be performed in the project vicinity using the following steps (modified after USEPA, 1993):

- Step 1: Walk the site and site vicinity to identify possible geomorphic or ground features that indicate faulting.
- Step 2: Collect and interpret aerial photographs, such as low sun angle photographs, that use shadows to accentuate topographic differences, infrared photographs that indicate temperature differences containing surface moisture content, and color photographs to study slight color changes.
- Step 3: Based on the above reconnaissance, draw a conclusion on the potential presence of active faults within the surveyed area.

Seismic source characterization can be a complex task, particularly in areas where the information available in the technical literature is incomplete or insufficient. Evaluation of *micro-seismicity*, interpretation of aerial photographs, and field reconnaissance studies should be performed by a geologist, seismologist, or geotechnical professional experienced in these areas and not by an unqualified geotechnical engineer.

3.2.3 Defining the Potential for Fault Movement

Movement within the Holocene Epoch (approximately the past 11,000 years), is generally regarded as the criterion for establishing that a fault is active (e.g., CDMG, 1986; USEPA, 1993). However, it is possible that the recurrence interval for major earthquakes may exceed 11,000 years on some faults. Furthermore, since not all faults rupture the ground surface and geomorphic evidence of fault displacement can be obliterated by natural and man-made activities, it may not be possible to definitely establish whether or not a fault has moved in the past 11,000 years. Therefore, lack of evidence of Holocene movement may not in itself be sufficient grounds to dismiss a fault as inactive. Nevertheless, evidence that a fault has not moved in Holocene time is generally considered sufficient evidence to dismiss the potential for ground surface rupture.

Most Holocene fault activity in North America has been west of the Rocky Mountains. Only two instances of ground surface rupture east of the Rocky Mountains in Holocene time have been conclusively established (the Meers fault in Oklahoma and the Ungava fault in Quebec). However, there have been several major earthquakes that caused widespread damage (e.g., Cape Ann, Massachusetts, 1775; New Madrid, Missouri, 1811 and 1812; and Charleston, South Carolina, 1886) and numerous smaller events causing local damage (e.g., Attica, New York, 1929; Massena, New York, 1944; Miramichi, New Hampshire, 1982) in the eastern and central United States in the past 250 years. Most of these damaging eastern and central United States events have had surface manifestations in the form of landslides, soil liquefaction, and ground cracking.

If the review of available geotechnical and seismological information and the preliminary site reconnaissance indicates the potential presence of active faults at the project site, then detailed geologic

investigation may be required to establish the location of faults and the recency of fault movement in the vicinity of the site. A detailed geologic surface reconnaissance study may be sufficient to identify fault locations and assess the magnitude and direction of past fault movements. The detailed reconnaissance study may be supplemented, if necessary, by a subsurface field investigation. The field investigation may include the following:

- use of geophysical methods such as resistivity, seismic refraction, seismic reflection, or magnetic survey methods to identify potential fault locations;
- excavation of exploratory trenches across potential faults and through "marked" beds of geologic strata to allow the detailed examination of the trench walls for evidence of the presence or absence of earthquake-induced displacements and recovery of material for stratigraphic age dating; and
- use of vertical and angled borings to locate fault zones and recover material for stratigraphic age dating.

The depth of the subgrade investigated by trenches and geophysical methods should be sufficient to encompass geologic activity within the Holocene Epoch. The depth of the boring may need to be significantly greater than the depth of Holocene strata if its purpose is to locate the fault trace. Radiocarbon dating of carbonaceous material encountered in the field investigation can be used to constrain the age of most recent fault offsets. A detailed description of soil-stratigraphic dating techniques is presented by Shlemon (1985). Sieh, *et al.* (1989) describe the application of high-precision radiocarbon dating for chronological analysis of active faulting. Jibson (1985) describes field investigation of geomorphic evidence (e.g., landsliding, liquefaction) of earthquake activity in an area in the central United States where fault rupture did not propagate up to the ground surface. Establishing that recent displacement has or has not occurred is greatly complicated if a limited soil profile over rock exists at the site, for example, in glacially polished terrain or if the Holocene zone is absent or otherwise disturbed.

3.2.4 Seismic Source Characterization in the Eastern and Central United States

In recent years, seismologists have expressed significant concern regarding the lack of understanding of the source of earthquakes, referred to as seismogenesis, in the eastern and central United States. Plate tectonic theories do not adequately explain the mechanisms associated with intra-plate earthquakes. Recent workshops and seminars on the seismogenesis and seismicity of the eastern United States (SSA, 1988; ATC, 1994) have shown that some widely accepted views on earthquake origins are inconsistent with recent observations and that a global perspective may be required to understand intra-plate seismogenesis. These concerns are beyond the scope of this document. It is, however, important to recognize several observations regarding earthquake/fault considerations in the eastern and central United States. These observations are described below.

- Earthquake source zones do appear to be related to subsurface crustal structure. However, these source zones do not appear to be related to surface expressions of faulting (ATC, 1994).
- The relationship between intra-plate earthquakes and the potential for surface faulting remains in question. This is in part due to the lack of either accumulated strain or recorded significant seismic events in the eastern and central United States.
- Detailed comparison of earthquake hypocenters and known surface fault locations have failed to indicate a correlation (Hynes, *et al.*, 1988).

- Only two faults on which fault rupture has propagated to the ground surface during the Holocene Epoch have been identified in North America east of the Rocky Mountains.

Current understanding of seismogenesis east of the Rocky Mountains strongly suggests that significant field reconnaissance efforts to define seismically active faults in this region may not be useful. The region where faults capable of rupturing the ground surface may be encountered reaches from the West Coast to the Meers fault in Oklahoma but clearly excludes most of the Midwest and all of the eastern United States. Therefore, seismic source characterization for the eastern and central United States depends primarily on micro-seismicity studies and the historic record of felt earthquakes with no direct surface expression of faulting.

3.3 DETERMINATION OF THE INTENSITY OF DESIGN GROUND MOTIONS

3.3.1 Introduction

Once the seismic sources capable of generating strong ground motions at a project site have been identified and characterized, the intensity of the ground motions which may be generated at the site are evaluated for use in design. Design ground motions can be evaluated in three different ways:

- from published codes and standards;
- from a deterministic seismic hazard analysis; or
- from a probabilistic seismic hazard analysis.

3.3.2 Published Codes and Standards

Information used for seismic source characterization can often be obtained from published codes and standards (e.g., local building codes, publications of the United States Geological Survey (USGS), or various state agencies). Published codes and standards are often used because they provide credibility for the designer and may give the engineer a feeling of security. However, due to the lag time between development and publication, published codes and standards may not incorporate recent developments on local or regional seismicity. Furthermore, published codes and standards are usually based upon rather broad, regional analyses and may not reflect local, site-specific conditions.

Building Codes often contain a seismic zone map that includes minimum required seismic design parameters. For example, the Applied Technology Council (ATC) map shown in Figure 3-3 in a reduced size format divides the United States into five zones that reflect the expected intensity of shaking in each zone. Typically, seismic coefficients for use in structural analyses are associated with the seismic zones presented on the map. An example of such a map is shown in Figure 3-4 (UBC, 1994). The seismic coefficients associated with these zones usually represent "effective" ground motions for structural analyses and are not suitable for use in geotechnical analyses. However, codes may occasionally provide minimum values of the seismic coefficient for use in slope stability analyses. In using building codes, it should be kept in mind that building codes are generally intended to mitigate collapse and loss of life and not necessarily prevent damage, and that a code presents a minimum standard of care for design.

Some published codes and standards provide information on the expected value of the peak earthquake ground motions. The California Department of Transportation (CALTRANS) has developed a statewide

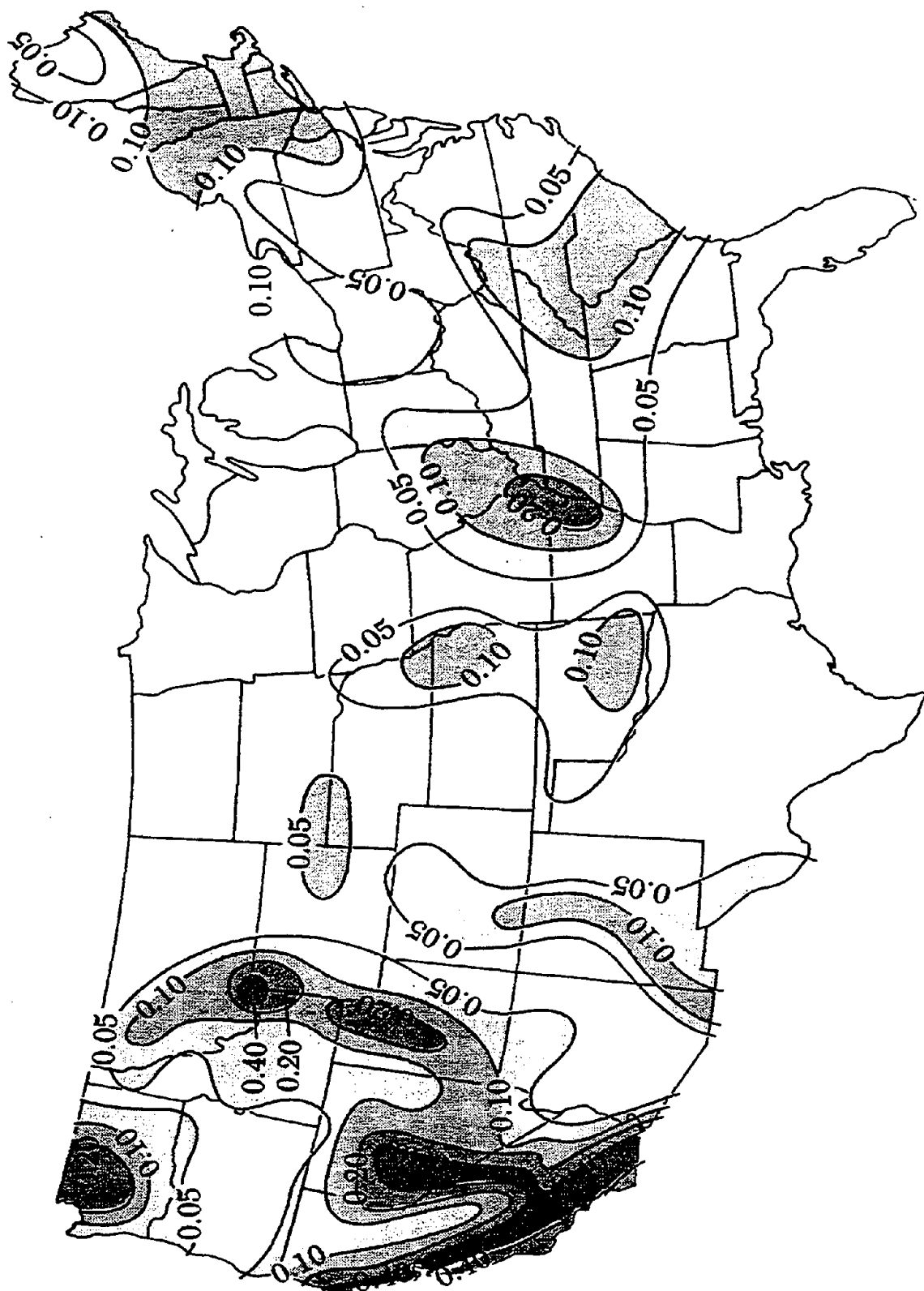


Figure 3-3: Effective Peak Acceleration Levels (In Decimal Fractions of Gravity) with a 10% Probability of Being Exceeded During a 50-year Period. (ATC, 1978, Reprinted by Permission of ATC)

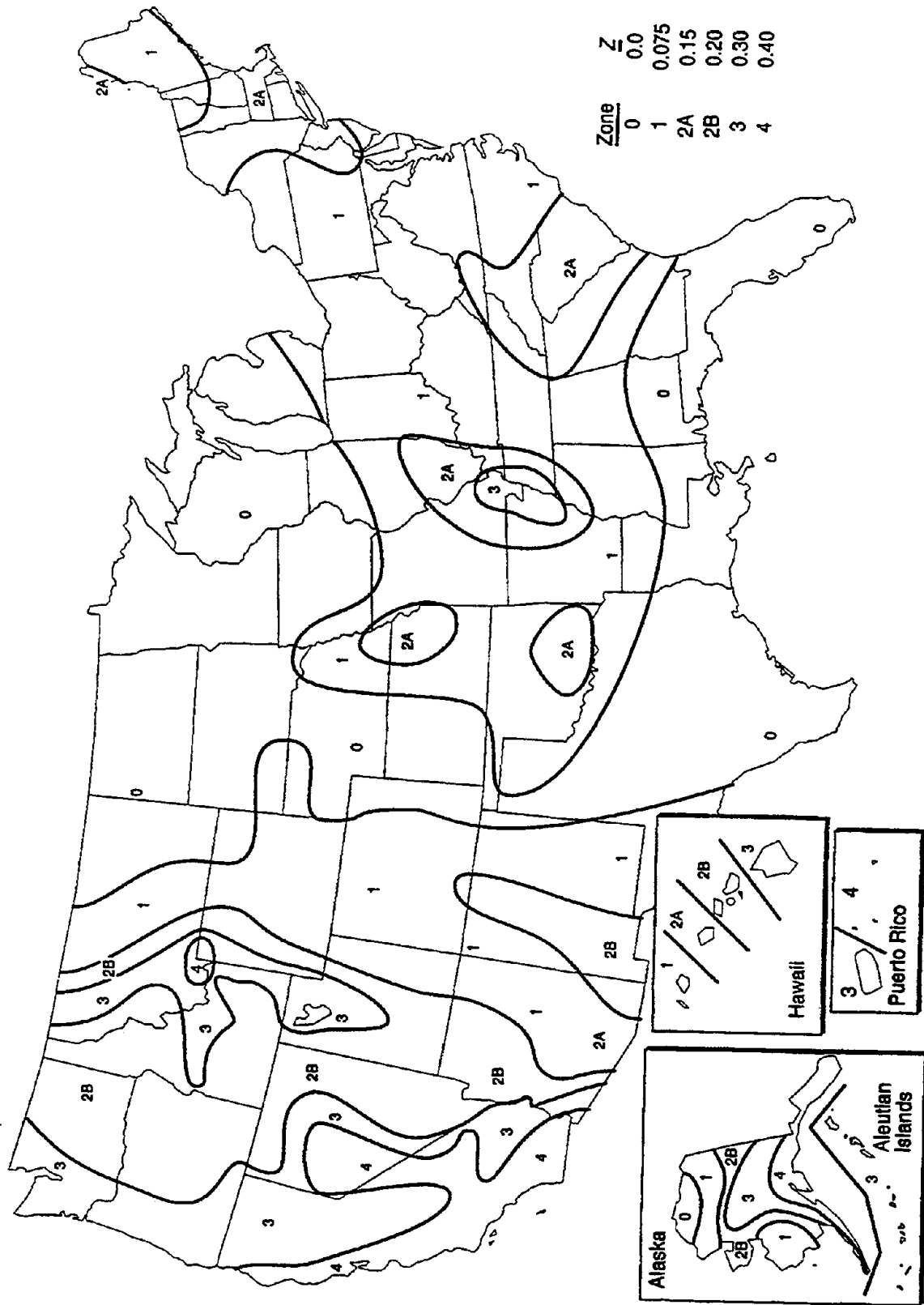


Figure 3-4: Map and Table for Evaluation of UBC Seismic Zone Factor, Z. (Reproduced from the Uniform Building Code™, Copyright© 1994, with the Permission of the Publisher, the International Conference of Building Officials)

map showing the peak ground acceleration in bedrock from the Maximum Credible Earthquake (MCE) (Mualchin and Jones, 1992; updated by Mualchin, 1995). The MCE is the regulatory design-basis earthquake in California for major bridges (e.g., toll bridges) and other important facilities (e.g., hospitals, earth dams). The USGS map presented in Figure 3-5 presents the estimated bedrock peak acceleration contours for Central and Eastern US, with a 90 percent probability of not being exceeded in 50 years (Frankel, et al., 1996). Historically, USGS provided maps for a 90 percent probability of not being exceeded for 10- and 50-year exposure periods for the peak values of acceleration (Algermissen et al., 1982, 1991). Recently, maps that include spectral acceleration values (in addition to the peak acceleration values) at various spectral periods (i.e., at 0.2, 0.3, and 1.0 second) have been developed by USGS under the National Earthquake Hazard Reduction Program (NEHRP). These maps can be accessed via the USGS Internet Website at "<http://geohazards.cr.usgs.gov/eq/>." This USGS website also provides a convenient "search by zip code" feature. Using this feature, map values for peak and spectral accelerations with a probability of being exceeded of 2 percent, 5 percent, and 10 percent in 50 years (corresponding to a 90 percent probability of not being exceeded in approximately 250, 100, 50 years, respectively) can be recovered in tabular form. An example of output data from the search at the USGS website is presented in the following:

```

The input zip-code is 11561.
ZIP CODE                11561
LOCATION                 40.5884 Lat.   -73.6560 Long.
DISTANCE TO NEAREST GRID POINT  3.9444 kms
NEAREST GRID POINT     40.6 Lat.   -73.7 Long.
Probabilistic ground motion values, in %g, at this point are:
      10%PE in 50 yr   5%PE in 50 yr   2%PE in 50 yr
PGA                5.46                10.15                20.75
0.2 sec SA        11.60                19.93                39.09
0.3 sec SA        8.40                 14.99                27.82
1.0 sec SA        2.71                 4.68                 8.91

```

If bedrock is not present at or near the ground surface, values from the CALTRANS or USGS maps may need to be modified to account for local site conditions.

The procedure for seismic hazard analysis using a published map is relatively simple:

- Step 1: Read the design peak ground acceleration from the map.
- Step 2: Assign a corresponding magnitude and distance to the peak design ground acceleration using information on regional seismic sources.

Historically, the CALTRANS, USGS, and other common seismic hazard maps typically did not provide information on the magnitude, distance, or duration of the earthquake associated with the map acceleration values. Therefore, representative values of these parameters, if necessary, had to be derived from ancillary data. Evaluation of these parameters from ancillary data is complicated by the fact that the acceleration values provided by the probabilistic maps are typically composed of contributions of earthquakes of many different magnitudes at many different distances (and therefore of many different durations). These maps provide a statistical estimate of the peak ground acceleration based on the estimated frequency of occurrence of earthquakes for the various seismic sources considered in the analysis. For many geotechnical analyses, knowledge of earthquake magnitude and, in some cases, distance and/or duration, is required. Therefore, if a map acceleration is to be used in a geotechnical analysis, a means of assigning a representative magnitude and/or distance to the design event may be needed.

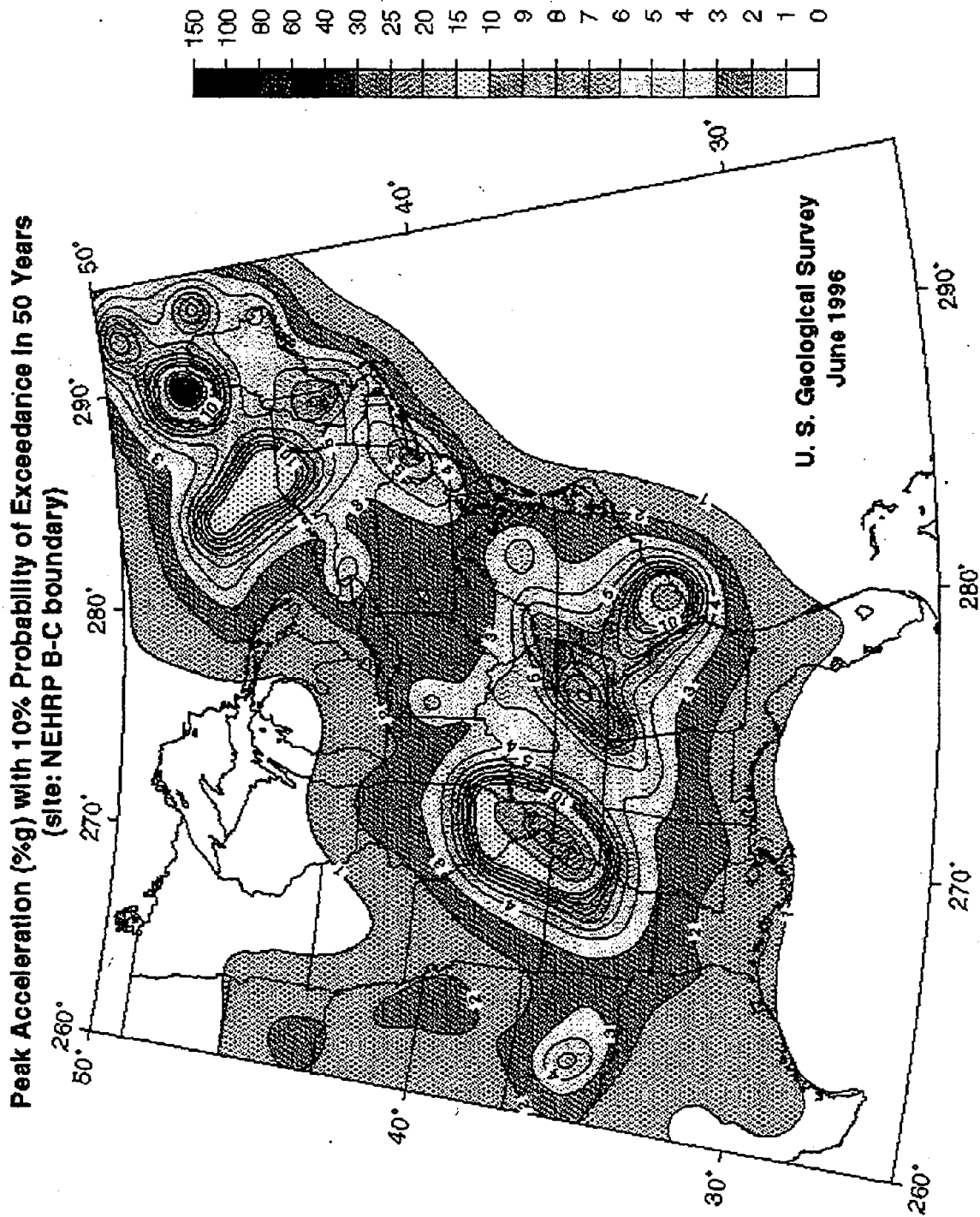


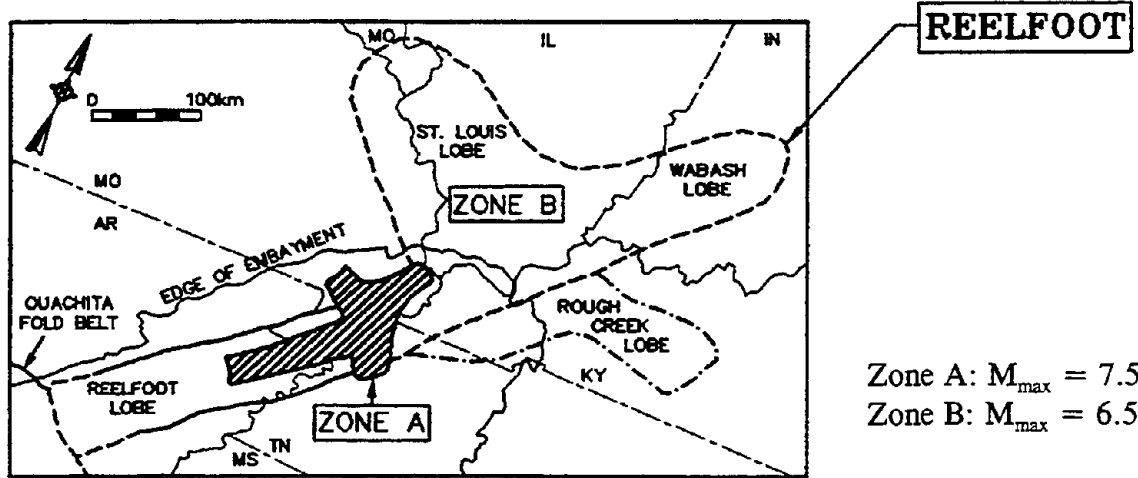
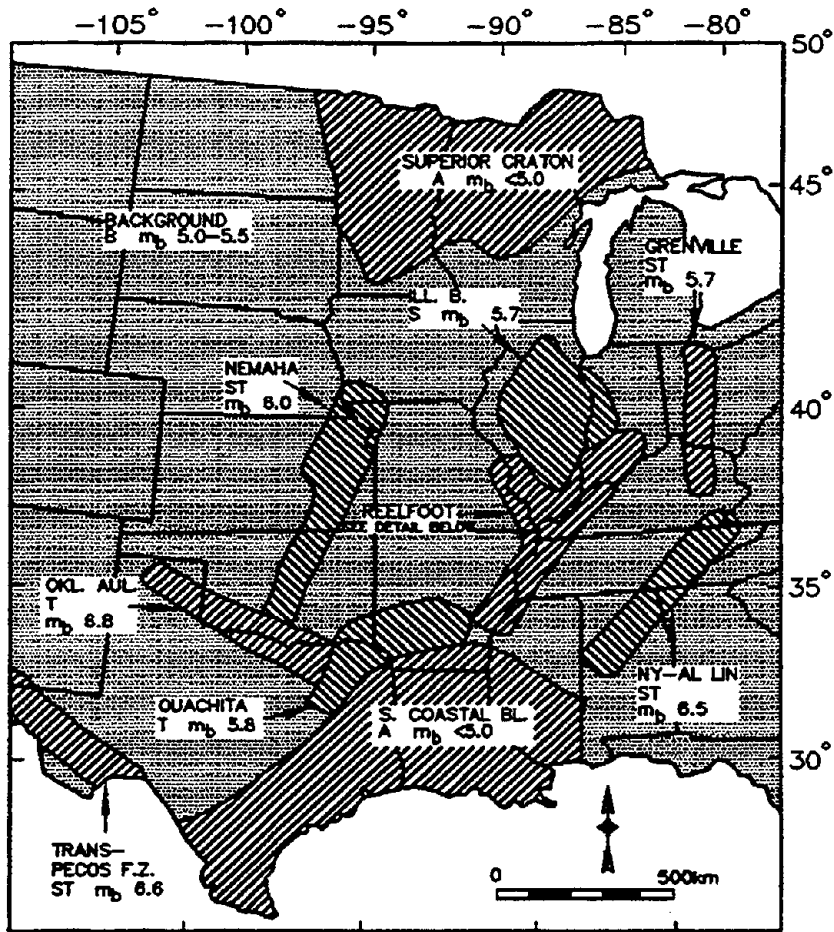
Figure 3-5: Peak Horizontal Ground Acceleration in Bedrock for Central and Eastern U.S. with a 10 Percent Probability of Exceedance in 50 Years. (Frankel, et al., 1996)

Another problem associated with using a map acceleration in a geotechnical analysis is that the earthquake generating the maximum peak ground acceleration at a site may not necessarily be the most damaging earthquake. An earthquake of lesser peak intensity but greater duration may be more damaging than the event associated with the maximum peak ground acceleration. In such cases, it may prove necessary to perform a site-specific seismic risk analysis.

Despite these shortcomings, peak acceleration values derived from published maps can be, and often are, used in geotechnical practice. Information on the location and magnitudes of earthquake sources can be obtained from either background information published with the map or from other sources of information. One conservative approach is to assign the maximum magnitude from all seismic sources contributing to the seismic hazard at the site to the published map acceleration value. Mualchin and Jones (1992) provided a listing of seismic sources and maximum magnitudes used to develop the CALTRANS map. Information on earthquake magnitudes associated with USGS map shown in Figure 3-5 can be found in Frankel, *et al.*, (1996). Figure 3-6 is a recent map of seismic sources for the central United States. The map in Figure 3-6 includes information on the maximum magnitude earthquake associated with each source zone, expressed in terms of body wave magnitude. Figure 3-7 is another example of a seismic source zone map. This map, developed especially for the central and eastern United States, and accompanying detailed information on source and background zones and earthquake magnitudes, can be found in a comprehensive, ten-volume seismic hazard study by EPRI (1986).

Alternatively, the USGS website discussed above provides information that can be used to estimate the representative magnitude and distance for a site in the continental United States to associate with a map peak or spectral acceleration value. This website provides the "deaggregated hazard", the distribution of earthquake magnitude and distance combinations contributing to the 1996 USGS map acceleration values, for a 2 percent probability of being exceeded in 50 years (corresponding to a 90 percent probability of not being exceeded in 250 years) for selected sites. The deaggregated hazard is provided for 56 cities in the Central and Eastern United States and 44 cities in the Western United States. The following output data from the website search provide an example of the deaggregated hazard information for Evansville, Illinois, one of the selected cities in the Central United States.

Deaggregated Seismic Hazard PE = 2% in 50 years pga								
Evansville IN 38.000 deg N 88.043 deg W PGA=0.32800 g								
M<=	5.0	5.5	6.0	6.5	7.0	7.5	8.0	
d<= 25.	13.888	13.372	9.591	5.787	2.447	1.584	0.000	
50.	1.507	3.176	4.624	5.054	2.818	2.440	0.000	
75.	0.093	0.349	0.927	1.737	1.449	1.757	0.000	
100.	0.011	0.060	0.247	0.670	0.591	0.938	0.000	
125.	0.002	0.017	0.095	0.348	0.250	0.488	0.000	
150.	0.000	0.004	0.030	0.143	0.114	0.269	0.000	
175.	0.000	0.001	0.008	0.050	0.051	0.146	15.718	
200.	0.000	0.000	0.002	0.019	0.023	0.083	6.904	
225.	0.000	0.000	0.001	0.007	0.010	0.042	0.000	
250.	0.000	0.000	0.000	0.003	0.004	0.020	0.000	
275.	0.000	0.000	0.000	0.001	0.002	0.012	0.000	
300.	0.000	0.000	0.000	0.000	0.001	0.006	0.000	
325.	0.000	0.000	0.000	0.000	0.000	0.003	0.000	
350.	0.000	0.000	0.000	0.000	0.000	0.002	0.000	
375.	0.000	0.000	0.000	0.000	0.000	0.002	0.000	
400.	0.000	0.000	0.000	0.000	0.000	0.001	0.000	
425.	0.000	0.000	0.000	0.000	0.000	0.001	0.000	



Zone A: $M_{max} = 7.5$
 Zone B: $M_{max} = 6.5$

Figure 3-6: Seismic Source Zones in the Central United States. (Johnston and Nava, 1994, reprinted by permission of ATC)

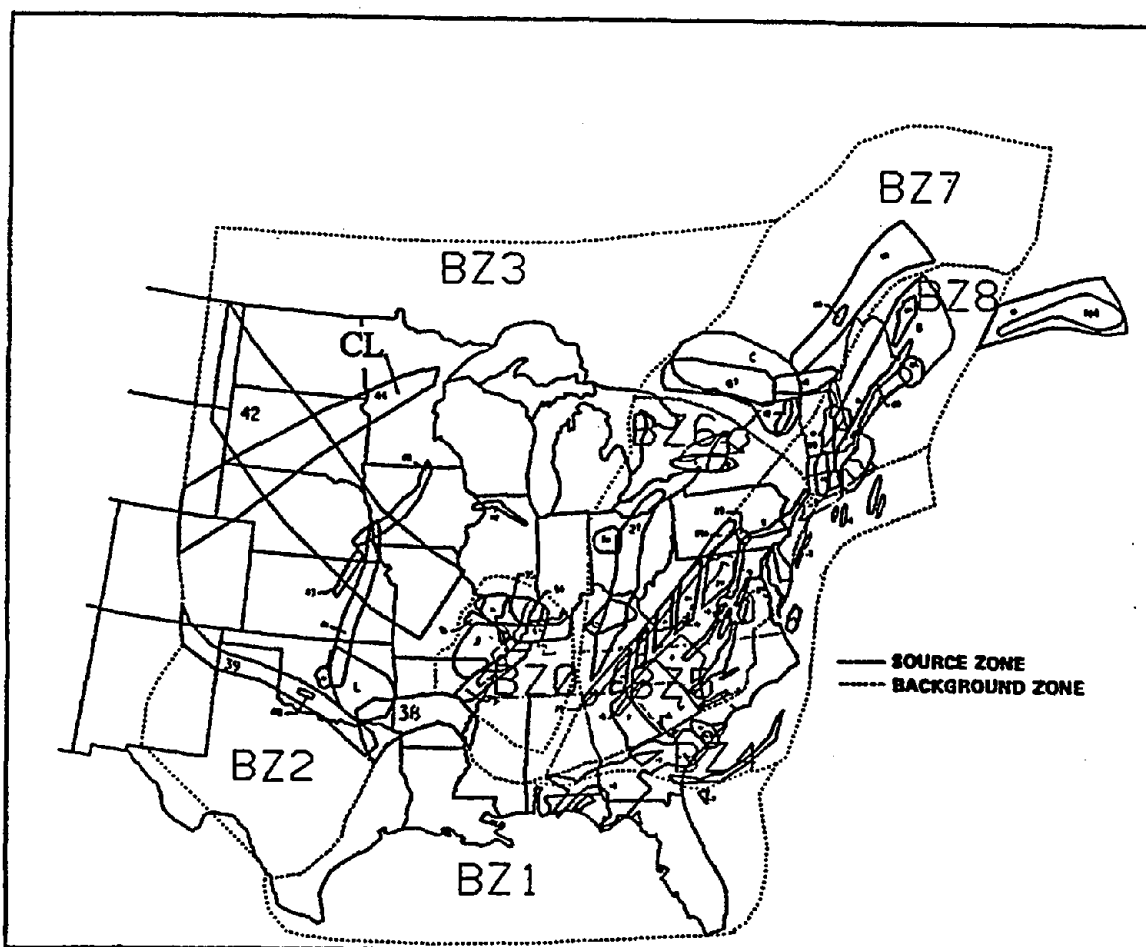


Figure 3-7: Seismic Source Zones in the Central and Eastern United States. (EPRI, 1986, reprinted by permission of ATC)

In using background zone and magnitude information to supplement PGA data from USGS, EERI, and other maps, the prudent engineer generally makes conservative assumptions to compensate for the uncertainty associated with published map data. For instance, the engineer may select the largest magnitude associated with the governing source zone for his project and locate it at the point within the zone closest to his site. If the governing source zone is uncertain, he may include multiple source zones in his analysis. To use the deaggregated seismic hazard information from the USGS website, the engineer generally recovers the data from the closest city of cities to the site. However, because the deaggregated data is provided for only selected cities and for one probability level and because the provided data represents multiple combinations of magnitude and distance, significant judgement is still required in choosing a representative value. Typically, the engineer will choose a magnitude and distance combination that encompasses 70 to 90 percent of the hazard (i.e., 70 to 90 percent of the hazard is from a smaller magnitude and a closer distance). In some cases, more than one combination of magnitude and distance may be required. The peak acceleration seismic hazard data presented above for Evanston illustrates such a case. These data indicate that most of the seismic hazard for Evanston is derived from earthquakes less than 25 km from the site with magnitudes between 5 and 6 (though the magnitude of some of these local events may be as great as 7.5). However, over 20 percent of the seismic hazard is from a distant earthquake more than 150 km from the site with a magnitude of 8.0. Therefore, for some projects in Evanston, the impact of both local and distant events may warrant consideration.

3.3.3 The Deterministic Approach

The objective of a deterministic seismic hazard analysis is to evaluate the magnitude of ground motion parameters (usually peak ground acceleration and acceleration response spectra) at a specific site from all the capable seismic sources with the potential for generating strong ground motions at the site. In some cases, particularly when soft soils capable of amplifying ground motions from earthquakes are present at the site, the seismic hazard analysis may include sources located over 100 km from the site.

In a deterministic seismic hazard analysis, the engineer or geologist performing the analysis first identifies the capable seismic sources and assigns a maximum magnitude to each source. Then, the intensity of shaking at the site from each capable source is calculated and the design earthquake is identified based on the source capable of causing the greatest damage. The steps in a deterministic seismic hazard analysis are as follows:

- Step 1: Establish the location and characteristics (e.g., style of faulting) of all potential earthquake sources that might affect the site. For each source, assign a representative earthquake magnitude.
- Step 2: Select an appropriate attenuation relationship and estimate the ground motion parameters at the site from each capable fault as a function of earthquake magnitude, fault mechanism, site-to-source distance, and site conditions.
- Step 3: Screen the capable (active) faults on the basis of magnitude and the intensity of the ground motions at the site to determine the governing source.

Engineers or engineering geologists performing deterministic seismic hazard analyses should consider all reasonable interpretations, models, and values in characterizing the seismic source zones. While all capable sources are usually treated equally in a deterministic analysis regardless of their likelihood of occurrence, the likelihood of occurrence may enter into the determination of whether or not a fault is capable of generating earthquakes of specified magnitudes. For instance, some bridges in California have been designed for the *Maximum Probable Earthquake* (MPE) defined by the California Division of Mines and Geology (CDMG) as the maximum earthquake anticipated in the next 100 years (CDMG, 1975). Therefore, active faults with long recurrence intervals may not be considered in evaluating the MPE, and the MPE magnitude may not be the largest magnitude earthquake of which the fault is capable.

Screening for the most damaging event in a deterministic seismic hazard analysis is typically based upon magnitude, intensity, and distance wherein events of smaller magnitude and lower intensity than events closer to the source are eliminated from consideration. However, it may not be possible to establish a single event that is most damaging based on the results of a deterministic analysis, as this process can result in a family of design events of increasing magnitude and distance with decreasing intensity. As there is no general method for evaluating the relative damage potential of one event with a large magnitude and low intensity compared to a smaller magnitude event of higher intensity, it may be necessary to consider multiple events in subsequent engineering analysis (unless the intensity discrepancy is so great or the magnitudes are so close that the choice is obvious).

Screening capable seismic sources on the basis of magnitude and distance prior to evaluating the intensity of ground motions at the site is not recommended as it can lead to errors due to the dependence of the mode of faulting on the intensity of ground motions. It is generally assumed that thrust faults generate higher intensity ground motions than strike slip faults of the same magnitude at the same distance.

Therefore, if the family of capable (active) faults includes faults with different modes of behavior, faults should not be screened on the basis of magnitude and distance only.

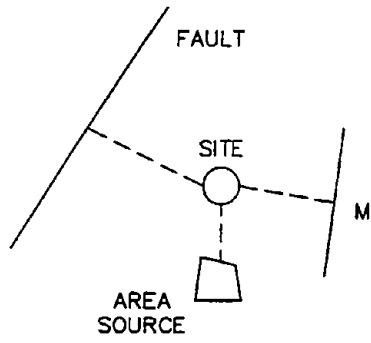
The intensity of the earthquake ground motions at the site generated by a capable (active) fault (or seismic zone) is evaluated using an attenuation relationship. Attenuation relationships that discriminate between different styles of faulting and between rock and soil sites are available. However, attenuation relationships associated with soil sites typically have greater uncertainty assigned to them than rock site attenuation relationships due to the greater observed variability in ground motions at soil sites. Therefore, it is generally more desirable to use attenuation relationships developed for rock sites in a seismic hazard analysis in combination with a site-specific analysis of the impact of local soil conditions on the design ground motions rather than to use a soil site attenuation relationship. Attenuation relationships are described in more detail in Chapter 4. Site-specific seismic response analyses are described in Chapter 6.

3.3.4 The Probabilistic Approach

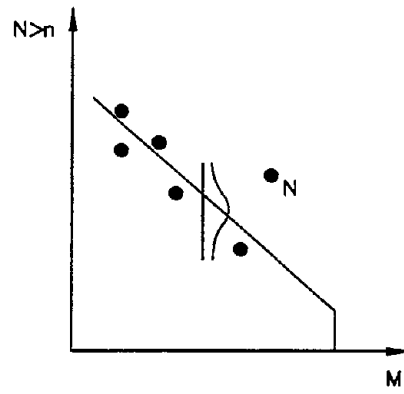
A probabilistic seismic hazard analysis incorporates the likelihood of a fault rupturing and the distribution of earthquake magnitudes associated with fault rupture into the assessment of the intensity of the design ground motion at a site. The objective of a probabilistic seismic hazard analysis is to compute, for a given exposure time, the probability of exceedance corresponding to various levels of a ground motion parameter (e.g., the probability of exceeding a peak ground acceleration of 0.2 g in a 100-year period). The ground motion parameter may be either a peak value (e.g., peak ground acceleration) or a response spectra ordinate associated with the strong ground motion at the site. The probabilistic value of the design parameter incorporates both the uncertainty of the attenuation of strong ground motions and the randomness of earthquake occurrences. A probabilistic seismic hazard analysis usually includes the following steps, as illustrated in figure 3-8:

- Step 1: Identify the seismic sources capable of generating strong ground motion at the project site.
- Step 2: Determine the minimum and maximum magnitude of earthquake associated with each source and assign a frequency distribution of earthquake occurrence to the established range of magnitudes. While the maximum magnitude is a physical parameter related to the fault dimensions, the minimum magnitude may be related to both the physical properties of the fault and the constraints of the numerical analysis. Use of a minimum magnitude less than 4.5 is not recommended, even if the seismic source is capable of generating smaller magnitude events, as inclusion of such small magnitude events can result in misleadingly high response values for extreme (low) probabilities of exceedance.
- Step 3: For each source, assign an attenuation relationship on the basis of the style of faulting. Uncertainty is usually assigned to the attenuation relationships based upon statistical analysis of attenuation in previous earthquakes.
- Step 4: Calculate the probability of exceedance of the specified ground motion parameter for a specified time interval by integrating the attenuation relationship over the magnitude distribution for each source and summing up the results.

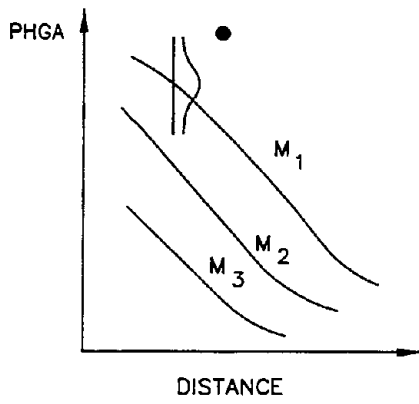
The Gutenberg-Richter magnitude-recurrence relationship (Gutenberg and Richter, 1942) is the relationship used most commonly to describe the frequency distribution of earthquake occurrence. This relationship, presented in Figure 3-9 (after Schwartz and Coppersmith, 1984) for the San Andreas Fault in southern



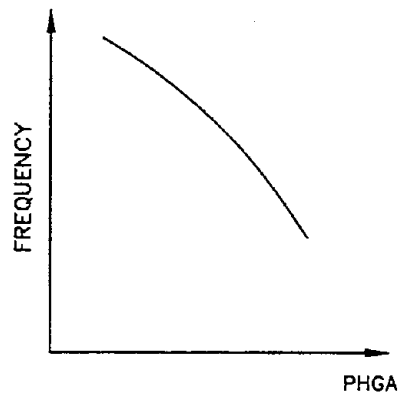
STEP 1
SOURCES



STEP 2
RECURRENCE



STEP 3
ATTENUATION



STEP 4
HAZARD CURVES

Figure 3-8: Probabilistic Seismic Hazard Analysis

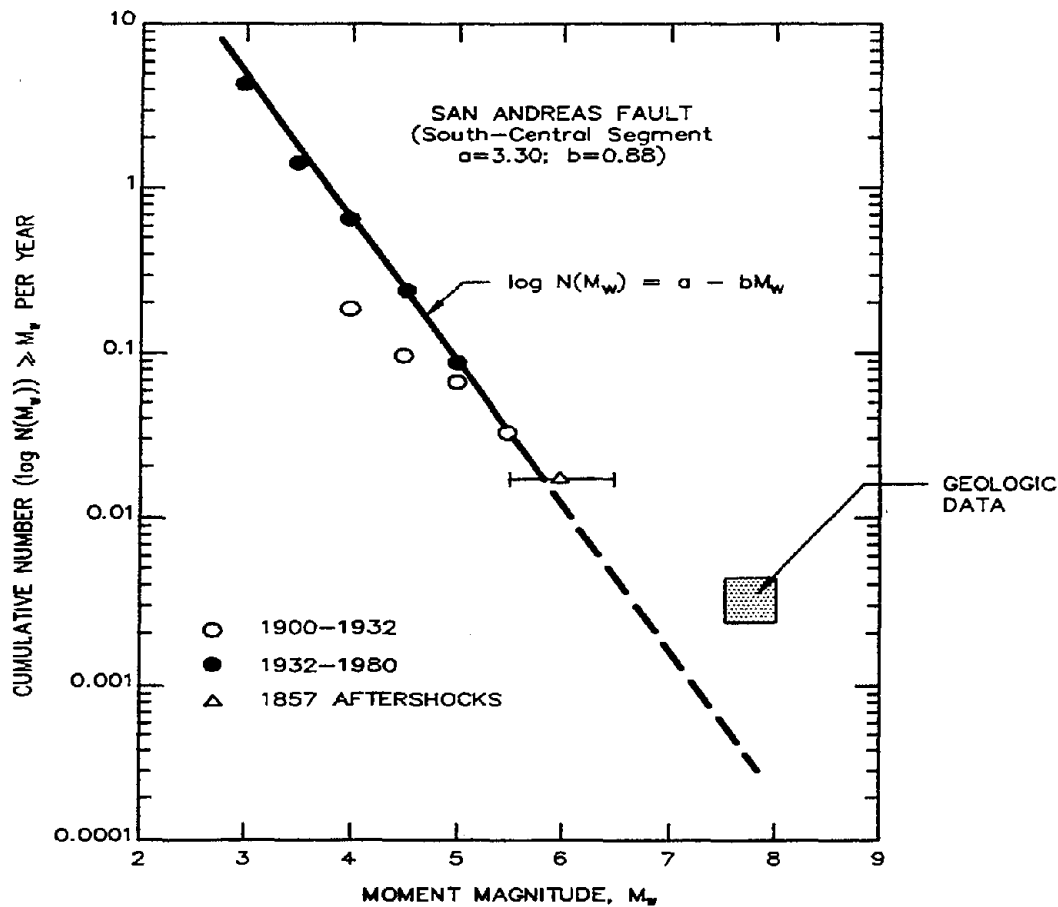


Figure 3-9: Cumulative Frequency-Magnitude Plot of Instrumental Seismicity; San Andreas Fault South-central Segment Data. (After Schwartz and Coppersmith, 1984 Fault Behavior and Characteristic Earthquakes: Examples from the Wasatch and San Andreas Fault Zones, *Journal of Geophysical Research*, Vol. 89, No. B7, pp. 5681-5698, Published by the American Geophysical Union)

California, describes an exponential-magnitude distribution relationship that corresponds to a straight line when magnitude versus the number of events (cumulative number) per year is plotted on semi-log paper. Because the historical record of large magnitude events with long recurrence intervals is "incomplete" (statistically non-representative due to the limited period over which records are kept), the Gutenberg-Richter recurrence relationship is often constructed using data for relatively low magnitude earthquakes and projected to predict the frequency of large earthquakes for which incomplete data exists.

An alternative method for establishing the magnitude-frequency of occurrence distribution for a seismic source is to use the geologic data on the historic occurrence of earthquakes and on regional tectonic movements. For some faults (e.g., the San Andreas fault zone in southern California, see Figure 3-9), field studies may provide reliable information on the magnitude and frequency of occurrence of major earthquakes. However, such instances are likely to be limited to a few major faults in the western United States. Alternatively, stratigraphic and seismologic data may be used to estimate regional tectonic deformation rates. These regional deformation rates may then be apportioned to individual faults and used to establish the magnitude-frequency of occurrence relationship for each individual fault. In many areas, this may be the only means of establishing the recurrence rate of major earthquakes, particularly for buried faults or faults with low rates of occurrence.

Seismicity that is not associated with known faults is typically incorporated into a probabilistic seismic hazard analysis using a "random" area source. A "random" earthquake is assigned an equal likelihood of occurrence at any point within the area source. The minimum and maximum magnitudes and the rate of occurrence are usually based upon the historical record for earthquake associated with faults not recognized prior to the event. The depth or depth range for the random earthquakes is typically based upon the depth at which micro-seismicity is observed to occur in the region.

Most probabilistic seismic hazard analyses are designed to provide information on the intensity of ground motions for design only, and not on the magnitude associated with the design intensity. While information on the distribution of magnitudes associated with the design intensity can be obtained from a probabilistic seismic hazard analysis, most commercially available computer programs do not readily provide this information. Furthermore, even if information on the distribution of earthquake magnitudes associated with the design intensity is available, there is no generally agreed upon method for determining the design magnitude from this information. Figure 3-10 illustrates the magnitude-distance distribution associated with the peak ground acceleration from a probabilistic seismic hazard analysis. As there is no generally accepted procedure for determining the design magnitude from a magnitude distribution like the one presented in Figure 3-10, engineering judgement is required to determine the design magnitude. For many projects, considering that the design acceleration is already based upon a low probability of occurrence, the expected magnitude value (the 50th percentile value) associated with the design acceleration may be used. Alternatively, a conservative approach in which the maximum magnitude or the magnitude with a 10 percent probability of being exceeded may be appropriate for some projects.

Additional information on procedures for performing both deterministic and probabilistic seismic hazard evaluations can be found in Krinitzsky, *et al.*, (1993).

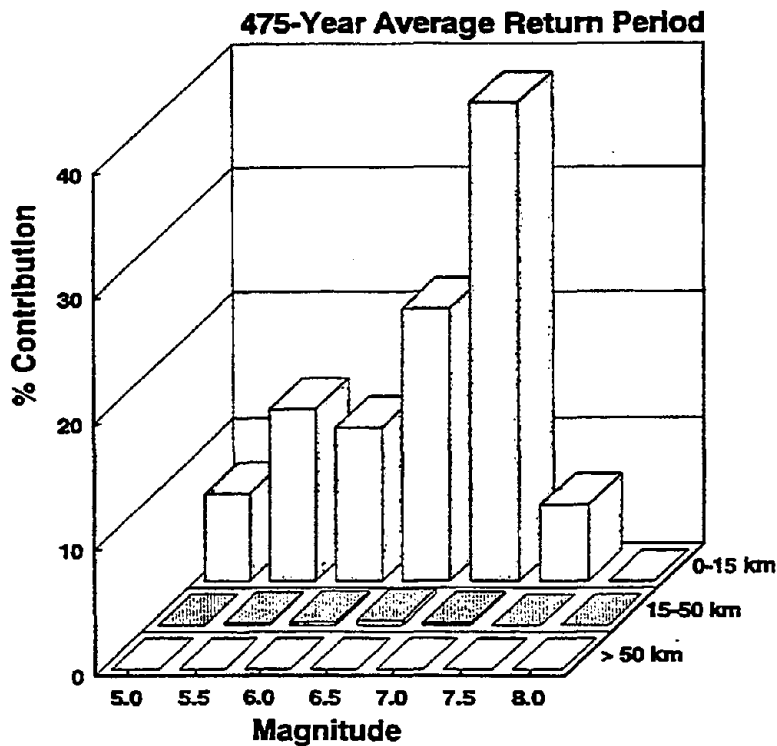


Figure 3-10: Magnitude-Distance Distribution for a Specified Peak Ground Acceleration. (Moriwaki, *et al.*, 1994, reprinted by permission of ATC)

CHAPTER 4.0 GROUND MOTION CHARACTERIZATION

4.1 BASIC GROUND MOTION CHARACTERISTICS

Results of the seismic hazard analysis will establish the peak horizontal ground acceleration (PHGA) for use in design analysis. However, PHGA is only one of the characteristics of the earthquake ground motion at a site that influence the potential for damage. The damage potential of seismically-induced ground motions may also depend upon the duration of strong shaking, the frequency content of the motion, the energy content of the motion, peak vertical ground acceleration (PVGA), peak ground velocity and displacement, and the intensity of the motion at times other than when the peak acceleration occurs, as elaborated below.

The acceleration response spectrum is one commonly used index of the character of earthquake ground motions. An acceleration response spectrum provides quantitative information on both the intensity and frequency content of the acceleration time history. However, while widely used in structural engineering, response spectra are of limited use in geotechnical analysis. The primary application of response spectra to geotechnical practice is as an aid in selection of time histories for input to site response and deformation analyses, for comparison of accelerograms, and for illustration and evaluation of the influence of local soil conditions on ground motions.

Other parameters used less frequently than PHGA and the acceleration response spectrum to describe the character of earthquake ground motions include various measures of the duration and energy content of the acceleration time history. Duration is sometimes expressed directly as the length of time from the initiation of strong shaking to its cessation. Alternatively, indirect measures of duration, including the number of equivalent cycles and the number of positive zero crossings of the acceleration time history, are sometimes employed in earthquake engineering practice.

The energy content of the strong ground motion may be expressed in terms of the *root-mean-square* (RMS) and duration of the acceleration time history or in terms of the Arias intensity. The RMS, discussed in detail in Section 4.4, represents an “average” or representative value for the acceleration over the defined duration of the strong ground motion. The Arias intensity is the square of the acceleration integrated over the duration of the motion. The time history of the normalized Arias intensity, referred to as a Husid plot, is sometimes used to define the duration of strong shaking.

These various indices of the character of strong ground motions (*ground motion parameters*) commonly used in engineering practice are defined and described in this chapter. Following their definition and description, procedures for using these indices for selection of representative time histories to characterize earthquake ground motions at a site are presented.

4.2 PEAK VALUES

4.2.1 Evaluation of Peak Parameters

Peak horizontal ground acceleration (PHGA) is the most common index of the intensity of strong ground motion at a site. The PHGA is directly related to the peak inertial force imparted by strong shaking to a structure founded on the ground surface and to the peak shear stress induced within the ground itself. Peak vertical ground acceleration (PVGA), peak horizontal ground velocity (PHGV), and peak horizontal

ground displacement (PHGD) are also used in some engineering analyses to characterize the damage potential of ground motions. For instance, PHGV is a common index of structural damage and PHGD may be used in analyses of retaining walls, tunnels, and underground pipelines. PVGA is an important parameter in the design of base-isolated structures.

Peak values for design analyses are evaluated on the basis of the seismic hazard analysis. For major projects, a site or project specific seismic hazard analysis may be performed. Alternatively, results from published regional seismic hazard analyses or from seismic hazard analyses performed for previous projects in the same vicinity may be used. Most published seismic hazard maps tend to be probabilistic in nature. Both deterministic and probabilistic project-specific analyses are used in practice.

4.2.2 Attenuation of Peak Values

A key step in both deterministic and probabilistic seismic hazard analyses is calculation of the ground motion parameter of interest at a given site from an earthquake of a given magnitude and site-to-source distance. These ground motion parameter values are typically evaluated using an *attenuation relationship*, an equation that relates the parameter value to the key variables on which the ground motion parameter depends (e.g., earthquake magnitude, site-to-source distance, style of faulting). Attenuation relationships may be developed either from statistical analyses of values observed in previous earthquakes or from theoretical models of the propagation of strong ground motions. These observations and analyses indicate that the most important factors influencing peak values of earthquake strong ground motions at a site are the magnitude of the earthquake, the distance between the site and the earthquake source, the style of faulting, and local ground conditions (e.g., rock or soil site conditions).

There are many different attenuation relationships that have been proposed. Campbell (1985), Joyner and Boore (1988), and Atkinson and Boore (1990) provide excellent summaries of many of the available attenuation relationships.

A large number of attenuation relationships are available for the western United States. These attenuation relationships are based primarily on statistical analysis of recorded data. For the eastern and central United States, where little to no recorded strong motion data are available for statistical analysis, relatively few attenuation relationships are available. The few attenuation relationships that do exist for the eastern and central United States are based primarily upon theoretical models of ground motion propagation due to the lack of observational data.

Even when restricted to a relatively narrow geographic locale like the northwestern United States, there may still be a need to use different attenuation relationships for different tectonic conditions. For example, Youngs, *et al.* (1988) found differences in attenuation of ground motions between earthquakes occurring along the interface between the subducting Juan de Fuca tectonic plate and the North American plate (interplate events) and earthquakes occurring within the subducting Juan de Fuca plate (intraplate events) in the Pacific northwest (see Figure 2-1).

PHGA attenuation relationships for shallow earthquakes that occur at the interface between the Pacific and American tectonic plates in the western United States have been developed by many investigators, including Campbell and Duke (1974), Campbell (1993), Campbell and Bozorgnia (1994), Boore, *et al.*, (1993), Boore and Joyner (1994), Sadigh, *et al.*, (1993), Geomatrix (1995), Silva and Abrahamson (1993), Abrahamson and Silva (1996), and Idriss (1995). Table 4-1 presents a summary of commonly used PHGA attenuation relationships in the western United States. These relationships consider earthquake magnitude, site-to-source distance, and local ground conditions (soil or rock). These relationships may also

TABLE 4-1
ATTENUATION RELATIONSHIPS FOR THE WESTERN UNITED STATES
(For Shallow Crustal Earthquakes)

Reference ⁽¹⁾	Magnitude Measure ⁽²⁾	Distance Measure ⁽³⁾	Limitation ⁽⁴⁾
Schnabel and Seed (1973)	$M^{(5)}$	Closest Horizontal Distance to the Zone of Energy Release, R_E	Available only in the form of charts. $3 \leq R_E \leq 1,000$ km
Campbell and Duke (1974)	M_S	Hypocentral Distance, R_H	Attenuation of I_A only. $15 \leq R_H \leq 110$ km
Kavazanjian, <i>et al.</i> (1985a)	M_w	Closest Distance to the Rupture Zone, R_R	Attenuation of RMSA only. $0 < R_R < 100$ km
Idriss (1993; 1995)	M_L if $M < 6$ M_S if $M > 6$	Closest Distance to the Rupture Zone, R_R	$1 \leq R_R \leq 60$ km
Joyner and Boore (1988); Boore, <i>et al.</i> (1993)	M_w	Closest <i>Horizontal</i> Distance to the Vertical Projection of the Rupture Zone, R_{JB}	$0 < R_{JB} \leq 80$ km
Geomatrix (1991, 1995); Sadigh, <i>et al.</i> (1993); Silva and Abrahamson (1993); Abrahamson and Silva (1996)	M_w	Closest Distance to the Rupture Zone, R_R	$0 < R_R \leq 100$ km
Campbell (1990; 1993); Campbell and Bozorgnia (1994)	M_L if $M < 6$ M_S if $M > 6$	Seismogenic Distance, R_S	$0 < R_S \leq 60$ km

- Notes: (1) Table lists main references and their latest updates. The following references also include coefficients for spectral values: Joyner and Boore (1988); Geomatrix (1991, 1995); Campbell (1990, 1993); and Idriss (1993). Relationship by Schnabel and Seed (1973) is shown by dashed lines in Figure 4-2. Relationship by Kavazanjian, *et al.* (1985) is shown in Figure 4-7. See Equation 4-4 for Campbell and Duke (1974) relationship.
- (2) M_w = Moment Magnitude, M_L = Local (Richter) Magnitude, M_S = Surface Wave Magnitude. Note that for $M < 6$, $M_L \approx M_w$ and for $M > 6$, $M_S \approx M_w$.
- (3) Refer to the original references for detailed definition of distance measures. Note that for design, it is commonly assumed that the rupture zone equals to the area of the fault plane.
- (4) I_A = Arias Intensity, as defined in Chapter 4.5; RMSA = Root Mean Square Acceleration as defined in Chapter 4.4.
- (5) Magnitude measure was not specified by Schnabel and Seed (1973).

discriminate on the basis of style of faulting, as statistical analysis shows that reverse (thrust) fault events generate peak ground accelerations approximately 20 to 30 percent greater than strike-slip events of the same magnitude at the same distance. Figure 4-1 compares mean value PHGA attenuation curves for magnitude 6.5 and 8.0 events on a strike-slip fault calculated by three commonly used attenuation relationships for western United States earthquakes.

Different attenuation relationships than those used for shallow crustal earthquakes are used for the subduction zone earthquakes that occur along the Pacific Coast in Alaska, Washington, Oregon, and the northwest corner of California. For subduction zone earthquakes, PHGA attenuation relationships by Cohee, *et al.*, (1991) and Youngs, *et al.*, (1988) are often used in earthquake engineering practice. Table 4-2 presents the relationships for attenuation of PHGA in subduction zone earthquakes developed by Cohee, *et al.* (1991) and Youngs, *et al.* (1988).

With respect to differences in ground motion attenuation between the western United States and the eastern and central United States, it is generally agreed that ground motions east of the Rocky Mountains attenuate more slowly than ground motions in the west. However, due to the much lower rates of seismicity and the absence of large magnitude earthquakes since the deployment of strong motion accelerographs in the eastern and central United States, there is insufficient data to characterize the attenuation of strong ground motions east of the Rocky Mountains using statistical methods. Therefore, attenuation relationships used for earthquakes occurring in eastern and central United States are based upon theoretical modeling of ground motion attenuation. Attenuation relationships for the eastern and central United States commonly used in engineering practice include relationships developed by Nuttli and Herrmann (1984), Boore and Atkinson (1987), McGuire, *et al.* (1988), Boore and Joyner (1991), and Atkinson and Boore (1995).

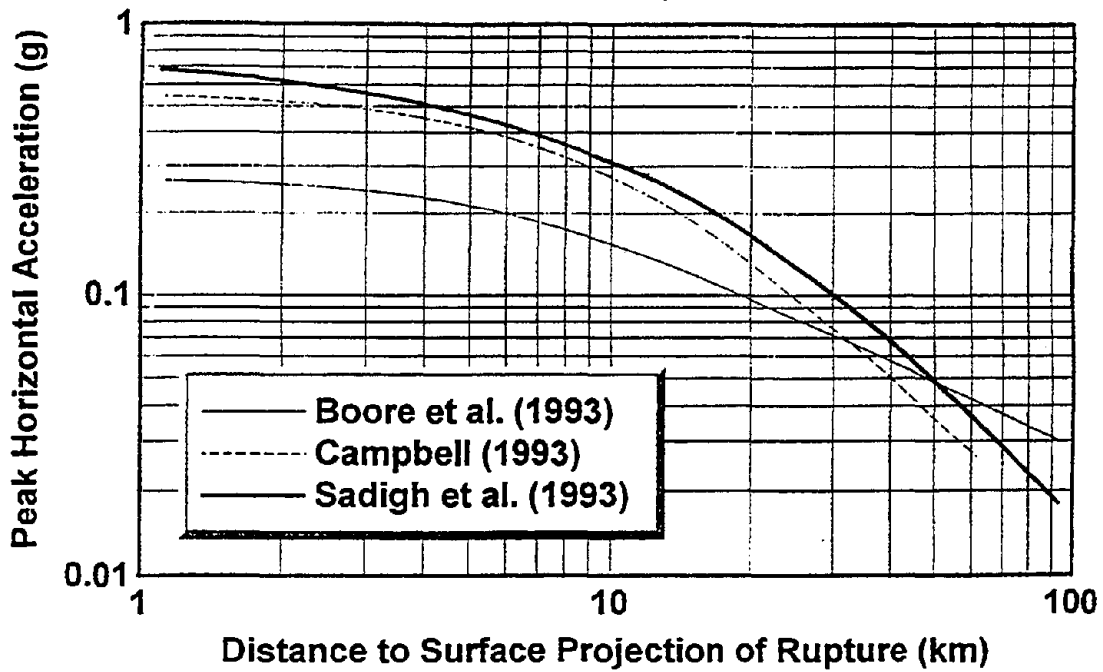
Table 4-2 includes the PHGA attenuation relationships developed by Toro, *et al.* (1997) for the Mid-Continent and Gulf Coast regions that were used in developing the 1996 USGS seismic hazard maps. Figure 4-2 compares typical PHGA attenuation relationship for the eastern and central United States to that used in the western United States (dashed lines).

Factors other than distance, magnitude, and style of faulting may influence the attenuation of strong ground motions. These factors include depth of earthquake hypocenter, the strike and dip of the fault plane (see Figure 2-6), location of the site relative to the hanging and foot walls of a thrust fault (see Figure 2-7), rupture directivity effects, topographic effects, depth to crystalline bedrock, velocity contrasts, asperities on the rupture surface, wave reflection, wave refraction, and wave scattering. Figure 4-3 presents a recent attenuation relationship developed by Abrahamson and Silva (1996) for reverse (thrust) faults showing the influence of the location of the site with respect to the hanging wall and the foot wall of the fault. Most other factors (e.g., directivity, rupture effects) are not explicitly considered in attenuation relationships and can only be accounted for by detailed seismologic modeling.

4.2.3 Selection of Attenuation Relationships

The engineer choosing an attenuation relationship for use in practice should keep in mind that new attenuation relationships are regularly being developed. Many of the investigators who have developed attenuation relationships for the western United States revise their relationships after almost ever major earthquake to include newly recorded motions. Therefore, when selecting an attenuation relationship, it is prudent to review the current literature and select the most appropriate relationship or relationships for the project site. When evaluating whether or not a certain attenuation relationship is appropriate, the engineer should thoroughly review the published information regarding its development, especially the tectonic regime for which it was developed, the ranges of magnitude and distance to which it is restricted,

ROCK SITE; $M_w = 6.5$



ROCK SITE; $M_w = 8.0$

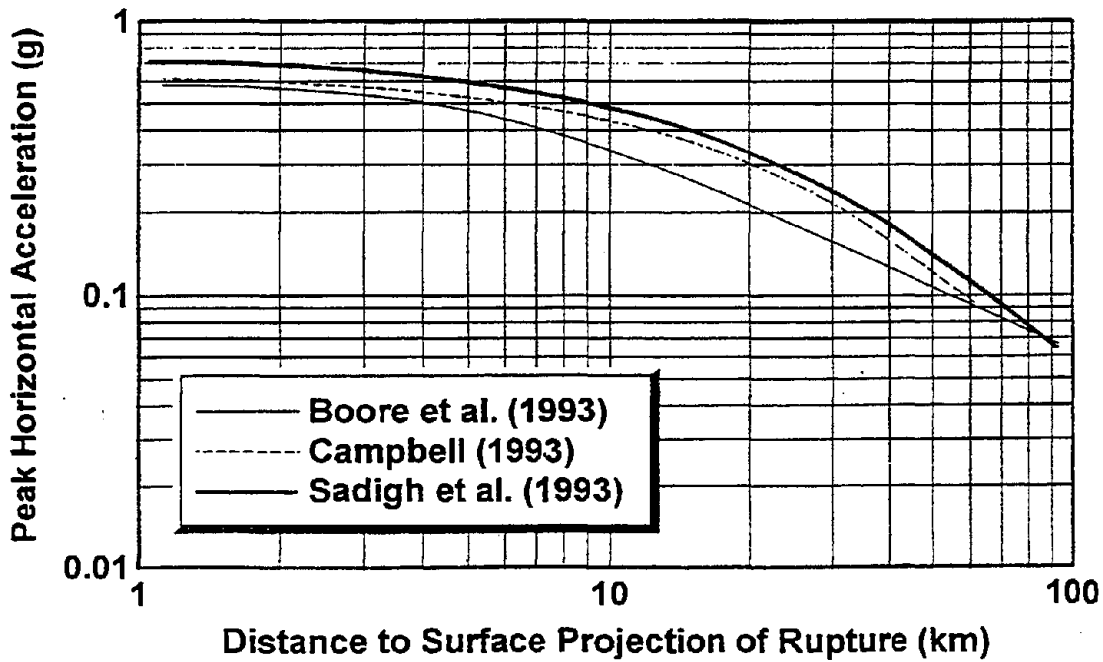


Figure 4-1: Comparison of Attenuation Relationships by Various Investigators. (For Strike-Slip Faults)

TABLE 4-2
ATTENUATION RELATIONSHIP FOR SUBDUCTION ZONE AND CENTRAL
AND EASTERN UNITED STATES EARTHQUAKES

Reference	Attenuation Relationship	Limitation ⁽¹⁾
Subduction Zone Youngs, <i>et al.</i> (1988)	$\ln(\text{PGA}) = 19.16 + 1.045M_w - 4.738 \ln[R_H + 205.5 \exp(0.0968M_w)] + 0.54Z_i$	$20 < R_H \leq 40 \text{ km}$ $M_w \leq 8$
Subduction Zone Youngs, <i>et al.</i> (1988)	$\ln(\text{PGA}) = 19.16 + 1.045M_w - 4.738 \ln[R_H + 154.7 \exp(0.1323M_w)]$	$20 < R_H \leq 40 \text{ km}$ $M_w > 8$
Subduction Zone Cohee, <i>et al.</i> (1991)	$\ln(\text{PGA}) = 1.5 - 3.33 \ln(R_S + 128) + 0.79s$	$25 < R_S < 175 \text{ km}$ $M_w \leq 8$
Subduction Zone Cohee, <i>et al.</i> (1991)	$\ln(\text{PGA}) = 2.8 - 1.26 \ln(R_R) + 0.79s$	$30 < R_R < 100 \text{ km}$ $M_w > 8$
Mid-Continent Toro, <i>et al.</i> (1997)	$\ln(\text{PGA}) = 2.20 + 0.81 (M_w - 6) - 1.27 \ln(R_m) - 0.11 \text{Max}[\ln(R_m/100), 0] - 0.0021 R_m$	
Gulf Coast Toro, <i>et al.</i> (1997)	$\ln(\text{PGA}) = 2.80 + 1.31 (M_w - 6) - 1.49 \ln(R_m) - 0.09 \text{Max}[\ln(R_m/100), 0] - 0.0017 R_m$	

Notes: M_w = Moment magnitude.
 R_H = Hypocentral distance.
 R_R = Closest distance to the rupture zone (fault plane).
 R_S = Seismogenic distance (closest distance from the fault asperity).
 R_m = $\sqrt{R_{JB}^2 + C_J^2}$
 C_J = 9.3 for Mid-Continent, 10.9 for Gulf Coast
 R_{JB} = Closest Horizontal Distance to Vertical Projection of Fault Plane (see Figure 2-7)
 Z_i = The tectonics term in Youngs, *et al.* (1988). Equal to 0 for interplate events, and 1 for intraplate events.
 s = The site term in Cohee, *et al.* (1991) relationship. Equal to 0 for rock sites and 1 for soil sites.
⁽¹⁾ = Refer to the original references for detailed description of distance measures and limitations.

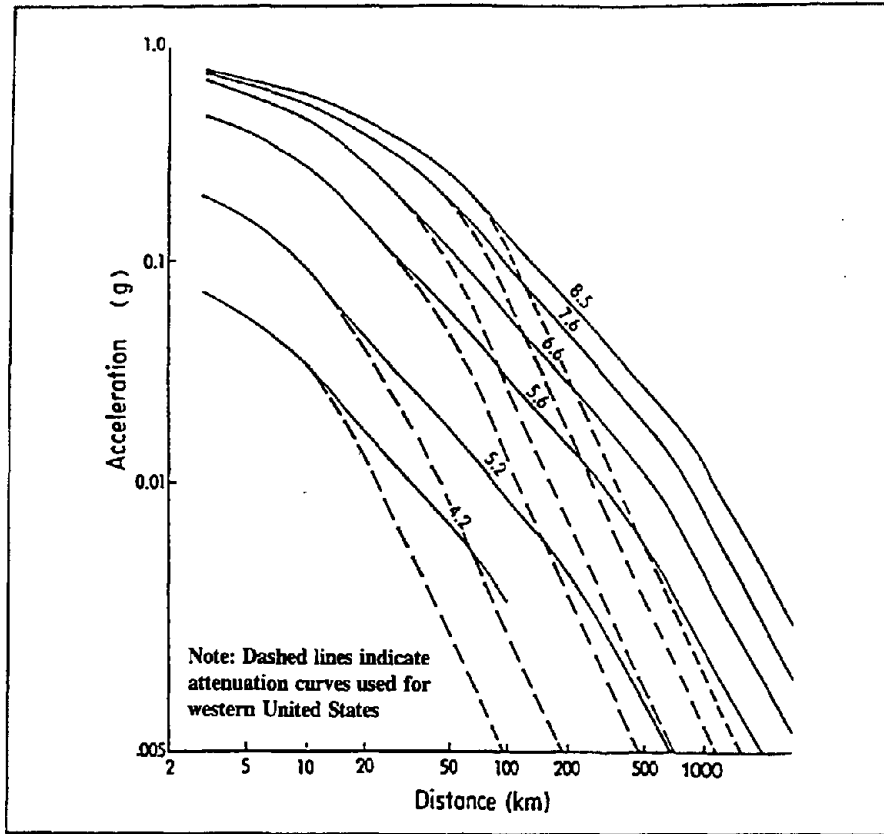


Figure 4-2: Comparison of Attenuation Relationship for Eastern and Central United States to Attenuation Relationship for Western United States.

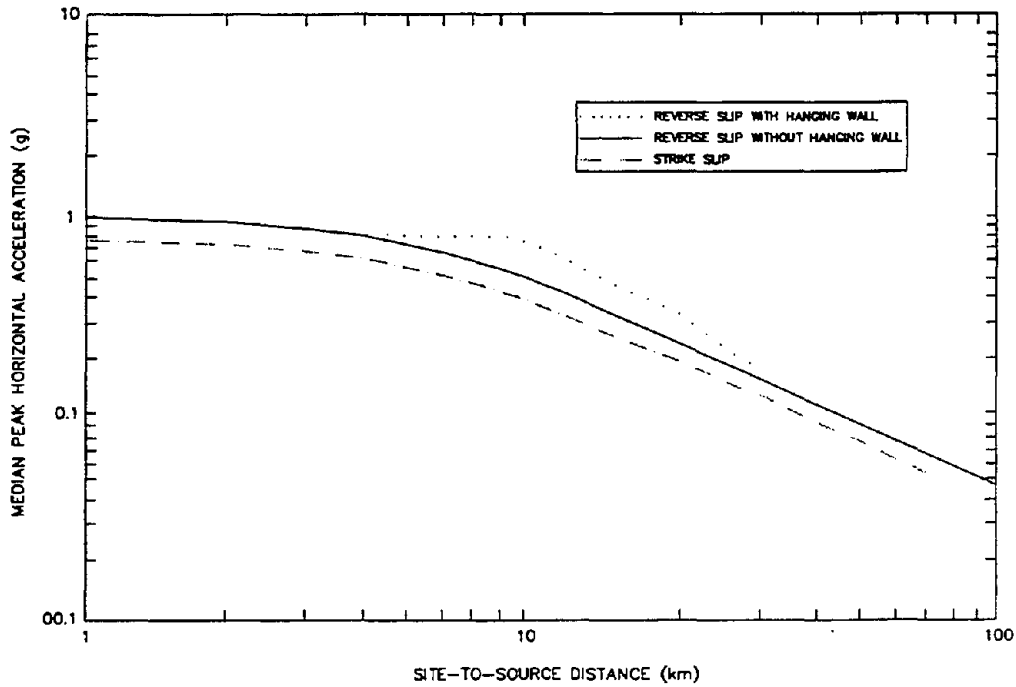


Figure 4-3: Abrahamson and Silva (1997) Attenuation Relationship

and the local ground conditions to which it applies. Frequently, several different attenuation relationships may be found to be equally appropriate. In such a case, the geometric mean (i.e., $\ln X_{\text{mean}} = (\Sigma \ln X_i)/n$) of the values calculated using all of the appropriate attenuation relationships is commonly employed in practice. By using the geometric mean of the values calculated by multiple relationships, bias inherent to individual relationships is minimized. However, when this approach is used, the multiple attenuation relationships *should not* include two generations of an attenuation relationship from the same investigator (e.g., Campbell, 1989 and Campbell and Bozorgnia, 1994):

Usually, attenuation relationships for both rock and soil sites will be available for use. Except for soil sites with less than 10 m of soil overlying bedrock and for soft soil sites where the average shear wave velocity over the top 30 m is less than 120 m/s, soil-site attenuation relationships may be used directly to characterize ground motions at a soil site. However, due to the variability in conditions at soil sites and the resulting uncertainty in soil site response, engineers often prefer to use a rock site attenuation relationship to characterize the design earthquake motions at a *hypothetical bedrock outcrop* at the geometric center of the project site and then conduct a site response analysis to evaluate the influence of local soil conditions on the earthquake motions at the site. The hypothetical bedrock outcrop concept is congruent with both the *free-field* (i.e., not affected by structure and/or topography) criterion used to develop the attenuation relationships and with the concepts used to specify motions for input to computer programs for seismic site response analyses (rock outcrop and transmitting boundary models, see Sections 6.4 and 6.5).

4.2.4 Selection of Attenuation Relationship Input Parameters

When using an attenuation relationship, it is important to use the magnitude scale consistent with the scale used to develop the attenuation relationship. In the eastern and central United States, the magnitude measure generally used in practice is body wave magnitude, m_b . In California, moment magnitude, M_w , local (Richter) magnitude, M_L , or surface wave magnitude, M_s , are used. The differences in these scales are due to the type of earthquake waves being measured, the type of instrument used to measure them, and local scaling factors. The relationship between these magnitude scales is shown on Figure 2-5.

Consistency with the site-to-source distance measure used in developing the attenuation relationship is also important, especially for near-field earthquakes. In the early days of development of attenuation relationships, the epicentral distance was often used because it was generally the most reliable distance measure (seismographs were too sparsely located to adequately constrain the focal depth). As seismographs became more numerous and portable arrays were deployed to measure aftershock patterns that roughly delineate the rupture zone, the focal depth and extent of the rupture surface were able to be better located. Statistical analyses indicate that measures of distance from the recording site to the rupture surface provide a more robust measure of seismic wave attenuation than epicentral distance. Therefore, most current attenuation relationships for the western United States use some measure of the distance to the rupture zone. In the eastern and central United States, hypocentral and epicentral distance measures are still commonly used due to the sparsity of strong-motion recordings from significant earthquakes.

4.2.5 Distribution of Output Ground Motion Parameter Values

All of the attenuation relationships commonly used in practice assume that the output ground motion parameter values are log-normally distributed (i.e., the logarithm of the parameter value is normally distributed). Most of the traditional attenuation relationships used in practice characterize the distribution of the output parameter values with a single, constant value for the log normal standard deviation, independent of earthquake magnitude. In these traditional relationships, the mean plus one standard

deviation peak acceleration values are typically about 1.5 times the corresponding mean values. Recently, Sadigh, *et al.* (1993), Idriss (1993), and Campbell and Bozorgnia (1994) have developed magnitude dependent values for the standard deviation, with smaller standard deviations for larger magnitudes.

4.3 FREQUENCY CONTENT

The importance of the frequency content of the earthquake ground motions with respect to the damage potential of the motions has been demonstrated repeatedly by damage surveys following earthquakes. Such damage surveys show strong correlations between damage to engineered structures, the natural period of the damaged structure, and the predominant frequency of the ground motion to which the structure was subjected. The frequency content of earthquake ground motions is generally characterized by the shape of the acceleration response spectrum. Velocity and displacement response spectra are also used in practice to characterize the frequency content of ground motions.

The same statistical analyses used to develop peak ground motion attenuation equations for the western United States have been used to develop attenuation relationships for spectral values. Joyner and Boore (1988), Geomatrix (1991), Campbell (1993), and Idriss (1993) present the coefficients for spectral acceleration attenuation for spectral periods of up to 7.5 seconds. These coefficients can be used to generate smoothed response spectra that illustrate the influence of magnitude and distance on the frequency content of strong ground motions.

Figure 4-4 compares smoothed acceleration response spectra for a rock site from Campbell (1993) for magnitude 5.5, 6.5, and 7.5 events at a distance of 15 km. For comparison purposes, these spectra are all normalized to a zero period (peak ground) acceleration value of 1.0. This figure clearly illustrates the increased damage potential of larger magnitude earthquakes. The larger magnitude events have larger peak spectral accelerations and larger spectral accelerations in the long period range where ground motions are often most damaging, even though all three spectra are scaled to the same peak acceleration value.

Figure 4-5 compares smoothed acceleration response spectra from three different investigators (Campbell, 1993; Sadigh, *et al.*, 1993; and Boore, *et al.*, 1993) for a rock site for a magnitude 6.5 event at a distance of 15 km. This figure illustrates the differences among attenuation relationships developed by different investigators using essentially the same data base. These differences are primarily due to the weighting scheme used in statistical analysis and the screening criteria used by each investigator in culling records from the common data base of world-wide strong motion records available for the analysis and theoretical assumptions on the shape of the attenuation relationship in the near field (whether or not it "saturates" (plateaus) at low distances) and the rate of decay of ground motion in the far field. The decision on which attenuation to use is a subjective one that is generally based on a comparison between the data base and assumptions used to develop the attenuation relationship and the problem at hand. Alternatively, the arithmetic average or geometric mean of multiple attenuation relationships may be used.

The smoothed acceleration response spectra illustrated in Figures 4-4 and 4-5 are important tools for selection of appropriate time histories for geotechnical analysis. When selecting or synthesizing ground motion time histories for use in engineering analysis, the smoothed spectra are used as a guide to the appropriateness of the time history frequency content. As illustrated in Figure 4-6, a suite of time histories for use in engineering analysis is selected such that the suite as a group conforms to the smoothed spectra, though no single time history is expected to conform to the spectra.

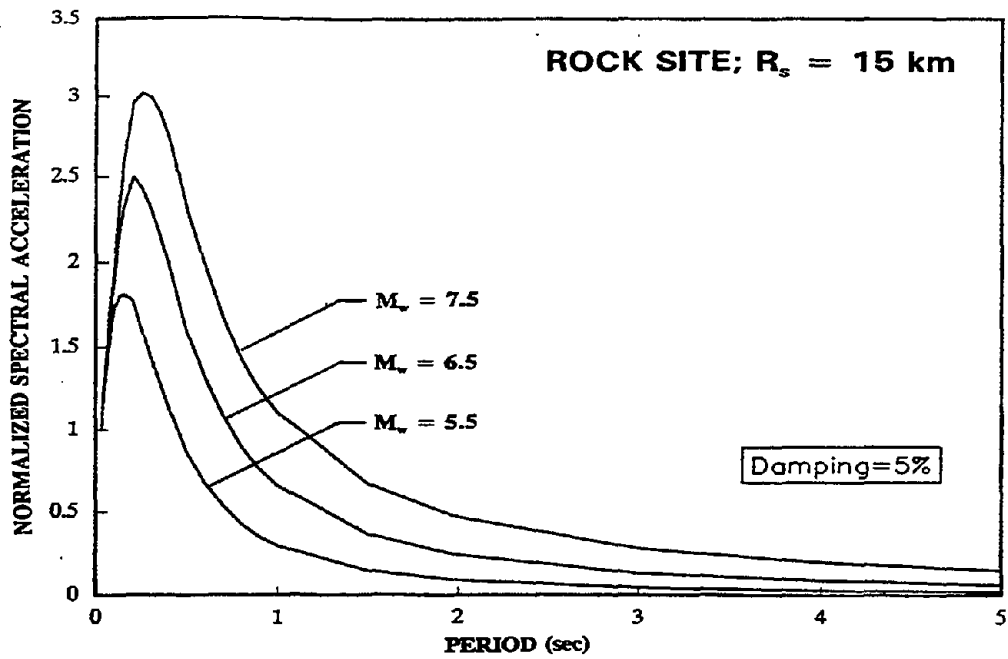


Figure 4-4: Comparison of Smoothed Acceleration Response Spectra for Various Earthquake Magnitudes. (Campbell, 1993 Attenuation Relationship)

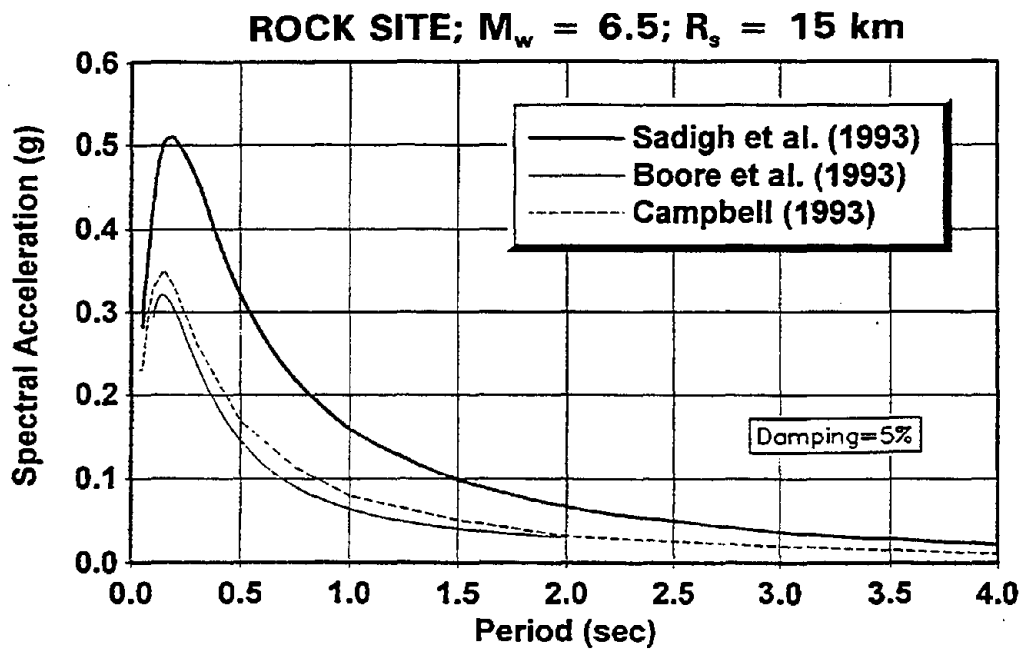


Figure 4-5: Comparison of Smoothed Acceleration Response Spectra by Various Investigators.

**OII LANDFILL
MONTEREY PARK, CALIFORNIA**

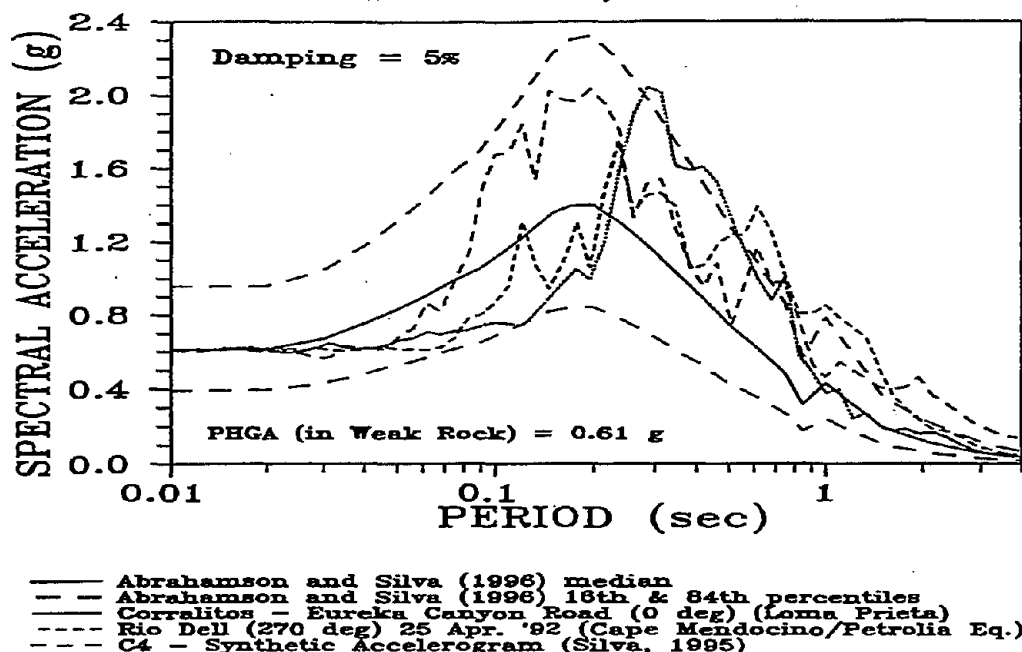


Figure 4-6: Real Spectra vs. Smoothed Spectra

4.4 ENERGY CONTENT

The *energy content* of the acceleration time history provides another means of characterizing strong ground motions. The energy content of the motion is proportional to the square of the acceleration. In engineering practice, the energy content of the motion is typically expressed in terms of either the *root-mean-square* (RMS) and duration of the acceleration time history or the *Arias intensity*, I_A . The RMS of the acceleration time history is the square root of the square of the acceleration integrated over the duration of the motion and divided by the duration:

$$RMSA = \sqrt{\frac{1}{t_r} \int_{t_{r0}}^{t_r} [a(t)]^2 dt} \quad (4-1)$$

where RMSA is the RMS of the acceleration time history, $a(t)$ is the acceleration time history, and t_r is the duration of strong ground shaking. The RMSA represents an average acceleration for the time history over the duration of strong shaking. The square of the RMSA multiplied by the duration of the motion is directly proportional to the energy content of the motion.

The value of the RMSA depends upon the definition of the duration of the motion. For instance, if the duration of the motion is defined such that it extends into the quiet period beyond the end of strong shaking, the RMSA value will be "diluted" by the quiet period at the end of the record. However, as the energy content of the motion is unchanged, the product of the RMSA and duration will remain constant. As the RMSA is not used as frequently as peak ground acceleration in engineering practice, RMSA attenuation relationships are not developed or revised as frequently as peak acceleration attenuation relationships. Figure 4-7 presents an attenuation relationship for RMSA at rock sites in the western United States developed by Kavazanjian, *et al.* (1985a) using the significant duration (Trifunac and Brady, 1975) defined in the next Section of this Chapter.

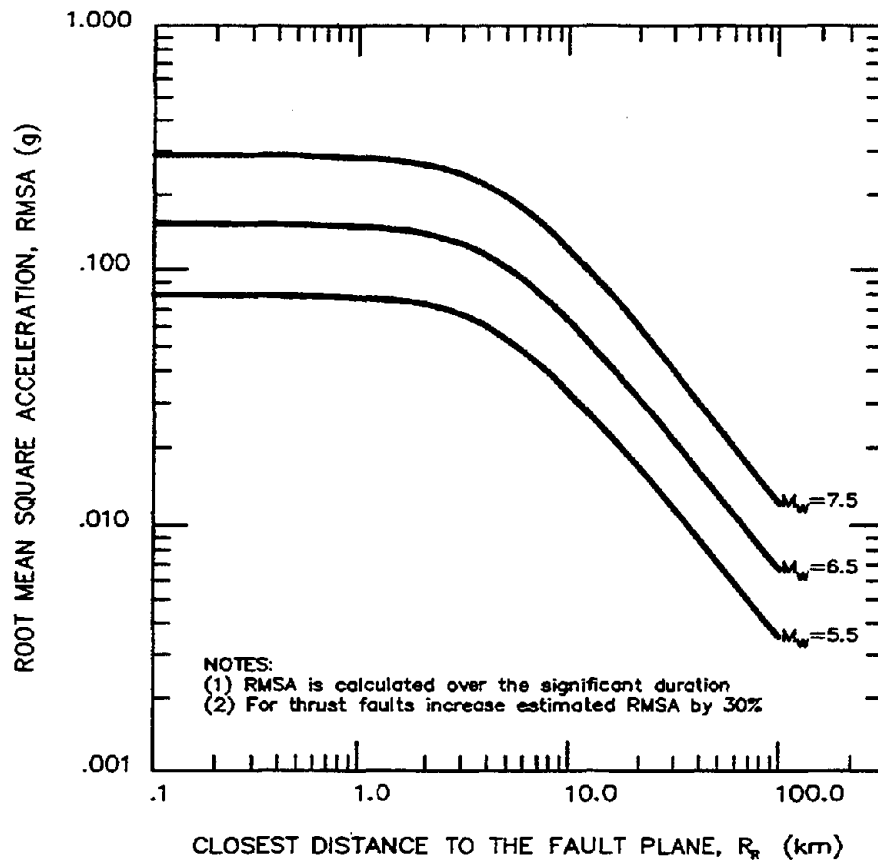


Figure 4-7: Attenuation of the Root Mean Square Acceleration. (Kavazanjian, *et al.*, 1985a, reprinted by permission of ASCE)

The *Arias intensity*, I_A , is proportional to the square of the acceleration integrated over the entire acceleration time history, $a(t)$:

$$I_A = \frac{\pi}{2g} \int_0^{t_f} [a(t)]^2 dt \quad (4-2)$$

where g is the acceleration of gravity and t_f is the duration of strong shaking. Arias (1969) showed that this integral is a measure of the total energy of the accelerogram. Arias intensity may be related to the RMSA as follows:

$$I_A = \frac{\pi}{2g} (\text{RMSA})^2 \cdot t_f \quad (4-3)$$

Figure 4-8 presents the attenuation relationship developed by Kayen and Mitchell (1997) for Arias intensity.

The specification of the duration of strong shaking for an acceleration time history can be somewhat arbitrary, as relatively low intensity motions may persist for a long time towards the end of the record. If the defined duration of strong motion is increased to include such low intensity motions, the Arias

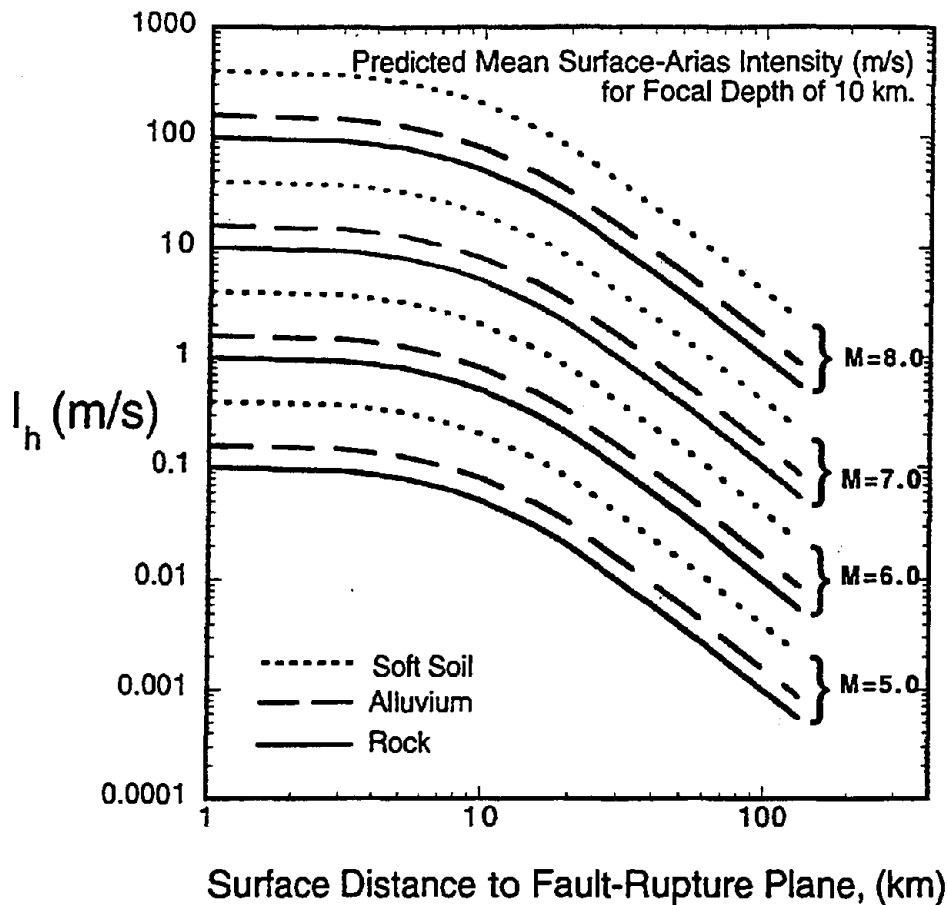


Figure 4-8: Arias Intensity Attenuation Relationship (Kayen and Mitchell, 1997)

intensity will remain essentially constant but the RMSA will decrease (as discussed above). Therefore, some investigators prefer Arias intensity to RMSA as a measure of energy content because the Arias intensity of a strong motion record is a more definite, essentially fixed value while the RMSA depends upon the definition of the duration of strong ground motion. A definition that results in a longer duration will result in a lower RMSA, but I_A will remain essentially unchanged.

Husid (1969) proposed plotting the evolution of the Arias intensity for an accelerogram versus time to study the evolution of energy release for the strong motion record. Figure 4-9 presents the acceleration time history recorded at Aloha Avenue in Saratoga during the 1989 M_w 6.9 Loma Prieta earthquake and the corresponding Husid plot.

Arias intensity and/or RMSA and duration are useful parameters in selecting time histories for geotechnical analysis. This is particularly true if a *seismic deformation analysis* is to be performed, as the deformation potential of a strong motion record is directly proportional to the energy content, which can be expressed as a function of either Arias intensity or the product of the RMSA and duration of the record.

4.5 DURATION

The duration of shaking is important to the response of a soil deposit and/or overlying structures if the materials are susceptible to cyclic pore pressure generation, loss of strength or stiffness during cyclic

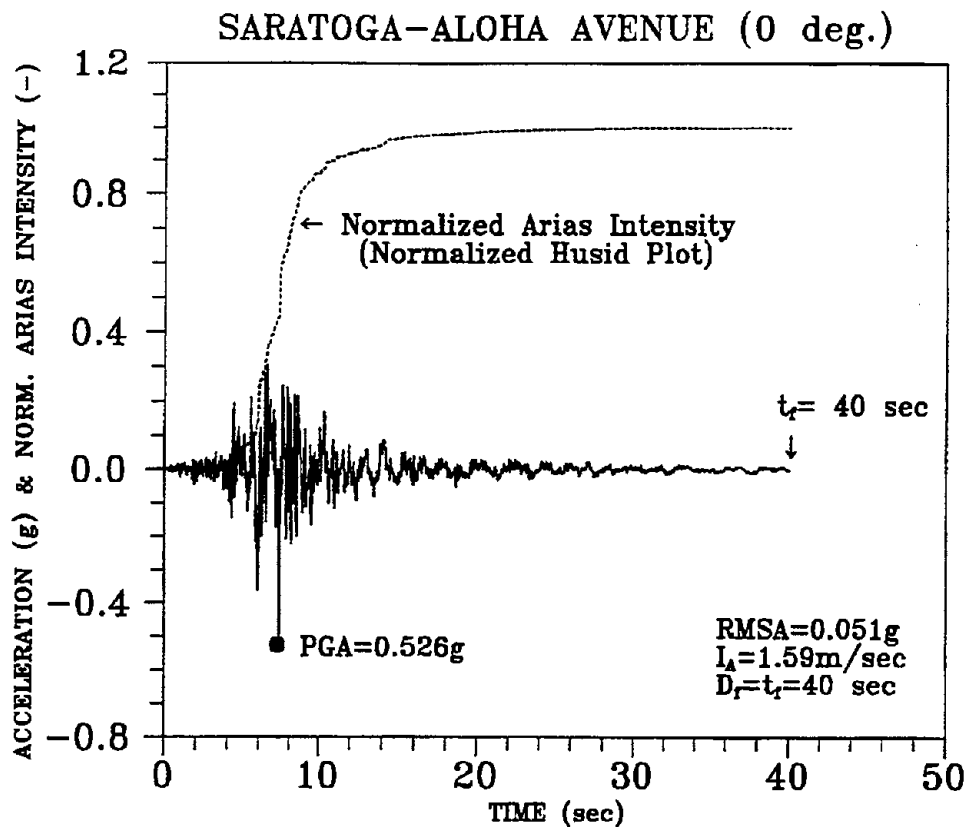


Figure 4-9: Accelerogram Recorded During the 1989 Loma Prieta Earthquake.

loading, or other forms of cumulative damage (e.g., permanent seismic deformation). Duration is often neglected or treated indirectly in evaluating the dynamic response of structures, but is usually implicitly (based upon magnitude) or explicitly accounted for in liquefaction and seismic deformation analyses.

The *bracketed duration of strong motion*, D_b , defined by Bolt (1973) as the elapsed time between the first and last acceleration excursion greater than a specified threshold level, is the definition most often found in strong motion catalogs. Figure 4-10 illustrates calculation of bracketed duration for Saratoga - Aloha Avenue accelerogram and a threshold acceleration of 0.05 g.

For problems dealing with cumulative damage during an earthquake, many engineers find the definition of *significant duration*, D_s , proposed by Trifunac and Brady (1975) to be the most appropriate duration definition. Trifunac and Brady (1975) defined the significant duration as the time interval between 5 and 95 percent of the total Arias intensity on a Husid plot. The Trifunac and Brady definition of duration is illustrated on the Husid plot in Figure 4-11.

The most recent study of significant duration available in the technical literature is by Dobry, *et al.* (1978). These investigators plotted significant duration versus earthquake magnitude for events less than and greater than 25 km from the source. Based upon the summary plot shown on Figure 4-12, these investigators suggested the following design equation for the significant duration at rock sites:

$$D_s = 10^{(0.432M_w - 1.83)} \quad (4-4)$$

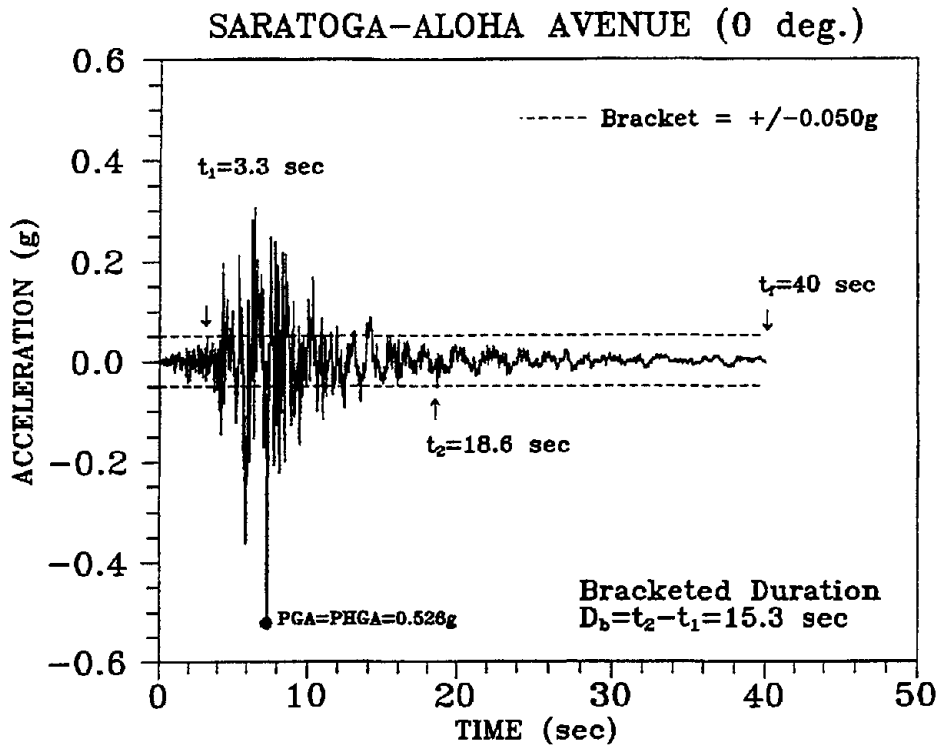


Figure 4-10: Bolt (1973) Duration of Strong Shaking.

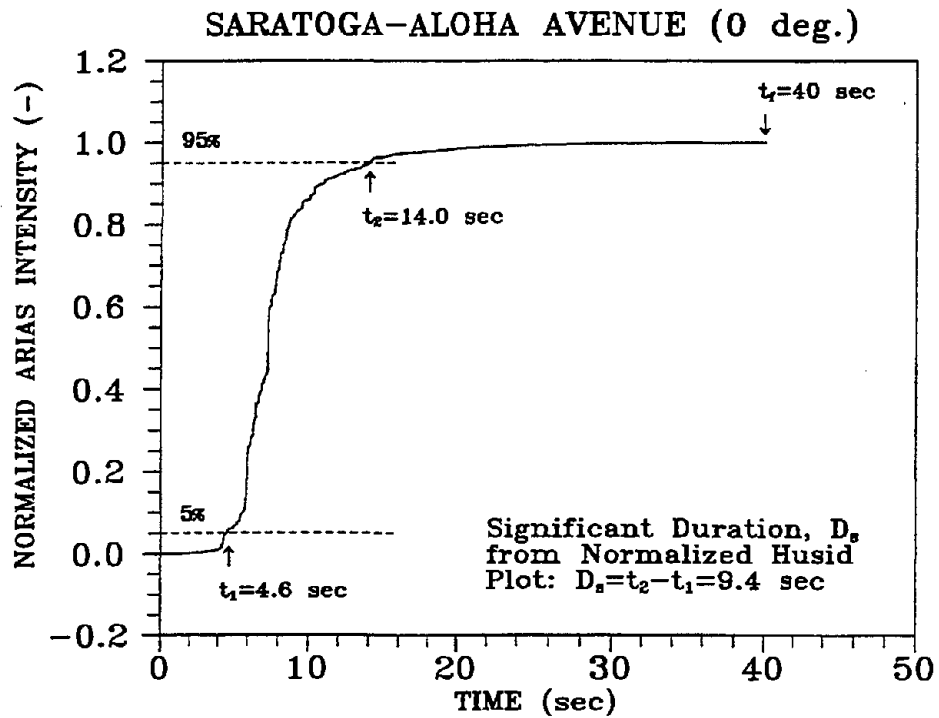


Figure 4-11: Trifunac and Brady (1975) Duration of Strong Shaking.

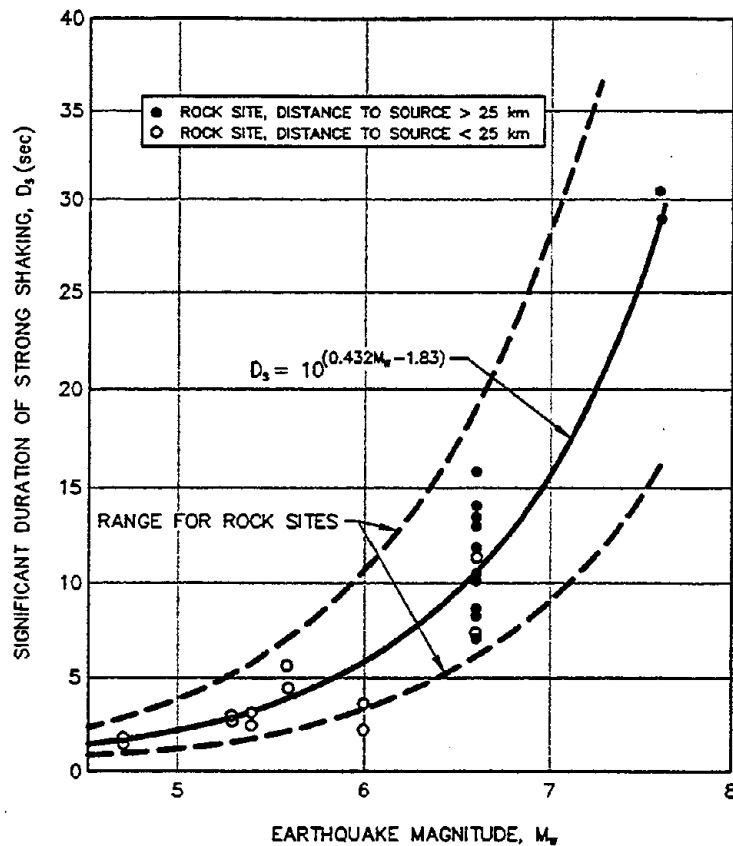


Figure 4-12: Duration Versus Earthquake Magnitude for the Western United States. (Dobry, *et al.*, 1978, reprinted by permission of SSA)

where D_s is the significant duration as defined by Trifunac and Brady (1975) and M_w is the moment magnitude of the design earthquake.

For problems related to soil liquefaction, duration is commonly expressed in terms of the *number of equivalent uniform cycles* (e.g., see Seed, *et al.*, 1975). The number of equivalent uniform cycles is typically expressed as a function of earthquake magnitude to reflect the general increase in duration with increasing magnitude. Recommendations for the number of equivalent uniform cycles as a function of earthquake magnitude for use in liquefaction and seismic settlement analyses are presented in Chapter 8.

4.6 INFLUENCE OF LOCAL SITE CONDITIONS

4.6.1 Local Site Effects

Qualitative reports of the influence of local soil conditions on the intensity of shaking and on the damage induced by earthquake ground motions date back to at least the 1906 San Francisco earthquake (Wood, 1908). Reports of localization of areas of major damage within the same city and of preferential damage to buildings of a certain height within the same local area from the Mexico City earthquake of 1957, the Skopje, Macedonia earthquake of 1963, and the Caracas, Venezuela earthquake of 1967 focused the attention of the engineering community on the influence of local soil conditions on the damage potential of earthquake ground motions.

Back-analysis by Seed (1975) of accelerograms from the moment magnitude M_w 5.3 Daly City (San Francisco) earthquake of 22 March 1957, presented in Figure 4-13, demonstrate the influence of local soil conditions on site response. Figure 4-13 shows peak acceleration, acceleration response spectra, and soil

stratigraphy data at six San Francisco sites approximately the same distance from the source of the 1957 earthquake. The peak acceleration and frequency content of the ground motion recorded at these six sites were dependent on the soil profile beneath each specific site.

At the sites shown in Figure 4-13, the local soil deposits attenuated the peak ground acceleration by a factor of approximately two compared to the bedrock sites. However, the acceleration response spectra for the soil sites clearly show amplification of spectral accelerations at longer periods (periods greater than 0.25 sec) compared to the rock sites. If the bedrock motions had larger spectral accelerations at the longer periods, a characteristic of larger magnitude events and of events from a more distant source, or if the natural period of the local soil deposits more closely matched the predominant period of the bedrock motions, amplification of the peak acceleration could have occurred at the soil sites.

The influence of local ground conditions can also be illustrated using the smoothed acceleration response spectra discussed in Section 4.3. Figure 4-14 presents smoothed acceleration response spectra calculated using the Campbell and Bozorgnia (1994) attenuation relationship for a magnitude 8 event at a distance of 5 km for both soil and rock sites. This figure clearly indicates the tendency for soil site motions to contain a larger proportion of their energy content at longer periods than rock site motions.

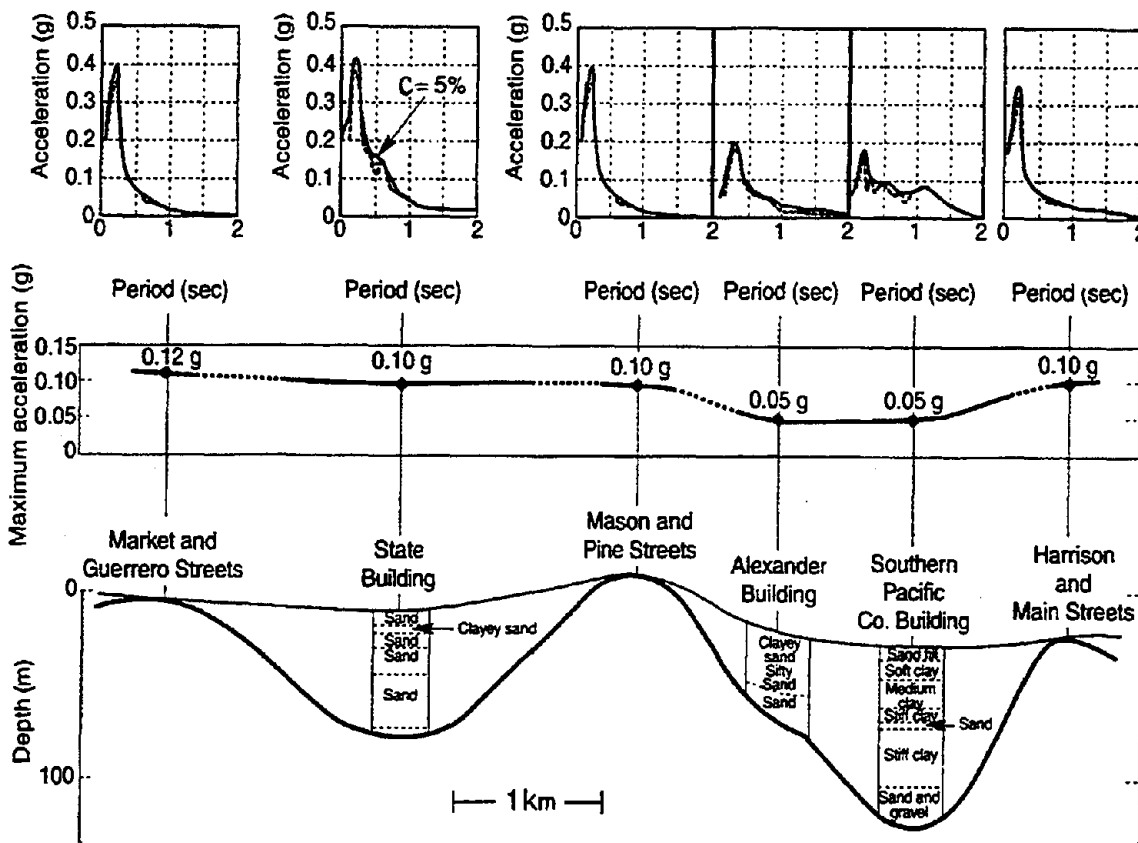


Figure 4-13: Soil Conditions and Characteristics of Recorded Ground Motions, Daly City (San Francisco) M_w 5.3 Earthquake of 1957. (Seed, 1975, reprinted by permission of Chapman and Hall)

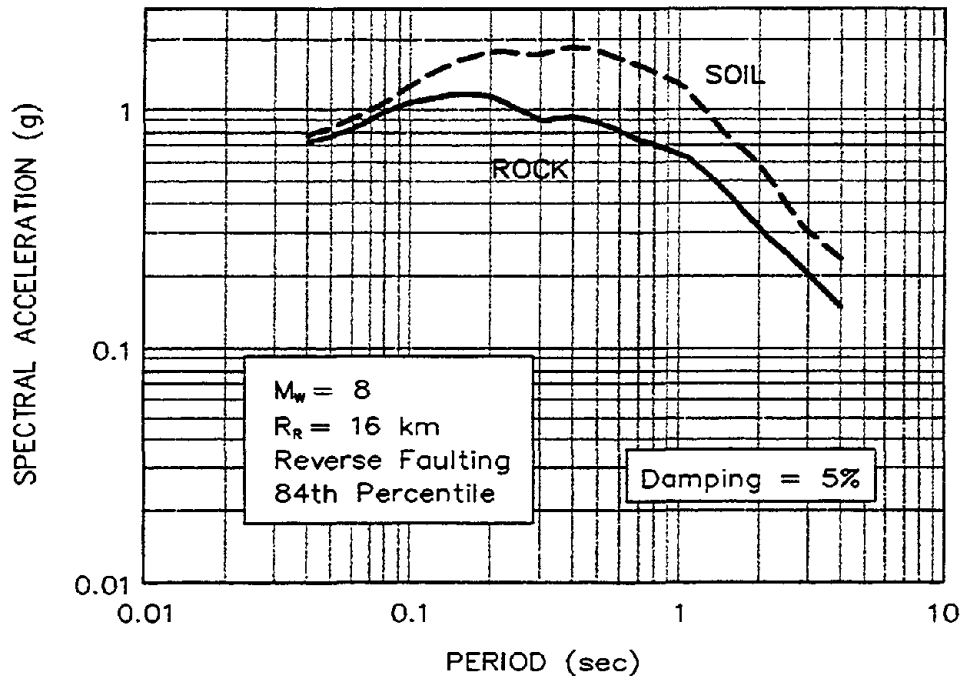


Figure 4-14: Comparison of Soil and Rock Site Acceleration Response Spectra for M_w 8 Event at 5 km. (Campbell and Bozorgnia, 1994, reprinted by permission of EERI)

The Richter Magnitude 8.0 Mexico City earthquake of 1985 provided dramatic evidence of the influence of local soil conditions on earthquake ground motions with respect to both peak ground acceleration and spectral acceleration. Figure 4-15 compares the peak ground acceleration measured at three soft soil sites in Mexico City to the peak acceleration values calculated from a conventional attenuation relationship at the mean plus one standard deviation level. As the figure shows, the peak ground accelerations at the three soft soil sites were significantly greater than the calculated mean plus one standard deviation acceleration values. The peak ground acceleration at one of these sites approached 0.2 g as compared to the mean plus one standard deviation value of 0.08 g for this earthquake, which occurred at a distance of 400 km from Mexico City. Figure 4-16 shows the effect of the local soil conditions at two of these three sites on spectral accelerations. The acceleration response spectra for the two soft clay sites show spectral amplification factors of up to 6 (i.e., a ratio of spectral acceleration to peak ground acceleration of up to 6) at the resonant site period.

4.6.2 Codes and Standards

The influence of local soil conditions on spectral shape may be illustrated using design spectra developed for building codes. For example, the 1994 version of the Uniform Building Code (UBC, 1994), defined three classes of site conditions when defining the shape of the normalized smoothed response spectra for structural design. These three classes of site conditions are rock (Type I), deep, cohesionless or stiff clay soil (Type II), and soft to medium stiff clays and sands (Type III). The smoothed normalized response spectra corresponding to these three site conditions, presented in Figure 4-17, again illustrate the increase in spectral acceleration at long periods for soil site motions compared to rock site motions.

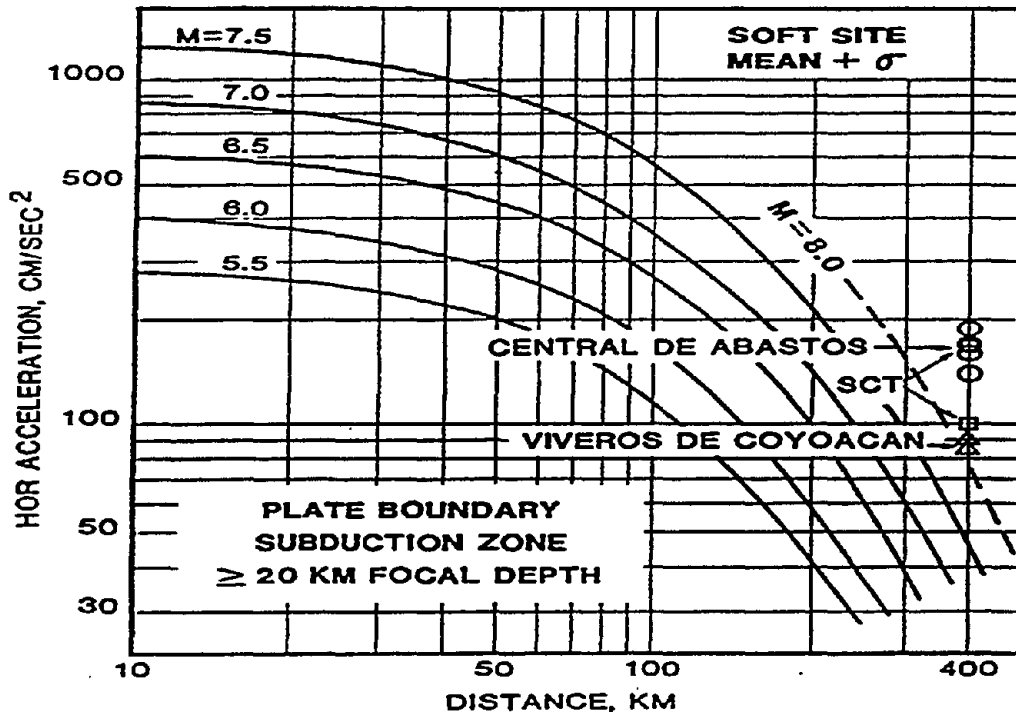


Figure 4-15: PGA Attenuation in 1985 Mexico City Earthquake (Krinitzky, 1986)

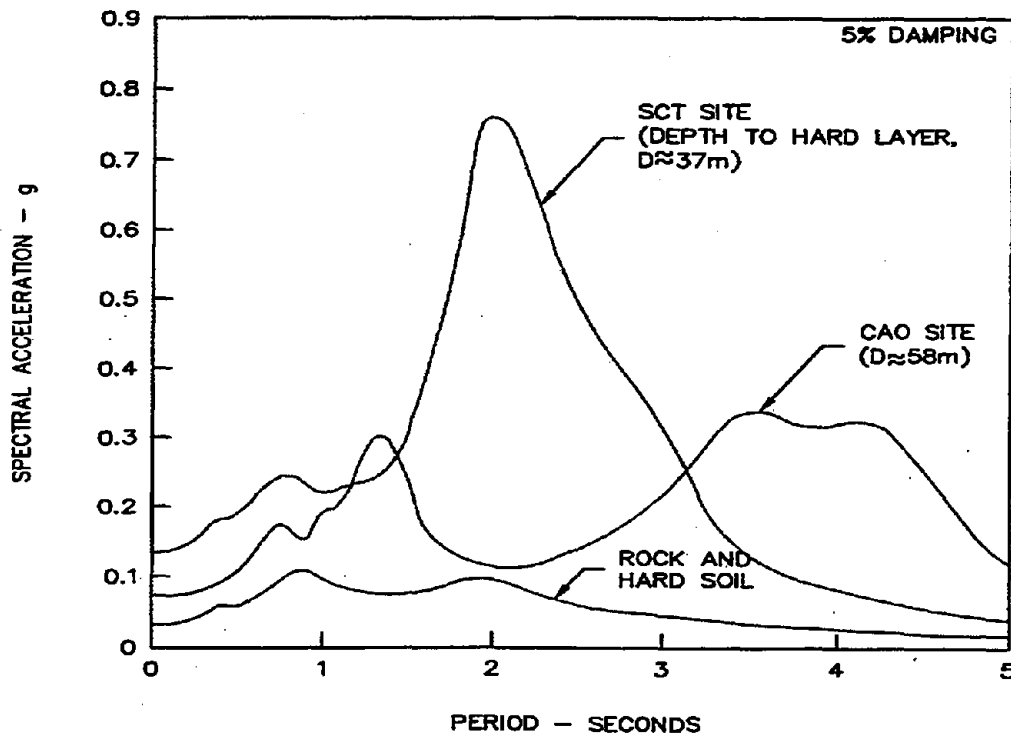


Figure 4-16: Spectral Amplification in 1985 Mexico City Earthquake (Romo and Seed, 1986)

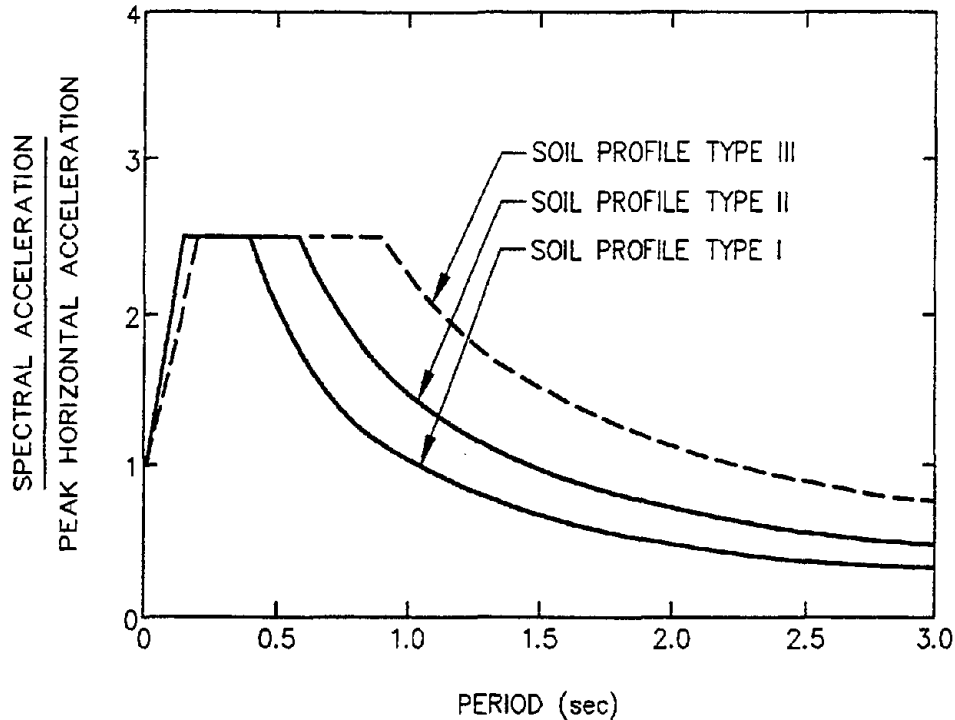


Figure 4-17: Normalized 1994 Uniform Building Code Response Spectra. (UBC, 1994, reproduced from the Uniform Building Code™, copyright© 1994, with the permission of the publisher, the International Conference of Building Officials)

The 1997 version of the UBC has six classes of site conditions and incorporates the effects of near-field ground motion. The six classes of site conditions incorporated in the 1997 UBC, designated S_A through S_F , are defined in Table 4-3 on the basis of the average shear wave velocity in the top 30 meters and other relevant geotechnical characteristics. The acceleration response spectra for classes S_A through S_E are based on Figure 4-18. For site class S_F , a site specific analysis is required to develop the response spectrum. The value of C_a , the spectral acceleration at zero period for the UBC spectra, is equal to the peak ground acceleration with a 10 percent probability of not being exceeded in 50 years. For site classes S_A through S_E , C_a may be taken from Table 4-4 in combination with the use of Figure 3-4 (to determine the Seismic Zone Factor, Z). For site class S_F , a site-specific analysis is required to evaluate C_a . The value of C_v for developing the UBC spectra described by Figure 4-18 is a function of the site class and UBC seismic zone factor (Figure 3-4 and Table 4-5).

For sites close to active faults (i.e. sites in zone 4), the Near Source Factors defined by Tables 4-6 through 4-8 should be applied to C_a and C_v . Vertical spectral accelerations are generally assumed equal to 2/3 of the horizontal spectral accelerations. However, for cases where a Near Source Factor greater than 1.0 is applied to the horizontal spectra, the UBC requires a site-specific analysis to develop the vertical response spectra.

While building code response spectra are useful to illustrate the effect of local soil conditions on ground response, these spectra represent effective spectral accelerations for use in structural design and are not intended to represent smoothed spectra from actual earthquakes. To represent an actual earthquake

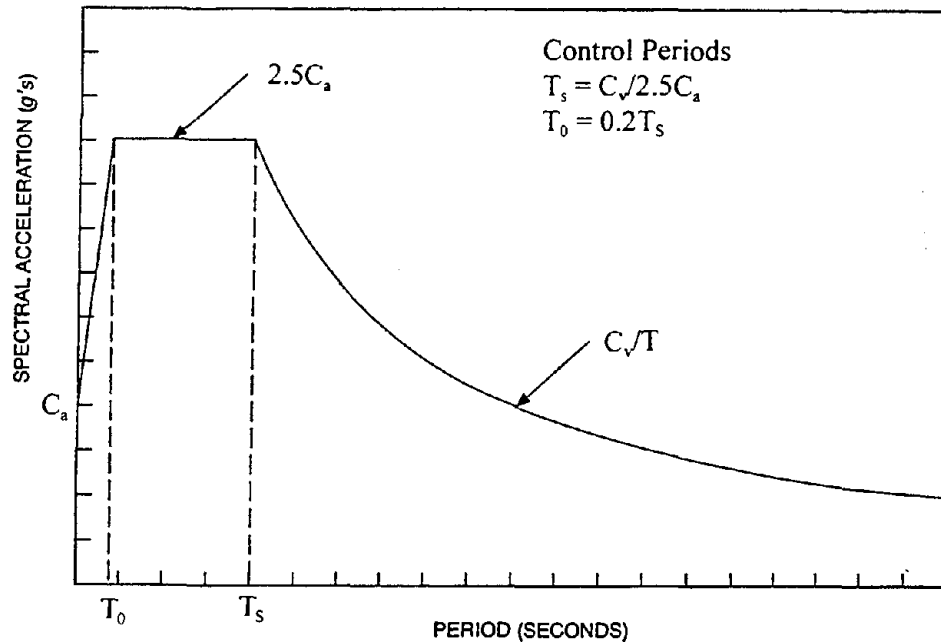


Figure 4-18: 1997 Uniform Building Code Design Response Spectra (UBC, 1997, reproduced from the Uniform Building Code™, copyright© 1997, with the permission of the publisher, the International Conference of Building Officials)

TABLE 4-3
1997 UBC SITE CLASSIFICATION

Designation	Site Class	Shear Wave Velocity ¹	Other Characteristics ²
S _A	Hard Rock	> 1500 m/s	
S _B	Rock	760 m/s to 1500 m/s	
S _C	Very Dense Soil and Soft Rock	360 m/s to 760 m/s	N > 50, S _u > 100 kPa
S _D	Stiff Soil	180 m/s to 360 m/s	15 < N < 50 50 kPa < S _u < 100 kPa
S _E	Soft Soil	Less than 180 m/s	More than 3m of soil with PI > 20, W _n > 40%, and S _u < 25 kPa
S _F	Special Soils		Collapsible, liquefiable, sensitive soils; More than 3m of peat or highly organic; More than 7.5m of clay with PI > 75; More than 36m of soft to medium clay.

- Notes: 1. Average shear wave velocity for upper 30m.
 2. N = standard Penetration Test Blow Count
 S_u = Undrained Shear Strength
 PI = Plasticity Index
 W_n = Moisture content

**TABLE 4-4
SEISMIC COEFFICIENT C_s**

Soil Profile Type	Seismic Zone Factor, Z				
	$Z = 0.075$	$Z = 0.15$	$Z = 0.2$	$Z = 0.3$	$Z = 0.4$
S_A	0.06	0.12	0.16	0.24	$0.32N_s$
S_B	0.08	0.15	0.20	0.30	$0.40N_s$
S_C	0.09	0.18	0.24	0.33	$0.40N_s$
S_D	0.12	0.22	0.28	0.36	$0.44N_s$
S_E	0.19	0.30	0.34	0.36	$0.36N_s$
S_F	See Footnote 1				

Notes: ¹ Site-specific geotechnical investigation and dynamic site response analysis shall be performed to determine seismic coefficients for Soil Profile Type S_F .

**TABLE 4-5
SEISMIC COEFFICIENT C_v**

Soil Profile Type	Seismic Zone Factor, Z				
	$Z = 0.075$	$Z = 0.15$	$Z = 0.2$	$Z = 0.3$	$Z = 0.4$
S_A	0.06	0.12	0.16	0.24	$0.32N_v$
S_B	0.08	0.15	0.20	0.30	$0.40N_v$
S_C	0.13	0.25	0.32	0.45	$0.56N_v$
S_D	0.18	0.32	0.40	0.54	$0.64N_v$
S_E	0.26	0.50	0.64	0.84	$0.96N_v$
S_F	See Footnote 1				

Notes: ¹ Site-specific geotechnical investigation and dynamic site response analysis shall be performed to determine seismic coefficients for Soil Profile Type S_F .

**TABLE 4-6
SEISMIC SOURCE TYPE¹**

Seismic Source Type	Seismic Source Description	Seismic Source Definition ²	
		Max. Moment Magnitude, M	Slip Rate, SR (mm/yr)
A	Faults that are capable of producing large magnitude events and that have a high rate of seismic activity	$M \geq 7.0$	$SR \geq 5$
B	All faults other than types A and C	$M \geq 7.0$ $M < 7.0$ $M \geq 6.5$	$SR < 5$ $SR > 2$ $SR < 2$
C	Faults that are not capable of producing large magnitude earthquakes and that have a relatively low rate of seismic activity	$M < 6.5$	$SR \leq 2$

Notes: ¹ Subduction sources shall be evaluated on a site-specific basis.

² Both maximum moment magnitude and slip rate conditions must be satisfied concurrently when determining the seismic source type.

**TABLE 4-7
NEAR-SOURCE FACTOR N_a ¹**

Seismic Source Type	Closest Distance to Known Seismic Source ^{2,3}		
	≤ 2 km	5 km	≥ 10 km
A	1.5	1.2	1.0
B	1.3	1.0	1.0
C	1.0	1.0	1.0

Notes: ¹ The Near-Source Factor may be based on the linear interpolation of values for distances other than those show in the table.
² The location and type of seismic sources to be used for design shall be established based on approved geotechnical data.
³ The closest distance to seismic source shall be taken as the minimum distance between the site and the area described by the vertical projection of the source on the surface. The surface projection need not include portions of the source depths of 10 km or greater. The largest value of the Near-Source Factor considering all sources shall be used for design.

**TABLE 4-8
NEAR-SOURCE FACTOR N_v ¹**

Seismic Source Type	Closest Distance to Known Seismic Source ^{2,3}			
	≤ 2 km	5 km	10 km	≥ 15 km
A	2.0	1.6	1.2	1.0
B	1.6	1.2	1.0	1.0
C	1.0	1.0	1.0	1.0

Notes: ¹ The Near-Source Factor may be based on the linear interpolation of values for distances other than those show in the table.
² The location and type of seismic sources to be used for design shall be established based on approved geotechnical data.
³ The closest distance to seismic source shall be taken as the minimum distance between the site and the area described by the vertical projection of the source on the surface. The surface projection need not include portions of the source depths of 10 km or greater. The largest value of the Near-Source Factor considering all sources shall be used for design.

spectrum, the spectrum generated from an attenuation relationship, or the spectrum from seismic site response analysis (see Chapter 6) should be used.

In May 1997, FHWA and the National Center for Earthquake Engineering Research (NCEER) jointly sponsored a workshop on the “National Representation of Seismic Ground Motion for New and Existing Highway Facilities” (Friedland, et. Al, 1997). Among the issues considered at the workshop were:

- Should the USGS maps and UBC code provisions be used for highway facilities;
- Should vertical and near-source ground motions be specified for design; and
- Should spatial variations of ground motions be specified for design?

While building code response spectra are useful to illustrate the effect of local soil conditions on ground motion, Workshop participants concluded that, while the 1996 USGS maps provide the basis for a national portrayal of seismic hazard for highway facilities, design of highway facilities to prevent collapse should consider design ground motions at probabilities lower than 10 percent probability of exceedence in 50 years that is currently in AASHTO and the UBC. The workshop participants recommended to develop seismic hazard maps for highway facilities similar to the 1997 National Earthquake Hazard Reduction Program (NEHRP) provisions for collapse- prevention design of building, wherein the USGS maps for 2% probability of exceedence in 50 years truncated by deterministic peak values in areas of high seismicity was recommended.

Workshop participants concluded that the 1997 UBC spectra, with separate sets of short and long period factors dependant on the intensity of ground shaking, with increased amplification for low levels of shaking, and 1/T decay at long periods, were more appropriate than the current AASHTO provisions for highway facilities design.

Workshop participants also concluded that because the high vertical motions in near-source regions can significantly impact bridge response, vertical ground motions should be specified for certain types of bridges in higher seismic zones. Furthermore, because near-source motions have certain unique characteristics not captured in current UBC or NEHRP spectral shapes, new approaches to specifying near field motions are needed. Workshop participants also recognized that the response of “ordinary” highway bridges is not greatly affected by spatial variations of ground motion, but that spatial variations can be important in some cases and that research is needed to define and address these cases.

4.6.3 Energy and Duration

Local soil conditions can also affect duration and energy content. Energy and durations on soil sites have greater scatter and tend to be longer than durations on rock sites. In fact, the range of energy and durations for rock sites appears to be a lower bound for soil site durations. The FHWA/NCEER workshop participants concluded that energy is a more fundamental parameter, influencing structural response. However, no accepted energy-based design procedures are currently available. For some geotechnical problems, duration may be as important as energy content.

4.6.4 Resonant Site Frequency

Amplification of long period bedrock motions by local soil deposits and constructed dams/embankments and soil retaining systems is now accepted as an important phenomenon that can exert a significant influence on the damage potential of earthquake ground motions. Significant structural damage has been attributed to amplification of both peak acceleration and spectral acceleration by local soil conditions. Amplification of peak acceleration occurs when the resonant frequency of the soil deposits or soil structure is close to the predominant frequencies of the bedrock earthquake motions (the frequencies associated with the peaks of the acceleration response spectra). The *resonant frequency*, f_o , of a horizontal soil layer (deposit) of thickness H can be estimated as a function of the average shear wave velocity of the layer, $(V_s)_{avg}$, using the following equation:

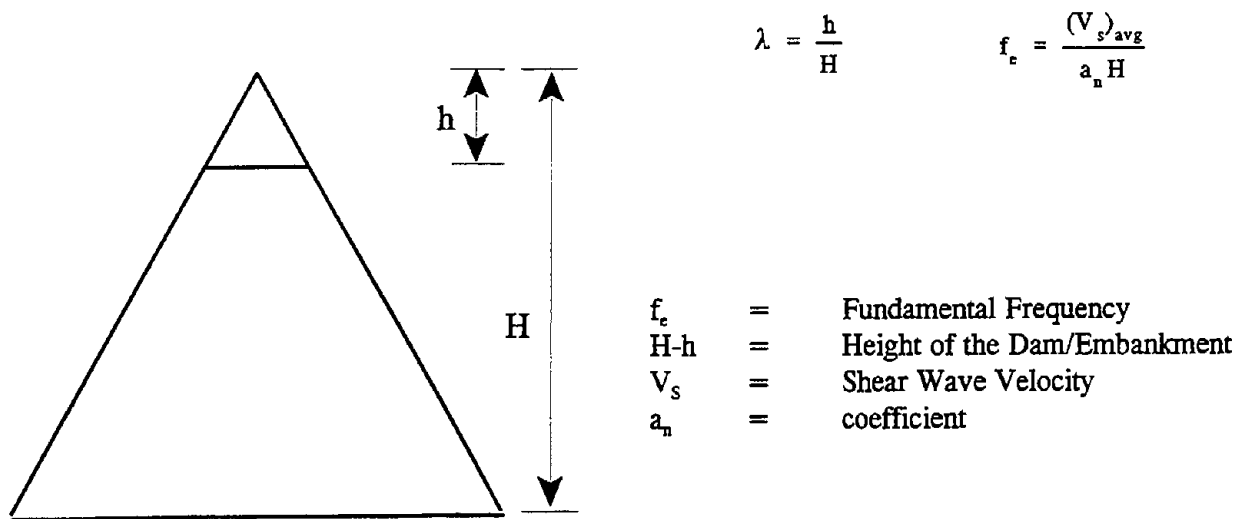
$$f_o = \frac{(V_s)_{avg}}{4H} \quad (4-5)$$

The resonant frequency of a trapezoidal embankment, f_e , can be estimated using a similar equation of the form:

$$f_e = \frac{(V_s)_{avg}}{a_n H} \quad (4-6)$$

where the coefficient a_n varies between 2.4 and 4 as shown in Figure 4-19.

Amplification of the spectral acceleration may occur at soil sites in any earthquake at frequencies around the resonant frequency of the soil deposit. Some of the most significant damage in recent earthquakes



λ	a_n
0.00	2.405
0.03	2.409
0.05	2.416
0.10	2.448
0.15	2.501
0.20	2.574
0.25	2.668
0.30	2.786
0.35	2.930
0.40	3.107
0.45	3.323
0.50	3.588
1.00	4.0

Note: For $0.5 \leq \lambda \leq 1.0$, a_n may be derived by linear interpolation from $a_n = 3.6$ for $\lambda = 0.5$ to $a_n = 4.0$ for $\lambda = 1.0$.

Figure 4-19: Fundamental Frequency of Trapezoidal Dam/Embankment

(e.g., building damage in Mexico City in the 1985 earthquake and damage to freeway structures in the Loma Prieta earthquake of 1989) has occurred in situations where the predominant frequencies of the bedrock motions and the resonant frequencies of both the local soil deposit and the overlying structure all fell within the same range.

4.7 SELECTION OF REPRESENTATIVE TIME HISTORIES

Earthquake time histories may be required for input to both seismic site response analyses (see Chapter 6) and seismic deformation analyses (see Chapter 7). There are several procedures that can be used to select earthquake ground motions at a site. These procedures include:

- selection of motions previously recorded for similar site conditions during a similar earthquake and at distances comparable to those under consideration;
- selection of generic, publicly available synthetic ground motions generated to represent an event of the target magnitude;
- estimation of a *target spectrum* (a spectrum representative of the design magnitude, site-to-source distance, and local geology (soil or rock) using either an attenuation relationship or a code or standard) and then selection of recorded or synthetic time histories whose special ordinates are either comparable to or envelope those of the target spectrum for the period range of interest; or
- use of simulation techniques to generate a project-specific synthetic time history, starting from the source and propagating the appropriate wave forms to the site to generate a suite of time histories that can then be used to represent the earthquake ground motions at the site of interest.

In selecting a representative time history from the catalog of available records, an attempt should be made to match as many of the relevant characteristics of the design earthquake as possible. Important characteristics that should be considered in selecting a time history include:

- earthquake magnitude;
- source mechanism (e.g., strike slip, dip slip, or oblique faulting);
- focal depth;
- site-to-source distance;
- site geology;
- peak ground acceleration;
- frequency content;
- duration; and
- energy content (RMSA or I_A).

The relative importance of these factors varies from case to case. For instance, if a bedrock record is chosen for use in a site response analysis to model the influence of local soil conditions, site geology will not be particularly important in selection of the input bedrock time history. However, if a soil site record is to be scaled to a specified peak ground acceleration, site geology can be a critical factor in selection of an appropriate time history, as the record must already include any potential influence of local soil conditions on the motion. Scaling of the peak acceleration of a strong motion record by a factor of more than two is not recommended, as the frequency characteristics of ground motions can be directly and indirectly related to the amplitude of the motion. Leeds (1992) and Naeim and Anderson (1993) present comprehensive databases of available strong motion records and their characteristics. These strong motion

records can be obtained in digital form (CD-ROM) from the National Geophysical Data Center (NGDC) in Boulder, Colorado. Also, Tao (1996) provides detailed information on several other sources from which accelerograms can be obtained directly via on-line systems or purchased in a variety of formats.

Due to uncertainties in the selection of a representative earthquake time history, response analyses are usually performed using a suite of time histories rather than a single time history. Engineers commonly use two to five time histories to represent each significant seismic source in a site response analysis. The 1997 UBC requires a minimum of three pairs of time histories from recorded events for time history analysis. For earthquakes in the western United States, it should be possible to find three to five representative time histories that satisfy the above criteria. However, at the present time, there are a limited number of bedrock strong motion records available from earthquakes of magnitude M_w 5.0 or greater in the central and eastern United States or Canada, including:

- eight records from the 1988 Saguenay, Quebec earthquake of magnitude M_w 5.9;
- three records from the 1985 Nahanni; Northwest Territories (Canada) Earthquake of Magnitude M_w 6.7; and
- the Loggie Lodge record with a peak horizontal acceleration of 0.4 g from the 1981 Mirimichi, New Brunswick earthquake of magnitude M_w 5.0.

Therefore, for analysis of sites east of the Rocky Mountains, records from a western United States site, an international recording site or synthetic accelerograms are often used to compile a suite of at least three records for analysis.

Generic, synthetically generated ground motions are available only for a limited number of major faults (fault systems). For example, Jennings, *et al.* (1968) developed the A1 synthetic accelerogram for soil site conditions for an earthquake on the southern segment of the San Andreas fault. Seed and Idriss (1969) developed a synthetic accelerogram for rock sites for an earthquake on the northern segment of the San Andreas fault. The Jennings, *et al.* (1968) A1 accelerogram has an energy content which is larger than the energy content of any accelerogram recorded to date. For this reason, the A1 record is often used to simulate major earthquakes in the Cascadia and New Madrid seismic zones. Appropriate synthetic accelerograms may also be available to the engineer from previous studies and may be used if they are shown to be appropriate for the site. Synthetic earthquake accelerograms for many regions of the country are currently being compiled by the Lamont-Doherty Earth Observatory of Columbia University under the auspices of the Multi-Disciplinary Center for Earthquake Engineering Research (formally National Center for Earthquake Engineering Research, NCEER) and can be downloaded from the NCEER website at "<http://nceer.eng.buffalo.edu>. A catalog of records representative on northeastern United States seismicity (i.e., Boston) was recently developed for a Federal Emergency Management Agency (FEMA) research project on the performance of steel buildings (Somerville, *et al.*, 1998). These records can be downloaded from the Earthquake Engineering Research Center (EERC) website at "http://quiver.eerc.berkeley.edu:8080/studies/system/ground_motions.html."

The *target spectrum* may be estimated from available attenuation relationships (see Section 4.3). These attenuation relationships, typically developed for a spectral damping of 5 percent, provide estimates of the median spectral ordinates and the log-normal standard deviation about the mean. Representative time histories are selected by trial-and-error on the basis of "reasonable" match with the target spectrum. A "reasonable" match does not necessarily mean that the response spectrum for the candidate record "hugs" the target spectrum. Particularly if a suite of time histories is used, a "reasonable" match only requires that the suite of response spectra averaged together approximates the mean target spectrum. Each individual spectrum may fluctuate within the plus and minus one standard deviation bounds over most of

the period range of interest. Natural and/or generic synthetic time histories can be screened in this type of selection process.

An alternative approach to trial-and-error matching of the target spectrum is computerized generation of a synthetic time history or a suite of time histories whose spectral ordinates provide a reasonable envelope to those of the target spectrum. Existing time histories can also be modified to be spectrum compatible. Several computer programs are available for these tasks (e.g., Gasparin and Vanmarcke, 1976; Ruiz and Penzien, 1969; Silva and Lee, 1987). However, generation of realistic synthetic ground motions is not within the technical expertise of most geotechnical engineering consultants. The simulation programs should only be used by qualified engineering seismologists and earthquake engineers. For this reason, these simulation techniques are beyond the scope of this guidance document.

CHAPTER 5.0 SITE CHARACTERIZATION

5.1 INTRODUCTION

This chapter describes the site characterization information required to evaluate the geotechnical parameters used for the seismic design of highway facilities. It is assumed that the basic geological, geotechnical, and hydrological investigations required for the general design of the structure under consideration have been (or will be) conducted according to the state of practice. The goal of site characterization for seismic design is to develop the subsurface profile and soil property information necessary for seismic analyses. Soil parameters required for seismic analyses include the initial (small strain) dynamic shear modulus, equivalent viscous damping ratio, shear modulus reduction and equivalent viscous damping characteristics, cyclic shear strength parameters, and liquefaction resistance parameters.

Three broad categories of site investigation activities can be included in a seismic site exploration program. The first category is conventional geotechnical site exploration, including a drilling program followed by laboratory testing on undisturbed or remolded samples. The second category is in situ testing, wherein the parameters that describe dynamic soil properties are estimated in situ using penetrometers and other types of probes and in situ testing devices. The third category is geophysical exploration.

All the three categories of site investigations are discussed in detail in Module 1 (Subsurface Investigations). Herein, only brief discussions related to characterization of site for seismic studies are presented.

The remainder of this chapter will describe the relevant soil parameters for seismic site characterization, their importance for seismic analyses, and the available evaluation techniques.

5.2 SUBSURFACE PROFILE DEVELOPMENT

5.2.1 General

As for all geotechnical engineering analyses, seismic analysis requires knowledge of the subsurface profile, or stratigraphy, at the site under study. The required stratigraphic information includes information on the water level, the soil stratigraphic profile, and the underlying bedrock. Stratigraphy can be obtained using classical investigation techniques (drilling and sampling), in situ tests, or geophysical means.

As in any geotechnical analysis, identification and quantification of relatively thin, weak layers can be an important part of seismic site characterization. However, the "weak" layer in a seismic analysis may differ from the "weak" layer in a static analysis. For instance, a saturated sand layer considered a suitable foundation material with respect to static loads may be susceptible to liquefaction under earthquake loads and thus becomes a weak layer in a seismic analysis. In other cases, such as soft material between beds of rock or stiff soil on a hillside, the same material that is a weak material for static analyses also represents a potential problem under earthquake loads.

5.2.2 Water Level

The groundwater level (or levels) should be established during a seismic site investigation. Groundwater may play an important role in seismic analysis, particularly if the soil deposits are liquefiable. Seasonal

variability in the water level should be considered in developing the stratigraphic profile and performing liquefaction potential analyses.

Groundwater level information is often obtained by observation of the depth to which water accumulates in an open borehole. However, water level observations in boreholes may be unreliable due to a variety of factors, including:

- insufficient time for equilibrium in borings in fine-grained soils;
- artesian pressures in confined aquifers; and
- perched water tables in coarser soils overlying fine-grained deposits.

Furthermore, borehole observations do not, in general, permit observations of seasonal fluctuations in water levels. Piezometers or observation wells installed in a borehole provide a much more reliable means of monitoring water levels in the subsurface. In deposits where layers of fine-grained soils are present and multiple water levels are suspected, multiple-point piezometers can be installed in a single borehole or multiple boreholes can be fit with single point piezometers.

A cone penetrometer (CPT) with pore pressure measuring capabilities, referred to as a piezocone, can also be used to estimate water level elevations. By holding the cone at a constant elevation and waiting until the pore pressure drops to a constant value, the piezocone can be used to determine the steady state pore pressure at a specified elevation. The potential for perched water tables or confined aquifers can be assessed with the piezocone by combining steady-state pore pressure readings at several elevations with stratigraphic information developed from the tip and sleeve resistance of the cone.

Geophysical stratigraphic profiling methods are generally not used to evaluate the depth to groundwater. Geophysical methods used to evaluate soil stratigraphy are often based upon shear wave or Rayleigh wave velocity and thus are generally insensitive to the water level. Some resistivity methods (e.g., down hole resistivity surveys) can detect the presence of water in the soil pores but cannot measure the pressure in the water. Therefore, in a fine-grained soil, such methods can neither distinguish between soil above the water table saturated by capillarity and soil below the water table nor measure an artesian pressure in a confined aquifer.

5.2.3 Soil Stratigraphy

The subsurface investigation should provide a detailed description of the soil stratigraphy at the site, including the thickness and elevation of the different layers. Potentially liquefiable soils should be clearly identified and quantified by one of the methods described later in this chapter. Both conventional boring and sampling and in situ testing using the CPT offer the possibility of development of a continuous soil profile in which layers as small as 75 mm can be identified. Thin continuous layers of weak or potentially liquefiable soil encountered between beds of more competent soil may prove to be the critical plane in seismic slope stability analyses. Borings offer the advantage of recovery of a sample for visual classification and, if desired, laboratory testing. In a boring in which continuous Standard Penetration Tests (SPT) sampling is performed, layers of soil can be visually identified from the sample recovered from the split spoon to develop a continuous stratigraphic profile. However, the SPT blow count, the primary measurement of cohesionless soil strength and consistency obtained using the SPT, generally applies only to the gross behavior of a relatively large 300 mm interval of the boring and thus cannot be used to characterize the liquefaction susceptibility of thin lenses of soil visually identified in the split-spoon sample. In the CPT, the resistance of the tip and sleeve of the cone to penetration can be used to develop continuous profiles of the shear strength of the soil that are applicable to layers as thin as 75 mm.

Geophysical methods will provide information on the stratigraphy of the soil with respect to the measured geophysical property. The measured geophysical property may be a physical property of direct interest in a seismic analysis (e.g., shear wave velocity) or may be correlated to a physical property of interest (e.g., electrical resistivity and water level). The ability of geophysical methods to resolve layering in the ground varies among the available methods and, in general, decreases with depth unless a down hole method is used (in which case a boring or in situ probe is required).

5.2.4 Depth to Bedrock

Ideally, the soil profile developed for a seismic analysis should extend to *competent bedrock*, where competent bedrock is defined as material with a shear wave velocity of at least 700 m/s, and the physical properties of the soil over the entire interval between the ground surface and competent bedrock should be defined. However, if competent bedrock is not reachable at a reasonable depth, the depth over which the physical properties of the soil for seismic analyses are defined should be at least 30 m. Furthermore, the depth to which the soil profile is developed should be at least as deep as required for conventional geotechnical analyses.

5.3 REQUIRED SOIL PARAMETERS

5.3.1 General

At a minimum, a seismic analysis requires the same parameters used to describe soil properties for static analyses of earth structures and foundations. During the course of a typical geotechnical investigation, the following information is obtained:

- soil classification and index parameters;
- unit weight of the soil; and
- compressibility and shear strength parameters of the soil.

For seismic design purposes, a series of other soil parameters and properties may need to be evaluated. For a seismic analysis, these may include:

- a measure of the relative density of the soil;
- shear wave velocity;
- cyclic stress-strain behavior; and
- peak and residual shear strength.

5.3.2 Relative Density

Measures of both the absolute and relative density of the soil skeleton are required for seismic analysis. The absolute density is usually expressed in terms of unit weight. The unit weight of the soil is used to calculate the total and effective vertical stresses for liquefaction and slope stability analyses. Unit weight is also an important parameter in dynamic response and stability analyses, as the inertia force of an element of soil is equal to the acceleration times the total weight. Total unit weight may be assessed on the basis of measured values from undisturbed samples, or from the water content and specific gravity of saturated soil.

Relative density is an important parameter with respect to the potential for soil liquefaction and seismically-induced settlement of cohesionless soils. The relative density is a measure of the relative consistency of

the soil.

Mathematically, relative density, D_r , is related to the maximum dry density ($\gamma_{d \max}$) or minimum void ratio e_{\min} (the densest state to which the material can be compacted) and the minimum density ($\gamma_{d \min}$) or maximum void ratio e_{\max} (the loosest state the material can attain) by:

$$D_r = \frac{e_{\max} - e_0}{e_{\max} - e_{\min}} = \frac{1 - \gamma_{d \min} / \gamma_{d_0}}{1 - \gamma_{d \min} / \gamma_{d \max}} 100\% \quad (5-1)$$

where e_0 is the in situ void ratio of the material and γ_{d_0} is the dry in situ unit weight. The relative density is an important parameter with respect to liquefaction and seismic settlement potential because it is related to the potential for a granular material to decrease in volume when subjected to disturbance.

Relative density is rarely measured directly. Generally, an index of the relative density is measured in situ. Commonly used indices of the relative density, or relative consistency, of soil in situ are the SPT blow count, N , and the normalized tip and sleeve resistance of the CPT probe, q_{cl} , and f_s , respectively. Table 5-1 presents the Terzaghi and Peck (1948) relationship between relative density and SPT blow count for sandy soils. Several of the indices used to evaluate relative density in situ have, in turn, been directly correlated to liquefaction and seismic settlement potential, often eliminating the need for direct evaluation of relative density in a seismic analyses.

TABLE 5-1
RELATIVE DENSITY OF SANDY SOILS
(After Terzaghi and Peck, 1948)

Relative Density, D_r (%)	Penetration Resistance, N (blows/300mm)	Descriptive Term
0-15	0-4	Very Loose
15-35	5-10	Loose
35-65	11-30	Medium
65-85	31-50	Dense
85-100	> 50	Very Dense

Note: See also Figure 5-4 for an alternative N- D_r correlation.

5.3.3 Shear Wave Velocity

The shear wave velocity of a soil is used to establish the stiffness of the soil at small strains. The small strain (initial) shear modulus of a soil, G_{\max} , is related to the shear wave velocity, V_s , and the mass density, ρ , of the soil by the equation:

$$G_{\max} = \rho \cdot V_s^2 \quad (5-2)$$

Mass density of the soil is related to the total unit weight of the soil, γ_t , by the acceleration of gravity, g :

$$\rho = \frac{\gamma_t}{g} \quad (5-3)$$

The mass density of most soils can be reasonably estimated from soil classification and location relative to the water table. Therefore, measurement of shear wave velocity can provide a reliable means for evaluating the small strain shear modulus of the soil if the stratigraphic profile is known.

Small strain (initial) Young's modulus, E_{\max} , is related to small strain shear modulus as a function of Poisson's ratio, ν , by the theory of elasticity:

$$E_{\max} = 2(1 + \nu)G_{\max} \quad (5-4)$$

For practical purposes, Poisson's ratio of soil can be assumed equal to 0.35 for sands and 0.45 for clays. Alternatively, if results of geophysical measurements are available, the following equation may be used to estimate ν .

$$\nu = 1 - \frac{1}{2(1 - (V_s/V_p)^2)} \quad (5-5)$$

where V_s and V_p are shear and compressional wave velocities, respectively. Young's modulus can also be evaluated from the compressional wave velocity and mass density of the soil. Consequently an efficient and reliable means of obtaining the small-strain elasticity properties of the soil is through the measurement of shear and compressional wave velocities.

5.3.4 Cyclic Stress-Strain Behavior

During an earthquake, a soil deposit is subjected to a complex system of stresses and strains resulting from the ground motions induced by the earthquake. In general, these stresses and strains will be cyclical due to the vibrational nature of the earthquake loading. To evaluate the seismic response of the soil deposit, it is necessary to estimate how it responds to this cyclic loading.

The earthquake-induced stresses and strains that produce the most damage in soils are generally considered to be due to cyclic shearing of the soil. Shear waves propagate primarily upward near the ground surface. Therefore, most geotechnical earthquake engineering analyses assume that earthquake ground motions are generated by vertically-propagating shear waves.

The cyclic stresses induced on a soil element by a vertically-propagating shear wave are schematically presented in Figure 5-1. The stress-strain response of soil to this type of cyclic loading is commonly characterized by a *hysteresis loop*. A typical hysteresis loop is shown on Figure 5-2. Various constitutive models have been developed to characterize soil hysteresis loops. The most common model used to represent the hysteretic behavior of soil in seismic analysis is the *equivalent-linear* model (Seed and Idriss, 1970). Various non-linear constitutive models (Kondner and Zelasko, 1963; Martin, 1975; Matasović and Vucetic, 1993) have also been developed to represent hysteretic soil behavior. Detailed discussion of non-linear constitutive models for the hysteretic behavior of soil is beyond the scope of this document.

The equivalent-linear model represents non-linear hysteretic soil behavior using an equivalent shear

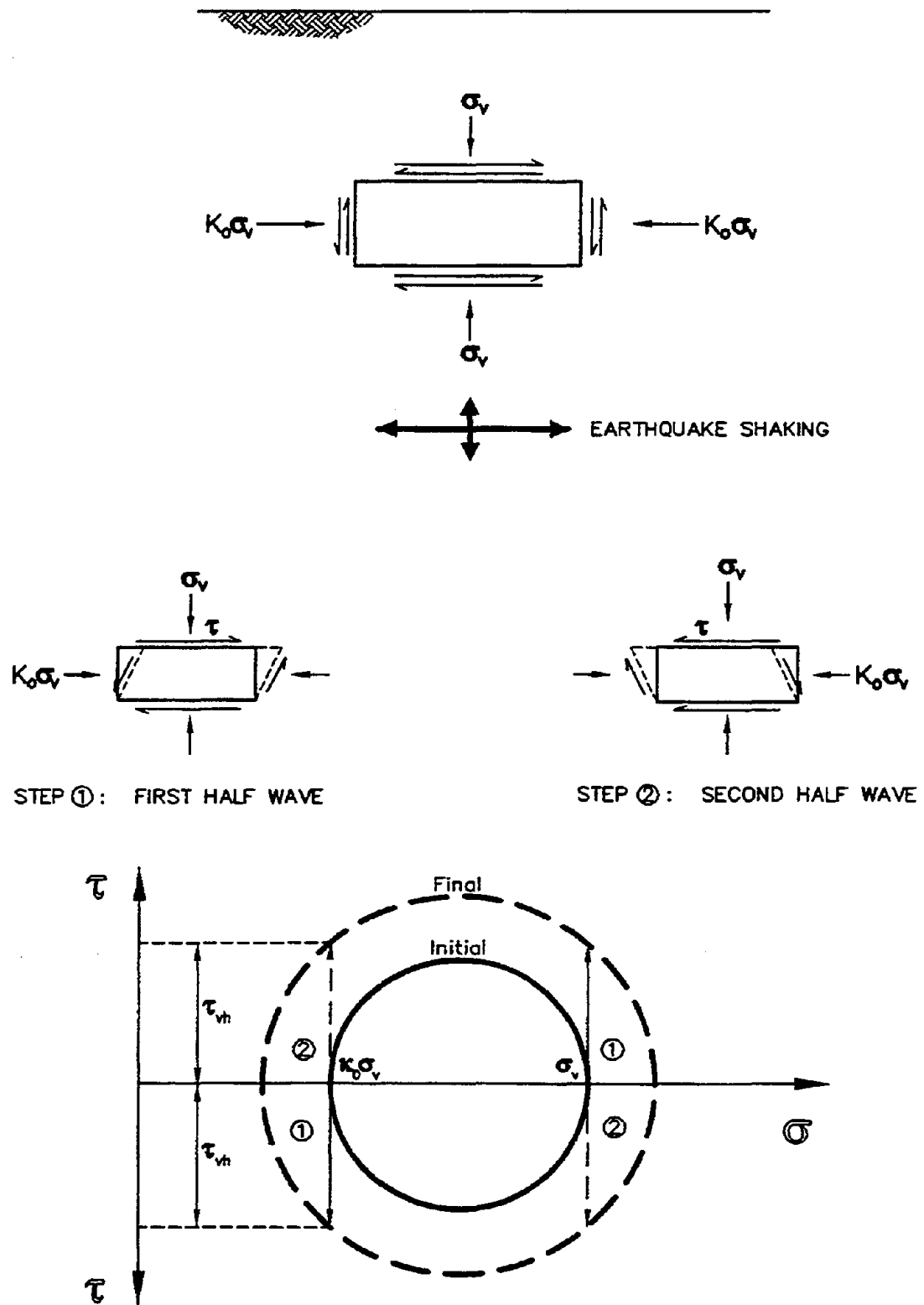


Figure 5-1: Stresses Induced in a Soil Element by Vertically Propagating Shear Wave.

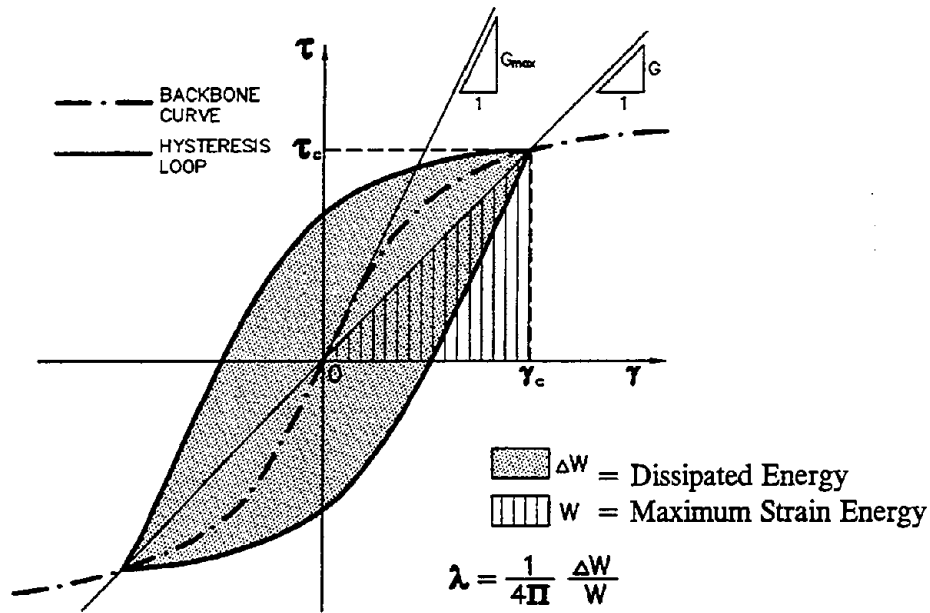


Figure 5-2: Hysteretic Stress-strain Response of Soil Subjected to Cyclic Loading.

modulus, G , equal to the slope of the line connecting the tips of the hysteresis loop and an equivalent viscous damping ratio proportional to the enclosed area of the loop. The equivalent modulus and damping ratio are strain-dependent. The strain dependence of the equivalent modulus and damping ratio are described by the *modulus reduction* and *damping curves* shown on Figure 5-3. The equivalent viscous damping ratio is evaluated from the area of the hysteresis loop as schematically shown on Figure 5-2. Modulus reduction and damping curves strictly apply only to uniform cyclic loading. However, these curves are typically also used to model the soil behavior under irregular (non-uniform) cyclic loading generated by earthquakes.

Cyclic loading can break the bonds between soil particles and rearrange the particles into a denser state. In a dry soil, this rearrangement will be manifested as compression of the soil and will result in seismic settlement. If the soil is saturated, volume change cannot occur instantaneously and the load carried by the soil skeleton is transferred to the pore water as the particles are rearranged. If the rearrangement is sufficient in magnitude, the soil skeleton can shed all of the load to the pore water, resulting in a pore pressure equal to the overburden pressure, complete loss of shear strength, and, consequently, liquefaction of the soil.

5.3.5 Peak and Residual Shear Strengths

Peak and residual shear strengths are important elements in the evaluation of seismic stability. The peak shear strength refers to the maximum shearing resistance an element of soil can sustain during and after cyclic loading. The peak shear strength may be used to calculate the *yield acceleration* of a soil (the horizontal acceleration above which permanent seismic deformations begin to accumulate) if the buildup of seismically-induced pore pressures is not anticipated. Residual shear strength refers to shear strength of the soil after significant static and/or cyclic shearing has occurred. Residual shear strength is often used to evaluate stability and calculate the accumulation of permanent seismic deformation in a post-liquefaction stability and deformation analysis for a foundation or earth structure.

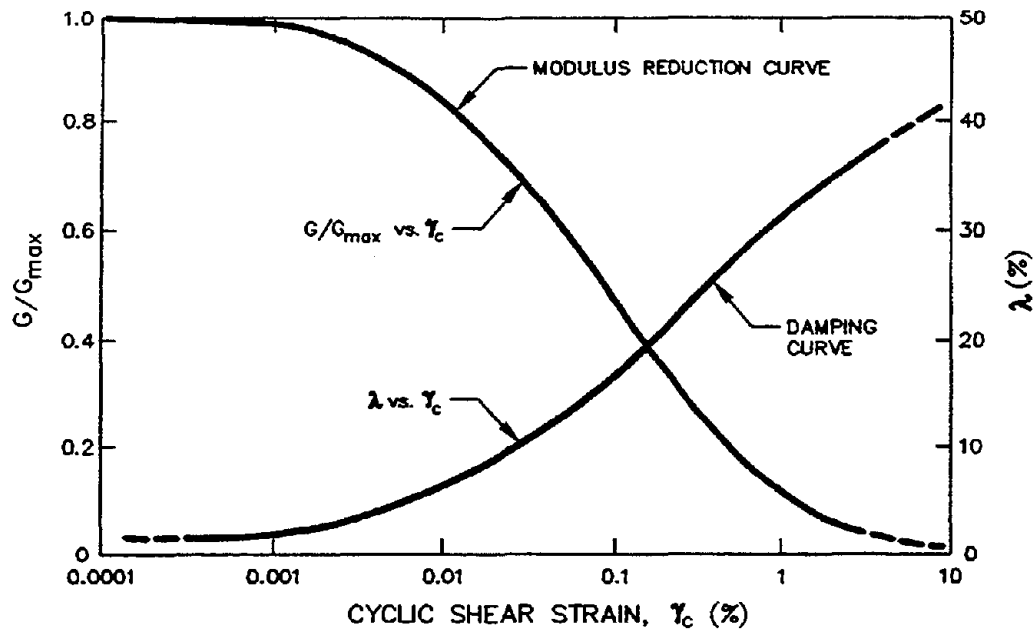


Figure 5-3: Shear Modulus Reduction and Equivalent Viscous Damping Ratio Curves.

While there is some limited information to indicate that the shear strength of soil increases with increasing strain rate, the peak shear strength of soil subjected to cyclic loading is generally assumed to be less than or equal to the peak static strength. If the soil is dry, the drained shear strength may be used. If the soil is saturated, even if the soil is relatively free draining, the undrained shear strength should be used for seismic analyses because of the rapid nature of earthquake loading.

Residual shear strength is used to represent the post-peak strength of the soil subsequent to both monotonic and cyclic loading. Many soils and geosynthetic interfaces show a marked decrease in shearing resistance when subjected to relatively large monotonic shear strains. If the seismic design philosophy for a foundation or earth structure calls for allowing the peak strength to be exceeded as long as cumulative deformations remain within a range defined as acceptable, the residual shear strength after monotonic loading is typically used to assess the post-liquefaction stability. The yield acceleration calculated using the residual shear strength can be used to assess cumulative seismic deformations on a conservative basis.

5.4 EVALUATION OF SOIL PROPERTIES

5.4.1 General

The key dynamic soil parameters required to perform a seismic response analysis are the shear wave velocity, modulus reduction and damping curves, peak and residual shear strength, and the parameters needed to evaluate soil liquefaction potential. A value for Poisson's ratio may also be required. These parameters can either be directly evaluated from laboratory test results or in situ test results or indirectly evaluated by correlation with index properties of soils. Laboratory tests generally provide the most direct means of evaluating soil parameters for seismic analyses. However, laboratory tests are subject to limitations on the recovery and testing of representative samples as well as on the testing itself. For some parameters (e.g., shear wave velocity), field testing provides a reliable and cost effective means of evaluation. However, in many cases, empirical correlation with index parameters and in situ test results is the most practical means of evaluating soil parameters for seismic analyses. Sometimes, for particular geographical areas and soils (e.g., Piedmont region residual soils, Borden, *et al.*, 1996) typical dynamic

soil parameters have been established.

5.4.2 In Situ Testing for Soil Profiling

Standard Penetration Testing (SPT)

Probably the most common in situ test used in geotechnical practice, the SPT, measures the resistance to penetration of a standard split-spoon sampler in a boring. The test method is rapid and yields useful data, although there are many factors that affect the results. The procedure used to perform the SPT is codified under ASTM Standard D 1586 and discussed in Module 1 (Subsurface Investigations). The SPT consists of driving a standard split barrel sampler with a 63.5 kg hammer dropping 762 mm in a free fall which theoretically delivers 60 percent of the energy to the drill rod. The (uncorrected) SPT blow count, N , is the result of the test.

Although widely recognized as an unsophisticated test, the SPT is performed routinely worldwide and, when performed properly, yields useful results. Extensive work has been conducted to understand the limitations of the test and develop reliable correction factors accounting for the influence of vertical stress, soil gradation, hammer efficiency, and other factors on test results. Correction factors to normalize and standardize the value of the SPT blow count, N , are discussed in Chapter 8. Corrected SPT blow count values can be used to:

- estimate the relative density of sand;
- estimate shear strength parameters of cohesionless soils;
- estimate bearing capacity;
- evaluate seismic settlement potential of sands;
- evaluate liquefaction potential of saturated sands; and
- estimate the shear modulus at very low strain.

Most soil mechanics text books contain correlations relating SPT blow counts to soil shear strength and foundation bearing capacity (e.g., Bowles, 1988). As discussed in Section 5.3.2 and presented in Table 5-1, SPT blow counts may also be used to estimate relative density of sand. Figure 5-4 presents a correlation between overburden pressure, relative density, and SPT blow count developed by Marcuson and Bieganousky (1977) for clean sand. As indicated in Figure 5-4, soils with the same relative density will have different SPT blow counts under different overburden pressures. Dynamic soil properties (e.g., cyclic resistance against liquefaction and residual undrained shear strength) are often related to the relative density of the soil. Therefore, to provide a consistent and stable parameter using SPT blow count numbers, field SPT N values should be corrected to account for the overburden pressure effects.

Hammer efficiency is another key factor in evaluating SPT blow count. Values of hammer efficiency, defined as the energy delivered to the sampler divided by the theoretical kinetic energy of the free-falling weight, measured in the field vary from 30 to 90 percent, with an average value of 60 percent, depending on the equipment, the operator, and other site-specific conditions. Field and analytical data indicate that the blow count is directly proportional to the energy delivered to the split spoon sampler (Seed, *et al.*, 1985). Measurement of efficiency made on the same day using the same equipment and operator has been known to vary by a factor of two. A two- to three-fold variation in efficiency will result in a two- to three-fold variation in blow count in a uniform soil. To mitigate this problem, i.e., to be able to relatively accurately standardize the blow count to correspond to the average efficiency of 60 percent, several companies have developed systems for measuring the energy delivered to the rods or split spoon sampler by the hammer. The services of these companies are available on a commercial basis and should seriously

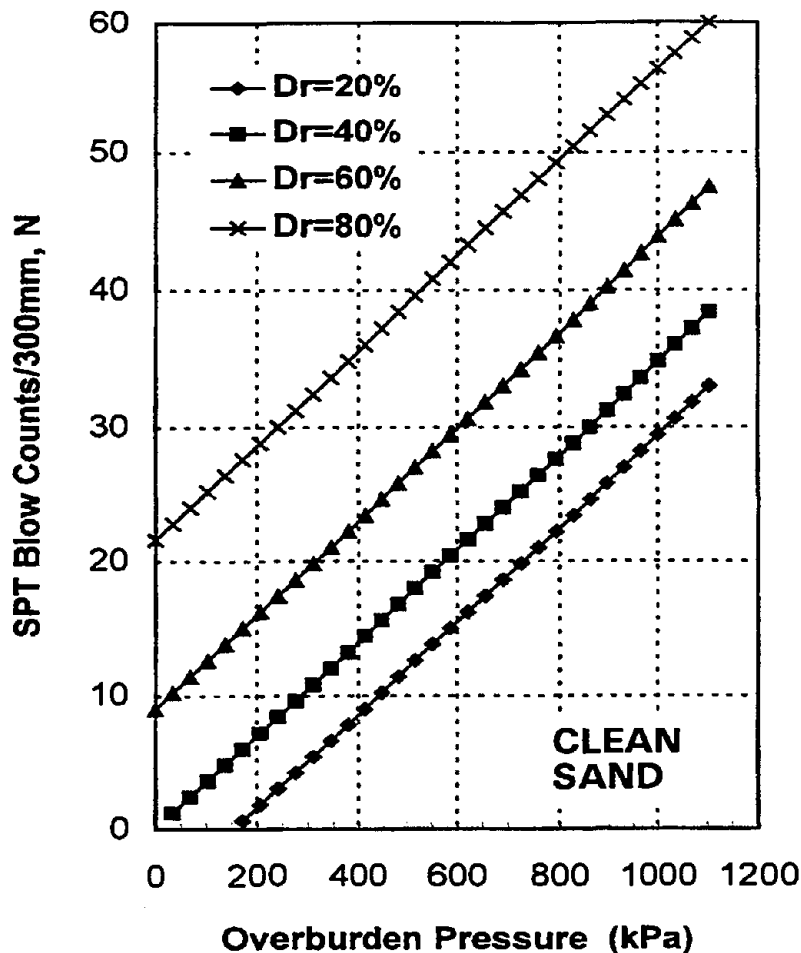


Figure 5-4: SPT-relative Density Correlation. (After Marcuson and Bieganousky, 1977, reprinted by permission of ASCE)

be considered for major projects or where liquefaction potential assessment is a critical issue.

The procedure used to account for the effects of energy variations and overburden pressure on the field SPT blow counts is presented below.

Step 1: Evaluate the *standardized* SPT blow count, N_{60} , which is the standard penetration test blow count for a hammer with an efficiency of 60 percent (60 percent of the nominal SPT energy is delivered to the drill rod). The "standardized" equipment corresponding to an efficiency of 60 percent is specified in Table 5-2. If nonstandard equipment is used, N_{60} is obtained from the equation:

$$N_{60} = N \cdot C_{60} \quad (5-6)$$

where C_{60} is the product of various correction factors. The equation for the global correction factor, C_{60} , in Equation 5-6 and the contributing correction factors recommended by various investigators for some common non-standard SPT configurations are provided in Table 5-3 (Richardson, *et al.*, 1995). The correction factors for non-standard hammer type, C_{HT} , and non-standard hammer weight or height of fall, C_{HW} , combine to represent a hammer energy factor, H_E :

$$H_E = C_{HT} \cdot C_{HW} \quad (5-7)$$

Therefore, the global SPT correction factor may be written as:

$$C_{60} = H_E \cdot C_{SS} \cdot C_{RL} \cdot C_{BD} \quad (5-8)$$

and C_{SS} , C_{RL} , and C_{BD} are the non-standard sampler setup, short rod length, and non-standard borehole diameter factors presented in Table 5-3.

For important projects, H_E may be calculated directly, by measuring the hammer energy. There are two commercially available methods for measuring hammer energy: the Force Squared (F2) method and the Force Velocity (FV) method. In the F2 method, strain gauge load cells are used to measure the force transmitted to the drill rods. The square of the force is integrated over time to calculate the hammer energy. In the FV method, the product of the force times the velocity is integrated over time. The FV method requires both load cells to measure the transmitted force and an accelerometer to measure the velocity time history. The equipment for making FV measurements is similar to pile driving analyzer equipment for dynamic load testing of driven piles.

In general, the F2 method is not considered as reliable as the FV method and is not recommended for correcting SPT blow counts. Using the energy measured by the FV method, F_{VE} the energy correction factor may be evaluated as:

$$H_E = \frac{F_{VE}}{0.6 F_{max}} \quad (5-9)$$

where F_{max} is the theoretical maximum energy of the SPT hammer (1,151 kg m²/s²).

If CPT data are available, N_{60} can be obtained from the chart relating N_{60} to q_c and D_{50} presented in Figure 5-7 (Robertson et al., 1983).

Step 2: Calculate the normalized and standardized SPT blow count, $(N_1)_{60}$. $(N_1)_{60}$ is the standardized blow count normalized to an effective overburden pressure of 96 kPa in order to eliminate the influence of confining pressure. The most commonly used technique for normalizing blow counts is via the correction factor, C_N , shown in Figure 5-5 (Seed, *et al.*, 1983). However, the closed-form expression proposed by Liao and Whitman (1986) may also be used:

$$C_N = 9.79 (1/\sigma'_v)^{1/2} \quad (5-10)$$

where σ'_v equals the vertical effective stress at the sampling point in kPa.

As shown in Figure 5-5, the Seed, *et al.* (1983) effective overburden correction factor curves are valid only for depths greater than approximately 3 m (approximately 50 kPa). A similar plot presented by Liao and Whitman (1986) suggests that C_N in Equation 5-10 should be limited to 2.0 at depths lower than 3 m.

Regardless of the manner in which C_N is estimated, the normalized and standardized blow count is calculated as:

$$(N_1)_{60} = C_N \cdot N_{60} \quad (5-11)$$

Other factors, such as grain size distribution, may influence C_N (Marcuson and Bieganousky, 1977). However, considering the uncertainties involved in the SPT itself, the application of equipment and overburden pressure correction factors should be sufficient for engineering purposes.

The use of SPT blow counts $(N_1)_{60}$ to evaluate soil liquefaction potential is described in detail in Chapter 8.

TABLE 5-2
RECOMMENDED "STANDARDIZED" SPT EQUIPMENT
(After Seed, *et al.*, 1985 and Riggs, 1986, Reprinted by Permission of ASCE)

Element	Standard Specification
Sampler	Standard split-spoon sampler with: (a) Outside Diameter, O.D. = 51 mm, and (b) Inside Diameter, I.D. = 35 mm (constant - i.e., no room for liners in the barrel)
Drill Rods	A or AW-type for depths less than 15.2 m; N- or NW-type for greater depths
Hammer	Standard (safety) hammer with: (a) weight = 63.5 kg; (b) drop = 762 mm (delivers 60% of theoretical free fall energy)
Rope	Two wraps of rope around the pulley
Borehole	100- to 130-mm diameter rotary borehole with bentonite mud for borehole stability (hollow stem augers where SPT is taken through the stem)
Drill Bit	Upward deflection of drilling mud (tricone or baffled drag bit)
Blow Count Rate	30 to 40 blows per minute
Penetration Resistance Count	Measured over range of 150 to 460 mm of penetration into the ground

Notes: ⁽¹⁾ If the equipment meets the above specifications, $N = N_{60}$ and only a correction for overburden is needed.

⁽²⁾ This specification is essentially the same to the ASTM D 1586 standard.

TABLE 5-3
CORRECTION FACTORS FOR NON-STANDARD SPT PROCEDURE AND EQUIPMENT
(Richardson, *et al.*, 1995; Youd and Idriss, 1997)

Correction for	Correction Factor	Reference
Nonstandard Hammer Type (DH = doughnut hammer; ER = energy ratio)	$C_{HT} = 0.75$ for DH with rope and pulley $C_{HT} = 1.33$ for DH with trip/auto & ER = 80	Seed, <i>et al.</i> (1985)
Nonstandard Hammer Weight or Height of Fall (H = height of fall in mm; W = hammer weight in kg)	$C_{HW} = \frac{H \cdot W}{63.5 \cdot 762}$	calculated per Seed, <i>et al.</i> (1985)
Nonstandard Sampler Setup (standard samples with room for liners, but used without liners)	$C_{SS} = 1.10$ for loose sand $C_{SS} = 1.20$ for dense sand	Seed, <i>et al.</i> (1985)
Nonstandard Sampler Setup (standard samples with room for liners, and liners are used)	$C_{SS} = 0.90$ for loose sand $C_{SS} = 0.80$ for dense sand	Skempton (1986)
Short Rod Length	$C_{RL} = 0.75$ for rod length 0-4 m $C_{RL} = 0.85$ for rod length 4-6 m $C_{RL} = 0.95$ for rod length 6-10 m $C_{RL} = 1.0$ for rod length 10-30 m $C_{RL} < 1.0$ for rod length > 30 m	Seed, <i>et al.</i> (1983); Youd and Idriss (1997)
Nonstandard Borehole Diameter	$C_{BD} = 1.05$ for 150 mm borehole diameter $C_{BD} = 1.15$ for 200 mm borehole diameter	Skempton (1986)

Notes: N = Uncorrected SPT blow count.

$$C_{60} = C_{HT} \cdot C_{HW} \cdot C_{SS} \cdot C_{RL} \cdot C_{BD}$$

$$N_{60} = N \cdot C_{60}$$

C_N = Correction factor for overburden pressure.

$$(N_1)_{60} = C_N \cdot N_{60} = C_N \cdot C_{60} \cdot N$$

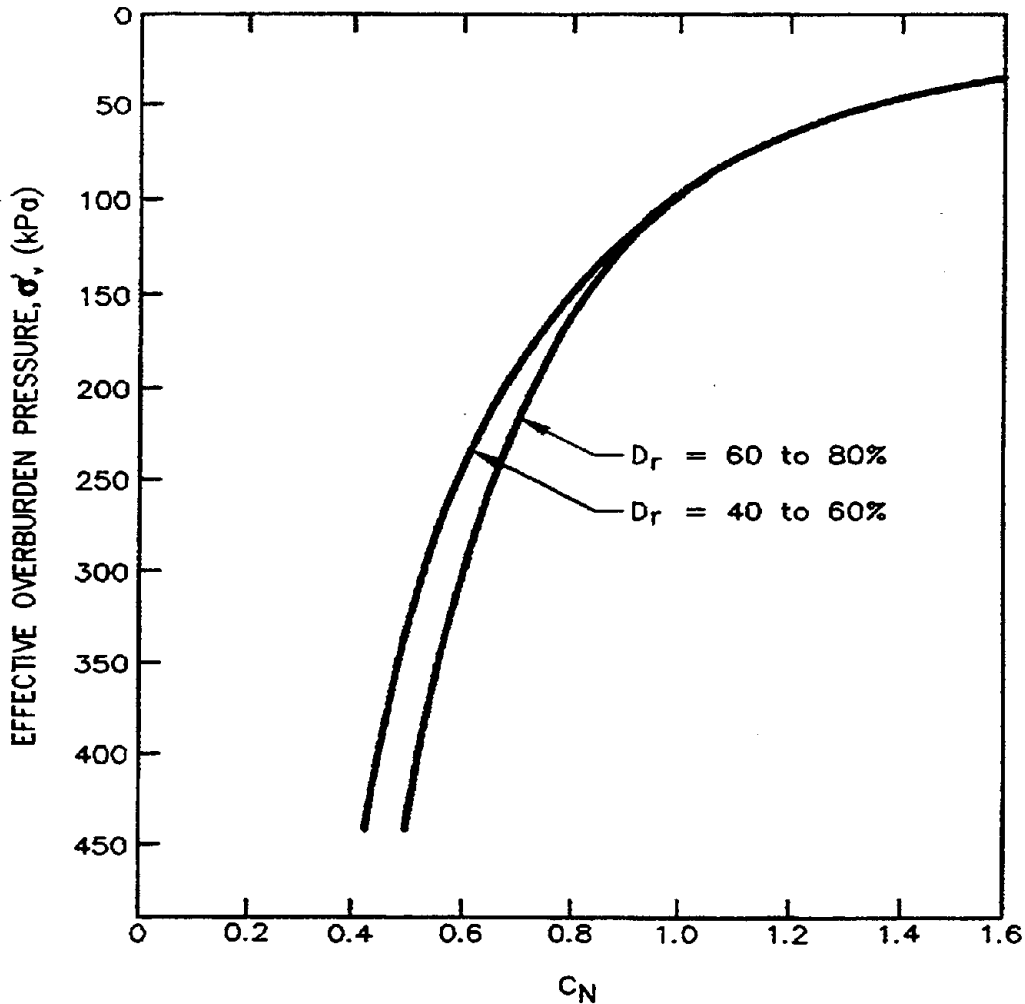


Figure 5-5: Correction Factor for the Effective Overburden Pressure, C_N . (Seed, *et al.*, 1983, reprinted by permission of ASCE)

Cone Penetration Testing (CPT)

The CPT test involves pushing a standard dimension conical probe into the ground at a constant rate and measuring the resistance of the tip of the cone and along the side of the cone to penetration. The cone tip resistance, q_c , combined with the friction ratio, f_s (the ratio between the side resistance and point resistance of the cone), has been shown to be strongly correlated to soil type and soil strength. In recent years, cone penetration testing probes have been fitted with pore pressure cells (piezocones) to measure pore pressure during penetrations and pore pressure dissipation after penetration, facilitating in situ measurement of consolidation properties and water table depth. The CPT can also be fitted with a geophone for use in "down hole" seismic profiling to determine shear wave velocity.

CPT testing is codified as ASTM Standard D 3441 and discussed in Module 1 (Subsurface Investigations). Recommendations for CPT testing are also provided by Riaund and Miran (FHWA Report No. FHWA-SA-91-043, 1992). The CPT is relatively easy to perform and provides a continuous profile of soil stratigraphy that can be invaluable in identifying the extent of liquefiable soils at a site. Figure 5-6 shows

a typical soil behavior type classification chart based on cone penetration resistance readings. Data from the CPT can also be used to establish allowable bearing capacity and for pile design (Riaund and Miran, 1992). In addition, correlations between SPT N values and CPT cone resistance have been developed to allow for the use of CPT data with relationships between SPT values and dynamic soil properties (e.g., liquefaction potential). Figure 5-7 presents the recommended chart (Robertson et al., 1983) which illustrates the relationship between cone resistance and SPT N values as a function of the mean grain size, D_{50} . Cone resistance has also been correlated to undrained shear strength, angle of internal friction, and relative density (Bowles, 1988; Meigh, 1987; Schmertmann, 1975; Riaund and Miran, 1992).

5.4.3 Soil Density

The total density of soil is usually expressed in terms of total unit weight. Typical values of the total unit weight are generally adequate for use in engineering analysis. If a higher degree of accuracy is required, unit weight can be evaluated from measurements made on undisturbed samples. In saturated cohesive soils, unit weight can be evaluated from the water content and the specific gravity.

Relative density, D_r , is rarely measured directly for geotechnical engineering purposes. Instead, an index of the relative density, usually the SPT blow count or the CPT resistance, is measured. Figure 5-4 presents one relationship between SPT blow count and the relative density of a clean sand.

5.4.4 Shear Wave Velocity

General

In general, shear wave velocity is directly measured in the field. However, shear wave velocity can also be estimated based upon soil type and consistency or by using the empirical correlations for small strain shear modulus described in Section 5.4.5 in conjunction with the soil density and Equation 5-2.

Shear wave velocity, or small strain shear modulus, can be evaluated in the laboratory using resonant column tests, as noted in Section 5.4.5. However, field geophysical measurements are used more commonly and reliably to estimate shear wave velocity.

Geophysical measurements of in situ wave velocities are typically based on measuring the wave travel time along a known propagation path. From knowledge of distance and travel time, the velocity is obtained. Wave velocity may be measured from intrusive methods such as boreholes and CPT soundings (seismic cone) or non-intrusively using seismic reflection, refraction, and surface wave profiling.

Geophysical Surveys

Geophysical techniques for subsurface exploration are described in detail in Module 1 (Subsurface Investigations) and by Woods (1994). Geophysical techniques commonly used in geotechnical practice are briefly summarized in the following paragraphs. Two general types of techniques are available to measure shear wave velocities in the field:

- intrusive techniques whereby measurements are made using probes and sensors that are lowered in boreholes or pushed into the ground; and
- non-intrusive techniques whereby the measurements are made from the ground surface.

$$q_{C1} = q_C (3.5 - 1.25 \log_{10} \sigma_v')$$

with σ_v' , q_C , q_{C1} in kPa.

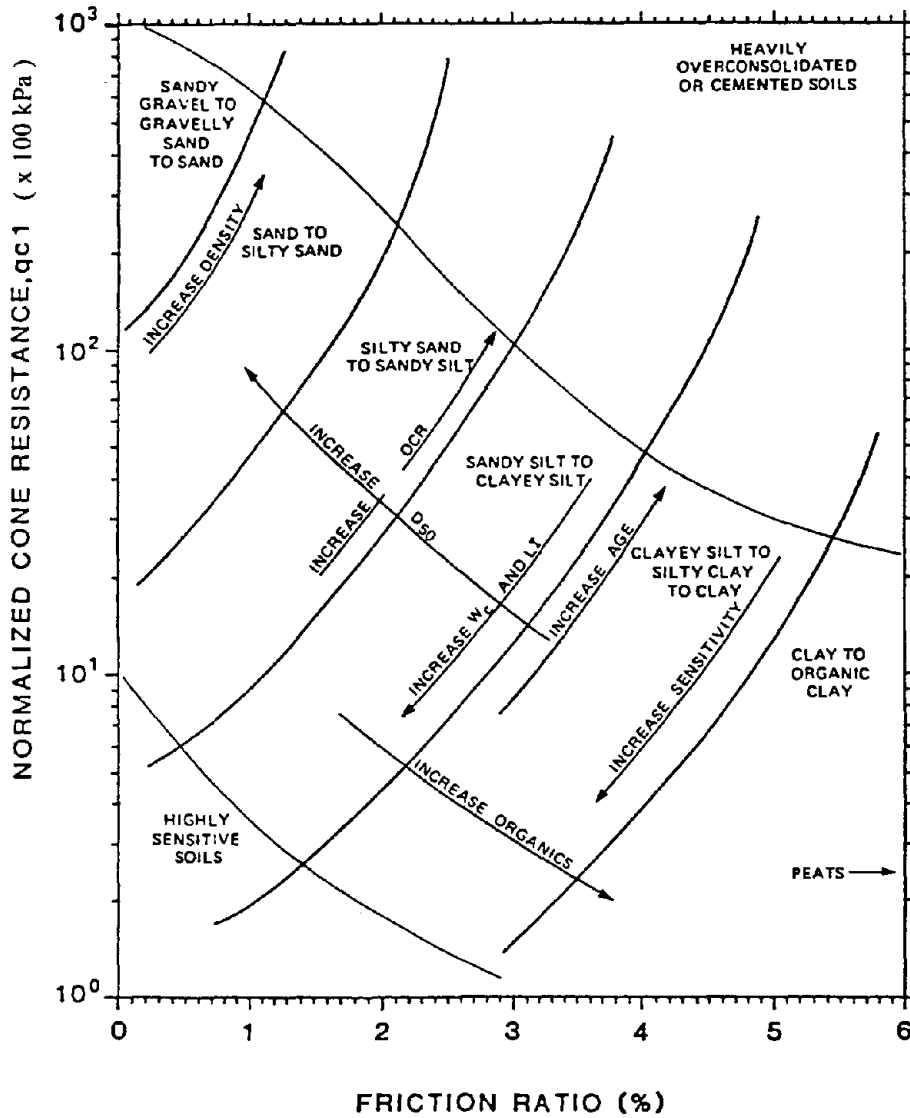


Figure 5-6: Soil Behavior Type Classification Chart Based on the CPT. (Douglas, 1984, 1981, reprinted from FHWA-SA-91-043, 1992.)

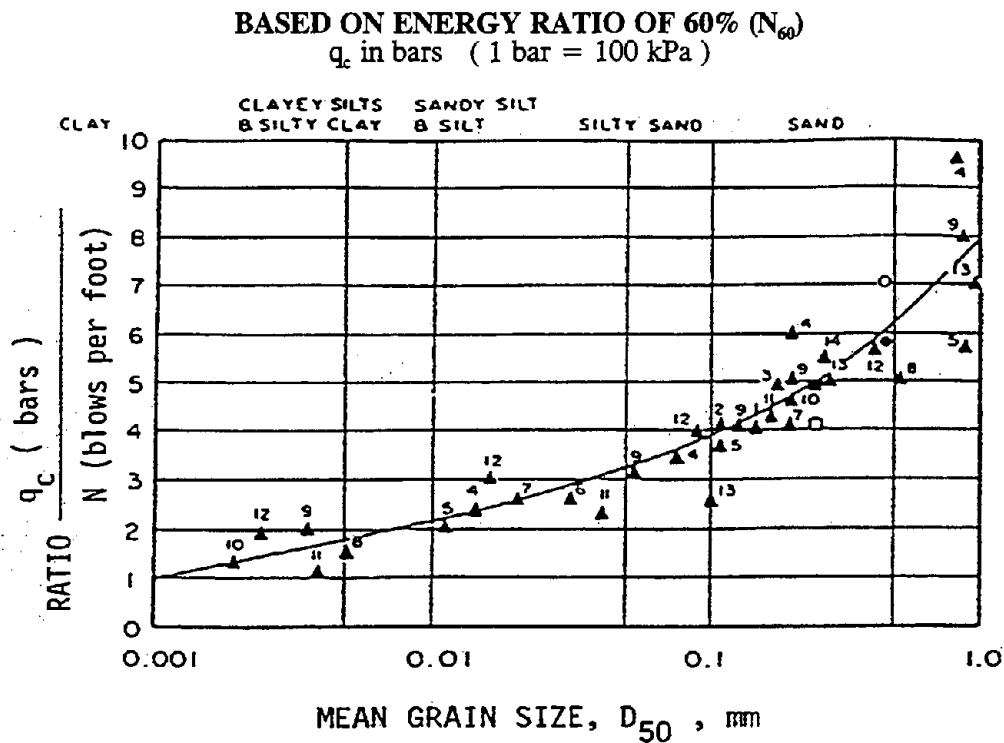


Figure 5-7: CPT-SPT Correlation Chart. (Robertson et al., 1983, reprinted from FHWA-SA-91-043, 1992.)

Borehole Surveys

In a borehole seismic survey, one or more boreholes are drilled into the soil to the desired depth of exploration. Wave sources and/or receivers are then lowered into the boreholes to perform the desired tests. There are three approaches to borehole seismic surveys:

- **Cross Hole Survey:** In a cross hole survey, the energy source is located in one boring and the detector (or detectors) is placed at the same depth as the energy source in one or more surrounding boreholes at a known spacing. Travel time between source and receiver is measured to determine the wave velocity. The cross hole survey method is illustrated by the sketch shown in Figure 5-8.
- **Down Hole Survey:** In a down hole survey, the energy source is located on the surface and the detector, or geophone, is placed in the borehole. The travel time is measured with the geophone placed at progressively increasing depth to evaluate the wave velocity profile. Figure 5-9 is a sketch showing the down hole survey method. Seismic cone penetration testing (SCPT) is another form of down hole survey, combined with conventional cone penetration testing (see Figure 5-10).
- **Up Hole Surveys:** Geophones are laid out on the surface in an array around the borehole. The energy source is set off within the borehole at successively decreasing depths starting at the bottom of the hole. The travel times from the source to the surface are analyzed to evaluate wave velocity versus depth. The energy source is usually either explosives or a mechanical pulse instrument composed of a stationary part and a hammer held against the side of the borehole by a pneumatic or hydraulic bladder.

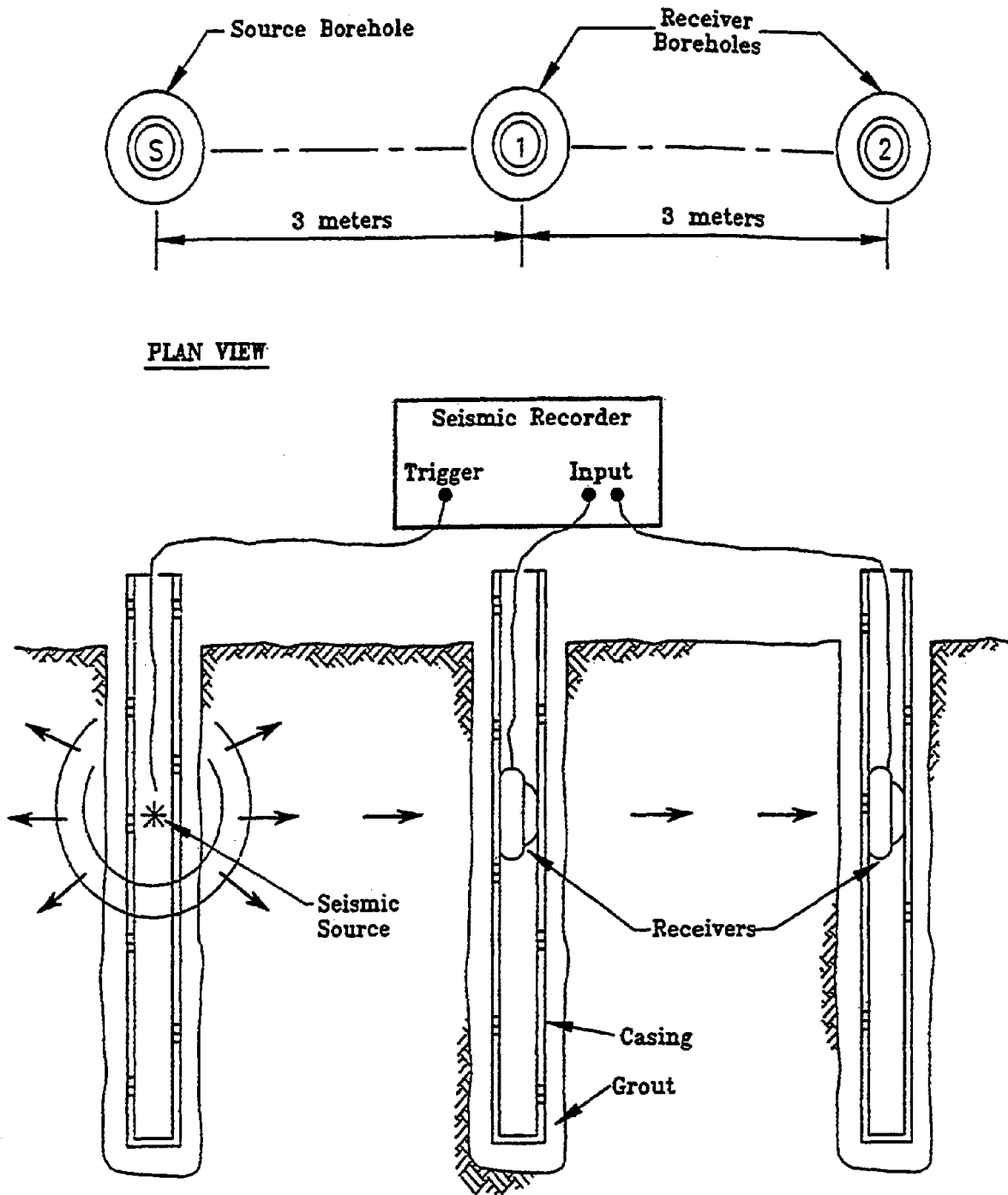


Figure 5-8: Schematic Sketch of Cross Hole Survey

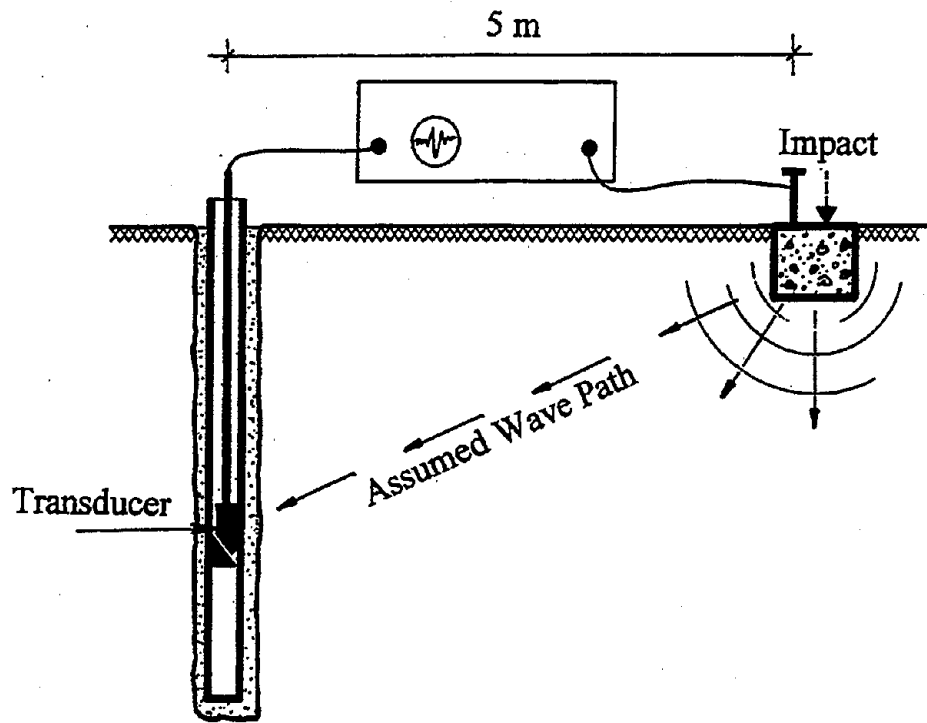


Figure 5-9: Schematic Sketch of Down Hole Survey

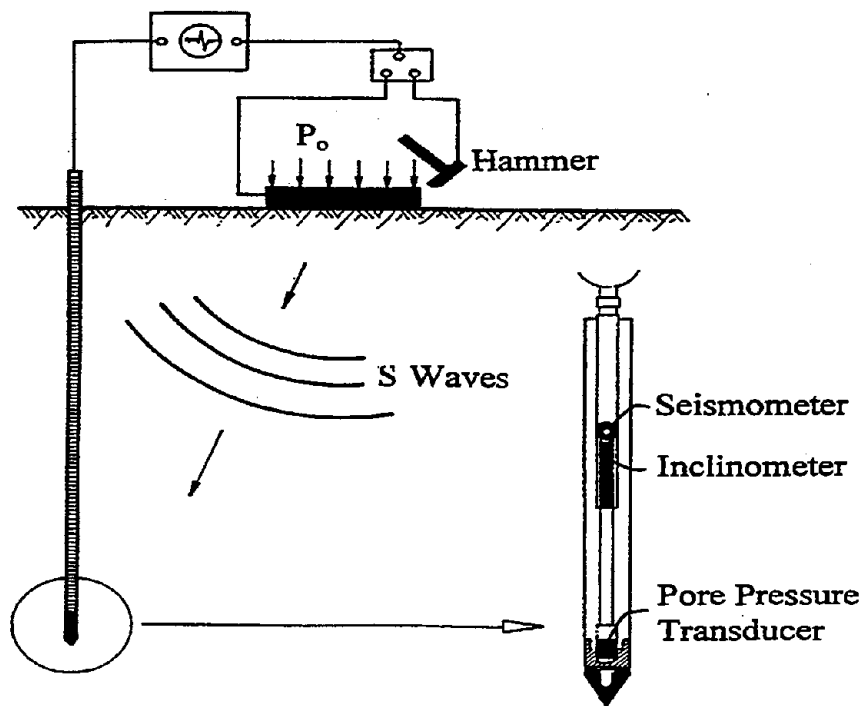


Figure 5-10: Schematic Sketch of Seismic Cone Penetration Testing (SCPT).

The cross hole technique is generally the preferred technique for a borehole survey as it offers the highest resolution and greatest accuracy. However, cross hole measurements require a very precise evaluation of the distance between the energy source and the detector. An inclinometer reading is generally performed in the boreholes used in a cross hole survey to correct the results for deviation of the boreholes from verticality. Cross hole geophysical testing is codified in ASTM Standard D 4428 and is discussed in Module 1 (Subsurface Investigations).

Seismic Refraction and Seismic Reflection Methods

Seismic refraction and reflection exploration surveys are conducted from the surface and do not require boreholes. The resolution of the methods is relatively poor and decreases with depth. These methods are most suitable as a means of identifying the depth to competent rock and the location of prominent soil horizons that have a large contrast in density and stiffness compared to the overlying soil.

Spectral Analysis of Surface Waves (SASW)

Spectral Analysis of Surface Waves (SASW) is a non-intrusive geophysical technique used primarily for evaluating subsurface shear wave velocity profiles. SASW testing evaluates shear wave velocity indirectly by direct measurement of Rayleigh, or surface wave, velocity. Rayleigh wave velocity is related to shear wave velocity by Poisson's ratio. The two velocities are usually within 5 percent of each other for most soils. SASW results are representative of the average properties of a relatively large mass of material, mitigating the potential for misleading results due to non-homogeneity. SASW can be a very cost-effective method of investigation. The ease and rapidity of field measurements and automated algorithms for data processing and inversion allow for evaluation of subsurface conditions at a relatively large number of points at a fraction of the cost of conventional intrusive exploration techniques.

A schematic representation of SASW testing is presented in Figure 5-11. Excitation at the ground surface is used to generate the Rayleigh, or surface, waves at various frequencies. By spectral analysis of the ground surface response (velocity or acceleration) at two points a known distance apart, the Rayleigh wave velocity can be obtained at discrete frequencies. Usually, an inversion process (trial and error) is used to determine the velocity profile. At sites where wave velocity increases gradually with depth, the velocity profile may be determined directly from the field data. The depth over which reliable measurements can be made depends upon the energy and frequency content of the source excitation and the consistency of the subgrade material. Measurements are not affected by the depth to the water table.

The concept of measuring the velocity of Rayleigh waves of different frequencies to determine the profile of shear wave velocity with depth was first proposed by Jones (1962), in Great Britain, for pavement surveys and by Ballard (1964), at the Waterways Experiment Station in Vicksburg, Mississippi, for geotechnical analyses. These investigators used impact loading as the source excitation and developed an analysis based upon the assumption of a uniform, homogeneous layer. Stokoe and Nazarian (1985) at the University of Texas, Austin, extended the analysis to consider multi-layered media. These investigators also used a surface impact as the source excitation and thus reliable measurements were typically limited to maximum depths on the order of 10 meters by the relatively low energy content of the excitation at relatively long wave lengths.

Satoh and his co-workers (1991) in Japan developed an electro-magnetic controlled vibrator for use as the source excitation. Large (2000 kg) mass, Controlled Source Spectral Analysis of Surface Waves (CSSASW) equipment capable of penetrating over 100 meters below the ground surface has recently been developed. Comparisons between SASW and down hole velocity measurements have been made (Nazarian and Stokoe, 1984) and show good agreement between the two methods.

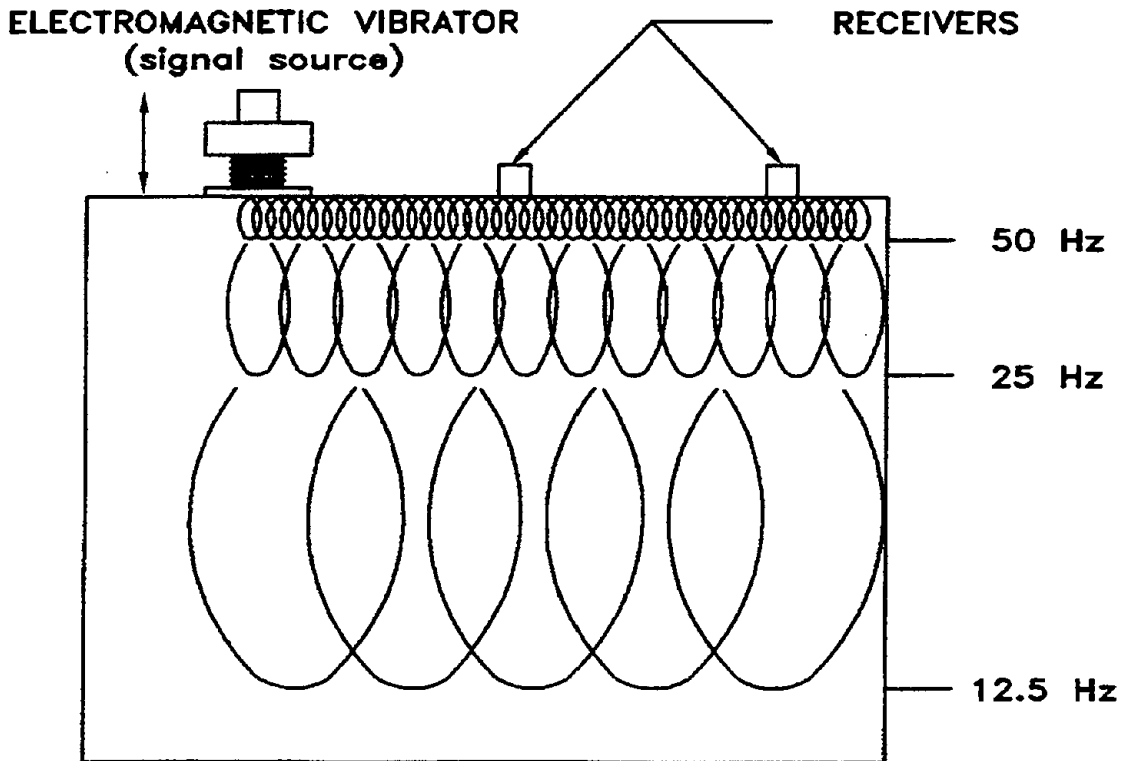
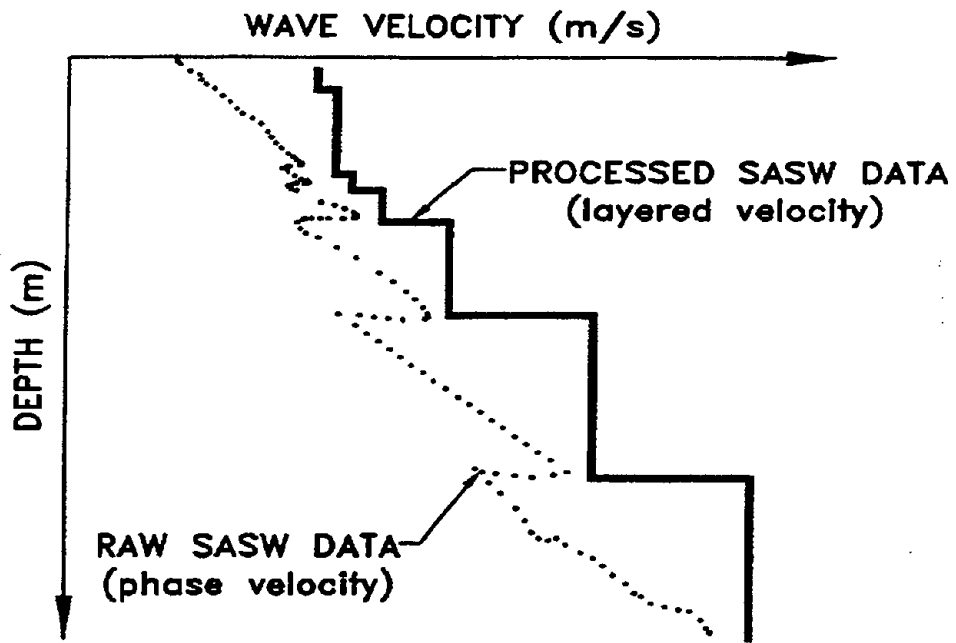


Figure 5-11: Schematics of SASW Testing. (Kavazanjian, *et al.*, 1994) and Stokoe, 1984) and show good agreement between the two methods.

Compressional Wave Velocity

Compressional wave velocity may sometimes be required for seismic analyses. Compressional wave velocity can be directly measured in a bore hole survey or in a laboratory test. Alternatively, the compressional wave velocity can be calculated from the shear wave velocity and Poisson's ratio using Equation 5-5.

5.4.5 Evaluation of Cyclic Stress-Strain Parameters

Laboratory Testing

Laboratory testing for evaluation of cyclic stress-strain parameters of soil is appealing to many engineers because direct measurements are made of the hysteretic stress-strain behavior of soils. However, cyclic laboratory testing is subject to a variety of constraints, including:

- difficulty in reproducing field stresses (or strains);
- difficulty in recovering and testing undisturbed cohesionless soil samples; and
- the time and expense associated with cyclic laboratory testing.

A summary of the different types of cyclic laboratory tests used in geotechnical practice and their advantages and limitations follows. More details on cyclic laboratory testing can be found in Kramer (1996).

Cyclic Direct Simple Shear Test

The cyclic direct simple shear (CyDSS) test may provide the most accurate representation of the stress state resulting from a vertically propagating shear wave in a horizontally layered soil deposit of any laboratory test. The simple shear device consists either of a rectangle box made of hinged plates or a cylindrical wire-reinforced membrane which surrounds the sample and restrains the sample from deforming laterally during the test. The apparatus includes either an arrangement for applying a constant vertical load or for maintaining a constant sample height while measuring the vertical load and a mechanism for applying a horizontal cyclic shear load. The sample is usually formed directly in the simple shear device. However, undisturbed samples of cohesive soil or frozen sand can be tested in the devices that use wire-reinforced membranes.

Cyclic Triaxial Test

The cyclic triaxial test was developed for geotechnical purposes by Seed and his co-workers at the University of California at Berkeley in the 1960s and has been used extensively to evaluate cyclic behavior of soils. The device consists of a regular triaxial cell and a cyclic, often sinusoidal loading machine attached to the loading piston. The sample is isotropically consolidated in the triaxial cell and then subjected to a cyclic axial load in extension and compression. The primary drawback of the cyclic triaxial tests is that it does not provide a good representation of the stress state induced in the ground by an earthquake (see Figure 5-1). The main difference in cyclic triaxial test stress conditions compared to the field conditions are: (1) the laboratory soil sample is isotropically consolidated, whereas the soil is under a K_0 condition in the field; (2) in the field there is a continuous reorientation of the principal stresses whereas in the triaxial test, the reorientation angle is either 0 or 90 degrees; (3) the cyclic shear stress is applied on a horizontal plane in the field but on a 45 degree plane in the triaxial test; and (4) the mean normal stress in the field is constant while the mean normal stress in the laboratory varies cyclically.

Torsional Simple Shear Test

In order to overcome some of the limitations of the CyDSS and triaxial tests, Ishibashi and Sherif (1974) developed a torsional simple shear test. The sample is "doughnut-like" in shape with outer to inner radius and outer to inner height ratios of about two. This doughnut-like shape ensures a relatively uniform shear strain on the horizontal plane throughout the sample. The torsional simple shear test offers several advantages over CyDSS and cyclic triaxial tests:

- simulates closely the field stress (strain) conditions like the CyDSS;
- it is possible to apply vertical and horizontal stresses independently; and
- permits the octahedral normal stress to remain unchanged during the test.

There are also some disadvantages associated with this test:

- interpretation of the results is rather complicated and the definition of liquefaction (Ishibashi and Sherif, 1974) does not permit correlation of torsional simple shear results with those of other tests;
- mobilization of enough interface shear between the sample and the top and bottom plates to prevent slippage may be difficult, however steel pins cast into porous stones will provide good contact between the sample and the plates; and
- the shape of the sample makes the device impractical for use in conventional practice, particularly for undisturbed samples.

Resonant Column Test

The resonant column test for determining dynamic properties of soils is based on the theory of wave propagation in rods. Either compression or shear waves can be propagated through the soil specimen in resonant column testing. Solid or hollow specimens can be used in the apparatus. Either a sinusoidal torque or a vertical compressional load is applied to the top of the sample through the top cap. The deformation of the top of the specimen is measured. The excitation frequency is adjusted until the specimen resonates. The wave velocity or modulus is computed from the resonant frequency and the geometric properties of the sample and driving apparatus. Damping is determined by switching off the current to the driving coil at resonance and recording the amplitude of decay of the vibrations. The decay of the amplitude with time is used to determine the *logarithmic decrement* (the percentage decay over one log cycle of time), which is directly related to the viscous damping ratio.

The primary problem associated with using resonant column tests to measure dynamic soil properties is that the test is generally limited to small to intermediate shear strains by the applied force requirements and resonant frequencies. Furthermore, at larger strains, hollow samples must be used to maintain a relatively constant shear strain across the sample. For these reasons, resonant column testing is primarily used to estimate small strain shear modulus. However, it can also be used to determine modulus reduction and equivalent viscous damping in intermediate strain range.

Use of Empirical Correlations

Parameters describing the cyclic soil properties required for a dynamic analyses include the initial (small strain) damping, λ , the initial (small strain) shear modulus at small shear strain, G_{\max} , and the modulus

reduction and damping curves for the soil. Small strain damping is difficult to evaluate. Therefore, an equivalent viscous damping ratio of 2 to 5 percent is commonly assumed in equivalent-linear analyses, while a viscous damping ratio of 0.5 to 1 percent is commonly assumed in non-linear analyses. The small strain shear modulus, commonly referred to as the *initial shear modulus*, G_{max} , can be obtained from site-specific investigations or by using empirical correlations with index soil properties. Geophysical methods for establishing G_{max} were previously described. Table 5-4 presents the typical range of G_{max} for several generic soil types.

**TABLE 5-4
TYPICAL VALUES OF INITIAL SHEAR MODULUS**

Type of Soil	Small-Strain Shear Wave Velocity, V_s (m/s)	Initial Shear Modulus, G_{max} (kPa)
Soft Clays	40 - 90	2,750 - 13,750
Firm Clays	65 - 140	6,900 - 34,500
Loose Sands	130 - 280	27,600 - 138,000
Dense Sands and Gravel	200 - 410	69,000 - 345,000

The parameter G_{max} has been empirically related to both the SPT N value and CPT point resistance, q_c . Correlations with SPT results by Seed, *et al.* (1984) and Imai and Tonouchi (1982) and with CPT results by Mayne and Rix (1993) are presented in Table 5-5.

Following the initial work of Hardin and Drnevich (1972), many researchers developed empirical relationships to estimate G_{max} of the following general form:

$$G_{max} = A \sigma'_m{}^{1/2} OCR^k f(e) \quad (5-11)$$

where $f(e)$ is some function of the void ratio, e , OCR is the overconsolidation ratio, A is a normalizing constant, k is the power factor, and σ'_m is the mean normal effective stress obtained as:

$$\sigma'_m = \left[\frac{1+2K_o}{3} \right] \sigma'_v \quad (5-12)$$

where σ'_v is the vertical effective stress and K_o is the coefficient of lateral earth pressure at rest.

Seed and Idriss (1970) developed a series of curves relating G_{max} to relative density and mean normal effective stress through a coefficient, $(K_2)_{max}$:

$$G_{max} = 1000 (K_2)_{max} (\sigma'_m)^{1/2} \text{ in psf} \quad (5-13)$$

$$G_{max} = 220 (K_2)_{max} (\sigma'_m)^{1/2} \text{ in kPa} \quad (5-14)$$

**TABLE 5-5
CORRELATIONS FOR ESTIMATING INITIAL SHEAR MODULUS**

Reference	Correlation	Units	Limitation
Seed, <i>et al.</i> (1984)	$G_{\max} = 220 (K_2)_{\max} (\sigma'_m)^{1/2}$ $(K_2)_{\max} \approx 20(N_1)_{60}^{1/3}$	kPa	$(K_2)_{\max} \approx 30$ for very loose sands and 75 for very dense sands; $\approx 80-180$ for dense well graded gravels; Limited to cohesionless soils
Imai and Tonouchi (1982)	$G_{\max} = 15,560 N_{60}^{0.68}$	kPa	Limited to cohesionless soils
Hardin (1978)	$G_{\max} = \frac{625}{(0.3 + 0.7 e_0^2)} (P_a \cdot \sigma'_m)^{0.5} \text{OCR}^k$	kPa ⁽¹⁾⁽³⁾	Limited to cohesive soils P_a = atmospheric pressure
Jamiolkowski, <i>et al.</i> (1991)	$G_{\max} = \frac{625}{e_0^{1.3}} (P_a \cdot \sigma'_m)^{0.5} \text{OCR}^k$	kPa ⁽¹⁾⁽³⁾	Limited to cohesive soils P_a = atmospheric pressure
Mayne and Rix (1993)	$G_{\max} = 99.5 (P_a)^{0.305} (q_c)^{0.695} / (e_0)^{1.13}$	kPa ⁽²⁾	Limited to cohesive soils P_a = atmospheric pressure

Notes: ⁽¹⁾ P_a and σ'_m in kPa

⁽²⁾ P_a and q_c in kPa

⁽³⁾ The parameter k is related to the plasticity index, PI , as follows:

PI	k
0	0
20	0.18
40	0.30
60	0.41
80	0.48
> 100	0.50

where $(K_2)_{\max}$ is a function of relative density and soil type (see Table 5-5). This approach has been further extended to estimate stress-dependent modulus reduction curves for sandy soils using the strain dependent parameter K_2 instead of $(K_2)_{\max}$. An example of a curve relating K_2 to shear strain is shown in Figure 5-12. Iwasaki, *et al.* (1978) found that the mean normal effective stress is the predominant factor that governs the modulus reduction of cohesionless soils and developed stress dependent curves shown in Figure 5-13. Note that the authors did not provide damping curves.

Vucetic and Dobry (1991) have shown that the relationships between modulus reduction and cyclic shear strain and between equivalent viscous damping and cyclic shear strain can, with a relatively high degree of confidence, be reduced to a set of curves that depend on the plasticity index, PI, of the soil. The Vucetic and Dobry modulus reduction and damping curves are presented in Figure 5-14. Note that the curves for PI equal to zero apply to sands, gravels, and other cohesionless soil. The Vucetic and Dobry PI = 0 damping curve may be used in conjunction with the Iwasaki, *et al.* (1978) stress-dependent modulus reduction curve to characterize the dynamic behavior of sandy soils.

The modulus reduction curves shown on Figures 5-12, 5-13, and 5-14 end at a shear strain level of 1 percent. In areas of high seismicity (e.g., California) cyclic strains in soils may exceed 1 percent. If necessary, modulus reduction curves can be extended to shear strain levels larger than 1 percent using a procedure developed by CALTRANS and elaborated upon in Jackura (1992).

5.4.6 Peak and Residual Shear Strength

The peak shear strength of soil not subject to strength degradation under cyclic loading may be evaluated using conventional methods, including laboratory and in situ testing and correlations with soil index properties. A key difference in seismic problems compared to static problems is that undrained strength parameters are typically used for the strength of saturated soils subjected to cyclic loading, even for cohesionless soils (e.g., sands, gravels) because of the relatively rapid rate of earthquake loading.

The dynamic undrained shear strength of a soil may be influenced by the amplitude of the cyclic deviator stress, the number of applied loading cycles, and the plasticity of the soil. For saturated cohesionless soils, even relatively modest cyclic shear stresses can lead to pore pressure rise and a significant loss of undrained strength. However, Makdisi and Seed (1978) point out that substantial permanent strains may be produced by cyclic loading of clay soils to stresses near the yield stress, while essentially elastic behavior is observed for large numbers of (>100) cycles of loading at cyclic shear stresses of up to 80 percent of the undrained strength. Therefore, these investigators recommend the use of 80 percent of the undrained strength as the "dynamic yield strength" for soils that exhibit small increases in pore pressure during cyclic loading, such as clayey materials, and partially saturated cohesionless soils.

Evaluation of the potential for shear strength reduction in a saturated or almost saturated cohesionless soil (low plasticity silt, sand, or gravel) subjected to dynamic loading may require sophisticated cyclic laboratory testing. Alternatively, a residual strength may be assigned to the soil based upon either undrained laboratory tests or in situ test results.

The residual shear strength after cyclic loading is of critical importance in assessing the post-liquefaction stability of a foundation or earth structure. Saturated soils which liquefy typically possess some "residual" shear strength even when in the liquefied state. In initially loose soils, this residual strength may be very small and of little consequence. In initially dense soils, particularly in dense granular soils which tend to

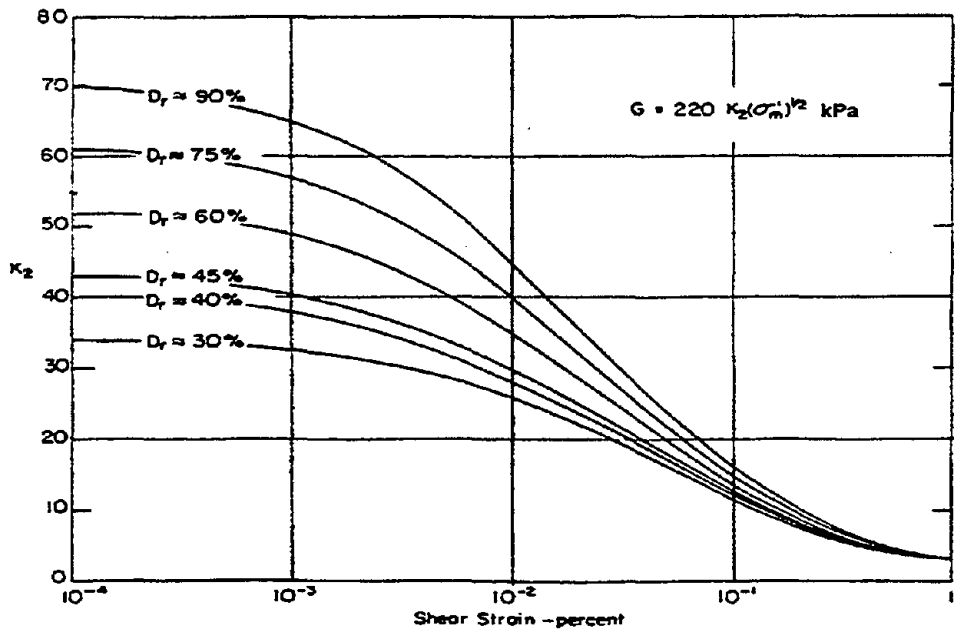
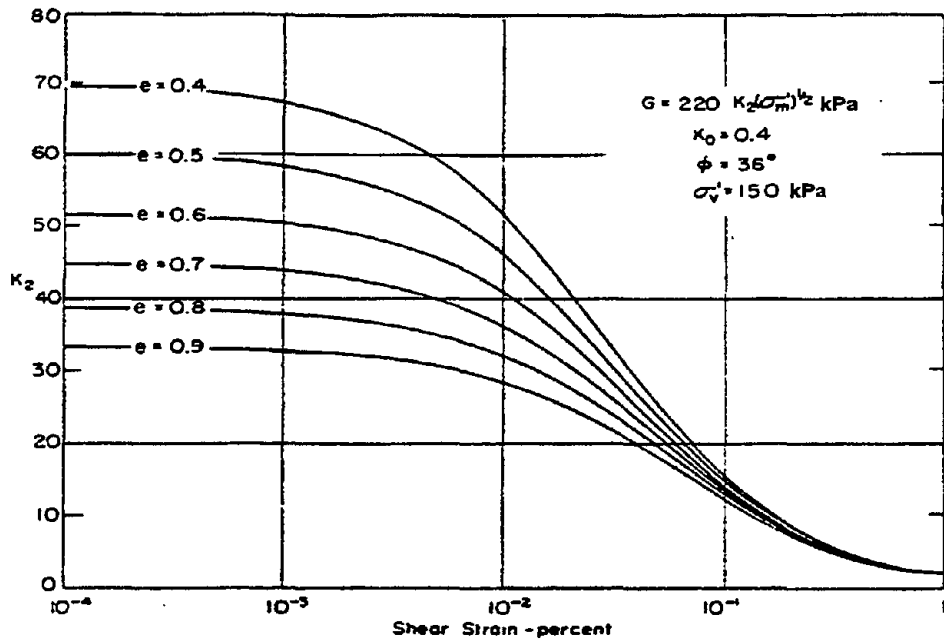


Figure 5-12: Shear Modulus Reduction Curves for Sands. (Seed and Idriss, 1970, reprinted by permission of ASCE)

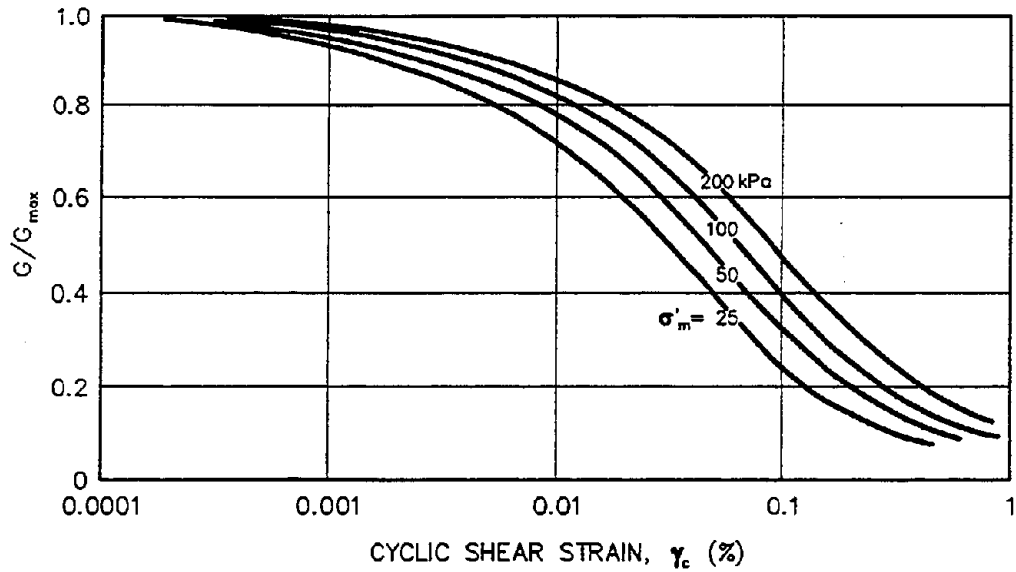


Figure 5-13: Shear Modulus Reduction Curves for Sands. (Iwasaki, *et al.*, 1978, reprinted by permission of Japanese Society of Soil Mechanics and Foundation Engineering)

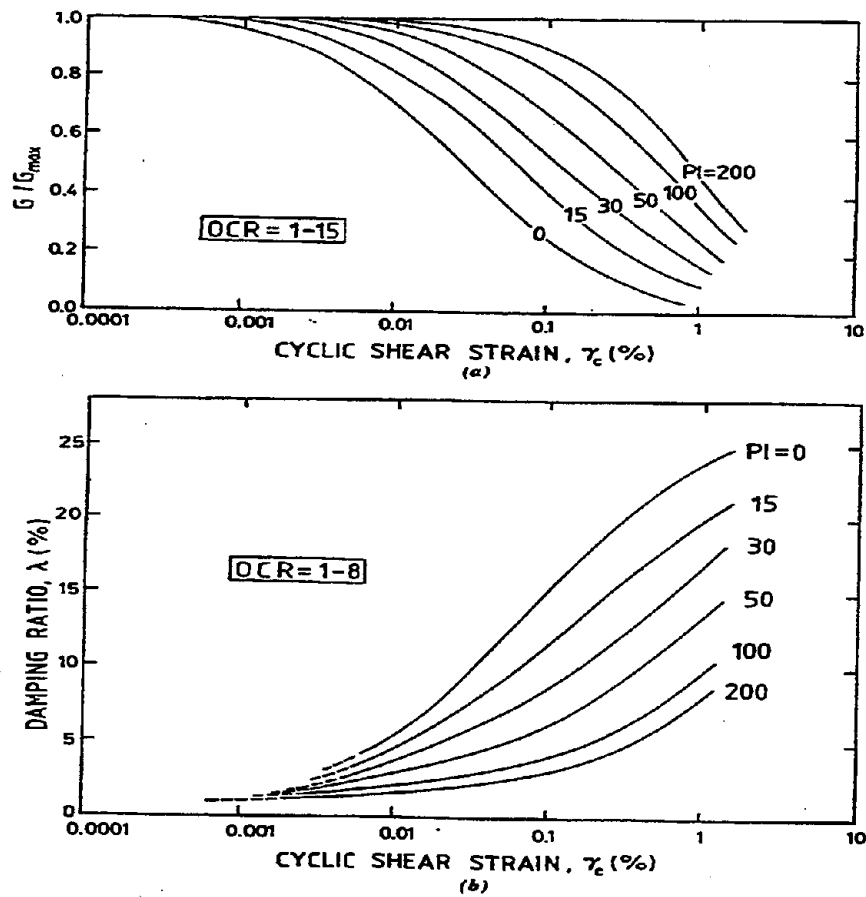


Figure 5-14: Shear Modulus Reduction and Damping Ratio as a Function of Shear Strain and Soil Plasticity Index. (Vucetic and Dobry, 1991, reprinted by permission of ASCE)

dilate, or expand in volume, when sheared, this residual strength can be significant and of great consequence in acting as a stabilizing force subsequent to liquefaction.

The *steady-state* shear strength, S_{su} , governs the behavior of liquefied soil. Poulos, *et al.* (1985) proposed a methodology for evaluation of the in situ S_{su} based on obtaining high-quality soil samples with minimal disturbance. The high-quality samples were tested in the laboratory and the laboratory strengths were then adjusted for field conditions using specially developed techniques to correct the resulting laboratory S_{su} values for effects of void ratio changes due to sampling, handling, and test set-up. Due to the very high sensitivity of S_{su} to even small changes in void ratio, the laboratory techniques proposed by Poulos, *et al.* presently do not appear to represent a reliable basis for engineering analyses unless very conservative assumptions and high factors of safety are employed to account for the considerable uncertainties involved.

Because of difficulties in measuring steady-state strength in the laboratory, Seed (1987) proposed an alternate technique for evaluation of in situ undrained residual shear strength based on the results of SPT testing. He back analyzed a number of liquefaction-induced failures from which residual strength could be calculated for soil zones in which SPT data was available, and proposed a correlation between *residual strength*, S_r , and $(N_1)_{60-cs}$. $(N_1)_{60-cs}$ is a "corrected" normalized standardized SPT blow count, as discussed in Section 5.4.2, with a correction, N_{corr} , for fines content to generate an equivalent "clean sand" blow count as:

$$(N_1)_{60-cs} = (N_1)_{60} + N_{corr} \quad (5-15)$$

where N_{corr} is a function of percent of fines. Recommendations for selecting N_{corr} are given in the insert of Figure 5-15. Since there is no guarantee that all the conditions for steady-state of deformation were satisfied in the case histories used to develop Figure 5-15, the term residual strength is used instead of steady-strength. Note that the fines correction on Figure 5-15 is not the same "fines" correction as is used in the liquefaction susceptibility analyses (see, e.g., Figure 8-5).

Figure 5-15 presents an updated and revised version of the Seed (1987) residual shear strength correlation developed by Seed and Harder (1990). Due to scatter and uncertainty and the limited number of case studies back analyzed to date, it is recommended that the lower-bound curve and the average $(N_1)_{60-cs}$ from all borings be used to estimate S_r . If lower bound, rather than average, $(N_1)_{60-cs}$ values are used, S_r may reasonably be estimated based upon the average of the lower and upper bound curves in Figure 5-15.

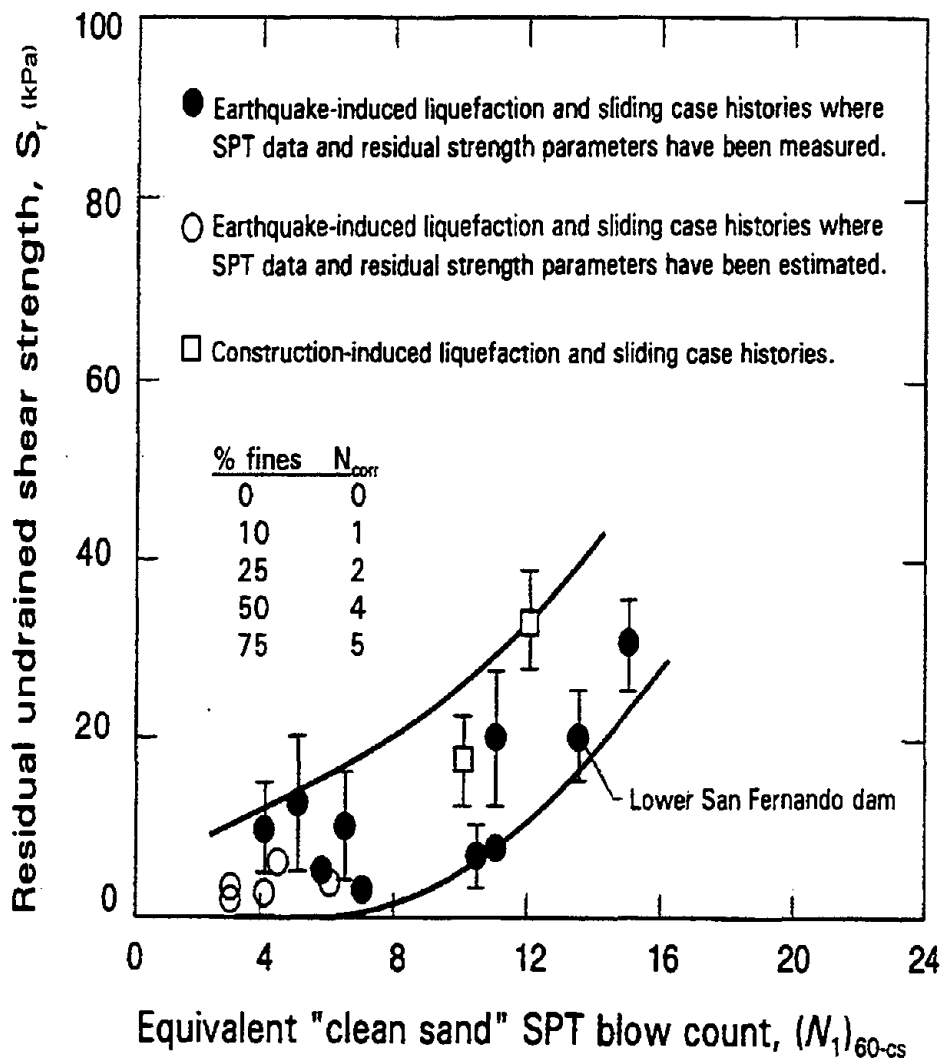


Figure 5-15: Relationship Between Corrected "Clean Sand" Blow Count $(N_1)_{60-cs}$ and Undrained Residual Strength (S_r) from Case Studies. (Seed and Harder, 1990)

CHAPTER 6.0

SEISMIC SITE RESPONSE ANALYSIS

6.1 GENERAL

The local soil profile at a project site can have a profound effect on earthquake ground motions. Local soil conditions can affect the intensity, frequency content, and duration of strong shaking. Amplification of peak bedrock acceleration by a factor of four or more and amplification of spectral accelerations by a factor of ten or more have been attributed to the response of the local soil profile to the bedrock ground motions.

The influence of local soil conditions on seismic ground motions can be assessed either in a gross empirical manner (using “soil-site” attenuation relationships, seismic hazard maps for soil sites, and/or code-prescribed response spectra for soil sites) or by conducting a site-specific seismic site response analysis. The choice of the approach to employ is usually a discretionary decision of the design engineer and depends on a variety of factors, including local seismicity, local soil conditions, type of facility, and the importance of the project. For major projects and critical facilities, when an analysis more accurate than a gross empirical analysis is desired, and for deep deposits of soft clay and other Special Study soil sites (see UBC, 1997 and Table 4-3), a site-specific site response analysis is usually warranted. A site-specific response analysis can be performed for foundation soils, for earthen embankments, or for the coupled response of foundation soil and an embankment, as discussed in the remainder of this chapter.

6.2 SITE-SPECIFIC SITE RESPONSE ANALYSES

Site-specific seismic site response analyses are generally based upon the assumption of a vertically propagating shear wave through uniform horizontal soil layers of infinite lateral extent. The assumption of that shear waves propagate vertically to the ground surface is, in general, a valid engineering assumption, as even if a shear wave is not propagating vertically at depth it will refract into a near vertical position as it approaches the ground surface. This refraction is due to the general decrease in shear wave velocity with decreasing distance from the ground surface, as illustrated in figure 6-1. This phenomenon is similar to the refraction of water waves at the beach such that they usually approach the shore with their crest aligned parallel to the shore line. The influence of vertical motions, compression waves, laterally non-uniform soil conditions, incoherence and spatial variation of ground motions are typically not accounted for in conventional seismic site response analyses. Evaluation solely of the impact of vertically propagating shear waves in a site response analysis is consistent with common design and code practices. It is also consistent with geotechnical engineering analyses for liquefaction potential and seismic slope stability, which consider only the horizontal component of the seismic motions. Three different levels of site-specific seismic site response analysis are available to the geotechnical engineer.

- simplified (empirical) analysis;
- equivalent-linear one-dimensional site response analyses; and
- advanced one- and two-dimensional site response analyses.

These three levels of site response analysis are discussed in detail in the remainder of this chapter.

6.3 SIMPLIFIED SEISMIC SITE RESPONSE ANALYSES

For screening purposes and preliminary analyses, the influence of local soil conditions on seismic site

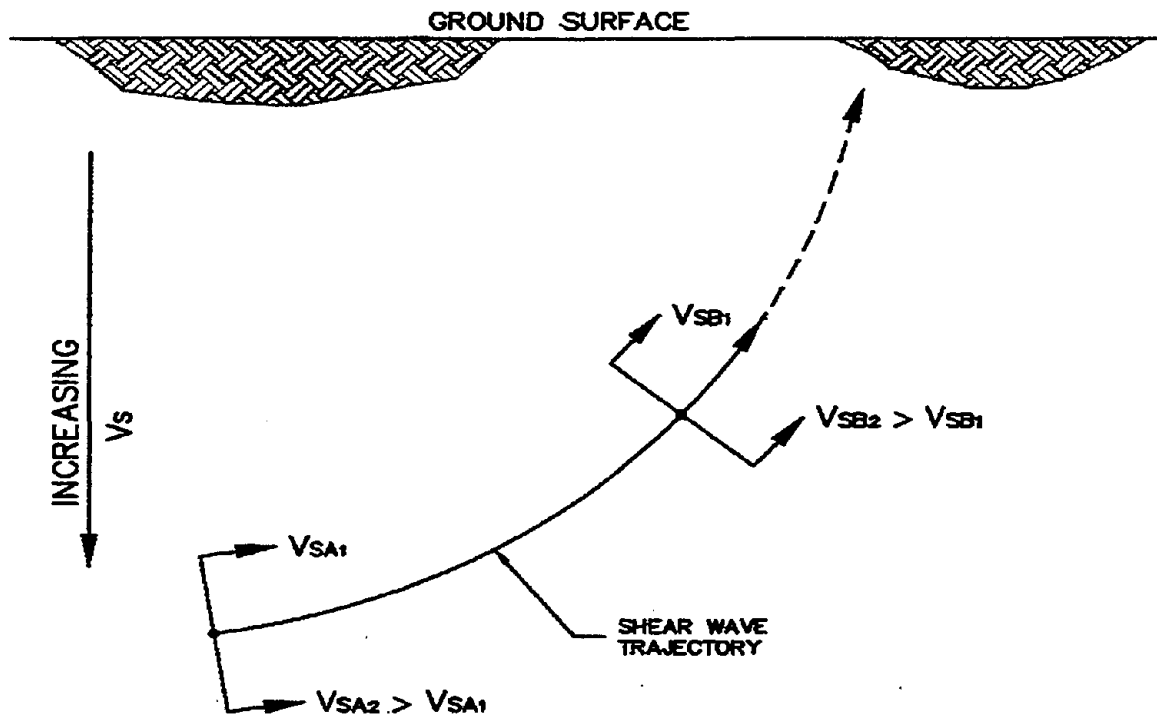


Figure 6-1: Refraction of Near Surface S-Waves

response can be assessed in a simplified manner using empirical relationships which correlate ground motions at rock sites to those at soil sites. These relationships, developed on the basis of both observations of ground motions in earthquakes and one-dimensional site response analysis, provide amplification factors that can be used to provide a rough estimate of the *free-field* (i.e., not affected by structure and/or topography) peak ground acceleration at soft and stiff soil sites from the free-field rock site peak ground acceleration determined in a seismic hazard analysis. Empirical relationships for the amplification of peak ground acceleration by earthen embankments have also been developed.

Whereas structural analyses typically require information on the spectral content of ground motions, and thus require a complete time history to characterize the design motion, geotechnical analyses frequently only require knowledge of either the peak ground acceleration or a combination of peak ground acceleration and earthquake magnitude. Earthquake magnitude and the peak acceleration at a hypothetical bedrock outcrop at the project site are generally evaluated as part of the seismic hazard analysis (see Chapter 3). Several investigators have developed empirical relationships between the peak ground acceleration at a hypothetical bedrock outcrop at the project site to the peak ground acceleration at a specific site as a function of the local soil conditions. The plot on Figure 6-2 shows a relationship developed by Seed and Idriss (1982) for soft soil and stiff soil site conditions. This plot was developed using SHAKE, a computer program for equivalent-linear one-dimensional site response analyses described in greater detail in Section 6.4.

Experience from recent earthquakes has shown that the curves shown on Figure 6-2 may significantly under-predict site amplification effects in many situations. Figure 6-3 shows an updated site amplification

relationship for free-field soft soil sites developed by Idriss (1990). This updated plot yields peak acceleration values significantly greater than the soft soil site curve from the 1982 Seed and Idriss plot. The updated plot was developed by Idriss (1990) from both SHAKE analyses and field observations of soft soil site response in recent earthquakes.

Figure 6-4 presents a comparison of peak acceleration values recorded at the base (usually bedrock) of several earthen dams and the corresponding transverse peak acceleration at the crest (Harder, 1991). Figure 6-4 indicates that larger amplification effects may be expected in earthen structures than at free-field soft soil sites due to two-dimensional effects. Note, however, that Figure 6-4 only applies to the transverse acceleration of embankments. For the longitudinal acceleration of embankments (e.g., for end slopes) and for the transverse acceleration of cut slopes, amplification effects may be expected to be significantly smaller than indicated by Figure 6-4.

The free-field soft soil site amplification curve presented in Figure 6-3 and the embankment response observational data presented in Figure 6-4 may be used in a simplified three- or four-step site response

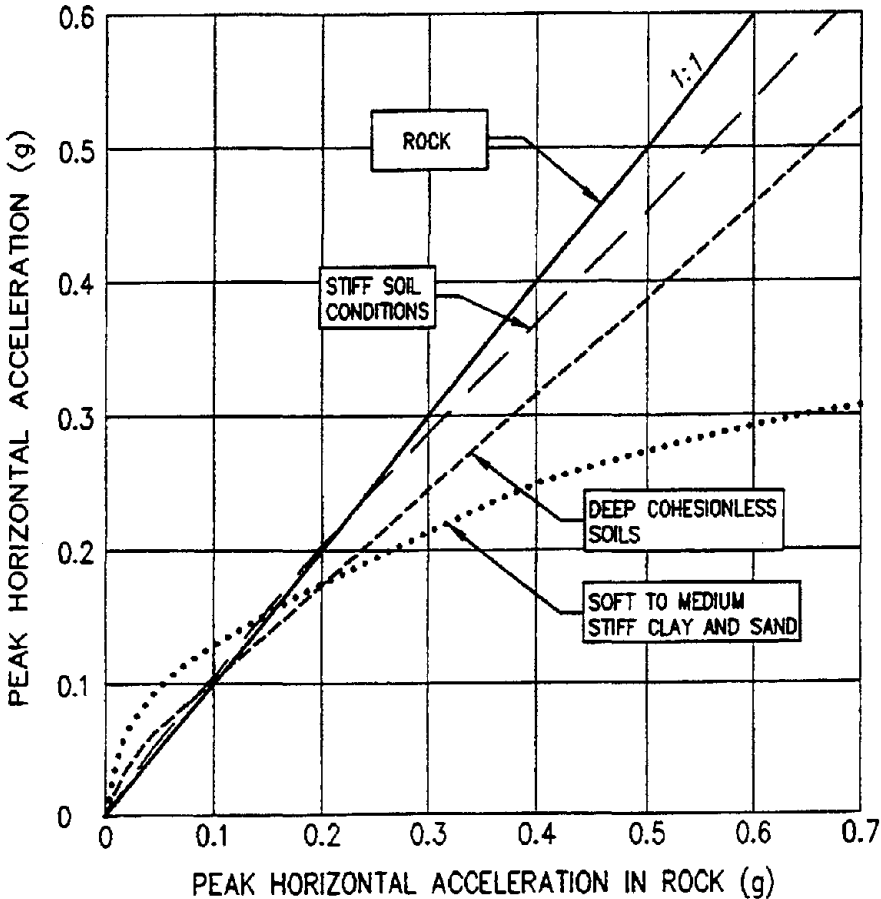


Figure 6-2: Relationship Between PHGA on Rock and on Other Local Site Conditions. (After Seed and Idriss, 1982, reprinted by permission of EERI)

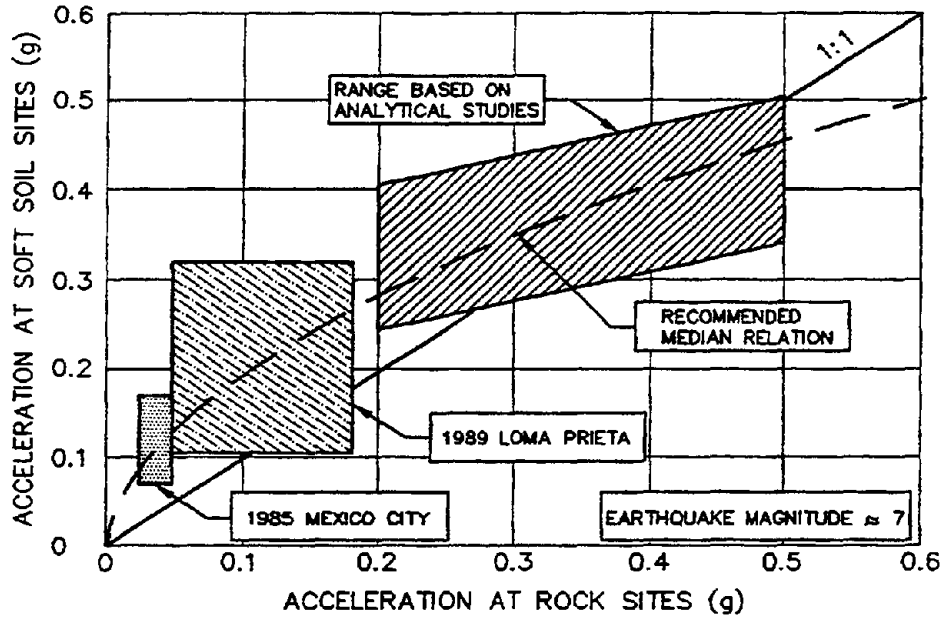


Figure 6-3: Relationship Between PHGA on Rock and on Soft Soil Sites. (Idriss, 1990)

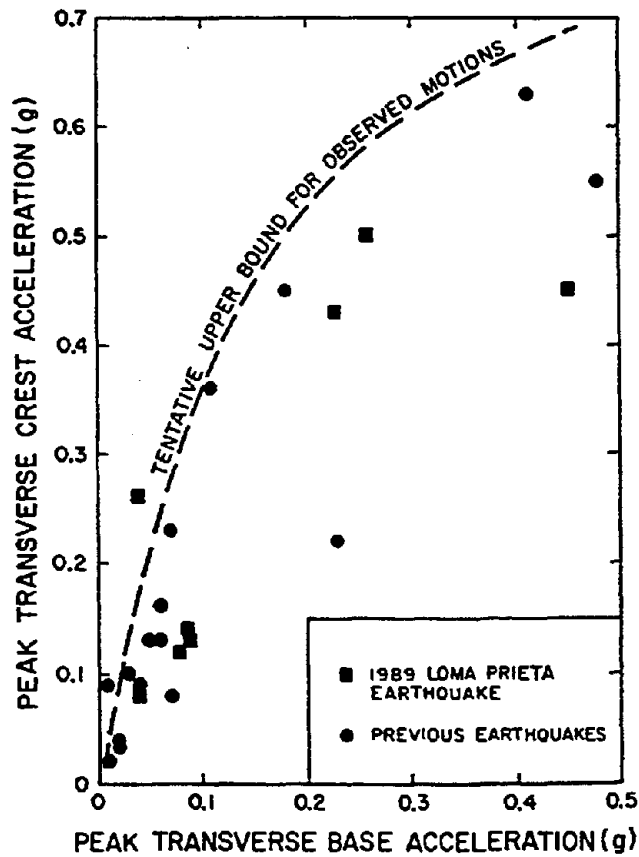


Figure 6-4: Comparisons of Peak Base and Crest Accelerations Recorded at Earth Dams. (Harder, 1991)

analysis procedure to account for the influence of local soil conditions and earthen embankments on the peak ground acceleration at a project site. The three- or four-step procedure, depending on whether an embankment is present, is as follows:

- Step 1: *Classify the site.* Using Table 4-3 (UBC, 1997), classify the site as a Special Study, soft, medium stiff, stiff, or rock on the basis of the average shear wave velocity for the top 30 meters of soil.
- Step 2: *Estimate the hypothetical free-field bedrock acceleration at the site.* Using one of the methods discussed in Chapter 3, estimate the free-field peak ground acceleration at a hypothetical bedrock outcrop at the project site.
- Step 3: *Estimate the free-field acceleration at the site.* Estimate the potential amplification of the hypothetical bedrock peak ground motion by the local soil conditions based upon the soil profile classification. For soft soils, use the curve shown on Figure 6-3 recommended by Idriss (1990). For medium stiff and stiff soil sites, for all acceleration levels, assume the free-field peak ground acceleration at the site is equal to the peak rock site acceleration. For Special Study soil sites, Figures 6-2 and 6-3 should not be used. Instead, site specific seismic response analyses such as those described in the next section of this chapter should be conducted.
- Step 4: *Estimate the peak acceleration at the top of the embankment.* Estimate the potential amplification of the peak acceleration at the top of the embankment, if an embankment is present, using the free-field peak soil acceleration derived in Step 3 and the earth dam amplification curve in Figure 6-4.

Step 4 in the procedure presented above is based upon a simplified, “decoupled” assumption that the peak acceleration at the base of the embankment is the same as the free-field peak acceleration, thereby ignoring interaction between the embankment mass and the ground. Analyses of the coupled response of embankments and foundation soils indicates that this simplified, decoupled analysis usually yield a conservative upper bound estimate of the acceleration at the base of the embankment (Bray, *et al.*, 1995). However, in general, this simplified approach is intended only to give a rough estimate of amplification effects at a site and is not intended for use in final design of highway facilities. The design engineer should decide if this approach is appropriate for the intended purpose or, if it is necessary to perform a more sophisticated analysis.

The peak acceleration at the top of an embankment estimated in Step 4 may also be used in preliminary analyses for various highway ancillary structures and for structures constructed on top of embankment fill. This acceleration is not, however, the appropriate peak acceleration for use in seismic stability and deformation potential calculations for an embankment mass or for bridge abutments. For these calculations, the *average acceleration* of the assumed failure mass, and not the acceleration at the top of the embankment, should be used. The average acceleration is directly proportional to the seismically-induced inertia forces and thus is the relevant response quantity. The peak average acceleration is always less than the peak ground acceleration due to spatial averaging.

For a given embankment height, h , and peak acceleration at the top of the embankment, a_{\max} , the peak average acceleration, k_{\max} , may be estimated at any elevation y within an embankment from the Makdisi and Seed (1978) chart. This chart, developed on the basis of one- and two-dimensional equivalent-linear site response analyses of earth dams, is shown on Figure 6-5. The Makdisi and Seed curve of Figure 6-5

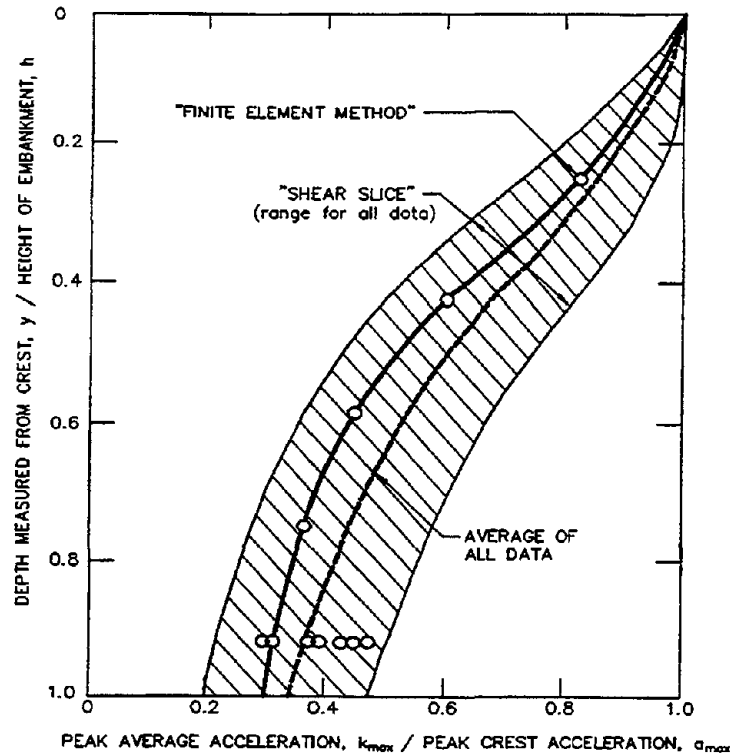


Figure 6-5: Variation of Peak Average Acceleration Ratio with Depth of Sliding Mass. (Makdisi and Seed, 1978, reprinted by permission of ASCE)

should not be used to evaluate the peak average acceleration for cut slopes and end slopes. For cut slopes and end slopes, the engineer should either do a formal response analysis or should use the r_d factor presented in Equation 8.2 and Figure 8.2 in Chapter 8 to estimate the peak average acceleration from the peak ground acceleration.

6.4 EQUIVALENT-LINEAR ONE-DIMENSIONAL SITE RESPONSE ANALYSES

When an analysis more accurate than the simplified analysis presented above is desired, a formal seismic site response analysis can be performed. Equivalent-linear one-dimensional analysis is by far the most common method used in engineering practice to analyze seismic site response. Even if a two-dimensional embankment or slope is to be analyzed, a one-dimensional response analysis can be used. Experience with response analyses of earth dams has shown that one-dimensional response analysis of vertical columns of soil within a two-dimensional earth structure provide a reasonable approximation of the two-dimensional response (Vrymoed and Calzascia, 1978).

In a one-dimensional equivalent-linear site response analysis, the soil profile is modeled as a horizontally layered, linear visco-elastic material characterized by an initial (small-strain) shear modulus and an equivalent viscous damping ratio. To account for the non-linear, strain-dependent behavior of soil, the equivalent-linear modulus and equivalent viscous damping ratio are evaluated from the modulus reduction and damping curves (see Chapter 5). The equivalent-linear material properties are evaluated in each iteration at the calculated *effective shear strain level*. The effective shear strain level is usually specified as:

$$\gamma_{\text{eff}} = n \cdot \gamma_{\text{max}} \quad (6-1)$$

where γ_{eff} is *effective strain*, γ_{max} is maximum absolute value of shear strain and n is the *effective strain factor*. Because γ_{eff} is not known prior to the start of the analysis, equivalent-linear response analyses are performed in an iterative manner, using the effective strain from one iteration of the analysis to evaluate the equivalent modulus and viscous damping ratio for the next iteration. Usually 5 to 10 iterations are needed for convergence.

The computer program SHAKE, originally developed by Schnabel, *et al.* (1972) and updated by Idriss and Sun (1992) as SHAKE91, is perhaps the most commonly used computer program for one-dimensional equivalent-linear seismic site response analysis. This program idealizes the site profile as a horizontally layered soil deposit overlying a uniform visco-elastic half-space, as illustrated in Figure 6-6. SHAKE91 is available from the National Information Service for Earthquake Engineering (NISEE) at the University of California at Berkeley for a nominal cost. Basic input to SHAKE91 includes the soil profile, soil parameters, and the input acceleration time history. Soil parameters used in SHAKE91 include the shear wave velocity or initial (small strain) shear modulus and unit weight for each soil layer. Also, curves relating the shear modulus reduction and equivalent viscous damping ratio to shear strain for each soil type are used. Evaluation of representative values for these soil properties is discussed in Chapter 5.

Once the soil profile and material properties have been specified, the only remaining input is the earthquake motion. Selection of representative acceleration time histories for the input motion is discussed in Chapter 4. The acceleration-time history may be input as either the motion at a *hypothetical bedrock outcrop* (most commonly used option because it is congruent with assumptions embedded in attenuation relationships) or at the bedrock-soil interface at the base of the soil column. Results of the analysis provide shear stress-, shear strain-, and acceleration-time histories and peak values for the ground surface, hypothetical bedrock outcrop, and for each layer within the soil profile.

Historically, the value of the effective strain factor used in SHAKE analyses to determine the equivalent-linear modulus and damping has been $n = 0.65$. However, based upon back analysis of strong motion records obtained at soil sites in recent earthquakes, several investigators have proposed that n be related to the earthquake magnitude. Equation 6-2 presents the relationship between earthquake magnitude, M_w , and n as proposed by Idriss and Sun (1992).

$$n = \frac{(M_w - 1)}{10} \quad (6-2)$$

In engineering practice, one-dimensional equivalent linear site response analyses such as those performed using SHAKE or similar computer programs are used for analysis of both one- and two-dimensional site response. Two-dimensional site response is modeled using one-dimensional profile and analysis by taking a series of vertical slices through the two-dimensional profile and analyzing each slice one-dimensionally. Figure 6-7 compares the results of one-dimensional equivalent linear site response analyses of vertical columns through a two-dimensional profile, expressed in terms of the maximum earthquake-induced shear stress versus depth, to the results of a two-dimensional equivalent linear analysis. The results from the one-dimensional analysis, performed using SHAKE, are generally within 5 to 10 percent of results of the two-dimensional analysis, performed using the computer program QUAD-4.

While it is relatively easy to set up SHAKE and perform a SHAKE analysis, the results of the analysis may be extremely sensitive to the details of the program input. Factors such as the thickness and number of sub-layers, selection of appropriate input motions, the digitization interval of the input time history, the "cut-off" frequency (the highest frequency used in the Fourier transformation of the input motion), the shear wave velocity and unit weight of the underlying half-space, and whether the input motion is specified

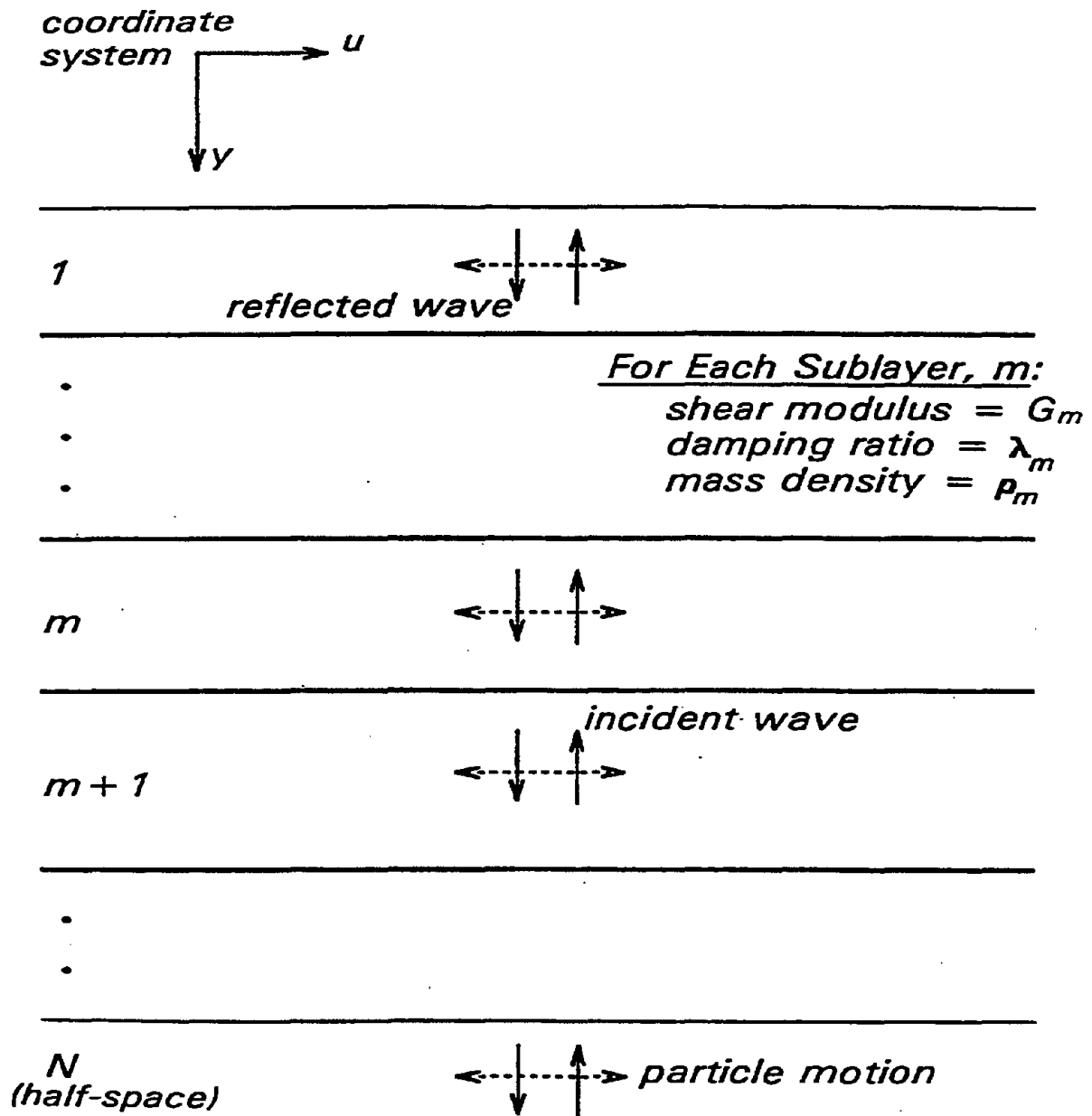


Figure 6-6: 1-Dimensional Column for SHAKE Analysis (Schnabel et al., 1972)

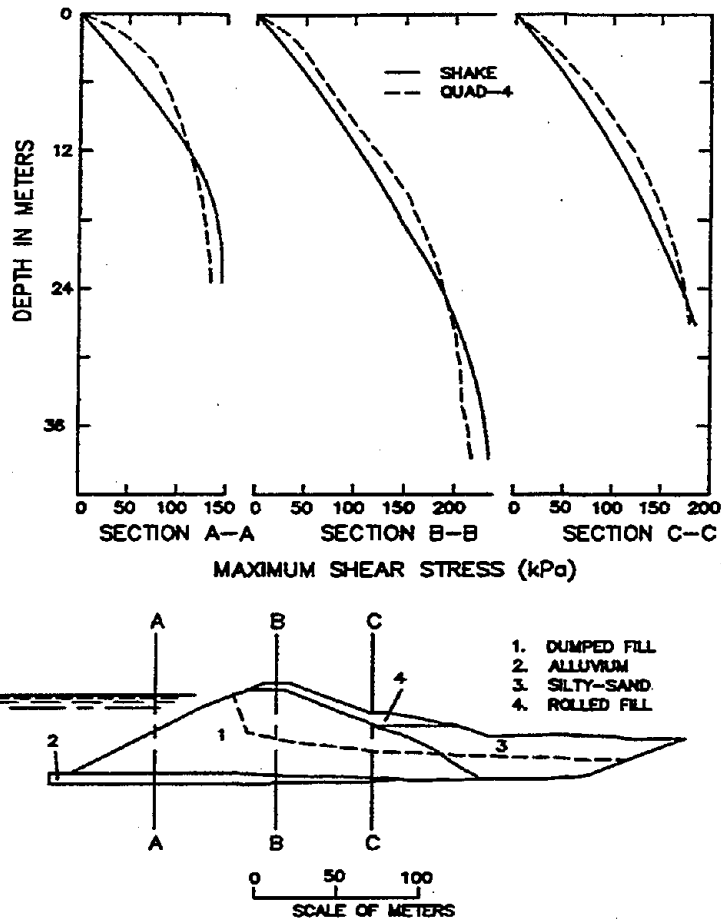


Figure 6-7: 1-Dimensional Analysis for 2-Dimensional Response

as a within profile motion or outcrop motion can significantly affect program output. Therefore, it is recommended that all formal seismic response analyses should be performed by, or at a minimum reviewed by, a qualified geotechnical professional familiar with the program being used and the problem being analyzed and experienced in seismic response analysis.

6.5 ADVANCED ONE- AND TWO-DIMENSIONAL SITE RESPONSE ANALYSES

6.5.1 General

An advanced seismic site response analysis may be necessary if one or more of the following project-specific conditions exists: (1) the project is considered important or critical (e.g., a "lifeline" structure); (2) irregular boundary conditions must be modeled; (3) the project includes an embankment founded on Special Study soils; and (4) an analysis more accurate than a one-dimensional equivalent-linear site response analysis is desired. Depending on the particular situation, either one-dimensional non-linear or two-dimensional equivalent-linear or non-linear site response analyses may be employed.

6.5.2 One-Dimensional Non-Linear Site Response Analyses

The primary difference between non-linear and equivalent-linear site response analyses is that non-linear analyses use a more realistic model to represent the behavior of soil subjected to cyclic loads. Essentially, a non-linear model traces the evolution of the hysteresis loops generated in a soil by cyclic loading in a

sequential manner, whereas the equivalent-linear model only approximates the representative soil stiffness and damping over the entire sequence of cyclic loads. The more realistic representation of the non-linear behavior of cyclically-loaded soils gives non-linear analyses a significant advantage over equivalent-linear seismic response analyses at higher levels of seismic shaking where non-linear effects tend to dominate.

In general, equivalent-linear site response analyses are considered unreliable at ground shaking levels in excess of 0.4 g (see Ishihara, 1986) or if calculated peak shear strains exceed approximately 2 percent. However, non-linear site response analyses are also subject to limitations. The material models used in non-linear site response analyses often require parameters for which readily obtainable or published values do not exist. Furthermore, computer programs for non-linear site response analysis are not readily available to the general engineering community. Therefore, even though non-linear site response analyses typically provide a more accurate and more versatile representation of seismic behavior, equivalent-linear site response analyses and other approximate solutions still dominate highway engineering practice.

The computer program DESRA-2, originally developed by Lee and Finn (1978), and its descendants, are perhaps the most commonly used computer programs for performing total stress, one-dimensional non-linear seismic site response analysis. Basic input to DESRA-2 includes the soil profile, parameters of the Kondner and Zelasko (1963) constitutive model, and the input time history of ground motions. The Kondner-Zelasko constitutive model uses a hyperbola to describe the backbone curve of the hysteresis loop. The backbone curve of a soil element is drawn by connecting the tips of the hysteresis loops generated during uniform cyclic loading. Hysteresis loops are generated from the backbone curve based upon the assumption of Masing (1926) behavior during cyclic loading. Parameters required for the Kondner-Zelasko (1963) model are the shear modulus at small strains and the shear strength of the soil. However, as noted by several researchers (see e.g., Ishihara, 1986), the relatively simple Kondner-Zelasko model can not accurately simulate the cyclic behavior of soil in the small shear strain range (i.e., for shear strain levels less than 0.1 percent).

Various derivative codes of DESRA-2 are also in use. In several of these codes, modifications have been made to improve the accuracy of the Kondner-Zelasko constitutive model at small strains. Chang, *et al.*, (1991) developed the computer program MARDES to study nonlinear ground response at a liquefied site in Taiwan. MARDES uses the three-parameter Martin-Davidenkov (Martin, 1975) constitutive model which enables a more accurate description of non-linear soil behavior than the Kondner-Zelasko model. Matasović (1993), while studying pore water pressure generation in saturated clay deposits, developed the computer program D-MOD. D-MOD employs a Modified Kondner and Zelasko (M-K-Z) constitutive model (Matasović and Vucetic, 1993) that also provides a better description of the actual soil behavior than the Kondner-Zelasko model. The M-K-Z parameters can be directly evaluated by curve-fitting of modulus reduction and damping curves. Li, *et al.* (1992) developed a computer program, SUMDES, which enables calculation of the seismic response of soil deposits subjected to multi-directional shaking. Computer programs with non-linear soil models can also be used for evaluation of pore pressure generation and liquefaction potential and of the impact of pore pressure generation on site response in an effective stress analysis.

6.5.3 Two-Dimensional Site Response Analyses

A variety of finite element and finite difference computer programs are available for use in two-dimensional seismic site response analyses. The computer program QUAD4, originally developed by Idriss and his co-workers (Idriss, *et al.*, 1973) and recently updated as QUAD4M by Hudson, *et al.* (1994), is among the most commonly used computer programs for two-dimensional site response analysis. QUAD4M uses an equivalent-linear soil model similar to the model used in SHAKE. Basic input to

QUAD4M includes the two-dimensional soil profile, equivalent-linear soil properties, and the time history of horizontal ground motion. Time history of vertical ground motion may also be applied at the base of the soil profile. The base can be modeled as a rigid boundary, with design motions input directly at the base, or as a *transmitting boundary* which enables application of ground motions as hypothetical rock outcrop motions. With respect to the input soil properties, QUAD4M is very similar to SHAKE91. However, the ability to analyze two-dimensional geometry and the option for simultaneous base excitation with horizontal and vertical acceleration components make QUAD4M a more versatile analytical tool than SHAKE91.

A major difference between the QUAD4M and SHAKE91 equivalent-linear models is that the damping ratio in QUAD4M depends on the frequency of excitation or rate of loading. In QUAD4M, the equivalent-linear viscous damping ratio is used to fix the frequency dependent damping curve at the natural frequency of the soil deposit in order to optimize the gap between model damping and the damping ratio. A major drawback of QUAD4M is its limited pre- and post-processing capabilities. These limited capabilities make finite element mesh generation and processing and interpretation of the results difficult and time consuming. QUAD4M is available from the National Information Service for Earthquake Engineering (NISEE) at University of California at Berkeley for a nominal cost.

Other two-dimensional equivalent-linear seismic site response analysis computer programs that are available to the public include program TELDYN (Pyke, 1995) and FLUSH (Lysmer, *et. al.*, 1975). TELDYN is an enhanced version of the original QUAD4 which can also be run in a nonlinear mode and is fully supported by its developer. FLUSH is a versatile frequency-domain program equipped with transmitting boundaries which enable calculations with a mesh of smaller size and a "quasi" three-dimensional analysis option. Because of the quasi three-dimensional analysis capabilities, FLUSH is popular for use in soil-structure interaction problems and for analyses of major earth dams.

Computer programs are also available for truly non-linear two-dimensional seismic site response analyses (e.g., Prevost, 1981; Finn, *et. al.*, 1986; Cundall and Board, 1988; Muraleetharan, *et. al.*, 1991; Bardet, 1992). However, these programs are not particularly "user-friendly" and usually require involvement of the developers to establish the parameters of constitutive models and boundary conditions. Therefore, such programs are not commonly used in geotechnical engineering practice.

CHAPTER 7.0 SEISMIC SLOPE STABILITY

7.1 BACKGROUND

The design, construction and maintenance of soil slopes in highway embankments and cuts are discussed in detail in Module 3 (Soil Slopes and Embankments). In this chapter, the seismic stability and deformation analysis of soil slopes are discussed in detail.

The ground accelerations associated with seismic events can induce significant inertia forces that may lead to instability and permanent deformations of natural and man-made slopes and embankments. There are, in general, two different but related methods used to evaluate the seismic stability of slopes and embankments in conventional geotechnical practice: (1) the seismic coefficient-factor of safety approach; and (2) the permanent seismic deformation approach. Both of these approaches to seismic stability assessment employ pseudo-static limit equilibrium analysis.

An essential element in both seismic coefficient-factor of safety analyses and permanent seismic deformation analyses to assess seismic slope stability is limit equilibrium slope stability analyses. In a pseudo-static limit equilibrium analysis, the earthquake inertia forces are represented by static loads applied at the center of gravity of each "slice" through the potential failure mass. Numerous limit equilibrium methods and procedures are currently available to evaluate static slope stability (Duncan, 1992). Most of these methods are, in some form, also suitable for pseudo-static seismic stability analysis. Pseudo-static limit equilibrium analyses required for both seismic coefficient and permanent seismic deformation analyses are generally carried out using the same model of the slope used in the static stability analysis. The cross sections are often reinterpreted using appropriate dynamic shear strength parameters. However, even if the cross section doesn't change, the search for the critical surface, i.e., the surface with the lowest factor of safety or yield acceleration, may have to be repeated because the critical surface from the static analysis is not necessarily the same as the critical surface for the dynamic analysis.

A wide variety of commercially available computer programs exist that can perform both static and pseudo-static limit equilibrium analyses. Most of these programs provide general solutions to slope stability problems with provisions for using the simplified Bishop, simplified Janbu, and/or Spencer's method of slices. Potential sliding surfaces, both circular or polygonal, can usually be pre-specified or randomly generated. Commonly used programs include PCSTABL4 (Carpenter, 1985) and PCSTABL5 (Achilleos, 1988) developed at Purdue University, UTEXAS3 (Wright, 1995) developed at the University of Texas at Austin, XSTABL (Sharma, 1994) developed at University of Idaho, Moscow, and SLOPEW distributed by Geo-Slope International.

In principle, pseudo-static limit equilibrium analysis can be performed using either a total or an effective stress analysis. Problems of estimating pore pressures induced by cyclic shearing are avoided by using a total stress analysis. The typical Corps of Engineers practice for pseudo-static stability analyses in sandy soils is to use a composite shear strength envelope based on consolidated drained (CD) test results at low confining pressures ("S" envelope) and on consolidated undrained (CU) test results at high confining pressures ("R" envelope), as shown on Figure 7-1. This strength envelope, which conservatively takes into account any possible dissipation of shear-induced negative pore pressures that might occur in the field in stiff clays and dense sands, is recommended for pervious soils. For soils of low permeability, in which undrained conditions are more likely to exist during an earthquake, a CU strength envelope is appropriate.

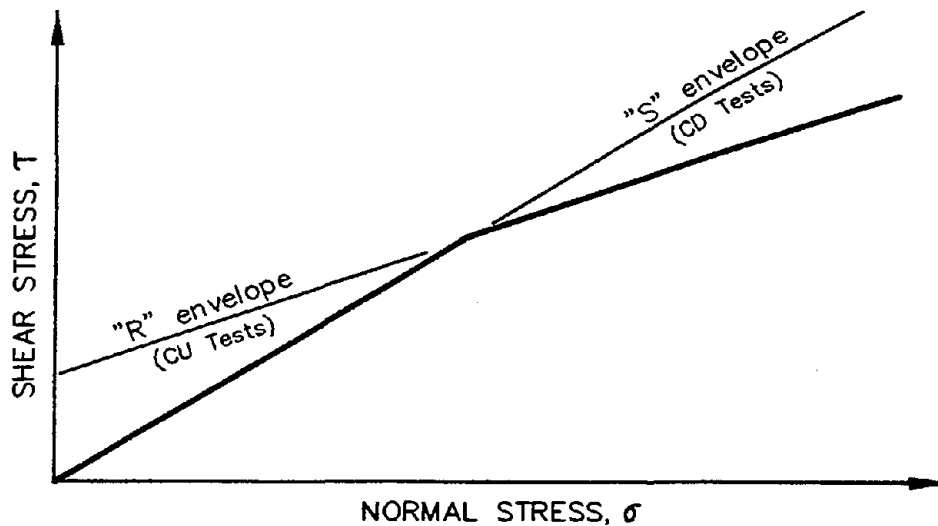


Figure 7-1: Composite Shear Strength Envelope.

In the seismic coefficient - factor of safety approach to pseudo-static limit equilibrium analysis, a seismic coefficient is used to represent the effect of the inertia forces imposed by the earthquake upon the potential failure mass. An allowable factor of safety is associated with the seismic coefficient in such a way that the behavior of the slope is within the range considered acceptable, i.e., the slope or embankment will experience acceptable deformation in the design earthquake. The seismic coefficient, k_s , is a dimensionless constant. The main drawback of the seismic coefficient - factor of safety approach lies in the difficulty of directly relating the value of the seismic coefficient to the characteristics of the design earthquake. Therefore, a considerable amount of conservatism is usually built into seismic coefficient - factor of safety analyses. Use of either the peak ground acceleration PGA, or the peak average horizontal acceleration of the failure mass, k_{max} , as the seismic coefficient (expressed as a function of gravity, i.e., $k_s = k_{max}/g$) in conjunction with a pseudo-static factor of safety of 1.0 has been shown to give excessively conservative assessments of slope performance in earthquakes. However, little guidance on selection of the seismic coefficient as a fraction of the peak acceleration is available to the engineer.

In contrast to the seismic coefficient-factor of safety approach, the permanent seismic deformation approach involves the explicit calculation of cumulative seismic deformation. In this approach, the potential failure mass is treated as a rigid body on a yielding base. The acceleration time history of the rigid body is assumed to correspond to the average acceleration time history of the failure mass. Deformation accumulates when the rigid body acceleration exceeds the yield acceleration of the failure mass, k_y , where k_y is defined as the horizontal acceleration that results in a factor of safety of 1.0 in a pseudo-static limit equilibrium analysis. The method, most commonly used for calculating the permanent seismic deformation of a slope or embankment, is termed the *Newmark method* (Newmark, 1965).

In a Newmark analysis, relative displacement is usually assumed to accumulate in only one direction, the downslope direction. Using this assumption, the yield acceleration in the other (upslope) direction is implicitly assumed to be larger than the peak acceleration of the failure mass being analyzed. Furthermore, vertical accelerations are typically ignored in a Newmark analysis.

For practical purposes, the seismic coefficient - factor of safety and permanent seismic deformation approaches may be combined into a unified seismic slope stability and deformation analysis, as discussed in Section 7.4.

7.2 SEISMIC COEFFICIENT - FACTOR OF SAFETY ANALYSES

7.2.1 General

The traditional pseudo-static limit equilibrium method of seismic stability analysis is illustrated in Figure 7-2. Simplifications made in using the pseudo-static approach to evaluate seismic slope stability include replacing the cyclic earthquake motion with a constant horizontal acceleration equal to $k_s \cdot g$, where k_s is the seismic coefficient, and g is acceleration of gravity, and assuming that this steady acceleration induces an inertia force $k_s W$ through the center of gravity of the potential failure mass, where W is the weight of the potential failure mass.

One of the most common questions asked about the traditional pseudo-static approach to limit equilibrium analysis is the impact of ignoring the vertical acceleration in the analysis. However, ignoring the vertical acceleration has been shown to be a reasonable engineering assumption. In general, studies have shown that application of a vertical pseudo-static force in limit equilibrium analysis will change the horizontal yield acceleration by no more than 10 percent as long as the vertical pseudo-static force is less than or equal to the horizontal pseudo-static force. This phenomenon is illustrated in Figure 7-3. Whether the change in the horizontal yield acceleration is an increase or decrease depends upon the direction of the vertical force. Vertical ground motions are generally out of phase with and of different frequency than horizontal ground motions. Therefore, the vertical pseudo-static force is as likely to be acting up on the potential failure mass as it is to be acting down when the inertia force is acting in a destabilizing direction (i.e., out of slope). As the direction of the vertical pseudo-static force is not correlated with direction of the horizontal pseudo-static force, vertical ground motion is as likely to increase the horizontal yield acceleration as it is to decrease it and whatever change does occur will be relatively small. On this basis, the net effect of vertical accelerations on a pseudo-static limit equilibrium analysis can reasonably be ignored.

In the seismic coefficient-factor of safety approach to pseudo-static stability analyses, the engineer attempts to select a seismic coefficient and allowable factor of safety such that the cumulative permanent deformation in the design earthquake is small enough to be acceptable. The seismic coefficient is always less than the peak average acceleration of the failure mass and the factor of safety is typically between 1.0 and 1.2. The reason the seismic coefficient is always less than the peak average acceleration is as follows: Earthquakes produce ground motions that in turn induce inertia forces of an alternating nature in slopes or embankments. The alternating inertia forces are of short duration and change direction many times. Therefore, even though the factor of safety during a cycle of earthquake loading may fall below one, it will usually remain below one for only a very brief period of time, until the load reverses. During the interval when the factor of safety is below one, permanent displacement will accumulate. However, only limited displacements will occur during the interval because of its short duration. Therefore, even though the seismic coefficient is less than the peak average acceleration of the failure mass, the cumulative deformation that occurs over the entire earthquake will be small provided the seismic coefficient and factor of safety are selected appropriately.

To perform pseudo-static slope stability analyses, estimates of the unit weight and the dynamic shear strength parameters of the various soils in the slope cross section are needed. Such data can be obtained directly through laboratory or in situ tests, from data in the literature, or evaluated indirectly through back analyses of representative case histories. The reader is referred to Chapter 5 for details on evaluation of the shear strength of soils subjected to seismic loading.

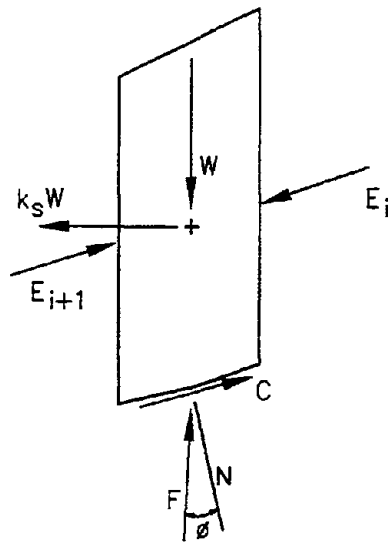
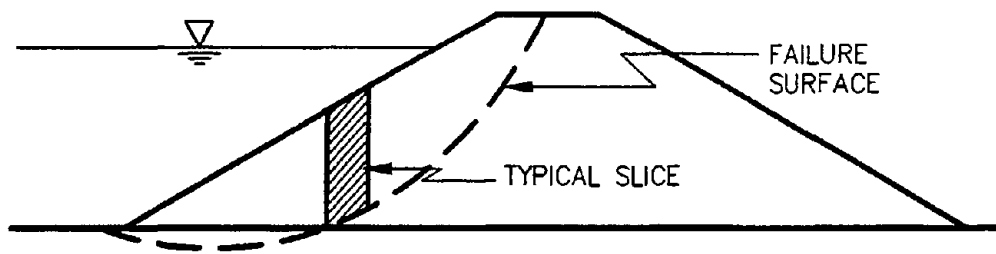


Figure 7-2: Pseudo-static Limit Equilibrium Analysis for Seismic Loads.

7.2.2 Selection of the Seismic Coefficient

A major difficulty in the application of the seismic coefficient-factor of safety approach to seismic stability analysis arises from the fact that there are many different views on how to define the seismic coefficient (Seed and Martin, 1966; Seed, 1979; Marcuson, 1981; Hynes and Franklin, 1984). In many building codes, empirical values based on judgement and experience are used ($k_s = 0.1$ to 0.25 is typical in the United States; $k_s = 0.15$ to 0.25 is typical in Japan). Seed (1979) reports that clay slopes and embankments with a pseudo-static factor of safety of 1.15 using a seismic coefficient of 0.15 have experienced "acceptable" deformations in earthquakes of magnitude as great as 8.5 subjected to peak acceleration levels as great as 0.75 g. Seed's definition of acceptable deformation appears to include deformations of up to one meter in some cases. Seed (1979) also recommends that, for earthquakes of magnitude 6.5 or less, a seismic coefficient of 0.10 combined with a factor of safety of 1.15 should be used. Seed's definition recognizes the importance of earthquake magnitude in determining the seismic coefficient. Unfortunately, this definition provides no guidance on selection of an appropriate value for k_s , for earthquakes with peak acceleration levels less than 0.75 g.

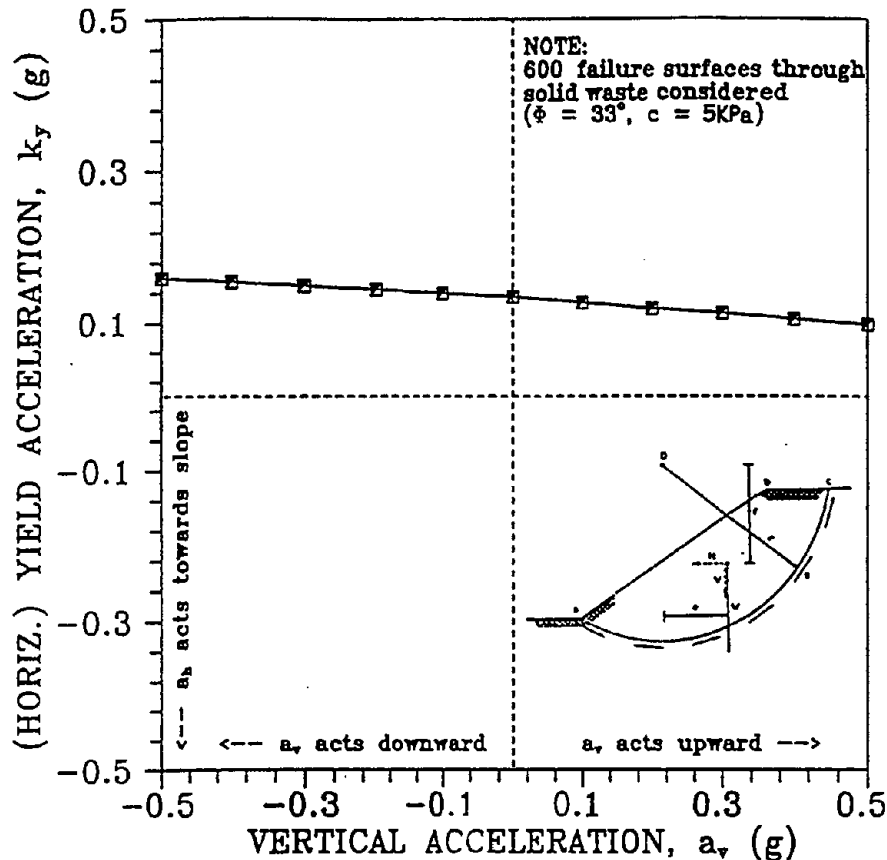


Figure 7-3: Influence of Vertical Seismic Coefficient on Horizontal Yield Acceleration

Other investigators have attempted to relate the seismic coefficient to the peak horizontal ground acceleration without considering earthquake magnitude. Figure 7-4 shows the results of Newmark seismic deformation analyses performed by Hynes and Franklin (1984) using 348 strong motion records (all soil/rock conditions; $4.5 < M_w < 7.4$) and 6 synthetic records. Based upon this data and their experience with seismic response analyses of slopes and embankments, Hynes and Franklin (1984) concluded that slopes and embankments designed with a yield acceleration k_y equal to half the peak ground acceleration a_{max} (i.e., a factor of safety of 1.0 for $k_s = 0.5 \cdot a_{max}/g$) would experience permanent seismic deformations, u , of less than one meter in any earthquake, even for embankments where amplification of peak accelerations by a factor of three occurs. In the absence of amplification, or if amplification is taken into account in determining the peak acceleration, the Hynes and Franklin "upper bound" curve presented in Figure 7-4 suggests that deformations will be less than 0.3 m for yield accelerations greater than or equal to one-half the peak acceleration for all cases. Therefore, based upon the work of Hynes and Franklin, it appears that a value of k_s equal to $0.5 \cdot k_{max}/g$ will limit permanent seismic deformations to less than 0.3 m, where k_{max} is peak horizontal average acceleration of the potential failure mass. The value of k_{max} can be estimated using the methods presented in Chapter 6.

The Hynes and Franklin curves illustrate the influence of the magnitude of the allowable deformation on selection of the seismic coefficient. When using the upper bound curve on Figure 7-4, the value of k_y/k_{max} is 0.17 for 1 m of permanent displacement. Thus, the Hynes and Franklin results indicate that deformations will be limited to less than 1 m if the yield acceleration is greater than 0.17 (approximately 1/6) of the peak average acceleration of the potential failure mass.

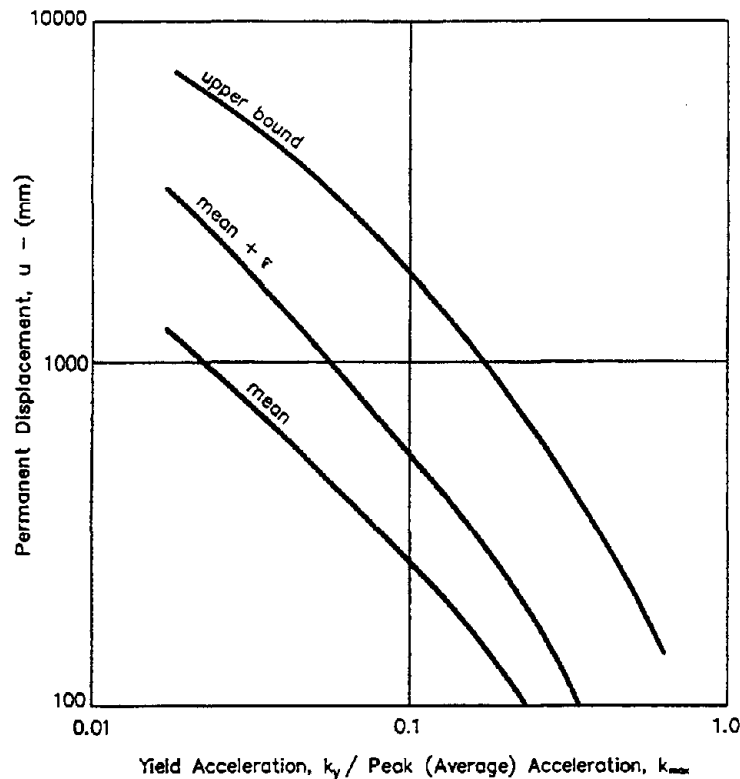


Figure 7-4: Permanent Seismic Deformation Chart. (Hynes and Franklin, 1984, reprinted by permission of U.S. Army Engineer Waterways Experiment Station)

7.3 PERMANENT SEISMIC DEFORMATION ANALYSES

7.3.1 Newmark Sliding Block Analysis

Permanent seismic deformation analyses for slopes and embankment are generally conducted using the Newmark method (1965) in which the failure mass is modeled as a block on a plane. The shearing resistance between the potential sliding mass and the underlying soil, or between the block and the plane, is evaluated in terms of the *yield acceleration*, k_y , the acceleration that will reduce the factor of safety obtained in a pseudo-static analysis to 1.0. The lowest yield acceleration for all possible failure surfaces passing through the slope or embankment should be used in the Newmark analysis.

In contrast to the seismic coefficient - factor of safety approach, the Newmark permanent seismic deformation approach involves the explicit calculation of cumulative seismic deformations. In the Newmark approach, the potential failure mass is treated as a rigid body on a yielding base. The acceleration time history of the rigid body is assumed to correspond to the average acceleration time history of the failure mass. Deformations accumulate when the rigid body acceleration exceeds its yield acceleration.

The calculation of permanent seismic deformations using the Newmark approach is depicted in Figure 7-5. Acceleration pulses in the time history that exceed the yield acceleration are double integrated to calculate cumulative relative displacement. In a Newmark analysis, relative displacement is often assumed to accumulate in only one direction, the downslope direction. With this assumption, the yield acceleration in the other (upslope) direction is implicitly assumed to be larger than the peak acceleration of the failure mass being analyzed. Analyses conducted by Yan, *et al.* (1996) demonstrate that the influence of the

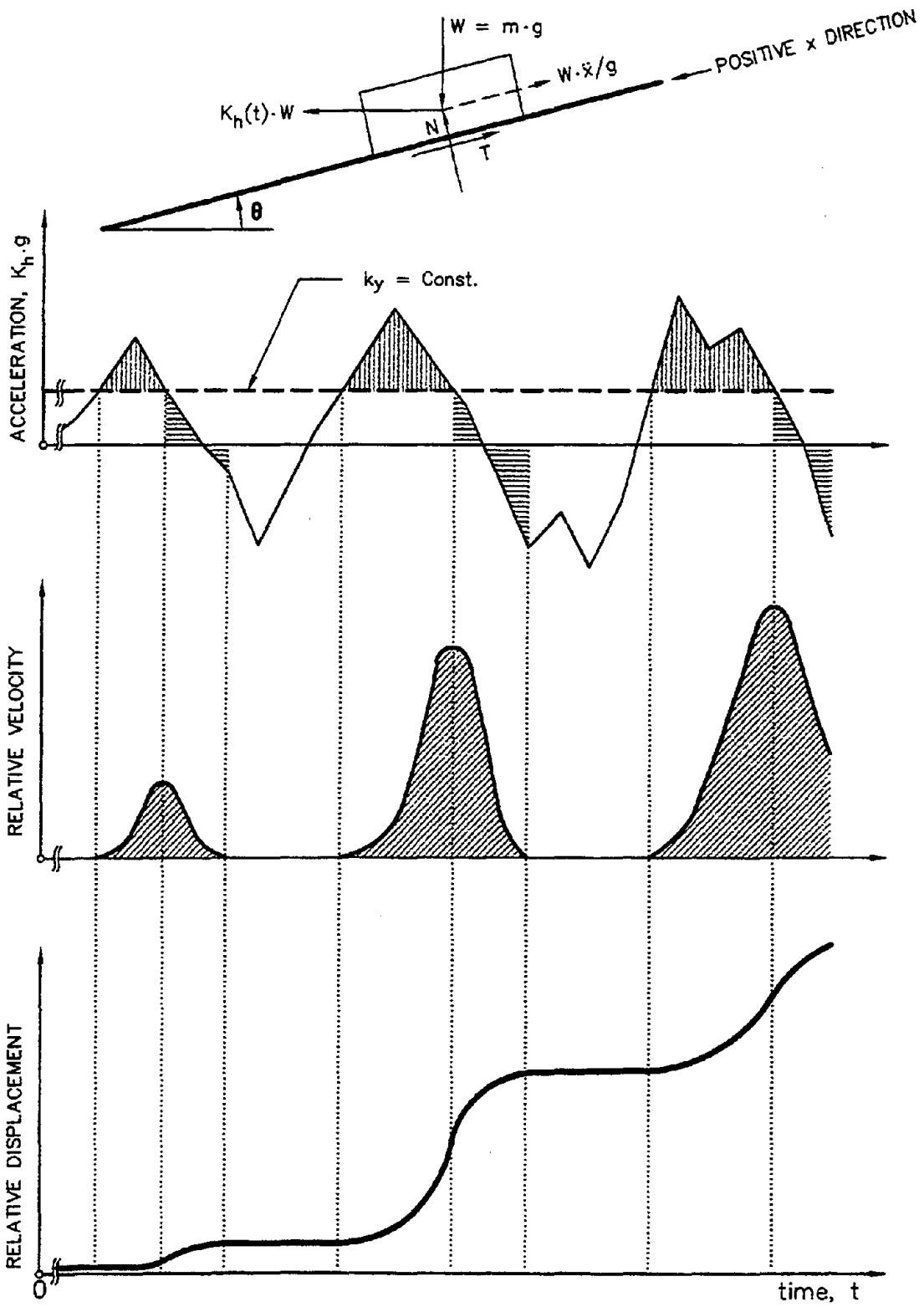


Figure 7-5 Basic Elements of Newmark Deformation Analysis. (Matasović, *et al.*, 1997)

vertical ground motion component in a Newmark analysis is generally relatively small for most situations encountered in practice.

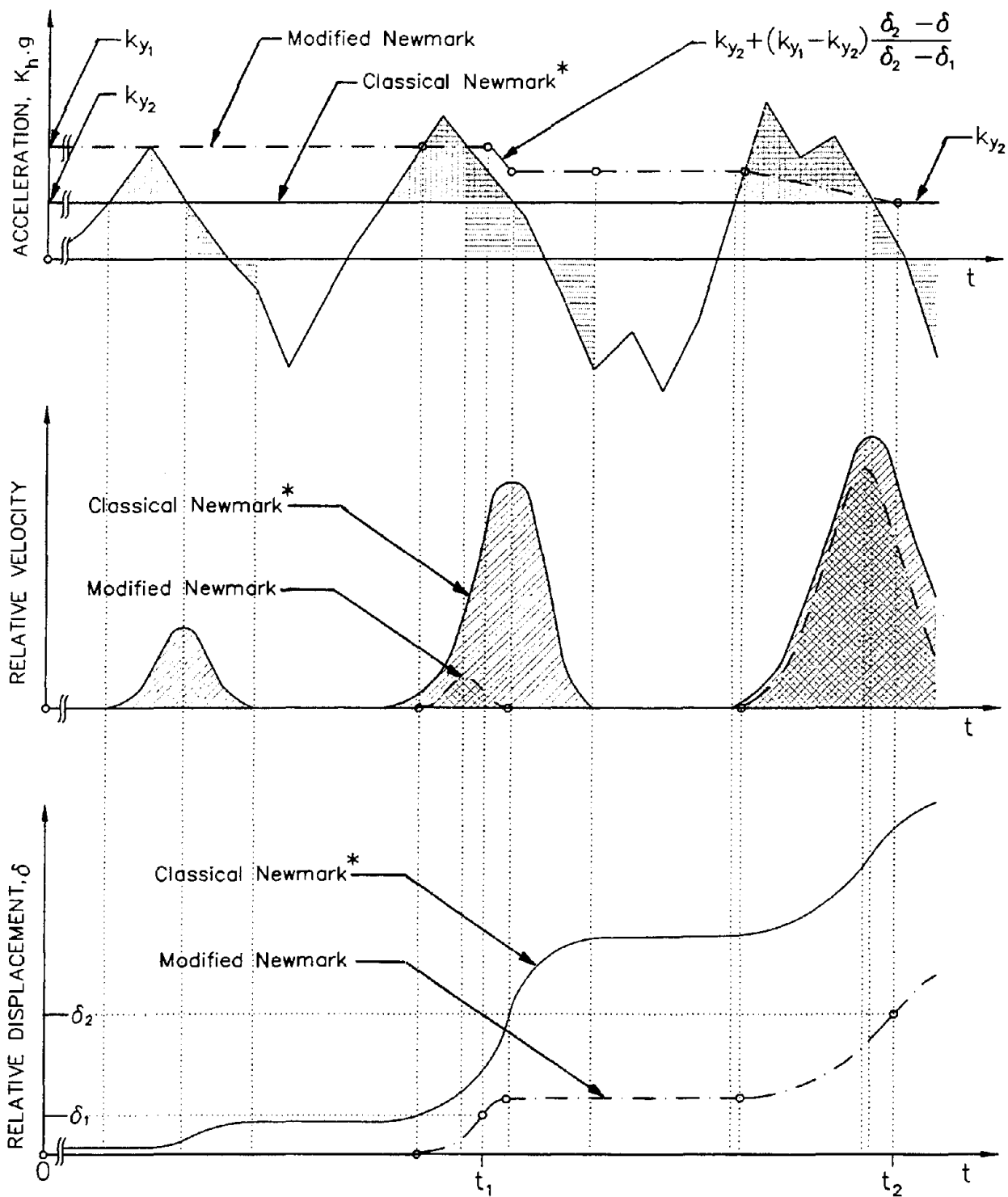
The results of the permanent seismic deformation analysis must be compared to the criterion established for acceptable deformations to determine if seismic performance is satisfactory. The criterion for satisfactory performance may depend on both the system component analyzed and the geometry of the failure surface. Cut slopes may be able to sustain several meters of permanent seismic displacement without jeopardizing the structural components of the highway system. Highway embankments with approach slabs may be able to accommodate substantial deformation perpendicular to the alignment of the approach slab but may not be able to sustain significant deformation parallel to the slab alignment. Establishing how much deformation a system component can accommodate in a seismic event is usually determined by the design engineer.

In using the acceleration time history from a one-dimensional site response analysis as the excitation in a Newmark sliding block analysis, the seismic response of a soil has been decoupled from its permanent seismic deformation. In other words, the influence of yielding and the accumulation of permanent seismic deformation has not been accounted for in the evaluation of the seismic response of the soil mass. Lin and Whitman (1986) have shown that this type of decoupled analysis overestimates seismic deformation by a minimum of 20 percent and by as much as a factor of 2 or 3 when the predominant period of the earthquake motion is close to the resonant period of the soil deposit. The predominant period of the earthquake motion can be determined from the acceleration response spectrum as the period at which the spectral acceleration is a maximum. The *fundamental period* of the soil deposit, T_0 , can be evaluated using Equation 4-5 as $T_0 = 1/f_0$.

While the residual shear strength is typically employed in practice to evaluate the yield acceleration, this common practice is another source of conservatism in permanent seismic deformation analyses. Deformations should not begin to accumulate until the seismic acceleration exceeds the yield acceleration corresponding to the peak shear strength. Furthermore, several centimeters of deformation may have to accumulate before the shear strength (and yield acceleration) fall from peak to residual values. Therefore, particularly for small calculated deformations, the use of residual shear strength to evaluate the yield acceleration for a Newmark deformation analysis can introduce considerable conservatism into the analysis.

Figure 7-6 illustrates the difference between the use of a constant shear strength based on residual strength in a conventional Newmark analysis and the use of a shear strength that degrades from the peak strength to a residual value as deformation accumulates in a modified Newmark analysis. Figure 7-7 compares the results from Newmark analyses using a constant strength equal to the peak strength to those from Newmark analyses using a constant strength equal to the residual strength to those from a Newmark analysis in which the strength degrades from peak strength to the residual strength. In the analyses shown in this figure, the residual strength was 70 percent of the peak strength and the strength degradation occurred linearly between a deformation of 20.1 mm and a deformation of 73 mm.

When performing a Newmark analysis, it is important to remember that the engineer must evaluate the deformation potential of all possible failure surfaces, much in the same way that the engineer must evaluate the factor of safety of all potential failure surfaces in a limit equilibrium stability analysis. It cannot be assumed *a-priori* that the surface with the largest permanent seismic deformation potential is either the surface with the lowest yield acceleration or surface with the highest peak average acceleration unless these are the same surface. In general, however, these are not the same surface, as illustrated in Figure 7-8, and the failure surface with the greatest permanent seismic deformation potential is the surface for which the



* Yield acceleration evaluated using large deformation shear strength parameters ($k_y = k_{y2}$).

Figure 7-6: Newmark Analysis Using Peak and Residual Shear Strengths (Matasovic, Kavazanjian and Giroud, 1998)

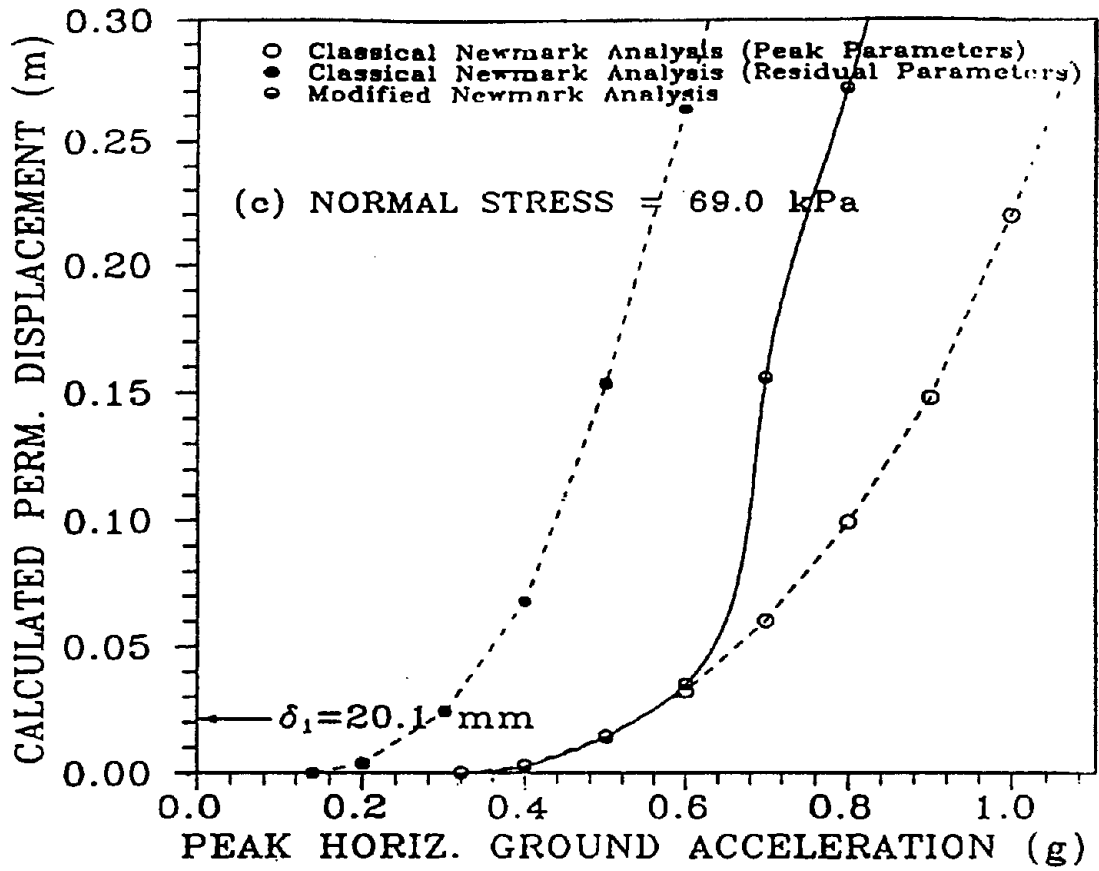


Figure 7-7: Comparison of Results from Newmark Analysis Using Peak and Residual Shear Strengths (Matasovic, Kavazanjian, and Giroud, 1998)

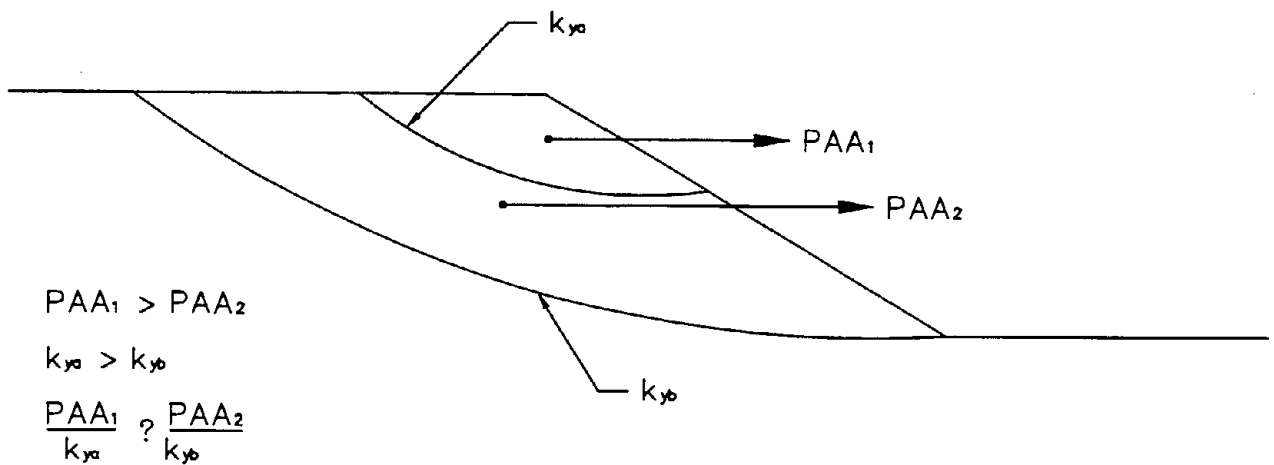


Figure 7-8: Inter-Relationship of Yield Acceleration and Peak Average Acceleration

ratio of the peak average yield acceleration to the peak average acceleration is the smallest. Not only must the design engineer search for surface with largest permanent seismic deformation potential, but the Design Engineer may also have to evaluate the permanent seismic deformation potential of other surfaces which pass through or under deformation-sensitive components of the highway system.

7.4 UNIFIED METHODOLOGY FOR SEISMIC STABILITY AND DEFORMATION ANALYSIS

The seismic coefficient-factor of safety and permanent seismic deformation analysis methods for seismic slope stability may be combined into a single, unified method for evaluation of slopes and embankments. First, a seismic coefficient-factor of safety analysis is performed using a suitably conservative value for the seismic coefficient. Then, if the seismic coefficient-factor of safety analysis results in an unacceptable factor of safety, a permanent seismic deformation analysis is performed.

The “unified” seismic stability and deformation analysis is carried out using the same basic model(s) of slopes used in the static analysis. Note, however, that the critical surface with the lowest yield acceleration or pseudo-static factor of safety may be very different from the surface with the lowest static factor of safety. The following steps are carried out to perform the unified seismic slope stability and deformation analysis:

- Step 1: Reinterpret the cross-sections analyzed in the static stability analysis and assign appropriate dynamic residual strength parameters. In cases where it is not clear whether drained or undrained shear strength parameters are appropriate for the dynamic analysis, follow guidelines presented in Duncan (1992) or use a composite consolidated drained-consolidated undrained strength envelope proposed by the Corps of Engineers for pervious soils and the consolidated undrained strength envelope for silts and clays. For fully saturated silts or clays of low sensitivity, multiply the undrained peak shear strength by 0.8 for the analysis. For sensitive soils, residual shear strength is often used to provide a conservative basis for design.
- Step 2: Select a seismic coefficient, k_s , for a minimum factor of safety of 1.0 based upon the work of Hynes and Franklin. If a permanent seismic deformation of 1 m is acceptable, a value of k_s equal to $0.5 \cdot a_{\max}/g$, where a_{\max} is peak horizontal acceleration at the ground surface, may be used for embankments. If a site response analysis has been performed to evaluate the peak average acceleration of the failure mass, a value of k_s equal to $0.17 \cdot a_{\max}/g$ may be used. For natural and cut slopes, where amplification effects are expected to be minimal, a value of k_s equal to $0.17 \cdot a_{\max}/g$ may also be used (see discussion in Section 7.3.2).
- Step 3: Perform the pseudo-static stability analysis. If the minimum factor of safety, FS_{\min} , exceeds 1.0, the seismic stability analysis is completed.
- Step 4: If the pseudo-static factor of safety is less than 1.0, perform a Newmark deformation analysis. This is done using the following three steps:
 - 1) Calculate the yield acceleration, k_y . The yield acceleration is calculated using a trial and error procedure in which the seismic coefficient is varied until $FS_{\min} = 1.0$ is obtained.
 - 2) Calculate the permanent seismic deformation. The permanent seismic deformation may be calculated using either simplified design charts (e.g., Figure 7-4), as described below,

or by performing a formal time-history analysis in which the excursions of the average acceleration time history above the yield acceleration are double integrated.

- 3) Compare the calculated permanent seismic deformation to the allowable maximum permanent displacement, u_{max} .

Several investigators have presented simplified charts based upon the results of Newmark deformation analyses for estimating permanent seismic deformations. The chart developed by Hynes and Franklin (1984) was presented in Figure 7-4. The Hynes and Franklin chart does not consider either site amplification or earthquake magnitude effects. Therefore, the Hynes and Franklin charts may be expected to give reasonable values for natural and cut slopes and low, broad embankments where amplification effects are expected to be small when subject to large earthquakes. For small earthquakes, the Hynes and Franklin charts may yield conservative values for such cases.

Makdisi and Seed (1978) developed the seismic deformation chart shown in Figure 7-9 from the results of two-dimensional finite element analyses of embankments. This chart includes the effect of amplification of seismic motions by the embankment and provides upper and lower bounds on the permanent deformation as a function of magnitude.

To calculate the permanent seismic deformation using either Figure 7-4 or 7-9, the following procedure should be used:

- Step 1: Calculate the yield acceleration for each potential failure surface of interest using limit equilibrium analysis as described previously in this section;
- Step 2: Calculate the peak average acceleration for each failure surface of interest based upon the seismic response considerations described in Section 6.3;
- Step 3: Calculate the ratio of the yield acceleration to the peak average acceleration for each failure surface of interest and evaluate the permanent seismic deformation from the appropriate curve in either Figure 7-4 or 7-9.

If Figure 7-4 is used, the upper bound curve should only be used for distant (site-to-source distance greater than 25 km), large magnitude (moment magnitude greater than 7.5) events. The average curve should only be used for small magnitude events (magnitude equal to or less than 5.5) or for intermediate magnitude events (magnitude between 5.5 and 6.5) with small site-to-source distance (site to source distance less than 10 km). For all other events, the mean plus one standard deviation curve should be used. If Figure 7-9 is used, the curve corresponding to the appropriate magnitude should be employed. Distance considerations may be used with judgement to determine where to choose the deformation from within the band for the appropriate magnitude.

If a seismic response analysis has been performed, a formal Newmark seismic deformation analysis can be performed by using the acceleration or shear stress time histories from the seismic site response analysis. Jibson (1993) describes the analytical procedure for performing such an analysis. To evaluate the permanent displacement of the sliding mass, the average acceleration time history of mass above the critical failure plane (the failure surface with the lowest yield acceleration) should be used.

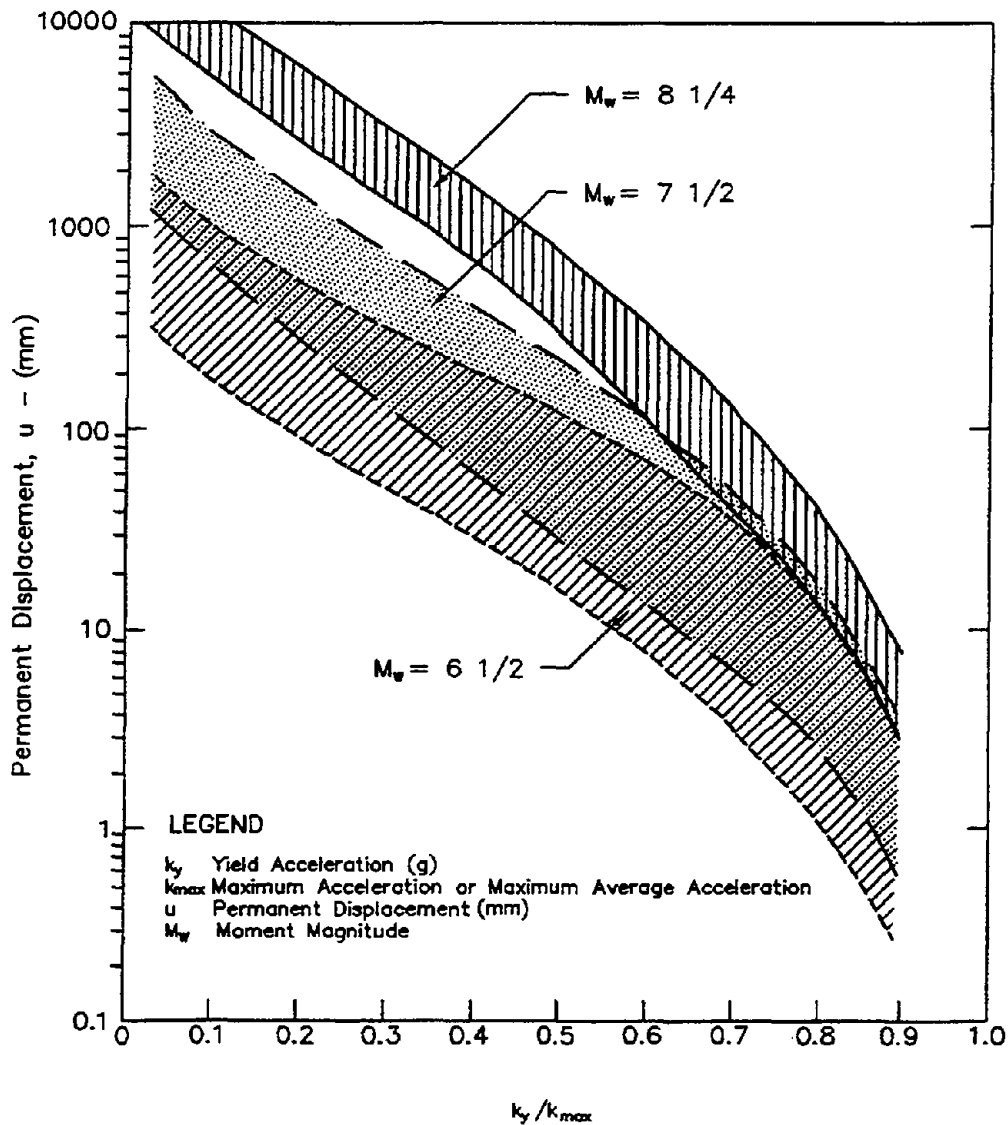


Figure 7-9: Permanent Displacement Versus Normalized Yield Acceleration for Embankments. (After Makdisi and Seed, 1978, reprinted by permission of ASCE).

7.5 ADDITIONAL CONSIDERATIONS

Stability of the underlying foundation soil is an important consideration in evaluating the overall performance of the embankment, particularly if a layer (or layers) in the foundation is susceptible to liquefaction. The potential for a liquefaction-induced flow failure may be analyzed using limit equilibrium analyses by employing residual shear strengths in the potentially liquefiable zones. In this type of post-earthquake stability assessment, the seismic coefficient should be set equal to zero (Marcuson, *et al.*, 1990). If the residual shear strength is conservatively assessed using minimum values of SPT blow counts (or CPT tip resistance) within the potentially liquefiable layer(s), a factor of safety of 1.1 may be considered as acceptable. Evaluation of residual shear strength for post-liquefaction stability analyses is discussed in Chapter 8.

CHAPTER 8.0 LIQUEFACTION AND SEISMIC SETTLEMENT

8.1 INTRODUCTION

During strong earthquake shaking, loose, saturated cohesionless soil deposits may experience a sudden loss of strength and stiffness, sometimes resulting in loss of bearing capacity, large permanent lateral displacements, and/or seismic settlement of the ground. This phenomenon is called *soil liquefaction*. In the absence of saturated or near-saturation conditions, strong earthquake shaking can induce compaction and settlement of the ground. This phenomenon is called *seismic settlement*.

Liquefaction and/or seismic settlement beneath and in the vicinity of highway facilities can have severe consequences with respect to facility integrity. Localized bearing capacity failures, lateral spreading, and excessive settlements resulting from liquefaction may damage bridges, embankments, and other highway structures. Liquefaction-associated lateral spreading and flow failures and seismically-induced settlement can also affect the overall stability of the roadway. Similarly, excessive total or differential settlement can impact the integrity and/or serviceability of highway facilities. Therefore, a liquefaction and seismic settlement potential assessment is a key element in the seismic design of highways.

This Section outlines the current state-of-the-practice for evaluation of the potential for, and the consequences of (should it occur), soil liquefaction and seismic settlement as they apply to the seismic design of highways. Initial screening criteria to determine whether or not a liquefaction analysis is needed for a particular project are presented in Section 8.2. The simplified procedure for liquefaction potential assessment commonly used in engineering practice is presented in Section 8.3. Methods for performing a liquefaction impact assessment, i.e., to estimate post-liquefaction deformation and stability, are presented in Section 8.4. The simplified procedures for seismic settlement of unsaturated sand evaluation commonly used in engineering practice are presented in Section 8.5. Methods for mitigation of liquefaction and seismic settlement potential and of the consequences of liquefaction are discussed in Section 8.6. Advanced methods for liquefaction potential assessments, including one- and two-dimensional fully-coupled effective stress site response analyses, are briefly discussed in Section 8.3.

8.2 FACTORS AFFECTING LIQUEFACTION SUSCEPTIBILITY

The first step in any liquefaction evaluation is to assess whether the potential for liquefaction exists at the site. A variety of screening techniques exist to distinguish sites that are clearly safe with respect to liquefaction from those sites that require more detailed study (e.g., Dobry, *et al.*, 1980). The following five screening criteria are most commonly used to make this assessment:

- *Geologic age and origin.* Liquefaction potential decreases with increasing age of a soil deposit. Pre-Holocene age soil deposits generally do not liquefy, though liquefaction has occasionally been observed in Pleistocene-age deposits. Table 8-1 presents the liquefaction susceptibility of soil deposits as a function of age and origin (Youd and Perkins, 1978).
- *Fines content and plasticity index.* Liquefaction potential decreases with increasing fines content and increasing plasticity index, PI. Data presented in Figure 8-1 (Ishihara, *et al.*, 1989) show grain size distribution curves of soils known to have liquefied in the past. This data serves as a rough guide for liquefaction potential assessment of cohesionless soils. Soils having greater than 15 percent (by

TABLE 8-1
SUSCEPTIBILITY OF SEDIMENTARY DEPOSITS
TO LIQUEFACTION DURING STRONG SHAKING
 (After Youd and Perkins, 1978, Reprinted by Permission of ASCE)

Type of Deposit	General Distribution of Cohesionless Sediments in Deposits	Likelihood that Cohesionless Sediments, When Saturated, Would Be Susceptible to Liquefaction (by Age of Deposit)			
		<500 Year	Holocene	Pleistocene	Pre-pleistocene
Continental Deposits					
River channel	Locally variable	Very high	High	Low	Very low
Flood plain	Locally variable	High	Moderate	Low	Very low
Alluvial fan and plain	Widespread	Moderate	Low	Low	Very low
Marine terraces and plains	Widespread	—	Low	Very low	Very low
Delta and fan-delta	Widespread	High	Moderate	Low	Very low
Lacustrine and playa	Variable	High	Moderate	Low	Very low
Colluvium	Variable	High	Moderate	Low	Very low
Talus	Widespread	Low	Low	Very low	Very low
Dunes	Widespread	High	Moderate	Low	Very low
Loess	Variable	High	High	High	Unknown
Glacial till	Variable	Low	Low	Very low	Very low
Tuff	Rare	Low	Low	Very low	Very low
Tephra	Widespread	High	High	Unknown	Unknown
Residual soils	Rare	Low	Low	Very low	Very low
Sebka	Locally variable	High	Moderate	Low	Very low
Coastal Zone					
Delta	Widespread	Very high	High	Low	Very low
Estuarine	Locally variable	High	Moderate	Low	Very low
Beach-high wave energy	Widespread	Moderate	Low	Very low	Very low
Beach-low wave energy	Widespread	High	Moderate	Low	Very low
Lagoonal	Locally variable	High	Moderate	Low	Very low
Fore shore	Locally variable	High	Moderate	Low	Very low
Artificial Deposits					
Uncompacted fill	Variable	Very high	—	—	—
Compacted fill	Variable	Low	—	—	—

weight) finer than 0.005 mm, a liquid limit greater than 35 percent, or an in-situ water content less than 0.9 times the liquid limit generally do not liquefy (Seed and Idriss, 1982).

- *Saturation.* Although unsaturated soils have been reported to liquefy, at least 80 to 85 percent saturation is generally deemed to be a necessary condition for soil liquefaction. In many locations, the water table is subject to seasonal oscillation. In general, it is prudent that the highest anticipated seasonal water table elevation be considered for initial screening.
- *Depth below ground surface.* While failures due to liquefaction of end-bearing piles resting on sand layers up to 30 m below the ground surface have been reported, shallow foundations are generally not affected if liquefaction occurs more than 15 m below the ground surface.
- *Soil penetration resistance.* According to the data presented in Seed and Idriss (1982), liquefaction has not been observed in soil deposits having normalized Standard Penetration Test (SPT) blow counts, $(N_1)_{60}$ larger than 22. Marcuson, *et al.* (1990) suggest a normalized SPT value of 30 as the threshold value above which liquefaction will not occur. However, Chinese experience, as quoted in Seed, *et al.* (1983), suggests that in extreme conditions liquefaction is possible in soils having normalized SPT blow counts as high as 40. Shibata and Teparaska (1988), based on a large number of observations, conclude that no liquefaction is possible if normalized Cone Penetration Test (CPT) cone resistance, q_{c1} , is larger than 15 MPa.

If three or more of the above criteria indicate that liquefaction is *not* likely, the potential for liquefaction may be considered to be small enough that a formal liquefaction potential analysis is not required. If, however, based on the above initial screening criteria, the potential for liquefaction of a cohesionless soil layer beneath the site cannot be dismissed, more rigorous analysis of liquefaction potential is needed.

Liquefaction susceptibility maps, derived on the basis of some (or all) of the above listed criteria, are available for many major urban areas in seismic zones (e.g., Kavazanjian, *et al.*, 1985b for San Francisco; Tinsley, *et al.*, 1985 for Los Angeles; Hadj-Hamou and Elton, 1988 for Charleston, South Carolina; Hwang and Lee, 1992 for Memphis). These maps may be useful for preliminary screening analyses for highway routing studies. However, as most new highways are sited outside major urban areas, these types of maps are unlikely to be available for many highway sites. Furthermore, most of these maps do not provide sufficient detail to be useful for site-specific studies or detailed design analyses.

Several attempts have been made to establish threshold criteria for values of seismic shaking that can induce liquefaction (e.g., minimum earthquake magnitude, minimum peak horizontal acceleration, maximum distance from causative fault). Most of these criteria have eventually been shown to be misleading, since even low intensity bedrock ground motions from distant earthquakes can be amplified by local soils to intensity levels strong enough to induce liquefaction, as observations of liquefaction in the 1985 Mexico City and 1989 Loma Prieta earthquakes demonstrate.

Most soil deposits known to have liquefied are sand deposits. However, as indicated on Figure 8-1, some deposits containing gravel particles (> 2 mm size) in a fine grained soil matrix may be susceptible to liquefaction. Discussion of the liquefaction potential of gravel deposits is beyond the scope of this document. The reader is referred to Ishihara (1985), Harder (1988), and Stark and Olson (1995) for a discussion of methods for evaluation of the liquefaction potential of gravels.

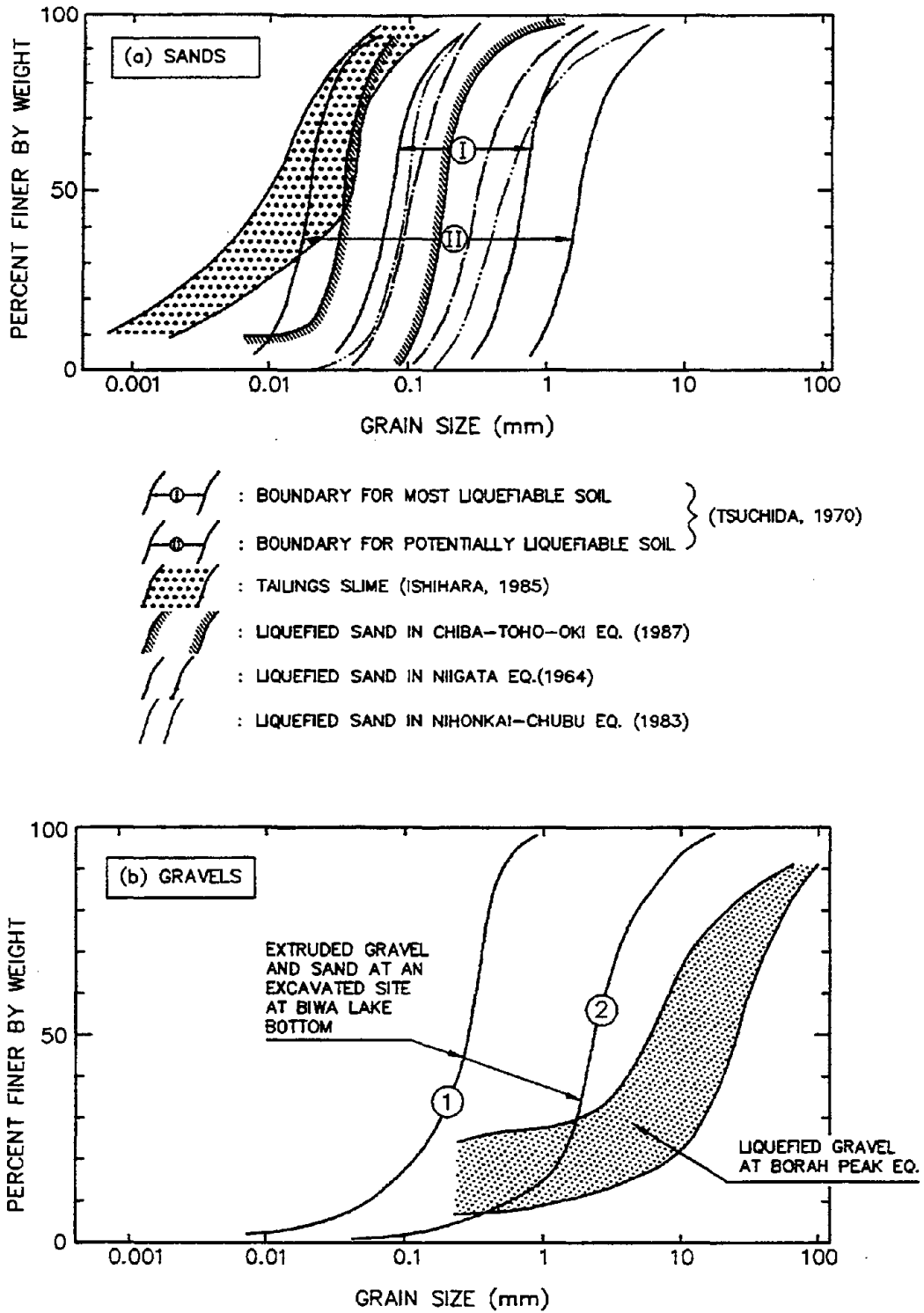


Figure 8-1: Grain Size Distribution Curves of Potentially Liquefiable Soils. (Modified after Ishihara, *et al.*, 1989, reprinted with permission of A.A. Balkema, Old Post Rd., Brookfield, VT 05036)

8.3 EVALUATION OF LIQUEFACTION POTENTIAL

8.3.1 Introduction

Due to the difficulties in obtaining and testing undisturbed representative samples from most potentially liquefiable soil materials, in situ testing is the approach preferred by most engineers for evaluating the liquefaction potential of a soil deposit. Liquefaction potential assessment procedures involving both the SPT and CPT are widely used in practice (e.g., Seed and Idriss, 1982; Ishihara, 1985; Seed and De Alba, 1986; Shibata and Teparaska, 1988; Stark and Olson, 1995). For gravelly soils, the Becker Penetration Test (BPT) is commonly used to evaluate liquefaction potential (Harder and Seed, 1986). Geophysical techniques for measuring shear wave velocity have recently emerged as potential alternatives for liquefaction potential assessment (Tokimatsu, *et al.*, 1991; Youd and Idriss, 1997).

8.3.2 Simplified Procedure

The most common procedure used in engineering practice for the liquefaction potential assessment of sands and silts is the *Simplified Procedure* originally developed by Seed and Idriss (1982). Since its original development, the original Simplified Procedure as proposed by Seed and Idriss has been progressively revised, extended, and refined (Seed, *et al.*, 1983; Seed, *et al.*, 1985; Seed and De Alba, 1986; Liao and Whitman, 1986). The Simplified Procedure may be used with either SPT or CPT data. Recent summaries of the various revisions to the Simplified Procedure are provided by Marcuson, *et al.*, (1990) and Seed and Harder (1990). A 1996 workshop sponsored by the National Center for Earthquake Engineering Research (NCEER) reviewed recent developments on evaluation of liquefaction resistance of soils and arrived consensus on improvements and augmentation to the simplified procedure (Youd and Idriss, 1997). Based primarily on recommendations from these studies, the Simplified Procedure for evaluating liquefaction potential at the site of highway facilities can be performed using the following steps:

- Step 1: From borings and soundings, in situ testing and laboratory index tests, develop a detailed understanding of the project site subsurface conditions, including stratigraphy, layer geometry, material properties and their variability, and the areal extent of potential problem zones. Establish the zones to be analyzed and develop idealized, representative sections amenable to analysis. The subsurface data used to develop the representative sections should include the location of the water table, either SPT blow count, N , or tip resistance of a standard CPT cone, q_c , mean grain size, D_{50} , unit weight, and the percentage of fines in the soil (percent by weight passing the U.S. Standard No. 200 sieve).
- Step 2: Evaluate the total vertical stress, σ_v , and effective vertical stress, σ_v' , for all potentially liquefiable layers within the deposit both at the time of exploration and for design. Vertical and shear stress design values should include the stresses resulting from facility construction. Exploration and design values for vertical total and effective stress may be the same or may differ due to seasonal fluctuations in the water table or changes in local hydrology resulting from project development. Note that for underwater sites, the total weight of water above the mudline should not be included in calculating the total vertical stress. Also evaluate the initial static shear stress on the horizontal plane, τ_{ho} , for design.
- Step 3: If results of a site response analysis are not available, evaluate the *stress reduction factor*, r_d as described below. The stress reduction factor is a soil flexibility factor defined as the ratio of the peak shear stress for the soil column, $(\tau_{max})_d$, to that of a rigid body, $(\tau_{max})_r$. There are several ways to obtain r_d . For non-critical projects, the following equations for r_d were recommended by

a panel of experts convened by the National Center for Earthquake Engineering Research (NCEER) in 1996 (Youd and Idriss, 1997):

$$\begin{aligned}
 r_d &= 1.0 - 0.00765 z && \text{for } z \leq 9.15 \text{ m} \\
 r_d &= 1.174 - 0.0267 z && \text{for } 9.15 \text{ m} < z \leq 23 \text{ m} \\
 r_d &= 0.744 - 0.008 z && \text{for } 23 < z \leq 30 \text{ m} \\
 r_d &= 0.5 && \text{for } z > 30 \text{ m}
 \end{aligned}
 \tag{8-1}$$

where z is the depth below the ground surface in meters. Mean values of r_d calculated from Equation 8-1 are plotted in Figure 8-2 along with the range of data proposed by Seed and Idriss (1971).

For critical projects warranting a site-specific response analysis, or if results of a site response analysis (see Chapter 6) are available, the maximum earthquake-induced shear stress at depth z , τ_{\max} , can be directly obtained from the results of the site response analysis. In this case, it may be convenient to calculate r_d from the site response results for use in spreadsheet calculations using the following equation:

$$r_d = \frac{(\tau_{\max})_{@depth=z}}{(\sigma_v)_{@depth=z} \cdot (a_{\max}/g)_{@surface}}
 \tag{8-2}$$

where σ_v is the total shear stress at depth z , a_{\max} is the peak ground surface acceleration, and g is the acceleration of gravity. The parameters σ_v and a_{\max} are also directly calculated by most site response computer programs described in Chapter 6.

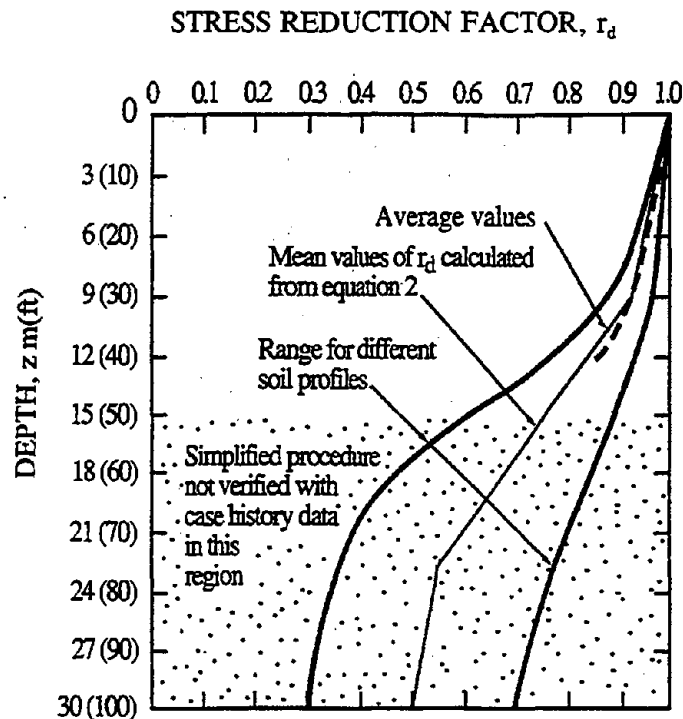


Figure 8-2: Stress Reduction Factor, r_d , Versus Depth Curves Developed by Seed and Idriss (1971) with Added Mean Value Lines from Equation 8-1.

Use of τ_{\max} from site response analysis (or use of the results of a site response analysis to evaluate r_d) is considered to be generally more reliable than any of the simplified approaches to estimate r_d , and is strongly recommended for sites that are marginal with respect to liquefaction potential (i.e., sites where the factor of safety for liquefaction is close to 1.0).

Step 4: Calculate the *critical stress ratio induced by the design earthquake*, CSR_{EQ} , as:

$$CSR_{EQ} = 0.65 (a_{\max}/g) r_d (\sigma_v/\sigma_v') \quad (8-3a)$$

If the results of a seismic site response analysis are available, CSR_{EQ} can be evaluated from τ_{\max} as:

$$CSR_{EQ} = 0.65 \tau_{\max}/\sigma_v' \quad (8-3b)$$

Note that the ratio τ_{\max}/σ_v' corresponds to the peak average acceleration denoted by k_{\max} in Chapter 6.

Step 5: Evaluate the *standardized SPT blow count*, N_{60} , using the procedure presented in Chapter 5.

Step 6: Calculate the normalized and standardized SPT blow count, $(N_1)_{60}$, using the procedure presented in Chapter 5

Step 7: Evaluate the critical stress ratio $CSR_{7.5}$ at which liquefaction is expected to occur during an earthquake of magnitude $M_w = 7.5$ as a function of $(N_1)_{60}$. Use the chart developed by Seed, *et al.* (1985) as modified by NCEER, shown in Figure 8-3, to find $CSR_{7.5}$. It should be noted that this chart was developed using a large database from sites where liquefaction did or did not occur during past earthquakes. The general conditions for the case history data presented in this chart are as follows: (1) all sites evaluated were under level ground condition, (2) the effective overburden pressure for all cases does not exceed 96 kPa, and (3) the magnitude of the earthquakes considered in all cases was in the neighborhood of 7.5.

Step 8: Calculate the *corrected* critical stress ratio resisting liquefaction, CSR_L . CSR_L is calculated as:

$$CSR_L = CSR_{7.5} \cdot k_M \cdot k_\sigma \cdot k_\alpha \quad (8-4)$$

where k_M is the correction factor for earthquake magnitudes other than 7.5, k_σ is the correction factor for stress levels larger than 96 kPa, and k_α is the correction factor for the initial driving static shear stress, τ_{ho} . Previous investigators have derived various recommendations on the magnitude correction factor, K_M , as shown in Figure 8-4. Upon review of all the data, the NCEER workshop participants have recommended a range of K_M values for design and analysis purposes. Their recommendations are presented in Figure 8-4. For effective confining pressures σ'_m larger than 96 kPa, k_σ can be determined from Figure 8-5 (Youd and Idriss, 1997). For σ'_m less than or equal to 96 kPa, no correction is required.

The value of k_α depends on both τ_{ho} and the relative density of the soil, D_r . On sloping ground, or below structures and embankments, τ_{ho} can be estimated using various closed-form elastic solutions (e.g., Poulos and Davis, 1974) or using the results of finite element (static) analyses. Once τ_{ho} and σ_v' are estimated, k_α can be determined from Figure 8-6, originally proposed by Seed

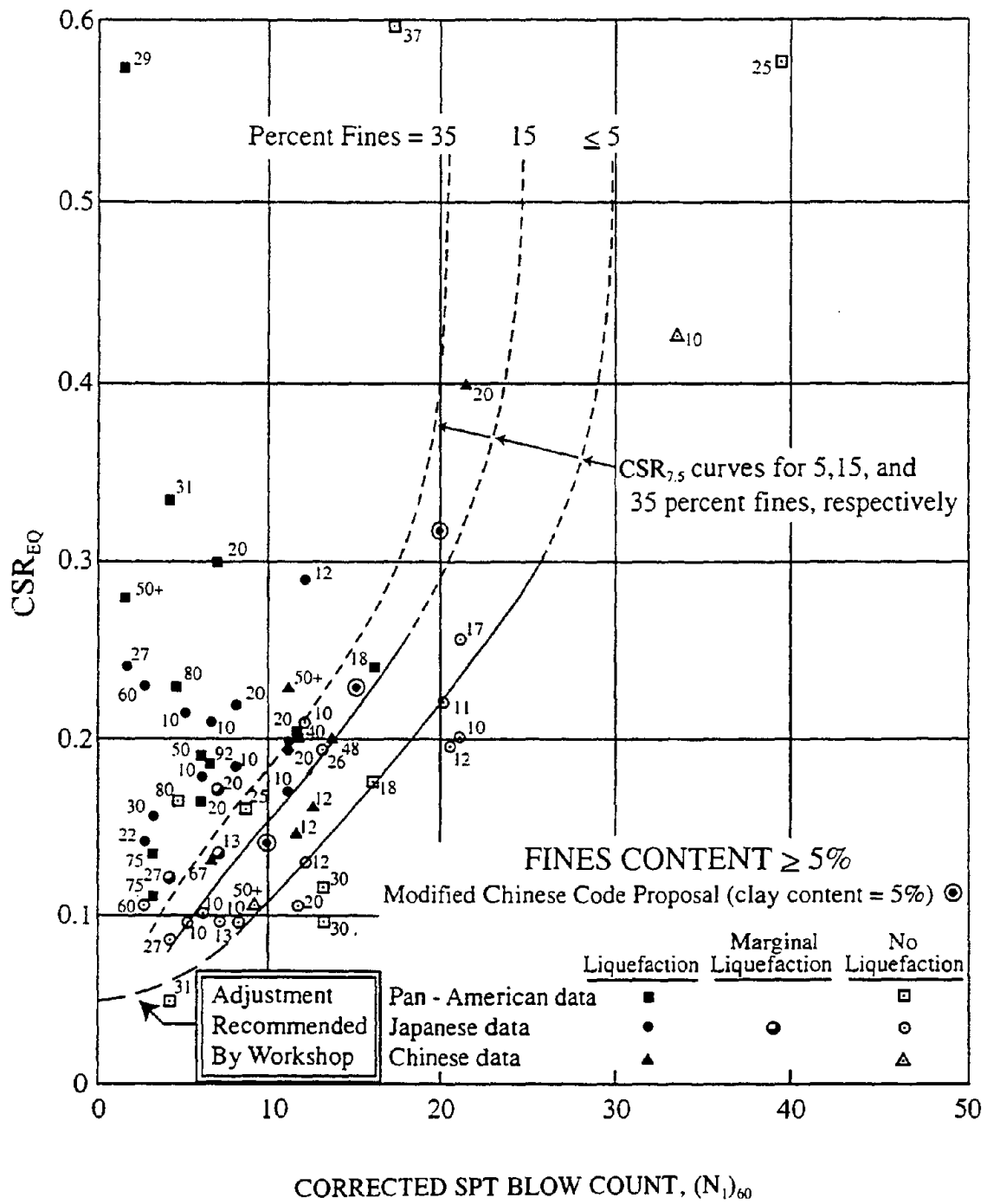


Figure 8-3: Relationship Between Cyclic Stress Ratio Causing Liquefaction and SPT (N₁)₆₀ Values for Sands for M = 7.5 Earthquakes (modified From Seed et al., 1985)

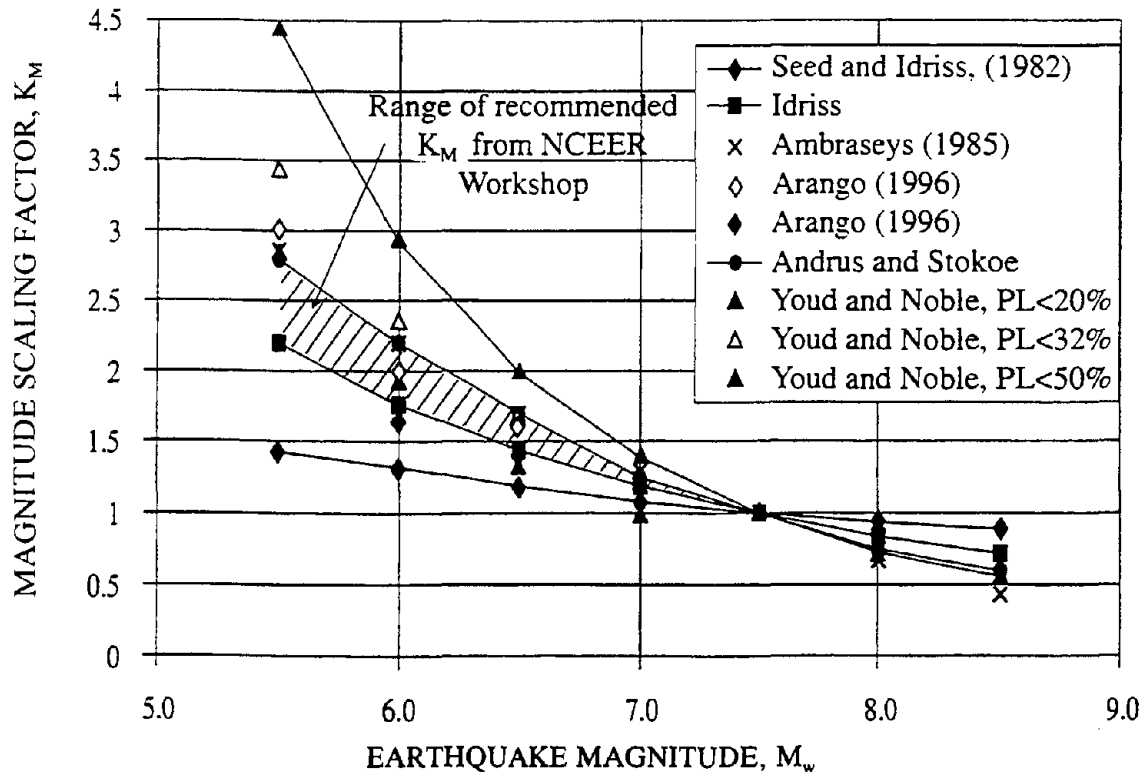


Figure 8-4: Magnitude Scaling Factors Derived by Various Investigators (After Youd and Idriss, 1997)

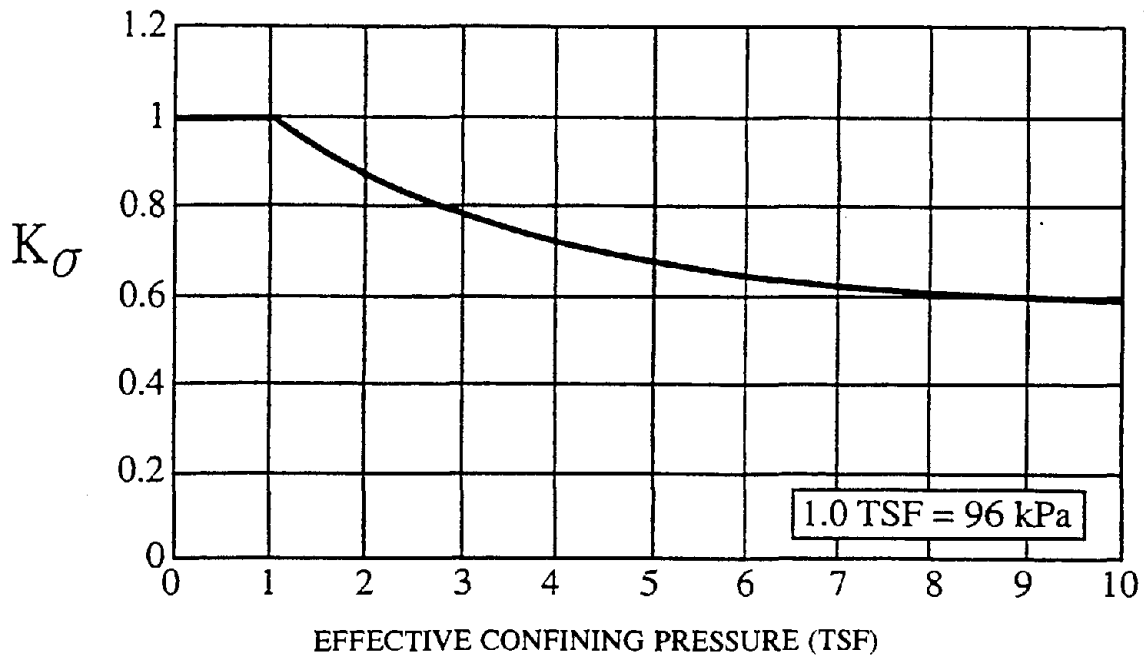


Figure 8-5: Recommended Correction Factor k_σ . (After Youd and Idriss, 1997)

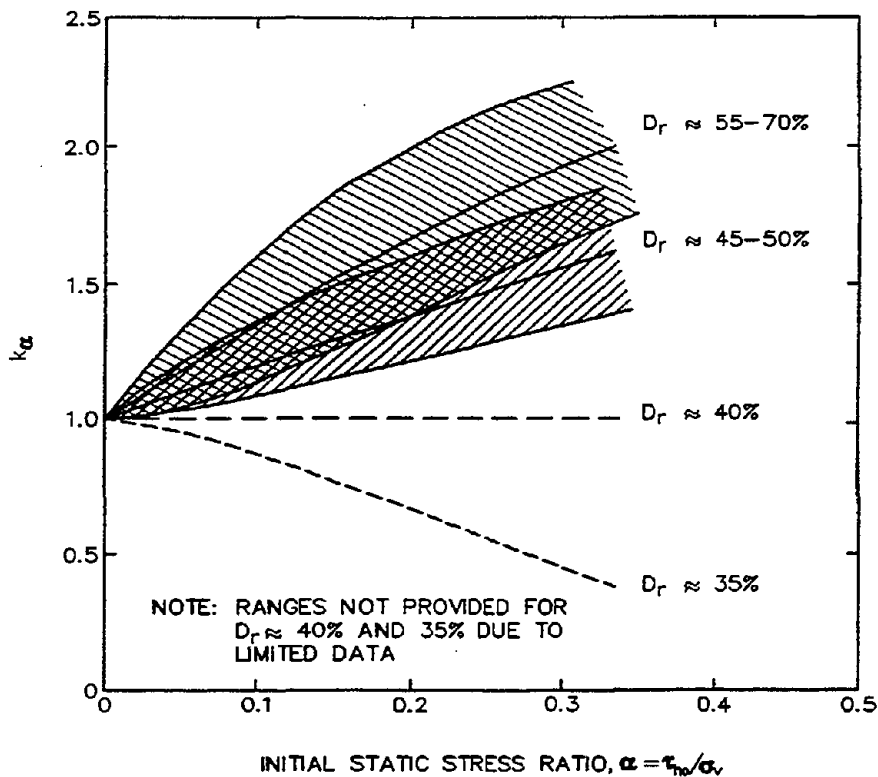


Figure 8-6: Curves for Estimation of Correction Factor, k_{α} . (Harder, 1988 and Hynes, 1988, as cited in Marcuson, *et al.*, 1990, reprinted by permission of EERI)

(1983) and modified by Harder (1988) and Hynes (1988). However, experts participating in the 1996 NCEER workshop on “Evaluation of Liquefaction Resistance of Soils” (1997) have concluded that due to the wide range of k_{α} values developed from previous studies and a lack of consistency of the results, general recommendations for use of k_{α} for design purposes are not advisable at this time. The evaluation of liquefaction resistance beneath sloping ground or embankments is not well understood and further research is required.

The effect of plasticity index on liquefaction resistance has also been reported (Ishihara, 1990). It is generally recognized that liquefaction resistance increases with soil plasticity. For example, many practitioners have been applying a 10 percent increase to the liquefaction resistance for soils with a plasticity index greater than 15 percent. However, a reliable correction relationship could not be formulated at this time due to the lack of data (Youd and Idriss, 1997).

Liquefaction resistance based on SPT (or CPT) measurements could not be reliably estimated for gravelly soils. Large gravel particles tend to increase the penetration resistance of the penetrometer unproportionately. To overcome this difficulty, large-diameter penetrometers have been used by some investigators. The Becker penetration test (BPT) has become the more effective and most widely used of this type of tools. There are correlations between Becker blowcount and SPT blowcount. The correlation proposed by Harder (1997) is recommended for liquefaction evaluation of gravelly soils in cases where Becker penetration testing data are available. Detailed information on the procedure is presented in the NCEER report (Youd and Idriss, 1997). In the absence of Becker penetration testing data, the effects of gravel content can be roughly estimated using the correlation curve shown in Figure 8-7 (Ishihara, 1985). The “Cyclic Strength of Sand

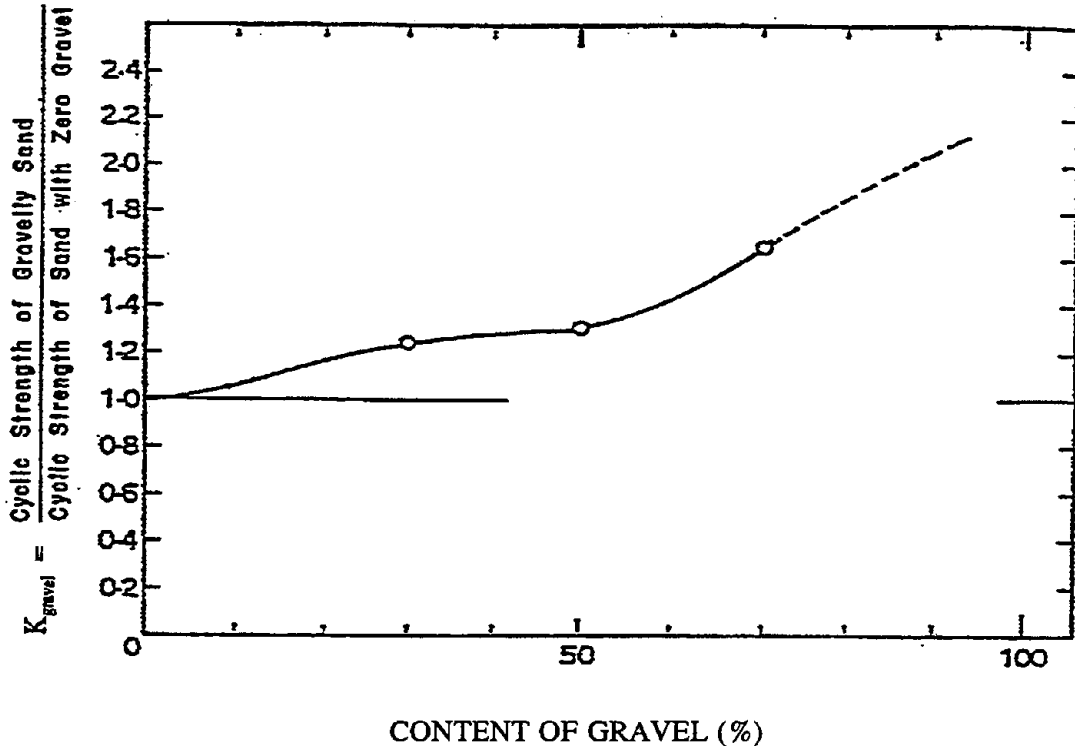


Figure 8-7: Effects of Gravel Content on Liquefaction Resistance of Gravelly Soils (Ishihara, 1985)

with Zero Gravel” cited in the figure should be obtained from the sand layers at the site in the vicinity of the gravelly soil deposit, provided that the sand layers (without gravel) and the gravelly soil layers were formed under the same geological conditions.

Step 9: Calculate the factor of safety against initial liquefaction, FS_L , as:

$$FS_L = \frac{CSR_L}{CSR_{EQ}} \quad (8-5)$$

There is no general agreement on the appropriate minimum factor of safety against liquefaction (NRC, 1985). There are cases where liquefaction-induced instability has occurred prior to complete liquefaction, i.e., with a factor of safety against initial liquefaction greater than 1.0. For regular highway bridge design, it is recommended that a minimum factor of safety of 1.1 against liquefaction be required.

It should be noted that the Simplified Procedure is aimed primarily at moderately strong ground motions ($0.2 g < a_{max} < 0.5 g$). If the peak horizontal acceleration is larger than 0.5 g, more sophisticated, truly non-linear effective stress-based analytical approaches may be advisable. Computer programs for evaluation of liquefaction potential as a part of a site response analysis include the one-dimensional response analysis computer program DESRA-2 (Lee and Finn, 1978) and its derivative codes MARDES (Chang, *et al.*, 1991), D-MOD (Matasović, 1993), and SUMDES (Li, *et al.*, 1992) as well as two-dimensional codes such as DYNAFLOW (Prevost, 1981), TARA-3 (Finn, *et al.*, 1986), LINOS (Bardet, 1992), DYSAC2 (Muraleetharan, *et al.*, 1991), and certain adaptations of FLAC (Cundall and Board, 1988) (e.g., Roth and Inel, 1993). These computer programs are briefly discussed in Chapter 6.

An example of a liquefaction analysis performed using the Simplified Procedure is presented in Part II of this document.

8.3.3 Variations on the Simplified Procedure

The principle variations on the simplified procedure used in practice include the use of CPT resistance and shear wave velocity, instead of the normalized SPT blow count to evaluate the critical stress ratio, causing liquefaction for a magnitude 7.5 earthquake, $CSR_{7.5}$. Figure 8-8 presents the relationship between corrected CPT tip resistance, q_{CIN} , and $CSR_{7.5}$, where q_{CIN} is evaluated from the tip resistance q_c as follows:

$$q_{CIN} = \left(\frac{P_a}{\sigma'_v} \right)^n \left(\frac{q_c}{P_a} \right) \quad (8-6)$$

where σ'_v is effective overburden pressure, P_a is atmospheric pressure (approximately 100 kPa) and n is an exponent that varies from 0.5 for clean sands, 0.7 for silty sands, and 0.8 for sandy silt.

It should be noted that Figure 8-8 is applicable for clean sands with fines less than 5%. To correct the normalized penetration resistance, q_{CIN} , of sands with fines greater than 5% to an equivalent clean sand value, $(q_{CIN})_{CS}$ the following relationship is used.

$$(q_{CIN})_{CS} = K_{CS} q_{CIN} \quad (8-7)$$

where K_{CS} varies from 1.0 for fines less than 5%, 1.4 for fines equal to 15%, to 3.35 for fines equal to 35%.

Simplified procedures using field measurements of small-strain shear wave velocity, V_s , to assess liquefaction resistance of granular soils have also been proposed. Figure 8-9 presents the relationship (Youd and Idriss, 1997) between $CSR_{7.5}$ and stress-corrected shear wave velocity, V_{s1} , where V_{s1} is calculated as:

$$V_{s1} = V_s \left(\frac{P_a}{\sigma'_v} \right)^{0.25} \quad (8-8)$$

The relationship shown in Figure 8-9 was developed based on data from many field sites (including the field performance data from the 1989 Loma Prieta earthquake) where liquefaction did or did not occur. Similar to the relationships developed using SPT and CPT data, the liquefaction resistance curves in Figure 8-9 are for magnitude 7.5 earthquakes and effective overburden pressures less than about 100 kPa. Appropriate correction factors as discussed in Section 8.3.2 should be applied to account for magnitudes other than 7.5 or effective overburden pressures greater than 100 kPa.

8.4 POST-LIQUEFACTION DEFORMATION AND STABILITY

For soil layers in which the factor of safety against initial liquefaction is unsatisfactory, a liquefaction impact analysis may demonstrate that the site will still perform adequately even if liquefaction occurs. Potential impacts of liquefaction include bearing capacity failure, loss of lateral support for piles, lateral spreading, and post-liquefaction settlement. These are all phenomena associated with large soil strains and

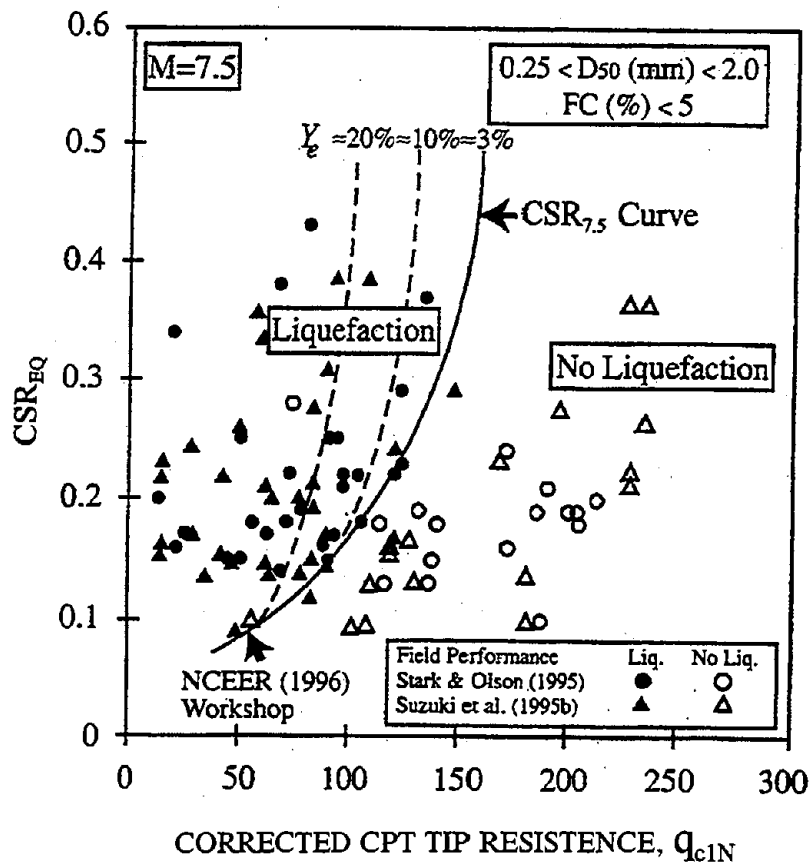


Figure 8-8: Relationship between Cyclic Stress Ratio Causing Liquefaction and CPT Tip Resistance, q_{c1N} for Sands for $M = 7.5$ (Robertson and Wride, 1997)

ground deformations. Relatively dense soils which liquefy may subsequently harden or stabilize at small deformations and thus have minimal impact on overlying highway structures. Conversely, relatively loose soils that liquefy will tend to collapse resulting in a much greater potential for post-liquefaction deformation. Methods for assessing the impact of liquefaction generally are based upon evaluation of the strain or deformation potential of the liquefiable soil. A liquefaction impact analysis for highway-related projects may consist of the following steps:

Step 1: Calculate the magnitude and distribution of liquefaction-induced settlement by multiplying the post-liquefaction volumetric strain, ϵ_v , by the thickness of the liquefiable layer, H .

The post-liquefaction volumetric strain can be estimated from the chart presented in Figure 8-10 (Tokimatsu and Seed, 1987). An alternative chart has recently been proposed by Ishihara (1993). Note that both charts were developed for clean sands and tend to overestimate settlements of sandy silts and silts. Application of Ishihara's chart requires translation of normalized SPT blow count $(N_1)_{60}$ values determined in Chapter 5 to Japanese-standard N_j values ($N_j = 0.833 (N_1)_{60}$; after Ishihara, 1993). The magnitude of liquefaction-induced settlement should be calculated at each SPT or CPT sounding location to evaluate the potential variability in seismic settlement across the project site.

Step 2: Estimate the free-field liquefaction-induced lateral displacement, Δ_L . The empirical equation proposed by Hamada, *et al.* (1987) may be used to estimate Δ_L in meters:

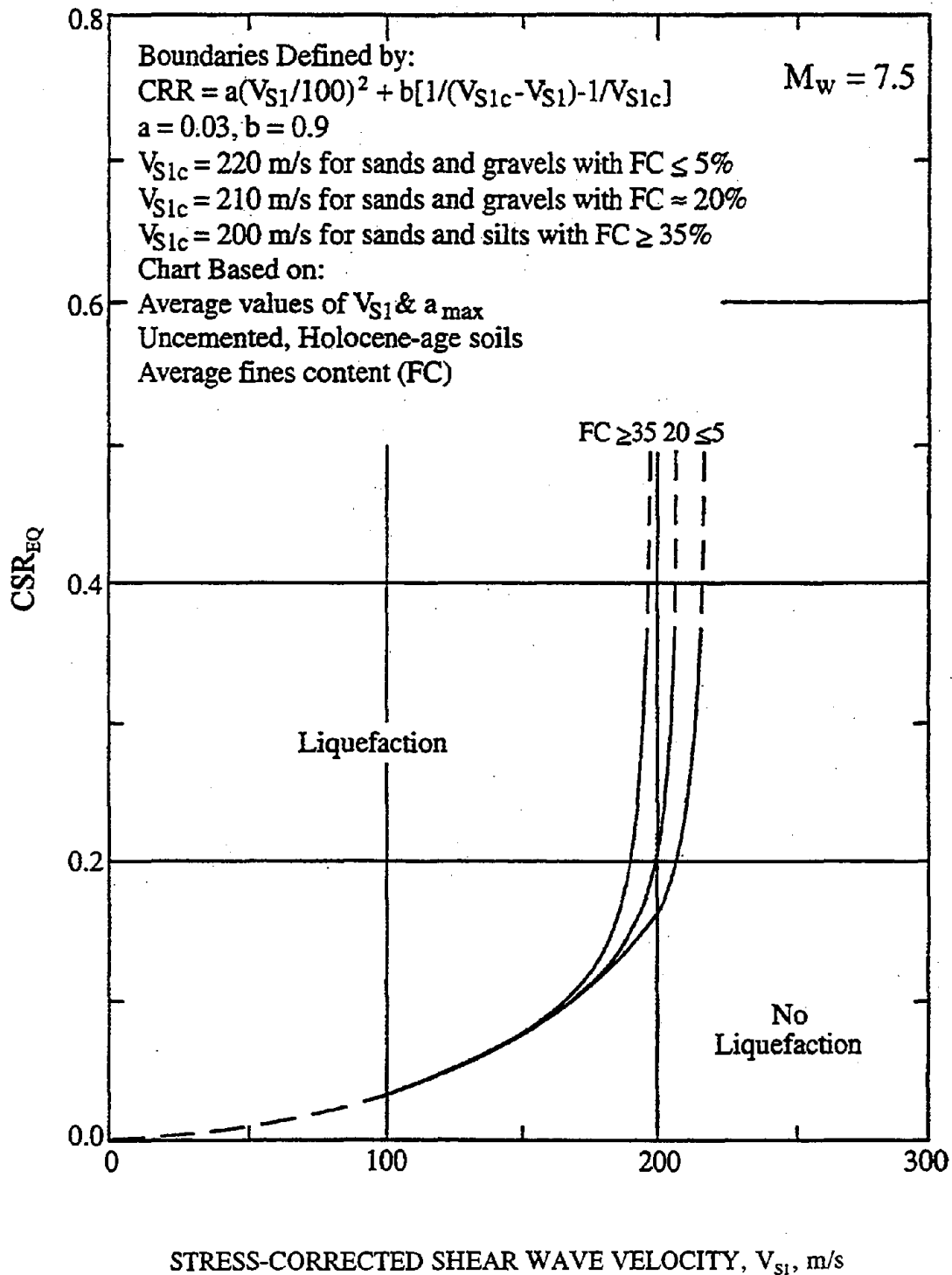


Figure 8-9: Relationship Between Cyclic Stress Ratio Causing Liquefaction and Shear Wave Velocity Values, V_{S1} , for Sands for $M=7.5$ Earthquakes (Youd and Idriss, 1997)

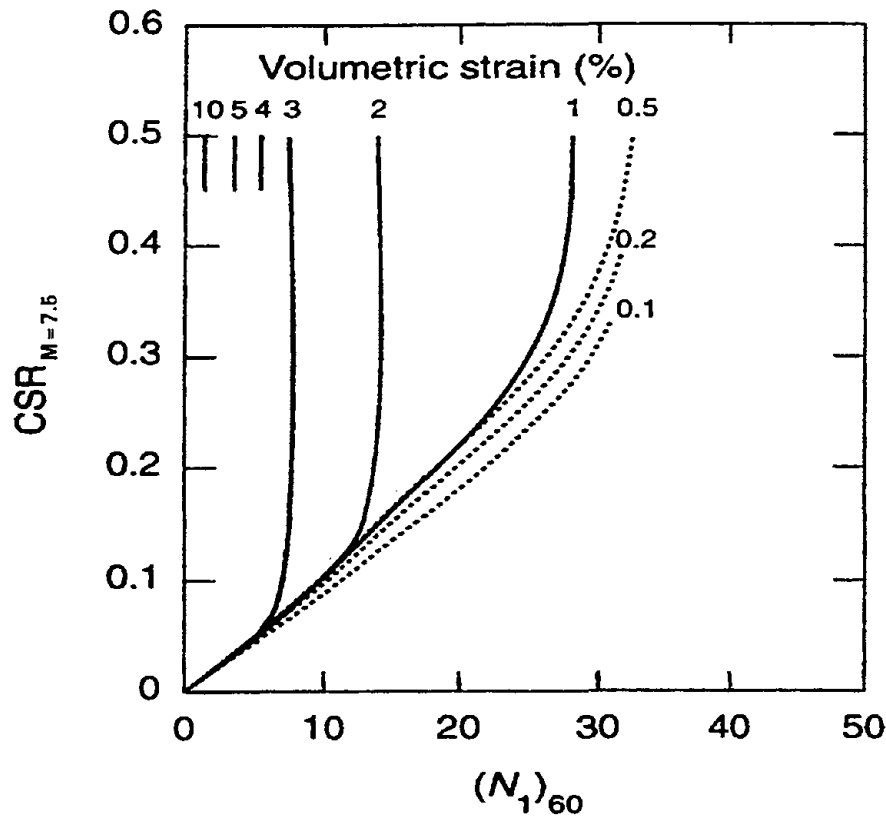


Figure 8-10: Curves for Estimation of Post-Liquefaction Volumetric Strain Using Spt Data and Cyclic Stress Ratio for M_w 7.5 Earthquakes. (Tokimatsu and Seed, 1987, reprinted by permission of ASCE).

$$\Delta_L = 0.75 (H)^{1/2} (S)^{1/3} \quad (8-9)$$

where H is the thickness of the liquefied layer in meters and S is the ground slope in percent.

The Hamada, *et al.* (1987) formula in Equation 8-9 is based primarily on Japanese data (for major earthquakes of magnitude 7.5 or greater) on observed liquefaction displacements of very loose sand deposits having a slope, S , less than 10 percent. Therefore, Equation 8-9 should be assumed to provide only a rough upper bound estimate of lateral displacement. Since Equation 8-9 does not reflect either the density, or $(N_1)_{60}$ value, of the liquefiable soil or the depth of the liquefiable layer, it likely provides a conservative estimate of lateral displacement for denser sands or for cases where the soil liquefies at depth. Estimates of lateral displacement obtained using Equation 8-9 may indicate excessive liquefaction-induced lateral displacements in areas of essentially flat ground conditions.

A more accurate empirical procedure for assessing lateral spreading was developed by Bartlett and Youd (1995). This procedure was developed from multiple linear regression analyses of U.S. and Japanese case histories. Two general types of lateral spreading are differentiated according to Bartlett and Youds' study: (1) lateral spread towards a free face, and (2) lateral spread down gentle ground slopes where a free face is absent. The procedure is summarized as follows:

- (1) If $(N_1)_{60}$ values are equal to or more than 15, the potential for lateral displacements would be small for earthquakes with magnitudes less than 8.0, and no additional

analyses are warranted.

- (2) If $(N_1)_{60}$ values are less than 15, then the evaluation of lateral displacement is performed using the following equations:

For free-face conditions:

$$\text{Log}\Delta_L = -16.366 + 1.178M - 0.927\text{Log } R - 0.013R + 0.657\text{Log } W \\ + 0.348\text{Log } H_{15} + 4.527\text{Log } (100 - F_{15}) - 0.922D50_{15} \quad (8-10a)$$

For ground slope conditions:

$$\text{Log}\Delta_L = -15.787 + 1.178M - 0.927\text{Log } R - 0.013R + 0.429\text{Log } S \\ + 0.348\text{Log } H_{15} + 4.527\text{Log } (100 - F_{15}) - 0.922D50_{15} \quad (8-10b)$$

Where:

- Δ_L = Estimated lateral ground displacement in meters
- H_{15} = Cumulative thickness of saturated granular layers with corrected blow counts, $(N_1)_{60}$, less than or equal to 15, in meters.
- $D50_{15}$ = Average mean grain size in granular layer included in H_{15} in mm.
- F_{15} = Average fines content for granular layers included in H_{15} in percent.
- M = Earthquake magnitude (moment magnitude).
- R = Horizontal distance from seismic energy source, in kilometers.
- S = Ground slope, in percent.
- W = Ratio of the height (H) of the free face to the distance (L) from the base of the free face to the point in question, in percent (i.e., $100H/L$).

Step 3: In areas of significant ground slope, or in situations when a deep failure surface may pass through the body of the facility or through underlying liquified layers, a flow slide can occur following liquefaction. The potential for flow sliding should be checked using a conventional limit equilibrium approach for slope stability analyses (discussed in Chapter 7) together with residual shear strengths in zones in which liquefaction may occur. Residual shear strengths can be estimated from the penetration resistance values of the soil using the chart proposed by Seed, *et al.* (1988) presented in Figure 5-15. Seed and Harder (1990) and Marcuson, *et al.* (1990) present further guidance for performing a post-liquefaction stability assessment using residual shear strengths.

If liquefaction-induced vertical and/or lateral deformations are large, the integrity of the highway facility may be compromised. The question the engineer must answer is "What magnitude of deformation is too large?" The magnitude of acceptable deformation should be established by the design engineer on a case-by-case basis. Calculated seismic deformations on the order of 0.15 to 0.30 m are generally deemed to be acceptable in current practice for highway embankments in California. For highway system components other than embankments, engineering judgement must be used in determining the allowable level of calculated seismic deformation. For example, components that are designed to be unyielding, such as bridge abutments restrained by batter piles, may have more restrictive deformation requirements than structures which can more easily accommodate foundation deformations. At the current time,

determination of allowable deformations remains a subject requiring considerable engineering judgement.

8.5 SEISMIC SETTLEMENT EVALUATION

Both unsaturated and saturated sands tend to settle and densify when subjected to earthquake shaking. If the sand is saturated and there is no possibility for drainage, so that constant volume conditions are maintained, the primary initial effect of the shaking is the generation of excess pore water pressures. Settlement then occurs as the excess pore pressures dissipate. In unsaturated sands, on the other hand, settlement may occur during the earthquake shaking under conditions of constant effective vertical stress (depending on the degree of saturation). In both cases (saturated and unsaturated soil), however, one result of strong ground shaking is settlement of the soil.

Liquefaction induced settlement of saturated sand is addressed as part of a post-liquefaction deformation and stability assessment as described in Section 8.4 of this Chapter. A procedure for evaluating the seismic settlement of unsaturated sand, following the general procedure presented in Tokimatsu and Seed (1987), is outlined below.

Seismic settlement analysis of unsaturated sand can be performed using the following steps:

Step 1: From borings and soundings, in situ testing and laboratory index tests, develop a detailed understanding of the project site subsurface conditions, including stratigraphy, layer geometry, material properties and their variability, and the areal extent of potential problem zones. Establish the zones to be analyzed and develop idealized, representative sections amenable to analysis. The subsurface data used to develop the representative sections should include normalized standardized SPT blow counts, $(N_1)_{60}$ (or results of some other test, e.g., the CPT from which $(N_1)_{60}$ can be inferred) and the unit weight of the soil.

Step 2: Evaluate the total vertical stress, σ_v , and the mean normal effective stress, σ'_m , at several layers within the deposit at the time of exploration and for design. The design values should include stresses resulting from highway facility construction. Outside of the highway facility footprint, the exploration and design values are generally the same.

Step 3: Evaluate the stress reduction factor, r_d , using one of the approaches presented in step 3 of Section 8.3 of this Chapter.

Step 4: Evaluate $\gamma_{\text{eff}} (G_{\text{eff}} / G_{\text{max}})$ using the Tokimatsu and Seed (1987) equation:

$$\gamma_{\text{eff}} (G_{\text{eff}} / G_{\text{max}}) = (0.65 \cdot a_{\text{max}} \cdot \sigma_v \cdot r_d) / (g \cdot G_{\text{max}}) \quad (8-11)$$

where $\gamma_{\text{eff}} (G_{\text{eff}} / G_{\text{max}})$ is a *hypothetical effective shear stress factor*, a_{max} is the peak ground surface acceleration, g is the acceleration of gravity, and G_{max} is the shear modulus of the soil at small strain. Note that $G_{\text{max}} = \rho \cdot V_s^2$, where V_s is the shear wave velocity and ρ is the mass density of the soil. Alternatively, G_{max} (in kPa) can be evaluated from the correlation given below (Seed and Idriss, 1970):

$$G_{\text{max}} = 4,400 [(N_1)_{60}]^{1/3} (\sigma'_m)^{1/2} \quad (8-12)$$

where $(N_1)_{60}$ is the normalized standardized SPT blow count defined before and σ'_m is mean normal effective stress in kPa. For unsaturated sands, σ'_m can be estimated using Equation 5-12.

However, for most practical purposes, the approximation $\sigma'_m \approx 0.65 \sigma'_v$ will suffice.

Step 5: Evaluate γ_{eff} as a function of $\gamma_{eff} (G_{eff}/G_{max})$ and σ_m using the chart reproduced in Figure 8-11.

Step 6: Assuming that $\gamma_{eff} \approx \gamma_c$, where γ_c is the cyclic shear strain, evaluate the volumetric strain due to compaction, ϵ_c , for an earthquake of magnitude 7.5 (15 cycles) using the chart reproduced in Figure 8-12.

Step 7: Correct for earthquake (moment) magnitude other than M_w 7.5 using the correction factors reproduced in Table 8-2.

Step 8: Multiply the volumetric strain due to compaction for each layer by two to correct for the multidirectional shaking effect, as recommended by Tokimatsu and Seed (1987), to get the representative volumetric strain for each layer.

Step 9: Calculate seismic settlements of each layer by multiplying the layer thickness by the representative volumetric strain evaluated in Step 8. Sum up the layer settlements to obtain the total seismic settlement for the analyzed profile.

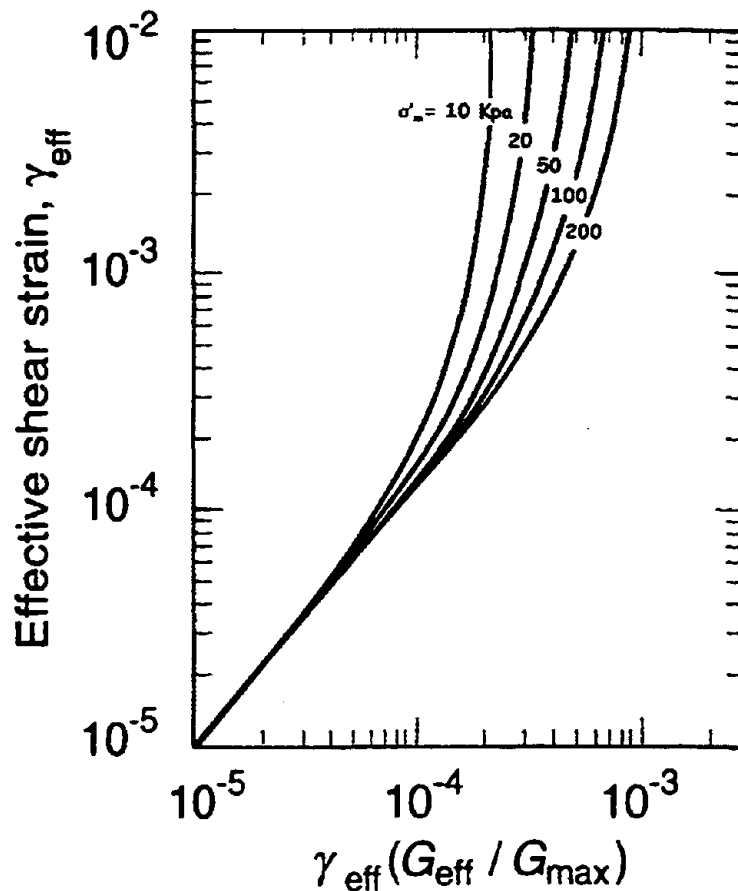


Figure 8-11: Plot for Determination of Earthquake-Induced Shear Strain in Sand Deposits. (Tokimatsu and Seed, 1987, reprinted by permission of ASCE)

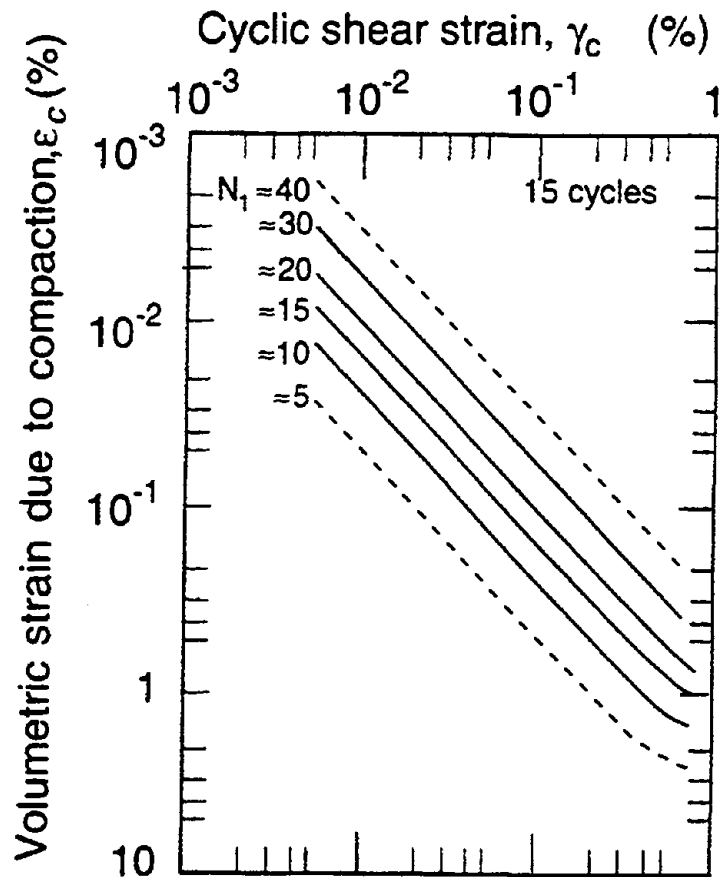


Figure 8-12: Relationship Between Volumetric Strain, Cyclic Shear Strain, and Penetration Resistance for Unsaturated Sands. (Tokimatsu and Seed, 1987, reprinted by permission of ASCE)

TABLE 8-2
INFLUENCE OF EARTHQUAKE MAGNITUDE
ON VOLUMETRIC STRAIN RATIO FOR DRY SANDS
 (After Tokimatsu and Seed, 1987, Reprinted by Permission of ASCE)

Earthquake Magnitude	Number of Representative Cycles at $0.65 \tau_{max}$	Volumetric Strain Ratio $\epsilon_{C,N}/\epsilon_{C,N=15}$
8.5	26	1.25
7.5	15	1.0
6.75	10	0.85
6	5	0.6
5.25	2-3	0.4

Considerable judgement is required when evaluating the performance of a highway facility based on an estimate of seismic settlement. The magnitude of calculated seismic settlement should be considered primarily as an indication of whether settlements are relatively small (several centimeters) or relatively large (several meters). A more precise evaluation of seismic settlement is not within the capabilities of conventional engineering analyses using the simplified methods presented herein.

8.6 LIQUEFACTION MITIGATION

If the seismic impact analyses presented in Sections 8.4 and 8.5 yield unacceptable deformations, consideration may be given to performing a more sophisticated liquefaction potential assessment and to evaluation of liquefaction potential mitigation measures. Generally, the engineer has the following options: (1) proceed with a more advanced analysis technique; (2) design the facility to resist the anticipated deformations; (3) remediate the site to reduce the anticipated deformations to acceptable levels; or (4) choose an alternative site. If a more advanced analysis still indicates unacceptable impacts from liquefaction, the engineer must still consider options (2) through (4). These options may require additional subsurface investigation, advanced laboratory testing, more sophisticated numerical modeling, and, in rare cases, physical modeling. Discussion of these techniques is beyond the scope of this document.

Options that may be considered when designing to resist anticipated deformation include the use of ductile pile foundations, reinforced earth, structural walls, or buttress fills keyed into non-liquefiable strata to resist the effects of lateral spreading. These techniques are described in detail elsewhere (e.g., Kramer and Holtz, 1991).

A variety of techniques exist to remediate potentially liquefiable soils and mitigate the liquefaction hazard. Table 8-3 presents a summary of methods for improvement of liquefiable soil foundation conditions (NRC, 1985). The cost of foundation improvement can vary over an order of magnitude, depending on site conditions (e.g., adjacent sensitive structures) and the nature and geometry of the liquefiable soils. Remediation costs can vary from as low as several thousand dollars per acre for dynamic compaction of shallow layers of clean sands in open areas to upwards of \$100,000 per acre for deep layers of silty soils adjacent to sensitive structures. Liquefaction remediation measures must be evaluated on a case-by-case basis to determine their economic viability.

The results of a number of post-earthquake settlement measurements made on Port Island and Rokko Island following the 1995 Kobe Earthquake in relation to site treatment methods are presented in Figure 8-13 (Yasuda, et al, 1995). The soil profile on these islands is typically 12 to 20 m of loose, hydraulically filled, decomposed granite sand underlain by several meters of soft, compressible alluvial clay. It should be noted that sand drains and preloading were used for the purpose of precompressing the soft clay for reducing future long term settlements under static loads. The results shown in Figure 8-13 suggest that sand drains and preloading, although have some beneficial effects on the liquefaction resistance, are not effective methods in preventing liquefaction from occurring. To mitigate liquefaction risk of loose, granular soils, proper methods of ground treatment have to be applied.

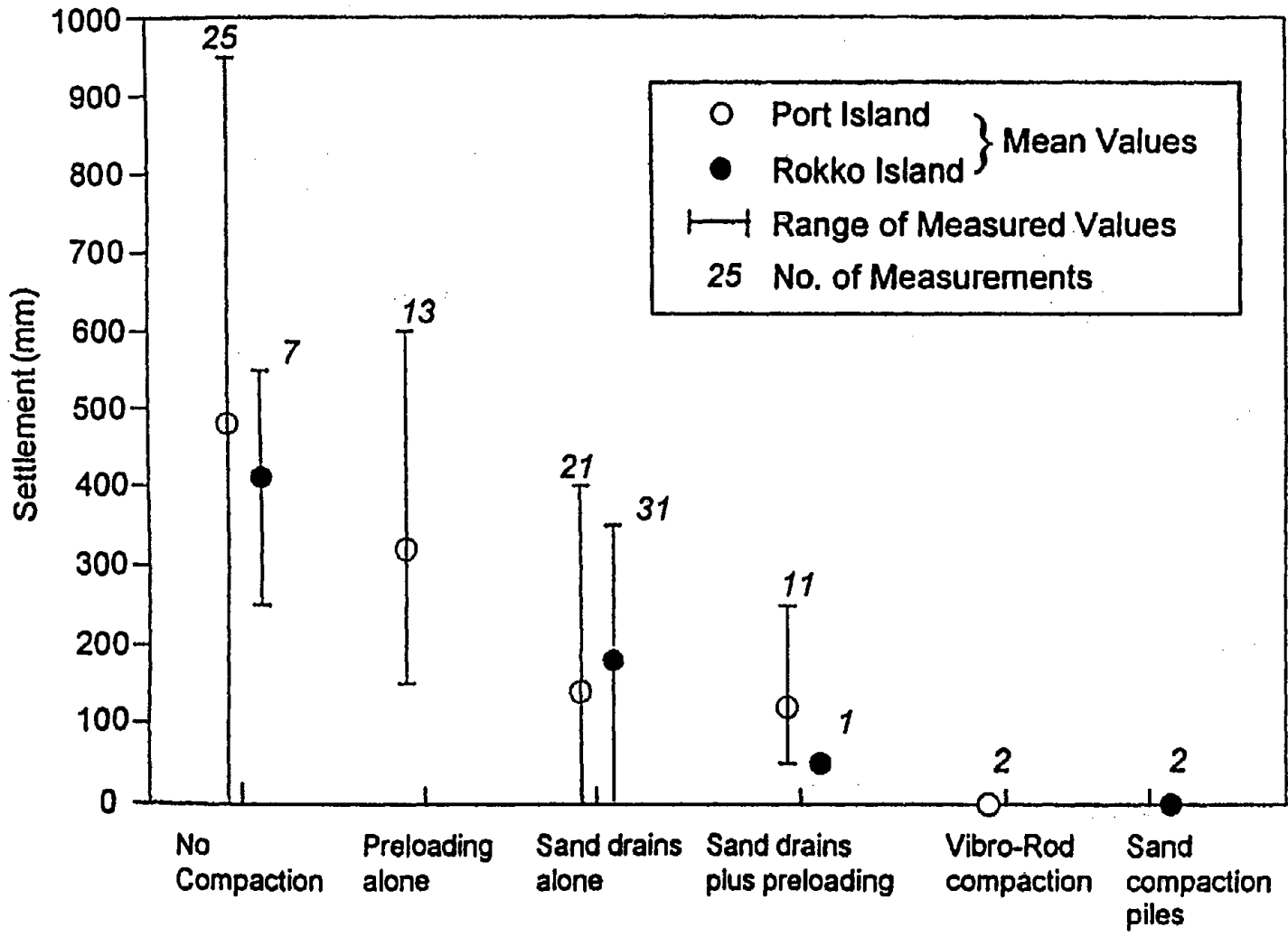


Figure 8-13: Post-Earthquake Settlements at Two Port Sites due to the 1995 Kobe Earthquake (Yasuda, et. al, 1995).

TABLE 8-3 IMPROVEMENT TECHNIQUES FOR LIQUEFIABLE SOIL FOUNDATION CONDITIONS (AFTER NRC, 1985)

Method	Principle	Most Suitable Soil Conditions/Types	Maximum Effective Treatment Depth	Economical Size of Treated Area	Ideal Properties of Treated Material ¹	Applications**	Case ¹	Relative Costs
In-Situ Deep Compaction								
(1) Blasting	Shock waves and vibrations cause limited liquefaction, displacement, remolding and settlement to higher density.	Saturated, clean sands; partly saturated sands and silts after flooding.	>40 m Solymar (1984)	Any Size	Can obtain relative densities of 70-80%; may get variable density; time-dependent strength gain.	Induce liquefaction in controlled and limited stages and increase relative density to potentially non-liquefiable range.	2 3	Low
(2) Vibratory Probe (a) Terraprob (b) Vibro-Rods (c) Vibro-Wing	Densification by vibration; liquefaction-induced settlement and settlement in dry soil under overburden to produce a higher density.	Saturated or dry clean sand; sand.	20 m routinely (ineffective above 3-4 m depth) > 30 m sometimes Mitchell (1981) Vibro-Wing-40 m Broms and Hansson (1984)	> 1,000 m ²	Can obtain relative densities of 80% or more. Ineffective in some sands.	Induce liquefaction in controlled and limited stages and increase relative density to potentially non-liquefiable range. Has been shown ineffective in preventing liquefaction.	2 3	Moderate
(3) Vibro-Compaction (a) Vibroflot (b) Vibro-Composer System (c) Soil Vibratory stabilizing method	Densification by vibration and compaction of backfill material of sand or gravel.	Cohesionless soils with less than 20% fins.	>30 m Solymar et al. (1984)	> 1,000 m ²	Can obtain high relative densities (over 85%), good uniformity.	Induce liquefaction in controlled and limited stages and increase relative densities to nonliquefiable condition. Is used extensively to prevent liquefaction. The dense column of backfill provides (a) vertical support, (b) drains to relieve pore water pressure and (c) shear resistance in horizontal and inclined directions. Used to stabilize slopes and strengthen potential failure surfaces or slip circles.	1 2 Δ ¹	Low to moderate
(4) Compaction Soils	Densification by displacement of pile volume and by vibration during driving, increase in lateral effective earth pressure.	Loose sandy soils; partly saturated clayey soils; loess.	>20 m Nataraja and Cook (1983)	> 1,000 m ²	Can obtain high densities, good uniformity. Relative densities of more than 80%.	Useful in soils with fines. Increases relative densities to nonliquefiable range. Is used to prevent liquefaction. Provides shear resistance in horizontal and inclined directions. Useful to stabilize slopes and strengthen potential failure surfaces or slip circles.	1 2 3	Moderate to High
(5) Heavy Tamping (dynamic compaction)	Repeated application of high-intensity impacts at surface.	Cohesionless soils best, other types can also be improved.	30 m (possibly deeper) Ménard and Broise (1975)	> 3,300 m ²	Can obtain high relative densities, reasonable uniformity. Relative densities of 80% or more	Suitable for some soils with fines; usable above and below water. In cohesionless soils, induces liquefaction in controlled and limited stages and increases relative density to potentially nonliquefiable range. Is used to prevent liquefaction.	2 3	Low

8 - 22 (Part I)

¹ SP, SW, or SM soils which have average relative density equal to or greater than 85 percent and the minimum relative density not less than 80 percent are in general not susceptible to liquefaction (TM 5-818-1). D'Appolonia (1970) stated that for soil within the zone of influence and confinement of the structure foundation, the relative density should not be less than 70 percent. Therefore, a criterion may be used that relative density increase into the 70-90 percent range is in general considered to prevent liquefaction. These properties of treated materials and applications occur only under ideal conditions of soil, moisture, and method application. The methods and properties achieved are not applicable and will not occur in all soils.

** Applications and results of the improvement methods are dependent on: (a) soil profiles, types, and conditions, (b) site conditions, (c) earthquake loading, (d) structure type and condition, and (e) material and equipment availability. Combinations of the methods will most likely provide the best and most stable solution.

¹ Site conditions have been classified into three cases; Case 1 is for beneath structures, Case 2 is for the not-under-water free field adjacent to a structure, and Case 3 is for the under-water free field adjacent to a structure.

¹ Δ means the method has potential use for Case 3 with special techniques required which would increase the cost.

TABLE 8-3 IMPROVEMENT TECHNIQUES FOR LIQUEFIABLE SOIL FOUNDATION CONDITIONS (AFTER NRC, 1985)

Method	Principle	Most Suitable Soil Conditions/Types	Maximum Effective Treatment Depth	Economical Size of Treated Area	Ideal Properties of Treated Material ¹	Applications**	Case ¹	Relative Costs
In-Situ Deep Compaction								
(6) Displacement/Compaction Grout	Highly viscous grout acts as radical hydraulic jack when pumped in under high pressure.	All soils.	Unlimited	Small	Grout bulbs within compressed soil matrix. Soil mass as a whole is strengthened.	Increase in soil relative density and horizontal effective stress. Reduce liquefaction potential. Stabilize the ground against movement.	1 2 3	Low to Moderate
Compression								
(7) Surcharge/Buttress	The weight of a surcharge/buttress increases the liquefaction resistance by increasing the effective confining pressures in the foundation.	Can be placed on any soil surface.		> 1,000 m ²	Increase strength and reduce compressibility.	Increase the effective confining pressure in a liquefiable layer. Can be used in conjunction with vertical and horizontal drains to relieve pore pressure. Reduce liquefaction potential. Useful to prevent movements of a structure and for slope stability.	2 3	Moderate if vertical drains used.
Pore-Water Pressure Relief								
(8) Drains (a) Gravel (b) Sand (c) Wick (d) Wells (for permanent dewatering)	Relief of excess pore-water pressure to prevent liquefaction. (Wick drains have comparable permeability to sand drains). Primarily gravel drains; sand/wick drains may supplement gravel drain or relieve existing excess pore water pressure. Permanent dewatering with pumps.	Sand, silt, clay.	Gravel and Sand >30 m Depth limited by vibratory equipment Wick >45 m Morrison (1982)	> 1,500 m ² Any size for wick.	Pore-water pressure relief will prevent liquefaction.	Prevent liquefaction by gravel drains. Sand and gravel drains are installed vertically; however, wick drains can be installed at any angle. Dewatering will prevent liquefaction but not seismically-induced settlements.	Gravel and Sand Δ ¹ Wick 1 2 3	Dewatering very expensive.
(9) Particulate Grouting	Penetration grouting - fill soil pores with soil, cement, and/or clay.	Medium to coarse sand and gravel.	Unlimited	Small	Impervious, high strength with cement grout. Voids filled so they cannot collapse under cyclic loading.	Eliminate liquefaction danger. Slope stabilization. Could potentially be used to confine an area of liquefiable soil so that liquefied soil could not flow out of the area.	1 2 3	Lowest of Grout Methods

8 - 23 (Part 1)

^{*} SP, SW, or SM soils which have average relative density equal to or greater than 85 percent and the minimum relative density not less than 80 percent are in general not susceptible to liquefaction (TM 5-818-1). D'Appolonia (1970) stated that for soil within the zone of influence and confinement of the structure foundation, the relative density should not be less than 70 percent. Therefore, a criterion may be used that relative density increase into the 70-90 percent range is in general considered to prevent liquefaction. These properties of treated materials and applications occur only under ideal conditions of soil, moisture, and method application. The methods and properties achieved are not applicable and will not occur in all soils.

^{**} Applications and results of the improvement methods are dependent on: (a) soil profiles, types, and conditions, (b) site conditions, (c) earthquake loading, (d) structure type and condition, and (e) material and equipment availability. Combinations of the methods will most likely provide the best and most stable solution.

¹ Site conditions have been classified into three cases; Case 1 is for beneath structures, Case 2 is for the not-under-water free field adjacent to a structure, and Case 3 is for the under-water free field adjacent to a structure.

¹ Δ means the method has potential use for Case 3 with special techniques required which would increase the cost.

TABLE 8-3 IMPROVEMENT TECHNIQUES FOR LIQUEFIABLE SOIL FOUNDATION CONDITIONS (AFTER NRC, 1985)

Method	Principle	Most Suitable Soil Conditions/Types	Maximum Effective Treatment Depth	Economical Size of Treated Area	Ideal Properties of Treated Material ¹	Applications ²	Case ³	Relative Costs
(10) Chemical Grouting	Solutions of two or more chemicals react in soil pores to form a gel or a solid precipitate.	Medium silts and coarser.	Unlimited	Small	Impervious, low to high strength. Voids filled so they cannot collapse under cyclic loading.	Eliminate liquefaction danger. Slope stabilization. Could potentially be used to confine an area of liquefiable soil so that liquefied soil could not flow out of the area. Good water shutoff.	1 2 3	High
(11) Pressure-Injected Lime	Penetration grouting - fill soil pores with lime.	Medium to coarse sand and gravel.	Unlimited	Small	Impervious to some degree. No significant strength increase. Collapse of voids under cyclic loading reduced.	Reduce liquefaction potential.	1 2 3	Low
Pore-Water Pressure Relief								
(12) Electrokinetic Injection	Stabilizing chemicals move into and fill soil pores by electro-osmosis or colloids into pores by electro-phoresis.	Saturated sands, silts, silty clays.	Unknown	Small	Increased strength, reduced compressibility, voids filled so they cannot collapse under cyclic loading.	Reduce liquefaction potential.	1 2 3	Expensive
(13) Jet Grouting	High-speed jets at depth excavate, inject, and mix a stabilizer with soil to form columns or panels.	Sands, silts, clays.	Unknown	Small	Solidified columns and walls.	Slope stabilization by providing shear resistance in horizontal and inclined directions which strengthens potential failure surfaces or slip circles. A wall could be used to confine an area of liquefiable soil so that liquefied soil could not flow out of the area.	1 2 3	High
Admixture Stabilization								
(14) Mix-in-Place Piles and Walls	Lime, cement, or asphalt introduced through rotating auger or special in-place mixer.	Sands, silts, clays, all soft or loose inorganic soils.	>20 m (60 m obtained in Japan) Mitchell (1981)	Small	Solidified soil piles or walls of relatively high strength.	Slope stabilization by providing shear resistance in horizontal and inclined directions which strengthens potential failure surfaces or slip circles. A wall could be used to confine an area of liquefiable soil so that liquefied soil could not flow out of the area.	1 2 3	High

8 - 24 (Part I)

¹ SP, SW, or SM soils which have average relative density equal to or greater than 85 percent and the minimum relative density not less than 80 percent are in general not susceptible to liquefaction (TM 5-818-1). D'Appolonia (1970) stated that for soil within the zone of influence and confinement of the structure foundation, the relative density should not be less than 70 percent. Therefore, a criterion may be used that relative density increase into the 70-90 percent range is in general considered to prevent liquefaction. These properties of treated materials and applications occur only under ideal conditions of soil, moisture, and method application. The methods and properties achieved are not applicable and will not occur in all soils.

² Applications and results of the improvement methods are dependent on: (a) soil profiles, types, and conditions, (b) site conditions, (c) earthquake loading, (d) structure type and condition, and (e) material and equipment availability. Combinations of the methods will most likely provide the best and most stable solution.

³ Site conditions have been classified into three cases; Case 1 is for beneath structures, Case 2 is for the not-under-water free field adjacent to a structure, and Case 3 is for the under-water free field adjacent to a structure.

TABLE 8-3 IMPROVEMENT TECHNIQUES FOR LIQUEFIABLE SOIL FOUNDATION CONDITIONS (AFTER NRC, 1985)

Method	Principle	Most Suitable Soil Conditions/Types	Maximum Effective Treatment Depth	Economical Size of Treated Area	Ideal Properties of Treated Material	Applications**	Case [†]	Relative Costs
Thermal Stabilization								
(15) In-Situ Vitrification	Melts soil in place to create an obsidian-like vitreous material.	All soils and rock.	>30 m Verbal from Battelle Laboratories	Unknown	Solidified soil piles or walls of high strength. Impervious; more durable than granite or marble; compressive strength, 9-11 ksi; splitting tensile strength, 1-2 ksi	Slope stabilization by providing shear resistance in horizontal and inclined directions which strengthens potential failure surfaces or slip circles. A wall could be used to confine an area of liquefiable soil so that liquefied soil could not flow out of the area.	1 2 3	Moderate
Soil Reinforcement								
(16) Vitro-Replacement Stone and Sand Columns (a) Grouted (b) Not Grouted	Hole jetted into fine-grained soil and backfilled with densely compacted gravel or sand hole formed in cohesionless soils by vibro techniques and compaction of backfilled gravel or sand. For grouted columns, voids filled with a grout.	Sands, silts, clays.	>30 m Limited by vibratory equipment.	> 1,500 m ² Fine-grained soils > 1,000 m ²	Increased vertical and horizontal load carrying capacity. Density increase in cohesionless soils. Shorter drainage paths.	Provides: (a) vertical support, (b) drains to relieve pore water pressure, and (c) shear resistance in horizontal and inclined direction. used to stabilize slopes and strengthen potential failure surfaces or slip circles. For grouted columns, no drainage provided but increased shear resistance. In cohesionless soil, density increase reduces liquefaction potential.	1 2 Δ [†]	Moderate
(17) Root Piles, Soil Nailing	Small-diameter inclusions used to carry tension, shear, compression.	All soils.	Unknown.	Unknown	Reinforced zone of soil behaves as a coherent mass.	Slope stability by providing shear resistance in horizontal and inclined directions to strengthen potential failure surfaces or slip circles. Both vertical and angled placement of the piles and nails.	1 2 3	Moderate to High

8 - 25 (Part I)

* SP, SW, or SM soils which have average relative density equal to or greater than 85 percent and the minimum relative density not less than 80 percent are in general not susceptible to liquefaction (TM 5-818-1). D'Appolonia (1970) stated that for soil within the zone of influence and confinement of the structure foundation, the relative density should not be less than 70 percent. Therefore, a criterion may be used that relative density increase into the 70-90 percent range is in general considered to prevent liquefaction. These properties of treated materials and applications occur only under ideal conditions of soil, moisture, and method application. The methods and properties achieved are not applicable and will not occur in all soils.

** Applications and results of the improvement methods are dependent on: (a) soil profiles, types, and conditions, (b) site conditions, (c) earthquake loading, (d) structure type and condition, and (e) material and equipment availability. Combinations of the methods will most likely provide the best and most stable solution.

† Site conditions have been classified into three cases; Case 1 is for beneath structures, Case 2 is for the not-under-water free field adjacent to a structure, and Case 3 is for the under-water free field adjacent to a structure.

‡ Δ means the method has potential use for Case 3 with special techniques required which would increase the cost.



CHAPTER 9.0 SEISMIC DESIGN OF FOUNDATIONS AND RETAINING WALLS

9.1 INTRODUCTION

This chapter addresses geotechnical aspects of seismic design of foundations, retaining walls, and other structural components of highway systems. In addressing these issues, it is assumed that the ground motions at the site have been determined by the project geologist and/or geotechnical engineer and that the earthquake-induced forces from the superstructure have been provided by the structural engineer. Guidelines are available for the seismic design of highway bridges which cover some of the issues related to seismic design of foundations and retaining walls. Of particular note are the AASHTO Standard Specifications for Highway Bridges (AASHTO, 1994), the seismic design course notes prepared by ABAM Engineering (ABAM, 1994), FHWA Guidelines for Seismic Design of Highway Bridge Foundations (Lam and Martin, 1986), Design and Construction of Driven Pile Foundations (Hannigan, et al., 1997), and Laterally-Loaded Piles (Reese, 1984). Much of the information contained in these guidelines will not be covered in detail herein, but will be incorporated by reference.

The discussions herein are intended to cover routine situations encountered in highway engineering. Specialty topics such as seismic retrofit of long span bridges require special considerations and are beyond the scope of this document.

9.1.1 Foundation Systems

In a manner similar to evaluation of the stability of a slope subject to earthquake ground motions (Chapter 7), earthquake effects on foundations can be modeled using either a pseudo-static approach, wherein the earthquake-induced loads are represented by static forces and/or moments to the foundation, or a dynamic approach, wherein the time history of transient cyclic earthquake forces is applied to the structure-foundation system.

In a pseudo-static analysis, the effects of the dynamic earthquake-induced loads on the foundation are represented using static forces and moments. The bearing capacity and lateral resistance of a foundation element is evaluated using static formulations and compared to the pseudo-static loads. However, the static shear strength may be either decreased or increased, depending on soil type and groundwater conditions, to account for dynamic loading conditions.

Earthquake induced loading on the foundation for a highway structure is typically dominated by the inertia forces from the superstructure. The earthquake-induced forces on the superstructure are predominantly horizontal. However, these horizontal forces are transmitted to the foundation in the form of horizontal and vertical forces and rocking and torsional moments. To represent the combined effect of the forces and moments induced by an earthquake, the resultant pseudo-static loads are applied to the foundation as shown in Figure 9-1. The resultant load may have to be inclined and applied eccentrically, as shown in Figure 9-2, to account for vertical loads and moment loading. Solutions for the bearing capacity of eccentrically loading footings may then be used to evaluate foundation performance (refer to Module 7 - Shallow Foundations). Alternatively, vertical bearing capacity and horizontal sliding resistance of the foundation can be considered independently. Note, however, that the influence of the applied moments on the vertical and horizontal loads must be considered in such analyses. Often (e.g., in the evaluation of shallow foundations), for "unimportant" structures, only the gross stability of the foundation is evaluated in the pseudo-static approach. Neither an assessment of the dynamic response of the foundation

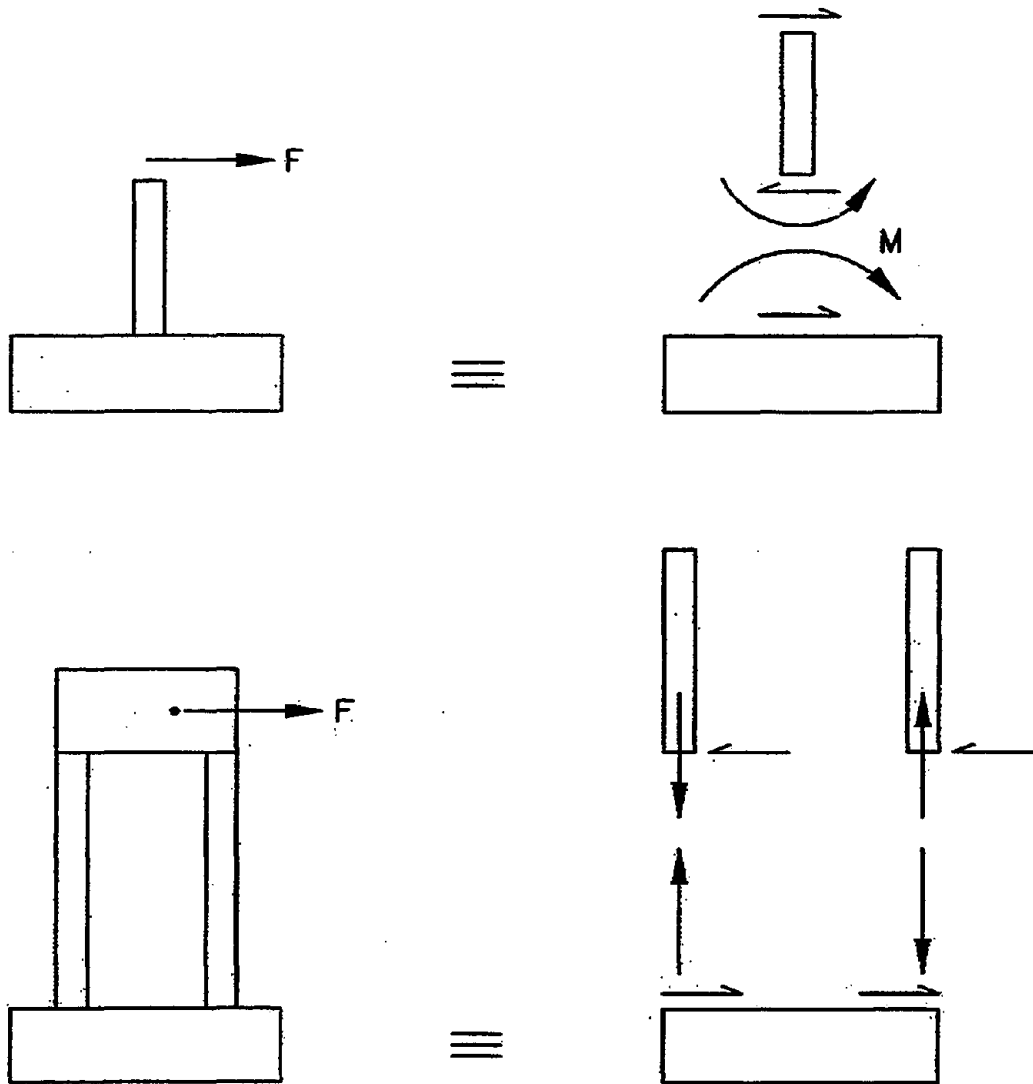


Figure 9-1: Superstructure Loads Resolved Into Components at Footing

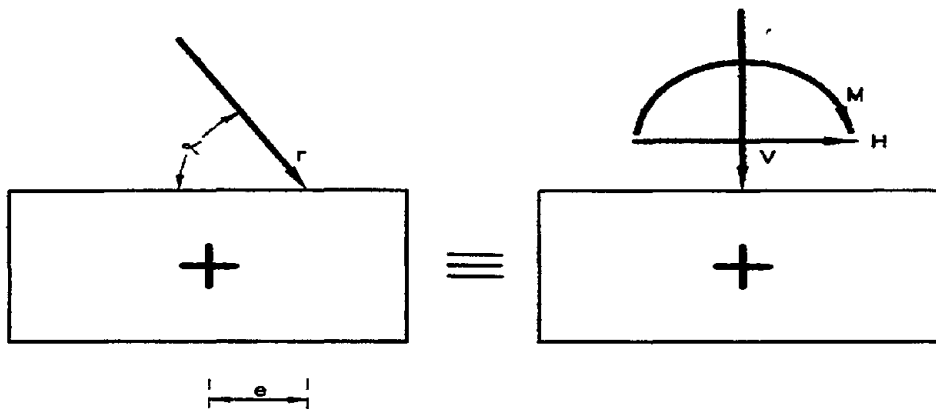


Figure 9-2: Principle of Superposition of Loads on Footing.

nor an evaluation of the interaction between the foundation and the superstructure is made. In other cases, (e.g., evaluation of the response of a laterally loaded pile), the stiffness or deformation of the foundation subject to the pseudo-static load is calculated in addition to a bearing capacity evaluation.

In a dynamic response analysis, the dynamic stiffness of the foundation is incorporated into an analytical model of the highway structure to evaluate the overall seismic response of the system. The foundation for a highway structure subject to dynamic excitation has six degrees of freedom (modes of motion): horizontal sliding in two orthogonal directions; vertical motions; rocking about two orthogonal horizontal axes; and torsion (rotation) about the vertical axis. Therefore, in the dynamic analysis of a highway structure, the response of the foundation to these modes of excitation is described by a 6 x 6 stiffness matrix with 36 stiffness coefficients, K_{ij} . The six modes of motion (degrees of freedom) of a shallow foundation and the corresponding stiffness matrix are shown in Figure 9-3. Each term K_{ij} of the stiffness matrix describes the deformation response of the foundation in coordinate direction i to a unit load in coordinate direction j (e.g., if mode i is horizontal motion in the y direction and mode j is rocking about the y axis, then K_{ij} is the horizontal translation under a unit horizontal force and K_{ji} is the rocking rotation in response to a unit horizontal force). It should be noted that the cross term coefficients K_{ij} , where $i \neq j$, are generally ignored for shallow footing analysis due to the negligibly small coupling effects. However, an exception may occur with respect to the rocking and sliding modes, which may be coupled as shown in Figure 9-4. A similar 6 x 6 matrix can be developed for the damping of the foundation, as discussed in Section 9.2.3. Internal damping of the soil is commonly incorporated in the site response model used to calculate design ground motions, as described in Chapters 5 and 6, and not in the foundation model itself. The geotechnical engineer provides the values of the foundation stiffness and damping coefficients to the structural engineer for use in the dynamic response analysis of the structure. Even when a dynamic response analysis is performed, the gross stability of the foundation should still be evaluated using a pseudo-static bearing capacity analysis. However, in this case, the applied loads on the foundation elements may be taken directly from the results of the dynamic response analysis by factoring the peak loads, as discussed in Section 9.2.2, Load Evaluation for Pseudo-Static Bearing Capacity Analysis.

9.1.2 Retaining Walls

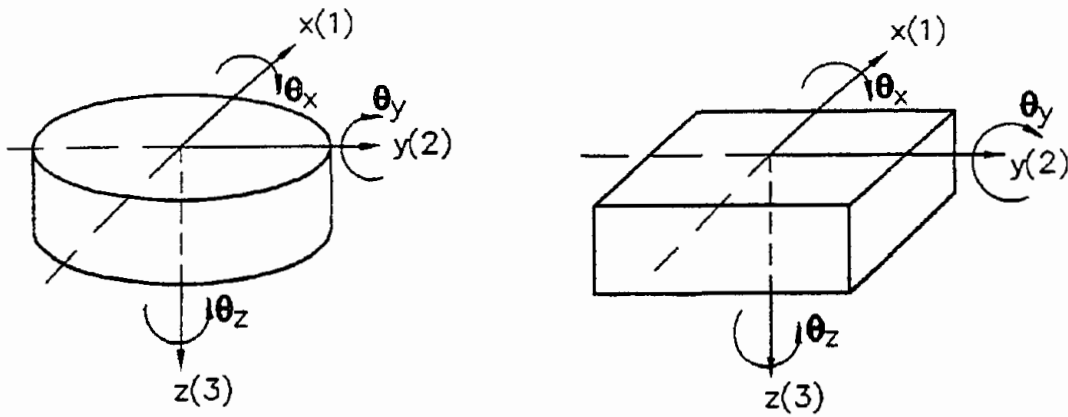
The seismic performance of retaining walls is an important component of earthquake engineering for highway systems. Retaining walls are used extensively for bridge abutments, depressed segments of highway alignments, and elevated highways. Retaining walls are generally designed to resist sliding, overturning, and structural failure due to lateral pressures. Most retaining structures are designed to resist seismic loads using pseudo-static analyses. For sliding of gravity walls, a deformation based design methodology (i.e., permissible displacement approach) is often used in practice.

9.2 DESIGN OF SHALLOW FOUNDATIONS

9.2.1 General

Shallow foundations are commonly used as foundations for bridge piers and abutment walls. Shallow foundations are suitable at rock sites or when firm soils are found at shallow depth provided the potential for landslide induced displacements is fairly low and the risk of liquefaction is very low or non-existent. In areas where deposits of compressible, expansive, or collapsible soils are found near the ground surface, shallow foundations may not be suitable. Where soil conditions are not suitable for the use of shallow foundations, deep foundations are used.

The seismic performance of shallow foundations may be evaluated using either pseudo-static limit



δ_x	δ_y	δ_z	θ_x	θ_y	θ_z
K_{11}	0	0	0	$-K_{15}$	0
0	K_{22}	0	K_{24}	0	0
0	0	K_{33}	0	0	0
0	K_{42}	0	K_{44}	0	0
$-K_{51}$	0	0	0	K_{55}	0
0	0	0	0	0	K_{66}

Figure 9-3: Degrees of Freedom of a Footing and Corresponding Stiffness Matrix.



Figure 9-4: Coupled Rocking and Sliding

equilibrium analysis or dynamic response analysis. The critical element in a pseudo-static analysis of a shallow foundation is the evaluation of the pseudo-static loads (forces and moments) for use in the analysis. The primary task of the geotechnical engineer in a dynamic response analysis of a structural system that employs shallow foundations is the evaluation of the coefficients of the stiffness matrix. If a dynamic response analysis of the structure is performed, the gross stability of the shallow foundation should still be evaluated using pseudo-static limit equilibrium analysis.

In addition to evaluating the gross stability of the shallow foundation under dynamic loads, the risk of excessive seismic settlement and soil liquefaction should also be evaluated for foundations founded upon saturated cohesionless soils. Evaluation of liquefaction and settlement potential is described in Chapter 8.

9.2.2 Pseudo-Static Analyses

General

Two alternative methods are commonly used in geotechnical practice to evaluate the ultimate bearing capacity of shallow foundations for highway structures:

- the general bearing capacity equation using bearing capacity factors derived from soil shear strength parameters (c , ϕ); and
- the bearing capacity equation based on Standard Penetration Test blow counts.

In theory, the two methods cited above should give similar results if the strength parameters used to represent the foundation soil are consistent with the SPT blow count. Some engineers prefer to use the blow count method for dynamic bearing capacity analysis because the SPT is a dynamic test and thus its use may take into account any tendency for the soil to lose strength when subjected to dynamic loading. However, the general bearing capacity equation method provides more flexibility in accounting for inclined and eccentric loading. Bearing capacity can also be evaluated using CPT results (Riaund and Miran, 1992).

Shallow foundations should also be designed to resist sliding under seismic loading. Sliding resistance is typically assessed using the interface friction and adhesion between the bottom of the foundation and the foundation soil to resist the applied seismic loads. Friction and adhesion on the sides of the foundation may also be included in evaluating the resistance of a foundation to sliding. Some engineers include the passive seismic soil resistance on the front of the footing when calculating sliding resistance. However, when passive resistance is employed in evaluating sliding resistance, the calculated passive seismic earth pressure is often divided by two to compensate for the relatively large lateral deformations required to mobilize the passive resistance of the soil. Furthermore, if the passive seismic resistance on the front of the footing is included in the analysis, the active seismic pressure on the back of the footing should also be considered. Evaluation of passive and active seismic earth pressures is discussed subsequently in Section 9.6.

Procedures for evaluating bearing capacity and sliding resistance of shallow foundations are presented in detail in Module 7 (Shallow Foundations). Herein, only guidance evaluating loads and resistances for pseudo-static analysis is presented.

Load Evaluation for Pseudo-Static Bearing Capacity Analysis

The foundation loads for use in a pseudo-static bearing capacity analysis for a shallow foundation may be

evaluated either by applying a pseudo-static load to the structure or from the results of a dynamic response analysis. In determining foundation loads by applying a pseudo-static force to the structure, both the horizontal and vertical inertial forces from the superstructure may be considered. These inertia forces are modeled by applying through the center of gravity of the superstructure, a load equal to the weight of the structure multiplied by a seismic coefficient. If applied centrally, the vertical load will generate only vertical forces on the foundation. However, if the vertical force is eccentrically applied to the foundation, it will generate a moment loading. The horizontal load typically generates both vertical forces and moments on the foundation. The peak vertical and horizontal dynamic loads are often considered separately, as it is highly unlikely that the peak vertical and horizontal forces will act simultaneously on the superstructure. In each case, the resultant forces and moments on the foundation elements are used in the pseudo-static bearing capacity analysis. Foundation performance should be evaluated for both compressive and tensile vertical seismic loads. Furthermore, the vertical and horizontal dead loads of the superstructure and foundation should be added to the seismic loads when analyzing the foundation system in either case.

There is no general agreement on establishing the seismic coefficient used in evaluation of the pseudo-static load for the seismic analysis of foundations. Based upon experience with the seismic stability of slopes (Chapter 7), the seismic coefficient for foundation design should be a fraction of the peak ground acceleration (PGA) expressed as a fraction of gravity. For many cases, the effective peak acceleration from AASHTO maps may be appropriate for use as the seismic coefficient in pseudo-static analysis, as this value is typically already reduced from the expected maximum peak ground acceleration. Alternatively, based upon experience with seismic deformation analyses of slopes and embankments, including back analyses of the performance of slopes and embankments in earthquakes, a value equal to one-half the PGA (expressed as a fraction of gravity) would appear to be reasonable. However, for structures that cannot tolerate foundation deformations of up to several centimeters and for structures founded on soils subject to progressive failure and/or a post-peak strength decrease, a value equal to the PGA (expressed as a fraction of gravity) may be appropriate. Furthermore, the potential for amplification of the PGA by the structure itself should be considered. For slender, flexible structures, it may be prudent to multiply the above values by an amplification factor provided by the structural engineer.

If the loads used in the pseudo-static foundation analysis are determined from the results of a dynamic response analysis of the structure, then the potential for amplification of the ground motion by the structure is included in the peak loads from the response analysis. In this case, the peak loads provided by the structural engineer should be factored in the same manner described above to evaluate the seismic coefficient from the PGA; that is, a factor of one-half would appear to be reasonable in most situations, while a value of one may be used for structures that cannot tolerate significant deformations and for structures founded on soils subject to progressive failure and/or post-peak strength decrease. When using the loads from a dynamic response analysis to evaluate foundation performance, peak loads that occur at different times in the analysis should not be superimposed. Loads used in combination should be loads that act upon the foundation at the same time. For instance, the peak horizontal load should be used in combination with the vertical loads imposed on the foundation by the peak horizontal load and with other vertical loads acting on the foundation at the same time as the peak horizontal load, but not in combination with the peak rocking moment or peak vertical load.

The General Bearing Capacity Equation

Terzaghi presented the first comprehensive theory for the evaluation of the ultimate bearing capacity of rough, shallow foundations. Using limit equilibrium analysis, Terzaghi expressed the ultimate bearing capacity as a function of the geometry of the foundation, the geometry of the assumed failure surfaces, and

the geotechnical properties of the foundation soil.

Terzaghi's early work was then expanded upon to provide formulations accounting for different foundation shapes, load inclination and load eccentricity, water table location, and other factors. These formulations are also based on the resolution of a limit equilibrium problem and the evaluation of the shear strength properties of the foundation soil.

Consequently, to account for eccentric loads, moments, inclined loads, and different foundation shapes, a series of correction factors were applied to the initial Terzaghi bearing capacity equation. Application of these correction factors results in a generalized bearing capacity equation of the form:

$$q_{ult} = c N_c s_c i_c + 0.5 \gamma B N_\gamma s_\gamma i_\gamma + q_s N_q s_q i_q \quad (9-1)$$

where q_{ult} is the ultimate bearing capacity, q_s is a uniform surcharge load applied at the ground surface adjacent to the foundation, B is the foundation width, s_c , s_γ , and s_q are foundation shape factors, i_c , i_γ and i_q are load inclination factors, c and γ are the cohesion and unit weight of the soil, and N_c , N_γ , and N_q are the bearing capacity factors. Note that the surcharge load q_s is equal to γD for a foundation embedded at a depth D below the ground surface.

The bearing capacity factors, N_c , N_γ , and N_q are a function of the friction angle of the soil, ϕ . Charts of bearing capacity factors versus ϕ are commonly available in geotechnical literature. For spread sheet calculations, the following equations may be used:

$$N_q = e^{\pi \tan \phi} \tan^2 \left(45 + \frac{\phi}{2} \right) \quad (9-2)$$

$$N_c = (N_q - 1) \cot(\phi) \quad (9-3)$$

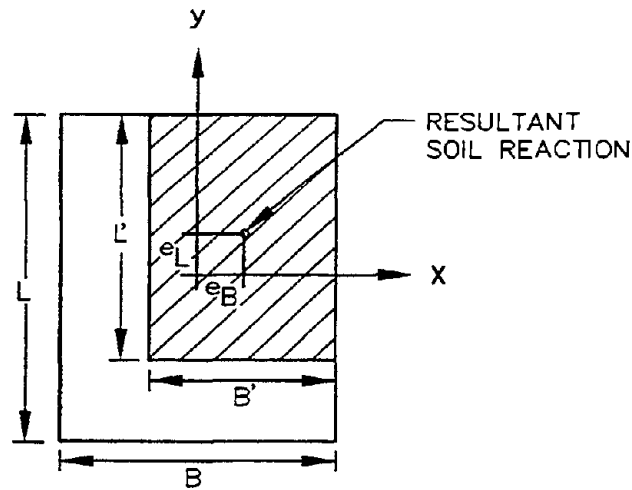
$$N_\gamma = (N_q - 1) \tan(1.4\phi) \quad (9-4)$$

Adjustments for Eccentric (Moment) Loading

The first step in a pseudo-static seismic bearing capacity analysis is to compute the pseudo-static loads. The pseudo-static and static loads are then combined into a single resultant force with an inclination α and an eccentricity, e , as illustrated in Figure 9-2.

Following computation of the resultant force, equivalent dimensions are computed for the footing to account for the eccentricity of the load on the footing. The load eccentricity is caused by the moment applied to the foundation. This applied moment creates a non-uniform pressure on the bottom of the footing and can lead to loss of contact pressure between the bottom of the footing and the ground. Therefore, the width of a footing subjected to an eccentric load is represented by a reduced, effective width, B' . The computation of equivalent dimensions to account for the load eccentricity is illustrated on Figure 9-5.

Some widely used relationships for the effective contact area are $B' = (B-2e)$, as recommended by



$$e_B = M_y/V, \quad e_L = M_x/V$$

$$B' = B - 2e_B, \quad L' = 2e_L$$

Maximum Soil Pressure (Linear Distribution):

$$q_{\max} = V [1 + (6 e_L/L)] / (BL) \quad \text{for } e_L < L/6$$

$$q_{\max} = 2V / [3B(L/2 - e_L)] \quad \text{for } L/6 < e_L < L/2$$

Figure 9-5: Evaluation of Overturning Moment.

Meyerhof (1953), and $B' = (3B/2 - 3e)$ corresponding to a linear soil pressure distribution. The calculated value tends to be conservative in that the actual contact area will usually be larger than the calculated values using these relationships.

To prevent uplifting of the footing edge, a limit is usually set on the allowable eccentricity of the dynamic load. Hansen (1953) showed that if $e \leq B/4$, there would be no uplift. Hansen (1953) recommended sizing the footing such that e is limited to $B/6$. In areas of high seismicity (ground motions in excess of 0.4 g), this may not be practical. In cases where it is not practical to limit e to $B/6$, it is recommended that e be limited to $B/4$.

An upwards vertical load on a foundation will tend to increase e . This will tend to reduce the effective footing area, which may lead to an increase in the calculated minimum soil pressure. Therefore, the foundation should be checked for both upwards and downwards vertical seismic loads.

Adjustment for Inclined (Lateral) Loading and Rectangular Shapes

Recommendations for the correction factors in Equation 9-1 for inclined loads and non-circular footing shapes are provided by Meyerhof (1953). These recommendations are as follows:

For inclined loads:

$$i_c = i_q [(1 - i_q)/(N_c \tan \phi)] \quad \text{for } \phi > 0 \quad (9-5a)$$

$$i_c = 1 - [nH/(BLcN_c)] \quad \text{for } \phi = 0 \quad (9-5b)$$

$$i_q = [1 - H/(V + BLc(\cot\phi))]^n \quad (9-5c)$$

$$i_\gamma = [1 - H/(V + BLc(\cot\phi))]^{(n+1)} \quad (9-5d)$$

where H and V are resultant horizontal and vertical seismic loads, respectively, and L and B are foundation length and width, respectively, and:

$$n = [(2 + L/B)/(1 + L/B)]\cos^2\theta + [(2 + B/L)/(1 + B/L)]\sin^2\theta \quad (9-6a)$$

where: $\theta = \tan^{-1}(e_b/e_L)$

If the load is applied parallel to the length L of the footing:

$$n = [2 + B/L]/(1 + B/L)]\cos^2\theta + [(2 + L/B)/(1 + L/B)]\sin^2\theta \quad (9-6b)$$

For rectangular footings with a length less than five times the width,

$$s_c = 1 + (B/L) (N_q/N_c) \quad (9-7a)$$

$$s_q = 1 + (B/L) \tan\phi \quad (9-7b)$$

$$s_\gamma = 1 - 0.4 (B/L) \quad (9-7c)$$

For eccentric loading, substitute B' for B in the above equations.

Other Cases

For complex situations such as multi-layer soils, inclined foundations, or foundations placed on or near a slope, alternative solutions for bearing capacity factors have been developed. Charts and tables to address such cases can be found elsewhere (e.g., AASHTO, 1994; NAVFAC, 1986).

Bearing Capacity From Penetration Tests

The bearing capacity of a shallow foundation on granular soils can be evaluated directly from SPT and CPT results. Bearing capacity evaluations based on SPT and CPT data are less reliable for foundations supported on cohesive soils.

Meyerhof (1956) proposed the following equation relating ultimate bearing capacity to SPT blow count:

$$q_{ult} = 0.1 N_{avc} \cdot B(C_{w1} + C_{w2} D_f/B)R_I \quad (9-8)$$

where q_{ult} is the ultimate bearing pressure in tons/ft², N_{avc} is the average blow count (blows/ft) adjusted for submergence effects, B is the footing width (least dimension), D_f is the depth to the base of the footing from the ground surface, R_I is the load inclination factor from Table 9-1, and C_{w1} and C_{w2} are correction factors that depend on the depth of the groundwater table, D_w , according to:

$$C_{w1} = C_{w2} = 1.0 \text{ for } D_w \geq D_f + 1.5B \quad (9-9a)$$

$$C_{w1} = 0.5 \text{ and } C_{w2} = 1.0 \text{ for } D_w = D_f \quad (9-9b)$$

$$C_{w1} = C_{w2} = 0.5 \text{ for } D_w = 0 \quad (9-9c)$$

Interpolation should be used to evaluate C_{w1} and C_{w2} for D_w in between 0 and D_f or between D_f and $D_f + 1.5B$.

The SPT blow count correction for submergence applies only to fine and silty sand. The submergence corrected blow count, N^* , is obtained as:

$$N^* = 15 + 0.5(N - 15) \text{ if } N > 15 \quad (9-10a)$$

$$N^* = N \quad \text{if } N \leq 15 \quad (9-10b)$$

where N is the measured blow count. The measured blow count value used in Equation 9-10 is averaged within the range of depth from the bottom of the footing to 1.5B below the bottom of the footing.

Load eccentricity can be accommodated using Equation 9-8 by substituting B' for B , where B' is evaluated in accordance with Figure 9-5. No correction factors for non-circular footings were proposed by Meyerhof for use with these equations. However, the general bearing capacity equations presented in the previous section can be used to calculate a correction factor for the bearing capacity of a non-circular footing.

Sliding Resistance of Shallow Foundations

The sliding resistance of a shallow foundation should be calculated independently of the bearing capacity. In calculating sliding resistance, the unit adhesion and/or frictional resistance of the base of the foundation to sliding is multiplied by the area of the base to determine the sliding resistance. The adhesion and interface frictional resistance of the base depend upon both the type of soil and the foundation material. Typically, for a concrete foundation, the adhesion and interface friction coefficient will be reduced by 20 to 33 percent from the cohesion and friction coefficient of the underlying soil. Navy Design Manual DM 7.2 (NAVFAC, 1986) provides recommendations for interface friction and adhesion values for

TABLE 9-1
INCLINATION FACTORS FOR BEARING CAPACITY OF SHALLOW FOUNDATIONS
 (After Meyerhof, 1956)

H/V	Square Footings Load Inclination Factor, R_f		
	$D_f/B=0$	$D_f/B=1$	$D_f/B=5$
0.10	0.75	0.80	0.85
0.15	0.65	0.75	0.80
0.20	0.55	0.65	0.70
0.25	0.50	0.55	0.65
0.30	0.40	0.50	0.55
0.35	0.35	0.45	0.50
0.40	0.30	0.35	0.45
0.45	0.25	0.30	0.40
0.50	0.20	0.25	0.30
0.55	0.15	0.20	0.25
0.60	0.10	0.15	0.20

H/V	Load Inclination Factor, R_f					
	Load Inclined in Width Direction			Load Inclined in Length Direction		
	$D_f/B=0$	$D_f/B=1$	$D_f/B=5$	$D_f/B=0$	$D_f/B=1$	$D_f/B=5$
0.10	0.70	0.75	0.80	0.80	0.85	0.90
0.15	0.60	0.65	0.70	0.70	0.80	0.85
0.20	0.50	0.60	0.65	0.65	0.70	0.75
0.25	0.40	0.50	0.55	0.55	0.65	0.70
0.30	0.35	0.40	0.50	0.50	0.60	0.65
0.35	0.30	0.35	0.40	0.40	0.55	0.60
0.40	0.25	0.30	0.35	0.35	0.50	0.55
0.45	0.20	0.25	0.30	0.30	0.45	0.50
0.50	0.15	0.20	0.25	0.25	0.35	0.45
0.55	0.10	0.15	0.20	0.20	0.30	0.40
0.60	0.05	0.10	0.15	0.15	0.25	0.35

dissimilar construction materials (e.g., sand/concrete, clay/steel). These values can be used for the design of both foundations and retaining walls against sliding. For eccentrically loaded foundations, the effective base area B' should be used in evaluating sliding resistance.

The vertical component of the seismic load on the footing should be included when evaluating the sliding resistance. Sliding resistance should be checked for both the maximum and minimum vertical loads (upwards and downwards seismic loading).

For embedded foundations, the passive seismic resistance in front of the foundation is often included in evaluation of the sliding resistance of a shallow footing. However, due to the relatively large deformations necessary for mobilization of the passive resistance, the passive earth pressure is typically reduced by a factor of two for use in sliding resistance analyses. Furthermore, the active seismic force on the front of the foundation should be either subtracted from the passive sliding resistance or added to the sliding driving force. The net result of factoring the passive seismic resistance and then subtracting the active seismic force may often be little to no change in the sliding resistance of the foundation.

Factors of Safety

Seismic loads represent an extreme loading condition, therefore relatively low factors of safety are generally considered acceptable in a pseudo-static analysis. Factors of safety on the order of 1.1 and 1.15 are typically used in practice for both bearing capacity and sliding resistance. The choice of the factor of safety and of the seismic coefficient (or peak load reduction factor) are intimately linked. For instance, if a seismic coefficient equal to the PGA (divided by the acceleration of gravity) has been used in the pseudo-static analysis because the foundation cannot tolerate large movements, there may be no need to increase the factor of safety beyond 1.0. Alternatively, if the seismic coefficient is one-half the PGA and the soil is susceptible to a post-peak strength decrease, it may be prudent use a factor of safety of 1.1 or 1.15.

9.2.3 Equivalent Foundation Stiffness

General

An accurate seismic response analysis requires the incorporation of the foundation system into the general dynamic model of the structure. The combined analysis is commonly referred to as the *soil-structure-interaction*, SSI analysis. In SSI analyses, the foundation system can either be represented by a system of springs (classical approach), or by a foundation stiffness (and damping) matrix. The latter approach, commonly used for SSI analyses of highway facilities, is commonly referred to as the *stiffness matrix method* approach.

The general form of the stiffness matrix for a rigid footing was presented in Figure 9-3. The 6 x 6 stiffness matrix can be incorporated in most structural engineering programs for dynamic response analysis to account for the foundation stiffness in evaluating the dynamic response of the structural system. The diagonal terms of the stiffness matrix represent the direct response of a mode of motion to excitation in that mode while the off diagonal terms represent the coupled response. Many of the off-diagonal terms are zero or close to zero, signifying that the two corresponding modes are uncoupled (e.g., torsion and vertical motion) and therefore may be neglected. In fact, for symmetric foundations loaded centrally, rocking and sliding (horizontal translation) are the only coupled modes of motion considered in a dynamic analysis.

Often, all of the off-diagonal (coupling) terms are neglected for two reasons: (1) the values of these off-

diagonal terms are small, especially for shallow footings; and (2) they are difficult to compute. However, the coupling of the two components of horizontal translation to the two degrees of freedom of rocking (tilting) rotation may be significant in some cases. For instance, coupled rocking and sliding may be important for deeply embedded footings where the ratio of the depth of embedment to the equivalent footing diameter is greater than five. The reader is referred to Lam and Martin (1986) for more guidance on this issue.

The stiffness matrix, K , of an irregularly shaped and/or embedded footing can be expressed by the following general equation:

$$K = \alpha \beta K_{ECF} \quad (9-11)$$

where K_{ECF} is the stiffness matrix of an equivalent circular surface footing, α is the foundation shape correction factor, and β is the foundation embedment factor. Each of these terms are discussed below.

Stiffness Matrix of a Circular Surface Footing

The solution for a circular footing rigidly connected to the surface of an elastic half space provides the basic stiffness coefficients for the various modes of foundation displacement. For vertical translation, the stiffness coefficient K_{33} can be expressed as:

$$K_{33} = 4GR/(1 - \nu) \quad (9-12a)$$

For horizontal translation, the stiffness coefficients K_{11} and K_{22} can be expressed as:

$$K_{11} = K_{22} = 8GR/(2 - \nu) \quad (9-12b)$$

For torsional rotation, the stiffness coefficient K_{66} can be expressed as:

$$K_{66} = 16GR^3/3 \quad (9-12c)$$

For rocking rotation, the stiffness coefficients K_{44} and K_{55} can be expressed as:

$$K_{44} = K_{55} = 8GR^3/3(1 - \nu) \quad (9-12d)$$

In Equation 9-12, G and ν are the dynamic shear modulus and Poisson's ratio for the elastic half space (foundation soil) and R is the radius of the footing.

The dynamic shear modulus, G , used to evaluate the foundation stiffness should be based upon the representative, or average, shear strain of the foundation soil. However, there are no practical guidelines for evaluating a representative shear strain for a dynamically loaded shallow foundation. Frequently, the value of G_{max} , the shear modulus at very low strain, is used to calculate foundation stiffness. However,

this is an artifact of the original development of the above equations for foundation stiffness for the design of machine foundations. For earthquake loading, it is recommended that values of G be evaluated at shear strain levels calculated from a seismic site response analysis using the modulus reduction curves presented in Chapter 5. If results of a site response analysis are not available, G may be evaluated using the modulus reduction curves presented in Chapter 5 and an assumed shear strain level that depends upon the magnitude of the earthquake, intensity of ground motion, and soil type. For events of magnitude 6.0 or less, and for ground motion intensities of 0.4 g or less, a value of G corresponding to a strain level of 0.1 percent appears to be appropriate. For larger magnitudes and/or higher intensity earthquakes, a larger strain level may be used. For very large magnitude events ($M > 7.5$) with very high shaking intensity ($PGA > 0.6$ g), a value of G corresponding to a shear strain of 1 percent is recommended.

Damping

One of the advantages of the stiffness matrix method over the classical approach is that a damping matrix can be included in SSI analysis. The format of the damping matrix is the same as the format of the stiffness matrix shown on Figure 9-3. While coefficients of the damping matrix may represent both an internal (material) damping and a radiation (geometric) damping of the soil, only radiation damping is typically considered in this type of analysis.

As discussed in Section 5.3.4, the internal damping of the soil is predominantly strain dependent and can be relatively accurately represented by the equivalent viscous damping ratio, λ . At the small strain levels typically associated with foundation response, λ is on the order of 2 to 5 percent. Radiation damping, i.e., damping that accounts for the energy contained in waves which “radiate” away from the foundation, is frequency-dependent and, in a SSI analysis, significantly larger than the material damping. Consequently, radiation damping dominates the damping matrix in SSI analyses.

The evaluation of damping matrix coefficients is complex and little guidance is available to practicing engineers. Damped vibration theory is usually used to form the initial foundation damping matrix. That theory, commonly used to study (small-strain) foundation vibration problems, assumes that the soil damping can be expressed via a damping ratio, D , defined as the ratio of the damping coefficient of the footing to the critical damping for the six-degree-of-freedom system.

The damping ratio for a shallow foundation depends upon the mass (or inertia) ratio of the footing. Table 9-2 lists the mass ratios and the damping coefficients and damping ratios for the various degrees of freedom of the footing. The damping ratios should be used as shown on Figure 9-3 to develop the damping matrix of the foundation system. It should be noted that this approach only partially accounts for the geometry of the foundations and assumes that small earthquake strains are induced in the soil deposit. For pile foundations or for complex foundation geometry, a more rigorous approach, commonly referred to as the *soil-foundation-structure-interaction* (SFSI) analysis, may be warranted. SFSI is beyond the scope of this document.

Rectangular Footings

Application of the foundation stiffness general equation 9-11 ($K = \alpha\beta K_{ECF}$) for rectangular footings involves the following two steps:

Step 1: Calculate the radius of an equivalent circular footing for the various modes of displacement using Table 9-2 and Figure 9-6. For vertical and horizontal (translational) displacements, the equivalent radius, r_e , is the radius of a circular footing with the same area as the rectangular footing. For

TABLE 9-2
EQUIVALENT DAMPING RATIOS FOR RIGID CIRCULAR FOOTINGS
 (After Richart, *et al.*, 1970)

Mode of Vibration	Mass (or Inertia) Ratio	Damping Coefficient	Damping Ratio	Equivalent Radius
Vertical Translation	$B_z = \frac{(1-\nu)}{4} \frac{m}{\rho r_o^3}$	$c_z = \frac{3.4 r_o^2}{1-\nu} \sqrt{\rho G}$	$D_z = \frac{0.425}{\sqrt{B_z}}$	$r_o = R_z = \sqrt{BL/\pi}$
Horizontal Translation (Sliding)	$B_x = \frac{(7-8\nu)}{32(1-\nu)} \frac{m}{\rho r_o^3}$	$c_x = \frac{4.6 r_o^2}{2-\nu} \sqrt{\rho G}$	$D_x = \frac{0.288}{\sqrt{B_x}}$	$r_o = R_x = \sqrt{BL/\pi}$
X- and Y-axis Rocking	$B_\psi = \frac{3(1-\nu)}{8} \frac{I_\psi}{\rho r_o^5}$	$c_\psi = \frac{0.8 r_o^4 \sqrt{\rho G}}{(1-\nu)(1+B_\psi)}$	$D_\psi = \frac{0.15}{(1+B_\psi)\sqrt{B_\psi}}$	$r_o = R_{\psi_x} = \left[\frac{16(B)(L)^3}{3\pi} \right]^{1/4}$ $r_o = R_{\psi_y} = \left[\frac{16(B)^3(L)}{3\pi} \right]^{1/4}$
Z-axis Rotation (Torsion)	$B_\theta = \frac{I_\theta}{\rho r_o^5}$	$c_\theta = \frac{4 \sqrt{B_\theta \cdot \rho G}}{1+2B_\theta}$	$D_\theta = \frac{0.5}{1+2B_\theta}$	$r_o = R_{\psi_z} = \left[\frac{16BL(B^2+L^2)}{6\pi} \right]^{1/4}$

Notes: m = mass of the foundation
 c = damping coefficient (c_z , c_x , c_ψ , c_θ)
 I = moment of inertia of the foundation
 ρ = mass density of foundation soil
 r_o = equivalent radius (R_x , R_y , R_ψ)
 B = width of the foundation (along axis of rotation for rocking)
 L = length of the foundation (in the plane of rotation for rocking)
 G = shear modulus of the soil
 ν = Poisson's ratio of the soil
 D = damping ratio (D_z , D_x , D_ψ , D_θ)

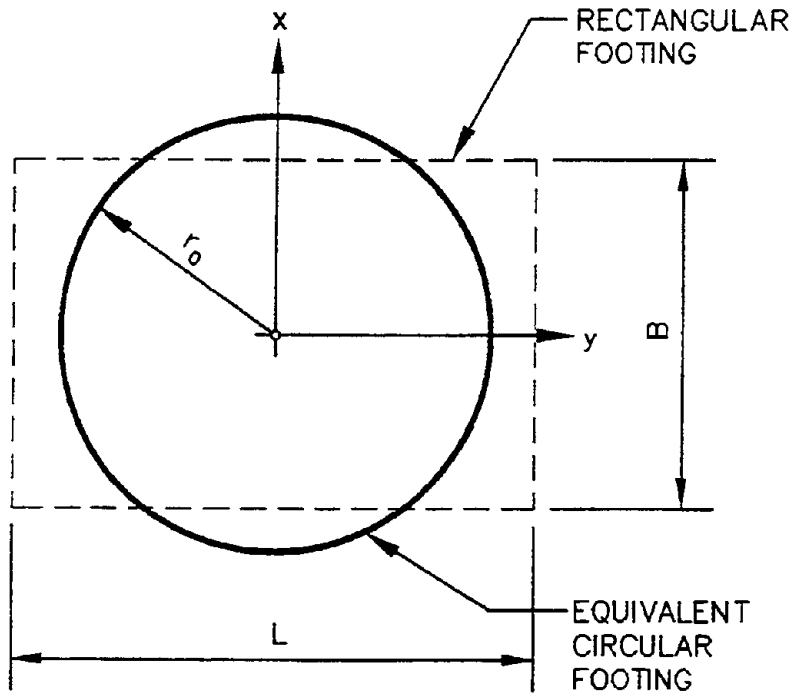


Figure 9-6: Calculation of Equivalent Radius of Rectangular Footing.

rocking and torsional motions, the calculation of the equivalent radius is more complicated, as it depends on the moment of inertia of the footing. The equivalent radius is then used in the equations from Section 9.2.3 to solve for the baseline stiffness coefficients K_{ECF} in Equation 9-11.

Step 2: Find the shape factor α to be used in Equation 9-11 using Figure 9-7. This figure gives the shape factors for various aspect ratios (L/B) for the various modes of displacement discussed in Section 9.2.3.

Embedment Effects

The influence of embedment on the response of a shallow foundation is described in detail in Lam and Martin (1986). The values of the foundation embedment factor β from that study are presented in Figure 9-8 for values of D/R less than or equal to 0.5 and in Figure 9-9 for values of D/R larger than 0.5. For cases where the top of the footing is below the ground surface, it is recommended that the thickness of the ground above the top of the footing be ignored and the thickness of the footing (not the actual depth of embedment D_f) be used to calculate the embedment ratio (D/R) in determining the embedment factor β .

Implementation of Dynamic Response Analyses

Typically, the geotechnical engineer provides values for terms of the stiffness matrix to the structural engineer for use in the dynamic response analysis. Based upon the results of the analysis, the structural engineer should then provide the peak dynamic loads and deformations of the foundation elements back to the geotechnical engineer. The geotechnical engineer then compares the dynamic loads and deformations to acceptable values to ascertain if the seismic performance of the foundation is acceptable.

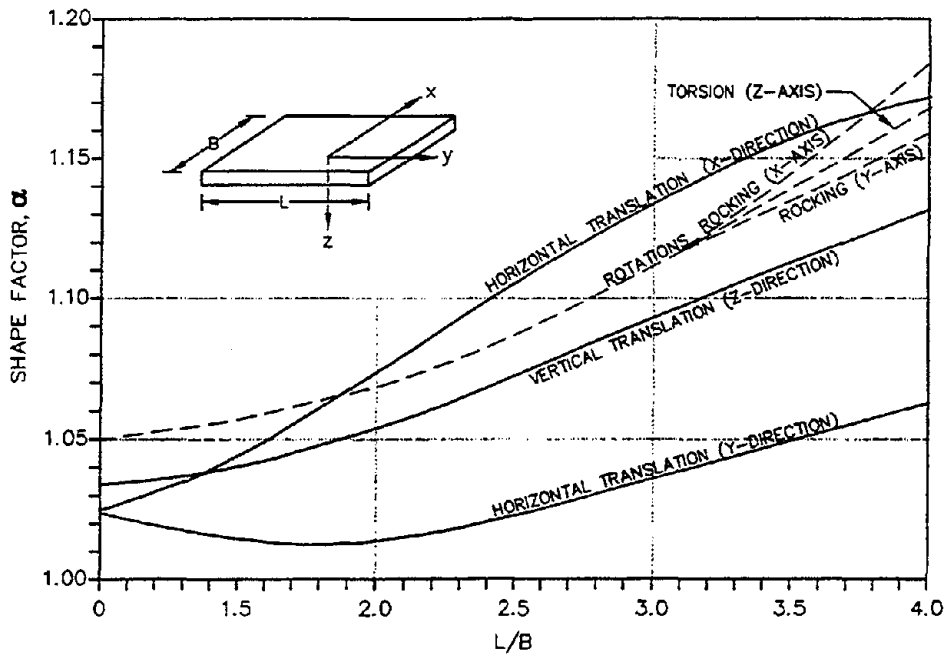


Figure 9-7: Shape Factor α for Rectangular Footings. (Lam and Martin, 1986)

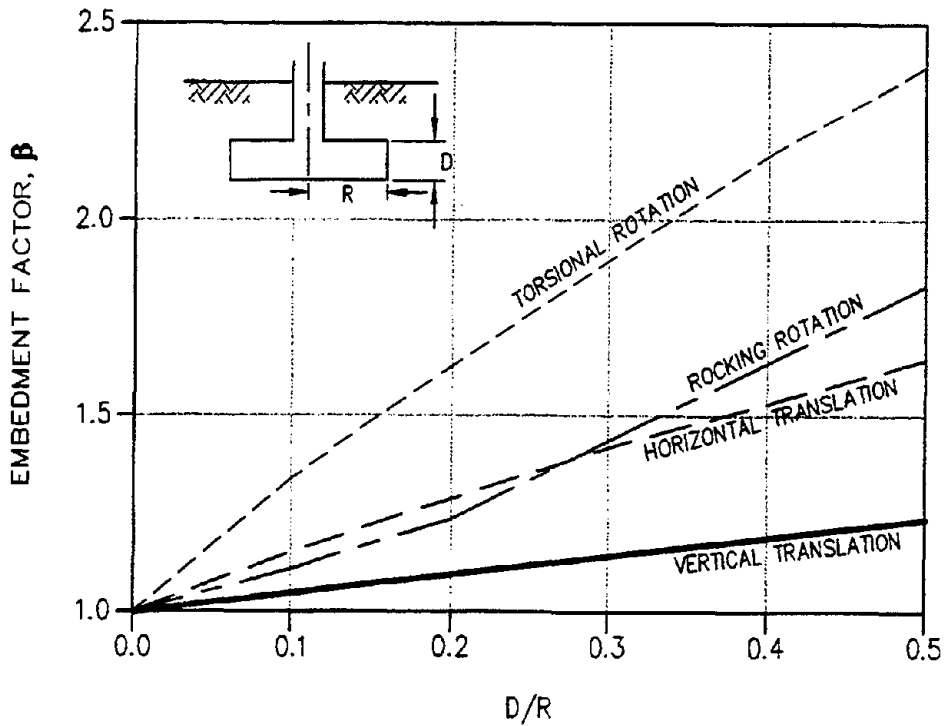


Figure 9-8: Embedment Factors for Footings with $D/R < 0.5$. (Lam and Martin, 1986)

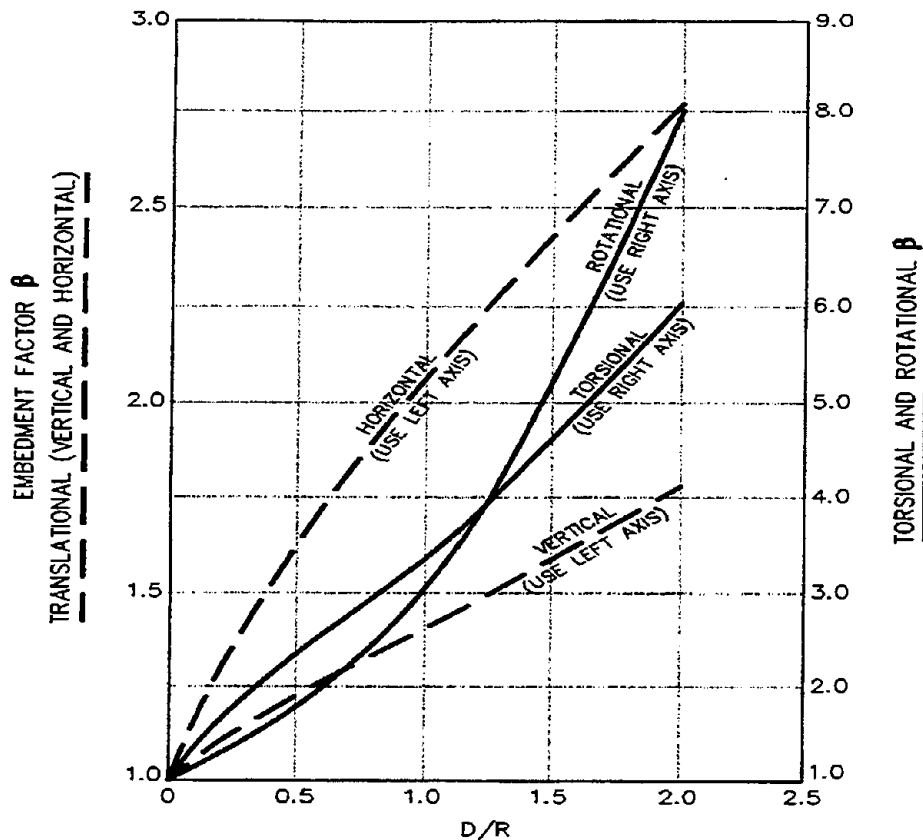


Figure 9-9: Embedment Factors for Footings with $D/R > 0.5$. (Lam and Martin, 1986)

If the foundation loads or deformations are unacceptable or if the stiffness coefficients depend upon the amount of deformation or on the magnitude of the dynamic load, iteration may be required to achieve a satisfactory foundation design. Even when a dynamic response analysis is employed to evaluate the seismic performance of a shallow foundation, the gross stability of the foundation must still be evaluated using pseudo-static analysis for bearing capacity and sliding resistance, as described in Section 9.2.2.

9.3 DESIGN OF DEEP FOUNDATIONS

9.3.1 General

Deep foundations are often used under the following foundation conditions (Lam and Martin, 1986):

- the upper soil strata are weak or compressible;
- the shallower soil layers are susceptible to liquefaction;
- footings cannot transmit inclined, horizontal, or uplift forces;
- excessive scour is likely to occur;
- future excavation is planned adjacent to the structure; or
- expansive or collapsible soils extend to a considerable depth.

Typical deep foundation systems for highway bridges include pile group (with or without battered piles), single column drilled shaft and pile bent foundations (see Figure 9-10). The pile group system (pile

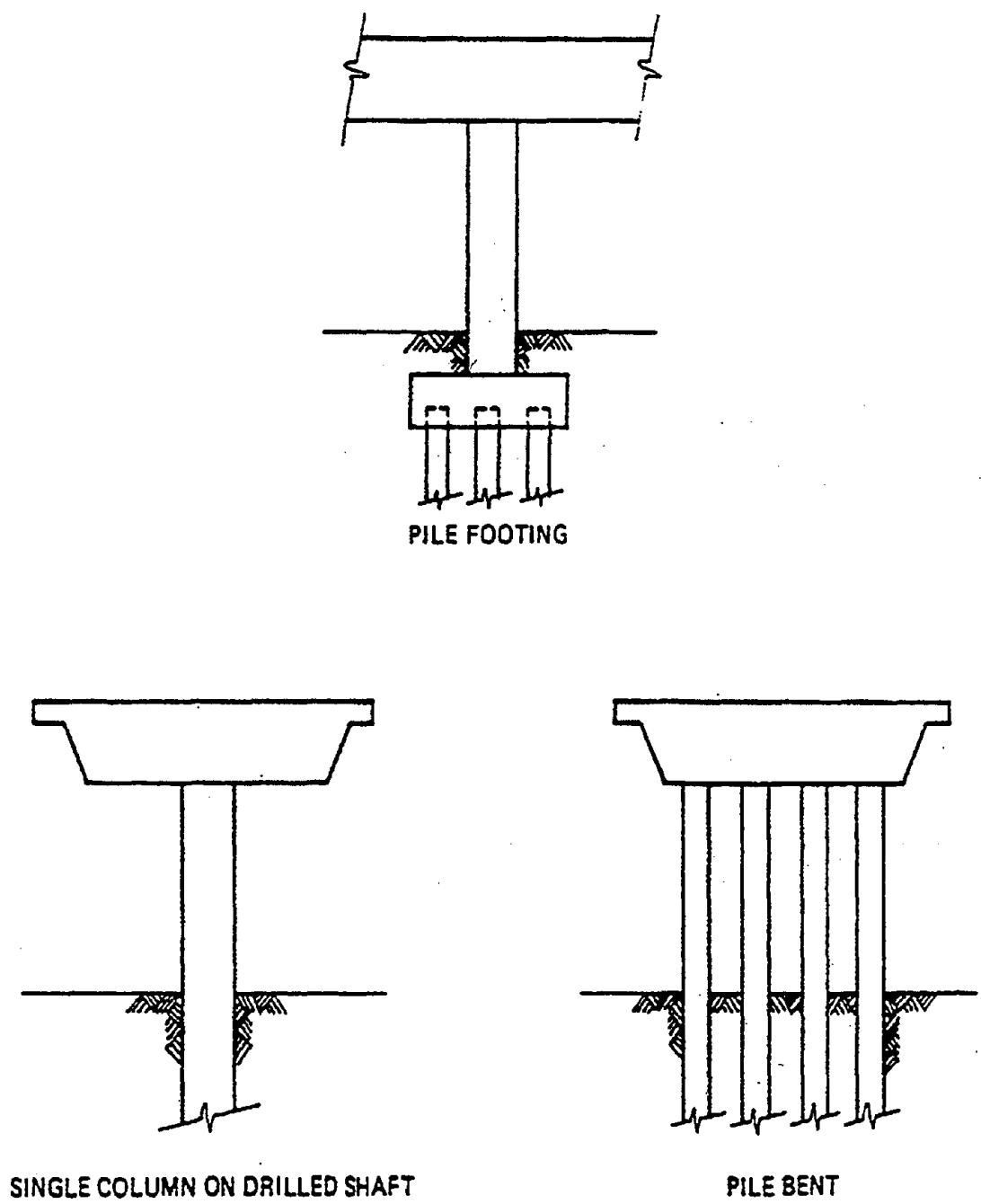


Figure 9-10: Commonly Used Deep Foundations for Highway Bridges. (Lam and Martin, 1986)

footings) is the most commonly used deep foundation system for support of highway bridge structures. Piles used for this system may include steel H piles, pipe piles (concrete filled or unfilled), timber piles, cast-in-place concrete piles, precast concrete piles, and precast-prestressed concrete piles. The single column drilled shaft and the pile bent foundations systems differ from the pile footing system in that no footings (or caps) are used and the substructures extends below ground as large diameter bridge drilled

shafts or smaller diameter pile extensions. In general, the rotational stiffness of the drilled shafts and pile extensions tend to be much lower than that of the pile footings. Therefore, foundation displacement evaluation and the consideration of foundation compliance in the bridge dynamic response analysis are particularly important for these foundation systems.

The construction aspects and design procedures for estimating axial load capacity of various pile/drilled shaft foundation systems are detailed in Module 8 (Deep Foundations). This chapter focuses on the evaluation and modeling procedures under seismic loading conditions. Since there are many common aspects in the behavior of piles and drilled shafts under seismic loading conditions, in the remainder of this chapter the term pile will be used to discuss the general seismic design methodologies for deep foundation. The discussion on piles also applies to other types of deep foundations, unless noted otherwise.

9.3.2 Seismic Vulnerability of Deep Foundations

Deep foundation failures may be divided into two types. The first type of failure involves large displacements of the foundation soil resulting from instability generated within the soil, such as that caused by liquefaction or embankment/slope instability. The mechanism for this type of failure is described in detail in Chapters 7 and 8. The second type of failure involves the yielding or failure of the foundation elements due to excessive seismic forces transmitted from the structure to the foundation. Figure 9-11 shows the potential failure modes for a typical pile footings. As indicated, the failure modes can be classified as follows (Buckle and Friedland, 1994):

- Tilting due to uplift or compression failure in the piling
- Pile pullout from the footing (or cap)
- Pile flexural or shear failure
- Concrete footing shear failure
- Concrete footing flexural failure
- Bond (anchorage) failure of the column steel

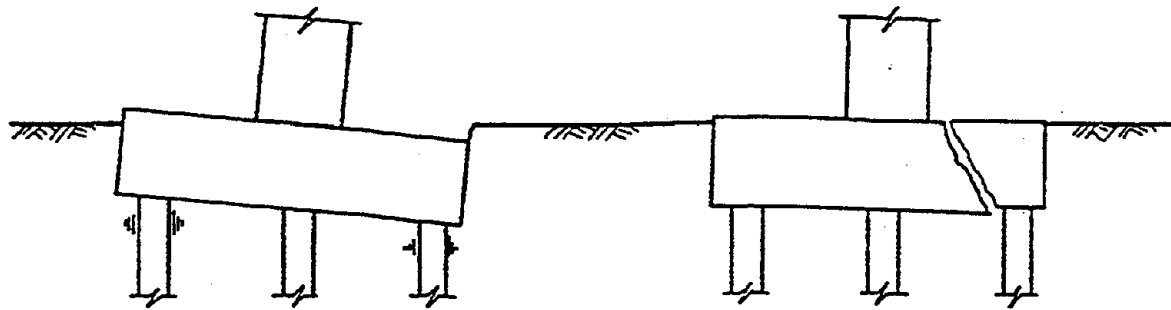
If the shear and flexural failures of the footing and the anchorage failure of the column steel will not occur, then the capacity of the foundation will be governed by pile failure. It should be noted that pile uplift may be limited by pullout of the pile from the footing or by insufficient soil frictional resistance along the pile.

In addition to the potential failure modes presented above, the design should also consider the lateral and rotational movements of the foundation. Foundation movements that are larger than desirable may be harmful to the superstructure and render the bridge unfunctional.

9.3.3 General Design Procedure

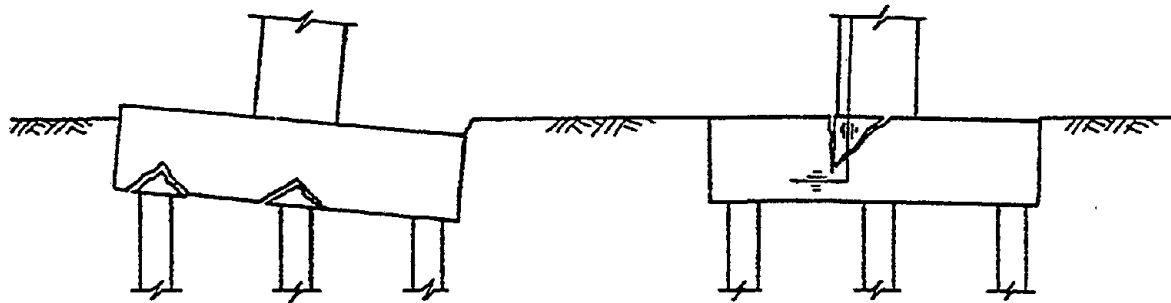
Design of a deep foundation system involves the following basic steps:

- (1) Using preliminary earthquake-induced forces (from the superstructure) provided by the structural engineer, perform a trial design by selecting initial pile/shaft size and arrangement (layout). The



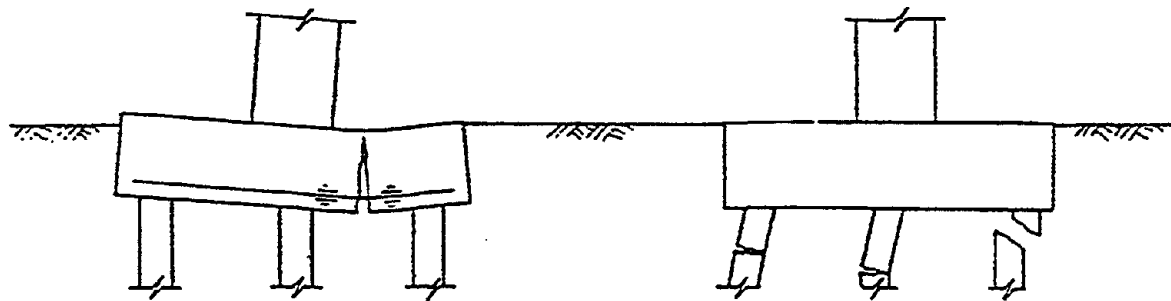
PILE OVERLOAD

CONCRETE SHEAR FAILURE



PILE PULLOUT

ANCHORAGE FAILURE



FLEXURAL YIELDING
OF REINFORCING

PILE FLEXURAL AND/OR
SHEAR FAILURE

Figure 9-11: Potential Failure Modes for Pile Foundations. (Buckle and Friedland, 1994)

earthquake-induced forces should include moments, shears and axial loads applied to the top of the pile/shaft group.

- (2) Determine the load distribution (of the earthquake-induced forces) to the individual pile/shaft elements in axial, shear and bending so that the pile/shaft can be properly sized for its structural as well as geotechnical capacity.
- (3) Compute the displacements and equivalent stiffness of the foundation (lateral as well as rotational). Check the foundation displacements against the allowable values, if applicable. Two methods have been widely used in design practice to model the foundation stiffness: (a) equivalent cantilever model, and (b) foundation stiffness matrix model. These two methods will be discussed in detail in Section 9.3.6.
- (4) Reanalyze the earthquake-induced forces (by structural engineers) incorporating the equivalent foundation stiffness derived in step (3) into the bridge response analysis. The displacements of the superstructure should also be checked to ensure the adequacy of the bridge performance during earthquakes.
- (5) With the new set of earthquake-induced forces, modify the pile/shaft design and adjust the foundation stiffness as required. Steps (2) through (5) are repeated until the forces are compatible with the foundation stiffness used.

9.3.4 Seismic Response of Pile Foundations

As shown in Figure 9-12, the basic problem of the seismic response of a pile foundation involves the distribution of a set of superstructure loads into the surrounding soil mass through the pile members. The general case involves consideration of the same six degrees of freedom considered in the design of shallow foundations; that is, three components of translational forces (an axial and two lateral shear forces) and three components of rotational moments (a torsional moment about the pile axis and two rotational moments about two orthogonal horizontal axes) along the pile member. For convenience in design analyses, the axial support characteristics of the pile are assumed to be independent of the lateral support characteristics. This assumption is usually justified because lateral soil reactions are usually concentrated along the top 5 to 10 pile diameters whereas the axial soil resistance of the pile is typically developed at greater depths. Therefore, the axial and lateral soil support behavior of the pile can be analyzed separately.

In evaluating the response of the pile or pile group to lateral loads, the lateral displacement of the pile or pile group is evaluated and compared to acceptable levels of displacement. In evaluating response to vertical loads, the loads on the pile are compared to the uplift and compressive capacities of the pile. In both lateral and vertical loading analyses, the structural capacity of the pile and pile cap must also be compared to the applied loads.

Under even relatively small lateral loads, some portion of the soil mass may yield during loading. Typically, this yielding will occur near the soil surface. Furthermore, in most situations, several different layers of soil will be encountered along the length of the pile. Therefore, a realistic approach to dynamic analysis of pile foundations should account for the nonlinear behavior of near-surface soils and the layered nature of typical soil profiles. In view of these constraints, current design practice usually models the soil support characteristics along the pile by discrete nonlinear springs. Analysis of such a soil-pile system usually involves modeling the pile as a beam-column supported by one set of lateral springs and another

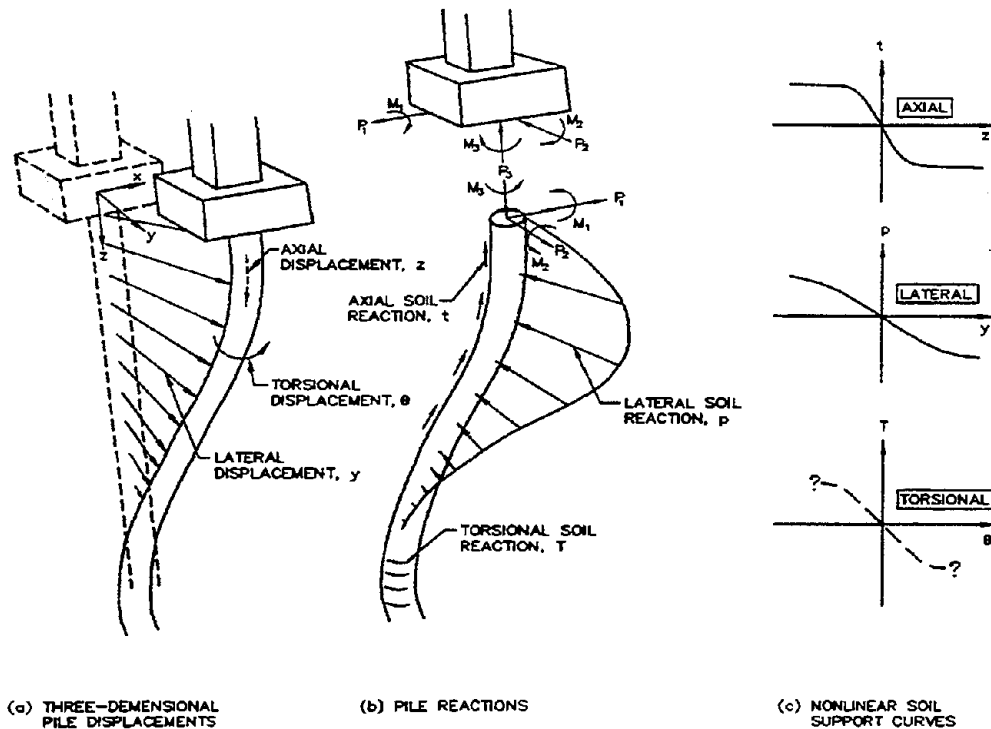


Figure 9-12: Three-Dimensional Soil Pile Interaction. (After Bryant and Matlock, 1977)

set of axial springs. The support curves characterizing the lateral soil reaction versus lateral pile deflection are usually referred to as *p-y curves*. The corresponding curves for the axial load transfer characteristics of the pile is referred to as *t-z curves*. Torsional resistance against rotation of individual piles is usually ignored or assumed to be negligible for highway bridges, as most deep highway foundations are supported by pile groups and torsional loads on pile groups become resolved as lateral loads on the individual piles.

The constraint at the head of a pile can have a significant influence on lateral load response of the pile. Piles free to rotate at the head will generally undergo larger lateral displacements than fixed-head piles subject to the same load. However, fixed-head piles may induce large moments at the head of the pile. Both the pile and pile cap must then be designed to accommodate this moment.

9.3.5 Method of Analysis

A comprehensive coverage on seismic analysis of pile foundations is provided in Lam and Martin (1986). Martin and Lam (1995) present additional, updated information on seismic design of pile foundations. The discussion provided herein will touch on only the key aspects of this problem. The readers are referred to Lam and Martin (1986), Martin and Lam (1995), and to the other references cited in this chapter for in-depth coverage of the subject.

Because of the inherently variable and nonlinear nature of soil, there is seldom any advantage in attempting to apply closed form mathematical solutions or in developing design charts for seismic design of pile foundations. Analysis of the response of piles to lateral loading is most conveniently accomplished using established computer programs. A variety of computer programs for the lateral and vertical load response

of piles and pile groups are commercially available. Most of these programs use methods developed by Reese and his co-workers (e.g., Reese, *et al.*, 1984; Wang and Reese, 1991). Many of these programs have user-friendly input and output routines and thus can be easily used by most geotechnical engineers, even those with limited computer training. Some of the widely used computer programs for this purpose include COM624P (FHWA-SA-91-048, 1993) for laterally loaded single pile analyses and GROUP (Reese, *et al.*, 1994) for laterally loaded pile group analyses. These programs analyze lateral pile/pile group response using finite-difference models of the pile along with non-linear springs (p-y and t-z springs) as depicted in Figure 9-13.

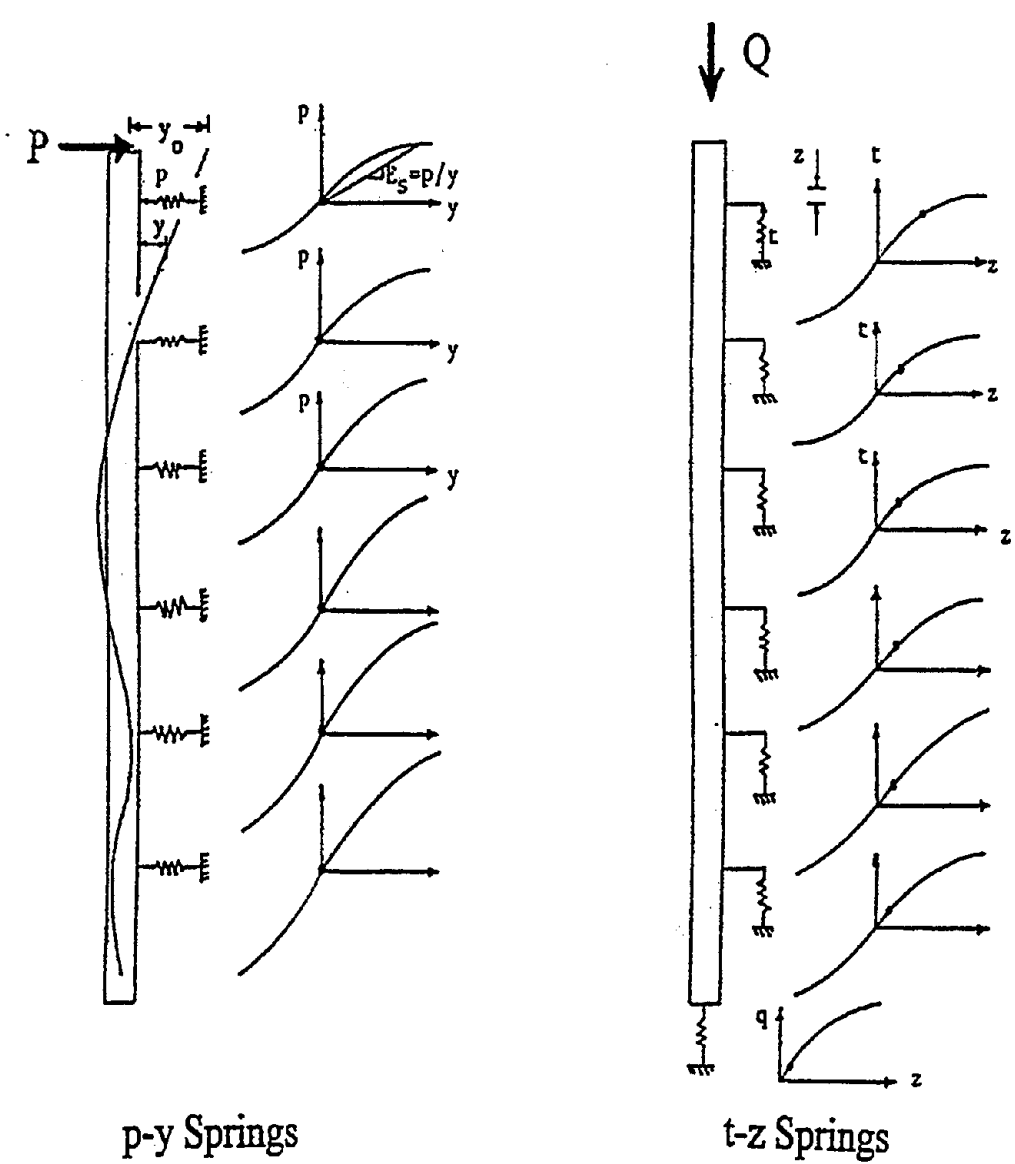


Figure: 9-13: Soil-Pile Characterization in Laterally Loaded Pile/Pile Group Analyses.

The construction of a full set of p-y curves for the analysis of a laterally loaded pile involves calculating p-y curves at selected depths along the length of the pile. Calculations for p-y curves for laterally loaded piles are described in detail by Reese, *et al.* (1984). These calculations are typically performed internally by the computer program based upon input soil types and shear strength parameters. For example, the COM624P program provides internally generated p-y curves for the following soil and water table conditions:

- Soft clay below water table
- Stiff clay below water table
- Stiff clay above water table
- Sand above or below water table

The required soil input parameters for generating these p-y curves typically consist of the following:

- Soil effective unit weight, γ'
- Soil strength parameters
 1. For cohesive soils
 - Cohesion, C_u
 - Strain at $\frac{1}{2}$ maximum principal stress, ϵ_{50}
 2. For cohesionless soils
 - Internal friction angle, ϕ
- Initial slope of soil modulus, K_i

Typical values of ϵ_{50} and K_i are presented in Table 9-3 (Hannigan, et al., FHWA-HI-97-013, 1997). A typical p-y curve for soft clay is shown in Figure 9-14, where the soil resistance p is normalized to the ultimate resistance of the soil, P_u , and the soil/pile deflection y is normalized to the deflection at $\frac{1}{2}$ the ultimate soil resistance, y_{50} . The ultimate soil resistance can be derived from C_u , and the value of y_{50} shown in Figure 9-14 is a function of ϵ_{50} .

In general, interpolations are done internally in the computer program to provide p-y characteristics at additional points between the points where p-y curves are input. The additional points generated by the computer should be spaced at about one-half the pile diameter to provide good resolution for the distributed soil support. Placement of p-y curves typically includes the top and bottom (or assumed bottom for a very long pile) of the pile. Since the lateral response of a pile is concentrated close to the soil surface, additional p-y curves are generally placed at closer spacings near the top of the pile. Usually, the pile response is relatively insensitive to p-y curves prescribed at greater depths. However, p-y curves should be placed at the top and bottom of all significant soil layers. In the analysis of a laterally loaded pile, the pile can usually be cut off at 30 to 40 diameters below the ground surface without affecting the lateral behavior of the upper part of the pile.

Typical output information from the laterally loaded pile analysis (e.g., using COM624P) includes the computed pile deflections, bending moments, stresses, shear, and soil reaction forces as functions of depths below the pile head. A typical graphical presentation of these output results is shown in Figure 9-15.

For evaluating the vertical response of piles subject to dynamic loading, t-z curves are generally calculated

TABLE 9-3
TYPICAL VALUES OF K_i AND ϵ_{50} (Hannigan, et al., 1997)

REPRESENTATIVE VALUES OF ϵ_{50} FOR CLAYS		
Clay Consistency	Average Undrained Shear Strength, c_u (kPa)	ϵ_{50}
Soft Clay	12 - 24	0.02
Medium Clay	24 - 48	0.01
Stiff Clay	48 - 96	0.007
Very Stiff Clay	96 - 192	0.005
Hard Clay	192 - 383	0.004

REPRESENTATIVE K_i VALUES FOR CLAYS AND SANDS				
Soil Type	Average Undrained Shear Strength, c_u (kPa)	Soil Condition	K_i - Static Loading (kN/m ³)	K_i - Cyclic Loading (kN/m ³)
Soft Clay	12 - 24	---	8,140	
Medium Clay	24 - 48	---	27,150	
Stiff Clay	48 - 96	---	136,000	54,300
Very Stiff Clay	96 - 192	---	271,000	108,500
Hard Clay	192 - 383	---	543,000	217,000
Loose Sand	---	Submerged	5,430	5,430
Loose Sand	---	Above Water Table	6,790	6,790
Med Dense Sand	---	Submerged	16,300	16,300
Med Dense Sand	---	Above Water Table	24,430	24,430
Dense Sand	---	Submerged	33,900	33,900
Dense Sand	---	Above Water Table	61,000	61,000

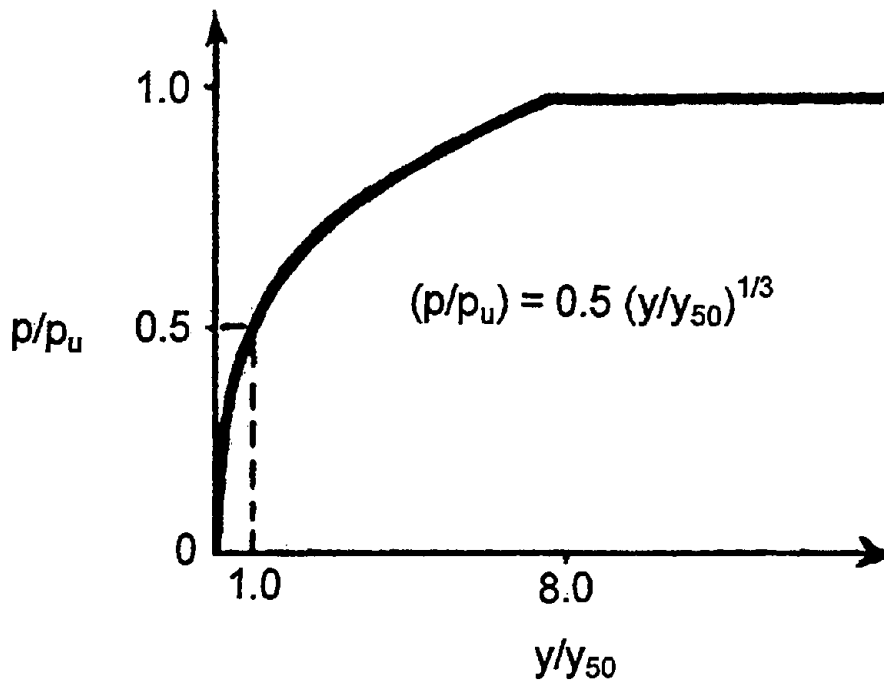


Figure 9-14: Typical p-y Curve for Soft Clay.

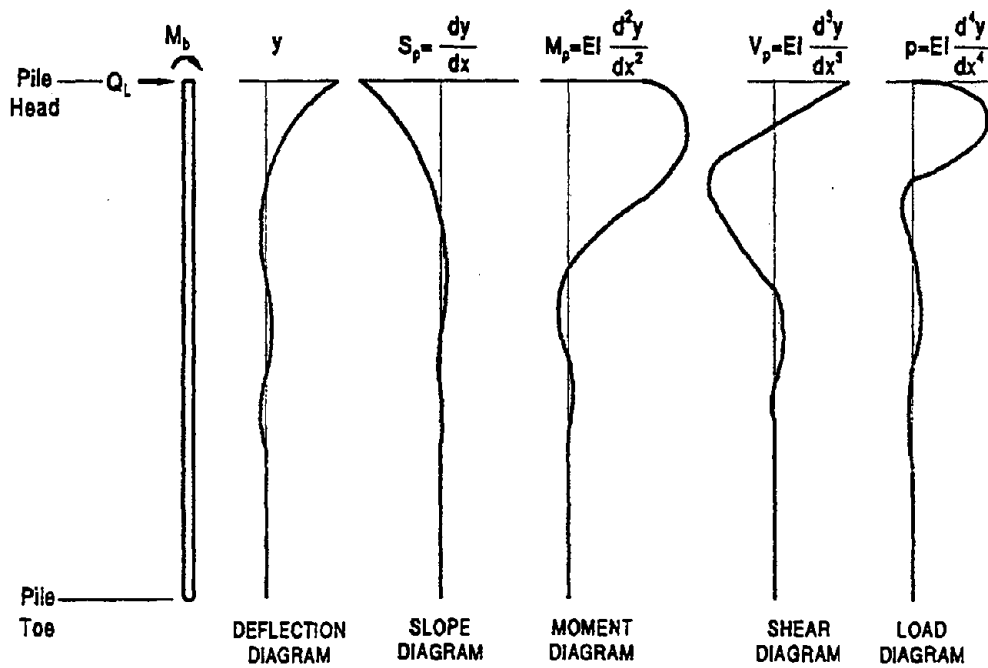


Figure 9-15: Graphical Presentation of Laterally Loaded Pile Analysis.

over the entire length of the pile. Rules for specifying t-z curves are similar to those cited above for specifying p-y curves. Procedures for evaluating t-z curves are provided by Lam and Martin (1986). Analysis of piles and pile groups subjected to dynamic vertical loads is also usually performed using commercially available computer programs.

Group Effects

One of the most difficult problems in evaluating the lateral response of pile foundations is the evaluation of group effects on pile stiffness. Historically, group effects have been generally addressed in two different manners. Either the stiffness of the p-y curves of the individual piles are decreased to account for group effects, or the pile group is analyzed as an equivalent single pile. As knowledge of the influence of group effects on the behavior of the individual piles has increased, use of equivalent single pile analyses has decreased. In practice today, equivalent single pile analyses should only be used for large groups of closely spaced piles where appropriate guidelines for the behavior of individual piles within the group are not available.

The behavior of individual piles within a 3 x 3 group of piles founded in sand has been discussed by Brown, *et al.* (1988), McVay, *et al.* (1995), and Pinto, *et al.* (1997). The findings of these investigations may be summarized as follows:

- for center-to-center spacing, S , greater than $5D$ (5 pile diameters), group effects are negligible and may be ignored;
- for center-to-center spacing of $5D$ or less, the behavior of individual piles within the group depends upon the relative density of the sand and position within the group;
- group efficiency, defined as the actual capacity of the group divided by the ideal capacity of the group if there was no group effect, decreases with decreasing spacing (capacity is defined as the lateral load at a lateral deformation of 76 mm); and
- the lead row of piles in the group shows a stiffer lateral load response than trailing rows.

Table 9-4 summarizes the results of centrifuge model tests in sand from Pinto, *et al.* (1997) illustrating these effects. The term "multipliers" in this table refers to the multiplier (or reduction factor) applied to the load term (p) of a single pile p-y curve in order to represent the behavior of the pile within the pile group, as illustrated in Figure 9-16. The p-y multipliers shown in this table are consistent with those recommended by Brown, *et al.* (1988). The reduction in stiffness and capacity for piles in the trailing rows is often referred to as the "shadow" effect. For groups of 4 x 4 or larger, piles in row 4 or greater may be assumed to behave similarly to the piles in the third row of the 3 x 3 group due to the shadow effect. While no similar data on group effects is available for piles in clay, pile groups in stiff clay may be assumed to behave like pile groups in dense sand and pile groups in soft clay may be assumed to behave like piles in loose sand with respect to the shadow effect.

Brown and Bollmann (1996) provided a general guideline in pile/shaft group design using the p-multiplier concept. The recommended "p-multiplier" values as a function of row position and pile spacing are presented in Table 9-5. It should be noted that these values are more representative of pile group effect when lateral deflection of the pile is on the order of about 10 percent of the pile diameter. For smaller deflections, the p-multiplier values tend to approach 1.0.

TABLE 9-4
p-MULTIPLIERS
SUMMARY OF CENTRIFUGE MODEL TESTS IN SAND
RESULTS (3 X 3 GROUP, FREE AND FIXED HEAD, PLUMB)
(Pinto, *et al.*, 1997)

Spacing	$D_r > 90\%$ ⁽¹⁾	$D_r = 55\%$	$D_r = 45\%$	$D_r = 33\%$	$D_r = 17\%$
Free Head (3D)					
P_{row}/P_{total}	.45 .32 .23	.41 .32 .27	.41 .32 .27	.37 .33 .30	.37 .33 .30
Multipliers	0.8 0.4 0.3	0.8 0.45 0.3		0.65 0.45 0.35	
Efficiency	0.74	0.73		0.73	
Load (kN)		1,050		807	
Free Head (5D)					
P_{row}/P_{total}		.36 .33 .31		.35 .33 .31	.36 .33 .31
Multipliers		1.0 0.85 0.7		1.0 0.85 0.7	
Efficiency		0.95		0.92	
Load (kN)		1,440		1,135	
Fixed Head (3D)					
Load (kN)		1,628 (+55%) ⁽²⁾		1,094 (+36%) ⁽²⁾	
Fixed Head (5D)					
Load (kN)		2,028 (+41%) ⁽²⁾		1,334 (+18%) ⁽²⁾	

Notes: ⁽¹⁾ Field Load Test by Brown, *et al.* (1988).

⁽²⁾ Increase in capacity relative to free head (at 76 mm of deflection).

TABLE 9-5
RECOMMENDED "p-MULTIPLIER" VALUES FOR PILE GROUP DESIGN
(Brown and Bollmann, 1996, Hannigan, *et al.*, 1997)

Row Spacing	Front Row	2nd Row	3rd & More Rows
3D	0.8	0.45	0.35
4D	0.9	0.65	0.55
5D	1.0	0.85	0.75

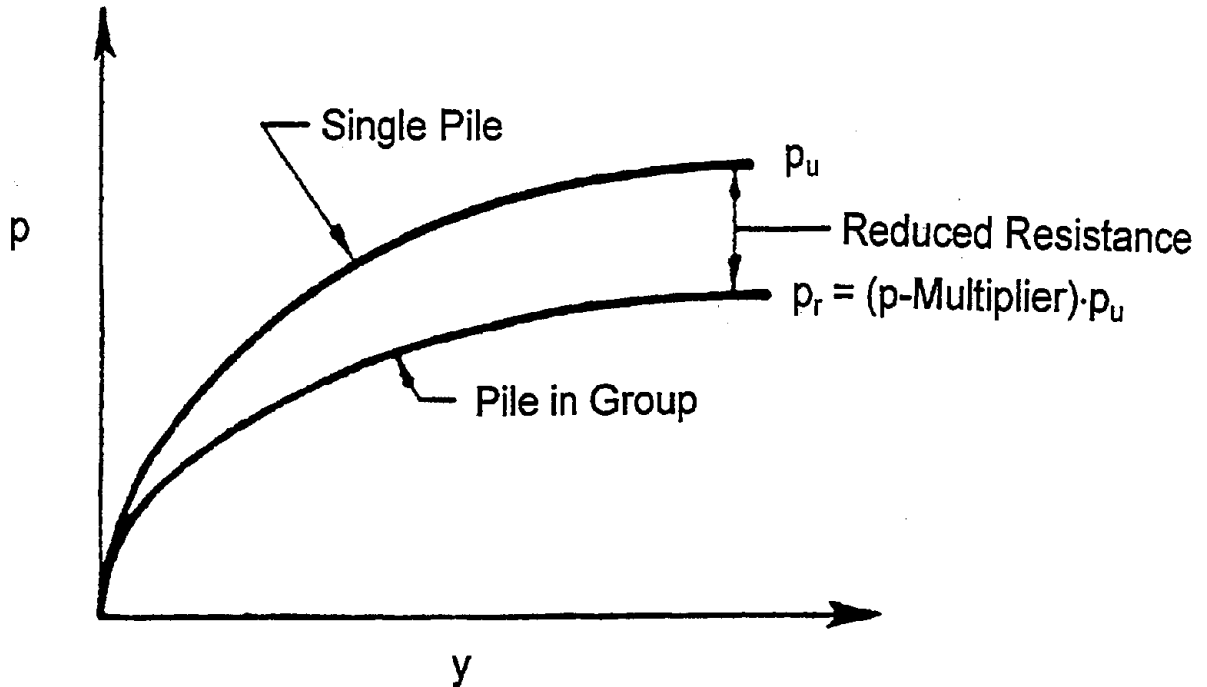


Figure 9-16: p-Multiplier for Group Effects.

9.3.6 Equivalent Foundation Stiffness

The foundation stiffness of pile/shaft foundations may vary widely. For instance, a pile/shaft supported footing foundation may display an equivalent rotational stiffness an order of magnitude that of a single column drilled shaft or pile extension foundation. The dynamic response of the overall bridge may be significantly affected by the foundation compliance. It affects the computation of the oscillator period of the structure and changes the distribution of the forces and moments in the structure. The magnitude of the superstructure displacement is also highly dependent on the foundation stiffness.

As discussed earlier, the stiffness of a pile/shaft foundation can be incorporated into the seismic response analysis of the bridge by various methods. The two most widely used methods are the equivalent cantilever method and the foundation stiffness matrix method (see Figure 9-17). The equivalent cantilever method has the advantage of simplicity, eliminating the need for a detailed foundation model. The foundation stiffness matrix method, on the other hand, is the most general method of representation of foundation stiffness and generally provides a more accurate assessment.

Equivalent Cantilever Method

This method assumes that an equivalent cantilever column can be used to model the pile/shaft foundation. The depth to the cantilever fixity is adjusted so as to give either the same stiffness at the ground level or the same maximum bending moment as in the actual pile/shaft system. Figure 9-18 is a schematic sketch showing the equivalent cantilever method based on the equal deflection (stiffness) assumption. The equivalent depth to fixity is primarily a function of the relative stiffness of the pile and soil. Typical ranges for the effective depth to fixity are from 3 to 9 pile diameter. The low end value corresponds to piles in very stiff sites.

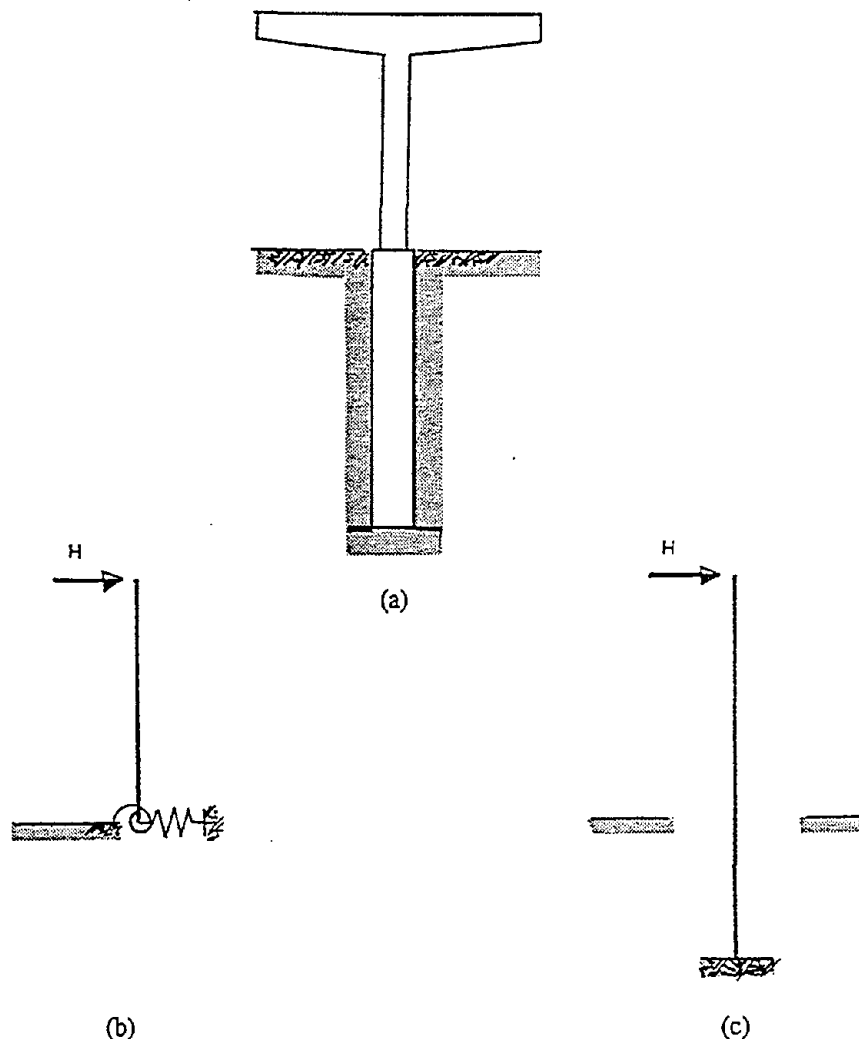


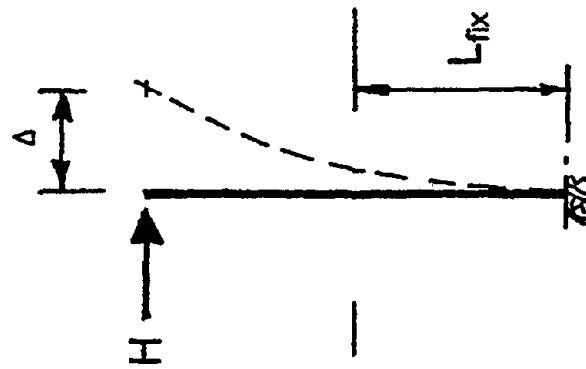
Figure 9-17: Methods for Representing Deep Foundation Stiffness, (a) Schematic of a Bridge-Pile System, (b) Foundation Stiffness Matrix Method, and (c) Equivalent Cantilever Method (Buckle et al., 1987).

In relatively competent sites, the use of this method will give satisfactory results. It is widely used for preliminary design purposes or for design of regular highway bridges that are not considered as critical structures.

Foundation Stiffness Matrix Method

The general form of the stiffness matrix for a pile/shaft foundation is the same as that for the shallow footing as presented in Figure 9-3, except that the cross coupling stiffness coefficient, which are generally ignored for shallow footings, are included for pile/shaft foundations. Calculations of these coefficient are normally done by performing laterally loaded pile or pile group analyses, as discussed in sections 9.3.4 and 9.3.5. In the analysis, a single pile or pile group is modeled explicitly in the soil mass, using non-linear spring (i.e., p-y and t-z curves) distributed along the pile length. A procedure proposed by Lam, Martin and Imbsen (1991) for a pile/shaft supported footing foundation is summarized as follows:

- (1) Solve for the stiffness matrix of a single pile under lateral loading. The computer program COM624P (1993) can be used for this purpose.



L_{fix} = Depth to Fixity
 (Based on Equal Deflection Assumption)

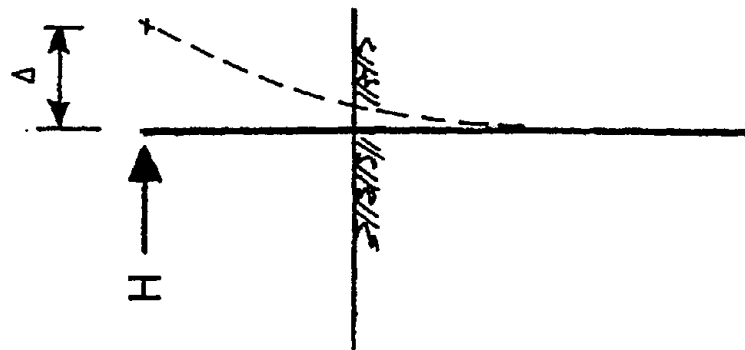


Figure 9-18: Equivalent Cantilever Method- Equal Deflection Assumption.

- (2) Solve for the stiffness of a single pile under axial loading.
- (3) Determine the pile group reduction factors (p -multipliers); refer to section 9.3.5.
- (4) Superimpose the stiffness of individual piles to obtain the pile group stiffness, taking into account the group reduction effect.
- (5) Determine the stiffness contribution of the pile cap. This additional stiffness results primarily from the passive resistance on the vertical surface of the cap.
- (6) Superimpose the stiffness of the pile cap to the pile group.

Strictly speaking, nonlinear pile solutions under lateral loading in layered soil deposits usually require the aid of computer models, such as the computer program COM624P cited above. Analysis using non-linear p - y curves is the state-of-practice for evaluating lateral pile stiffness for highway bridges. However, linear representation of the soil stiffness can also yield solutions of reasonable accuracy provided that the soil conditions are not highly variable and the expected lateral deflection of the pile is within a reasonable range (i.e., between 10 mm and 25 mm). This type of solutions can be derived using the horizontal subgrade reaction model, which assumes the support springs along the pile are elastic and the stiffness of the springs is independent of the pile diameter and vary linearly with depth. The recommended coefficients of variation of subgrade modulus for sand and for clay are presented in Figure 9-19 and Figure 9-20, respectively.

Using the subgrade reaction model described above, Lam (1995) has developed a series of linear pile-head stiffness charts to expedite soil-pile analysis under lateral loading, as shown in Figure 9-21 through 9-27. These design charts reflect the relationship between applied pile head lateral loads and moments and the corresponding lateral deflections. The design charts provide stiffness values for various pile-head embedment and boundary conditions, which significantly affects pile stiffness. It is important that the pile-cap connection be properly accounted for. For example, an assumption of a free pile head may be appropriate for timber and steel pile with minimal pile head embedment into the pile-cap. On the other hand, an assumption of fixed head condition may be warranted for concrete piles with proper reinforcement steel/dowels into the pile-cap. Because of the ease of their use, these simplified design charts are particularly useful for preliminary design or sensitivity evaluations.

9.3.7 Other Design Issues

Foundation Design Forces

The earthquake-induced design forces for the foundation are generally taken as twice the seismic forces in the column. Alternatively, the foundation can also be designed to resist the forces corresponding to the column yield demands. (i.e., forces corresponding to column plastic hinges). The intent of these design requirements is to ensure the failure would not occur in the foundation components and limit the damage to exposed locations.

Single column drilled shafts and pile extensions (see Figure 9-10) are the exceptions to the design philosophy to avoid seismic damage below ground level. Historically, there has been a number of foundation problems associated with pile extensions. However, drilled shafts tend to performed better. This may be attributed to the large diameter of the shaft allowing more ductile details as compared to conventional piles used for pile extensions.

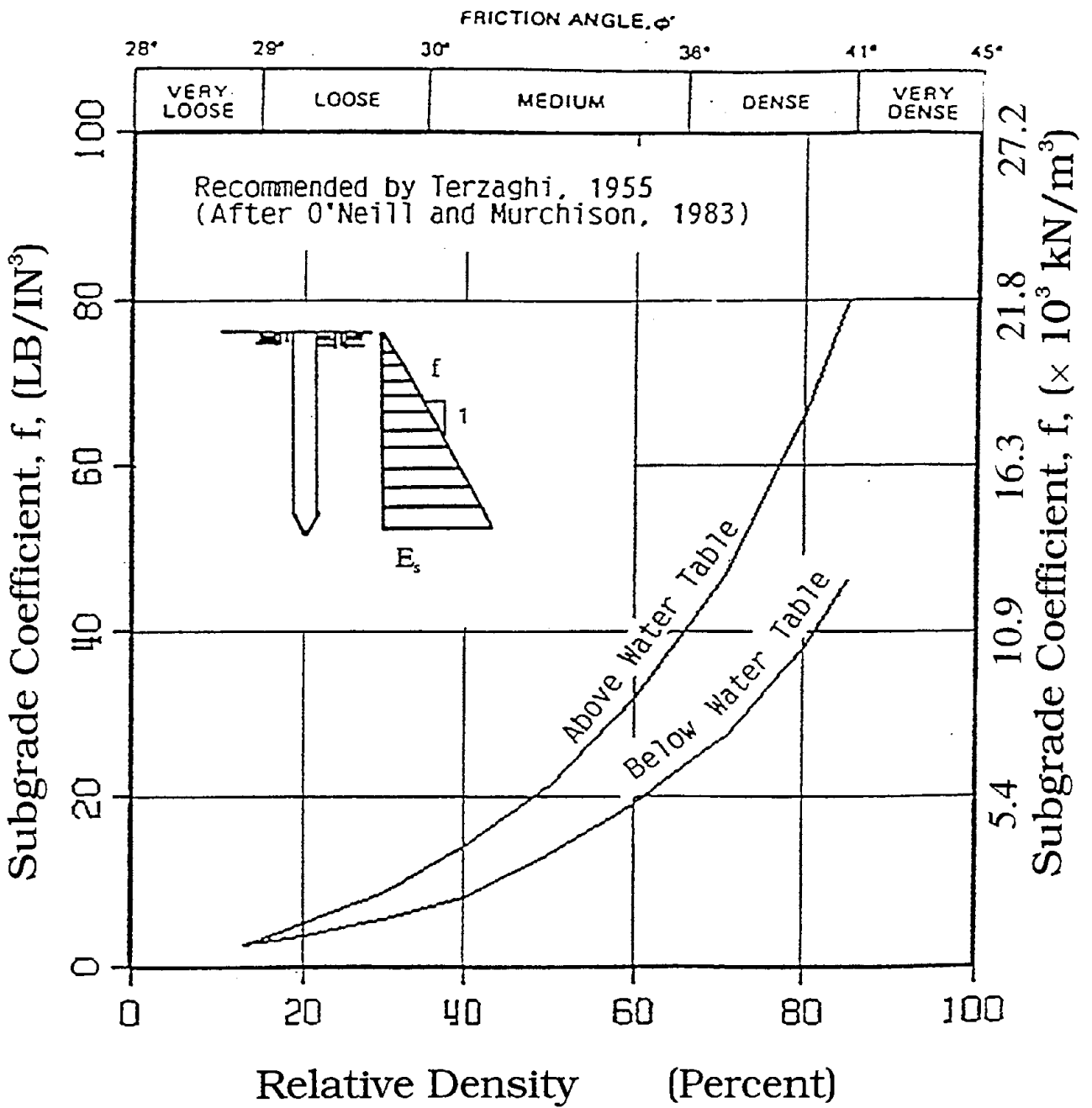


Figure 9-19: Coefficient of Variation of Subgrade Modulus for Sand.

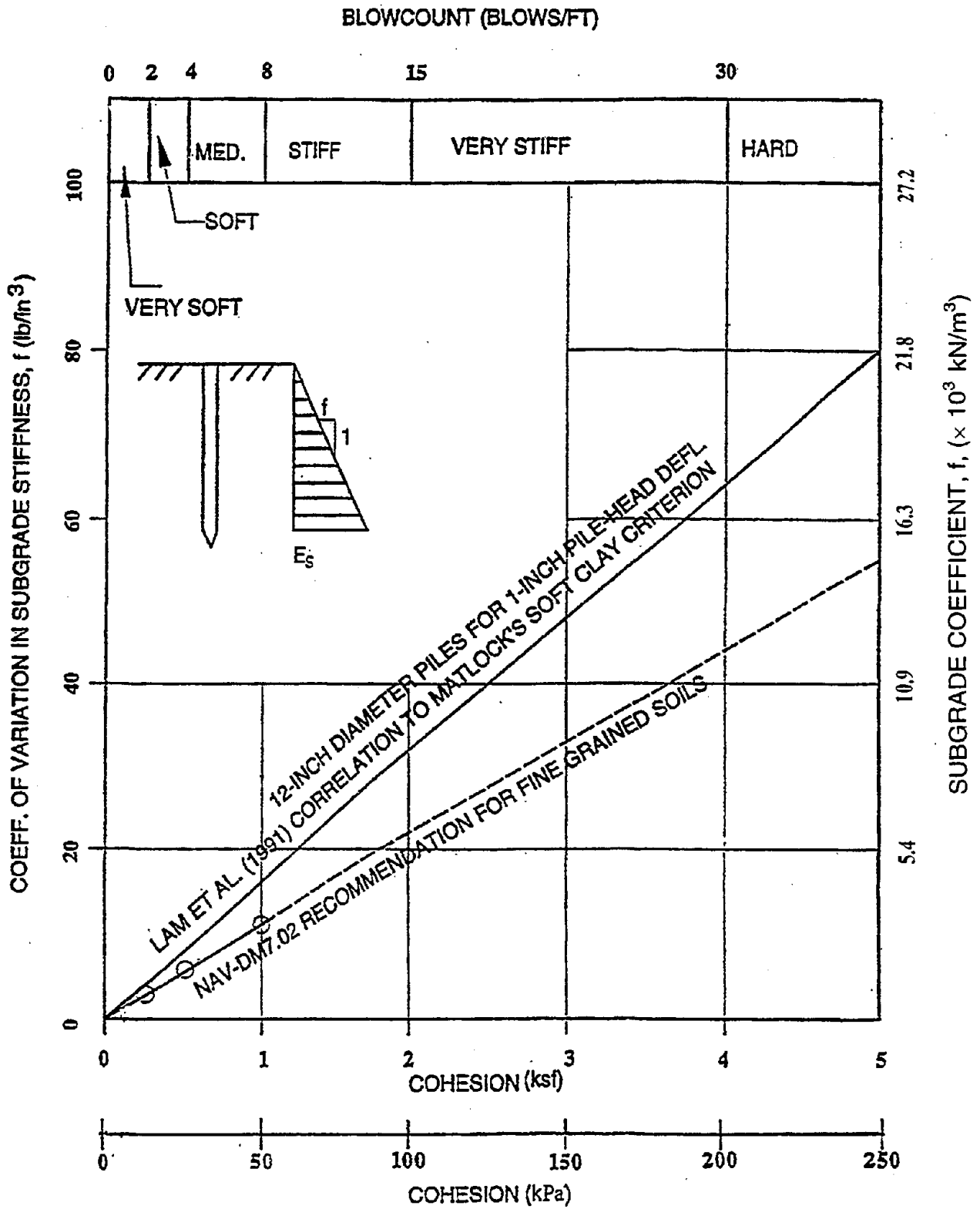
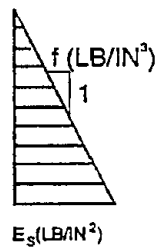
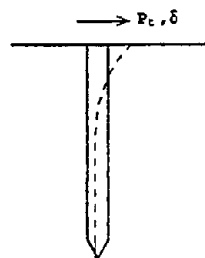
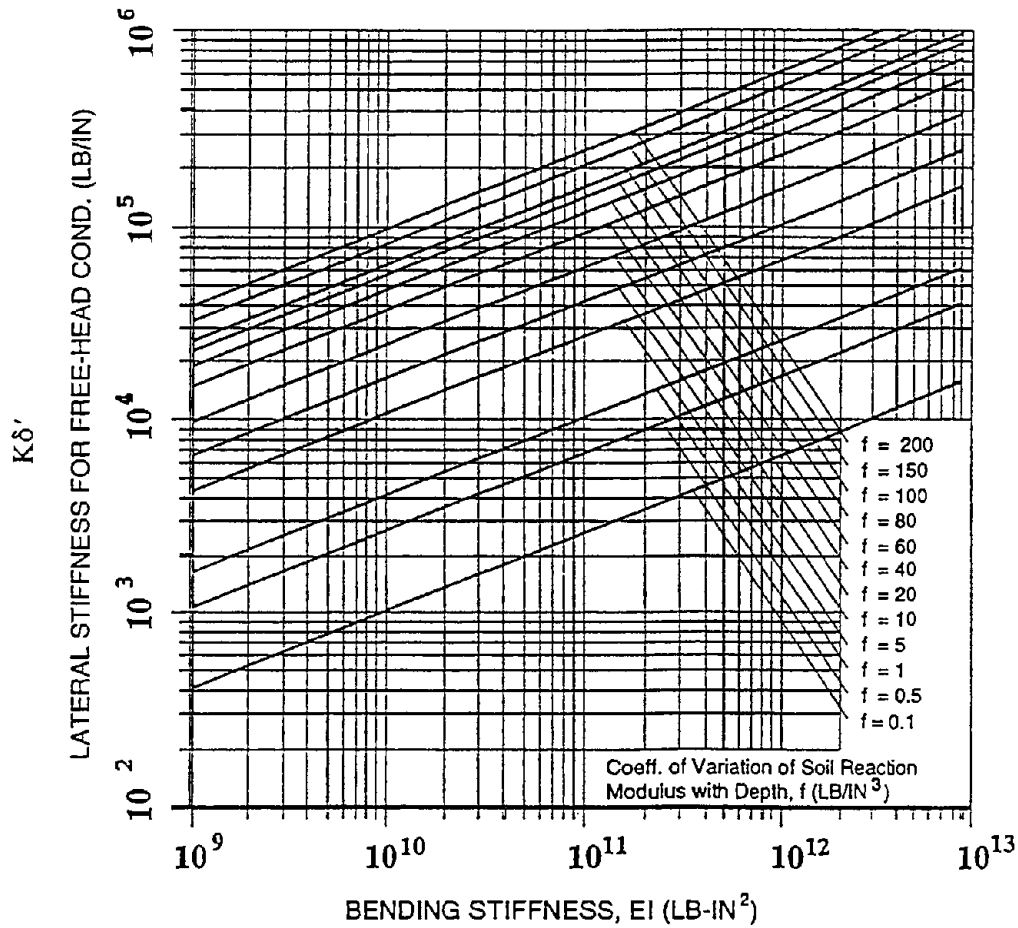


Figure 9-20: Coefficient of Variation of Subgrade Modulus for Clay.



FREE HEAD PILE STIFFNESS $K\delta'$

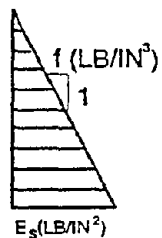
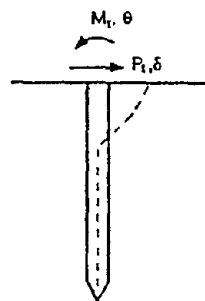
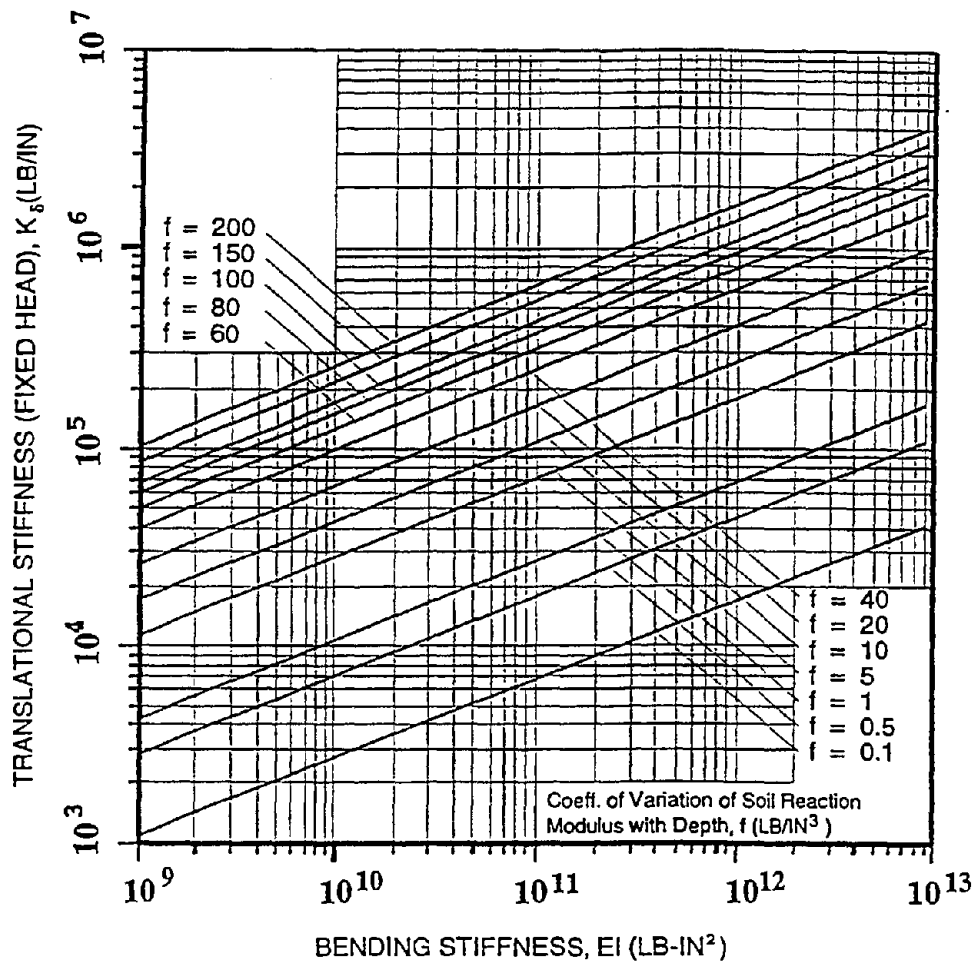
$$= K_{\delta} \cdot \frac{K_{\delta\theta}^2}{K_{\theta}}$$

$$= 0.41 \frac{E \cdot I}{T^3}$$

$$T = \left(\frac{E \cdot I}{f} \right)^{1/5}$$

- 1 lb/in³ = 272 kN/m³
- 1 ksf = 48 kPa
- 1 lb/in = 0.1752 kN/m
- 1 lb-in² = 2.87 × 10⁻⁶ kN-m²

Figure 9-21: Lateral Stiffness of Free-Headed Piles.



$$P_t = K_\delta \cdot \delta + K_{\delta\theta} \cdot \theta$$

$$M_t = K_{\delta\theta} \cdot \delta + K_\theta \cdot \theta$$

$$K = \frac{1.0765 \cdot E \cdot I}{T^3}$$

$$T = \left(\frac{E \cdot I}{f} \right)^{1/5}$$

$$1 \text{ lb/in}^3 = 272 \text{ kN/m}^3$$

$$1 \text{ ksf} = 48 \text{ kPa}$$

$$1 \text{ lb/in} = 0.1752 \text{ kN/m}$$

$$1 \text{ lb-in}^2 = 2.87 \times 10^{-6} \text{ kN-m}^2$$

Figure 9-22: Lateral Stiffness of Fixed Head Piles.

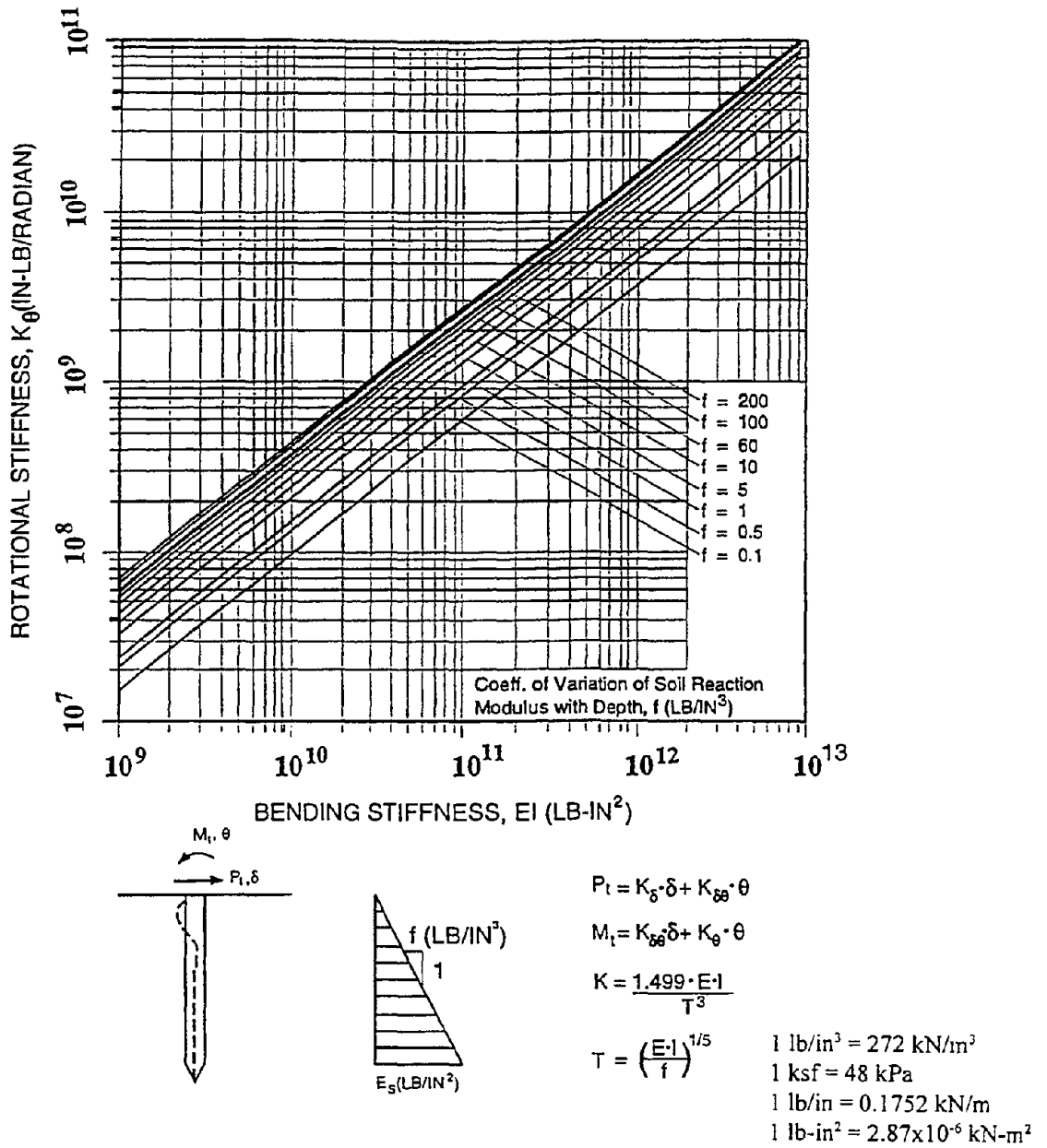
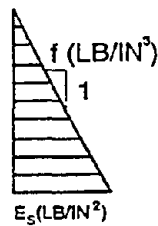
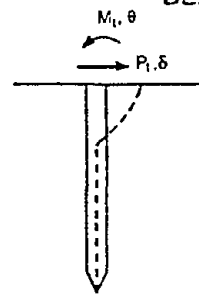
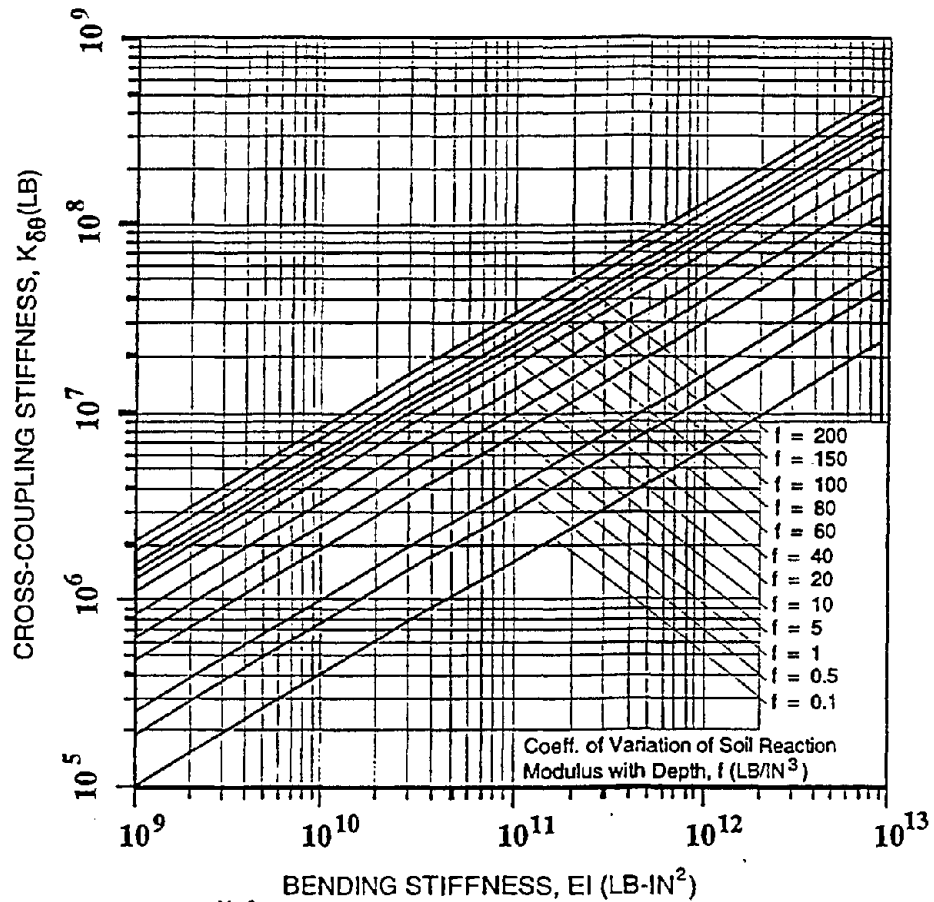


Figure 9-23: Rotational Stiffness at Pile Head.



$$P_t = K_\delta \cdot \delta + K_{\delta\theta} \cdot \theta$$

$$M_t = K_{\delta\theta} \cdot \delta + K_\theta \cdot \theta$$

$$K_{\delta\theta} = \frac{0.999 \cdot E \cdot I}{T^2}$$

$$T = \left(\frac{E \cdot I}{f} \right)^{1/5}$$

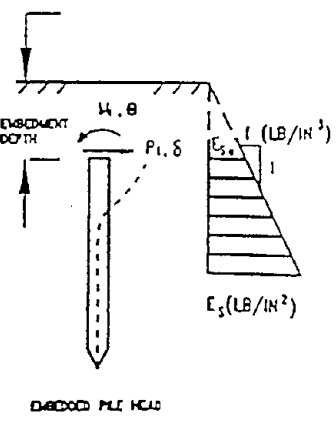
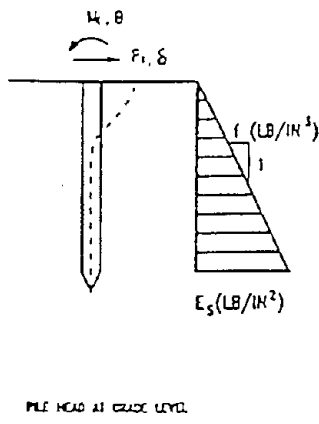
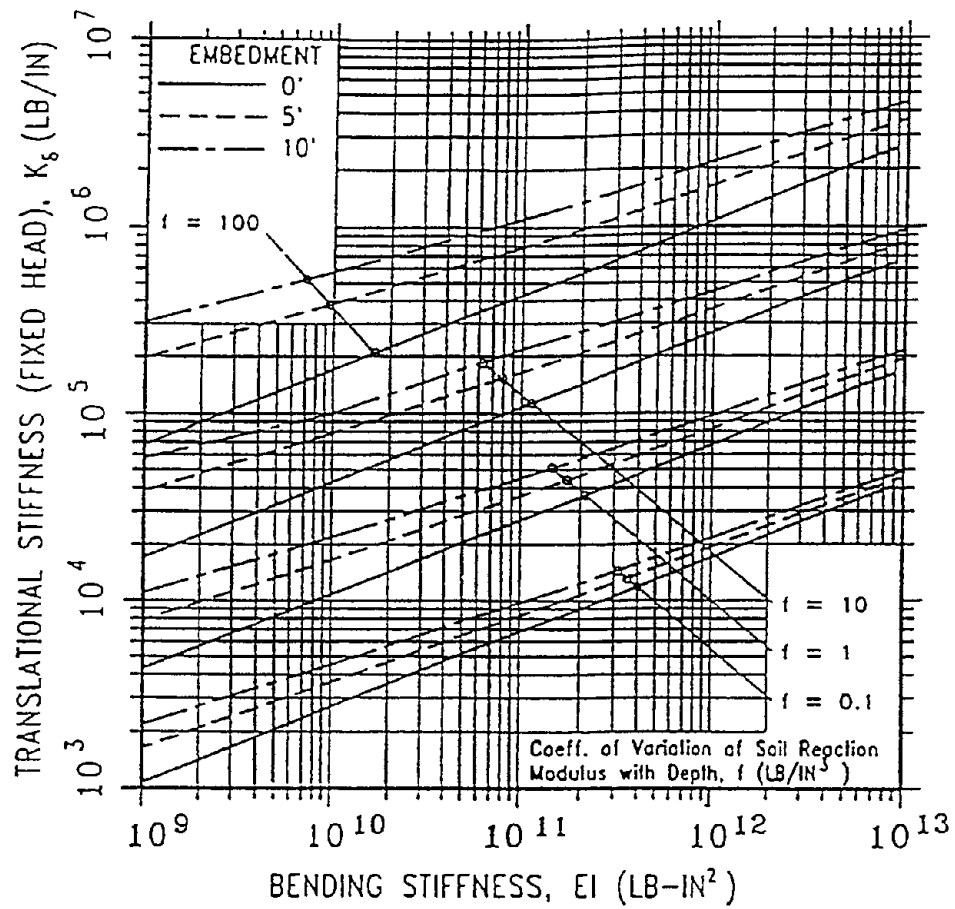
$$1 \text{ lb/in}^3 = 272 \text{ kN/m}^3$$

$$1 \text{ ksf} = 48 \text{ kPa}$$

$$1 \text{ lb/in} = 0.1752 \text{ kN/m}$$

$$1 \text{ lb-in}^2 = 2.87 \times 10^{-6} \text{ kN-m}^2$$

Figure 9-24: Cross-Coupling Stiffness at Pile-Head.

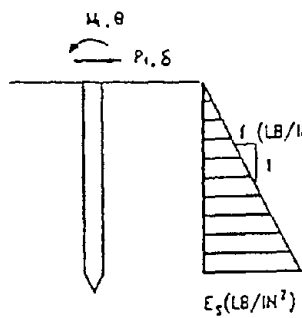
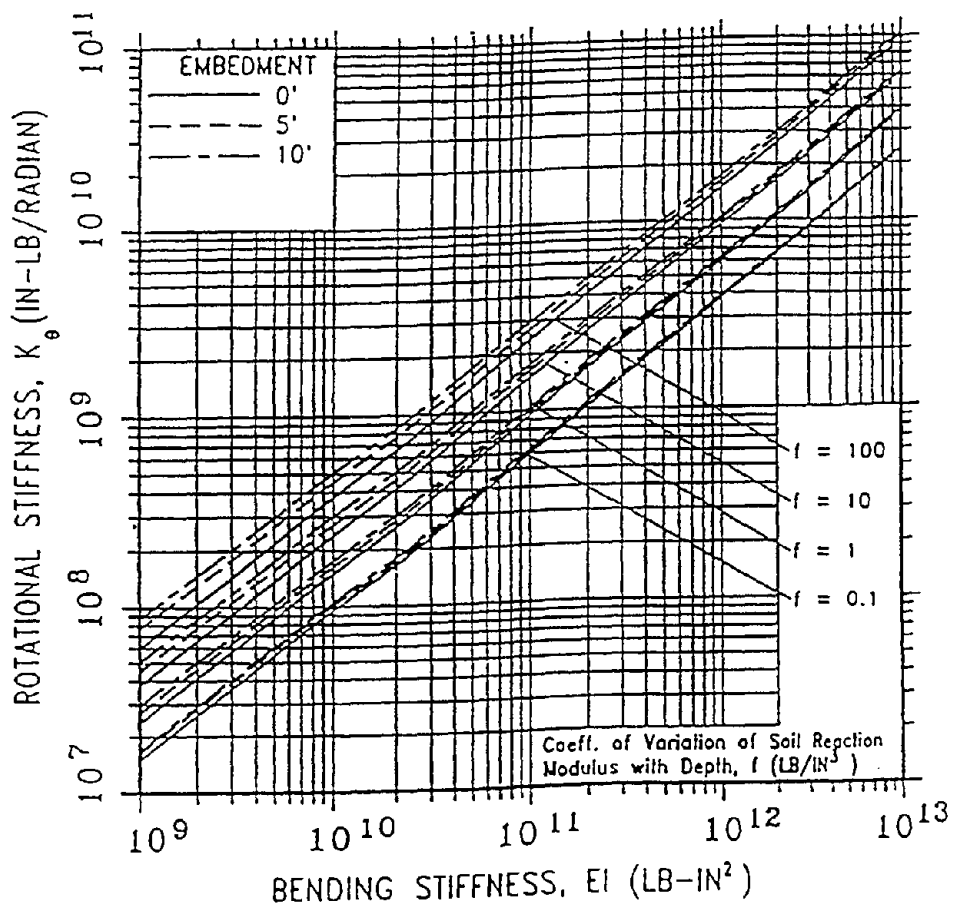


$$P_i = K_s \cdot \delta + K_{s1} \cdot \theta$$

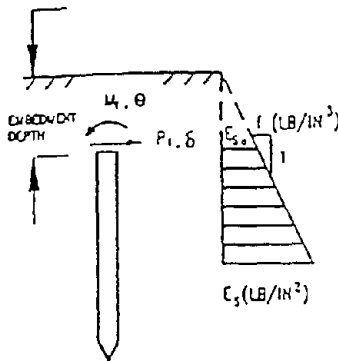
$$M_i = K_{s1} \cdot \delta + K_s \cdot \theta$$

- 1 lb/in³ = 272 kN/m³
- 1 ksf = 48 kPa
- 1 lb/in = 0.1752 kN/m
- 1 lb-in² = 2.87x10⁻⁶ kN-m²

Figure 9-25: Embedment Effects on Lateral Stiffness of Fixed Head Piles.



PILE HEAD AT GRADE LEVEL



EMBEDDED PILE HEAD

$$P_i = K_s \cdot \delta + K_r \cdot \theta$$

$$M_i = K_{rs} \cdot \delta + K_r \cdot \theta$$

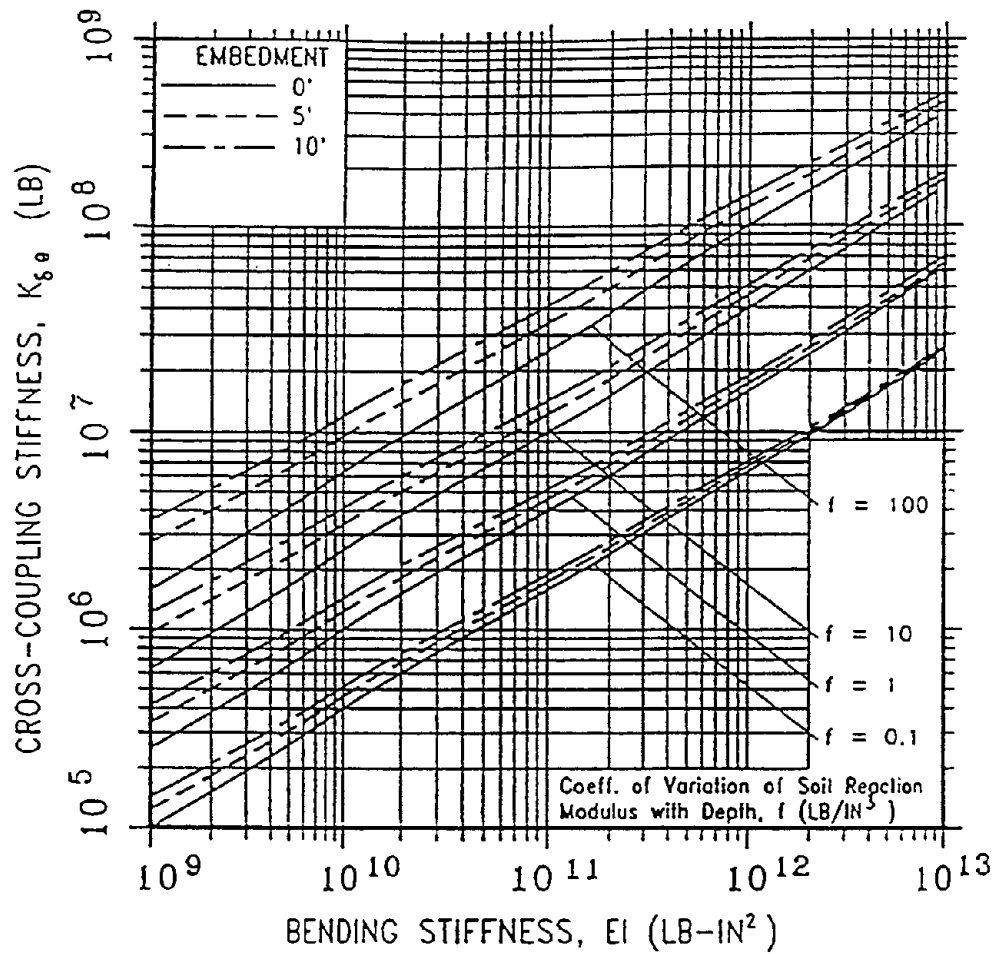
$$1 \text{ lb/in}^3 = 272 \text{ kN/m}^3$$

$$1 \text{ ksf} = 48 \text{ kPa}$$

$$1 \text{ lb/in} = 0.1752 \text{ kN/m}$$

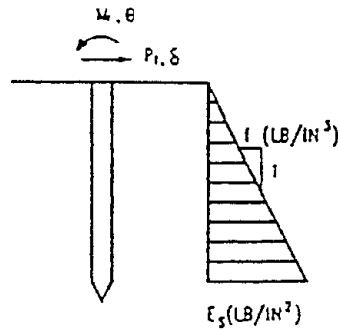
$$1 \text{ lb-in}^2 = 2.87 \times 10^{-6} \text{ kN-m}^2$$

Figure 9-26: Embedment Effects on Rotational Stiffness.

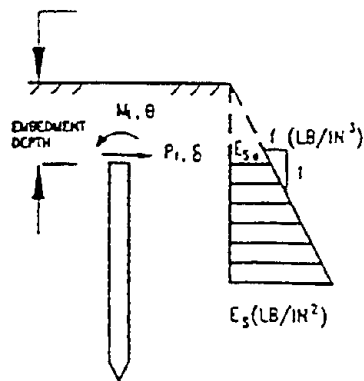


$$P_i = K_{\delta} \cdot \delta + K_{\delta\theta} \cdot \theta$$

$$M_i = K_{\theta\delta} \cdot \delta + K_{\theta} \cdot \theta$$



PILE HEAD AT GRADE LEVEL



EMBEDDED PILE HEAD

- 1 lb/in³ = 272 kN/m³
- 1 ksf = 48 kPa
- 1 lb/in = 0.1752 kN/m
- 1 lb-in² = 2.87x10⁻⁶ kN-m²

Figure 9-27: Embedment Effect on Cross-Coupling Stiffness.

Soil Strength

Lam and Martin (1986) performed a sensitivity study to examine the effects of various factors on the overall pile behavior. These factors include the p-y curve shape, the gapping effects at the pile head, and the shear strength of soil. The results indicate that the overall pile behavior is relatively insensitive to minor variations of the p-y curve (e.g., initial stiffness and curve shape). Primary emphasis should be placed on assessing the soil strength. This is particularly the case when saturated loose sand and soft clay foundation soils are encountered. Current FHWA/AASHTO guidelines recommend the consideration of potential for strength and stiffness degradation under repeated cyclic loading in these soils (refer to Chapter 5).

It should also be noted that current design practice is to use the ultimate capacity of the foundation supporting medium in designing for seismic loads. Because of the transient nature of these loads, even when the ultimate capacity is reached the foundation is expected to experience limited deformation and collapse of the structure is unlikely. This assumption enables cost effective design and construction of foundations in highly seismic area.

Pile Uplift Capacity

It is not unusual for piles in pile groups to be subjected to significant uplift resulting from seismic loading. The moment applied by the seismic lateral force to the pile cap is typically resisted by axial loads in the piles. Thus, the outermost piles in the group can be subjected to relatively large cyclic axial loads. Experience with seismic analysis of pile foundations for seismic retrofitting of bridges in California indicates that foundation piles, subjected to such uplift loads, reach or exceed their tensile capacity. This is particularly the case for single column bent pile footings where additional uplift capacity is necessary to resist large overturning moments. Numerous pile foundations for bridges in California have been and/or are currently scheduled for retrofit due to inadequate tensile capacity compared to peak seismic uplift loads.

Analogy with the seismic response of embankments and slopes would indicate that the tensile capacity of piles should only have to be a portion of the peak uplift load during seismic loading. Exceeding the uplift capacity for only a few cycles of loading should result in only limited permanent deformation of the pile. The analogy can also be interpreted as follows. In a multi-pile group, the pile cap should not suffer any permanent deformation until all piles in the "outboard" half of the pile group have reached their tensile capacity. If even one pile subject to uplift remains within the load limit, unrecoverable rotation of the cap should not occur. Lam and Martin (1997) have demonstrated the tradeoff between the additional capacity derived by allowing some of the piles in a group to yield in tension and the resulting permanent displacement of the pile caps. In general, permanent displacements are small provided at least one pile in the cap has not yielded. The above discussion is consistent with AASHTO (1994) recommendations. In Section 6.4.2(b), AASHTO suggests that some separation between end bearing foundations and the subsoil is permitted, provided that the foundation soil is not susceptible to loss of strength under the imposed cyclic loading. For pile groups, the separation may reach up to one-half the end bearing area of the pile group. In Section 6.4.2(c), AASHTO recommends that the ultimate capacity of the piles be used in designing the foundation for uplift forces. However, these recommendations should be considered with structural requirements including embedment length of the pile in the pile cap and the detailing of the connections.

Specifically, AASHTO requires that all piles be properly anchored to the pile footing or cap. The embedment length of concrete piles should be sufficient to develop uplift forces but should not be less than

the development length required for the reinforcement. For concrete-filled pipe piles, the pile head should be anchored into the footing or cap by at least 4 reinforcing steel dowels. For timber and steel H piles, including unfilled pipe piles, special anchoring devices should be provided to develop the full uplift forces. In general, steel piles, including concrete filled pipe piles, are more favored in highly seismic areas because their superior characteristics in ductility and shear resistance. Concrete piles tend to hinge or shatter at the location immediately below the pile cap, thereby requiring reduced tie spacing for better concrete confinement.

Liquefaction

Pile-supported structures have performed extremely well in areas subject to liquefaction in recent earthquakes. Notable examples include the performance of pile-supported container cranes at the Port of Oakland in the Loma Prieta earthquake of 1989 and the performance of pile-supported buildings on Port Island in the Kobe earthquake of 1995.

In many earthquakes where liquefaction occurs, the soil may not liquefy until the end of the earthquake. Therefore, during an earthquake piles may still be able to rely on the vertical and lateral support of the soil in the potentially liquefied zone. However, due to uncertainties as to exactly when liquefaction will occur, it seems prudent to assign a reduced vertical and lateral resistance to potentially liquefiable soil surrounding a pile if the pile is expected to function as a load carrying member during and after an earthquake. Preliminary results by Dobry, *et al.* (1996) suggests that the lateral resistance of a pile in liquefied ground is approximately 10 percent of the lateral resistance in non-liquefied ground. In characterizing the p-y relationship of the liquefied zone, it is important that the residual shear strength of the soil be used. Additionally, this residual shear strength should be limited to a value that does not exceed the drained strength of the liquefied materials. If a pile foundation in potentially liquefiable soil is expected to carry lateral loads after the surrounding soil liquefies, batter piles may be required to provide adequate lateral support. If batter piles are used, the pile cap connections should be designed to sustain concentrated shears and moment loads induced by lateral movements and the batter piles should be designed to sustain loads due to soil settlement.

Ground Displacement Loading

In addition to the inertial superstructure forces (applied to the pile cap), the pile/shaft foundation may also experience earthquake loading in the form of ground displacements. The sources of this form of loading may include: (1) free-field ground displacement, (2) unstable embankments/slopes, and (3) liquefaction-induced lateral spreading.

Ground displacements impose forces acting along the length of the piles and pile cap. For the free-field ground displacement, the forces can be estimated by imposing the peak free-field ground displacement profile on the pile through p-y springs. The free-field site response analysis program SHAKE can be used to develop the peak free-field ground displacement profile. In competent sites, the free-field ground displacement normally does not govern the pile design primarily because the curvature of the ground displacement profile is small, thereby causing insignificant bending moment in the pile. Nevertheless, large curvatures could develop at interfaces between soft and stiff soil layers. In such cases the emphasis should be placed on using flexible ductile piles. Dobry (1990) provided a simplified chart for estimating bending moment of pile at interfaces between soil layers having a large stiffness contrast.

Ground displacements due to an unstable embankment/slope or liquefaction-induced lateral spreading present a more difficult case. Analysis of this problem is similar to that described above except that the

ground displacements are generally much larger. The procedures for estimating the ground displacements due to an unstable embankment/slope and liquefaction-induced lateral spreading are presented in Chapters 7 and 8 respectively. Designing a pile foundation to resist this form of loading is generally not feasible. Instead, various forms of ground treatment and/or modification of design configuration are often considered.

9.4 RETAINING STRUCTURES

9.4.1 General

A comprehensive discussion of various types of earth retaining structure systems used for highway applications is presented in Module 6 (Earth Retaining Structures). Also included in Module 6 are detailed discussions on wall selection, contracting issues, bidding documents and static design and analysis procedures for each type of earth retaining structures. The materials presented in the following sections focus on the seismic design aspects of the retaining structures.

Gravity earth retaining walls subjected to seismic loading have suffered large movements and extensive damage in earthquakes, even though the retaining structures had been designed with adequate factors of safety against static earth pressures. In some cases, this damage has been attributed to liquefaction. However, in some cases, the damage has been attributed to the increase in the magnitude of the lateral earth pressure during seismic events. Seed and Whitman (1970) have reported several cases of failure of gravity retaining walls in earthquakes by rotation about the wall-top as a result of the dynamic earth pressure. Descriptions of damage to gravity retaining structures subjected to earthquakes are also given by Seed and Whitman (1970), Nazarian and Hadjian (1979), and others. Mechanically Stabilized Earth (MSE) walls, and soil-nailed walls have, in general, performed very well in earthquakes with no reports of significant damage. Anchored walls have performed reasonably well in the U.S.. However, when used as waterfront structures, anchored walls are often vulnerable.

Damage to retaining structures due to earthquakes can be classified using three main categories:

- *Damage to gravity retaining walls with saturated backfill:* Damage of this type has been frequently reported for port and harbor structures such as quay walls. Seed and Whitman (1970) suggest that failure in quay walls from dynamic loads is primarily due to a combination of the increase in the lateral soil pressure behind the wall, a reduction in water pressure in front of the wall, and possibly liquefaction of the foundation soil. Liquefaction of retaining wall backfill created large lateral pressures that are believed to be responsible for outward movements of quay walls as great as 8 meters during recent earthquakes in Japan.
- *Damage to gravity retaining walls with unsaturated backfill:* Fewer cases of failure of retaining walls with unsaturated backfill have been reported than for walls with saturated backfill. Jennings (1971) and Evans (1971) reported movements and failures in retaining walls and bridge abutments in the San Fernando earthquake. Ross, *et al.* (1969) reported that as a result of the 1964 Alaskan earthquake, the flexible deck of a bridge structure buckled due to the movement of retaining walls in the abutments. Conventional gravity retaining walls supporting elevated portions of the Shinkansen ("bullet" train) track alignment failed in Kobe in the 1995 earthquake.
- *Damage to MSE walls, anchored walls, and soil-nailed walls:* Tatsuoka, *et al.* (1995) report that mechanically stabilized earth walls (reinforced earth walls) along the same stretch of the alignment where conventional gravity walls failed performed very well in the 1995 Kobe earthquake.

Mechanically stabilized earth walls also performed well in the 1989 Loma Prieta earthquake. There have been no reports of serious damage to anchored walls in earthquakes in the U.S. This includes several anchored walls in the epicentral region of the Northridge earthquake. In Japan, however, anchored wall have been shown to suffer significant damage either due to liquefaction in the backfill soil or the combined effect of dynamic earth pressure and hydrodynamic forces. Felio, *et al.* (1990) report that eight soil-nailed walls in the San Francisco Bay area showed no signs of significant distress as a result of shaking during the Loma Prieta earthquake.

9.4.2 Gravity Type Retaining Walls

The seismic performance of gravity type retaining walls is most commonly evaluated using pseudo-static dynamic earth pressure analysis, where the dynamic lateral earth force is estimated as a sum of the initial static earth force and the increment in active earth force due to the seismic loading. For some cases, alternative permissible displacement-based approach is also adopted.

Dynamic Earth Pressure Approach

During earthquakes, the soil behind a retaining wall exerts a horizontal dynamic earth thrust that is greater than the static force. The method most frequently used for the calculation of this dynamic earth thrust is that developed by Mononobe (1929) and Okabe (1926). This pseudo-static approach was developed for dry cohesionless materials and was based on the following assumptions:

- The wall yields sufficiently to produce minimum active pressure during earthquakes. When a wall is not allowed to yield sufficiently, the dynamic earth pressure tends to increase and the pseudo-static approach needs to be adjusted. A recommendation on this adjustment will be presented later.
- The active failure wedge developed behind the wall behaves as a rigid body so that the accelerations are uniform throughout the soil mass and the effect of earthquake motion is represented by a pseudo-static inertial force ($k_h W_s$) and ($k_v W_s$), where W_s is the weight of the active failure wedge, as shown in Figure 9-28. This is a reasonable assumption in most cases, except for very high walls where more detailed analyses may be justified.
- The soils behind the wall are not saturated and liquefaction will not occur. When liquefaction occurs in the backfill zone, soil pressure may be greatly increased due to the loss of strength of the soil. Furthermore, the effect of hydrodynamic forces of the liquefied soil should also be addressed.

Using this approach, the **total** dynamic active earth thrust, P_{ac} , is expressed by the following equation:

$$P_{ac} = \frac{1}{2} \gamma H^2 (1 - k_v) K_{ac} \quad (9-13a)$$

where K_{ac} is given by

$$K_{ac} = \frac{\cos^2(\phi - \psi - \theta)}{\cos\psi \cos^2\theta \cos(\delta + \theta + \psi) \left[1 + \sqrt{\frac{\sin(\phi + \delta) \sin(\phi - \psi - \beta)}{\cos(\delta + \theta + \psi) \cos(\beta - \theta)}} \right]^2} \quad (9-13b)$$

Figure 9-29, from Lam and Martin (1986), presents values for K_{ac} for values of ϕ from 20 to 45 degrees for vertical walls with level backfill and a wall/backfill interface friction angle equal to $\phi/2$ for horizontal seismic coefficients and vertical seismic coefficients (i.e., k_h and k_v) from 0 to 0.5 and from 0 to 0.2, respectively.

It should be noted that the total dynamic earth thrust calculated using Eq. (9-13a) consists of two components: (1) the static active earth force, P_a , and (2) the incremental dynamic earth force, ΔP_{ac} . The static active earth force can be calculated by assuming $k_h = k_v = 0$ and $\psi = 0$. The incremental dynamic earth force is simply the difference between the total dynamic earth thrust and the static active earth force ($\Delta P_{ac} = P_{ac} - P_a$).

Besides the magnitude of the seismic earth pressure, the distribution of the seismic earth pressure or the location of the dynamic earth pressure resultant is needed for analyses. The height at which the resultant of the total dynamic earth thrust, P_{ac} , acts on the wall can be divided into two parts. The static force, i.e., with no dynamic effect involved, acts at $H/3$ from the bottom of the retaining wall. The incremental dynamic force, ΔP_{ac} , should be taken to act at a height of $0.6H$ from the bottom. For practical purposes, it may be assumed that the total seismic active earth pressure is uniformly distributed over the height of the wall, meaning that the earth pressure resultant acts at the midheight of the wall (i.e., at $0.5H$). This assumption appears appropriate for most highway problems in moderate to high seismic areas.

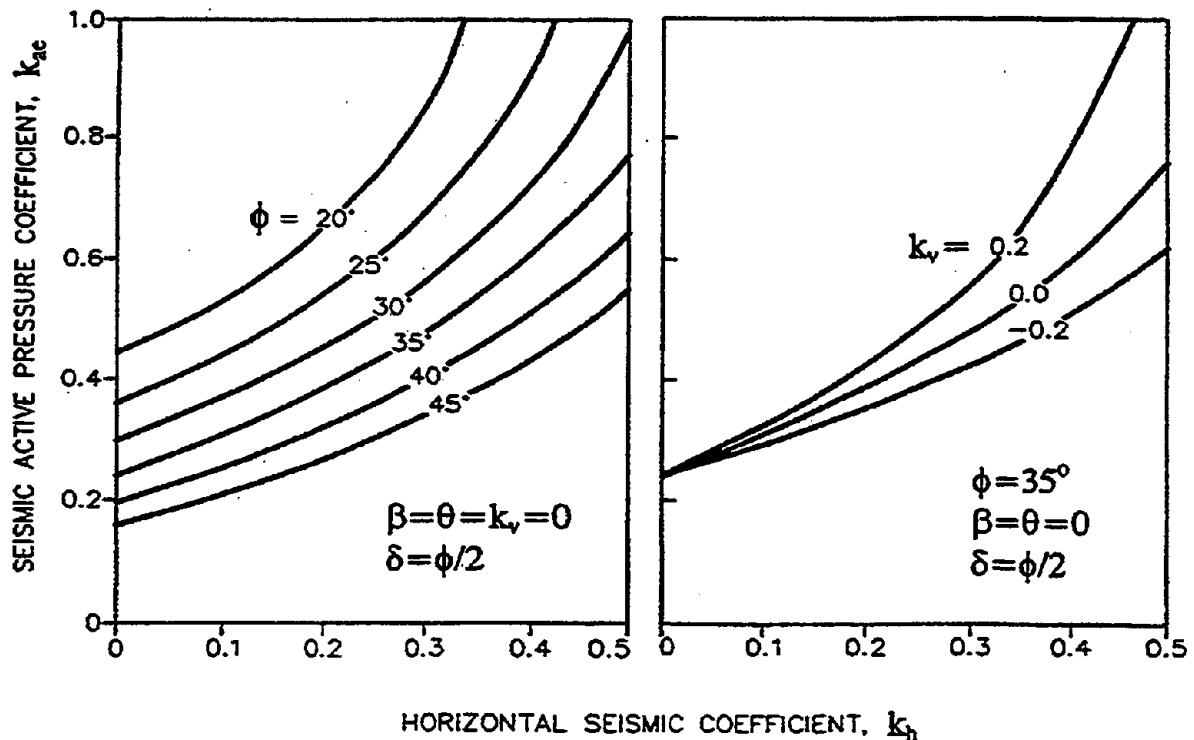


Figure 9-29: Effect of Seismic Coefficients and Friction Angle on Seismic Active Pressure Coefficient. (Lam and Martin, 1986)

In using the Mononobe-Okabe approach, it is necessary to note that the inertial effect of the retaining wall itself is not taken into account. For gravity type retaining walls, this effect need to be included in stability analysis (e.g., against sliding and overturning). It should also be noted that, the vertical acceleration is usually ignored in practice in the design of retaining walls (i.e., $k_v=0$)

The procedure for seismic stability evaluation of gravity type retaining walls is summarized as follows:

- (1) Select an appropriate seismic coefficient, k_h , based on the design earthquake, and assume $k_v=0$.
- (2) Calculate the horizontal inertial force of the gravity wall itself, $k_h W$, and the dynamic earth thrust, P_{ae} , using the Mononobe-Okabe equation presented above.
- (3) Evaluate sliding, overturning and seismic bearing capacity stability using procedures presented in Module 6, "Earth Retaining Structures".

Like any pseudo-static analysis, the major challenge in applying the Mononobe-Okabe theory is selection of an appropriate seismic coefficient. Evidence from shaking table and centrifuge model testing, summarized by Whitman (1990), indicates that the peak ground acceleration should be used to evaluate the peak lateral earth pressure on a retaining wall. Thus, for critical facilities with walls that can accommodate very little deformations, use of the peak ground acceleration divided by the acceleration of gravity as the seismic coefficient may be warranted. In some extreme cases, where the walls are rigid and restrained from any lateral movements such that active soil wedge behind the wall cannot be mobilized, the dynamic earth force will be greater than that given by the Mononobe-Okabe analysis. For very critical structures under this condition, it is recommended that the incremental dynamic component of the earth force, ΔP_{ae} , be increased by a factor of 1.5. It is a design practice to allow lower factors of safety for retaining wall stability analyses under the design seismic loading condition. Generally, if the seismic coefficient, k_h , is assumed to be equal to the peak ground acceleration value, factors of safety between 1.0 to 1.1 are considered acceptable for bearing capacity and sliding resistance. For overturning stability, factors of safety ranging from 1.3 to 1.5 are typically used in practice. If a reduced seismic coefficient is used (as discussed in the following paragraphs) it is recommended that factors of safety between 1.1 and 1.2 be used for bearing capacity and sliding stability evaluations and a minimum factor of safety of 1.5 for overturning stability evaluation.

However, for retaining walls that are allowed to accommodate some limited deformations, the design may become overly conservative if the peak ground acceleration is used, particularly in high seismic areas. Most retaining walls for highway applications can accommodate a small amount of displacement without jeopardizing their functions. To provide a more economical structure, a reduced seismic acceleration coefficient smaller than the peak ground acceleration may be used, provided that the wall is detailed to accommodate a small tolerable displacement. This so-called "Permissible Displacement Approach" procedure is recommended by FHWA (Lam and Martin, 1986) and will be presented next.

Permissible Displacement Approach

Several theories were developed to account for the displacement and rotation of walls during an earthquake. Richards and Elms (1979) extended the work of Franklin and Chang (1977) on seismic deformation of earth dams to gravity retaining walls. The approach is similar to the method suggested by Newmark (1965) to evaluate the amount of slip displacements occurring in dams and embankments during earthquakes (see Chapter 7 of this module). The results of their study along with those obtained by Newmark (1965) and Franklin and Chang (1977) are shown in Figure 9-30. This figure is a plot of the

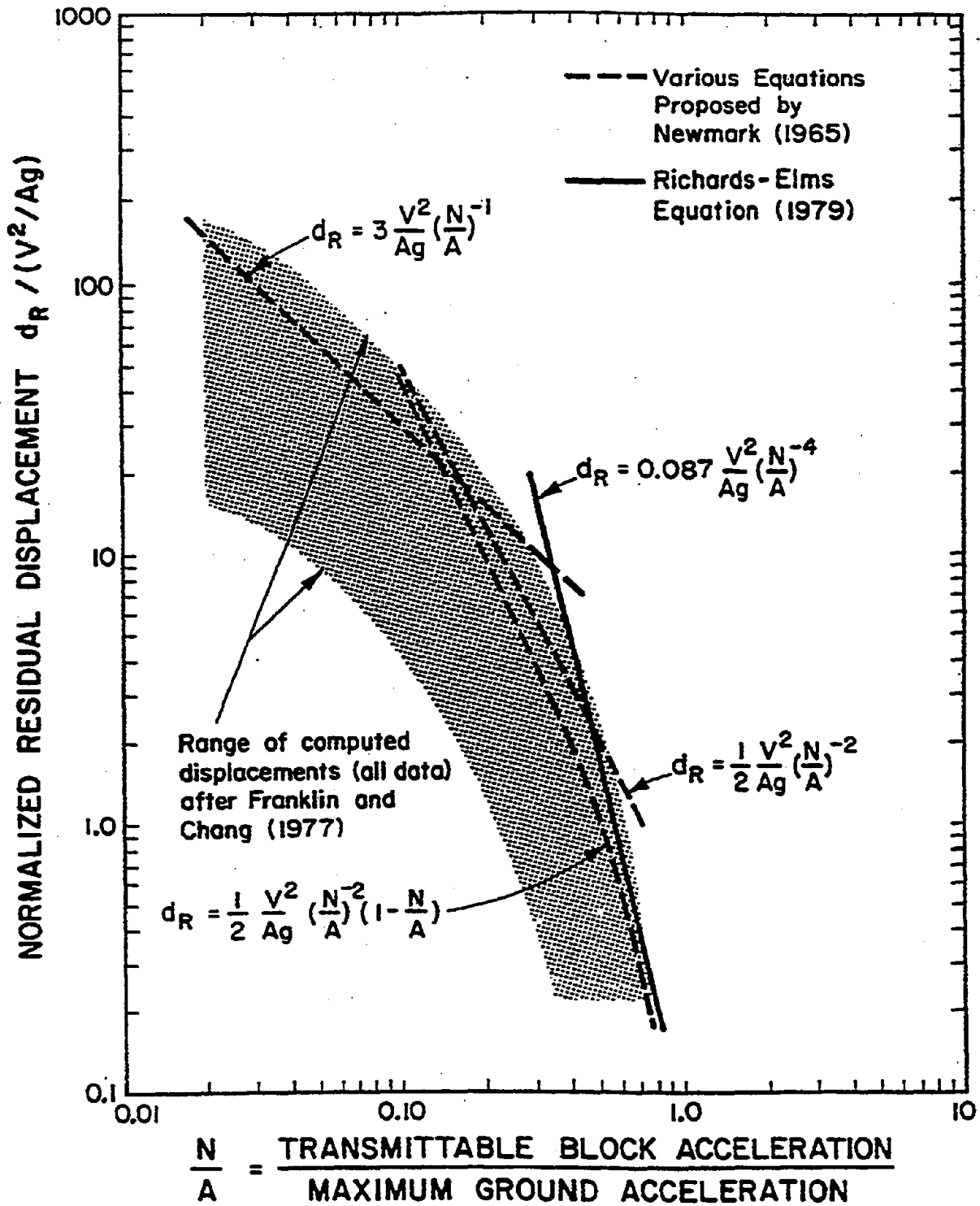


Figure 9-30: Range of Normalized Displacements Using Newmark Sliding Block Model, and Various Equations Approximating the Upper Envelope (Richard and Elms, 1979).

normalized residual displacement, d_r , versus the ratio of transmittable acceleration, N , to peak ground acceleration, A . These data were obtained from numerous strong motion records from previous earthquakes. It is clear that there is considerable scatter in the calculated displacements, primarily due to the differing characteristics of the various earthquake records. The figure also shows several formula suggested by various other investigators. As indicated, these formula tend to yield upper bound estimates of the residual displacements. Since in most applications the ratio N/A ranges between 0.3 and 0.7, AASHTO has recommended to use the formula derived by Richards and Elms (1979), expressed in any consistent set of units, for the displacement of a gravity wall.

$$d_r = 0.087 (V^2/A \cdot g) \cdot (N/A)^4 \quad (9-14)$$

where d_r is the displacement, V is the peak velocity of the earthquake record, N is the peak seismic resistance coefficient sustainable by the wall before it slides (equal to the yield acceleration coefficient of the retaining wall divided by gravity), and A is the peak ground acceleration.

In the absence of information on the time history of velocity, the following values may be used:

$$V = 760 (A) \text{ (mm/s)} \quad (9-15)$$

A design procedure employing the permissible displacement approach for a gravity type retaining wall is outlined as follows:

- (1) Determine the allowable displacement, d , of the wall. The allowable displacement will depend on the allowable settlement that may be tolerated in the backfill, the alignment of the wall, any impact on adjacent facilities, and others.
- (2) Select an appropriate peak ground acceleration coefficient, A , and peak ground velocity, V , based on the design earthquake.
- (3) Derive the seismic resistance coefficient, N , sustainable by the wall using Eq 9-14 and the parameters A , V and $d_r (=d)$ determined above.
- (4) Using $K_h = N$ and assuming $K_v = 0$, calculate the horizontal inertial force of the gravity wall itself, $K_h W$, and the dynamic active earth thrust, P_{ae} , using the Mononobe-Okabe equation presented previously.
- (5) Evaluate sliding, overturning and seismic bearing capacity stability using procedures presented in Module 6 (Earth Retaining Structures).

For most design purposes, it has been shown (Elms and Martin, 1979) that a design value of $K_h = 0.5A$ is adequate, provided that the wall can accommodate an outward displacement of up to about $250A$ mm.

9.4.3 Mechanically Stabilized Earth (MSE) Walls

Seismic design and analysis of MSE walls are, in many aspects, very similar to that for gravity type retaining walls. The primary difference is that an internal seismic stability analysis should also be performed as part of the design for MSE walls. The internal stability analysis incorporates the effects of the inertial force generated by the reinforced soil volume on individual reinforcing element during an earthquake as a pseudo-static horizontal load. The FHWA has recently published design guidelines for seismic design and analysis for MSE walls (Elias and Christopher, 1996). According to these guidelines,

the external stability analysis for MSE walls follows a procedure similar to that presented for gravity type retaining walls, except that different assumptions were used in the selection of design seismic coefficient and in the consideration of the inertial forces of the reinforced soil mass and the backfill. A detailed design procedure for MSE walls (Elias and Christopher, 1996) is presented below.

External Seismic Stability

During an earthquake, the retained fill exerts an incremental dynamic horizontal thrust, ΔP_{ac} , on the MSE wall in addition to the static thrust, P_s . Moreover, the reinforced soil mass is subjected to a horizontal inertia force $P_{IR} = M A_m$, where M is the mass of the active portion of the reinforced wall section assumed at a base width of $0.5H$, and A_m is the maximum horizontal acceleration in the reinforced soil wall (see Figure 9-31).

The force ΔP_{ac} can be evaluated by the Mononobe-Okabe analysis (presented for the gravity type retaining walls) and added to the static forces acting on the wall (weight, surcharge, and static thrust). The dynamic stability with respect to external stability is then evaluated. Allowable minimum dynamic safety factors are assumed as 75 percent of the static safety factors.

The seismic external stability evaluation is performed as follows:

- (1) Select a peak horizontal ground acceleration (free field peak acceleration) based on the design earthquake. If a site-specific seismic hazard analysis is not performed, the peak free field ground acceleration coefficient may be obtained from Division 1A of current AASHTO where it is given as A , Acceleration Coefficient.
- (2) Calculate the maximum acceleration A_m developed in the wall:

$$A_m = (1.45 - A)A \quad (9-16)$$

where A = maximum free field ground acceleration coefficient, AASHTO, Division 1A.
 A_m = maximum wall acceleration coefficient at the centroid of the wall mass.

- (3) Calculate the horizontal inertia force P_{IR} and the incremental dynamic earth thrust ΔP_{ac} :

$$P_{IR} = 0.5 A_m \gamma_r H^2 \quad (9-17)$$

$$\Delta P_{ac} = 0.375 A_m \gamma_r H^2 \quad (\text{Horizontal Backslope}) \quad (9-18)$$

where γ_r is the unit weight of the reinforced soil mass and γ_f is the unit weight of the retained backfill. Note that the equation for ΔP_{ac} shown above was developed assuming a friction angle of 30 degrees and may be adjusted for the other soil friction angles using the Mononobe-Okabe analysis.

- (4) Add to the static force P_s (see Figure 9-31) acting on the structure, 50 percent of the seismic thrust ΔP_{ac} and the full inertial force P_{IR} . The reduced ΔP_{ac} is used because these two forces are unlikely to peak simultaneously.

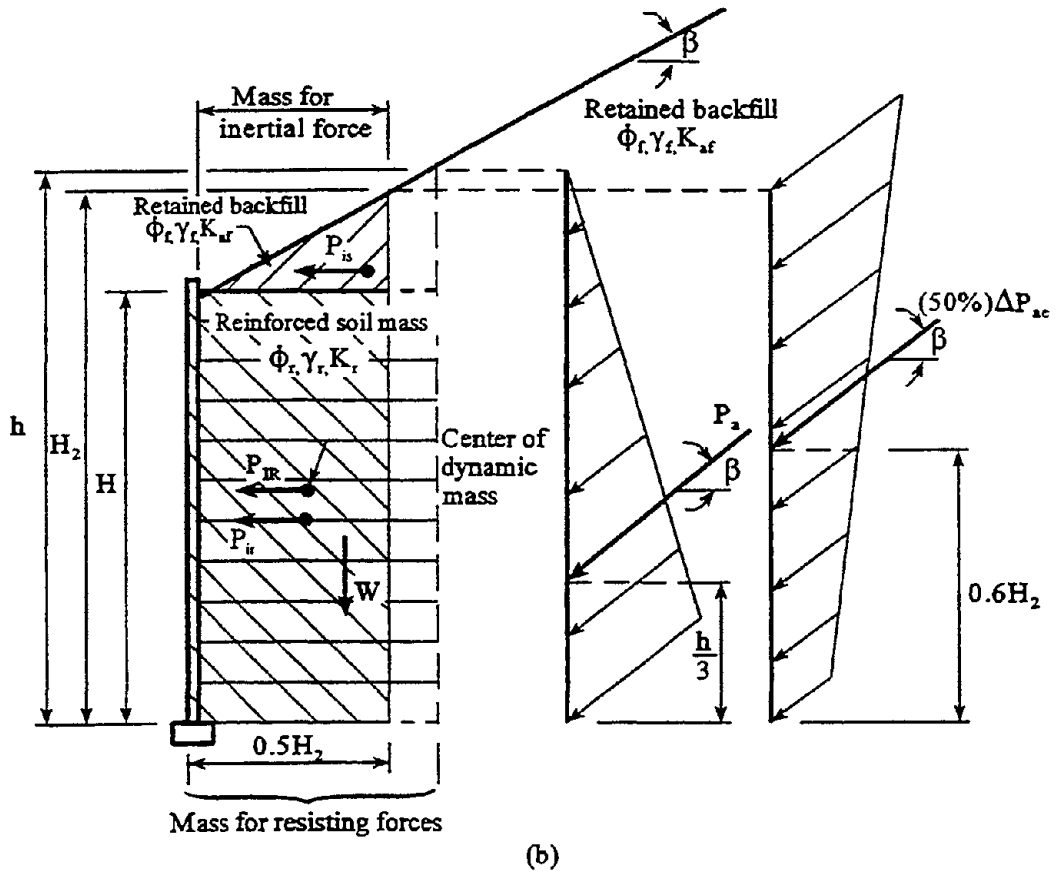
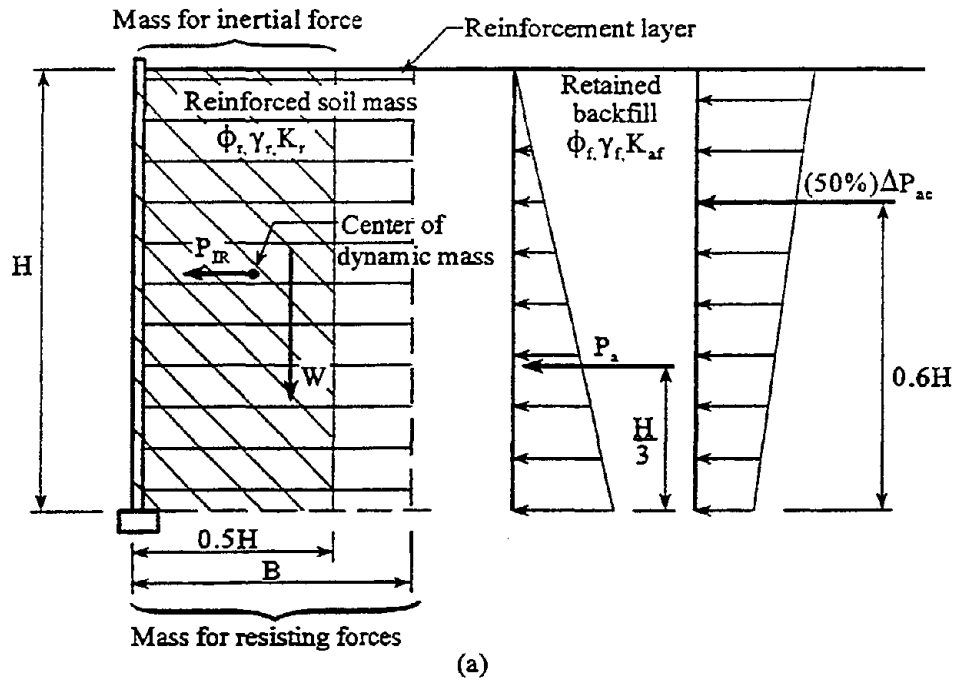


Figure 9-31: Seismic External Stability of a MSE Wall. (Module 6, 1997)

- (5) For structures with sloping backfills, the inertial force (P_{IR}) and the dynamic horizontal thrust (ΔP_{ae}) shall be based on a height H_2 near the back of the wall determined as follows:

$$H_2 = H + \frac{\tan\beta \cdot 0.5H}{(1 - 0.5\tan\beta)} \quad (9-19)$$

Δp_{ae} may be adjusted for sloping backfills using the Mononobe-Okabe method, with the horizontal acceleration K_h equal to A_m and K_v equal to zero. A height of H_2 should be used to calculate ΔP_{ae} in this case. P_{IR} for sloping backfills should be calculated as follows:

$$P_{IR} = P_{ir} + P_{is} \quad (9-20)$$

where:

$$P_{ir} = 0.5 A_m \gamma_r H_2 H \quad (9-21)$$

$$P_{is} = 0.125 A_m \gamma_f (H_2)^2 \tan\beta \quad (9-22)$$

and
$$\Delta P_{ae} = 0.5 \gamma_f H_2^2 \Delta K_{ae} \quad (\text{Sloping backfill}) \quad (9-22b)$$

where P_{ir} is the inertial force caused by acceleration of the reinforced backfill and P_{is} is the inertial force caused by acceleration of the sloping soil surcharge above the reinforced backfill, with the width of mass contributing to P_{IR} equal to $0.5H_2$. P_{IR} acts at the combined centroid of P_{ir} and P_{is} as shown in Figure 9-31. ΔK_{ae} should be computed as $\Delta K_{ae} = K_{ae} - K_a$, where K_{ae} is given by Eq. 9-13b presented previously for gravity type walls and K_a is the static earth pressure coefficient, which can be calculated using the same equation with $\psi=0$.

- (6) Evaluate sliding, overturning and seismic bearing capacity stability as detailed in the previous sections.
 (7) Check that the computed safety factors are equal to or greater than 75 percent of the minimum static safety factors.

Note that seismic loads may be reduced if the wall is designed to allow horizontal displacements. The permissible displacement method presented in Section 9.4.2 for the gravity type retaining walls is also applicable for the MSE wall design

Internal Seismic Stability

Seismic loads produce an inertial force P_I acting horizontally within the active zone (see Figure 9-32), in addition to the existing static forces.

This force will lead to incremental dynamic increases in the maximum tensile forces in the reinforcements. It is assumed that the location and slope of the maximum tensile force line does not change during seismic loading (this assumption is conservative relative to pullout resistance). Calculation steps for internal stability analyses with respect to seismic loading are as follows (see Figure 9-32).

- (1) Calculate the maximum acceleration in the wall and the force P_I per unit width acting above the base:

$$P_I = A_m W_A \quad (9-23)$$

$$A_m = (1.45 - A)A \quad (9-24)$$

where, W_A is the weight of the active zone (shaded area on Figure 9-32) and A is the AASHTO site acceleration coefficient.

- (2) Calculate the total maximum static load applied to the reinforcement T_{max} in each reinforcement layer per unit width following the procedures outlined in Module 6 (Earth Retaining Structures):

$$T_{max} = s_v \sigma_h \quad (9-25)$$

Where s_v is the vertical spacing between reinforcements and σ_h is the horizontal stress (static) at the reinforcement level of interest. The horizontal stress should consider those due to the weight of the retained fill $\gamma_r Z$ plus, if present, uniform surcharge load q and concentrated surcharge loads:

$$\sigma_h = K \gamma_r Z + qK_a + \Delta\sigma_v K_a \quad (9-26)$$

where

$K = K(Z)$ = horizontal earth pressure coefficient for MSE walls (see Figure 9-33 for K values)

Z = depth below top of the wall

γ_r = unit weight of the soil in the reinforced zone

q = uniform surcharge, if present

K_a = active earth pressure coefficient

$\Delta\sigma_v$ = equivalent additional vertical stress due to concentrated vertical loads.

- (3) Calculate the dynamic increment T_{md} directly induced by the inertia force P_I in the reinforcements by distributing P_I in the different reinforcements proportionally to their "resistant area" (L_{ei}) on a load per unit wall width basis. This leads to:

$$T_{md} = P_I \frac{L_{ei}}{\sum_{i=1}^n (L_{ei})} \quad (9-27)$$

which is the resistant area of the reinforcement at the i th level divided by the sum of the resistant area for all reinforcement levels.

- (4) The maximum total tensile force is:

$$T_{total} = T_{max} + T_{md} \quad (9-28)$$

Check stability with respect to breakage and pullout of the reinforcement, with seismic safety factors of 75 percent of the minimum allowable static safety factors. Refer to Module 6 (Earth Retaining Structures) for procedures for evaluating the breakage and pullout stability.

9.4.4 Soil-Nailed Walls

The general principles of seismic design and analysis of soil-nailed walls are very similar to those for the MSE walls. The seismic loading is accounted for by applications of a seismic coefficient as a pseudostatic inertia force. The following guidance is recommended in defining the appropriate design seismic coefficient. The detailed seismic design procedure for soil-nailed walls, including the evaluation of internal

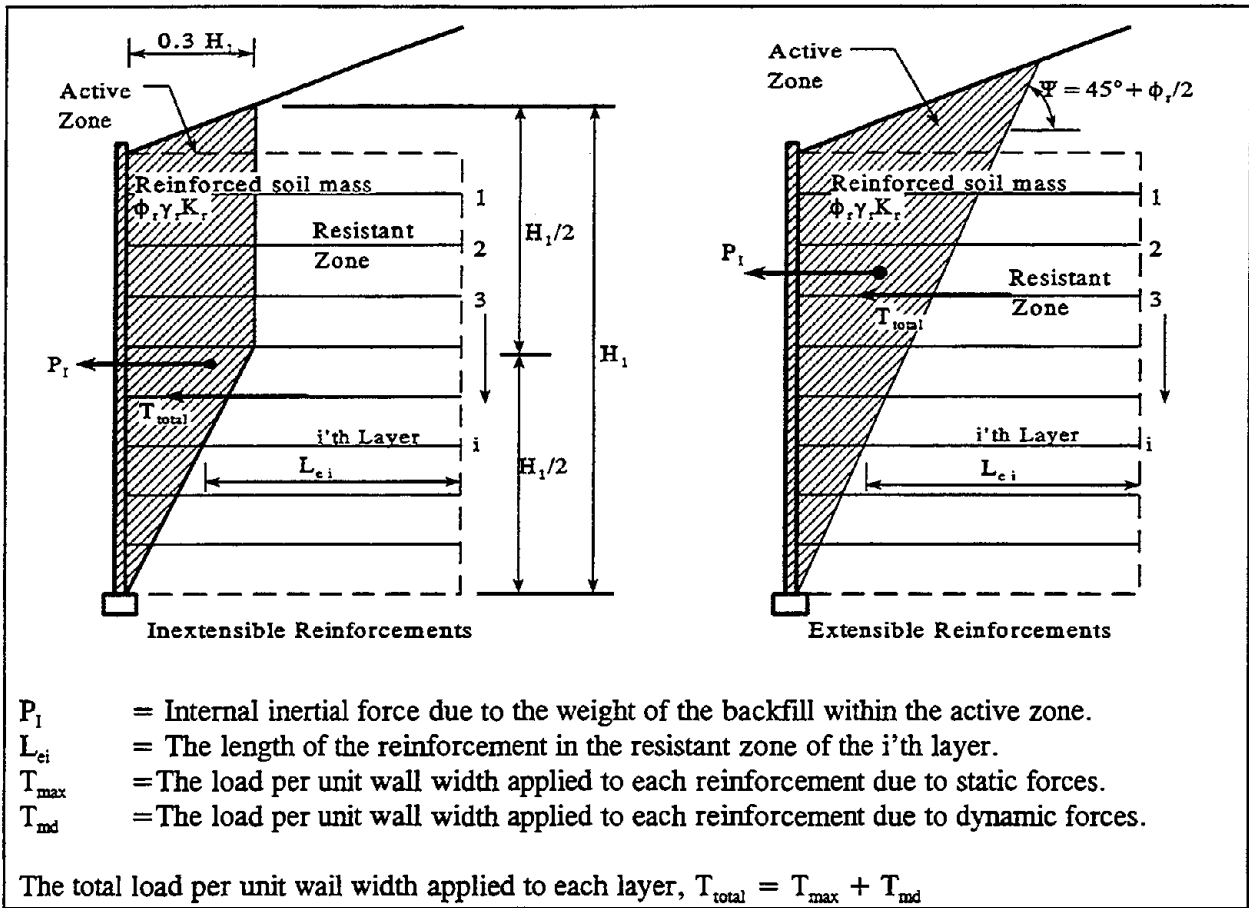


Figure 9-32: Seismic Internal Stability of a MSE Wall. (Modified from Module 6, 1997)

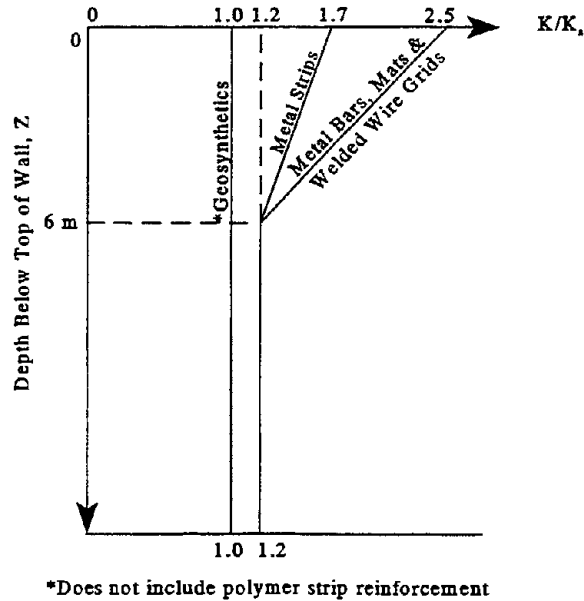


Figure 9-33: Design Value of the Lateral Earth Pressure Coefficient, K , for Various Types of Soil Reinforcement Systems. (Module 6, 1997)

stability as well as external stability, has been documented in a recent FHWA publication (Byrne, et al., 1997).

- Select a peak horizontal ground acceleration (free field peak acceleration) based on the design earthquake. In the absence of site specific data or local seismic map, the acceleration coefficient, A , can be taken off the current AASHTO Division 1A map.
- For slip surfaces that are primarily “internal” in nature (i.e., intersect the nail reinforcement), define a design seismic coefficient, $A_m = (1.45-A)A$ in accordance with that recommended for MSE walls. This design seismic coefficient is applied to “internal” slip modes as a pseudostatic earthquake acceleration.
- For slip surfaces that are primarily “external” in nature, the design pseudostatic seismic coefficient, A_m , will vary depending on the permanent displacements that the retaining wall can tolerate during the design event. For example, if the wall can tolerate a permanent displacement of up to $250A$ mm then a design seismic coefficient equal to $0.5A$ can be assumed. For other tolerable permanent displacements, the appropriate seismic acceleration coefficient can be determined in accordance with the permissible displacement approach presented in Section 9.4.2 of this chapter.
- For assessment of seismic bearing capacity stability of the reinforced soil block, a design seismic coefficient equal to $0.5A$ is recommended.

9.4.5 Anchored Walls

For ease of discussion, this type of retaining structures include those constructed of sheet piles, soldier piles and lagging, and other relatively flexible, externally supported structural walls. Earthquake failures of such structures are primarily due to increased dynamic active pressure combined with the decreased passive resistance in front of the pile/wall embedment as well as the anchor. When this type of walls are used as waterfront bulkhead structures retaining saturated loose backfill, liquefaction and hydrodynamic forces often lead to failure during major earthquakes. In this case, the structure should be carefully evaluated and solutions by ground treatment methods may need to be considered.

Figure 9-34 shows the seismic effects on anchored walls (Elms and Richards, 1990). Basically, there are three main considerations:

- The incremental dynamic active earth thrust, ΔP_{ae} , in addition to the static active force, P_a .
- The reduction of the static passive soil resistance, P_p , by a decrement ΔP_{pe} .
- The increased interference between the passive wedge in front of the anchor (or tiebacks) and the dynamic active failure wedge behind the wall. This interference will reduce the anchor resistance if anchors are not placed far enough behind the wall.

Evaluation steps for seismic design and analysis of anchored walls are as follows:

- (1) Select an appropriate seismic coefficient, K_h , based on the design earthquake, and assume $k_v=0$.

- (2) Calculate the dynamic active earth thrust, P_{ae} , using the Mononobe-Okabe equation (active earth thrust case) presented in Section 9.4.2.
- (3) Calculate the reduced passive resistance, P_{pe} , within the pile/wall embedment using the equivalent Mononobe-Okabe passive equation as follows:

$$P_{pe} = \frac{1}{2} \gamma H^2 (1 - k_v) K_{pe} \quad (9-29a)$$

where K_{pe} is given by

$$K_{pe} = \frac{\cos^2(\phi - \psi + \theta)}{\cos\psi \cos^2\theta \cos(\delta - \theta + \psi) \left[1 - \sqrt{\frac{\sin(\phi + \delta) \sin(\phi - \psi + \beta)}{\cos(\delta - \theta + \psi) \cos(\beta - \theta)}} \right]^2} \quad (9-29b)$$

- (4) Determine the dynamic failure surface of the active wedge. Calculate the active failure surface inclination, α_{ae} , from horizontal as follows:

$$\alpha_{ae} = (\phi - \psi) + \arctan \left\{ \frac{\sqrt{F_1(F_1 + F_2)(1 + F_3 F_2)} - F_1}{1 + F_3(F_1 + F_2)} \right\} \quad (9-30)$$

where

$$\begin{aligned} F_1 &= \tan(\phi - \psi - \beta) \\ F_2 &= \cot(\phi - \psi - \theta) \\ F_3 &= \tan(\delta + \theta + \psi) \end{aligned}$$

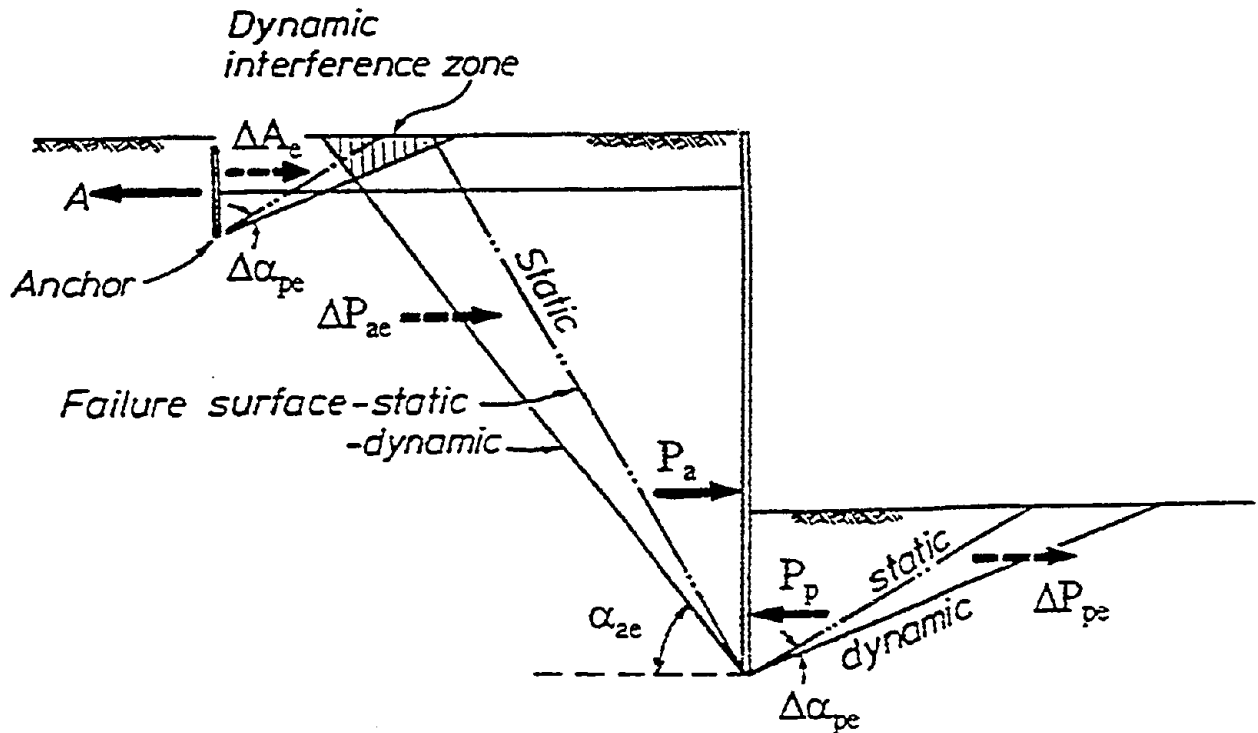


Figure 9-34: Seismic Effects on Anchored Bulkheads (Elms and Richards, 1990).

- (5) Using dynamic active and passive earth forces obtained from steps (2) and (3) above, calculate the required wall embedment depth and anchor load through moment equilibrium (with respect to the anchor point at the wall face) and horizontal force equilibrium analyses. Refer to Module 6 (Earth Retaining Structures) for detailed calculation procedure.
- (6) Design anchors (or tiebacks) to be located beyond the potential dynamic active failure surface (defined by the angle α_a) to minimize the interference effect on anchor passive resistance.

9.4.6 Stiffness of Abutment Walls

Lam and Martin (1986) presents equations for incorporating the stiffness of abutment walls into a dynamic model of a bridge system. The stiffness is intended for bridge analysis when the wall is displaced into the backfill by longitudinal inertial loading from the bridge superstructure. These investigators propose the following equations for the translational stiffness, K_s , and the rotational stiffness, K_θ , of an integral abutment wall:

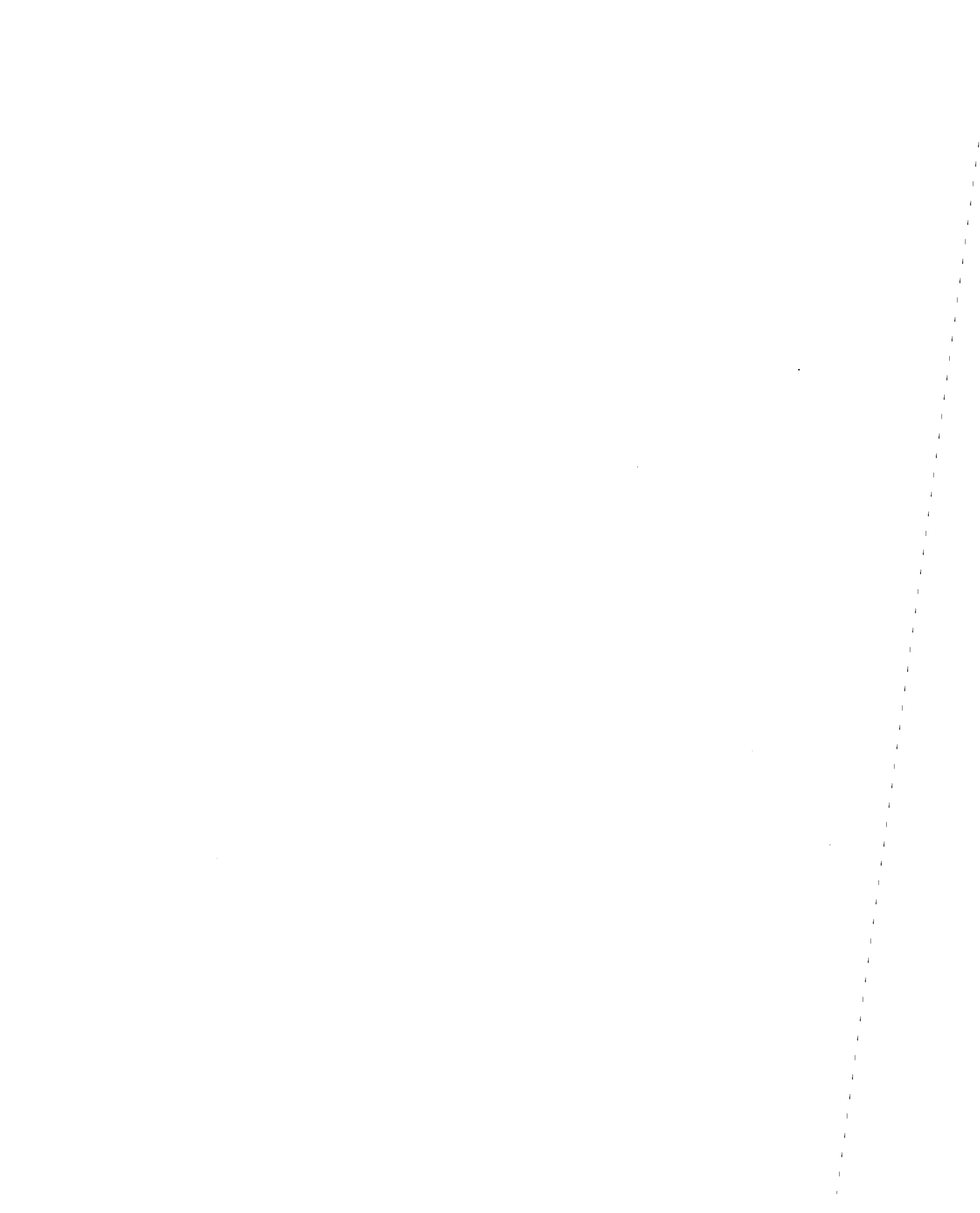
$$K_s = 0.425 E_s \cdot B \quad (9-31)$$

$$K_\theta = 0.072 E_s \cdot B \cdot H^2 \quad (9-32)$$

where H is the wall height, E_s is the Young's modulus of the soil, and B is the width of the abutment wall. Equations 9-31 and 9-32 are used when the stiffness of the abutment wall is incorporated in the dynamic response analysis of the bridge structure.

The Young's modulus for the soil, E_s , used in Equations 9-31 and 9-32 can be evaluated using the equations in Chapter 5. Use of strain-compatible Young's modulus values in Equations 9-31 and 9-32 is recommended. The strain-compatible moduli values can be estimated from the shear strains calculated in site response analyses assuming that the reduction of Young's modulus follows the same modulus reduction curves as the shear modulus. If the results of a site response analysis are not available, strain-compatible Young's modulus may be evaluated using the same modulus reduction curves and assuming a shear strain level depending upon the magnitude of the earthquake, intensity of ground motion, and soil type. For events of magnitude 6.0 or less, and for ground motion intensities of 0.4 g or less, E_s at a strain level of 0.1 percent may be used. For larger magnitudes and/or higher intensity earthquakes, a value of E_s corresponding to a shear strain of 1 percent is recommended.

The location of the resultant force due to wall translation may be applied at 0.6 H from the base of the wall and the resultant force from wall rotation may be applied at 0.37 H from the base of the wall.



CHAPTER 10.0 REFERENCES

- ABAM (1994), "Draft-Seismic Design Course," ABAM Engineers, Course Notes Prepared for the United States Department of Transportation, Federal Highway Administration, Central Federal Lands Highway Division, 28 December.
- Abrahamson, N.A. and Silva, W.J. (1997), "Empirical Response Spectral Attenuation Relations for Shallow Crustal Earthquakes," *Seismological Research Letters*, Vol. 68, No. 1, pp. 94-127.
- Abrahamson, N.A. and Silva, W. (1996), "Preliminary Attenuation Relations for Horizontal Response Spectra Including Data from the 1994 Northridge Earthquake," Draft Report to Brookhaven National Laboratory, New York.
- Achilleos, E. (1988), "User Guide for PCSTABL 5M," Joint Informational Report JHRP-88/19, Indiana Department of Highways and Purdue University School of Civil Engineering, West Lafayette, Indiana, 132 p.
- Algermissen, S.T., Perkins, D.M., Thenhaus, P.C., Hanson, S.L. and Bender, B.L. (1982), "Probabilistic Estimates of Maximum Acceleration and Velocity in Rock in the Contiguous United States," United States Geological Survey, Open-File Report 82-1033.
- Algermissen, S.T., Perkins, D.M., Thenhaus, P.C., Hanson, S.L. and Bender, B.L. (1991), "Probabilistic Earthquake Acceleration and Velocity Maps for the United States and Puerto Rico," United States Geological Survey, Miscellaneous Field Studies Map MF-2120.
- AASHTO (1994), "Standard Specifications for Highway Bridges," 16th Edition, American Association of State Highway and Transportation Officials, Washington, D.C.
- ASTM (1994), "Annual Book of ASTM Standards, Section 4, Construction," American Society for Testing and Materials, Philadelphia, Pennsylvania, 978 p.
- Arango, I. (1996), "Magnitude Scaling Factors for Soil Liquefaction Evaluations," *Journal of Geotechnical Engineering*, ASCE, Vol. 122, No. 11, pp. 929-936.
- Arias, A. (1969), "A Measure of Earthquake Intensity," In: *Seismic Design for Nuclear Power Plants*, R. Hansen, Editor, Massachusetts Institute of Technology Press, Cambridge, Massachusetts.
- ATC (1978), "Tentative Provisions for the Development of Seismic Regulations for Buildings," Report ATC 3-06, Applied Technology Council, San Francisco, California.
- ATC (1994), "Seminar on New Developments in Earthquake Ground Motion Estimation and Implications for Engineering Design Practice," Applied Technology Council, ATC 35-1, Redwood City, California.
- Atkinson, G.M. and Boore, D.M. (1990), "Recent Trends in Ground Motion and Spectral Response Relations for North America," *Earthquake Spectra*, Vol. 6, No. 1, pp. 15-35.

- Atkinson, G.M. and Boore, D.M. (1995), "Ground-Motion Relations for Eastern North America," *Bulletin of the Seismological Society of America*, Vol. 85, No. 1, pp. 17-30.
- Ballard, R.F., Jr. (1964), "Determination of Soil Shear Moduli at Depth by In Situ Vibratory Techniques," *Miscellaneous Paper No. 4-691*, U.S. Army Waterways Experiment Station, Vicksburg, MS, USA.
- Bardet, J.P. (1992), "LINOS, a Nonlinear Finite Element Program for Geomechanics and Geotechnical Engineering," *User's Manual*, Research Center for Computational Geomechanics, University of Southern California, Los Angeles, 145 p.
- Barker, R.M., Duncan, J.M., Rojiani, K.B., Ooi, P.S.K., Tan, C.K. and Kim, S.G. (1991), "Manuals for the Design of Bridge Foundations," *NCHRP Report No. 343*, 308 p.
- Bartlett, S.F., and Youd, T.L. (1995), "Empirical Prediction of Liquefaction-Induced Lateral Spread," *Journal of Geotechnical Engineering, ASCE*, Vol. 121, No. 4, pp. 316-329.
- Bathurst, R.J. and Cai, Z. (1995), "Pseudo-Static Seismic Analysis of Geosynthetic-Reinforced Sequential Retaining Walls," *Geosynthetics International*, Vol. 2, No. 5, pp. 787-830.
- Bolt, B.A. (1973), "Duration of Strong Ground Motion," *Proc. 5th World Conference on Earthquake Engineering*, Rome, Italy.
- Bolt, B.A. (1988) Earthquakes, W.H. Freeman and Company, New York
- Bonilla, M.G., Mark, R.K., and Lienkaemper, J.J. (1984), "Statistical Relations Among Earthquake Magnitude, Surface Rupture Length and Surface Fault Displacement," *Journal of Geophysical Research*, Vol. 74, Vol. B6, pp. 2379-2411.
- Boore, D.M. and Atkinson, G.M. (1987), "Prediction of Ground Motion and Spectral Response Parameters at Hard-Rock Sites in Eastern North America," *Bulletin of the Seismological Society of America*, Vol. 77, No. 2, pp. 440-467.
- Boore, D.M. and Joyner, W.B. (1991), "Estimation of Ground Motion at Deep-Soil Sites in Eastern North America," *Bulletin of the Seismological Society of America*. Vol. 81, No. 6, pp. 2167-2185.
- Boore, D.M., Joyner, W.B. and Fumal, T.E. (1993), "Estimation of Response Spectra and Peak Accelerations From Western North America Earthquakes: An Interim Report," *United States Geological Survey, Open File Report 93-509*.
- Boore, D.M. and Joyner, W.B. (1994), "Prediction of Ground Motion in North America," *Proc. Seminar on New Developments in Earthquake Ground Motion Estimation and Implication for Engineering Design Practice*, Applied Technology Council Publication No. ATC 35-1, Redwood City, California, pp. 6-1 - 6-41.
- Borcherdt, R.D. (1994), "New Developments in Estimating Site Response Effects on Ground Motion," *Proc. Seminar on New Developments in Earthquake Ground Motion Estimation and Implications for Engineering Design Practice*, Applied Technology Council, ATC 35-1, Redwood City, California, pp. 10-1 - 10-44.

- Borden, R.H., Shao, L., and Gupta, A. (1996), "Dynamic Properties of Piedmont Residual Soils," *Journal of Geotechnical Engineering*, ASCE, Vol. 122, No. 10, pp. 813-821.
- Bowles, J.E. (1988), "Foundation Analyses and Design," 4th Edition, McGraw-Hill Book Company, New York, 1004 p.
- Bray, J.D., Augello, A.J., Leonards, G.A., Repetto, P.C. and Byrne, R.J. (1995), "Seismic Stability Procedures for Solid-Waste Landfills," *Journal of Geotechnical Engineering*, ASCE, Vol. 121, No. 2, pp. 139-151.
- Broms, B.B. and Hansson, O. (1984), "Deep Compaction with the Vibro-Wing Method," *Ground Engineering*, Vol. 17, No. 5.
- Brown, D.A., Morrison, C., and Reese, L.C. (1988), "Lateral Load Behavior of a Pile Group in Sand," *Journal of Geotechnical Engineering*, ASCE, Vol. 114, No. 11, pp. 1261-1276.
- Brown, D. and Bollmann, H.T. (1996), "Pile Group Design for Lateral Loading using COM624," *Proc. The Design of Bridges for Extreme Events*, Atlanta, Georgia, pp. 1-46.
- Bryant, L.M. and Matlock, H. (1977), "Three Dimensional Analysis of Framed Structures with Nonlinear Pile Foundations," *Proc. 9th Annual Offshore Technology Conference*, Houston, Texas, Paper No. 2955.
- Byrne, R.J., Cotton, D., Porterfield, J., Wolschlag, C., and Veblacker, G. (1997), "Manual for Design and Construction Monitoring of Soil Nail Walls," Report No. FHWA-SA-96-069, U.S. Department of Transportation, Federal Highway Administration, Washington, District of Columbia, 468 p.
- Campbell, K.W., and Duke, C.M. (1974), "Bedrock Intensity, Attenuation, and Site Factors from San Fernando Earthquake Records," *Bulletin of the Seismological Society of America*, Vol. 64, No. 1, pp. 173-185.
- Campbell, K.W. (1985), "Strong Motion Attenuation Relations: a Ten-Year Perspective," *Earthquake Spectra*, Vol. 1, No. 4, pp. 759-804.
- Campbell, K.W. (1989), "Empirical Prediction of Near-Source Ground Motion for the Diablo Canyon Power Plant Site, San Luis Obispo County, California," *United States Geological Survey, Open-File Report 89-484*.
- Campbell, K.W. (1990), "Empirical Prediction of Near-Source Soil and Soft-Rock Ground Motion for the Diablo Canyon Power Plant Site, San Luis Obispo County, California," *Dames & Moore, Report Prepared for Lawrence Livermore National Laboratory, Evergreen, Colorado*.
- Campbell, K.W. (1993), "Empirical Prediction of Near-Source Ground Motion From Large Earthquakes," *Proc. International Workshop on Earthquake Hazard and Large Dams in the Himalaya*, Sponsored by the Indian National Trust for Art and Cultural Heritage (INTACH), New Delhi, India, January 15-16.

- Campbell, K.W. and Bozorgnia, Y. (1994), "Near Source Attenuation of Peak Horizontal Acceleration From Worldwide Accelerographs Recorded From 1957 to 1993," Proc. 5th U.S. National Conference on Earthquake Engineering, Chicago, Illinois, Vol. 3, pp. 283-292.
- Carpenter, J.R. (1985), "PCSTABL4 User Manual," Joint Highway Research Project No. JHRP-85-7, School of Civil Engineering, Purdue University, West Lafayette, Indiana.
- CDMG (1986), "Guidelines for Evaluating the Hazard of Surface Fault Rupture," Technical Note 49, California Division of Mines and Geology, Sacramento, California, 2 p.
- CDMG (1975), "Recommended Guidelines for Determining the Maximum Credible and the Maximum Probable Earthquakes," Technical Note No. 43, California Division of Mines and Geology, Sacramento, California, 1 p.
- CDMG (1995), "The Northridge, California Earthquake of 17 January 1994," Mary C. Woods and W. Ray Seiple Editors, California Division of Mines and Geology Special Publication 116, Sacramento, California.
- Chang, C.-Y., Mok, C.M., Power, M.S. and Tang, Y.K. (1991), "Analysis of Ground Response Data at Lotung Large Scale Soil-Structure Interaction Experiment Site," Report No. NP-7306-SL, Electric Power Research Institute, Palo Alto, California.
- Cluff, L.S., Hansen, W.R., Taylor, C.L., Weaver, K.D., Brogan, G.E., Idriss, I.M., McClure, F.E. and Blayney, J.A. (1972), "Site Evaluation in Seismically Active Regions - An Interdisciplinary Team Approach," Proc. International Conference on Microzonation for Safety Construction, Research and Application, Seattle, Washington, Vol. 2, p. 9-57 - 9-87.
- Cohee, B.P., Somerville, P.G. and Abrahamson, N.A. (1991), "Simulated Ground Motions for Hypothesized $M_w = 8$ Subduction Earthquakes in Washington and Oregon," Bulletin of the Seismological Society of America, Vol. 81, No. 1, pp. 28-56.
- Cundall, P.A. and Board, M. (1988), "A Microcomputer Program for Modelling Large-Strain Plasticity Problems," In: Numerical Methods in Geomechanics, C. Swoboda, Ed., A.A. Balkema, Rotterdam, The Netherlands, pp. 2101-2108.
- D'Appolonia, E. (1970), "Dynamic Loadings," Journal of the Soil Mechanics and Foundations Division, ASCE, Vol. 96, No. SM1.
- DePolo, C.M. and Slemmons, D.B. (1990), "Estimation of Earthquake Size for Seismic Hazards," Krinitzsky, E.L. and Slemmons, D.B., Neotectonics in Earthquake Evaluation, Chapter 1, Geological Society of America, Vol. 8.
- Dobry, R., Idriss, I.M. and Ng, E. (1978), "Duration Characteristics of Horizontal Components of Strong-Motion Earthquake Records," Bulletin of the Seismological Society of America, Vol. 68, No. 5, pp. 1487-1520.
- Dobry, R., Powell, D.J., Yokel, F.Y. and Ladd, R.S. (1980), "Liquefaction Potential of Saturated Sand - The Stiffness Method," Proc. 7th World Conference on Earthquake Engineering, Istanbul, Turkey, Vol. 3, pp. 25-32.

- Dobry, R., Abdoun, T., and O'Rourke, T.D. (1996), "Evaluation of Pile Response to Liquefaction-Induced Lateral Spreading of the Ground," Proc. 4th CALTRANS Seismic Research Workshop, Sacramento, California, 10 p.
- Douglas, B.J., and Olsen, R.S. (1981), "Soil Classification Using Electric Cone Penetrometer," Symposium on Cone Penetration Testing and Experience, ASCE National Convention, St. Louis, Missouri, pp. 209-227.
- Duncan, J. M. (1992), "State-of-the-Art: Static Stability and Deformation Analysis," Proc. Stability and Performance of Slopes and Embankments - II, Vol. 1, pp. 222-266.
- EERI (1989), "Loma Prieta Earthquake, October 17, 1989," Preliminary Reconnaissance Report, Earthquake Engineering Research Institute, Oakland, California, 51 p.
- EERI (1995), "The Hyogo-Ken Nanbu Earthquake, January 17, 1995," Preliminary Reconnaissance Report, Earthquake Engineering Research Institute, Oakland, California, 116 p.
- Elias, V. and Christopher, B.R. (1996), "Mechanically Stabilized Earth Walls and Reinforced Soil Slopes, Design and Construction Guidelines," Report No. FHWA-SA-96-071, U.S. Department of Transportation, Federal Highway Administration, Washington, D.C.
- EPRI (1986), "Seismic Hazard Methodology for the Central and Eastern United States," EPRI Report NP-4726, (10 Volumes), Electric Power Research Institute, Palo Alto, California.
- Evans, G.L. (1971), "The Behavior of Bridges Under Earthquakes," Proc. New Zealand Reading Symposium, Vol. 2.
- Felio, G.Y., Vucetic, H., Hudson, M., Bara, P., and Chapman, R. (1990), "Performance of Soil Nailed Walls During the October 17, 1989 Loma Prieta Earthquake," Proc. of the 43rd Canadian Geotechnical Conference, Quebec, Canada, pp. 165-173.
- Frankel, F., Mueller, C., Bernard, T., Perkins, D., Leyendecker, E.V., Dickman, N., Hanson, S. And Hopper, M. [1996], "Interim National Hazard Maps: Documentation," Draft Report, US Geological Survey, Denver, Colorado.
- Friedland, I.M., Power, M.S., and Mayes, R.L., editors (1997), "Proceedings of the FHWA/NCEER Workshop on the National Representation of Seismic Ground Motion for New and Existing Highway Facilities," Burlingame, California, May 29-30, 1997, NCEER Report No. 97-0010.
- Finn, L.W.D., Yogendrakumar, M., Yoshida, N. and Yoshida, H. (1986), "TARA-3: A Program for Nonlinear Static and Dynamic Effective Stress Analysis," Department of Civil Engineering, University of British Columbia, Vancouver, British Columbia, Canada.
- Franklin, A.G. and Chang, F.K. (1977), "Earthquake Resistance of Earth and Rock-Fill Dams," Report 5: Permanent Displacement of Earth Embankments by Newmark Sliding Block Analysis, Misc. Paper 5-71-17, Soils and Pavements Laboratory, US Army Engineer Waterways Experiment Station, Vicksburg, Mississippi.

- Gasparin, D.A. and Vanmarcke, E.H. (1976), "SIMQKE - A Program for Artificial Motion Generation," Department of Civil Engineering, Massachusetts Institute of Technology, Cambridge, Massachusetts.
- Geomatrix (1991), "Seismic Ground Motion Study for West San Francisco Bay Bridge," Draft Report to CALTRANS, Division of Structures, Sacramento, California, March (note in February 1993: this report has been completed and was issued in final form in December, 1992).
- Geomatrix (1995), "Adjustments to Rock Response Spectra for CALTRANS Toll Bridges in Northern California," Report to CALTRANS, Division of Structures, Sacramento, California.
- Gere, J.M., and Shah, H.C. (1984), "Terra Non Firma," Stanford Alumni Association, Stanford, California.
- Gutenberg, B. and Richter, C.F. (1942), "Earthquake Magnitude, Intensity, Energy, and Acceleration," Seismological Society of America Bulletin, Vol. 32, pp. 163-191.
- Hadj-Hamou, T. and Elton, D.J. (1988), "A Liquefaction Potential Map for Charleston, South Carolina," Report No. GT-88-1, Tulane University, New Orleans, Louisiana, 67 p.
- Hamada, M. Towhata, I., Yasuda S. and Isoyama, R. (1987), "Study on Permanent Ground Displacements Induced by Seismic Liquefaction," Computers and Geomechanics Vol. 4, pp. 197-220.
- Hanks, T.C. and Kanamori, H. (1979), "A Moment Magnitude Scale," Journal of Geophysical Research, Vol. 84, No. B8, pp. 2348-2350.
- Hannigan, P.J., Goble, G.G., Thendean, G., Likins, G.E. and Raushe, F. (1996), "Design and Construction of Driven Pile Foundations," Workshop Manual, NHI Course Nos. 13221 and 13222, U.S. Department of Transportation, Federal Highway Administration, Office of Technology Applications, Washington, District of Columbia.
- Hansen, B. (1953), "Earth Pressure Calculations," Teknisk Forlag, Copenhagen.
- Harder, L.F. and Seed, H.B. (1986), "Determination of Penetration Resistance for Coarse-Grained Soils Using the Becker Hammer Drill," Report No. UCB/EERC-86/06, Earthquake Engineering Research Center, University of California at Berkeley, California.
- Harder, L.F., Jr. (1988)*, "Use of Penetration Tests to Determine the Cyclic Loading Resistance of Gravelly Soils During Earthquake Shaking," Ph.D. Dissertation, University of California, Berkeley, California.
- Harder, L.F., Jr. (1991), "Performance of Earth Dams During the Loma Prieta Earthquake," Proc. Second International Conference on Recent Advances in Geotechnical Earthquake Engineering and Soil Dynamics, University of Missouri, Rolla, pp. 11-15.

* Available through University Microfilms International, (800) 521-0600, Ext. 3879.

- Hardin, B.O. and Drnevich, V. (1972), "Shear Modulus and Damping in Soils: Design Equations and Curves," *Journal of the Soil Mechanics and Foundation Division, ASCE*, Vol. 98, No. SM7, pp. 667-692.
- Hardin, B.O. (1978), "The Nature of Stress-Strain Behavior of Soils," *Proc. Earthquake Engineering and Soil Dynamics, ASCE, Pasadena, California*, Vol. 1, pp. 3-89.
- Hart, E.W. (1980), "Fault-Rupture Hazard Zones in California," *Alquist-Priolo Special Studies Zones Act of 1972 with index to Special Studies Zones Maps*. In: *California Division of Mines and Geology Special Publication 42 (Revised edition)*, 24 p.
- Heaton, T.H., Tajima, F. and Mori, A.W. (1986), "Estimating Ground Motions Using Recorded Accelerograms," *Surveys in Geophysics*, Vol. 8, pp. 23-83.
- Hudson, M., Idriss, I.M. and Beikae, M. (1994)*, "QUAD4M - A Computer Program to Evaluate the Seismic Response of Soil Structures using Finite Element Procedures and Incorporating a Compliant Base," *User's Manual, Center for Geotechnical Modeling, Department of Civil and Environmental Engineering, University of California, Davis, California*, 27 p. (plus Appendices).
- Husid, R.L. (1969), "Análisis de Terremotos: Análisis General," *Revista del IDEM*, No. 8, Santiago, Chile, pp. 21-42.
- Hwang, H. and Lee, C.S. (1992), "Evaluation of Liquefaction Potential in Memphis Area, USA," *Proc. 10th World Conference on Earthquake Engineering*, pp. 1457-1460.
- Hynes, M.E. and Franklin, A.G. (1984), "Rationalizing the Seismic Coefficient Method," *Miscellaneous Paper GL-84-13, U.S. Army Engineer Waterways Experiment Station, Vicksburg, Mississippi*, 34 p.
- Hynes, M.E. (1988)*, "Pore Pressure Generation Characteristics of Gravel Under Undrained Cyclic Loading," *Ph.D. Dissertation, University of California, Berkeley, California*.
- Idriss, I.M., Lysmer, J., Hwang, R. and Seed, H.B. (1973), "QUAD4 - A Computer Program for Evaluating the Seismic Response of Soil Structures by Variable Damping Finite Element Procedures," *Report No. EERC 73-16, Earthquake Engineering Research Center, University of California, Berkeley, California*, 67 p.
- Idriss, I.M. (1990), "Response of Soft Soil Sites During Earthquakes," *Proc. Memorial Symposium to Honor Professor H.B. Seed, Berkeley, California*.
- Idriss, I.M. and Sun, J.I. (1992)**, "User's Manual for SHAKE91," *Center for Geotechnical Modeling, Department of Civil and Environmental Engineering, University of California, Davis, California*, 13p. (plus Appendices).
- Idriss, I.M. (1993), "Procedures for Selecting Earthquake Ground Motions at Rock Sites," *National Institute of Standards and Technology, NIST GCR 93-625*, 7 p.

* Available through University Microfilms International, (800) 521-0600, Ext. 3879.

** Available through NISEE / Computer Applications, (510) 642-5113.

- Idriss, I.M. (1995), "An Overview of Earthquake Ground Motions Pertinent to Seismic Zonation," Proc. 5th International Conference on Seismic Zonation, Nice, France, Vol. 3, pp. 1-16.
- Imai, T. and Tonouchi, K. (1982), "Correlation of N-Value with S-Wave Velocity and Shear Modulus," Proc. 2nd European Symposium on Penetration Testing, Amsterdam, The Netherlands, pp. 67-72.
- Ishibashi, I. and Sherif, M.A. (1974), "Soil Liquefaction by Torsional Simple Shear Device," Journal of the Geotechnical Engineering Division, ASCE, Vol. 100, No. GT 8, pp. 871-888.
- Ishihara, K. (1985), "Stability on Natural Deposits During Earthquakes," Proc. 11th International Conference on Soil Mechanics and Foundation Engineering, San Francisco, California, Vol. 1, pp. 321-376 (Please order from A.A. Balkema, Old Post Road, Brookfield, Vermont 05036, Tel. (802) 276-3162, fax (802) 276-3837, Price \$995).
- Ishihara, K., "Evaluation of Liquefaction Potential and Consequent Deformations in Sandy Fills," Proceedings of the Seismic Workshop on the Port of Los Angeles, 1990.
- Ishihara, K. (1986), "Evaluation of Soil Properties for Use in Earthquake Response Analysis," In: Geomechanical Modelling in Engineering Practice, R. Dungar and J.A. Studer, Eds., A.A. Balkema, Rotterdam, the Netherlands, 241 - 275.
- Ishihara, K., Kokusho, T. and Silver, M.L. (1989), "Recent Developments in Evaluating Liquefaction Characteristics of Local Soils," State-of-the-Art Report, Proc. 12th International Conference on Soil Mechanics and Foundation Engineering, Rio de Janeiro, Brazil, Vol. 4, pp. 2719-2734.
- Ishihara (1993), "Liquefaction and Flow Failure During Earthquakes," Géotechnique, Vol. 43, No. 3., pp. 351-415.
- Iwasaki, T., Tatsuoka, F. and Takagi, Y. (1978), "Shear Moduli of Sands Under Cyclic Torsional Shear Loadings," Soils and Foundations, JSSMFE, Vol. 18, No. 1, pp. 39-56.
- Jackura, K.A. (1992), "CALTRANS Procedures for Development of Site-Specific Acceleration Response Spectra," California Department of Transportation, Office of Geotechnical Engineering, Sacramento, California, 18 p.
- Jamiolkowski, M., Leroueil, S. and Lo Presti, D.C.F. (1991), "Theme Lecture: Design Parameters from Theory to Practice," Proc. Geo-Coast '91, Yokohama, Japan, pp. 1-41.
- Jennings, C.P. (1971), "Engineering Features of San Fernando Earthquake, February 1971," Report of Earthquake Engineering Research Laboratory, California Institute of Technology, Pasadena, California.
- Jennings, P.C., Housner, R.W. and Tsai, N.C. (1968), "Simulated Earthquake Motions," Research Report, Earthquake Engineering Research Laboratory, California Institute of Technology, Pasadena, California.

- Jennings, C.W. (1994), "An Explanatory Text to Accompany the Fault Activity Map of California and Adjacent Areas," California Department of Conservation, Division of Mines and Geology, Sacramento, California, 92 p.
- Jibson, R.W. (1985)*, "Landslides Caused by the 1811-12 New Madrid Earthquakes," Ph.D. Dissertation, Stanford, California, Stanford University, 234 p.
- Jibson, R.W. (1993), "Predicting Earthquake-Induced Landslide Displacements Using Newmark's Sliding Block Analysis," Transportation Research Record 1411, Transportation Research Board, National Research Council, Washington, D.C., pp. 9-17.
- Johnston, A.C. and Nava, S.J. (1994), "Seismic Hazard Assessment in the Central United States," Proc. Seminar on New Developments in Earthquake Ground Motion Estimation and Implications for Engineering Design Practice, Applied Technology Council, AT C35-1, Redwood City, California, pp. 2-1 - 2-12.
- Jones, R. (1962), "Surface Wave Technique for Measuring Elastic Properties and Thickness of Roads: Theoretical Development," British Journal of Applied Physics, Vol. 13, pp. 21-29.
- Joyner, W.B. and Boore, D.M. (1988), "Measurement, Characterization, and Prediction of Strong Ground Motion." In: Von Thun, J.L., Ed., Earthquake Engineering and Soil Dynamics II, Recent Advances in Ground Motion Evaluation, ASCE Geotechnical Special Publication No. 20, pp. 43-102.
- Kavazanjian, E., Jr., Echezuria, H. and McCann, M.W. (1985a), "RMS Acceleration Hazard for San Francisco," Soil Dynamics and Earthquake Engineering, Vol. 4, No. 3, pp. 106-123.
- Kavazanjian, E. Jr., Roth, R.A. and Echezuria, H. (1985b), "Liquefaction Potential Mapping for San Francisco," Journal of Geotechnical Engineering, ASCE, Vol. 111, No. 1, pp. 54-76.
- Kavazanjian, E., Jr., Snow, M.S., Matasović, N., Poran, C. and Satoh, T. (1994), "Non-Intrusive Rayleigh Wave Investigations at Solid Waste Landfills," Proc. 1st International Congress on Environmental Geotechnics, Edmonton, Alberta, pp. 707-712.
- Kayen, R.E., and Mitchell, J.K., (1997), "Assessment of Liquefaction Potential During Earthquakes by Arias Intensity," American Society of Civil Engineers, *Journal of Geotechnical and Geoenvironmental Engineering*, Vol. 123, No. 12, December 1997, pp. 1162-1174.
- Kondner, R.L. and Zelasko, J.S. (1963), "A Hyperbolic Stress-Strain Formulation of Sands," Proc. 2nd Pan American Conference on Soil Mechanics and Foundation Engineering, Sao Paulo, Brazil, pp. 289-324.
- Kramer, S.L. (1996), "Geotechnical Earthquake Engineering," Prentice-Hall, Inc., Upper Saddle River, New Jersey, 653 p.

* Available through University Microfilms International, (800) 521-0600, Ext. 3879.

- Kramer, S.L. and Holtz, R.D. (1991), "Soil Improvement and Foundation Remediation with Emphasis on Seismic Hazards," A Report of a Workshop Sponsored by the National Science Foundation, University of Washington, Seattle, Washington.
- Krinitzky, E.L., (1986) "Empirical Relationships for Earthquake Ground Motions in Mexico City," in Proceedings of the International Conference on *The Mexico City Earthquake-1985: Factors Involved and Lessons Learned*, Cassaro, M.A., and Romero, E.M., editors, American Society of Civil Engineers, Mexico City, Mexico, September 1986, pp. 96-118.
- Krinitzky, E.L., Gould, J.P. and Edinger, P.H. (1993), "Fundamentals of Earthquake-Resistant Construction," John Wiley & Sons, New York, New York.
- Lam, I.P. and Martin, G.R. (1986), "Seismic Design of Highway Bridge Foundations - Vol. II. Design Procedures and Guidelines," Report No. FHWA/RD-86-102, U.S. Department of Transportation, Federal Highway Administration, McLean, Virginia, 167 p.
- Lam, I.P. and Martin, G.R. (1997), "Current Developments in Seismic Design of Bridge Foundations," Proc. Transportation Research Board 76th Annual Meeting, Session No. 236, Washington, District of Columbia, 21 p.
- Lee, M.K.W. and Finn, W.D.L. (1978), "DESRA-2, Dynamic Effective Stress Response Analysis of Soil Deposits with Energy Transmitting Boundary Including Assessment of Liquefaction Potential," Soil Mechanics Series No. 36, Department of Civil Engineering, University of British Columbia, Vancouver, Canada, 60 p.
- Leeds, D.L. (1992), "State-of-the-Art for Assessing Earthquake Hazards in the United States: Report 28, Recommended Accelerograms for Earthquake Ground Motions," Misc. Paper S-73-1, Geotechnical Laboratory, U.S. Army Waterways Experiment Station, Vicksburg, Mississippi, 171 p. (plus Appendices).
- Liao, S.S.C. and Whitman, R.V. (1986), "Overburden Correction Factors for SPT in Sand," Journal of Geotechnical Engineering, ASCE, Vol. 112, No. 3, pp. 373-377.
- Li, X.S., Wang, Z.L. and Shen, C.K. (1992), "SUMDES - A Nonlinear Procedure for Response Analysis of Horizontally-Layered Sites Subjected to Multi-Directional Earthquake Loading," Department of Civil Engineering, University of California, Davis, California.
- Lin, S.J. and Whitman, R.V. (1986), "Earthquake Induced Displacements of Sliding Blocks," Journal of Geotechnical Engineering, ASCE, Vol. 112, No. 1, pp. 44-59.
- Lysmer, J., Udaka, T., Tsai, C.F. and Seed, H.B. (1975), "FLUSH - A Computer Program for Approximate 3-D Analysis of Soil-Structure Interaction Problems," Report No. EERC-75/30, Earthquake Engineering Research Center, University of California, Berkeley.
- Makdisi, F.I. and Seed, H.B. (1978), "Simplified Procedure for Estimating Dam and Embankment Earthquake-Induced Deformations," Journal of the Geotechnical Engineering Division, ASCE Vol. 104, No. GT7, pp. 849-867.

- Marcuson, W.F., III and Bieganousky, W.A. (1977), "Laboratory Standard Penetration Tests on Fine Sands," *Journal of the Geotechnical Engineering Division, ASCE*, Vol. 103, No. GT6, pp. 565-588.
- Marcuson, W.F., III (1981), "Earth Dams and Stability of Slopes Under Dynamic Loads," *Moderators Report, Proc. 1st International Conference on Recent Advances in Geotechnical Earthquake Engineering and Soil Dynamics, St. Louis, Missouri*, Vol. 3, pp. 1175.
- Marcuson, W.F., III, Hynes, M.E. and Franklin, A.G. (1990), "Evaluation and Use of Residual Strength in Seismic Safety Analysis of Embankments," *Earthquake Spectra*, Vol. 6, No. 3, pp. 529-572.
- Martin, G.R. (1992), "Evaluation of Soil Properties for Seismic Stability Analysis of Slopes," In: *Stability and Performance of Slopes and Enhancements II, Geotechnical Special Publication No. 31, ASCE*, Vol. 1, pp. 116-142.
- Martin, G.R., and Lam, I.P. (1995), "Seismic Design of Pile Foundations: Structural and Geotechnical Issues," *State of the Art (SOA4), Proc. 3rd International Conference on Recent Advances in Geotechnical Earthquake Engineering and Soil Dynamics, St. Louis, Missouri*, Vol. 3, pp. 1491-1515.
- Martin, P.P. (1975)*, "Non-Linear Methods for Dynamic Analysis of Ground Response," Ph.D. Thesis, University of California, Berkeley.
- Masing, G. (1926), "Eigenspannungen und Verfestigung beim Messing," *Proc. 2nd International Congress on Applied Mechanics, Zurich, Switzerland*, 332-335.
- Matasović, N. and Vucetic, M. (1993), "Cyclic Characterization of Liquefiable Sands," *Journal of Geotechnical Engineering, ASCE*, Vol. 119, No. 11, pp. 1805-1822.
- Matasović, N., Kavazanjian, E., Jr., and Giroud, J.P., (1998) "Newmark Seismic Deformation Analysis for Geosynthetic Covers," *Geosynthetics International, International Geosynthetics Society*, Vol. 5, Nos. 1-2, pp.237-264.
- Matasović, N. (1993)*, "Seismic Response of Composite Horizontally-Layered Soil Deposits," Ph.D. Dissertation, Civil and Environmental Engineering Department, University of California, Los Angeles, 452 p.
- Matasović, N., Kavazanjian, E. Jr., and Yan, L. (1997), "Newmark Deformation Analysis with Degrading Yield Acceleration," *Proc. Geosynthetic '97, Long Beach, California*, Vol. 2, pp. 989-1000.
- Mayne, P.W. and Rix, G.J. (1993), " G_{max} - q_c Relationships for Clays," *Geotechnical Testing Journal, ASTM*, Vol. 16, No. 1, pp. 54-60.

* Available through University Microfilms International, (800) 521-0600, Ext. 3879.

- McGuire, R.K., Toro, G.R. and Silva, W.J. (1988), "Engineering Model of Earthquake Ground Motion for Eastern North America," Technical Report NP-6074, Electric Power Research Institute, Palo Alto, California.
- McVay, M.C., Casper, R., and Shang, T. (1995), "Lateral Response of Three-Row Groups in Loose to Dense Sands at 3D and 5D Pile Spacing," *Journal of Geotechnical Engineering, ASCE*, Vol. 121, No. 5, pp. 436-441.
- Meigh, A.C. (1987), "Cone Penetration Testing: Methods and Interpretation," CIRIA Ground Engineering Report: In Situ Testing, Butterworths, 141 p.
- Ménard, L. and Broise, Y. (1975), "Theoretical and Practical Aspects of Dynamic Consolidation," *Geotechnique*, Vol. 15, No. 1.
- Meyerhof, G.G. (1953), "The Bearing Capacity of Foundations under Eccentric Loads," *Proc. 3rd International Conference on Soil Mechanics and Foundation Engineering*, Vol. 1, pp. 440-445.
- Meyerhof, G.G. (1956), "Penetration Tests and Bearing Capacity of Cohesionless Soils," *Journal of the Soil Mechanics and Foundations Division, ASCE*, Vol. 82, SM1, pp. 1-19.
- Mitchell, J. K. (1981), "Soil Improvement: State of the Art," *Proc. 10th International Conference on Soil Mechanics and Foundation Engineering*, Vol. 4, pp. 509-565.
- Mitchell, J. K., Baxter, C.D.P., and Munson, T.C. (1995), "Soil Improvement for Earthquake Hazard Mitigation," *Geotechnical Special Publication No. 49, American Society of Civil Engineers*.
- Mononobe, N. (1929), "Earthquake-Proof Construction of Masonary Dams," *Proc. World Engineering Conference*, Vol. 9, p. 275.
- Moriwaki, Y., Tan, P. and Somerville, P. (1994), "Some Recent Site-Specific Ground Motion Evaluations - Southern California Examples and Selected Issues," *Proc. Seminar on New Developments in Earthquake Ground Motion Estimation and Implication for Engineering Design Practice, Applied Technology Council ATC 35-1, Redwood City, California*, pp. 14-1 - 14-25.
- Morrison, A. (1982), "The Booming Business in Wick Drains," *Civil Engineering, ASCE*, Vol. 53, No. 3.
- Mualchin, L. and Jones, A.L. (1992), "Peak Acceleration From Maximum Credible Earthquakes in California (Rock and Stiff Soil Sites)," *California Department of Conservation, Division of Mines and Geology, Open-File Report 92-1, Sacramento, California* (updated in 1995 by L. Mualchin).
- Muraleetharan, K.K., Mish, K.D., Yogachandran, C. and Arulananadan, K. (1991), "User's Manual for DYSAC2: Dynamic Soil Analysis Code for 2-Dimensional Problems," *Research Report, Department of Civil Engineering, University of California, Davis, California*.
- Naeim, F. and Anderson, J.C. (1993), "Classification and Evaluation of Earthquake Records for Design," *Report No. CE 93-08, Department of Civil Engineering, University of Southern California, Los Angeles*, 288 p.

- Nataraja, M.S. and Cook, B.E. (1983), "Increase in SPT N-Values Due to Displacement Piles," Technical Note, Journal of the Geotechnical Engineering Division, ASCE, Vol. 109, No. 1, pp. 108-113.
- NAVFAC (1986), "Foundations and Earth Structures," Design Manual DM 7.02, Naval Facilities Engineering Command, Department of the Navy, Alexandria, Virginia.
- Nazarian, H.N. and Hadjian, A.H. (1979), "Earthquake-Induced Lateral Soil Pressures on Structures," Journal of the Geotechnical Engineering Division, ASCE, Vol. 105, No. GT9, pp. 1049-1066.
- Nazarian, S. and Stokoe, K.H. II (1984), "In Situ Shear Wave Velocities from Spectral Analysis of Surface Waves," Proc. 8th World Conference on Earthquake Engineering, San Francisco, California, Vol. 3, pp. 31-38.
- NEHRP (1991), "NEHRP Recommended Provisions for the Development of Seismic Regulations for New Buildings," Part 1: Provisions, Building Seismic Safety Council, Washington, District of Columbia, 199 p.
- Newmark, N.M. (1965), "Effects of Earthquakes on Dams and Embankments," Géotechnique, Vol. 15, No. 2, pp. 139-160.
- Nigam, N.C. and Jennings, P.C. (1968)**, "SPECEQ/UQ - Digital Calculation of Response Spectra from Strong-Motion Earthquake Records," CALTECH, Earthquake Engineering Research Laboratory, Pasadena, California, 65 p. (plus Appendix).
- NRC (1985), "Liquefaction of Soils During Earthquakes," National Research Council, Committee on Earthquake Engineering, Washington, District of Columbia.
- Nuttli, O.W. (1974), "Seismic Hazard of the Rocky Mountains," Preprint 2195, ASCE, National Structural Engineering Meeting, Cincinnati, Ohio.
- Nuttli, O.W. and Herrmann, R.B. (1984), "Ground Motion of Mississippi Valley Earthquakes," Journal of Technical Topics in Civil Engineering, ASCE, Vol. 110, No. 1, pp. 54-69.
- Okabe, S. (1926), "General Theory of Earth Pressures," Journal of the Japan Society of Civil Engineering, Vol. 12, No. 1.
- Park, R.G. (1983), "Foundations of Structural Geology," Blackie Publishing, Chapman and Hall, New York, New York.
- Pinto, P., McVay, M., Hoyt, M. and Lai, P. (1997), "Centrifuge Testing of Plumb and Battered Pile Groups in Sand," Proc. Transportation Research Board, 17th Annual Meeting, Washington, District of Columbia, Paper No. 551, pp. 1-17.
- Poulos, S.J., Castro, G. and France, W. (1985), "Liquefaction Evaluation Procedure," Journal of Geotechnical Engineering Division, ASCE, Vol. 111, No. 6, pp. 772-792.

** Available through NISEE / Computer Applications, (510) 642-5113.

- Poulos, H.G. and Davis, E.M. (1974), "Elastic Solutions for Soil and Rock Mechanics," John Wiley and Sons, Inc., New York, 410 p. (reprinted in 1991 by Centre for Geotechnical Research, University of Sydney, Australia).
- Prakash, S. and Basavanna, B.M. (1969), "Earth Pressure Distribution Behind Retaining Walls During Earthquakes," Proc. 4th World Conference on Earthquake Engineering, Santiago, Chile.
- Prevost, J.H. (1981), "DYNAFLOW: A Nonlinear Transient Finite Element Analysis Program," Department of Civil Engineering and Operational Research, Princeton University, (Last update January 1994).
- Pyke, R. (1995), "TELDYN - User's Manual," TAGA Engineering Systems & Software, Lafayette, California.
- Reese, L.C. (1984), "Handbook on Design of Piles and Drilled Shafts Under Lateral Load," FHWA IP-84-11, U.S. Department of Transportation, Federal Highway Administration, McLean, Virginia, 360 p.
- Reese, L.C., Cooley, L.A. and Radhakrishnan, N. (1984), "Laterally Loaded Piles and Computer Program COM 624G," Technical Report K-84-2, U.S. Army Engineer, Lower Mississippi Valley.
- Riaund, J. and Miran, J. (1992), "The Cone Penetrometer Test," FHWA-SA-91-043, USDOT FHWA, U.S. Department of Transportation, Federal Highway Administration, Washington, District of Columbia, 161 p.
- Richards, R. Jr. and Elms, D.G. (1979), "Seismic Behavior of Gravity Walls," Journal of the Geotechnical Engineering Division, ASCE, Vol. 105, No. GT4, pp. 449-464.
- Richardson, G.N., Kavazanjian, E., Jr. and Matasović, N. (1995), "RCRA Subtitle D (258) Seismic Design Guidance for Municipal Solid Waste Landfill Facilities," EPA/600/R-95/051, United States Environmental Protection Agency, Cincinnati, Ohio, 143 p.
- Richart, F.E., Jr., Woods, R.D. and Hall, J.R., Jr. (1970), "Vibrations of Soils and Foundations," Prentice-Hall, Inc., Englewood Cliffs, New Jersey, 414 p.
- Richter, C.F. (1958), "Elementary Seismology," W.H. Freeman and Company, San Francisco, California.
- Riggs, C.O. (1986), "North American Standard Penetration Test Practice," In: Use of In Situ Tests in Geotechnical Engineering, ASCE Geotechnical Special Publication No. 6, pp. 949-965.
- Robertson, P.K., and Campanella, R.G., (1983), "Interpretation of Cone Penetration Tests- Part I (Sand)," Canadian Geotechnical Journal, Vol. 20, No. 4, pp. 734-745.

- Romo, M.P., and Seed, H.B., (1986) "Analytical Soil Modeling of Dynamic Soil Response in the Mexico City Earthquake," in Proceedings of the International Conference on *The Mexico City Earthquakes-1985: Factors Involved and Lessons Learned*, Cassaro, M.A., and Romero, E.M., editors, American Society of Civil Engineers, Mexico City, Mexico, September 1986, pp. 148-162.
- Ross, G.A., Seed, H.B. and Migliaccio, R.R. (1969), "Bridge Foundation Behavior in Alaska Earthquake," *Journal of the Soil Mechanics and Foundations Division, ASCE*, Vol. 95, No. SM4, pp. 1007-1036.
- Roth, W.H. and Inel, S. (1993), "An Engineering Approach to the Analysis of VELACS Centrifuge Tests," *Proc. International Conference on the Verifications of Numerical Procedures for the Analysis of Soil Liquefaction Problems*, Davis, California, Vol. 1, pp. 1209-1229.
- Ruiz, J. and Penzien, J. (1969), "PSEQGN - Artificial Generation of Earthquake Accelerograms," Report No. EERC 69-3, Earthquake Engineering Research Center, University of California, Berkeley, California.
- Sadigh, K., Chang, C.-Y., Abrahamson, N.A., Chiou, S.J. and Power, M.S. (1993), "Specification of Long-Period Ground Motions: Updated Attenuation Relationships for Rock Site Conditions and Adjustment Factors for Near-Fault Effects," *Proc. Seminar on Seismic Isolation, Passive Energy Dissipation, and Active Control*, Vol. 1, Applied Technology Council, ATC 17-1, pp. 59-70.
- Satoh, T., Poran, C.J., Yamagata K. and Rodriguez, J.A. (1991), "Soil Profiling by Spectral Analysis of Surface Waves," *Proc. 2nd International Conference on Recent Advances in Geotechnical Earthquake Engineering and Soil Dynamics*, St. Louis, Missouri, Vol. 2, pp. 1429-1434.
- Satoh, T. (1989), "On the Controlled Source Spectral Rayleigh Wave Excitation and Measurement System," VIC Ltd., Tokyo, Japan.
- Schmertmann, J.H. (1975), "The Measurement of In-Situ Shear Strength," *Proc. ASCE Specialty Conference In-Situ Measurement of Soil Properties*, Vol. 2, pp. 57-138.
- Schnabel, P.B., Lysmer, J. and Seed, H.B. (1972), "SHAKE: A Computer Program for Earthquake Response Analysis of Horizontally Layered Sites," Report No. EERC 72-12, Earthquake Engineering Research Center, University of California, Berkeley, California.
- Schnabel, P.B. and Seed, H.B. (1973), "Accelerations in Rock for Earthquakes in the Western United States," *Bulletin of the Seismological Society of America*, Vol. 63, No. 1, pp. 501-516.
- Schwartz, D.P. and Coppersmith, K.J. (1984), "Fault Behavior and Characteristic Earthquakes: Examples from the Wasatch and San Andreas Fault Zones," *Journal of Geophysical Research*, Vol. 89, No. B7, pp. 5681-5698.
- Seed, H.B. (1975), "Earthquake Effects on Soil-Foundation Systems," In: *Foundation Engineering Handbook*, H.F. Winterkorn and H.Y. Fang (Eds.), Van Nostrand Reinhold, New York, pp. 700-732.

- Seed, H.B. (1979), "Considerations in the Earthquake-Resistant Design of Earth and Rockfill Dams," *Géotechnique*, Vol. 29, No. 3, pp. 215-263.
- Seed, H.B. and Martin, G.R. (1966), "The Seismic Coefficient in Earth Dam Design," *Journal of Soil Mechanics and Foundations Division, ASCE*, Vol. 92, No. SM3, pp. 25-58.
- Seed, H.B. (1983), "Earthquake-Resistant Design of Earth Dams," *Proc., Symposium on Seismic Design of Embankments and Caverns, ASCE, Philadelphia*, pp 6-10.
- Seed, H.B. (1987), "Design Problems in Soil Liquefaction," *Journal of Geotechnical Engineering Division, ASCE*, Vol. 113, No. 8, pp. 827-845.
- Seed, H.B. and Idriss, I.M. (1969), "Rock Motion Accelerograms for High Magnitude Earthquakes," Report No. EERC 69-7, Earthquake Engineering Research Center, University of California, Berkeley, California, 8 p.
- Seed, H.B. and Whitman, R.V. (1970), "Design of Earth Retaining Structures for Dynamic Loads," *Proc. Specialty Conference on: Lateral Stresses in Ground and Design of Earth Retaining Structures, Cornell University, Ithaca, New York*.
- Seed, H.B. and Idriss, I.M. (1970), "Soil Moduli and Damping Factors for Dynamic Response Analyses," Report No. EERC 70-10, Earthquake Engineering Research Center, University of California, Berkeley, California, 40 p.
- Seed, H.B., Idriss, I.M., Makdisi, F. and Bannerje, N. (1975), "Representation of Irregular Stress Time Histories by Equivalent Uniform Stress Series in Liquefaction Analyses," Report EERC 75-29, College of Engineering, University of California, Berkeley.
- Seed, H.B. and Idriss, I.M. (1982), "Ground Motions and Soil Liquefaction During Earthquakes," Monograph No. 5, Earthquake Engineering Research Institute, Berkeley, California, 134 p.
- Seed, H.B., Idriss, I.M. and Arango, I. (1983), "Evaluation of Liquefaction Potential Using Field Performance Data," *Journal of Geotechnical Engineering, ASCE*, Vol. 109, No. 3, pp. 458-482.
- Seed, H.B., Wong, R.T., Idriss, I.M. and Tokimatsu, K. (1984), "Moduli and Damping Factors for Dynamic Analyses of Cohesionless Soils," Report No. UCB/EERC-84/14, Earthquake Engineering Research Center, University of California, Berkeley, California.
- Seed, H.B., Tokimatsu, K., Harder, L.F. and Chung, R.M. (1985), "Influence of SPT Procedures in Soil Liquefaction Resistance Evaluations," *Journal of Geotechnical Engineering, ASCE*, Vol. 111, No. 12, pp. 1425-1445.
- Seed, H.B. and De Alba, P. (1986), "Use of SPT and CPT Tests for Evaluating the Liquefaction Resistance of Sands." In: *Use of In-Situ Tests in Geotechnical Engineering, ASCE Geotechnical Special Publication No. 6*, pp. 281-302.

- Seed, H.B., Seed, R.B., Harder, L.F., Jr. and Jong, H.-L. (1988), "Re-Evaluation of the Slide in the Lower San Francisco Dam in the Earthquake of February 9, 1971," Report No. UCB/EERC-88/04, Earthquake Engineering Research Center, University of California, Berkeley, California.
- Seed, R.B. and Harder, L.F., Jr. (1990), "SPT-Based Analysis of Cyclic Pore Pressure Generation and Undrained Residual Strength," In: H.B. Seed Memorial Symposium, J.M. Duncan, Editor, Tech Publishers Ltd., Vancouver, Canada, Vol. 2, pp. 351-376.
- Sharma, S. (1988), "XSTABL - An Integrated Slope Stability Analysis Program for Personal Computers," Reference Manual, Interactive Software Designs, Inc., Moscow, Idaho, 214 p.
- Shibata, T. and Taparaska, W. (1988), "Evaluation of Liquefaction Potentials of Soils Using Cone Penetration Tests," Soils and Foundations, JSSMFE, Vol. 28, No. 2, pp. 49-60.
- Shlemon, R.J. (1985), "Application of Soil-Stratigraphic Techniques to Engineering Geology," Bulletin of the Association of Engineering Geologists, Vol. XXII, No. 2, pp. 129-142.
- Sibol, M.S., Bollinger, G.A., and Mathena, E.C., (1985) "Seismicity of the Southeastern United States, January 1, 1985 - June 30, 1985," Southeastern U.S. Seismic Network Bulletin No. 16, Seismological Observatory, Virginia Polytechnic Institute and State University, Department of Geological Sciences, Blacksburg, Virginia, December 1985.
- Sieh, K., Stuiver, M. and Brillinger, D. (1989), "A More Precise Chronology of Earthquakes Produced by the San Andreas Fault in Southern California," Journal of Geophysical Research, Vol. 94, No. B1, pp. 603-623.
- Silva, W.J. and Abrahamson, N. A. (1993), "Attenuation of Long Period Strong Ground Motions," Proc. American Society of Military Engineers PVP Conference, Denver, Colorado.
- Silva, W.D. and Lee, K. (1987), "State-of-the-Art for Assessing Earthquake Hazards in the United States: Report 24, WES RASCAL Code for Synthesizing Earthquake Ground Motions," Misc. Paper S-73-1, Geotechnical Laboratory, U.S. Army Waterways Experiment Station, Vicksburg, Mississippi.
- Skempton, A.W. (1986), "Standard Penetration Test Procedures and the Effects in Sands of Overburden Pressure, Relative Density, Particle Size, Ageing and Overconsolidation," Géotechnique, Vol. 36, No. 3, pp. 425-447.
- Solyman, Z.V. (1984), "Compaction of Alluvial Sands by Deep Blasting," Canadian Geotechnical Journal, Vol. 21.
- Somerville, P., Anderson, D., Sun, J., Punyamurthula, S., and Smith, N. (1998) "Generation of Ground Motion Time Histories for Performance-Based Seismic Engineering," Proceedings of the Sixth U.S. National Conference on Earthquake Engineering, Paper No. 222 (on CD ROM), Earthquake Engineering Institute, Oakland, CA, 12 pages.

- SSA (1988), "National Workshop on Seismogenesis in the Eastern United States," A.C. Johnston, A.C. et al., Eds. (presented in *Seismological Research Letters*, Vol. 59, No. 4, Seismological Society of America).
- Stark, T.D. and Olson, S.M. (1995), "Liquefaction Resistance Using CPT and Field Case Histories," *Journal of Geotechnical Engineering*, ASCE, Vol. 121, No. 12, pp. 856-869.
- Stokoe, K.H., II and Nazarian, S. (1985), "Use of Rayleigh Waves in Liquefaction Studies," Proc. Session on Measurement and Use of Shear Wave Velocity for Evaluating Soil Dynamic Properties, ASCE National Convention, Denver, Colorado, pp. 1-17.
- Tao, D. (1996)***, "News from the Information Service - Increased Availability of Strong Motion Records," *NCEER Bulletin*, Vol. 10, No. 3, pp. 15-17.
- Tatsuoka, F., Koseki, J. and Tateyama, M. (1995), "Performance of Geogrid-Reinforced Soil Retaining Walls during the Great Honshin-Awaji Earthquake, January 17, 1995," Proc. 1st International Conference for Earthquake Geotechnical Engineering, Tokyo, Japan, Vol. 1, pp. 55-62.
- Terzaghi, K. and R.B. Peck (1967), "Soil Mechanics in Engineering Practice," 2nd Edition, John Wiley and Sons, New York. The first edition was published in 1948.
- Tinsley, J.C., Youd, T.L., Perkins, D.M. and Chen, A.T.F. (1985), "Evaluating Liquefaction Potential," In: J.I. Ziony, Ed., *Evaluating Earthquake Hazards in the Los Angeles Region, an Earth Science Perspective*, U.S. Geological Survey Professional Paper 1360, pp. 263-315.
- Tokimatsu, K. and Seed, H.B. (1987), "Evaluation of Settlements in Sands due to Earthquake Shaking," *Journal of Geotechnical Engineering*, ASCE, Vol. 113, No. 8, pp. 861-879.
- Tokimatsu, K., Tamura, S. and Kuwayama, S. (1991), "Liquefaction Potential Evaluation Based on Rayleigh Wave Investigation and its Companion with Field Behavior," Proc. 2nd International Conference on Recent Advances in Geotechnical Earthquake Engineering and Soil Dynamics, St. Louis, Missouri, Vol. 1, pp. 357-364.
- Toro, G.R., Abrahamson, N.A., and Schneider, J.F. (1997) "Model of Strong Ground Motions from Earthquakes in the Central and Eastern North America: Best Estimates and Uncertainties," *Seismological Research Letters*, Volume 68, Number 1, January/February 1997, pp. 41-57.
- Trautmann, C.H. and Kulhawy, F.H. (1983), "Data Sources for Engineering Geologic Studies," *Bulletin of the Association of Engineering Geologists*, Vol. XX, No. 4, pp. 439-454.
- Trifunac, M.D. and Brady, A.G. (1975), "A Study of the Duration of Strong Earthquake Ground Motion," *Bulletin of the Seismological Society of America*. Vol. 65, pp. 581-626.
- UBC (1994), "Uniform Building Code, Volume 2 - Structural Engineering Design Provisions," International Conference of Building Officials, Whittier, California.

*** Available from NCEER, (716) 645-3391.

- USEPA (1993), "Technical Manual: Solid Waste Disposal Facility Criteria" United States Environmental Protection Agency, EPA/530/R-93/017, United States Environmental Protection Agency, Washington, District of Columbia.
- Vrymoed, J.L. and Calzascia, E.R. (1978), "Simplified Determination of Dynamic Stresses in Earth Dams," in Proceedings of the Specialty Conference on *Earthquake Engineering and Soil Dynamics*, American Society of Civil Engineers, Pasadena, California, June 1978, pp. 991-1006.
- Vucetic M. and Dobry, R. (1991), "Effect of Soil Plasticity on Cyclic Response," *Journal of Geotechnical Engineering*, ASCE, Vol. 117, No. 1, pp. 89-107.
- Wang, S-T and Reese, L.C. (1991), "Analysis of Piles under Lateral Load - Computer Program COM624P for the Microcomputer," FHWA-SA-91-002, U.S. Department of Transportation, Federal Highway Administration, 229 p.
- Wesnousky, S.G. (1986), "Earthquakes, Quaternary Faults and Seismic Hazard in California," *Journal of Geophysical Research*, Vol. 91, No. B12, pp. 12587-12631.
- Whitman, R.V. (1990), "Seismic Design of Gravity Retaining Walls," *Proc. Design and Performance of Earth Retaining Structures*, ASCE Geotechnical Special Publication No. 25, pp. 817-842.
- Winterkorn, H.F. and Fang, H.Y. (1975), "Foundation Engineering Handbook," Van Nostrand Reinhold, New York (2nd Edition published in 1991).
- Wood, H.O. (1908), "Distribution of Apparent Intensity in San Francisco," In: *The California Earthquake of April 18, 1906*, Report of the State Earthquake Investigation Commission, Carnegie Institution of Washington, District of Columbia, pp. 220-245.
- Woods, R.D. (1994), "Geophysical Characterization of Sites," *Proc. 12th International Conference on Soil Mechanics and Foundation Engineering*, Special Volume Prepared by TC 10, New Delhi, India.
- Woodward-Clyde Consultants (1979), "Report of the Evaluation of Maximum Earthquake and Site Ground Motion Parameters Associated With the Offshore Zone of Faulting, San Onofre Nuclear Generating Station," Unpublished Report for Southern California Edison Company, 241 p.
- Wright, S. (1995), "UTEXAS3 - A Computer Program for Slope Stability Calculations," *User's Manual*, Shinoak Software, Austin, Texas (originally coded in 1990).
- Wyss, M. (1979), "Estimating Maximum Expectable Magnitude of Earthquakes from Fault Dimensions," *Geology*, Vol. 7. pp. 336-340.
- Yan, L., Matasović, N. and Kavazanjian, E., Jr. (1996), "Seismic Response of Rigid Block on Inclined Plane to Vertical and Horizontal Ground Motions Acting Simultaneously," *Proc. 11th ASCE Engineering Mechanics Conference*, Fort Lauderdale, Florida, Vol. 2, pp. 1110-1113.
- Yasuda, S., Ishihara, K., Harada, K. And Shinkawa, N. (1996), "Effectiveness of the Ground Improvement on the susceptibility of Liquefaction Observed During the 1995 Hyogoken Nambu (Kobe) Earthquake," *World Conference on Earthquake Engineering*, Mexico.

- Youd, T.L. (1995), "Liquefaction-Induced Lateral Ground Displacement," Proc. 3rd International Conference on Recent Advances in Geotechnical Earthquake Engineering and Soil Dynamics, St. Louis, Missouri, Vol. 2, pp. 911-925.
- Youd, T.L. and Hose, S.N. (1976), "Liquefaction during 1906 San Francisco Earthquake," Journal of the Geotechnical Engineering Division, ASCE, Vol. 102, No. GT5, pp. 425-439.
- Youd, T.L. and Idriss, I.M. (1997), "Proceedings of the NCEER Workshop on Evaluation of Liquefaction Resistance of Soils," National Center of Earthquake Engineering Research, Technical Report NCEER - 97-0022.
- Youd, T.L. and Perkins, D.M. (1978), "Mapping Liquefaction-Induced Ground Failure Potential," Journal of Geotechnical Engineering, ASCE, Vol. 104, No. GT4, pp. 433-446.
- Youngs, R.R., Day, S.M. and Stevens, J.L. (1988), "Near Field Ground Motions on Rock for Large Subduction Earthquakes," Earthquake Engineering and Soil Dynamics II - Recent Advances in Ground-Motion Evaluation, ASCE Geotechnical Special Publication No. 20, pp. 445-462.

PART II

DESIGN EXAMPLES

LIST OF FIGURES

<u>No.</u>	<u>Caption</u>	<u>Page</u>
2-1	Cross Section of Proposed Bridge and Soil Stratigraphy	2-2
2-2	Location of the Example 1 Test Boring	2-3
2-3	Corrected SPT Results for Example 1 Test Borings	2-5
3-1	Cross Section of Superstructure	3-2
3-2	Typical Span Resting on Two Bents	3-3
3-3	Typical Example 2 Boring Log	3-4
3-4	Corrected SPT Results for Example 2 Test Borings	3-6
3-5	Pile Cap Configuration	3-7
3-6	Pile and Idealized SPT Profile	3-9
4-1	Site Profile for Site Response Analysis	4-2
4-2	Design Response Spectra	4-8
4-3a	Design Ground Motions- Peak Acceleration Scaling	4-11
4-3b	Design Ground Motions- Spectral Acceleration Scaling	4-12
4-4	Free-Field Acceleration Response Spectra- Peak Acceleration Scaling	4-13
4-5	Free-Field Acceleration Response Spectra- Spectral Acceleration Scaling	4-14
4-6	Acceleration Response Spectra- Peak Acceleration Scaling (Input vs. Free-Field for Nahanni Record).	4-15
4-7	Acceleration Response Spectra- Spectral Acceleration Scaling (Input vs. Free-Field for Nahanni Record).	4-16
4-8	Acceleration Response Spectra- SHAKE Analysis vs. Target Spectra	4-17
4-9	Maximum Shear Stresses with Depth.	4-18
4-10	Acceleration Response Spectra- Embankment vs. Free-Field for Saguenay	4-19
5-1	Original Topography and Proposed Grading	5-2
5-2	Example 4 Boring Log	5-4
5-3	Shear Strength Envelopes for Site Materials	5-5
5-4	Calculation of MCE Peak Ground Acceleration	5-7
5-5	Critical Failure Mechanisms for Bench 1, Static Loading	5-8
5-6	Critical Failure Mechanisms for Bench 1, Pseudo-Static Loading	5-9
5-7	Critical Deep-Seated Failure Mechanism, Static Loading	5-10
5-8	Critical Deep-Seated Failure Mechanism, Pseudo-Static Loading	5-11
5-9	Wedge Analysis of Anchor System	5-13
6-1	Example 5 Site Location and Seismic Source	6-2
6-2	Recurrence Relationship for Blind Thrust and Fold Belt	6-4
6-3	Seismic Hazard Curves	6-5
6-4	Stratigraphic Profile Under Embankment	6-8
6-5	Example 5 Boring Log	6-9
6-6	Field Uncorrected SPT N Value Distribution	6-10
6-7	Shear Wave Velocity Profile in Channel	6-11
6-8	Critical Failure Surface for OLE	6-13
6-9	Critical Failure Surface for CLE	6-14
6-10	Post-Liquifaction Slope Stability Analysis	6-16

6-11 Permanent Seismic Deformation Chart 6-17
6-12 Response Spectra from SHAKE Analysis for OLE Events 6-21
6-13 Response Spectra from SHAKE Analysis for CLE Events 6-22
6-14 Design Response Spectra 6-23

LIST OF TABLES

No.	<u>Caption</u>	<u>Page</u>
1-1	Brief Description of Volume II Examples	1-2
2-1	Summary of Soil Properties	2-4
2-2	Geometry of Bridge Foundations	2-6
2-3	Coefficients of Stiffness Matrix	2-6
2-4	Normalization of SPT Blow Counts	2-8
2-5	Summary of Bearing Capacity Coefficients	2-9
2-6	Results of Equivalent Radius Calculations	2-11
2-7	Results of Stiffness Coefficient Calculation for Equivalent Circular Footing	2-13
2-8	Results of Stiffness Coefficient Calculation for Central Pier Footing	2-14
2-9	Results of Stiffness Coefficient Calculation for Abutment Wall Footing	2-14
2-10	Evaluation of Seismic Settlement	2-19
3-1	Dynamic Loading Characteristics	3-8
3-2	Stratigraphy and Strength Parameters for the Two Layers	3-10
3-3	Loads on Individual Piles (Transverse Direction)	3-12
3-4	Loads on Individual Piles (Longitudinal Direction)	3-13
3-5	Combined Longitudinal and Transverse Moments on Individual Piles	3-13
4-1	Summary of Available Information	4-7
4-2	Summary of Available Properties	4-7
4-3	Summary of Deaggregated Peak Ground Acceleration	4-7
6-1	Summary of Design Earthquake Parameters	6-7
6-2	Main Characteristics of Candidate CLE Accelerograms	6-19
6-3	Main Characteristics of Candidate OLE Accelerograms	6-20
6-4	Liquefaction Potential in the Free-Field	6-26
6-5	Liquefaction Potential Under the Centerline of the Embankment	6-29

CHAPTER 1.0 INTRODUCTION

In the United States, design of constructed facilities to resist the effects of earthquakes is often considered a problem restricted to areas west of the Rocky Mountains. However, historical records show that damaging earthquakes can, and do, also occur over broad areas of the eastern and central United States. In fact, the areas over which damaging earthquakes may reasonably be expected to occur cover more than 40 percent of the continental United States. Until recently, highway facilities in many of these areas have not been designed for seismic loading. However, in response to a growing awareness of both the potential for strong motions due to earthquakes in the eastern and central United States and the impact of even the modest levels of shaking on facilities not designed to resist earthquake effects, most states now require some consideration of seismic loading in design of new highway facilities.

This reference manual has been prepared to provide geotechnical engineers with general guidance on the seismic design of highway facilities. The manual is divided into two parts. Part I presents the principles of geotechnical earthquake engineering for highway projects. This second part (Part II) presents a series of five design examples illustrating the application of the design principles presented in Part I.

The examples presented in Part II are based upon actual problems encountered in geotechnical earthquake engineering practice. Each example is self-supporting and contains all the necessary information to conduct the required analyses. In example 1, the seismic bearing capacity and dynamic stiffness matrix of a shallow bridge foundation is evaluated. Example 2 is devoted to the seismic design of a deep foundation constructed with driven piles for a four-lane highway bridge. In example 3, a complete site specific seismic response analysis for a design earthquake is conducted for a highway project in the northeastern United States. The seismic stability analysis of a cut slope in soft rock is presented in example 4. Example 5 illustrates the evaluation of liquefaction potential.

Table 1-1 summarizes the topics covered in each of the five examples presented in this part of the manual. In each example, reference is made to the appropriate chapters in Part I. For each example, a concise statement of the problem to be solved is presented along with the necessary information, detailed calculations, and the final recommendations for design. Equation numbers which appear in the right-hand margin of the calculation sheets refer back to Part I.

TABLE 1-1
BRIEF DESCRIPTION OF Part II EXAMPLES

Example	Chapter	Title	Part I Topics Covered
1	2	Seismic Analysis of a Shallow Bridge Foundation	<ul style="list-style-type: none"> • Correction of SPT N values • Static and dynamic bearing capacity • Dynamic stiffness matrix for shallow footings • Dynamic stiffness coefficient for shallow abutment wall • Seismic settlement evaluation
2	3	Seismic Design of a Deep Foundation System	<ul style="list-style-type: none"> • Deep foundation static and dynamic bearing capacity • Lateral deflection of a pile group • Vertical deflection of a pile
3	4	Site Specific Seismic Response Analysis	<ul style="list-style-type: none"> • Simplified seismic hazard analysis • Seismic response analysis • Derivation of Dynamic Soil Properties
4	5	Slope Stability Analysis	<ul style="list-style-type: none"> • Deterministic seismic hazard analysis • Pseudo-static slope stability analysis
5	6	Liquefaction Potential Analysis	<ul style="list-style-type: none"> • Seed and Idriss simplified method for liquefaction potential evaluation • Probabilistic seismic hazard analysis • Seismic slope stability and deformation analysis • Post-liquefaction stability analysis • Liquefaction mitigation measures

CHAPTER 2.0

SEISMIC ANALYSIS OF A SHALLOW BRIDGE FOUNDATION

2.1 INTRODUCTION

2.1.1 Description of the Project

This project involves a foundation performance evaluation for the construction of a new bridge in an alluvial valley. The geotechnical engineer has been asked to evaluate the allowable seismic bearing capacity of the proposed spread footing foundation and provide the structural engineer with the dynamic stiffness matrix for the footings and abutment walls. The bridge is 38 m long with a 5-m clearance. It is a composite structure with steel girders and precast concrete slabs forming the deck. The cross section of the bridge and soil profile are shown on Figure 2-1. The bridge is 24 m wide, including sidewalks and barriers, as shown in Figure 2-2. The seismic hazard and site response analyses were performed as part of earlier, preliminary, design work and are not part of this problem. The maximum credible earthquake design event is characterized by a moment magnitude equal to 7.5 and a peak horizontal ground acceleration equal to 0.55 g. Seismically-induced peak shear strains calculated in site response analyses were on the order of 0.02 percent.

2.1.2 Source Materials Required

The source materials necessary to solve this problem include:

- the configuration of the bridge;
- geotechnical subsurface information (e.g., boring logs with blow counts); and
- Part I of this document.

2.2 SITE GEOLOGY

Soil conditions in the valley are dominated by deep Holocene alluvium. Available information on the regional geology indicates that the site is underlain by up to 450 m of this Holocene alluvium. Information obtained during initial site reconnaissance, from a review of surficial geology maps, and from a review of data from previous subsurface investigations in the vicinity of the site indicates that the soils at the site consist of sand, silty sands, sandy silts, and gravelly sands.

2.3 GEOTECHNICAL EXPLORATION

Soil conditions at the site were obtained from two soil borings (B-7 and B-8) located at the ends of the proposed bridge, as shown on Figure 2-1. Borings were advanced using a 0.2 m diameter hollow stem auger mounted on a CME-75 drill rig. The boring program included standard penetration tests (SPT) (ASTM D 1586) and California Drive Sampling (ASTM D 3550) in predominantly cohesionless soils. Standard penetration tests and drive sampling were performed alternately at 1.5-m intervals using a donut hammer with rope and pulley.

Borings B-7 and B-8 were drilled to refusal at depths of 24 m and 21 m, respectively, at the locations shown on Figure 2-2. Groundwater was not encountered in either boring. The soil profile developed based on information from these borings is reported on Figure 2-1.

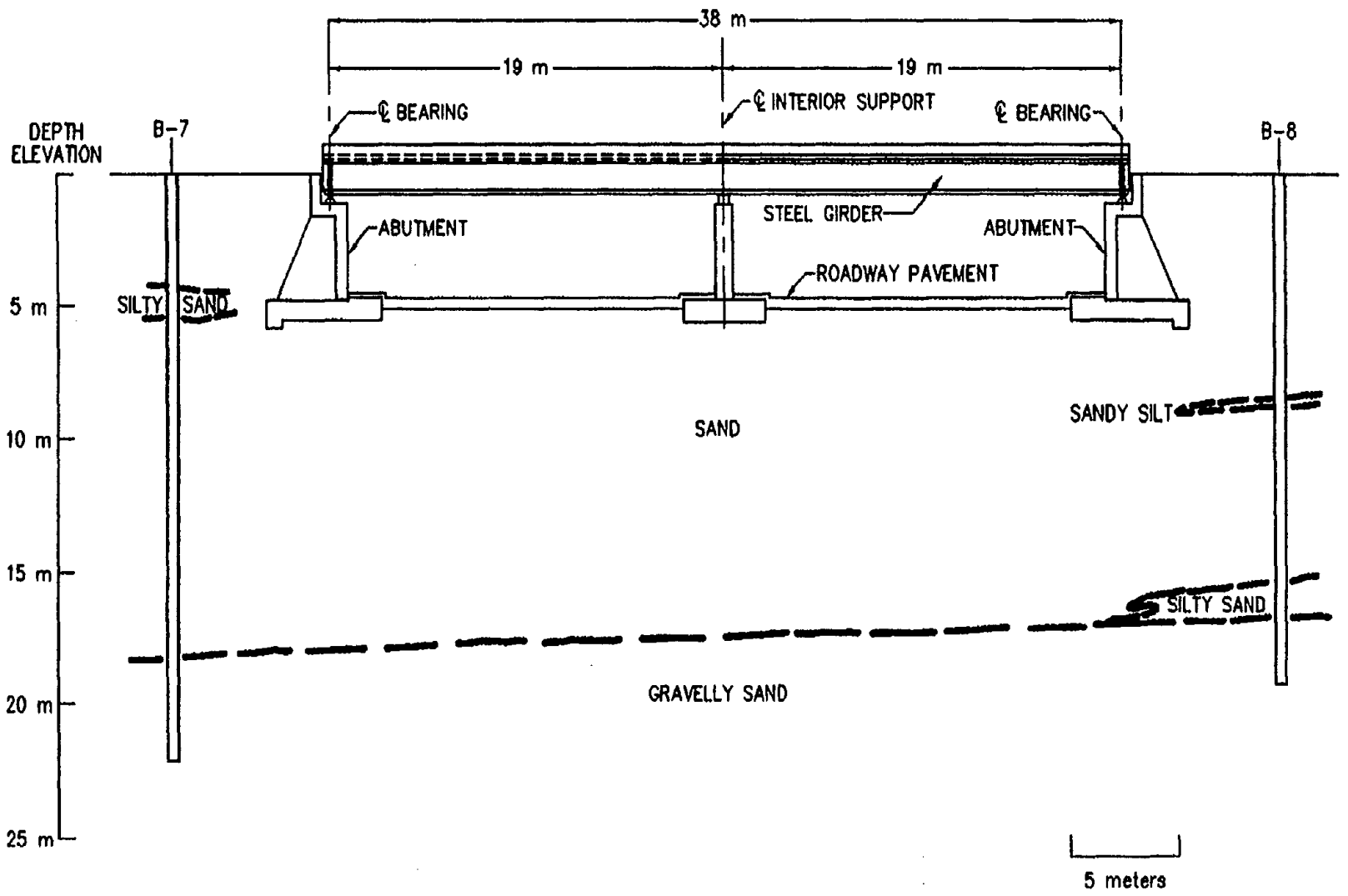


Figure 2-1: Cross Section of Proposed Bridge and Soil Stratigraphy.
2 - 2 (Part II)

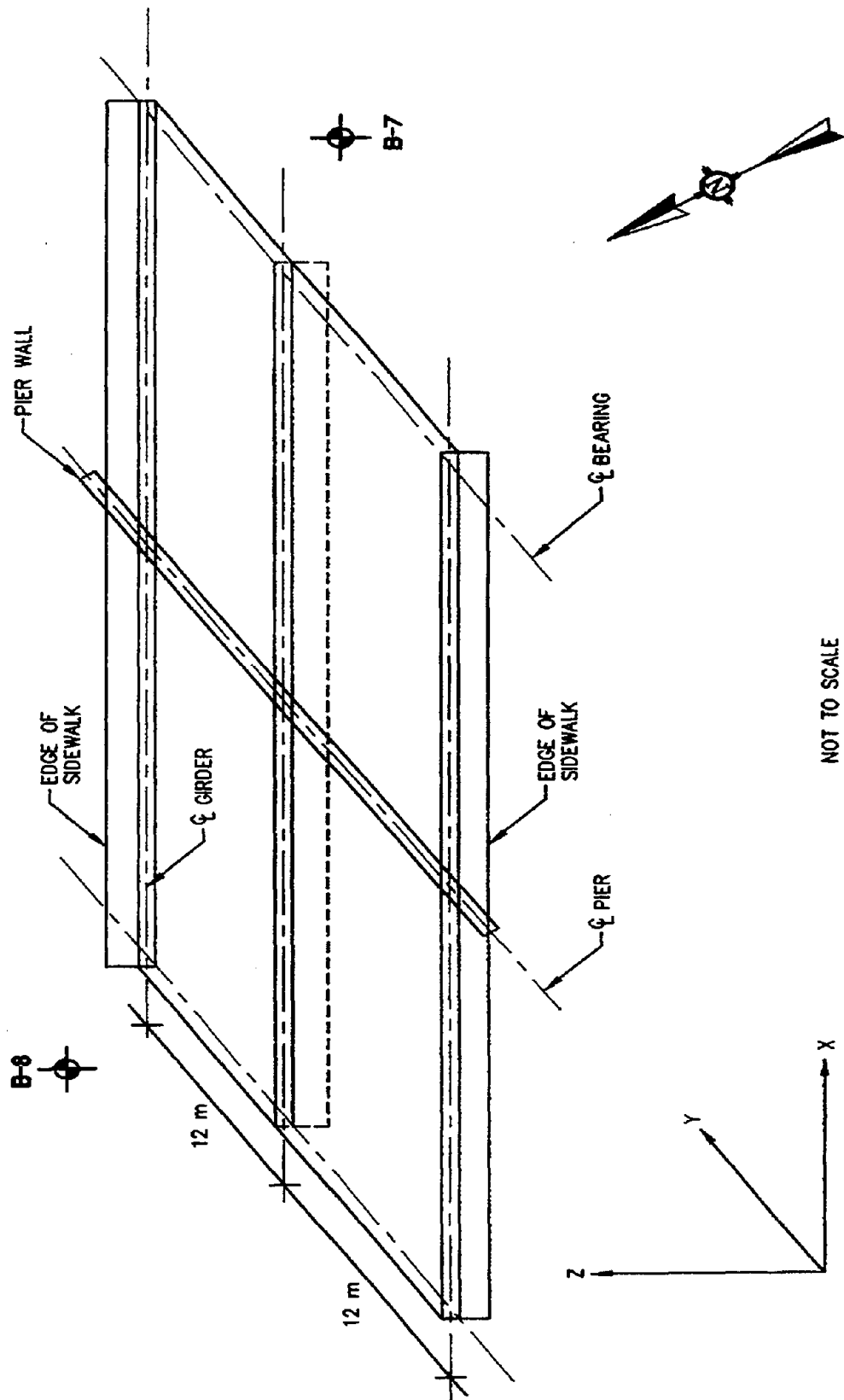


Figure 2-2: Location of the Example 1 Test Boring.

Based upon the results of the laboratory and field tests, the site stratigraphy was idealized for engineering analysis. Table 2-1 presents this idealized soil profile and relevant soil parameters obtained from the laboratory test results and empirical correlations for use in the bearing capacity analysis.

**TABLE 2-1
SUMMARY OF SOIL PROPERTIES**

Depth (m)	Soil Type (USCS)	Dry Unit Weight (kN/m ³)	Total Unit Weight (kN/m ³)	Friction Angle (°)	Cohesion (kPa)
0-18	SP-SM	16.5	17.2	35	0
18-21	SP-GP	17.3	18.1	38	0

Note: Groundwater was not encountered in either boring.

The field blow counts and blow counts normalized to 96 kPa overburden pressure and standardized for 60 percent hammer efficiency are reported on Figure 2-3. Details of the normalization and standardization procedures are provided in the attached calculation sheets. In general, the blow counts increase with depth. Average normalized and standardized values vary from approximately 25 blows per 300 mm at shallow depths (0 to 10 m) to approximately 30 blows per 300 mm at greater depths (11 to 20 m). Both borings were terminated due to refusal at the bottom of the hole (depths 21 m and 24 m). Refusal and the isolated high blow counts at shallower depths may be attributed to the presence of gravel, which is known to result in high blow counts.

2.4 DESIGN OF SHALLOW FOUNDATION

The proposed bridge will be supported by a central pier resting on a rectangular footing and two cast-in-place concrete abutment walls, as shown on Figure 2-1. The bearing capacity and stiffness matrix of the central pier footing and the footings for the two abutment walls are needed by the structural engineer for the seismic analysis. The structural engineer also requires the rotational and translational stiffness of the abutment walls. The analysis was carried out in two phases. For the initial phase, an estimate of the static bearing capacity was made to enable the engineer to assess the adequacy of the dimensions of the footings. The footing dimensions were then used to evaluate the stiffness matrix. Using the stiffness matrix, the structural engineer performed the seismic response computations and provided the geotechnical engineer with estimates of the vertical and horizontal loads which may be imposed on the footings during the design earthquake. In the second phase, the bearing capacity of the footings under dynamic conditions was assessed the loads from the dynamic analysis.

The geometry of the foundations shown on Figure 2-1 is summarized in Table 2-2.

The allowable static bearing capacity was calculated using the method described in Section 9.2.2 of Part I. The allowable static bearing capacity, including a factor of safety of 3, is approximately 420 kPa for the central pier footing and 580 kPa for the abutment wall footings. This static capacity is for vertical loads only and was used to size the foundations. The dynamic bearing capacity will be estimated once the magnitude of the seismic loads, and hence the magnitude and direction of the resultant force, are obtained from the structural engineer.

SPT Blow Counts (Blows/300mm)

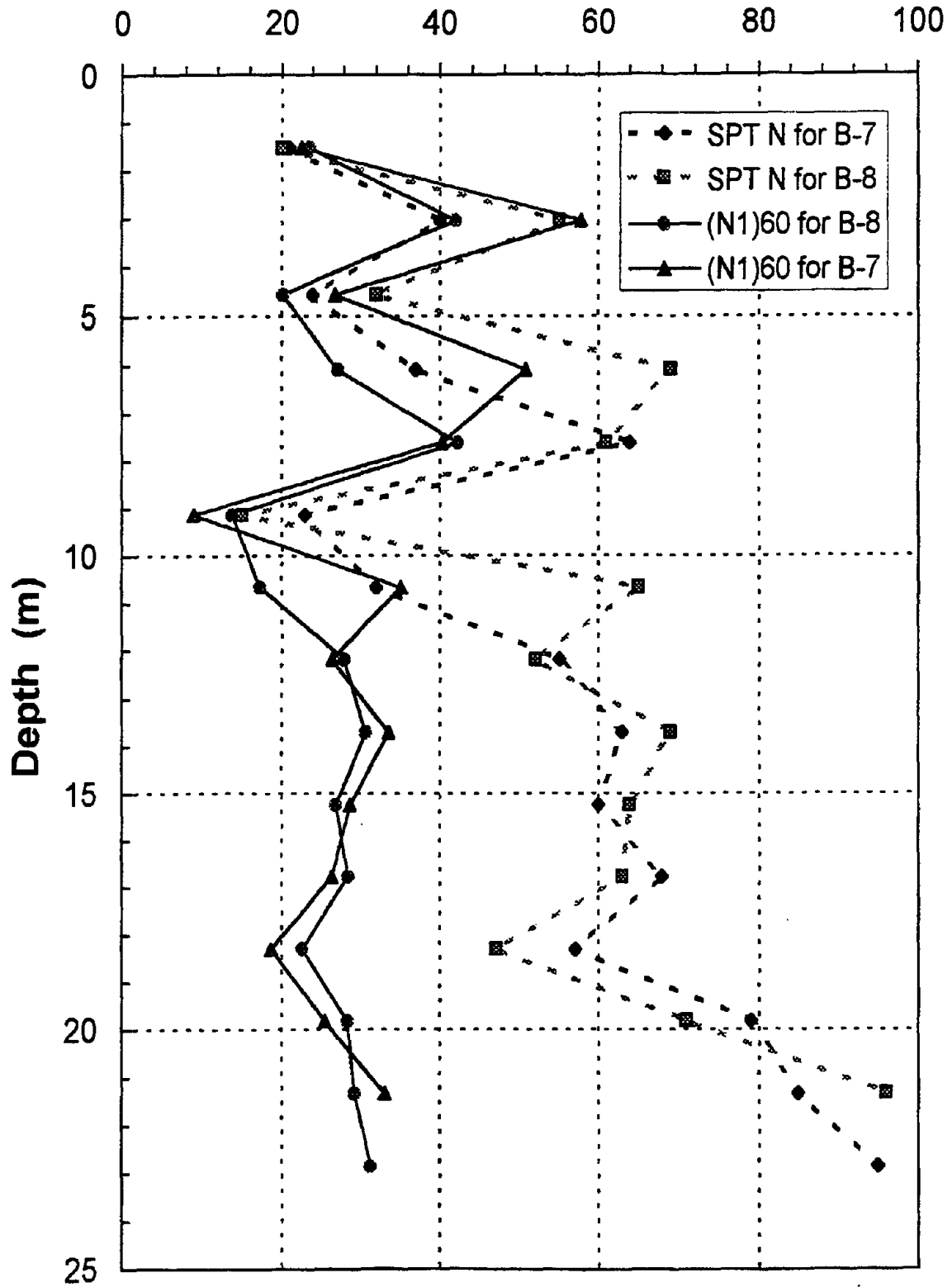


Figure 2-3: Corrected SPT Results for Example 1 Test Borings.

**TABLE 2-2
GEOMETRY OF BRIDGE FOUNDATIONS**

Foundation	Length (m)	Width (m)	Depth Below Grade (m)
Central Pier Footing	25	4.25	5.5
Abutment Wall Footings	25	6.0	5.5

The stiffness matrix for the footings for soil-structure interaction computations was obtained using the procedure detailed in Section 9.2.3 of Part I. The elements of the stiffness matrix for the footings are listed in Table 2-4 below and the detailed calculations are provided in the calculation sheets at the end of this example.

The rotational and translational stiffness of the abutment walls were calculated using the procedure detailed in Section 9.4.6 of Part I. The rotational stiffness was calculated as 4,294 MPa/m and the translational stiffness was calculated as 1,147 MPa/m². Detailed calculations are provided in the calculation sheets at the end of this example.

**TABLE 2-3
COEFFICIENTS OF STIFFNESS MATRIX**

Motion	Central Pier Footing (MPa · m)	Abutment Wall Footings (MPa · m)
Vertical	$K_{33} = 4,015$	$K_{33} = 4,679$
Horizontal	$K_{11} = K_{22} = 3,430$	$K_{11} = K_{22} = 3,814$
X-Axis Rocking	$K_{44} = 2,992,156$	$K_{44} = 3,875,628$
Y-Axis Rocking	$K_{55} = 224,544$	$K_{55} = 486,130$
Z-Axis Rotation (Torsion)	$K_{66} = 2,800,657$	$K_{66} = 3,645,971$

Using the stiffness coefficients provided by the geotechnical engineer, estimates of the dynamic horizontal and vertical loads were provided by the structural engineer and are incorporated into the final check of the dynamic bearing capacity of the footing. For the central pier, the following dynamic loads were calculated:

$$\text{Peak Dynamic Vertical Load: } (P_v)^{\text{DYN}} = 7,000 \text{ kN}$$

$$\text{Peak Dynamic Horizontal Load: } (P_H)^{\text{DYN}} = 14,000 \text{ kN}$$

The calculations for the dynamic bearing capacity of the central pier are included in the attached calculation sheets.

2.5 SEISMIC SETTLEMENT AND LIQUEFACTION POTENTIAL

The seismic settlement of the foundation soil in the design earthquake was evaluated using the method described in Section 8.5 of Part I. The calculated seismic settlement is 22 mm. The calculations are provided in the calculation sheets. The potential for earthquake-induced liquefaction is negligible because groundwater was not encountered in either of the borings, indicating that groundwater was at least 24 m below ground surface.

2.6 CALCULATIONS

The calculations for Example 1, "Seismic Analysis of a Shallow Bridge Foundation" are presented in Section 2.8.

2.7 SUMMARY AND CONCLUSIONS

Preliminary dimensions for the shallow foundations for a highway bridge were estimated based upon the static loads. The stiffness matrix and dynamic bearing capacity for the proposed bridge foundations were evaluated based upon these dimensions. The structural engineer used the stiffness matrix provided by the geotechnical engineer to evaluate the seismic response of the bridge structure. Using the foundation loads calculated by the structural engineer in the seismic response analysis, the geotechnical engineer checked the dynamic bearing capacity and sliding resistance of the foundations and found them to be acceptable.

Liquefaction was not of concern due to the absence of groundwater within 24 m of the ground surface and the high blow count values encountered at depths greater than 20 m. Seismic-induced settlement was calculated to be 24 mm. This value was deemed to be acceptable by the structural engineer.

2.8 DETAILED CALCULATIONS - EXAMPLE 1 - SEISMIC ANALYSIS OF A SHALLOW BRIDGE FOUNDATION

Equation numbers that appear in the right hand margin of the calculations refer back to Part I.

Correlation of SPT N Values

1. Standardization

The standardized SPT blow count N_{60} is the standard penetration blow count for a hammer with an efficiency of 60 percent. If non-standard equipment is used, N_{60} is obtained from Equation 5-6 of Part I.

$$N_{60} = N \cdot C_{60} \quad (5-6)$$

where N is the SPT blow count measured in the field.
 C_{60} is the product of various correlative factors.

$$C_{60} = C_{HT} \cdot C_{HW} \cdot C_{SS} \cdot C_{RL} \cdot C_{BD}$$

Values of the different factors are provided in Table 5-3 of Part I.

The equipment used at the site included a donut hammer with rope and pulley. Other elements of the SPT equipment met the recommended standards listed in Table 5-2 of Part I.

From Table 5-3 of Part I:

$$\begin{aligned}
 C_{HT} &= 0.75 \\
 C_{HW} &= 1.0 \\
 C_{SS} &= 1.0 \\
 C_{RL} &= 1.0 \text{ (Assume the effect of rod length is negligible.)} \\
 C_{BD} &= 1.0 \\
 \Rightarrow C_{60} &= (0.75)(1.0)(1.0)(1.0)(1.0) = 0.75
 \end{aligned}$$

2. Normalization

$(N_1)_{60}$ is the standardized blow count normalized to an effective stress of 96 kPa (1 ton per square foot) in order to eliminate the influence of confining pressure.

$$(N_1)_{60} = C_N \cdot N_{60} \quad (5-11)$$

where C_N is read from Figure 5-5 of Part I (use Table 5-1 or Figure 5-4 from Part I for N-D_r correlation) or obtained using Equation 5-10. A spreadsheet was developed to perform the calculation of the standardized normalized blow count at the site. The distributions with depth of both field measured and normalized and standardized blow count are shown in Figure 2-3 of this example.

**TABLE 2-4
NORMALIZATION OF SPT BLOW COUNTS**

Depth	Vertical Effective Stress	C_N (Figure 5-5)	C_{60} (Table 5-3)	N		$(N_1)_{60} = N \cdot C_N \cdot C_{60}$	
				B-7	B-8	B-7	B-8
1.5 m	25.2 kPa	1.50	0.75	21	20	23.6	22.5
3.0 m	50.4 kPa	1.40	0.75	40	55	42.0	57.8
4.6 m	75.6 kPa	1.12	0.75	24	32	20.2	26.9
6.1 m	100.8 kPa	0.98	0.75	37	69	27.2	50.7
7.6 m	126.0 kPa	0.88	0.75	64	61	42.2	40.3
9.1 m	151.2 kPa	0.80	0.75	23	15	13.8	9.0
10.7 m	176.4 kPa	0.72	0.75	32	65	17.3	35.1
12.2 m	201.6 kPa	0.68	0.75	55	52	28.1	26.5
13.7 m	226.8 kPa	0.65	0.75	63	69	30.7	33.6
15.2 m	252.0 kPa	0.60	0.75	60	64	27.0	28.8
16.8 m	277.2 kPa	0.56	0.75	68	63	28.6	26.5
18.3 m	302.4 kPa	0.53	0.75	57	47	22.7	18.7
19.8 m	343.2 kPa	0.48	0.75	79	71	28.4	25.6
21.3 m	369.6 kPa	0.46	0.75	85	96	29.3	33.1
22.9 m	396.0 kPa	0.44	0.75	95	—	31.4	—

Allowable Bearing Capacity

Allowable bearing capacity is evaluated using the procedure described in Section 9.2.2 of Part I. The equation for ultimate bearing capacity can be written as:

$$q_{ult} = c N_c s_c i_c + 0.5 \gamma B N_\gamma s_\gamma i_\gamma + q_s N_q s_q i_q \quad (9-1)$$

Step 1: Evaluate the Coefficients and Soil Parameters (Section 9.2.2 of Part I)

$$N_q = e^{\pi \tan \phi} \tan^2 (45 + \phi/2) \quad (9-2)$$

$$N_c = (N_q - 1) \cot \phi \quad (9-3)$$

$$N_\gamma = (N_q - 1) \tan (1.4\phi) \quad (9-4)$$

For preliminary calculations, it is assumed that the applied loads are vertical. This implies that, with respect to the load inclination factors in Equation 9-1, $i_c = i_q = i_\gamma = 1$.

The foundation shape factors are given by (Section 9.2.2 of Part I):

$$s_c = 1 + \frac{B}{L} (N_q / N_c) \quad s_q = 1 + \frac{B}{L} \tan \phi \quad s_\gamma = 1 - 0.4 \left(\frac{B}{L} \right) \quad (9-7a,b,c)$$

As the proposed foundations are shallow foundations, the soil parameters for the upper 18 m thick soil layer are used for this analysis. From Table 2-1, these parameters are:

$$\begin{aligned} \phi &= 35^\circ \\ \gamma &= 17.2 \text{ kN/m}^3 \end{aligned}$$

The footing length, L, was set at 25 m, the width of the bridge. After several trials, a footing width, B, of 4.25 m was established for the central pier, and a width of 6 m was established for the abutment wall.

Based upon these values, the following bearing capacity coefficients were calculated:

**TABLE 2-5
SUMMARY OF BEARING CAPACITY COEFFICIENTS**

Factor	Central Pier; B = 4.25 m, L = 25 m	Abutment Wall; B = 6 m, L = 25 m
N_q	33.3	33.3
N_γ	37.2	37.2
N_c	46.1	46.1
s_q	1.12	1.17
s_γ	0.93	0.90
s_c	1.12	1.17

Step 2: Evaluate Bearing Capacity

For this computation, it is assumed that the footings are founded directly at the proposed grade elevation (no embedment). The effect of embedment on the bearing capacity of the abutment wall footings and the effect of the horizontal seismic loads on bearing capacity will be included in later analyses.

Therefore, the equation of bearing capacity (Equation 9-1 in Part I), with $c = 0$ (cohesionless), $q_s = 0$ (no surcharge), and $i_r = 1$ (no inclination), can be written as:

$$q_{ult} = 0.5\gamma B N_\gamma s_\gamma$$

Assuming a factor of safety $FS = 3$ the allowable bearing capacities for static loading calculated using this equation are:

$$\text{Central Pier Footing: } q_a = \frac{1,265}{3} = 420 \text{ kPa}$$

$$\text{Abutment Wall Footings: } q_a = \frac{1728}{3} = 580 \text{ kPa}$$

The estimated loads on each footing were:

Central Pier Footing: 44,625 kN

Abutment Wall Footing: 87,000 kN

As the bridge is 25 m wide, and therefore the footings are 25 m long ($L=25$ m), the following footing widths were established for each footing.

$$\text{Central Pier Footing: } B_{min} = \frac{44,625}{(420)(25)} = 4.25 \text{ m}$$

$$\text{Abutment Wall Footing: } B_{min} = \frac{87,000}{(25)(580)} = 6.00 \text{ m}$$

These results indicated that 4.25 m was an acceptable width for the central pier and that 6 m was an acceptable width for the abutment wall.

Stiffness Matrix

The equation for the general footing stiffness matrix, K , is:

$$K = \alpha \beta K_{ECF} \quad (9-11)$$

where: α = foundation shape correction factor (Section 9.2.3 of Part I)
 β = foundation embedment factor (Section 9.2.3 of Part I)
 K_{ECF} = stiffness matrix of an equivalent circular surface footing, composed of coefficients K_{ij} , as described in Section 9.2.3 of Part I.

The stiffness coefficients of a circular footing of radius R are: (Section 9.2.3 of Part I)

$$\text{Vertical Translation} \quad K_{33} = \frac{4GR}{1-\nu} \quad (9-12a)$$

$$\text{Horizontal Translation} \quad K_{11} = K_{22} = \frac{8GR}{2-\nu} \quad (9-12b)$$

$$\text{X \& Y-Axis Rocking} \quad K_{44} = K_{55} = \frac{8GR^3}{3(1-\nu)} \quad (9-12d)$$

$$\text{Z-Axis Rotation (Torsion)} \quad K_{66} = \frac{16GR^3}{3} \quad (9-12c)$$

where G is the shear modulus of soil and ν is Poisson's ratio.

Step 1: Evaluation of Equivalent Radius

Using the equations for evaluating the equivalent circular radius of a rectangular footing given in Table 9-2 of Part I, the equivalent radius is calculated for each mode as follows:

$$\text{Translational modes:} \quad R_z = R_x = \sqrt{\frac{BL}{\pi}} \quad (\text{Vertical and Horizontal Translation})$$

$$\begin{aligned} \text{Rotational modes:} \quad R_{\psi_x} &= \left[\frac{(16B)(L)^3}{3\pi} \right]^{1/4} && \text{X-Axis Rocking} \\ R_{\psi_y} &= \left[\frac{16(B)^3(L)}{3\pi} \right]^{1/4} && \text{Y-Axis Rocking} \\ R_{\psi_z} &= \left[\frac{16BL(B^2 + L^2)}{6\pi} \right]^{1/4} && \text{Z-Axis Rotation (Torsion)} \end{aligned}$$

where the x-axis is parallel to the B-dimension (width of the footing), the y-axis is parallel to the L-dimension (length of the footing) and Z is the vertical axis. Results of the calculations are presented in the following table:

TABLE 2-6
RESULTS OF EQUIVALENT RADIUS CALCULATION

Motion	Equivalent Radius	
	Central Pier Footing (m)	Abutment Wall Footings (m)
Vertical and Horizontal Translation	$R_z = R_x = 5.82$	$R_z = R_x = 6.91$
X-Axis Rocking	$R_{\psi_x} = 18.32$	$R_{\psi_x} = 19.97$
Y-Axis Rocking	$R_{\psi_y} = 7.56$	$R_{\psi_y} = 9.78$
Z-Axis Rotation (Torsion)	$R_{\psi_z} = 15.52$	$R_{\psi_z} = 17.03$

Step 2: Evaluation of the Shear Modulus

As no direct measurements of the shear modulus or shear wave velocity are available, the small strain shear modulus of the upper layer of medium dense sand and silty sand at the site must be estimated for use in evaluating the stiffness coefficients. Available methods for estimating shear wave velocity or modulus include: (1) correlations using SPT blow count values; (2) typical values for dense sandy soils; or (3) empirical correlations such as those described in Section 5.4.5 and Table 5-5 of Part I.

Compute $G = G_{\max}$ at a depth approximately equal to the equivalent radius for translation of the foundation. Use 6.5 meters as average value for both footings and use the properties reported in Table 2-1 and Figure 2-3 for the soils between 1 and 6.5 meters:

$$N_{60} = 28; \phi = 35^\circ; \gamma = 17.2 \text{ kN/m}^3$$

Two different methods are used herein to calculate G_{\max} : (1) the Seed, *et al.* (1984) empirical correlation based upon mean normal effective stress and blow count; and (2) the Imai and Tonouchi (1982) equation based solely on the SPT blow count values.

(1) Seed, *et al.* (1984):

$$G_{\max} = 220 (K_2)_{\max} (\sigma'_m)^{1/2}$$

$$\sigma'_m = \left(\frac{1 + 2K_o}{3} \right) \sigma'_v$$

$$\sigma'_v = (6.5)(17.2) = 112 \text{ kPa}$$

$$K_o = 1 - \sin\phi = 1 - \sin(35^\circ) = 0.43$$

$$\sigma'_m = \left(\frac{1 + 2(0.43)}{3} \right) (112) = 69 \text{ kPa}$$

$$(K_2)_{\max} = 20(N_{60})^{1/3} = (20)(28)^{1/3} = 60.73$$

$$G_{\max} = 220(60.73)(69)^{1/2} = 110,982 \text{ kPa}$$

$$G_{\max} = 110 \text{ MPa}$$

(2) Imai and Tonouchi (1982):

$$G_{\max} = 15,560 (N_{60})^{0.68}$$

$$= 15,560 (28)^{0.68} = 149,995 \text{ kPa}$$

$$G_{\max} = 150 \text{ MPa}$$

Using average value from methods (1) and (2):

$$G_{\max} = 130 \text{ MPa}$$

Based on the results of a seismic site response analysis, it is assumed that the design earthquake will induce shear strains of about 0.02 percent. Therefore, following the recommendations from Part I, Section 9.2.3, and using modulus reduction curve for sand shown on Figure 5-12 of Part I ($\sigma'_m \approx 100$ kPa), the small strain shear modulus will be reduced by 30 percent to 91 MPa for use in calculating the footing stiffness coefficients.

Step 3: Evaluation of the Stiffness Coefficient for Circular Footing

Using the G_{max} value calculated above (including the 30 percent reduction), the equivalent radius values computed in Step 1, and an assumed value of Poisson's ratio, $\nu = 0.35$ (see Part I, Section 5.3.3), the stiffness coefficients for a circular footing are calculated using Equations 9.12a through 9.12d. The results of this calculation are shown in the following table.

**TABLE 2-7
RESULTS OF STIFFNESS COEFFICIENT CALCULATION
FOR EQUIVALENT CIRCULAR FOOTING**

Motion	Stiffness Coefficient for Circular Footing	
	Central Pier Footing MPa·m	Abutment Wall Footings MPa·m
Vertical Translation	$K_{33} = 3,260$	$K_{33} = 3,870$
Horizontal Translation	$K_{11} = K_{22} = 2,568$	$K_{11} = K_{22} = 3,049$
X-Axis Rocking	$K_{44} = 2,295,478$	$K_{44} = 2,973,247$
Y-Axis Rocking	$K_{55} = 161,310$	$K_{55} = 349,231$
Z-Axis Rotation (Torsion)	$K_{66} = 1,814,326$	$K_{66} = 2,397,088$

Step 4: Evaluation of Rectangular Footing Stiffness Coefficient

Once the stiffness coefficients for an “equivalent” circular footing are calculated, they can be multiplied by the shape and embedment factors α and β to get the stiffness coefficient for the embedded rectangular footing in accordance with Equation 9-11. The shape and embedment factors, α and β , are functions of depth of embedment, dimensions of the footings, and type of motion. Values for these factors may be taken from Figures 9-7 and 9-8 from Part I and combined with the stiffness values calculated in Step 3 to calculate the stiffness coefficients for the bridge foundations.

For both footings, use a footing thickness $D = 1$ m from the design drawings.

Since $L = 25$ m and $B = 4.25$ m, $L/B = 5.9$. To calculate the shape and embedment factors, use asymptotic values for $L/B = 4$ and D/R calculated with $D = 1$ and R from the table on page 2-11. The resulting values of α and β (see Figures 9-7 and 9-8 in Part I) and the calculated stiffness values for the central pier footing are given in the following table.

**TABLE 2-8
RESULTS OF STIFFNESS COEFFICIENT CALCULATION FOR CENTRAL PIER FOOTING**

Motion	D/R	β	α	K_{PIER} (MPa·m)
Vertical Translation	0.172	1.09	1.13	$K_{33} = 4,015$
Horizontal Translation	0.172	1.26	1.06	$K_{11} = K_{22} = 3,430$
X-Axis Rocking	0.055	1.1	1.185	$K_{44} = 2,992,156$
Y-Axis Rocking	0.13	1.2	1.16	$K_{55} = 224,544$
Z-Axis Rotation (Torsion)	0.06	1.3	1.17	$K_{66} = 2,800,657$

For the Abutment Wall Footings:

Since $L = 25$ m and $B = 6$ m, $L/B = 4.2$. Use asymptotic values for $L/B = 4$ and D/R calculated with $D = 1$ and R from the table on page 2-11. The resulting values of α and β and the calculated stiffness values for the abutment footings are given in the following table:

**TABLE 2-9
RESULTS OF STIFFNESS COEFFICIENT CALCULATION
FOR ABUTMENT WALL FOOTING**

Motion	D/R	β	α	$K_{ABUTMENT}$ (MPa·m)
Vertical Translation	0.145	1.07	1.13	$K_{33} = 4,679$
Horizontal Translation	0.145	1.18	1.06	$K_{11} = K_{22} = 3,814$
X-Axis Rocking	0.05	1.1	1.185	$K_{44} = 3,875,628$
Y-Axis Rocking	0.10	1.2	1.16	$K_{55} = 486,130$
Z-Axis Rotation (Torsion)	0.06	1.3	1.17	$K_{66} = 3,645,971$

Stiffness Coefficient for Abutment Wall

The translational and rotational stiffness coefficients for the abutment walls are computed below using Equations 9-31 and 9-32 from Part I.

$$K_s = 0.425 E_s B \quad (9-31)$$

$$K_\theta = 0.072 E_s B H^2 \quad (9-32)$$

where B and H are the width and height of the wall and E_s is the Young's modulus of the soil. Values for B and H were obtained from the design drawings and are equal to 25 m and 4.7 m, respectively.

The shear modulus of the backfill, G , is estimated from the values listed in Table 5-4 of Part I.

Silty sand, medium compaction:

$$G = 80 \text{ MPa}$$

$$E_s = 2(1 + \nu) G = 2(1 + 0.35) 80 = 216 \text{ MPa}$$

As recommended in Section 9.4.6 of Part I, the value of Young's modulus is reduced to reflect a strain level of 0.02 percent. Following the logic used previously for the shear modulus and using modulus reduction curves for sand shown on Figure 5-13 of Part I ($\sigma'_m \approx 25 \text{ kPa}$), E_s will be reduced by 50 percent.

$$E_s = (0.5)(216) = 108 \text{ MPa}$$

$$K_s = (0.425)(108)(25) = 1,147 \text{ MPa} \cdot \text{m}$$

$$K_e = (0.072)(108)(25)(4.7)^2 = 4,294 \text{ MPa} \cdot \text{m}^2$$

Evaluate Dynamic Bearing Capacity of Central Pier Footing

Following performance of a seismic response analysis for the bridge, the structural engineer has provided the following estimates of the peak dynamic vertical and horizontal loads on top of the central pier footing:

$$(P_v)^{\text{DYN}} = 7,000 \text{ kN}$$

$$(P_H)^{\text{DYN}} = 14,000 \text{ kN}$$

These loads must be checked against the dynamic bearing capacity of the footing and the sliding resistance. Note that cited horizontal forces used in this example are transverse loads (perpendicular to the roadway). For actual design, the calculations also need to be performed for horizontal loads along the longitudinal direction of the bridge.

The footing is subjected to a combined vertical load and horizontal load. This combined system of loads is first replaced by a single inclined load. Then, the footing is analyzed for two load conditions, one in which the vertical load is assumed to act upwards (maximum dynamic load inclination) and another where the vertical load is assumed to act downwards (maximum vertical load).

- Maximum dynamic load inclination.

$$V = (P_v)^{\text{STAT}} - (P_v)^{\text{DYN}}$$

where $(P_v)^{\text{STAT}}$ is the static vertical load ($Q_a = 44,625 \text{ kN}$)

$$V = 44,625 - 7,000 = 37,625 \text{ kN}$$

This loading condition governs sliding, but it will also be used to evaluate bearing capacity.

Since $H = (P_H)^{\text{DYN}} = 14,000 \text{ kN}$, the load is inclined at an angle α from the horizontal evaluated as:

$$\alpha = \tan^{-1} \frac{37,625}{14,000} = 70^\circ$$

The magnitude of the load is evaluated as:

$$P = \sqrt{H^2 + V^2} = \sqrt{14,000^2 + 37,625^2} = 40,145 \text{ kN}$$

Since the central pier footing is founded directly at the proposed grade elevation on a cohesionless soil, the bearing capacity Equation 9-1 reduces to:

$$q_{ult} = 0.5\gamma BN_{\gamma}s_{\gamma}i_{\gamma} \quad (9-1)$$

For zero cohesion, i_{γ} is given by:

$$i_{\gamma} = \left[1 - \frac{H}{V}\right]^n \quad (9-5d)$$

and

$$n = \left[\left(2 + \frac{L}{B}\right) / \left(1 + \frac{L}{B}\right) \right] \cos^2\theta + \left[\left(2 + \frac{B}{L}\right) / \left(1 + \frac{B}{L}\right) \right] \sin^2\theta \quad (9-6a)$$

where: $\theta = \tan^{-1}(e_B/e_L)$

The parameters e_B and e_L are the load eccentricity factors (offset distances) in the transverse and longitudinal directions, respectively.

Since there is no eccentricity, $\theta = 0$ and:

$$\begin{aligned} n &= \left[\left(2 + \frac{L}{B}\right) / \left(1 + \frac{L}{B}\right) \right] \\ &= \left[\left(2 + \frac{25}{4.25}\right) / \left(1 + \frac{25}{4.25}\right) \right] = 1.145 \end{aligned}$$

$$i_{\gamma} = \left(1 - \frac{14,000}{37,625}\right)^{1.145} = 0.59$$

$$q_{ult} = (0.5)(17.2)(4.25)(37.2)(0.93)(0.59) = 746 \text{ kPa (ultimate bearing capacity for the maximum dynamic load inclination).}$$

$$q_{max} = \frac{P}{A} = \frac{40,145}{4.25(25)} = 378 \text{ kPa}$$

The factor of safety is then given by:

$$FS = \frac{746}{378} = 1.97$$

Sliding Resistance

The frictional capacity is given by: $F = V(\tan \phi) r$, where r is a reduction factor varying from 0.67

to 0.8 (see Section 9.2.2 of Part I for further discussion) that is applied to the friction coefficient of the soil to obtain the footing-soil interface friction coefficient. For concrete on sand, $r = 0.8$, so:

$$F = (37,625)(0.8)(\tan(35)) = 21,076 \text{ kN}$$

The factor of safety is then given by:

$$FS = \frac{20,006}{14,000} = 1.43$$

- **Maximum vertical load**

This maximum load occurs when the dynamic vertical load acts down and is combined with the static load:

$$\begin{aligned} V_{\max} &= (P_V)^{\text{STAT}} + (P_V)^{\text{DYN}} \\ &= 44,625 + 7,000 = 51,625 \text{ kN} \end{aligned}$$

Since $H = (P_H)^{\text{DYN}} = 14,000 \text{ kN}$, the load is inclined at an angle α from the horizontal evaluated as:

$$\alpha = \tan^{-1} \frac{51,625}{14,000} = 74.8^\circ$$

The magnitude of the load is evaluated as:

$$P = \sqrt{H^2 + V^2} = \sqrt{14,000^2 + 51,625^2} = 53,490 \text{ kN}$$

Since the central pier footing is founded directly at the proposed grade elevation on a cohesionless soil, the bearing capacity Equation 9-1 reduces to:

$$q_{\text{ult}} = 0.5\gamma B N_{\gamma} s_{\gamma} i_{\gamma} \quad (9-1)$$

For zero cohesion, i_{γ} is given by:

$$i_{\gamma} = \left[1 - \frac{H}{V} \right]^n \quad (9-5d)$$

and

$$n = \left[\left(2 + \frac{L}{B} \right) \right] \left[\left(1 + \frac{L}{B} \right) \right] \cos^2 \theta + \left[\left(2 + \frac{B}{L} \right) \right] \left[\left(1 + \frac{B}{L} \right) \right] \sin^2 \theta \quad (9-6a)$$

where: $\theta = \tan^{-1}(e_b/e_v)$

Since there is no eccentricity, $\theta = 0$ and:

$$n = \left[\left(2 + \frac{L}{B} \right) / \left(1 + \frac{L}{B} \right) \right]$$

$$= \left[\left(2 + \frac{25}{4.25} \right) / \left(1 + \frac{25}{4.25} \right) \right] = 1.145$$

$$i_y = \left(1 - \frac{14,000}{51,625} \right)^{1.145} = 0.70$$

$$q_{ult} = (0.5)(17.2)(4.25)(37.2)(0.93)(0.70) = 885 \text{ kPa (ultimate bearing capacity for the maximum vertical load).}$$

$$q_{max} = \frac{P}{A} = \frac{53,490}{4.25(25)} = 503 \text{ kPa}$$

The factor of safety is then given by:

$$FS = \frac{885}{503} = 1.76$$

Note that sliding need not be checked for this case, as the factor of safety against sliding will exceed that calculated for the upwards vertical load (since i_y is greater for this case than when the load acts upwards). Also, the abutment footing must be checked for bearing capacity and sliding resistance. As these evaluations are similar to those for the central pier footing, they are not presented in this example.

Evaluate Liquefaction Potential

As discussed in Section 8.2 of Part I, the first step in assessing liquefaction potential is evaluating whether or not a potential for liquefaction exists. Five screening criteria are listed in Section 8.2 of Part I. Of relevance to this problem are the depth to groundwater and soil penetration resistance. Groundwater was not encountered in either boring. Therefore, it can be assumed that the water table is at least 24 m below ground surface (the maximum boring depth). Furthermore, for depths deeper than 20 m, the normalized and standardized blowcounts are in excess of 60 blows per 300 mm. Given the depth of the groundwater table and the high blow counts, liquefaction is not expected at the site.

Estimate Seismic Settlement

The step by step method outlined in Section 8.5 of Part I provides a means of evaluating the seismic settlement potential. The calculations are performed by subdividing the top 20 m into two 10-m-thick layers. These calculations are presented in the table below. Note that it was assumed that the seismic strains in the layers at depths greater than 20 m will be negligible due to the high blow counts (normalized and standardized blow counts greater than 60).

TABLE 2-10
EVALUATION OF SEISMIC SETTLEMENT

Equation Reference	0 to 10 m	10 to 20 m
σ_v at mid-depth = σ'_v	$(5 \cdot 17.2) = 86 \text{ kPa}$	$(15)(17.2) = 258 \text{ kPa}$
$\sigma'_m = 0.65 \sigma'_v$	$(0.65)(86) = 55.9 \text{ kPa}$	$(0.65)(258) = 167.7 \text{ kPa}$
(Equation 8-1 of Part I)	$1 - 0.00765 z = 0.962$	$1.174 - 0.0267 z = 0.774$
G_{\max} (see calculation below) ^(*)	93,950 kPa	162,700 kPa
$\gamma_{\text{eff}} (G_{\text{eff}}/G_{\max}) =$ $= (0.65 a_{\max} \sigma_v r_d)/(g \cdot G_{\max})$ where $a_{\max} = 0.55 g$ (given)	$3.1 \cdot 10^4$	$4.4 \cdot 10^4$
$\gamma_{\text{eff}} =$ (Figure 8-11 of Part I)	$1.0 \cdot 10^{-3}$	$1.2 \cdot 10^{-3}$
$\Delta_h = \gamma_{\text{eff}} \cdot H$	$(1.0 \cdot 10^{-3})(10) = 1.0 \cdot 10^{-2} \text{ m}$	$(1.2 \cdot 10^{-3})(10) = 1.2 \cdot 10^{-2} \text{ m}$
$\Delta H_{\text{TOTAL}} = 1.0 \cdot 10^{-2} + 1.2 \cdot 10^{-2} = 2.2 \cdot 10^{-2} = 0.022 \text{ m} = 22 \text{ mm}$		

(*) G_{\max} was obtained for both depths using Seed, *et al.* (1984) method used in the evaluation of the stiffness coefficients in this example.

$$G_{\max} = 220 (K_2)_{\max} \sigma'_m{}^{1/2}$$

$$\sigma'_m = \frac{1 + 2K_o}{3} \sigma'_v$$

$$(K_2)_{\max} = 20 (N)_{60}^{1/3}$$

with $(N)_{60} = 25$ [average blow count (for both depths)]

Depth 5m: $\sigma_v = 86 \text{ kPa} = \sigma'_v$

$$\sigma'_m = \frac{1 + 2(0.43)}{3} (86) = 53 \text{ kPa}$$

$$(K_2)_{\max} = (20)(25)^{1/3} = 58.48$$

$$\Rightarrow G_{\max} = (220)(58.48)(53)^{1/2} = 93,950 \text{ kPa}$$

Depth 15 m: $\sigma_v = 258 \text{ kPa} = \sigma'_v$

$$\sigma'_m = \frac{1 + 2(0.43)}{3} (258) = 160 \text{ kPa}$$

$$(K_2)_{\max} = (20)(25)^{1/3} = 58.48$$

$$\Rightarrow G_{\max} = (220)(58.48)(160)^{1/2} = 162,700 \text{ kPa}$$

CHAPTER 3.0 SEISMIC DESIGN OF A DEEP FOUNDATION SYSTEM

3.1 INTRODUCTION

3.1.1 Description of the Project

Portions of a new highway will be built on a viaduct over an existing roadway and railroad tracks. To minimize disruption to existing traffic and because of the low bearing capacity of the top few meters of soil, a driven pile foundation will be employed for the viaduct. The viaduct will be composed of simply supported sections resting on pile-supported bents. Each bent will consist of three columns, each 1 m in diameter, transferring the load to a cast-in-place pile cap on top of the foundation piles.

To accommodate four lanes of traffic, the central barrier, shoulders, and side barriers, the viaduct is about 25 m wide. Figure 3-1 shows a cross section of the superstructure. The superstructure is composed of nine AASHTO standard precast type VI I-beams. The typical span is 43 m long resting on two bents as shown in Figure 3-2. The bottom of the bent is about 5 m above the top of the pile cap.

The structural engineer has made a preliminary estimate of the loads transferred to the bottom of the columns in the design earthquake. The geotechnical engineer must evaluate the lateral load-deformation behavior and the ultimate uplift and compressive capacities of the proposed pile foundation for use in final design.

3.1.2 Source Materials Required

The source materials necessary to solve this problem include:

- geotechnical information on subsurface conditions;
- the configuration of the bridge and anticipated foundation loads;
- Part I of this document;
- National Highway Institute manual for design and construction of driven pile foundations (NHI, 1996); and
- COM624 computer program for analysis of laterally loaded piles (Reese, *et al.*, 1984; or Wang and Reese, 1991).

3.2 GEOTECHNICAL EXPLORATION

Three borings were drilled at the ends of the bridge. The borings were drilled to depths ranging from 23 to 25 m. Standard Penetration Tests (SPTs) were performed at 1.5-m intervals in the borings. The general stratigraphy at the site consists of sands and silty sands with a few lenses of low plasticity silts and clays. Figure 3-3 shows a typical boring log from the site. Groundwater was not encountered in any of the borings. Samples were recovered from the SPT split spoon for soil classification purposes. The distribution of normalized and standardized SPT blow count values with depth is shown on Figure 3-4. The blow counts show that the material gets progressively denser with depth. The top 5 m are characterized by very variable normalized and standardized SPT values with an average value of about 10.

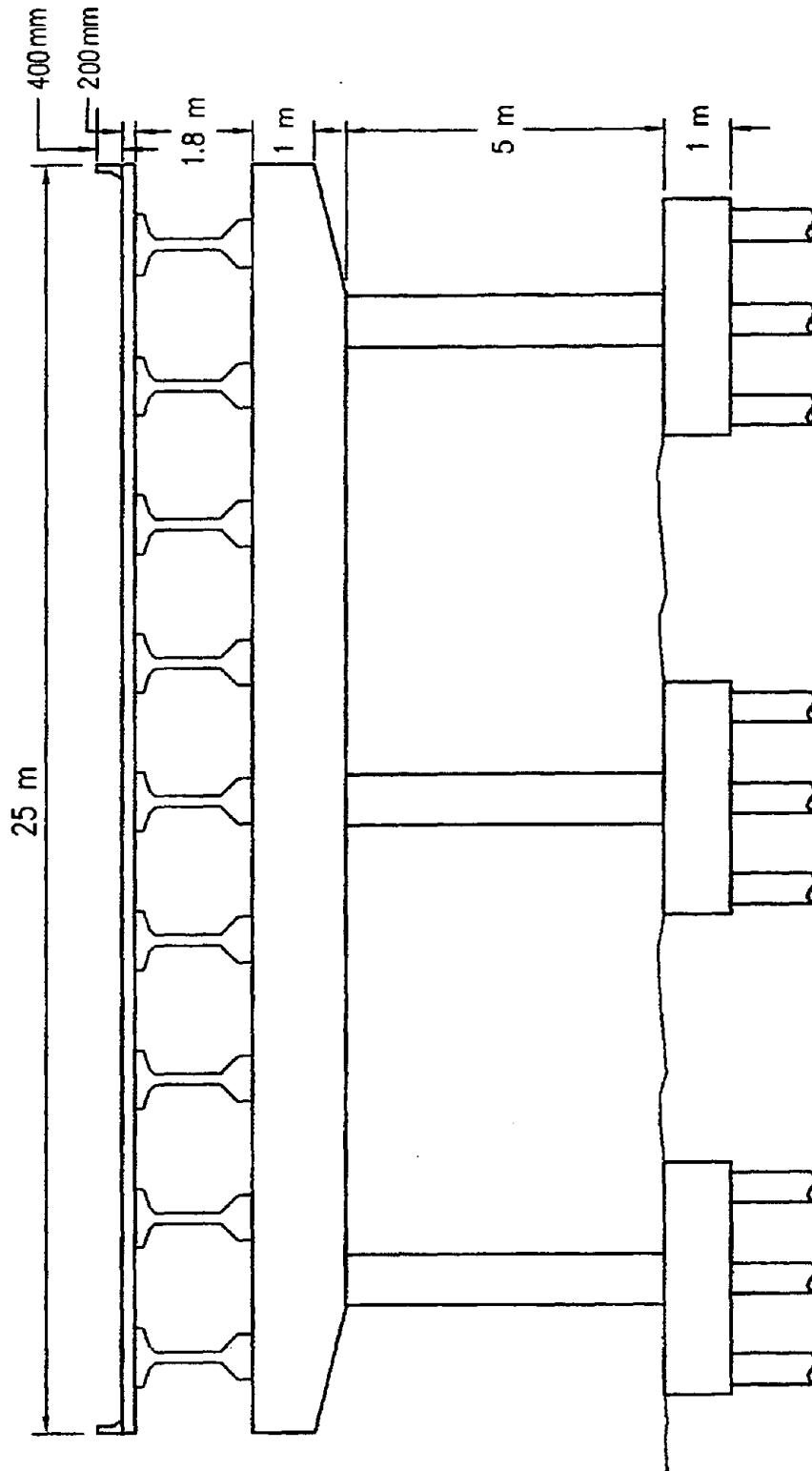


Figure 3-1: Cross Section of Superstructure.

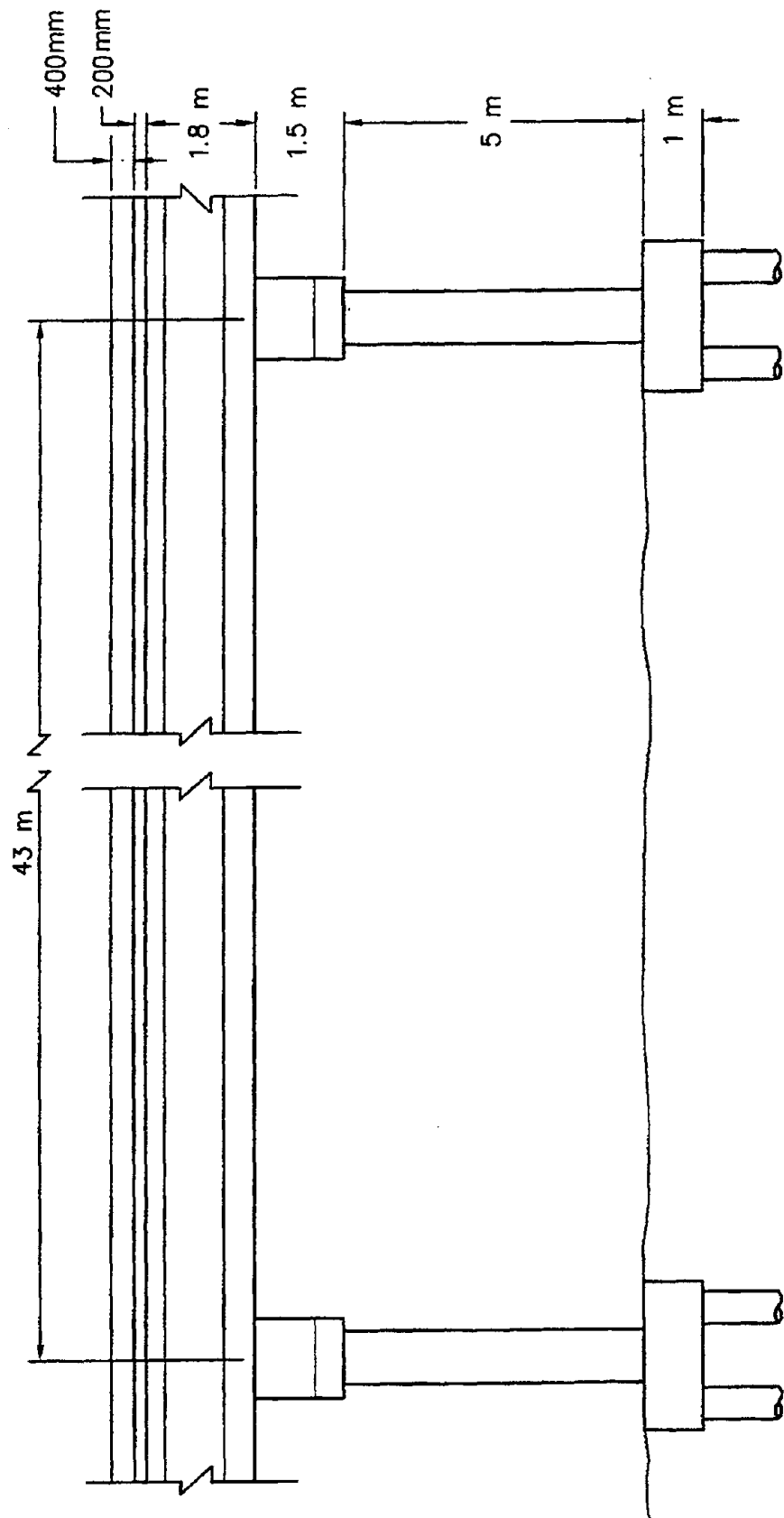


Figure 3-2: Typical Span Resting on Two Bents.

DEPTH BGS (m)	MATERIAL DESCRIPTION	SYMBOLIC LOG	EL. ABOVE MSL (m)	SAMPLES				
				NUMBER	SYMBOL	SPT VALUES		
						REC & ROD (%) OR REC (%)	BLOWS PER 150mm	N
5.0	Grey-brown, loose, fine to medium, sand		-30-	s-1			2-2-3	5
				s-2			3-5-4	9
				s-3			5-6-6	12
9.0	Dark brown, dense, silty sand with clay seams.		-20-	s-4			8-10-12	22
				s-5			12-14-12	26
				s-6			12-15-13	28
16.0	Dark brown, dense, sand.		-10-	s-7			8-22-23	45
				s-8			20-26-27	53
				s-9			26-26-29	55
17.0	Dark brown, silt			s-10			26-28-30	58
23.0	Very dense, silty sand.		-10-	s-11			32-35-35	70
				s-12			30-32-35	67
				s-13			30-34-36	70
				s-14			33-43-47	90
	End of drilling at 23 m.			s-15			42-46-55	101
				s-16			Refusal	

Figure 3-3: Typical Example 2 Boring Log.

From 5 to about 9 m below ground surface, the normalized and standardized SPT values are about 25 and then increase to about 50 from 9 to about 15 m below grade. At a depth of 16 m, the normalized and standardized SPT blow counts increase to about 70. The blow counts eventually reach refusal in a dense gravelly sand layer 24 to 30 m below grade. The idealized normalized and standardized SPT profile used for design is shown on Figure 3-4.

The isolated cohesive silt and clay seams and lenses encountered in the borings were of low plasticity and were not saturated. For the purposes of design analyses, the subsurface profile was simplified as a uniform layer of cohesionless soil that is progressively denser with depth. A total unit weight of 19 kN/m³ was assigned to the soil and the friction angle was assumed to vary from 33 degrees at depths from 0 to 9 m to 38 degrees from 9 to 16 m. These friction angles were estimated using the normalized and standardized SPT blow counts and empirical correlations.

3.3 DESIGN OF PILE FOUNDATIONS

Preliminary values for the loads transferred from the superstructure to the top of the pile caps were provided by the structural engineer. The following preliminary loads were used for design analysis of the pile cap:

Static Load per Pile Cap

- Vertical Compressive Load (Q) = 3,110 kN

Dynamic Load per Pile Cap

- Horizontal Load Along Bridge, Longitudinal Axis (H_x) = 180 kN
- Horizontal Load Perpendicular to Bridge, Longitudinal Axis (H_y) = 602 kN
- Longitudinal Moment (M_x) = 903 kN·m
- Transverse Moment (M_y) = 3,010 kN·m

Based on the preliminary loads, octagonal 0.4-m-diameter driven concrete piles were selected for use in the foundation. Given the general stratigraphy of the site, it was decided to embed the pile in the denser sand layer that starts at 9 m depth. To provide sufficient end bearing capacity, the tip elevation was set at a depth of 12 m. Six 12-m-long piles, configured as shown in Figure 3-5, were proposed for the cap under each column, resulting in a static vertical load of approximately 520 kN/pile. To minimize group effects, the center-to-center spacing of piles in each cap was set at five pile diameters (i.e., 2.0 m). A pile cap embedment depth equal to 2.5 pile diameters (1 m) was used to fix the pile head with respect to the pile cap (no rotation of the pile head in the lateral load analysis). The ultimate static vertical compressive bearing capacity of a 12 m long, 0.4-m-diameter driven concrete pile at the site is on the order of 2,515 kN, resulting in a static factor of safety of almost 5. The detailed calculations are provided.

In addition to the vertical compressive capacity of the piles, calculations were performed to evaluate vertical uplift capacity and lateral stiffness of the piles. The lateral capacity of the pile group was evaluated using the computer program COM624 (Reese, *et al.*, 1984). The p-y curves representing the lateral resistance of the soils were generated internally by the program based upon recommendations made by Reese, *et al.* (1984) for cohesionless soils. Because the pile heads were fixed, the sand was medium dense to dense, and the piles were spaced at 5 pile diameters (center-to-center), group interaction behavior was ignored (the p-y curve for the trailing piles in the group was not modified). If the pile heads were free to rotate, "p-multipliers" of 0.85 and 0.75 would have been used to modify the p-y curves for the second and third row of piles, respectively, based upon the values presented in Table 9-4 of Part I. The lateral load-deformation behavior of the cap would be calculated by assuming each pile deflected the same amount and summing up the lateral load carried by each pile to calculate the group load.

Normalized and Standardized SPT N Values (Blows/300mm)

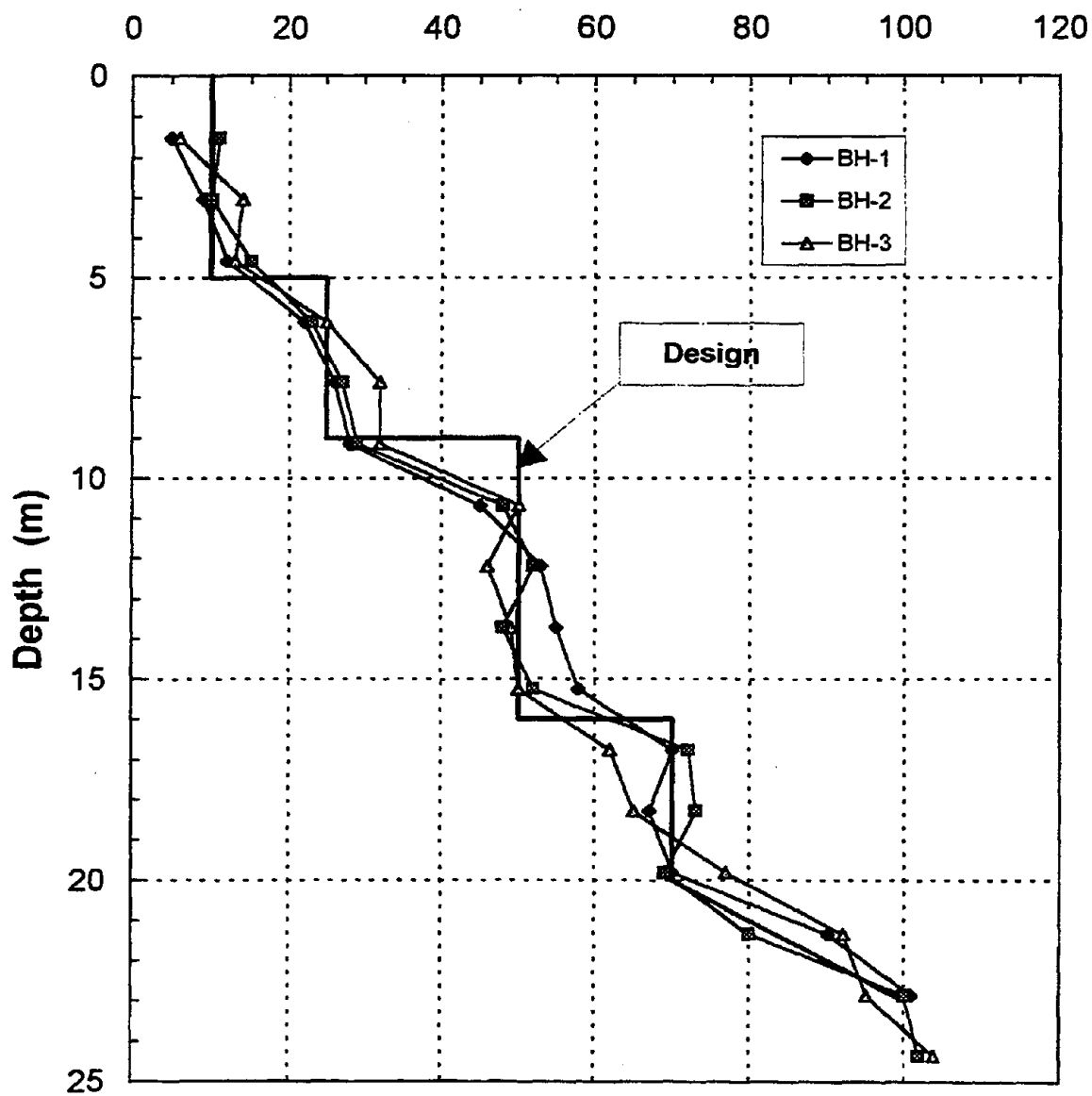


Figure 3-4: Corrected SPT Results for Example 2 Test Borings.

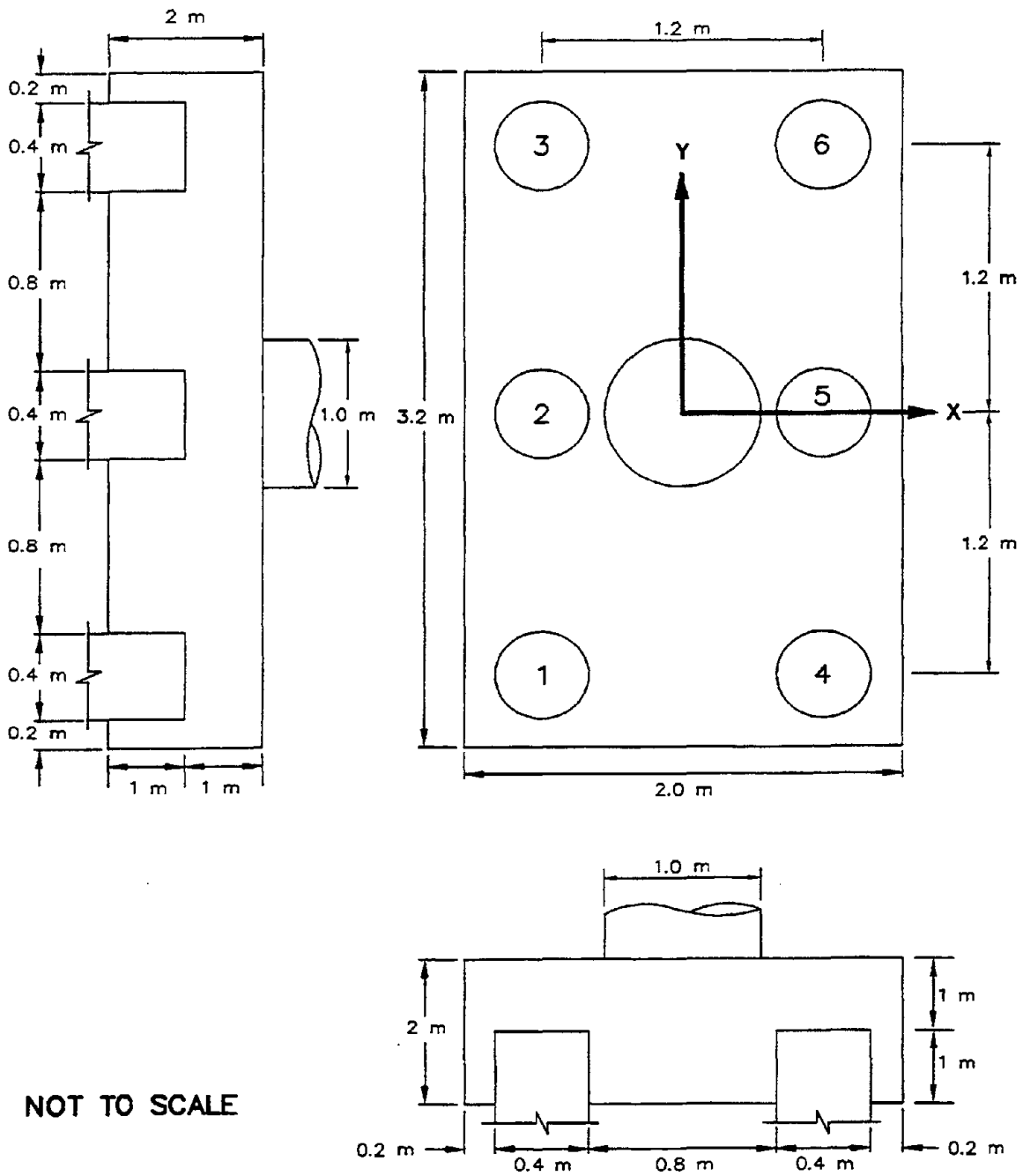


Figure 3-5: Pile Cap Configuration.

The loads provided by the structural engineer were resolved into individual pile loads, as shown in the calculations in Section 3.4 (see Step 3) and summarized in Table 3-1. Note that the vertical load on the pile analyzed for stiffness capacity was increased from the static load of 518 kN to 1,045 kN to account for the vertical load induced by moment loading (see calculations in Section 3.4). Also listed in Table 3-1 is the factor of safety against uplift or compression failure and the expected vertical and lateral deflection of the pile under the dynamic loads.

**TABLE 3-1
DYNAMIC LOADING CHARACTERISTICS**

Type of Load	Maximum Load Per Pile (kN)	Factor of Safety (FS)	Deflection ⁽¹⁾ (mm)
Compression	1,045	FS = 2.4	6 ⁽²⁾
Uplift	9	FS > 1	N/A
Horizontal	100	N/A	5

Notes: ⁽¹⁾ Calculated deflections based on allowable capacities.

⁽²⁾ Reported value is incremental deflection under seismic load.

3.4 DETAILED CALCULATIONS

EXAMPLE 2 - SEISMIC DESIGN OF A DEEP FOUNDATION SYSTEM

Step 1: Design of Pile Group

- Piles are 12 m long
- Piles are octagonal 0.4 m diameter, driven concrete piles
- Piles are spaced 5 diameters apart (i.e., 2 m) center to center
- Piles are embedded 1 m (2.5 diameters) into the pile cap
- Each cap contains 6 piles
- Layout of piles is shown in Figure 3-5

Step 2: Evaluate Static Bearing Capacity

Static bearing capacity is evaluated using the Nordlund Method as outlined in NHI (1996). The idealized normalized and standardized SPT profile and the pile profile are shown in Figure 3-6. The ultimate bearing capacity, q_{ult} , is composed of a shaft resistance, R_s , tip resistance, R_T , such that $q_{ult} = R_s + R_T$.

$$q_{ult} = R_s + R_T$$

$$q_{ult} = \left[\sum_{d=0}^{d=D} K_{\delta} C_F p_d \frac{\sin(\delta + \omega)}{\cos \omega} C_d \Delta d \right] + [\alpha_t N'_q A_t p_t]$$

Normalized and Standardized SPT N Values (Blows/300mm)

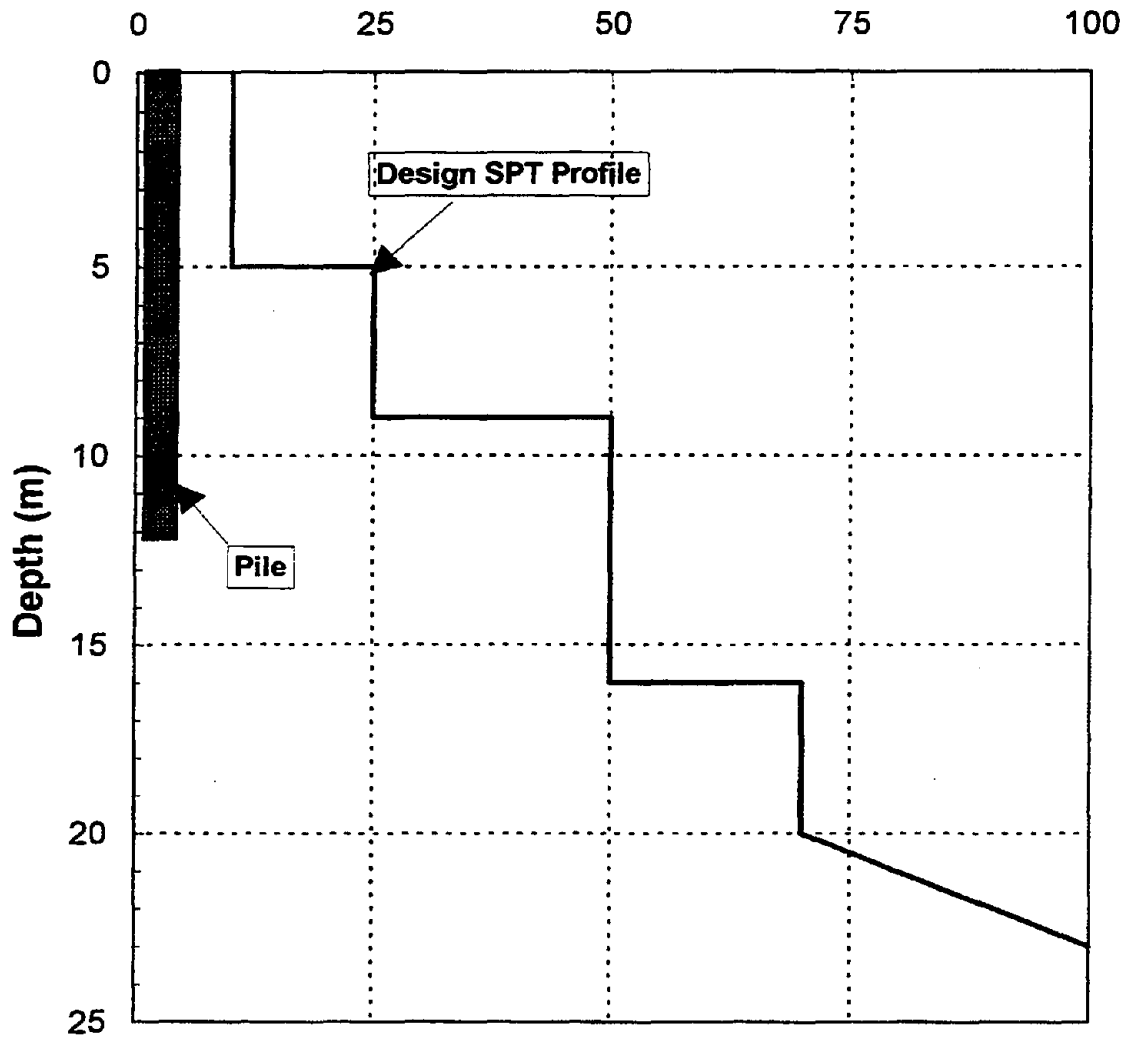


Figure 3-6: Pile and Idealized SPT Profile.

where: d = depth;
 D = embedded pile length;
 K_δ = coefficient of lateral earth pressure at depth d ;
 C_F = correction factor of K_δ when $\delta \neq \phi$;
 p_d = effective overburden pressure at the center of depth increment d ;
 δ = soil-pile friction angle;
 ω = angle of pile taper;
 C_d = pile perimeter at depth d ;
 Δd = length of pile segment;
 α_t = dimensionless factor (dependent on pile depth-width relationship);
 N'_q = bearing capacity factor;
 A_t = pile tip area; and
 p_t = effective overburden pressure at the pile tip.

- Compute Tip Resistance, R_T

$$R_T = \alpha_T N'_q A_t p_t$$

$$\alpha_T = 0.7 \text{ for } \phi = 38^\circ \text{ (NHI, 1996)}$$

$$N'_q = 100 \text{ for } \phi = 38^\circ \text{ (NHI, 1996)}$$

$$A_t = \pi r^2 = \pi(0.4 \text{ m}/2)^2 = 0.126 \text{ m}^2$$

$$p_t = (12 \text{ m})(19 \text{ kN/m}^3) = 228 \text{ kPa}$$

The limiting value of p_t is 150 kPa (NHI, 1996), therefore, $p_t = 150 \text{ kPa}$ and $R_T = (0.7)(100)(0.126 \text{ m}^2)(150 \text{ kPa}) = 1,325 \text{ kN}$

However, R_T is limited to $R_T = q_L A_t$.
 $q_L = 12,000 \text{ kPa}$ for $\phi = 38^\circ$ (NHI, 1996)
 $R_T \text{ limiting} = (12,000 \text{ kPa})(0.126 \text{ m}^2) = 1,510 \text{ kN}$ (does not govern)

$$\therefore R_T = 1,325 \text{ kN}$$

- Compute Shaft Resistance, R_s

$$R_s = \sum_{d=1}^{d=D} K_\delta C_F p_d \frac{\sin(\delta + \omega)}{\cos \omega} C_d \Delta d$$

For this calculation, the soil deposit has been divided into two layers as follows:

TABLE 3-2
STRATIGRAPHY AND STRENGTH PARAMETERS FOR THE TWO LAYERS

Layer	Depth Interval (m)	Friction Angle, ϕ (deg)
1	0-9	33
2	9-12	38

(see Section 3.2 of this document for a discussion of the values of ϕ)

Determine approximate circumference of pile, C_d .

$$C_d \approx 2\pi r = 2\pi(0.4\text{m}/2) = 1.26 \text{ m}$$

This is constant over the length of pile, i.e., the angle of the pile taper, $\omega = 0$.

Determine δ , the friction angle between pile and soil based on soil friction angle, ϕ . For a pre-cast concrete pile, $\delta/\phi = 0.72$ (NHI, 1996)

$$\delta_1 = (0.72)(33^\circ) = 24^\circ$$

$$\delta_2 = (0.72)(38^\circ) = 27^\circ$$

Determine for each material based upon displaced soil volume, V (NHI, 1996)

$$V_1 = V_2 = \frac{\pi r^2 \cdot 1\text{m}}{1\text{m}} = \frac{\pi \left(\frac{0.4}{2}\right)^2 \cdot 1\text{m}}{1\text{m}} = 0.126 \frac{\text{m}^3}{\text{m}}$$

for $\omega = 0$ (pile has no taper), using $V = 0.093 \text{ m}^3/\text{m}$ curve (approx.)

$$K_{\delta_1} = 1.15 + (0.6)(1.75-1.15) = 1.51$$

(interpolating between plots for $\phi = 30^\circ$ and $\phi = 35^\circ$)

$$K_{\delta_2} = 1.75 + (0.6)(3.00-1.75) = 2.5$$

(interpolating between plots for $\phi = 35^\circ$ and $\phi = 40^\circ$)

Determine correction factor, C_F , to be applied to K_s if $\delta \neq \phi$ (NHI, 1996)

$$C_{F_1} = 0.85 \text{ for } \delta/\phi = 0.72 \text{ and } \phi = 33^\circ$$

$$C_{F_2} = 0.80 \text{ for } \delta/\phi = 0.72 \text{ and } \phi = 38^\circ$$

Determine effective overburden pressure at midpoint of each layer, P_d .

$$P_{d_1} = (19 \text{ kN/m}^3)(4.5 \text{ m}) = 85.5 \text{ kPa}$$

$$P_{d_2} = (19 \text{ kN/m}^3)(10.5 \text{ m}) = 199.5 \text{ kPa}$$

Compute shaft resistance, R_s

$$R_s = R_{s_1} + R_{s_2}$$

$$R_s = (1.51)(0.85)(85.5 \text{ kPa})(\sin 24^\circ)(1.26 \text{ m})(9 \text{ m}) + (2.5)(0.80)(199.5 \text{ kPa})(\sin 27^\circ)(1.26 \text{ m})(3 \text{ m}) = 1,190 \text{ kN}$$

Compute Static Bearing Capacity

$$q_{ult} = R_s + R_t$$

$$q_{ult} = 1,325 \text{ kN} + 1,190 \text{ kN} = 2,515 \text{ kN}$$

Step 3: Calculate Loads on Piles

- Compute vertical loads on piles from preliminary values provided by the structural engineer using the average vertical compressive load and the load induced by the moment distribution:

$$p = \frac{Q}{n} \pm \frac{M \cdot d_i}{\sum_{i=1}^n d_i^2}$$

where: p = vertical load on pile;
 Q = static vertical load on pile cap;
 n = number of piles in group (6 for this example);
 d_i = distance from center of gravity of pile group to pile i ; and
 M = design moment.

Transverse direction (y direction):

$$Q = 3,110 \text{ kN}$$

$$M_y = 3,010 \text{ kN} \cdot \text{m}$$

$$\sum_1^6 d_i^2 = 4 \cdot (2\text{m})^2 + 2 \cdot (0\text{m})^2 = 16\text{m}^2$$

Piles on outer edge will experience the highest load. Calculated loads on each pile are listed on the following table:

**TABLE 3-3
LOADS ON INDIVIDUAL PILES (TRANSVERSE DIRECTION)**

Pile	Q/n (kN)	d (m)	$M_y d / \sum d^2$ (kN)
1	518	2	-376
2	518	0	0
3	518	2	376
4	518	2	-376
5	518	0	0
6	518	2	367

Note that the direction of action of M_y is arbitrary and piles 1 and 4 are symmetrical with respect to piles 3 and 6.

Longitudinal direction (x direction):

$$Q = 3,110 \text{ kN}$$

$$M_x = 903 \text{ kN} \cdot \text{m}$$

$$\sum_1^6 d_i^2 = 6 \cdot (1\text{m})^2 = 6\text{m}^2$$

TABLE 3-4
LOADS ON INDIVIDUAL PILES (LONGITUDINAL DIRECTION)

Pile	Q/n (kN)	d (m)	$M_x d / \Sigma d^2$ (kN)
1	518	1	-151
2	518	1	-151
3	518	1	-151
4	518	1	151
5	518	1	151
6	518	1	151

Note that the direction of action of M_x is arbitrary and piles 1, 2, and 3 are symmetrical with respect to piles 4, 5, and 6.

Calculate maximum and minimum pile loads by superimposing longitudinal and transverse moment loads.

TABLE 3-5
COMBINED LONGITUDINAL AND TRANSVERSE MOMENTS ON INDIVIDUAL PILES

Pile	Q/n (kN)	$M_y d / \Sigma d^2$ (Transverse Direction) (kN)	$M_x d / \Sigma d^2$ (Longitudinal Direction) (kN)	P (kN)
1	518	-376	-151	-9
2	518	0	-151	367
3	518	376	-151	743
4	518	-376	151	293
5	518	0	151	669
6	518	376	151	1,045

Step 4: Verify Factors of Safety

- Compression Loads

Maximum static load on any pile = 518 kN

Maximum vertical load on any pile = 1,045 kN

Ultimate compression capacity of each pile = 2,515 kN

$$FS_{\text{STATIC}} = \frac{2,515\text{kN}}{518\text{kN}} = 4.9$$

$$FS_{\text{SEISMIC}} = \frac{2,515\text{kN}}{1,045\text{kN}} = 2.4$$

These factors of safety are considered acceptable.

- Uplift Forces
The maximum uplift force on any pile is 9 kN. This force is significantly less than the ultimate capacity of the pile, so uplift capacity is adequate.

Step 5: Evaluate pile deflections

- Lateral deflection of the pile group

The effect of lateral forces on the piles was estimated using the program COM624 (Wang and Reese, 1991) in accordance with NHI, 1996 recommendations. Because pile spacing was 5D and the sand was dense, group interaction effects were ignored. Deformation of the pile is estimated to be 5 mm. COM624 input and output files are attached following these computation sheets.

Note: Maximum moment in pile from COM624 output (2.95×10^6 in. · lbs (333 m · kN)) must be compared to pile capacity for structural adequacy.

- Vertical deflection of foundation pile.

Maximum vertical seismic deflection is calculated assuming that all load is carried at the pile tip. This is a conservative assumption. More detailed computations can be made using the t - z curve method (see Chapter 9, Part I)

The vertical deflection of the foundation pile is calculated as the sum of the elastic deformation of the pile and the settlement of the soil at the pile tip. That is, $\delta_T = \delta_{PILE} + \delta_{SOIL AT TIP}$.

$$\delta_{PILE} = \frac{P_f \cdot L}{A \cdot E} = \frac{(527 \text{ kN})(12 \text{ m})}{(0.126 \text{ m}^2)(30,000,000 \text{ kPa})} \approx 2 \text{ mm} \approx 0.002 \text{ m}$$

where: E = Young's modulus (30,000,000 kPa for concrete);

A = cross sectional area of pile;

P_f = the maximum vertical load imposed by the earthquake including the effect of the moments = 376 kN + 151 kN = 527 kN; and

L = Length of pile.

$$\delta_{SOIL AT TIP} = \frac{0.96 P_f \sqrt{B} I_f}{(N_1)_{60}} \quad (\text{NHI, 1996})$$

$$\delta_{SOIL AT TIP} = \frac{0.96 \cdot 299 \cdot \sqrt{2.4} \cdot 0.5}{50} = 4.4 \text{ mm} = 0.004 \text{ m}$$

where: $\delta_{SOIL AT TIP}$ = estimated total settlement (mm) of soil;

$N' \approx (N_1)_{60}$ = average normalized and standardized SPT N value within a depth B below pile tip level;

P_f = foundation pressure due to seismic load (kPa);

I_f = influence factor for group embedment = $1 - [D / 8B] \geq 0.5$;

D = pile embedment depth (m);

B = width of pile group (m);

$$P_f = \frac{(527 \text{ kN/piles})(6 \text{ piles})}{(4.4 \text{ m})(2.4 \text{ m})} = 299 \text{ kPa}$$

$$I_f = 1 - [D / 8B] = 1 - [12 \text{ m} / 8 (2.4 \text{ m})] = 0.0375 \therefore I_f = 0.5$$

The vertical deflection of the pile is:

$$\delta_T = \delta_{\text{PILE}} + \delta_{\text{SOIL AT TIP}} \approx 2 \text{ mm} + 4 \text{ mm} \approx 6 \text{ mm} \approx 0.006 \text{ m}$$

Input Data COM624 Sample Printout

***** UNIT DATA. *****

SYSTEM OF UNITS
(UP TO 16 CHAR.)
ENGL

***** PILE DATA. *****

NO. INCREMENTS PILE IS DIVIDED	NO. SEGMENTS WITH DIFFERENT CHARACTERISTICS	LENGTH OF PILE	MODULUS OF ELASTICITY	DEPTH
48	1	.472E+03	.300E+08	.000E+00
TOP OF SEGMENT	DIAMETER OF PILE	MOMENT OF INERTIA	CROSS-SECT. AREA	
.000E+00	.160E+02	.302E+04	.195E+03	

***** SOIL DATA. *****

NUMBER OF LAYERS
2

LAYER NUMBER	P-Y CURVE CONTROL CODE	TOP OF LAYER	BOTTOM OF LAYER	INITIALSOIL MODULI CONST.	FACTOR 'A'	FACTOR 'F'
1	5	.000E+00	.354E+03	.225E+03	.000E+00	.000E+00
2	5	.354E+03	.472E+03	.225E+03	.000E+00	.000E+00

***** UNIT WEIGHT DATA. *****

NO. POINTS FOR PLOT
OF EFF. UNIT WEIGHT
VS. DEPTH
2

DEPTH BELOW TOP TO POINT	EFFECTIVE UNIT WEIGHT
.000E+00	.700E-01
.600E+03	.700E-01

***** PROFILE DATA. *****

NO. POINTS FOR
STRENGTH PARAMETERS
VS. DEPTH
3

DEPTH BELOW TOP OF PILE	UNDRAINED SHEAR STRENGTH OF SOIL	ANGEL OF INTERNAL FRICTION IN RADIANS	STRAIN AT 50% STRESS LEVEL
.000E+00	.000E+00	.576E+00	.200E-01
.354E+03	.000E+00	.663E+00	.200E-01
.500E+03	.000E+00	.663E+00	.200E-01

***** P-Y DATA. *****

NO. OF
P-Y CURVES
4

NO. POINTS ON

P-Y CURVES
9

X-COORD. TO
INPUT P-Y CURVE
.590E+02

DEFLECTION	SOIL RESISTANCE
.000E+00	.000E+00
.200E-01	.890E+02
.700E-01	.171E+03
.110E+00	.199E+03
.160E+00	.220E+03
.200E+00	.237E+03
.240E+00	.252E+03
.600E+00	.355E+03
.160E+02	.355E+03

X-COORD. TO
INPUT P-Y CURVE
.177E+03

DEFLECTION	SOIL RESISTANCE
.000E+00	.000E+00
.200E-01	.444E+03
.700E-01	.133E+04
.110E+00	.196E+04
.160E+00	.238E+04
.200E+00	.269E+04
.240E+00	.296E+04
.600E+00	.494E+04
.160E+02	.494E+04

X-COORD. TO
INPUT P-Y CURVE
.295E+03

DEFLECTION	SOIL RESISTANCE
.000E+00	.000E+00
.200E-01	.800E+03
.700E-01	.240E+04
.110E+00	.337E+04
.160E+00	.396E+04
.200E+00	.447E+04
.240E+00	.492E+04
.600E+00	.821E+04
.160E+02	.821E+04

X-COORD. TO
INPUT P-Y CURVE
.413E+03

DEFLECTION	SOIL RESISTANCE
.000E+00	.000E+00
.200E-01	.107E+04
.700E-01	.320E+04
.110E+00	.449E+04
.160E+00	.528E+04
.200E+00	.596E+04
.240E+00	.656E+04
.600E+00	.109E+05
.160E+02	.109E+05

**Output Data
COM624 Sample Printout**

DATA OUTPUT CODE	OUTPUT INCREMENT CODE	P-Y PRINTOUT CODE	NO. DEPTHS TO PRINT FOR P-Y CURVES
1	2	1	7

DEPTH FOR
PRINTING
P-Y CURVES

.500E+02
 .100E+03
 .150E+03
 .200E+03
 .250E+03
 .300E+03
 .350E+03

***** PILE HEAD (BOUNDARY) DATA. *****

BOUNDARY CONDITION CODE	NO. OF SETS OF BOUNDARY CONDITIONS	PILE HEAD PRINTOUT CODE	LATERAL LOAD AT TOP OF PILE	VALUE OF SECOND BOUNDARY CONDITION	AXIAL LOAD ON PILE
2	2	0	.220E+05	.000E+00	.226E+05
		1	.220E+05	.000E+00	.000E+00

***** CYCLIC DATA. *****

CYCLIC(0) OR STATIC(1) LOADING	NO. CYCLES OF LOADING
0	.000E+00

***** PROGRAM CONTROL DATA. *****

MAX. NO. OF ITERATIONS	TOLERANCE ON SOLUTION CONVERGENCE	PILE HEAD DEFLECTION FLAG (STOPS RUN)
200	.100E-02	.140E+02

COMG24G INPUT DATA
 OUTPUT DATA

GENERATED P-Y CURVES

THE NUMBER OF CURVES = 7
 THE NUMBER OF POINTS ON EACH CURVE = 17

***** WARNING *****

P-Y CURVES CANNOT BE GENERATED IN LAYERS WHERE
 P-Y CURVES ARE INPUT

1 1 CASE

UNITS--ENGL

 O U T P U T I N F O R M A T I O N

NO. OF ITERATIONS = 5
 MAXIMUM DEFLECTION ERROR = .991E-03 IN
 MAXIMUM MOMENT IMBALANCE FOR ANY ELEMENT = -.828E-01 IN-LBS
 MAX. LAT. FORCE IMBALANCE FOR ANY ELEMENT = .570E-02 LBS
 COMPUTED LATERAL FORCE AT PILE HEAD = .22000E+05 LBS
 COMPUTED SLOPE AT PILE HEAD = .14113E-17 IN/IN
 THE OVERALL MOMENT IMBALANCE = -.662E-01 IN-LBS
 THE OVERALL LATERAL FORCE IMBALANCE = -.578E-08 LBS
 PILE HEAD DEFLECTION = .171E+00 IN
 MAXIMUM BENDING MOMENT = -.295E+07 IN-LBS
 MAXIMUM TOTAL STRESS = .794E+04 LBS/IN**2
 MAXIMUM SHEAR FORCE = .426E+05 LBS

NO. OF ITERATIONS = 1
 MAXIMUM DEFLECTION ERROR = .181E-03 IN

PILE LOADING CONDITION

LATERAL LOAD AT PILE HEAD = .220E+05 LBS
 SLOPE AT PILE HEAD = .000E+00 IN/IN
 AXIAL LOAD AT PILE HEAD = .000E+00 LBS

X	DEFLEC	MOMENT	TOTAL STRESS	DISTR. LOAD	SOIL MODULUS	FLEXURAL RIGIDITY
IN	IN	LBS-IN	LBS/IN**2	LBS/IN	LBS/IN**2	LBS-IN**2

```

*****
.00 .171E+00 -.295E+07 .781E+04 .000E+00 -.526E+04 .906E+11
19.67 .165E+00 -.236E+07 .626E+04 .000E+00 -.311E+04 .906E+11
39.33 .149E+00 -.158E+07 .418E+04 .000E+00 -.875E+03 .906E+11
59.00 .126E+00 -.739E+06 .196E+04 .000E+00 .164E+04 .906E+11
78.67 .999E-01 .198E+05 .523E+02 .000E+00 .462E+04 .906E+11
98.33 .740E-01 .603E+06 .160E+04 .000E+00 .788E+04 .906E+11
118.00 .507E-01 .966E+06 .256E+04 .000E+00 .112E+05 .906E+11
137.67 .313E-01 .111E+07 .294E+04 .000E+00 .149E+05 .906E+11
157.33 .167E-01 .108E+07 .285E+04 .000E+00 .192E+05 .906E+11
177.00 .663E-02 .918E+06 .243E+04 .000E+00 .222E+05 .906E+11
196.67 .464E-03 .702E+06 .186E+04 .000E+00 .252E+05 .906E+11
216.33 -.271E-02 .480E+06 .127E+04 .000E+00 .281E+05 .906E+11
236.00 -.382E-02 .286E+06 .758E+03 .000E+00 .311E+05 .906E+11
255.67 -.371E-02 .138E+06 .365E+03 .000E+00 .341E+05 .906E+11
275.33 -.299E-02 .377E+05 .999E+02 .000E+00 .370E+05 .906E+11
295.00 -.210E-02 -.198E+05 .526E+02 .000E+00 .400E+05 .906E+11
314.67 -.128E-02 -.451E+05 .119E+03 .000E+00 .422E+05 .906E+11
334.33 -.653E-03 -.493E+05 .130E+03 .000E+00 .444E+05 .906E+11
354.00 -.231E-03 -.421E+05 .111E+03 .000E+00 .467E+05 .906E+11
373.67 .114E-04 -.305E+05 .809E+02 .000E+00 .489E+05 .906E+11
393.33 .124E-03 -.191E+05 .505E+02 .000E+00 .511E+05 .906E+11
413.00 .154E-03 -.998E+04 .264E+02 .000E+00 .533E+05 .906E+11
432.67 .141E-03 -.398E+04 .105E+02 .000E+00 .533E+05 .906E+11
452.33 .110E-03 -.860E+03 .228E+01 .000E+00 .533E+05 .906E+11
472.00 .746E-04 .000E+00 .000E+00 .000E+00 .533E+05 .906E+11

```

OUTPUT VERIFICATION

```

THE MAXIMUM MOMENT IMBALANCE FOR ANY ELEMENT = -.632E-01 IN-LBS
THE MAX. LATERAL FORCE IMBALANCE FOR ANY ELEMENT = .485E-02 LBS

COMPUTED LATERAL FORCE AT PILE HEAD = .22000E+05 LBS
COMPUTED SLOPE AT PILE HEAD = .00000E+00 IN/IN

THE OVERALL MOMENT IMBALANCE = .317E-01 IN-LBS
THE OVERALL LATERAL FORCE IMBALANCE = -.560E-08 LBS

```

OUTPUT SUMMARY

```

PILE HEAD DEFLECTION = .171E+00 IN
MAXIMUM BENDING MOMENT = -.295E+07 IN-LBS
MAXIMUM TOTAL STRESS = .781E+04 LBS/IN**2
MAXIMUM SHEAR FORCE = .426E+05 LBS
1 1 CASE

```

S U M M A R Y T A B L E

LATERAL LOAD (LBS)	BOUNDARY CONDITION BC2	AXIAL LOAD (LBS)	YT (IN)	ST (IN/IN)	MAX. MOMENT (IN-LBS)	MAX. STRESS (LBS/IN**2)
.220E+05	.000E+00	.226E+05	.171E+00	.141E-17	-.295E+07	.794E+04
.220E+05	.000E+00	.000E+00	.171E+00	.000E+00	-.295E+07	.781E+04

End COM624 Sample Output

3.5 SUMMARY AND CONCLUSIONS

A new highway will be built on a viaduct over an existing roadway and railroad tracks. Due to the relatively low bearing capacity of the near-surface soils and because it was necessary to minimize disruption to traffic, a pile foundation was selected. Precast concrete piles, 0.4 m in diameter driven in groups of six were used to support each column. The vertical and lateral static and pseudo-static loads were provided by the structural engineers.

The geotechnical investigation indicated that the top 5 m consisted of very loose fine sand underlain by about 4 m of silty sand with clay lenses. The bearing layer was identified to be a dense sand layer starting at depths of 10 m.

The static bearing capacity of each pile in the group was estimated based on methods presented in NHI (1996) to be 2,515 kN. The static factor of safety for the piles was 4.9.

The maximum pseudo-static load on any pile was calculated to be 1,045 kN, resulting in a seismic factor of safety of 2.4 for compressive loading. The maximum pseudo-static uplift force on any pile was estimated to be 9 kN, resulting in an adequate seismic factor of safety for uplift loading.

The lateral deflection due to seismic loading was estimated using the computer program COM624. The seismically-induced lateral deflection was estimated to be 5 mm. The upper bound vertical deformation was evaluated using NHI methods and assuming that all vertical loads were carried by the pile tip. The vertical incremental deflection due to seismic loading was estimated to be 6 mm.

CHAPTER 4

SITE RESPONSE ANALYSIS

4.1 INTRODUCTION

4.1.1 Description of the Project

A 4-m-high embankment will be built across a 12-m-thick clay deposit as part of a highway project in the northeast United States. The geotechnical engineer has been asked to evaluate both the free-field site response for design of an adjacent viaduct and the response of the embankment to ground motions with a 2-percent probability of being exceeded in 50 years. To perform the site response analysis, the following tasks need to be performed:

- develop the subsurface profile for dynamic analysis;
- evaluate seismicity information and select appropriate design earthquake parameters; and
- perform a site specific seismic response analysis for the design earthquake.

The site is located just outside of Boston, Massachusetts.

4.1.2 Source Materials Required

- Part 1 of this document;
- subsurface profile information;
- probabilistic earthquake acceleration maps (peak and spectral acceleration) for the continental United States (Frankel et. al, 1996);
- access to a catalog of strong motion records (USGS, NOAA, NCEER); and
- the computer program SHAKE91 (Idriss and Sun, 1992).

4.2 SITE CONDITIONS

4.2.1 Subsurface Profile

Figure 4-1 shows the subsurface profile for the site from the geotechnical investigation. Also shown on this figure is the geometry of the proposed embankment. As shown on Figure 4-1, the soil profile at the site consists of 2 m of high-plasticity organic silt underlain by 12 m of normally consolidated clay. The clay sits on top of 6 m of glacial till overlying weathered metamorphic rock bedrock. The water table is at the ground surface.

Beneath the embankment, the organic silt will be excavated and replaced with well-compacted sand backfill. The embankment itself will be built out of the same sand backfill material. The embankment will rise 4 m above grade and will be 40 m wide at the crest and 56 m wide at the base (i.e., side slopes will be at 2H:1V). The pile caps for the viaduct will be founded on top of the clay layer.

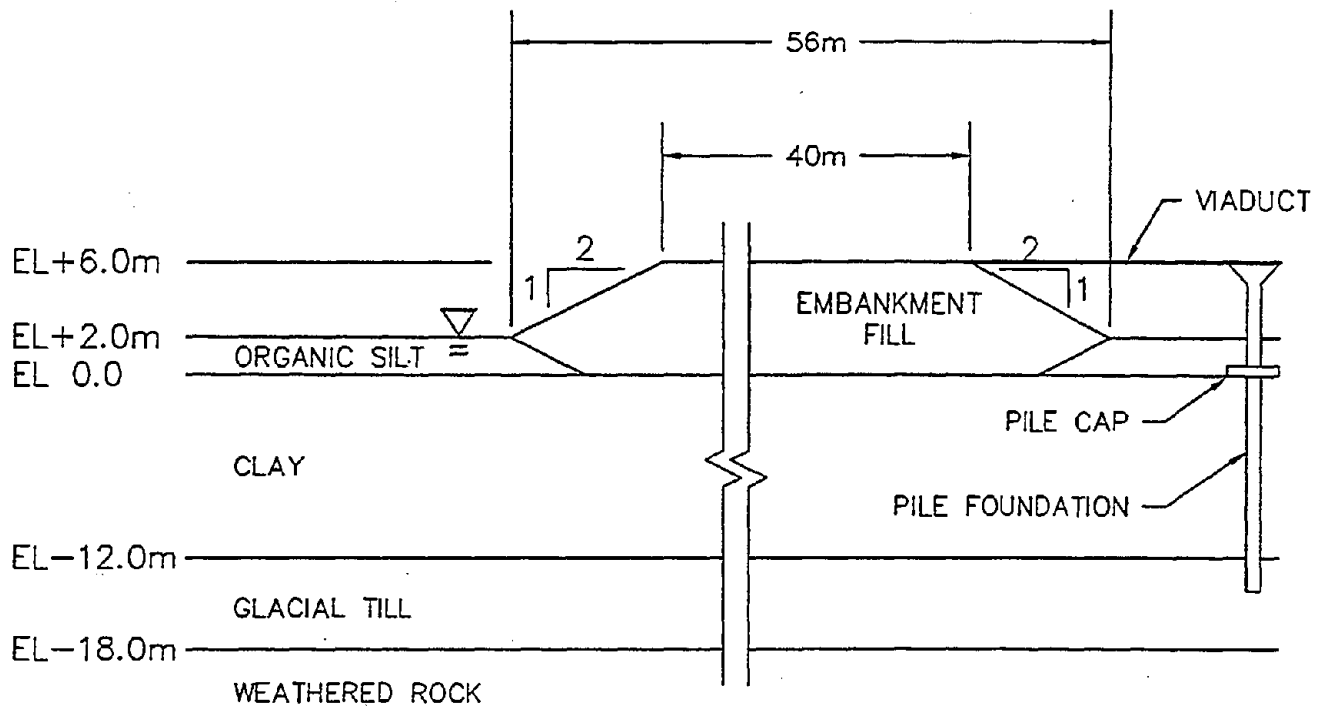


Figure 4-1: Site Profile for Site Response Analysis

4.2.2 Dynamic Soil Properties

Dynamic soil properties were estimated based upon the available geotechnical information and correlations with index properties. Table 4-1 presents a summary of available information from the geotechnical investigation. Available data indicated that the plasticity index for the organic silt was over 50, the total unit weight was 12 kN/m^3 , and the void ratio was 3. The mean effective stress at the center of the silt layer was estimated using Equation 5-12 from Part I and assuming $K_0 = 0.5$ as 1.47 kPa . Based upon the correlation of Jamiolkowski, et. al in Table 5-5 of Part I, the small strain shear modulus, G_{\max} , at the center of the silt layer was estimated as:

$$G_{\max} = \frac{625}{3^{1.3}} (100 \times 1.47)^{0.5} \times 1^k = 1,820 \text{ kPa}$$

The shear wave velocity for the silt was estimated using Equations 5-2 and 5-3 from Part I as:

$$V_s = \sqrt{G/\rho} = \left(1,820 \times \frac{9.8}{12} \right)^{0.5} = 39 \text{ m/s} \quad (5-2 \ \& \ 5-3)$$

The clay was normally consolidated with a plasticity index of 15, a total unit weight of 16 kN/m^3 , and a void ratio of 1.2 at the top of the layer and 1.0 at the bottom of the layer. Assuming $K_0 = 0.5$, the mean effective stress at the top of the clay was evaluated as 2.93 kPa . In the free-field at the top of the clay layer, G_{\max} was evaluated using the Jamiolkowski, et. al equation as:

$$G_{\max} = \frac{625}{12^{1.3}} (100 \times 2.93)^{0.5} \times 1^k = 8,440 \text{ kPa}$$

and the shear wave velocity was estimated as:

$$V_s = \left(8,440 \times \frac{9.8}{16} \right)^{0.5} = 72 \text{ m/s}$$

In the free-field at the bottom of the clay layer, the mean effective stress was calculated as 52.5 kPa, and G_{\max} was evaluated as:

$$G_{\max} = \frac{625}{1^{1.3}} (100 \times 52.5)^{0.5} \times 1^k = 45300 \text{ kPa}$$

and the shear wave velocity was estimated as:

$$V_s = \left(45300 \times \frac{9.8}{16} \right)^{0.5} = 167 \text{ m/s}$$

For the glacial till, the average normalized blow count was approximately 75. Therefore, based upon the Imai and Tonouchi equation in Table 5-5 of Part I, G_{\max} was estimated as:

$$G_{\max} = 15560(75)^{0.68} = 293000 \text{ kPa}$$

Assuming a total unit weight of 20.5 kN/m³, the shear wave velocity was estimated as:

$$V_s = \left(293000 \times \frac{9.8}{20.5} \right)^{0.5} = 375 \text{ m/s}$$

The weathered bedrock was assigned a unit weight of 21.2 kN/m³ and a shear wave velocity of 760 m/s (corresponding to the boundary between UBC Soil profiles S_b and S_c in Table 4-3 of Part I).

The embankment soil was assumed to be sand compacted to a relative density of 75 percent and a total unit weight of 19.5 kN/m³. Using the Seed, et. al equation in Table 5-5 of Part I and Figure 5-12 of Part I, G_{\max} at a depth 1 m below the top of the embankment was estimated assuming $K_o = 1$ (for near-surface compacted soil) as:

$$G_{\max} = 220(62)(19.5)^{0.5} = 60230 \text{ kPa}$$

and V_s was estimated as:

$$V_s = \left(60230 \times \frac{9.8}{19.5} \right)^{0.5} = 174 \text{ m/s}$$

One meter below the ground surface (1 m above the top of the clay), G_{\max} in the compacted sand backfill was estimated assuming $K_o = 0.6$ as:

$$G_{\max} = 220(62) \left(\frac{87.7 + 2(0.6)87.7}{3} \right)^{0.5} = 109390 \text{ kPa}$$

and V_s was estimated as:

$$V_s = \left(109390 \times \frac{9.8}{19.5} \right)^{0.5} = 234 \text{ m/s}$$

Calculations were also conducted for the shear wave velocity in the clay layer beneath the centerline of the embankment after embankment construction. At the top of the clay after embankment construction, G_{\max} was estimated using the Jamiolkowski, et. al correlation from Table 5-5 of Part 1 and assuming $K_o = 0.5$ as:

$$G_{\max} = \frac{625}{1^{1.3}} (100 \times 649)^{0.5} \times 1^k = 50350 \text{ kPa}$$

and the shear wave velocity was estimated as:

$$V_s = \left(50350 \times \frac{9.8}{16} \right)^{0.5} = 175 \text{ m/s}$$

At the bottom of the clay layer after embankment construction, G_{\max} was estimated as:

$$G_{\max} = \frac{625}{0.9^{1.3}} (100 \times 1145)^{0.5} \times 1^k = 76700 \text{ kPa}$$

and the shear wave velocity was estimated as:

$$V_s = \left(76700 \times \frac{9.8}{16} \right)^{0.5} = 217 \text{ m/s}$$

Modulus reduction and damping curves were assigned to the various materials using the curves in Figure 5-14 of Part 1 as follows:

- PI = 50 for the organic silt;
- PI = 15 for the soft clay;
- PI = 5 for the glacial till;
- PI = 0 for the embankment; and
- engineering judgement for the weathered rock.

Table 4-2 summarizes the dynamic properties for the various materials.

4.2.3 Fundamental Period

Using the properties summarized in Table 4-2, the fundamental period was calculated using Equation 4-5 from Part 1 for the following cases:

- the clay layer in the free-field;
- the clay layer beneath the embankment; and
- the embankment.

The average shear wave velocity of the clay layer in the free-field was calculated from the values in Table 4-2 for the top and bottom of the layer as:

$$(V_{s,AVE})_{FF} = (72+167)/2 = 120m/s$$

The fundamental period of the 12-m-thick clay layer was calculated as:

$$(T_o)_{FF} = \frac{4 \times 12}{120} = 0.4 s$$

The average shear wave velocity of the clay layer beneath the embankment was calculated from the values in Table 4-2 as:

$$(V_{s,AVE})_{BE} = (175+217)/2 = 196m/s$$

The fundamental period of the clay beneath the embankment was calculated as:

$$(T_o)_{BE} = \frac{4 \times 12}{196} = 0.25s$$

The fundamental period of the embankment was calculated using Figure 4-19 in Part I. Taking the height of the embankment as 6 m (including the compacted sand below ground surface), the embankment aspect ratio, λ , was calculated as:

$$\lambda = \frac{h}{H} = \frac{10}{16} = 0.625$$

Using linear interpolation, the factor a_n for Figure 4-19 of Part I is calculated as:

$$a_n = \frac{0.625-0.5}{1-0.5} (4.0-3.588) + 3.588 = 3.69$$

The average shear wave velocity of the embankment is calculated from the values at the top and bottom of the embankment in Table 4-2 as:

$$(V_{s,avg})_E = (174 + 234) / 2 = 204 \text{ m/s}$$

and the fundamental period of the embankment is calculated as:

$$(T_o)_E = \frac{3.69 \times 6}{204} = 0.11 \text{ s}$$

4.3 SEISMIC HAZARD ANALYSIS

4.3.1 Introduction

The seismic hazard analysis was based upon the maps produced by the USGS for the National Earthquake Hazard Reduction Project (NEHRP). Because of the importance of the facility and because of the uncertainty associated with use of a regional map, the decision was made to use a ground motion with a 2 percent probability of being exceeded in 50 years as the basis for design.

4.3.2 Response Spectra

Peak and spectral acceleration values corresponding to the design basis were downloaded from the USGS website at <http://geohazards.cr.usgs.gov/eq> using the "search by zip code" option. The response spectrum from the downloaded values is shown in Figure 4-2 along with the response spectra constructed using the 1997 Uniform Building Code. The peak acceleration from the USGS map for the site is 0.16 g and the peak spectral acceleration at 0.2, 0.3, and 1 second period are 0.31 g, 0.23 g, and 0.09 g, respectively. Beyond 1 second period, the spectral acceleration was assumed to decay as 1/T.

4.3.3 Magnitude Distribution

The distribution of earthquake magnitudes contributing to the response spectrum shown in Figure 4-2 was evaluated by downloading the deaggregated hazard values for Boston from the USGS website. Table 4-3 summarizes the magnitude contributions to the peak acceleration hazard from the deaggregated hazard data. Table 4-3 indicates that the magnitude contributions to the seismic hazard are broadly distributed from magnitudes less than 5.0 to as great as 7.5. While approximately 45 percent of the peak acceleration hazard is from events of magnitude equal to or less than magnitude 5.5, approximately 22 percent of the hazard is from events of magnitude greater than 6.5. The smaller magnitude events tend to be associated with distances of less than 25 km while the larger magnitude events tend to be associated with distances in the 50 to 100 km range. The spectral accelerations at larger periods are influenced more by the larger magnitude, more distant events. For instance, approximately 30 percent of the hazard for the spectral acceleration at 1 Hz frequency (1 second period) is from events of magnitude 7 to 7.5 with a predominant distance of 75 to 100 km and a mean distance of 225 to 250 km.

**TABLE 4-1
SUMMARY OF AVAILABLE INFORMATION**

	Unit Weight kN/m ³	PI (%)	OCR	(N ₁) ₆₀	D _r (%)	e _o
Embankment Fill	19.5	0	—	—	75	—
Organic Silt	12.0	50	1	—	—	3
Clay	16.0	15	1	—	—	1 - 1.2
Glacial Till	20.5	5	> 10	75	—	—
Weathered Rock	21.2	—	—	—	—	—

**TABLE 4-2
SUMMARY OF MATERIAL PROPERTIES**

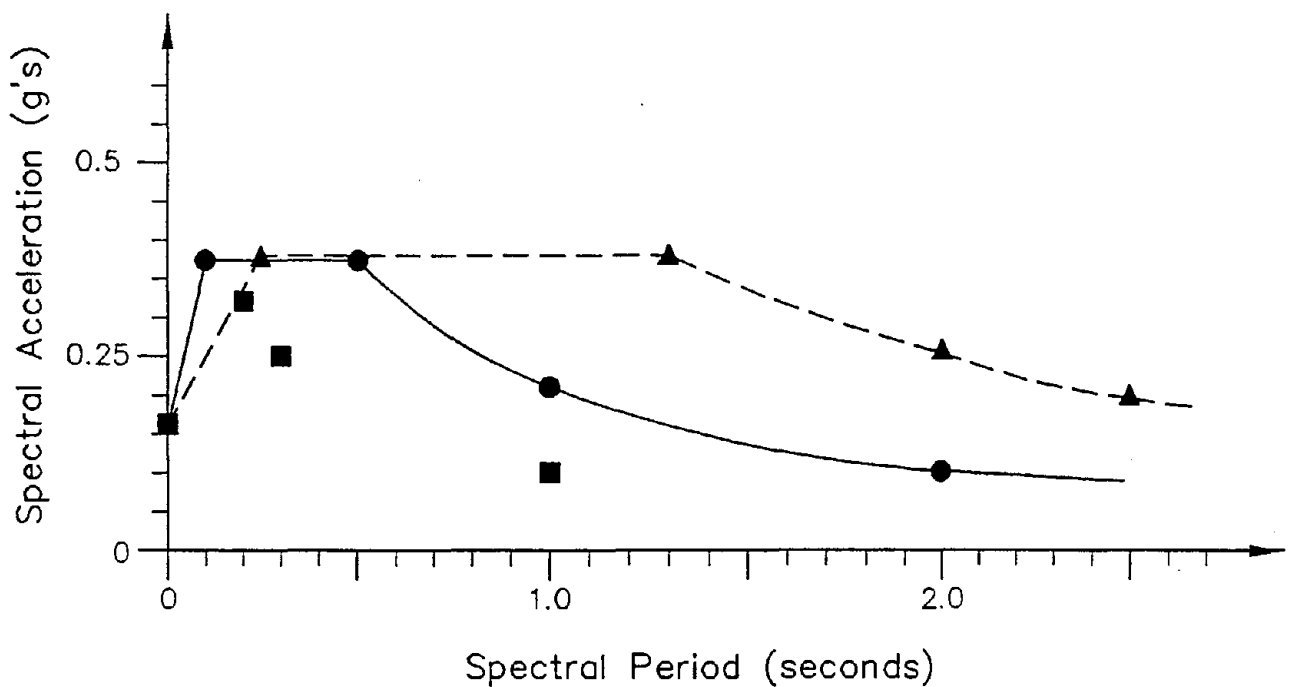
Material	Location	γ kN/m ³	σ' _v kPa	σ' _m kPa	G _{max} kPa	V _s m/s	Modulus Reduction and Damping
Embankment	1 m from top 1 m above clay	19.5	19.5	19.5	60,230	174	PI = 0
			87.7	64.3	109,390	234	
Organic Silt	Middle	12	2.2	1.5	1,820	39	PI = 50
Clay	Top	16	4.4	2.9	8,440	72	PI = 15
	Bottom		78.8	52.5	45,300	167	
	Top w/ Embankment		97.4	64.9	50,350	175	
	Bottom w/ Embankment		171.8	114.5	76,700	217	
Till	Middle	20.5	110.9	N/A	293,000	375	PI = 5
Bedrock	Everywhere	21.2	N/A	N/A	N/A	760	Judgement

**TABLE 4-3
SUMMARY OF DEAGGREGATED PEAK GROUND ACCELERATION
HAZARD DATA FOR BOSTON**

Magnitude ≤	5.0	5.5	6.0	6.5	7.0	7.5
Percent Contribution	22.3	21.3	18.5	16.2	10.7	11.0
Predominant Distance (km)	≤ 25	≤ 25	25-50	25-50	50-75	50-75
Mean Distance (km)	≤ 25	25-50	25-50	50-75	50-75	75-1

4.3.4 Selection of Time Histories

A suite of three time histories were selected to represent the design earthquake from the catalog of available strong motion records. These time histories were chosen from a collection of 10 pairs of time histories (20 records total) selected to represent earthquake ground motions in the northeastern United States for a Federal Emergency Management Agency-sponsored research project on the performance of steel structures (Somerville, et. al, 1998). These records may be downloaded from the website at "http://quiver.eerc.berkeley.edu:8080/studies/system/ground_motions.html" by U.C. Berkeley Earthquake Engineering Research Center (EERC). The selected ground motions include records from:



- USGS - 2% in 50 years (S_B - S_C Boundary)
- 1997 UBC Firm Ground (S_B - S_C Boundary)
- ▲ 1997 UBC Soft Soil (S_E)

Figure 4-2: Design Response Spectra

- the 1985 M_w 6.9 Nahanni Earthquake in the Northwest Territories (Canada);
- the 1988 M_w 5.9 Saguenay, Quebec earthquake; and
- a synthetic record for a simulated M_w 6.5 event.

The response spectra for the three selected time histories scaled to the design value of the peak ground acceleration are shown plotted against the target spectra in Figure 4-3a. Scaling to the target peak ground acceleration is typical for geotechnical analysis. The response spectra for the selected time histories scaled to the design value of the spectral acceleration at the fundamental period of the clay layer in the free-field, approximately 0.4 seconds, are plotted against the target spectra in Figure 4-3b. Scaling to the spectral acceleration of interest is typical for structural analysis.

4.4 SEISMIC RESPONSE ANALYSIS

4.4.1 Method of Analysis

Seismic response analyses were performed using the computer program SHAKE91. The following three different sets of analyses were conducted:

- free-field response analyses using time histories scaled to the peak ground acceleration;
- free-field response analyses using time histories scaled to the spectral acceleration at the 0.4 s spectral period; and
- embankment response using time-histories scaled to the peak ground acceleration.

The essential input on soil properties to SHAKE91 is summarized in Table 4-2. The effective strain factor used in the SHAKE91 analyses for each of the three time histories cited in Section 4.3.4 was different and was based upon the magnitude of the particular record and Equation 6-2 of Part I. The SHAKE91 input files for the free-field response and embankment analyses are presented at the end of this section.

4.4.2 Results of the Analysis

Figures 4-4 through 4-7 portray the results of the free-field response analyses. Figures 4-4 and 4-5 present the acceleration response spectra for the top of the clay layer plotted against the target response spectra for the input motions for the two different input motion cases (peak acceleration scaling and spectral acceleration scaling). Figures 4-6 and 4-7 compares the input motion response spectra for one time history, the Nahanni record, to the response spectrum at the top of the clay from the response analysis for both cases. These figure show the amplification of ground motions that occurs around the degraded fundamental period of the clay layer of approximately 0.6 s (the fundamental period of the clay increases as the modulus softens).

Figures 4-8 through 4-10 illustrate the results of the embankment response analyses. Figure 4-8 shows the response spectra at the top of the embankment from the three motions compared to the input motion target spectrum. Figure 4-9 shows the maximum shear stress versus depth within the embankment (proportional to the peak average acceleration) from each of the three motions. Figure 4-10 compares the response spectrum at the base of the embankment, the response spectrum at the top of the embankment, and the response spectrum from the free-field analyses (peak acceleration scaling) for the Nahanni record to illustrate the effect of the embankment on the free-field site response.

Figure 4-9 was used by the geotechnical engineer in pseudo-static slope stability analysis. The peak shear stress from the Saguenay record in this figure was divided by the overburden stress to evaluate the peak average acceleration for use in simplified Newmark analyses using the Hynes and Franklin and Makdisi and Seed charts (Figures 7-4 and 7-9 in Part I). The “smoothed” spectra in Figure 4-5 was provided to the structural engineer for analysis of the viaduct structural response.

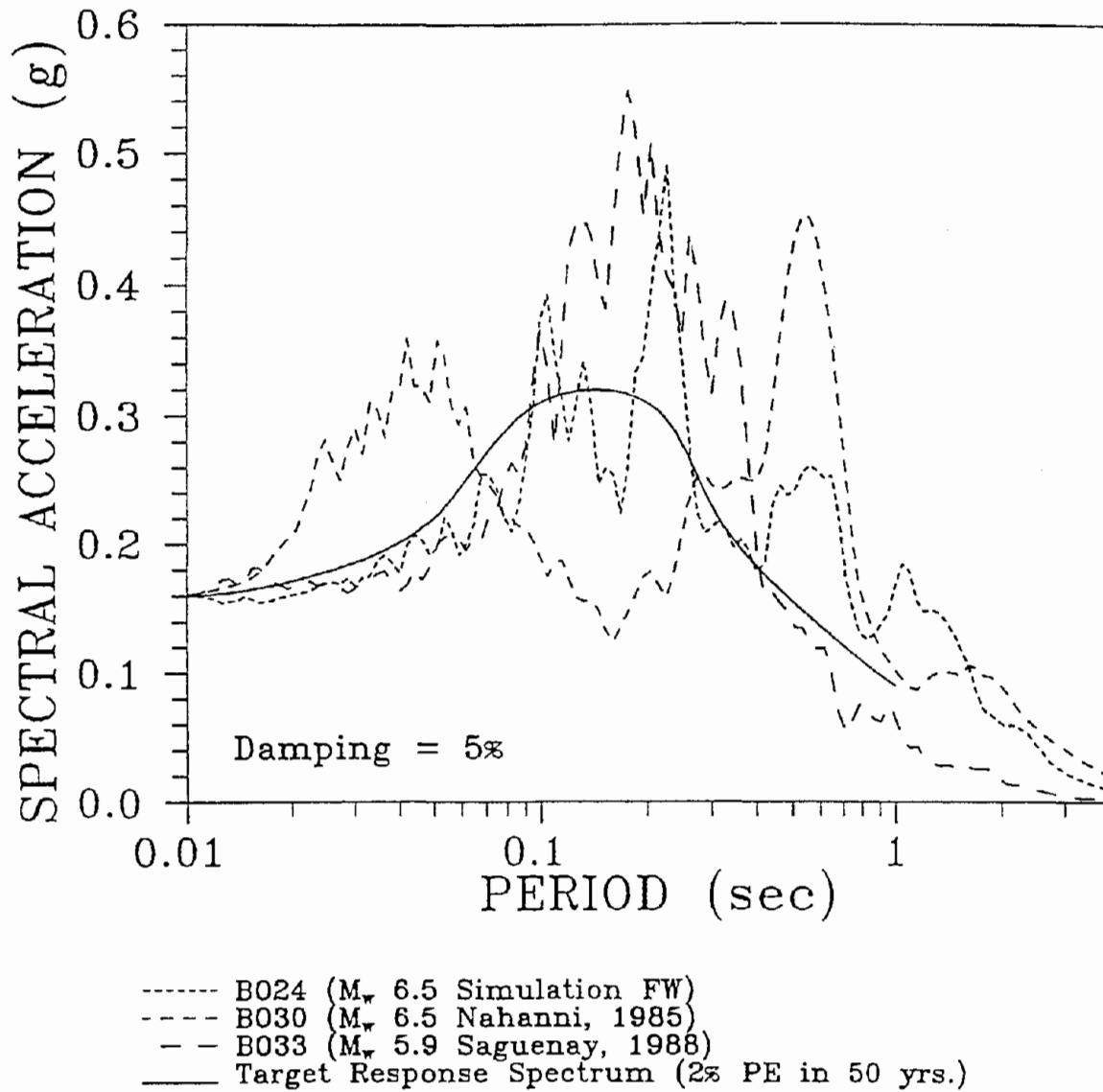


Figure 4-3a: Design Ground Motions- Peak Acceleration Scaling

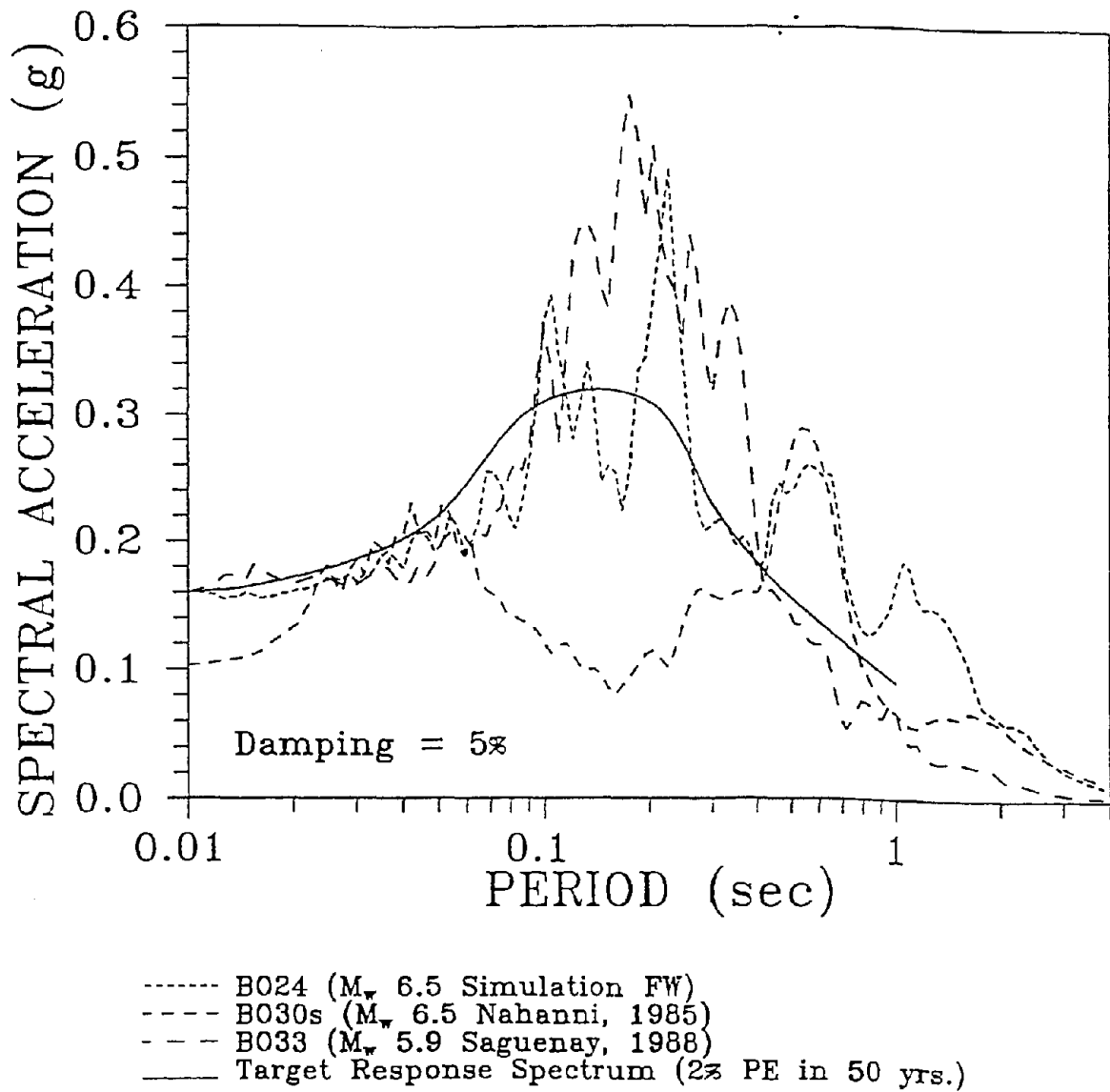


Figure 4-3b: Design Ground Motions- Spectral Acceleration Scaling

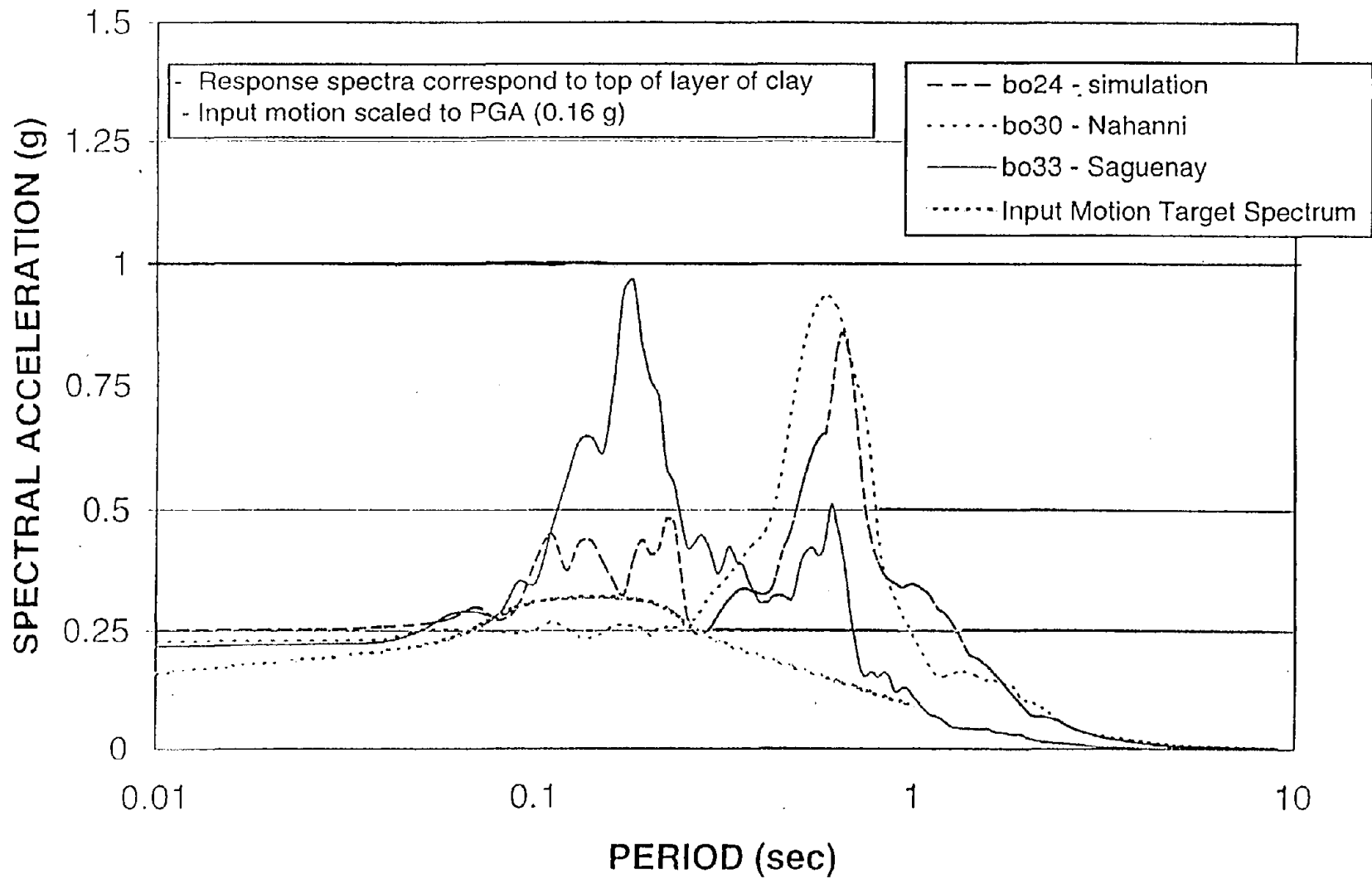


Figure 4-4: Free-Field Acceleration Response Spectra- Peak Acceleration Scaling

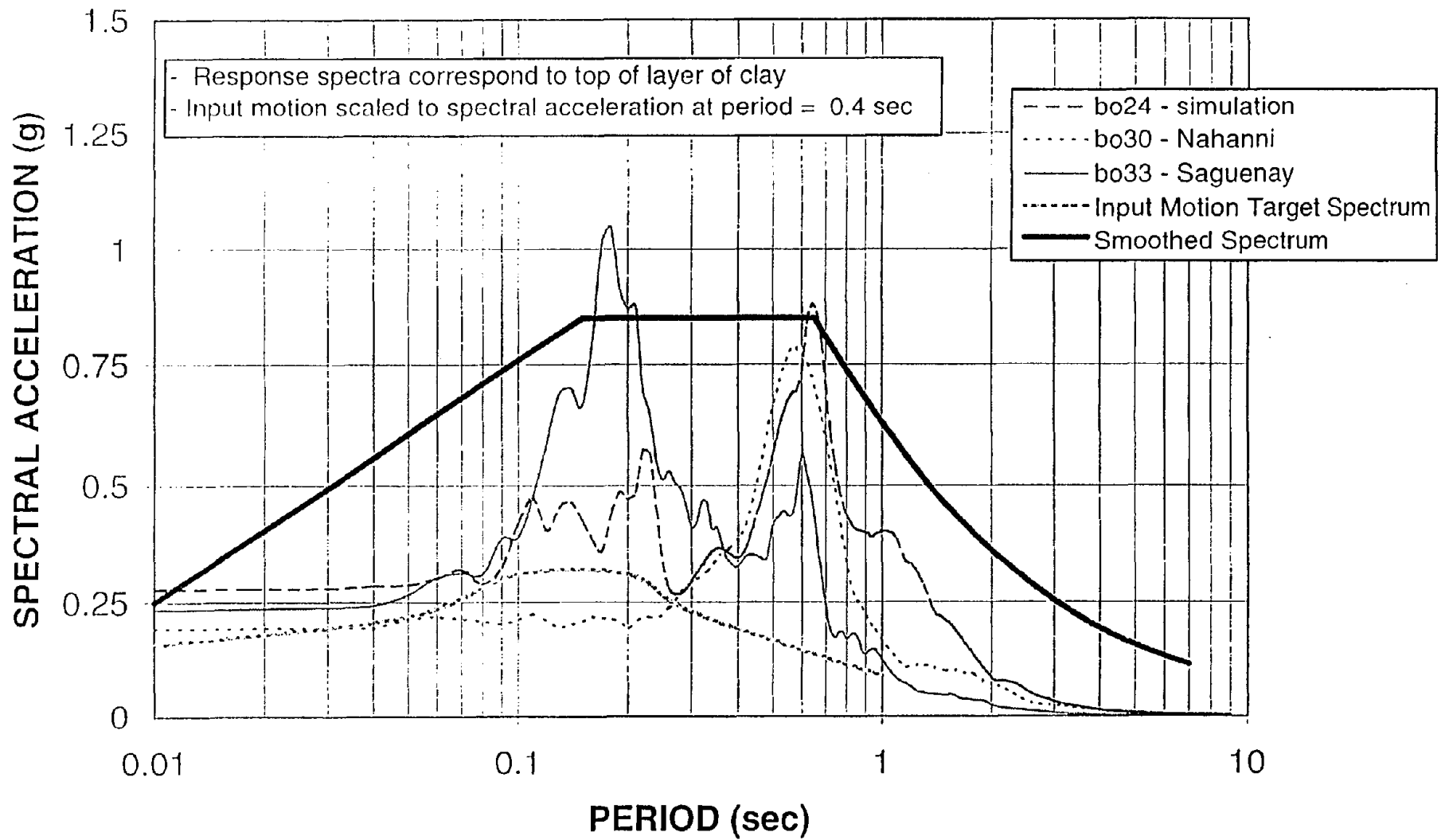


Figure 4-5: Free-Field Acceleration Response Spectra- Spectral Acceleration Scaling

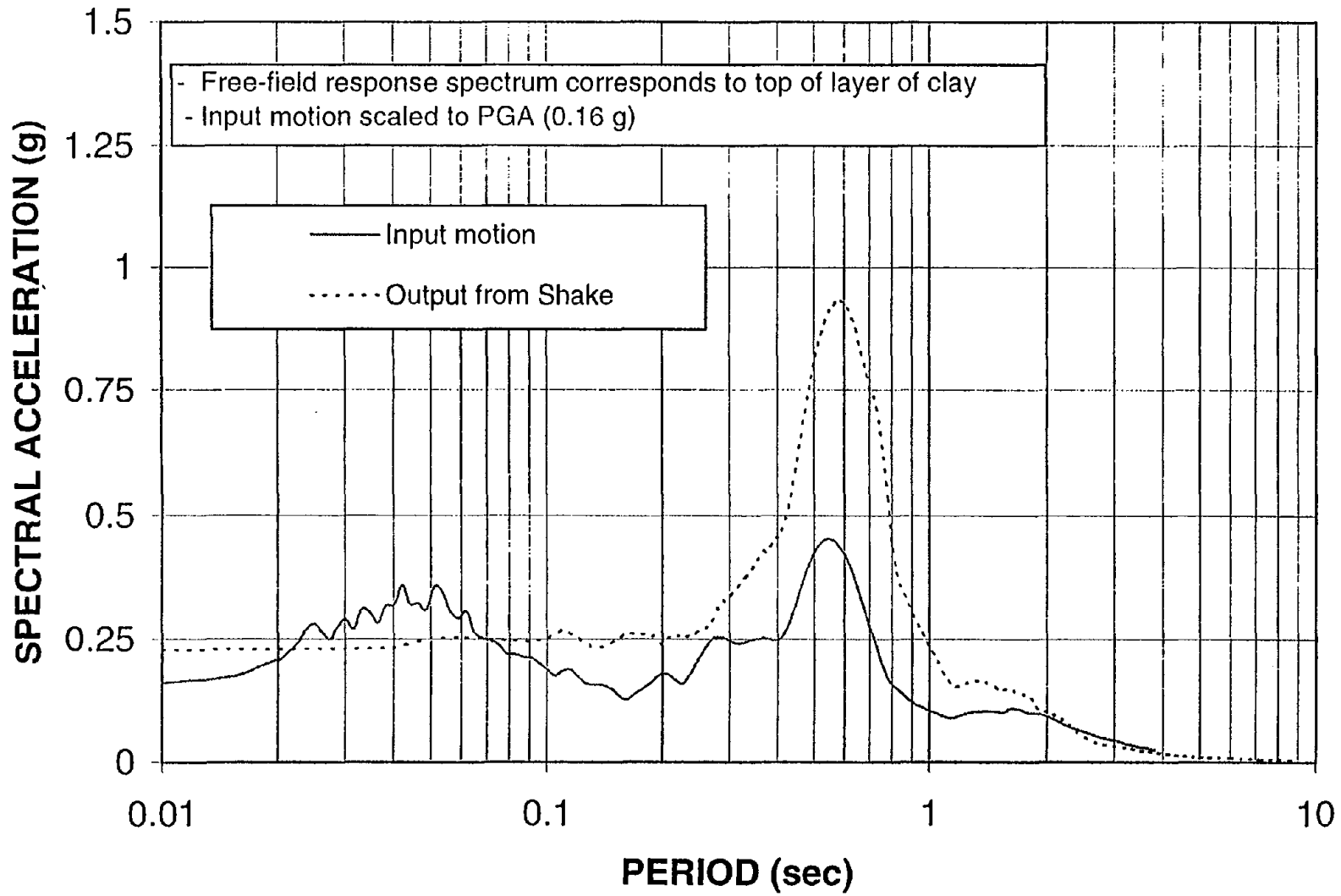


Figure 4-6: Acceleration Response Spectra- Peak Acceleration Scaling (Input vs. Free-Field for Nahanni Record).

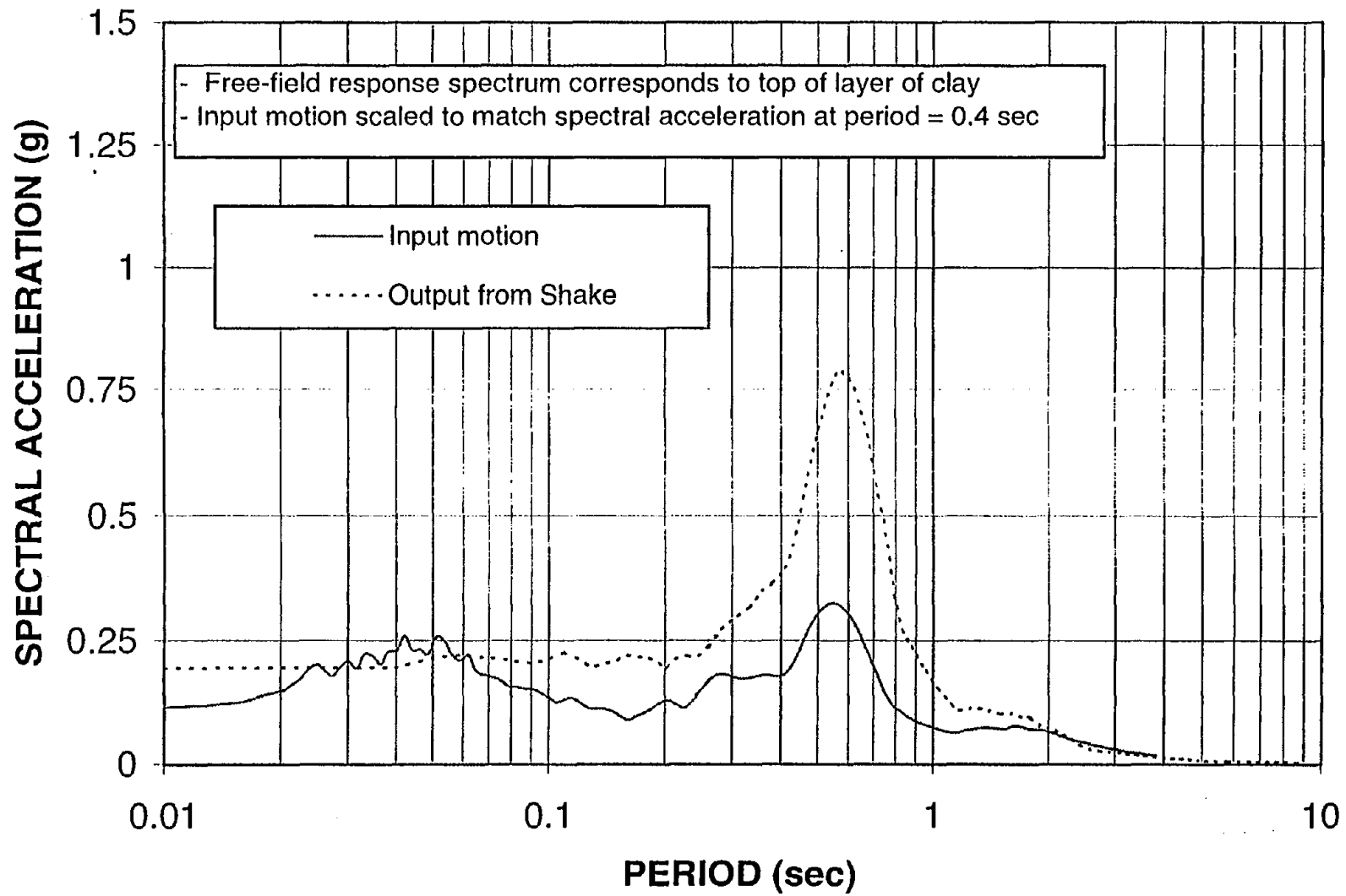


Figure 4-7: Acceleration Response Spectra- Spectral Acceleration Scaling (Input vs. Free-Field for Nahanni Record).

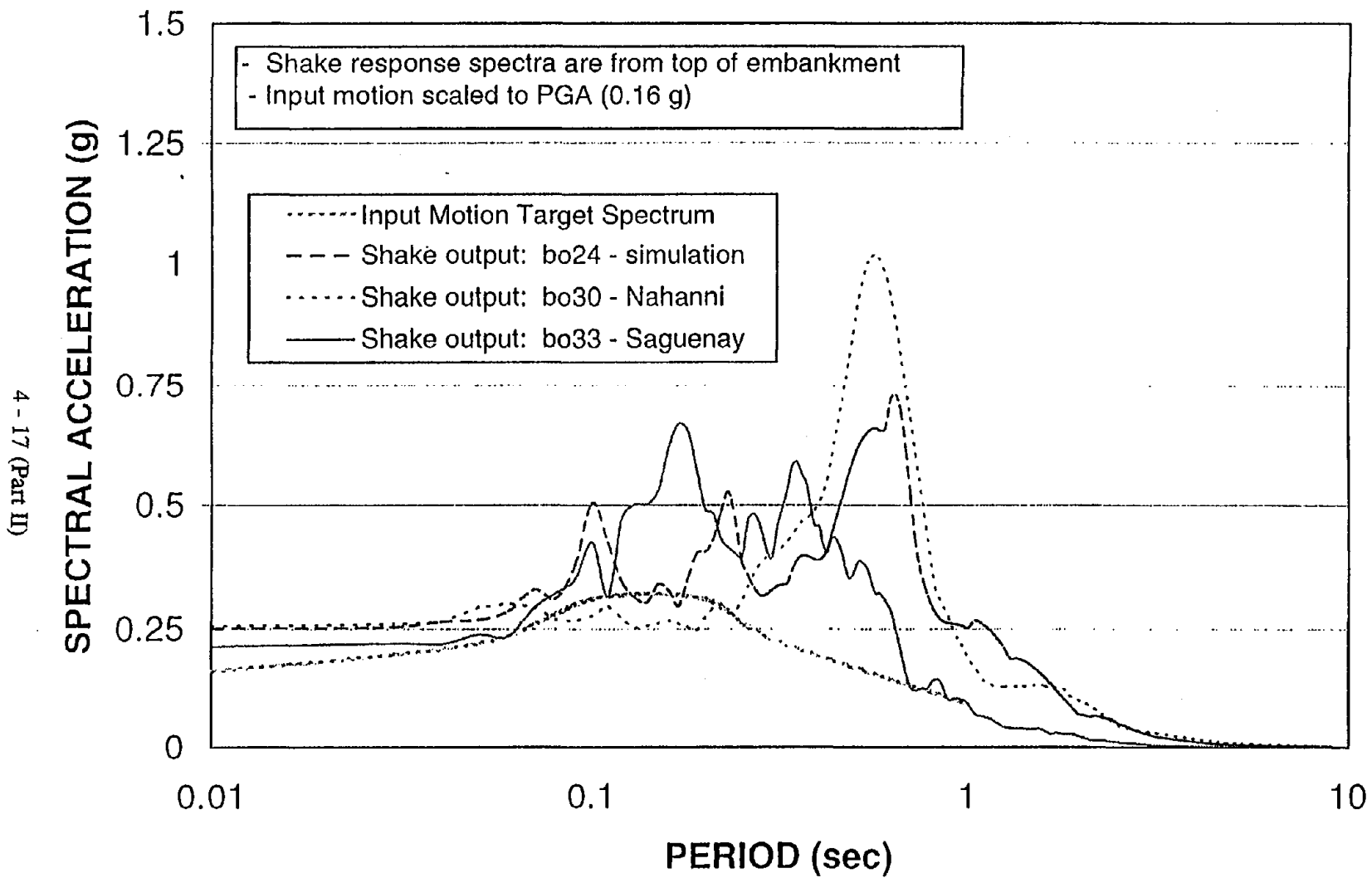


Figure 4-8: Acceleration Response Spectra- SHAKE Analysis vs. Target Spectra

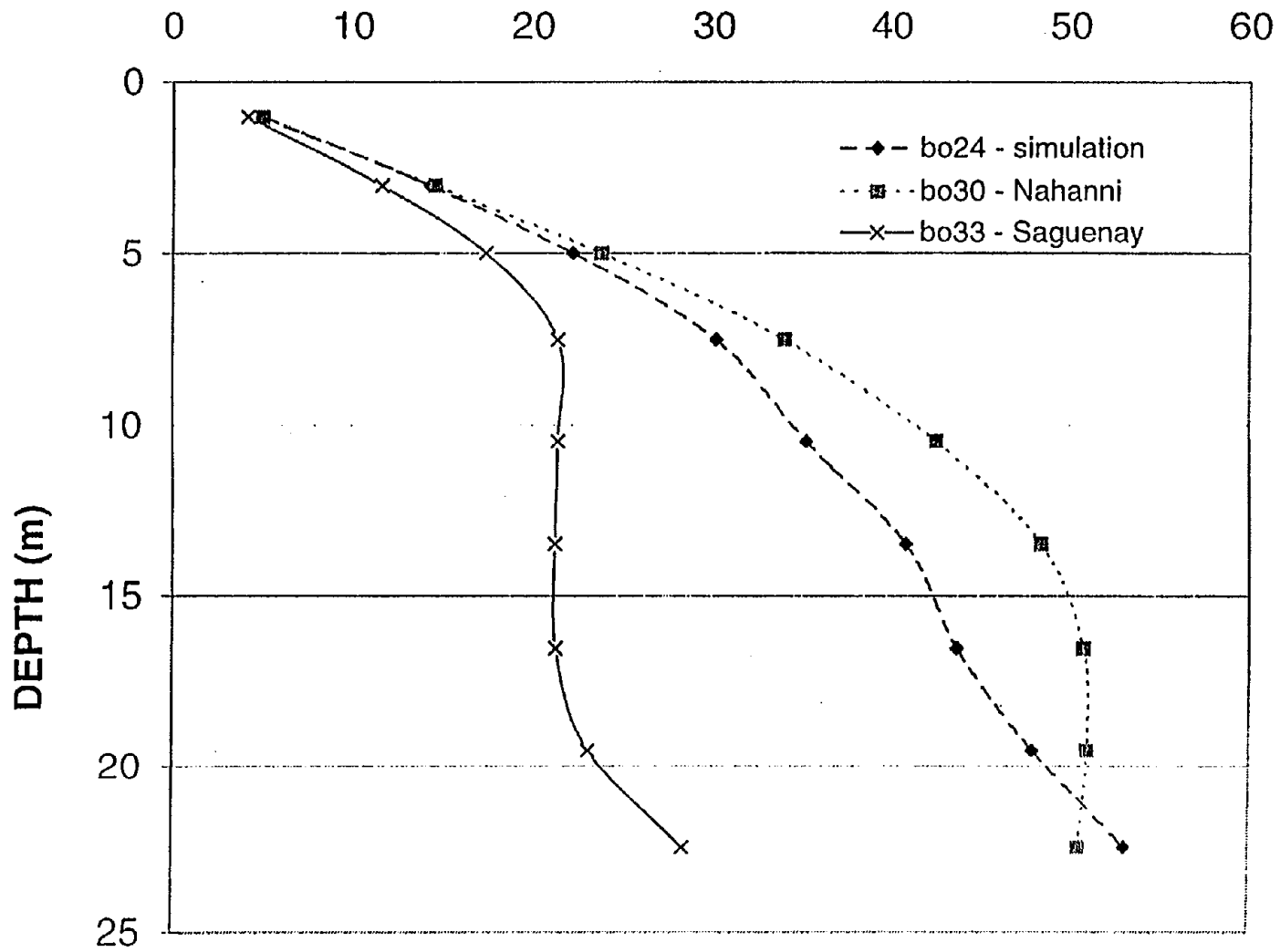


Figure 4-9: Maximum Shear Stresses with Depth.

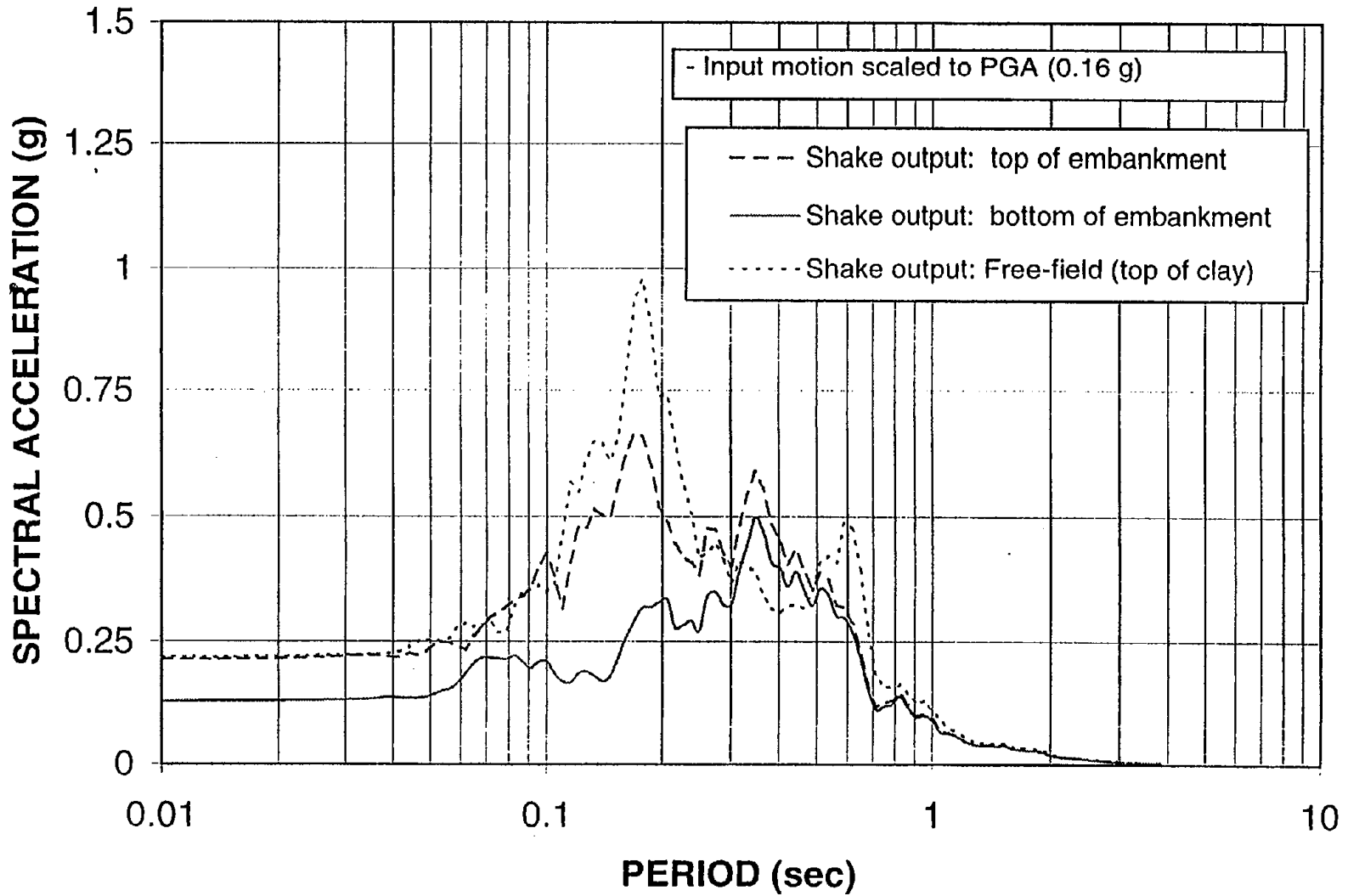


Figure 4-10: Acceleration Response Spectra- Embankment vs. Free-Field for Saguenay Record.

```

OPTION 1 - dynamic soil properties - (max is thirteen):
1
5
9 #1 Modulus for sand (PI=0) (Vucetic and Dobry, 1991)
0.0001 0.000316 0.001 0.00316 0.01 0.0316 0.1 0.316
1.
1.000 1.0 .960 0.87 0.715 0.49 0.25 0.1
0.02
9 #1 Damping for sand (PI=0) (Vucetic and Dobry, 1991)
0.0001 0.000316 0.001 0.00316 0.01 0.0316 0.1 0.316
1.
2.0 2.0 2.0 3.0 5.5 10.5 16.0 20.0
24.0
10 #2 Modulus for silt (PI=50) (Vucetic and Dobry, 1991)
0.0001 0.000316 0.001 0.00316 0.01 0.0316 0.1 0.316
1.
1.000 1.000 1.000 0.99 0.95 0.83 0.67 0.45
0.22
10 #2 Damping for sil (PI=50) (Vucetic and Dobry, 1991)
0.0001 0.000316 0.001 0.00316 0.01 0.0316 0.1 0.316
1.
2.0 2.0 2.0 2.0 3.0 4.1 6.0 9.3
13.2
9 #3 Modulus for CL (PI=15) (Vucetic and Dobry, 1991)
0.0001 0.0003 0.001 0.00316 0.01 0.0316 0.1 0.316
1.
1.000 1.000 1.000 0.95 0.810 0.63 0.400 0.200
0.1
9 #3 Damping for CL (PI=15) (Vucetic and Dobry, 1991)
0.0001 0.0003 0.001 0.00316 0.01 0.0316 0.1 0.316
1.
2.580 2.580 2.580 2.580 4.645 7.77 11.67 16.085
20.12
9 #4 Modulus for till (PI=5) (Vucetic and Dobry, 1991)
0.0001 0.0003 0.001 0.00316 0.01 0.0316 0.1 0.316
1.
1.000 1.000 0.980 0.900 0.77 0.51 0.32 0.16
0.06
9 #4 Damping for till not yet (PI=5) (Vucetic and Dobry, 1991)
0.0001 0.0003 0.001 0.00316 0.01 0.0316 0.1 0.316
1.
2.0 2.000 2.2 2.6 4.6 9.0 14.0 19.5
23.8
8 #5 ATTENUATION OF ROCK AVERAGE
.0001 0.0003 0.001 0.003 0.01 0.03 0.1 1.0
1.000 1.000 0.9875 0.9525 0.900 0.810 0.725 0.550
5 #5 DAMPING IN ROCK
.0001 0.001 0.01 0.1 1.
0.4 0.8 1.5 3.0 4.6
5 1 2 3 4 5
OPTION 2 -- Soil Profile
2
1 8 FHWA without embankment
1 2 6.56 0.05 0.076 128
2 3 9.84 0.05 0.102 275
3 3 9.84 0.05 0.102 353
4 3 9.84 0.05 0.102 431
5 3 9.84 0.05 0.102 509
6 4 9.84 0.05 0.131 1230
7 4 9.84 0.05 0.131 1230

```

```

8 5 0.10 0.135 2493
OPTION 3 -- input motion:
3
3752 4096 .005 bo30.sar (BF9.6)
0.16 25. 2 8
OPTION 4 -- sublayer for input motion (within (1) or outcropping (0):
4
8 0
OPTION 5 -- number of iterations & ratio of avg strain to max strain
5
0 8 0.59
OPTION 9 -- RESPONse
9
2 1
1 0 981
0.05
STOP -- execution will stop when program encounters 0
0

```

```

OPTION 1 - dynamic soil properties - (max is thirteen):
  1
  5
  9 #1 Modulus for sand (PI=0) (Vucetic and Dobry, 1991)
0.0001 0.000316 0.001 0.00316 0.01 0.0316 0.1 0.316
  1.
1.000 1.0 .960 0.87 0.715 0.49 0.25 0.1
  0.02
  9 #1 Damping for sand (PI=0) (Vucetic and Dobry, 1991)
0.0001 0.000316 0.001 0.00316 0.01 0.0316 0.1 0.316
  1.
2.0 2.0 2.0 3.0 5.5 10.5 16.0 20.0
24.0
  10 #2 Modulus for silt (PI=50) (Vucetic and Dobry, 1991)
0.0001 0.000316 0.001 0.00316 0.01 0.0316 0.1 0.316
  1.
1.000 3.16
  0.22 0.02
  10 #2 Damping for silt (PI=50) (Vucetic and Dobry, 1991)
0.0001 0.000316 0.001 0.00316 0.01 0.0316 0.1 0.316
  1.
2.0 2.0 2.0 2.0 3.0 4.1 6.0 9.3
13.2 18.0
  9 #3 Modulus for CL (PI=15) (Vucetic and Dobry, 1991)
0.0001 0.0003 0.001 0.00316 0.01 0.0316 0.1 0.316
  1.
1.000 1.000 1.000 0.95 0.810 0.63 0.400 0.200
  0.1
  9 #3 Damping for CL (PI=15) (Vucetic and Dobry, 1991)
0.0001 0.0003 0.001 0.00316 0.01 0.0316 0.1 0.316
  1.
2.580 2.580 2.580 2.580 4.645 7.77 11.67 16.085
20.12
  9 #4 Modulus for till (PI=5) (Vucetic and Dobry, 1991)
0.0001 0.0003 0.001 0.00316 0.01 0.0316 0.1 0.316
  1.
1.000 1.000 0.980 0.900 0.77 0.51 0.32 0.16
  0.06
  9 #4 Damping for till not yet (PI=5) (Vucetic and Dobry, 1991)
0.0001 0.0003 0.001 0.00316 0.01 0.0316 0.1 0.316
  1.
2.0 2.000 2.2 2.6 4.6 9.0 14.0 19.5
23.8
  8 #5 ATTENUATION OF ROCK AVERAGE
.0001 0.0003 0.001 0.003 0.01 0.03 0.1 1.0
1.000 1.000 0.9875 0.9525 0.900 0.810 0.725 0.550
  5 #5 DAMPING IN ROCK
.0001 0.001 0.01 0.1 1.
0.4 0.8 1.5 3.0 4.6
  5 1 2 3 4 5
OPTION 2 -- Soil Profile
  2
  1 10 FHWA with embankment
  1 1 6.56 0.05 0.124 571
  2 1 6.56 0.05 0.124 669
  3 1 6.56 0.05 0.124 768
  4 3 9.84 0.05 0.102 591
  5 3 9.84 0.05 0.102 626
  6 3 9.84 0.05 0.102 660
  7 3 9.84 0.05 0.102 695

```

```

  8 4 9.84 0.05 0.131 1230
  9 4 9.84 0.05 0.131 1230
  10 5 0.10 0.135 2493
OPTION 3 -- input motion:
  3
3752 4096 .005 bo30.sar (8F9.6)
  0.16 25. 2 8
OPTION 4 -- sublayer for input motion (within (1) or outcropping (0):
  4
  10 0
OPTION 5 -- number of iterations & ratio of avg strain to max strain
  5
  0 8 0.59
OPTION 9 -- RESPONSE
  9
  1 1
  1 0 981
  0.05
STOP -- execution will stop when program encounters 0
  0

```


CHAPTER 5.0

SLOPE STABILITY ANALYSIS

5.1 INTRODUCTION

5.1.1 Description of the Project

Construction of a new highway will require extensive excavation and regrading of a hillside. Figure 5-1 shows the original topography and the proposed final grading. The highest cut slope rises approximately 44 m above grade. The existing topography is at an average inclination of 2.9H:1V (Horizontal:Vertical) and the proposed final grading calls for 1.5H:1V slopes. In general, the hillside is composed of interbedded weak sedimentary rock that, in some cases, dips out of slope. To complete the seismic design of the slope, the following tasks need to be performed:

- develop a representative geological and geotechnical profile;
- perform a pseudo-static stability of the cut slope; and
- design slope stabilization measures, if needed.

The local highway department required minimum factors of safety of 1.5 for static conditions and 1.1 for pseudo-static conditions with a seismic coefficient equal to one-half the peak ground acceleration.

5.1.2 Source Materials Required

The source materials necessary to solve this problem includes:

- topography of the proposed cut;
- geologic and geotechnical information;
- seismological data;
- slope stability computer program such as STABL4; and
- Part I of this document.

5.2 SITE GEOLOGY

Previous investigations identified two bedrock formations and five classes of surficial deposits within the area. The surficial deposits include terrace deposits, landslide debris, colluvium, alluvium, and artificial fill. The bedrock formations consist of marine sediments. The bedrock formations are divided into an upper group of Miocene formations and an underlying group of Pliocene age formations.

The Pliocene formation group is a siltstone unit, exposed over much of the area. It is described in boring logs as a light tan sandy siltstone, clayey siltstone, and silty sandstone with local silty claystone interbed seams. It was reported that the siltstone bedrock materials are massive with thin interbedded sandstone layers and abundant gypsum- and clay-lined joints. Weak seams are typically parallel to bedding and, by definition, have lower shear strengths than the predominant bedrock. In slope areas where adverse (i.e., out-of-slope) bedding is present, these weak seams may provide a mechanism for slope instability.

Regionally, bedding planes generally dip toward the north except where there has been local deformation due to faulting and folding. This regional trend is inferred to exist at the site based upon previous mapping.

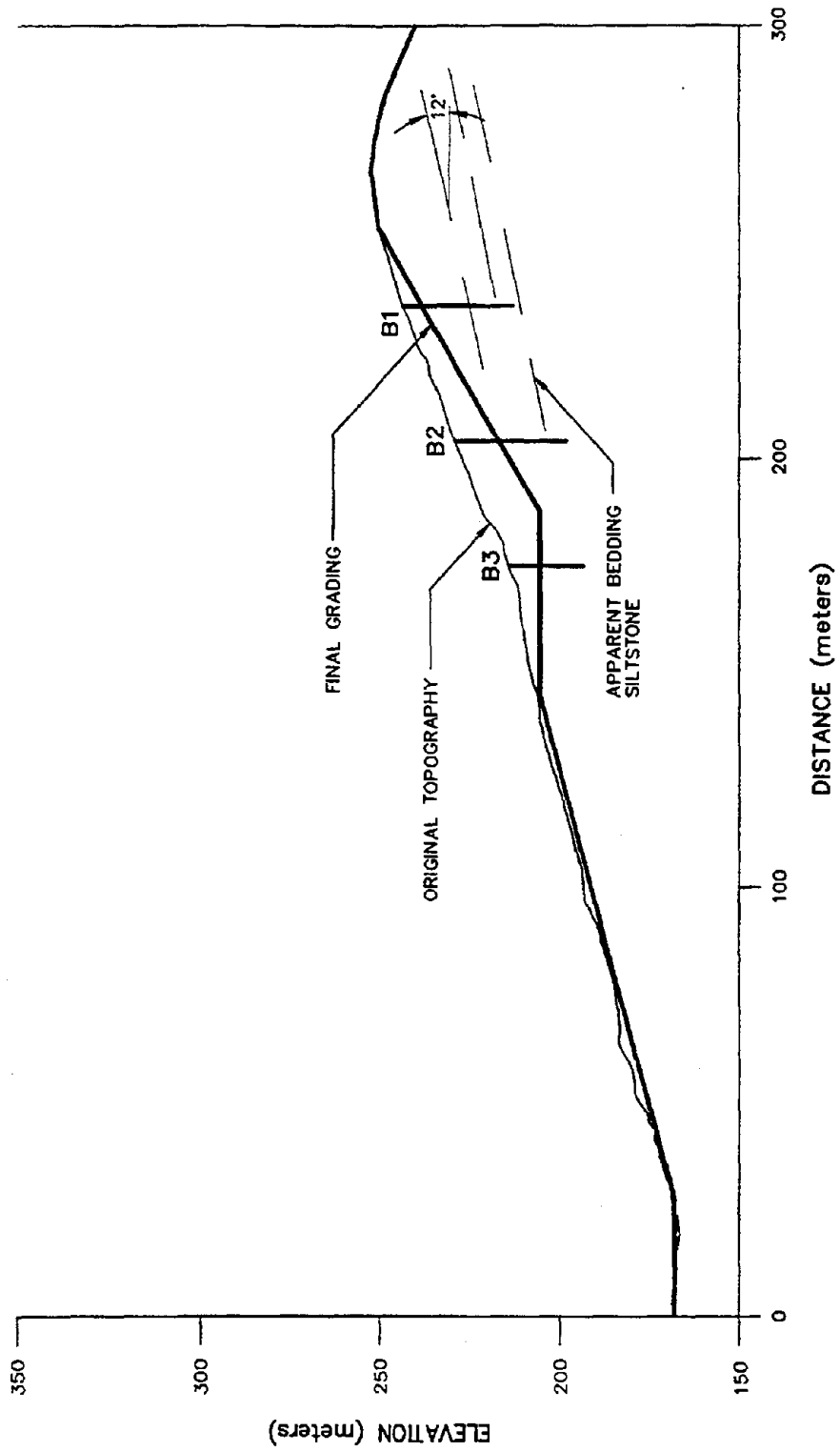


Figure 5-1: Original Topography and Proposed Grading.

5.3 GEOTECHNICAL EXPLORATION

5.3.1 General

Data from previous exploration programs and knowledge of the local geology indicate that the geomorphology will have a great influence on the stability of the cut slopes. Consequently, the geotechnical exploration program was designed to provide information on the orientation of the beds and on the shear strength of both the rock mass of the bedrock and on the bedding plane interfaces and weak seam material. To that effect, and to complement traditional borings and sampling procedures, a series of three 0.6-m-diameter test borings were excavated with a bucket auger. Downhole logging was performed in these borings to note bedding attitudes and to collect block samples for direct shear testing along bedding planes. The log of Boring B-1 is reported on Figure 5-2. The geologic lithology of the section analyzed in this example is predominantly siltstone. The bedding dips out of the proposed cut slope at an apparent angle of approximately 12 degrees.

5.3.2 Geotechnical Properties

Intact Rock

The claystone and siltstone materials within the different bedrock formations exhibit similar shear strength parameters. Based upon laboratory test results, a cohesion of 50 kPa, a friction angle of 35 degrees, and a unit weight of 18.8 kN/m³ were assigned to intact claystone and siltstone bedrock.

Bedding Plane/Claystone and Siltstone Seam Material

A limited number of laboratory direct shear and triaxial shear test results were performed on intact and remolded samples of claystone and siltstone material. Data on other claystone and siltstone strata of similar origins but different locations were also available. Due to the similarity in the index properties reported for these strata and those reported for material from the project site, and considering that these bedrock formations are marine deposits that are typically relatively uniform over large areas, the data from the other claystone and siltstone strata in the area were used in developing shear strength parameters for the stability analyses. In addition to this laboratory data, there were a number of landslides in the area from which shear strengths could be back calculated.

Analysis of this data indicated that the peak shear strength of the claystone and siltstone materials could be conservatively characterized by a lower bound strength envelope with a friction angle of 19 degrees and cohesion of 50 kPa. Based largely on strength parameters back-analyzed from landslides in the same formations, a friction angle of 12 degrees and a cohesion value of 10 kPa were assigned to the residual shear strength parameters for the claystone and siltstone seam material. A unit weight of 18.8 kN/m³ was assigned to the claystone and siltstone seam material. The shear strength envelopes for the different materials are reported on Figure 5-3.

5.4 DETERMINISTIC SEISMIC HAZARD ANALYSIS

The project site is located about 7.5 km from a strike-slip fault capable of generating a maximum credible earthquake (MCE) with a moment magnitude, M_w , of 7. In order to evaluate the value of maximum horizontal acceleration at the site from the MCE, five different attenuation relationships for rock sites were considered.

LAYER DEPTH (M)	MATERIAL DESCRIPTION	ATTITUDE	SYMBOLIC LOG	EL. (M)	SAMPLES		COMMENTS
					NUMBER	SYMBOL	
	Bedrock on surface, very dry Buff colors some gravel, siltstone some sand.						Monitor with PID: Oppm O2 = 16.3 at bottom exp = 0% Will pump O2 downhole during logging
4.0	Light to medium grey, clayey diatomaceous siltstone	N85W 19S		805			
6.0	3 cm. Sandstone, grey, ironstained Back to dense grey siltstone as above						
9.0	Slickenside surface in clayey siltstone 2 cm. thick very clayey, medium to dark grey silty claystone with slickensides. Orange stained sand 1/4 to 1/2" thick Dense, medium grey siltstone again	N88E 21S		800	S1		
		N45W 45NE		785			
15.0	Dense siltstone as above	N80E 20S		790	S2	90	
		N10E 25SE					
21.0					S2		
22.5	21-22.5 m. Hard brittle zone (hard and chipped) breaks irregularly - a bit cemented in siltstone still. Siltstone as above	N85W 24S		785			
25.5	Hard zone same as 21-22.5 m. above						
27.0	27-28 m. Hard cemented siltstone tan to medium grey Back to medium grey siltstone, more cemented than as above - shaley siltstone, hard to chip out.			780	S3		
31.0	15 cm. very well cemented siltstone, light tan as zone 27-28 m. Grey siltstone, cemented	N56W 22SW			S4		
34.0		N35E 8SE		775			
35.0	large gravel/cobbles cemented siltstone 4" thick light tan/orange tan highly cemented siltstone. Back to grey siltstone, firm and hard thin bedded	N75W 22SW N8E 6SE		770	S4	95	
40.0	Due to unstable rock, downhole logging completed at Total depth 40 m						
		N55W 13SW					

CONTRACTOR		NORTHING	776.7
EQUIPMENT	CME 75	EASTING	2816.6
DRILL MTHD	BUCKET AUGER	ANGLE	Vertical
DIAMETER	24 cm	BEARING	---
LOGGER TW/EH	REVIEWER THH	PRINTED	18 MAR 96

REMARKS:
SEE KEY SHEET FOR SYMBOLS AND ABBREVIATIONS

Figure 5-2: Example 4 Boring Log.

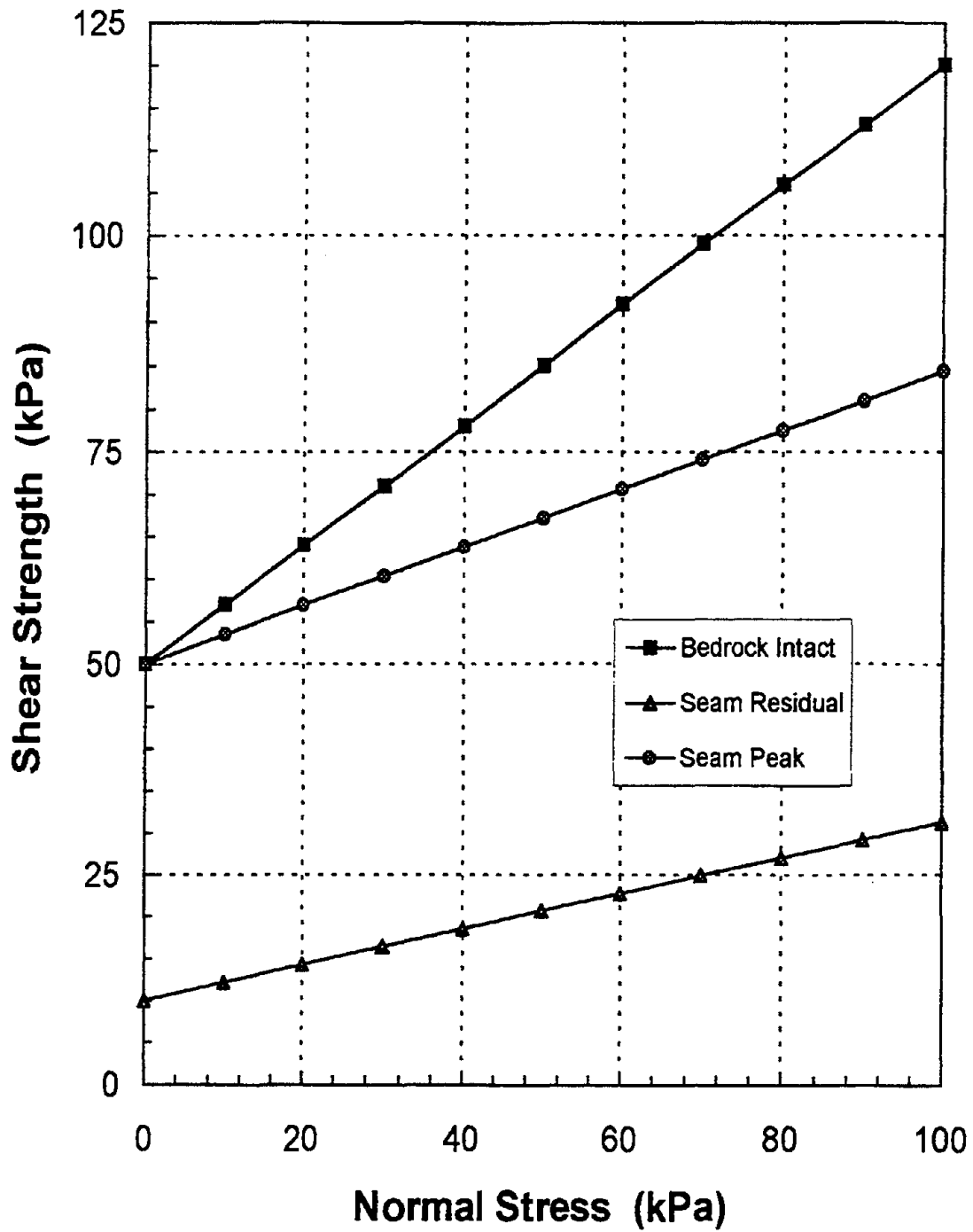


Figure 5-3: Shear Strength Envelopes for Site Materials.

Figure 5-4 illustrates the calculation of the MCE peak ground acceleration. This figure provides the reference for each attenuation relationships and the mean and mean plus one standard deviation peak ground acceleration at the site for each attenuation relationship.

The average of the mean values of peak ground acceleration, 0.4 g, will be used in the design.

5.5 SLOPE STABILITY ANALYSIS

5.5.1 Design Criteria

The slope stability criteria imposed by local regulators required a minimum static factor of safety of 1.5. For seismic conditions, a factor of safety of 1.0 when using a seismic coefficient equal to $0.5 a_{\max}/g$ in a pseudo-static limit equilibrium analysis was considered acceptable. The rationale for this seismic design criterion is discussed in Section 7.2.2 of Part I. The seismic coefficient established using this criteria was $(0.5)(0.4g)/g = 0.20$.

The shear strength parameters used in the long term static stability were the peak values for the intact rock and the residual values for the claystone and siltstone seams. The shear strength parameters used in the pseudo-static seismic (short term) analysis were the peak values for both the intact rock and the claystone and siltstone seams.

5.5.2 Stability Analyses

The computer program STABL4 (Lovell, *et al.*, 1984) was used to assess the stability of the slope. STABL4 employs limit equilibrium principles to provide general solutions to slope stability problems using the Modified Bishop or Modified Janbu methods to calculate factors of safety. Potential sliding surfaces can be pre-specified or randomly generated. The Modified Janbu method was used for the slope stability analyses performed herein.

Both circular and planar failure surfaces were evaluated. Planar failure surfaces generated for analysis considered the presence of weak zones such as the claystone and siltstone seams. The locations of the potential failure surfaces were varied in the slope stability analyses to evaluate the depth to the potential failure surface (the seam of weak material along the bedding).

The STABL4 input and output for the critical surface (the surface with the lowest pseudo-static factor of safety) are provided following this design example.

5.6 RESULTS

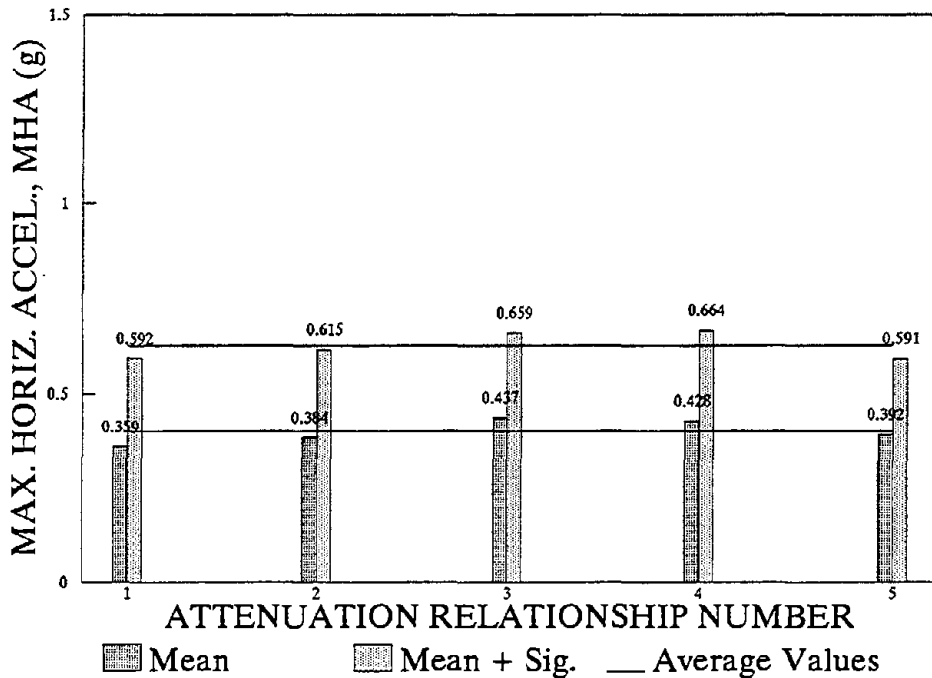
Figure 5-5 shows the most critical failure mechanisms for the slope. A wedge analysis was performed assuming sliding along the weak seam dipping at a 12-degree angle out of slope. The minimum calculated factor of safety under static loading conditions is 0.95. Under a seismic coefficient of 0.2, the pseudo-static factor of safety of the slope is 0.93, which is also not sufficient, as shown on Figure 5-6.

Figures 5-7 and 5-8 show the stability analysis for circular deep seated failures under static and pseudo-static conditions. The analyses using circular surfaces give higher factors of safety than the wedge analyses, indicating that stability is controlled by the strength of the weak seams in the rock mass.

MHA VALUES BY SELECTED ATTENUATION RELATIONSHIPS

Mw = 7.0

SITE TO SOURCE DISTANCE = 7.5 km



Attenuat. Relat. Number	SELECTED ATTENUATION RELATIONSHIPS ROCK SITES / STRIKE-SLIP FAULTS		MAX. HORIZONTAL ACCELERATION	
	Reference	Summary	Mean	Mean + Sig.
1	Campbell, K.W. (1993) "Empirical Prediction of Near-Source Ground Motion From Large Earthquakes," Proc. Internat. Workshop on Earthquake Hazard and Large Dams in the Himalaya, Sponsored by the Indian National Trust for Art and Cultural Heritage (INTACH), New Delhi, India, 7 p. (plus Appendices).	Hard Rock (< 10 m of Sediments) Updated by Near Source Events Strong Earthquakes (M = 8) World-Wide Data Set Focal Depth < 25 km	0.359	0.592
2	Boore, D.M., Joyner, W.B. and Fumal, T.E. (1993) "Estimation of Response Spectra and Peak Accelerations From Western North America Earthquakes: An Interim Report," U.S. Geological Survey Open File Report 93-509, 15 p.	M _w Western U.S. Data Set M < 7.5; R < 80 km Shallow Earthquakes (< 20 km) <i>Prediction of Larger Horizont. Comp.</i>	0.384	0.615
3	Sadigh, K., Chang, C.-Y., Abrahamson, N.A., Chiou, S.J., and Power, M.S. (1993) "Specification of Long-Period Ground Motions: Updated Attenuation Relationships for Rock Site Conditions and Adjustment Factors for Near-Fault Effects," Proc. ATC-17 Seminar on Seismic Isolation, Passive Energy Dissipation, and Active Control, Applied Technology Council, Vol. 1, 59-70.	Rock Sites West. U.S. + World-Wide Data Set Shallow Earthquakes (< 20 km) M = < 8; Near Fault Option <i>Both Horiz. Components Considered</i>	0.437	0.659
4	Silva, W.J. and Abrahamson, N.A. (1993) "Attenuation of Long Period Strong Ground Motions," Proc. American Society of Military Engineers PVP Conference, Denver, Colorado, 5 p.	Rock Sites World-Wide M 6+ Data Set <i>Average of Horiz. Components Used</i>	0.428	0.664
5	Idriss, I.M. (1993) "Procedures for Selecting Earthquake Ground Motions at Rock Sites," Report NIST GCR 93-625, U.S. Department of Commerce, National Institute of Standards and Technology, Gaithersburg, Maryland, 7 p.	Rock Sites 4.6 < M < 7.4; 1 < R < 60 km <i>Randomly Oriented Horizontal Comp.</i>	0.392	0.591

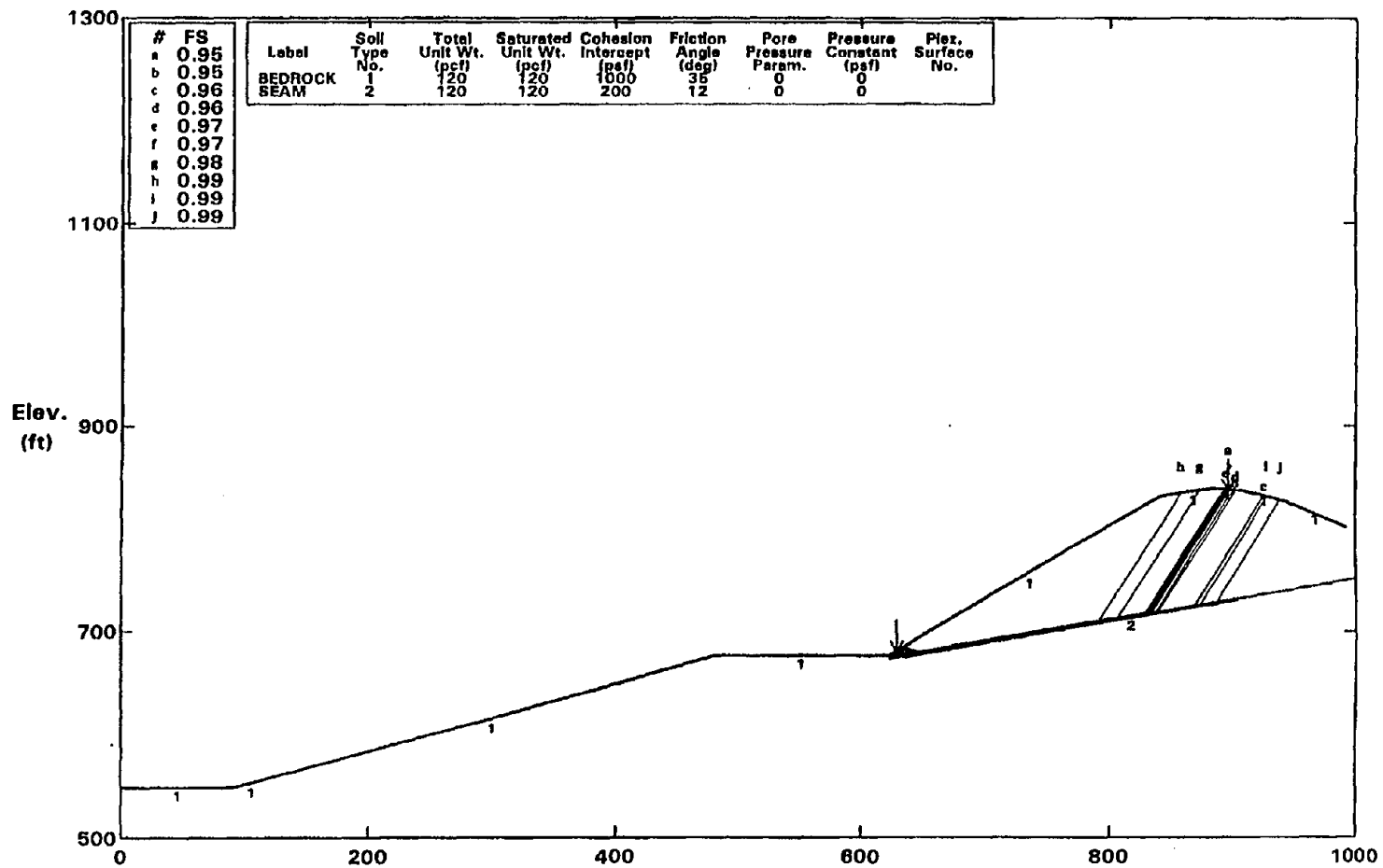
6 AVERAGE OF THE FIVE PGA VALUES LISTED ABOVE:

0.400 0.624

Figure 5-4: Calculation of MCE Peak Ground Acceleration.

Highway Cut - GEC#2 - Static Analysis Seam daylight at road level

Ten Most Critical. R:GEC-F23.PLT By: THH 09-03-96 11:56am



PCSTABL5 FSmin = 0.95 X-Axis (ft)

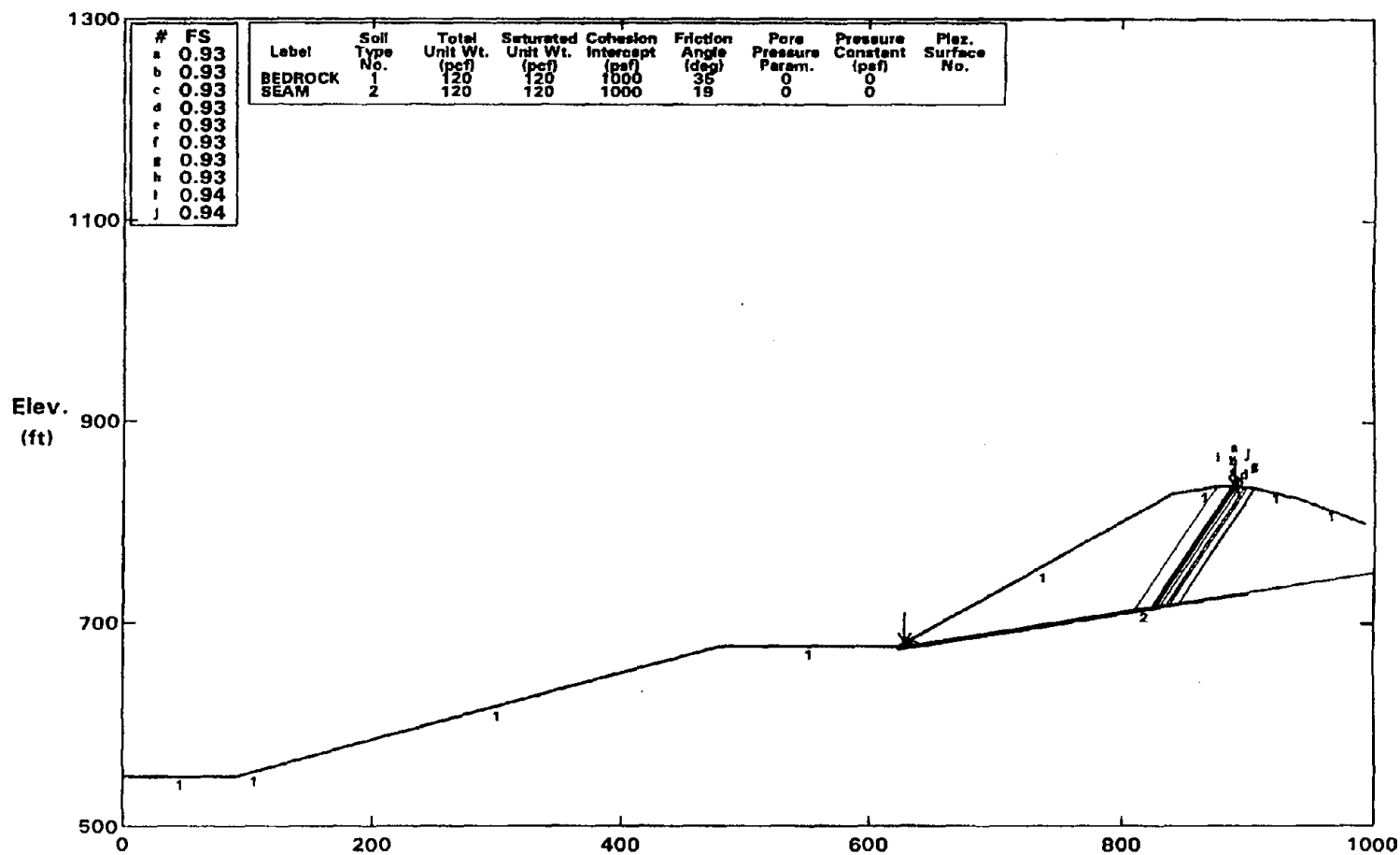
Factors Of Safety Calculated By The Modified Janbu Method

Note: 1 ft=0.3048 m, 1 psf=47.9 N/m², 1 pcf = 0.157 kN/m³

Figure 5-5: Critical Failure Mechanisms for Bench 1, Static Loading.
5 - 8 (Part II)

Highway Cut - GEC#2 - Seismic Analysis Seam daylight at first bench

Ten Most Critical. R:GEC-F24.PLT By: THH 09-03-96 11:58am



PCSTABLE5 FSmin = 0.93 X-Axis (ft)

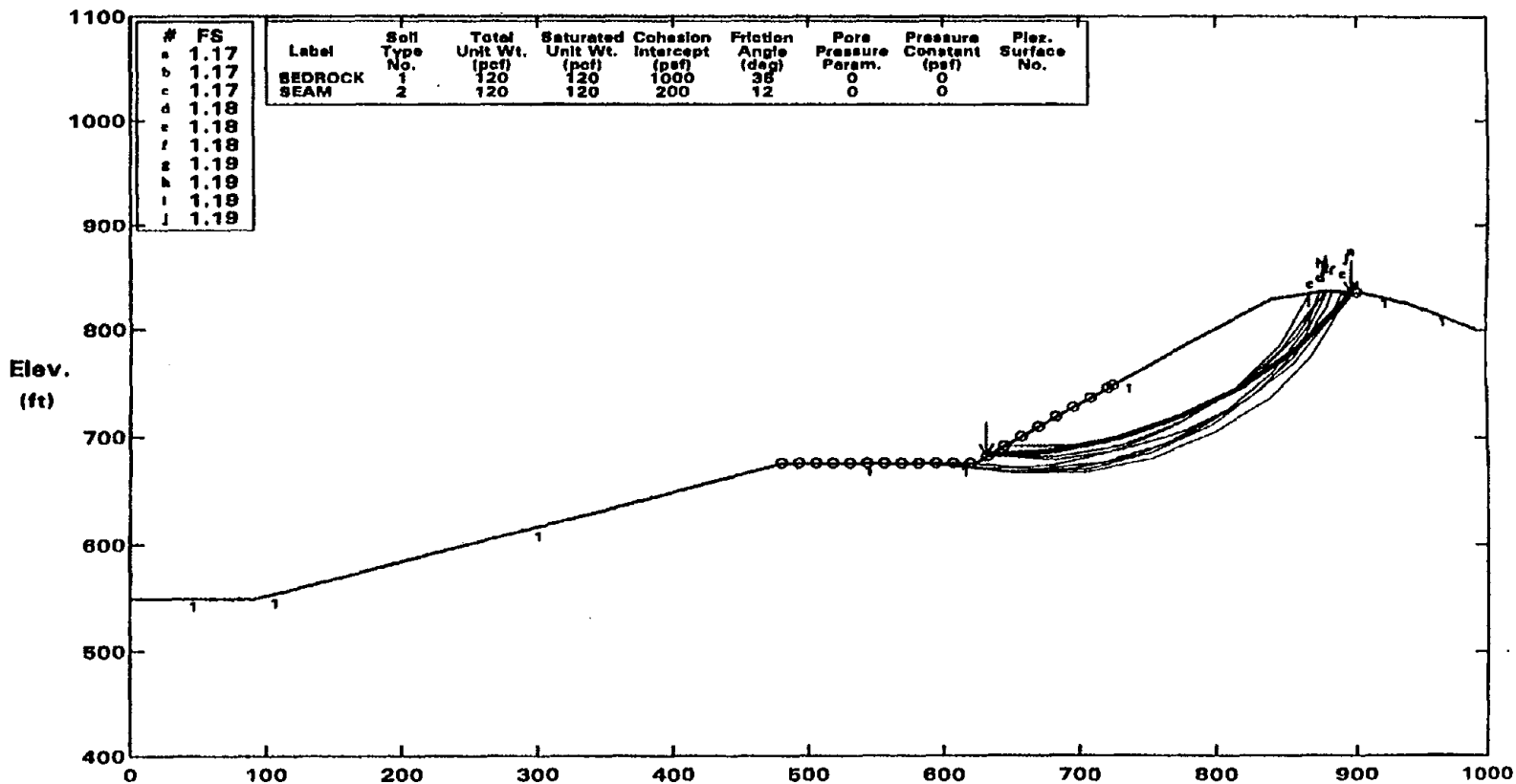
Factors Of Safety Calculated By The Modified Janbu Method

Note: 1 ft=0.3048 m, 1 psf=47.9 N/m², 1 pcf= 0.157 kN/m³

Figure 5-6: Critical Failure Mechanisms for Bench 1. Pseudo-Static Loading.

Highway Cut - GEC#2 - Static analysis - Deep seated circular mechanism

Ten Most Critical. R:GEC-F25N.PLT By: THH 09-03-96 10:10am



PCSTABL FSmin = 1.17 X-Axis (ft)
 Factors Of Safety Calculated By The Modified Janbu Method
 Note: 1 ft=0.3048 m, 1 psf=47.9 N/m², 1 pcf = 0.157 kN/m³

Figure 5-7:

Critical Deep-Seated Failure Mechanism, Static Loading.

Highway Cut - GEC#2 - Seismic analysis - Deep seated circular mechanism
 Ten Most Critical. R:GEC-F26N.PLT By: THH 09-03-96 10:12am

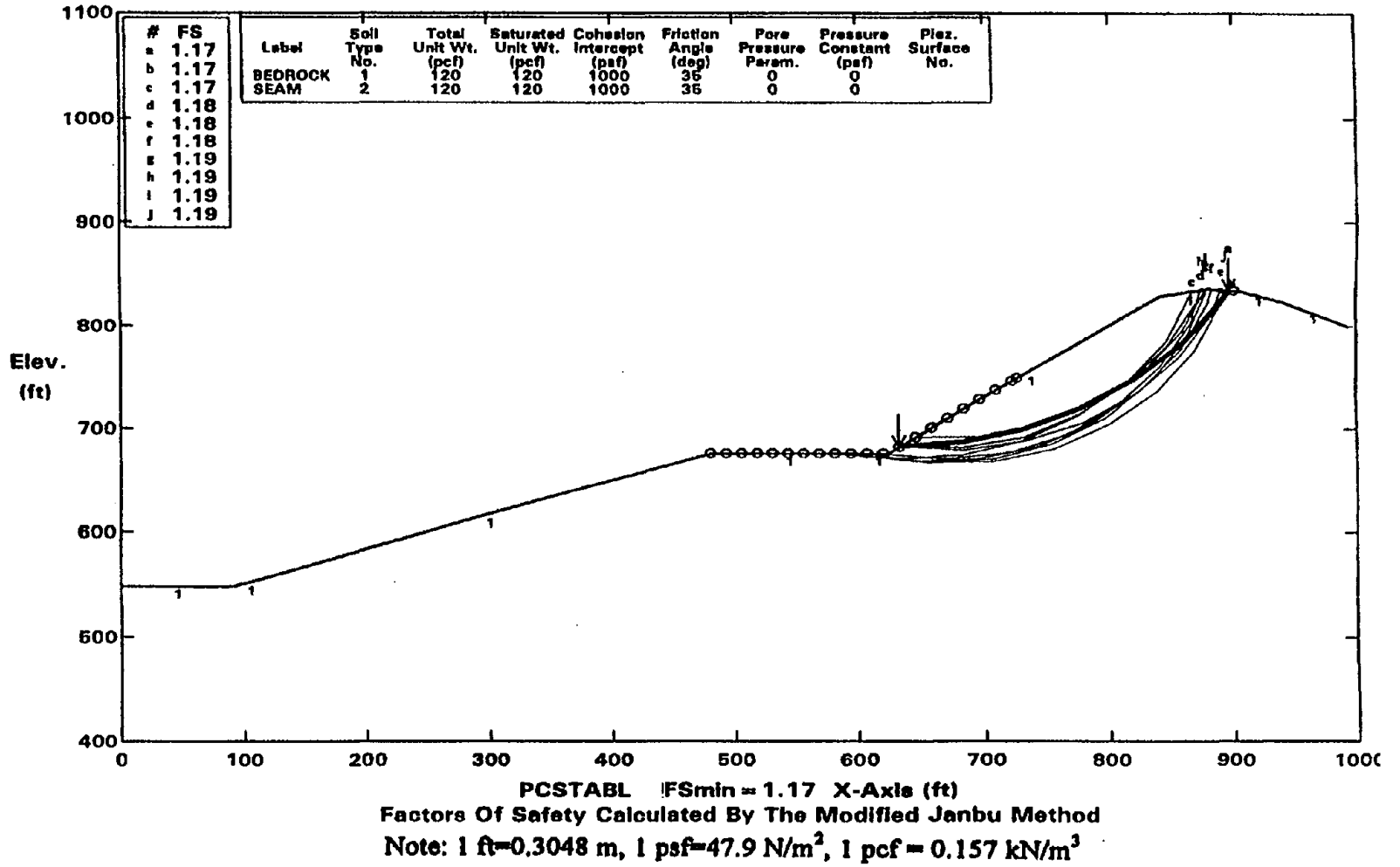


Figure 5-8: Critical Deep-Seated Failure Mechanism, Pseudo-Static Loading.

The results indicate that the proposed grading plan for the highway cut does not meet the requirements for either static or seismic conditions. Geometric constraints did not allow the engineers to flatten the slopes to increase stability. Therefore, structural stabilization solutions were investigated.

5.7 REMEDIAL SOLUTION

To increase the factors of safety to the required level, structural stabilization of the slope was required. The proposed stabilization system consisted of three rows of soil anchors located on benches. In general, the lowest row of anchors was designed to stabilize a global potential failure surface that extends parallel to the apparent dip and would daylight at road level or pass under the proposed roadway. The upper two rows of anchors were designed to stabilize the potential failure mass contained within the 1.5H:1V slopes. While many engineers prefer not to use benches on slopes above highways due to the potential for rockfalls, that potential was considered relatively low for this slope and the benches facilitate both access to the anchors for maintenance and monitoring and surface water drainage control.

The required anchor capacities were computed using hand calculations. Anchor loads were evaluated for all surfaces with a factor of safety below the desired value to find the required anchor capacity. The pseudo-static load due to a seismic coefficient of 0.20 was included in these calculations. The critical failure mechanisms were modeled as 4-block wedge mechanisms consisting of an upper (active) wedge, two middle sliding blocks, and a lower (passive) wedge, as shown on Figure 5-9. The 4-block wedge slope stability hand calculations were performed using force equilibrium. In these inclinations, the interslice forces were assumed to be inclined at 12 degrees to the horizontal (i.e., parallel to the weak bedding plane). The calculation used an iterative approach to find a set of four normal forces, three interslice forces, and an anchor force that produced the required factor of safety against instability. The set of simultaneous equations were programmed into commercially available spreadsheet software.

The purpose of this chapter is not to show the detailed design of anchors; however, it is important to note that there are several potential failure mechanisms that need to be considered in anchor design:

- failure of the grout-reinforcement interface in shear;
- failure of the anchor reinforcement in tension (i.e., breakage of the anchor);
- failure of the soil-grout interface in shear (i.e., pullout of the anchor); and
- pull out of the anchor from the moving soil mass.

The anchors were installed on the benches from the top row down as the cut progressed. Each anchor was designed to resist the calculated anchor force and to develop this resistance below the potential failure surfaces (i.e., below the weak bedding plane). Information on the analysis and design of permanent ground anchors can be found in Module 6 (Earth Retaining Structures).

5.8 SUMMARY AND CONCLUSIONS

Construction of a new highway required regrading of a hillside. The highest cut slope rose about 44 m above grade at an inclination of 1.5H:1V. The site geology is characterized as sedimentary bedrock of marine origin. It is described as a light tan sandy siltstone with local interbedded clay seams. The bedding dips out at the proposed cut slope at an apparent angle of 12 degrees. The site is located about 7.5 km from a strike-slip fault capable of generating earthquakes of moment magnitude (M_w) of 7.0. A seismic

hazard analysis was conducted using five attenuation relationships, resulting in a maximum horizontal ground acceleration of 0.4 g for use in design at the site.

Slope stability criteria called for a static factor of safety of 1.5 and a pseudo-static factor of safety of 1.1 for a seismic coefficient of 0.2 (one-half the peak ground acceleration). Initial slope stability analyses indicated that the proposed grading design would not meet the static and pseudo-static criteria.

A remedial solution was developed to stabilize the slope. The solution was based on using permanent ground anchors located on benches. The ground anchors were also designed for a seismic coefficient of 0.2 g.

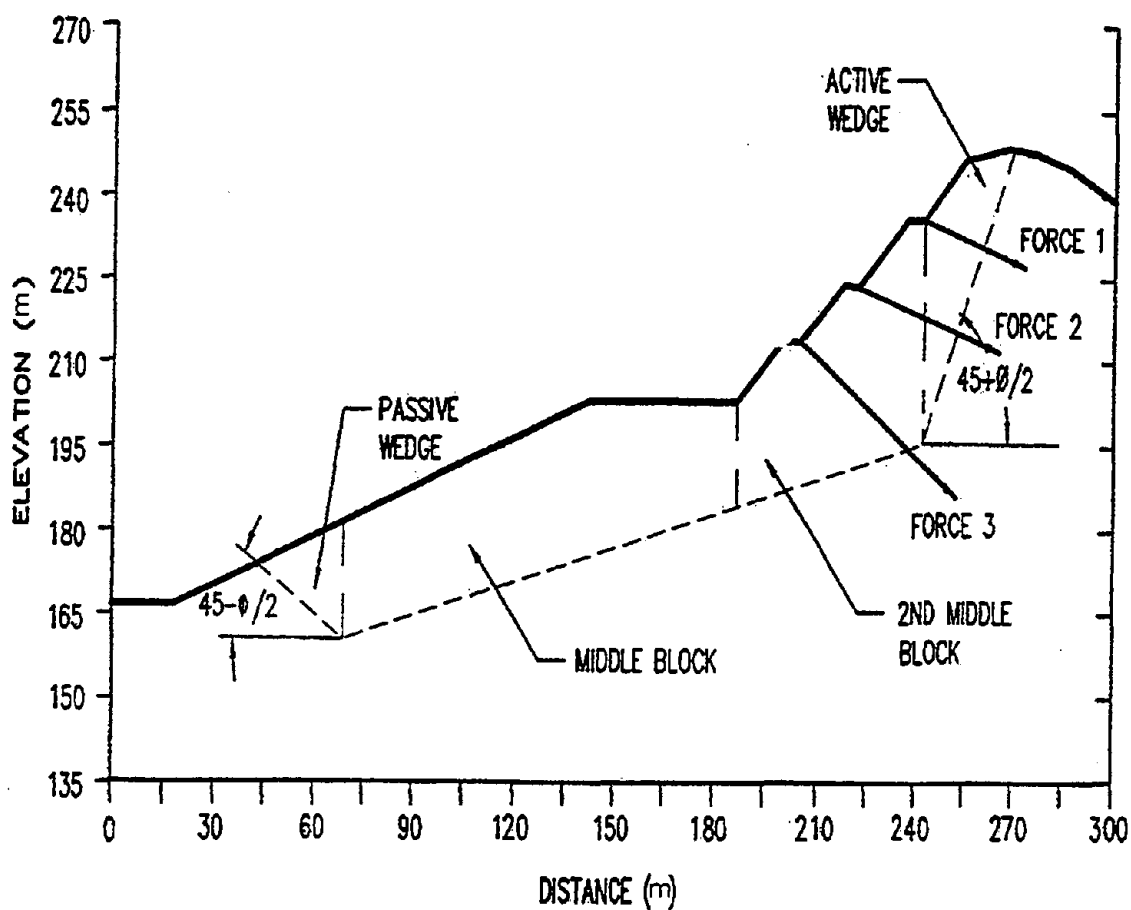


Figure 5-9: Wedge Analysis of Anchor System.

**EXAMPLE 4 - SLOPE STABILITY ANALYSIS
PCSTABL Output File**

** pcSTABL4 **
by
Purdue University

1 --Slope Stability Analysis--
 Simplified Janbu Method of Slices
 or Simplified Bishop Method

Run Date:
Time of Run:
Run By:
Input Data Filename: gec-f23.inp
Output Filename: gec-f23.ouu

PROBLEM DESCRIPTION Highway Cut - GEC#2 - Static Analysis
 Seam daylight at first bench

BOUNDARY COORDINATES

 9 Top Boundaries
 10 Total Boundaries

Boundary No.	X-Left (ft)	Y-Left (ft)	X-Right (ft)	Y-Right (ft)	Soil Type Below End
1	.00	49.00	90.00	49.00	1
2	90.00	49.00	110.00	55.00	1
3	110.00	55.00	480.00	176.00	1
4	480.00	176.00	623.00	176.00	1
5	623.00	176.00	840.00	330.00	1
6	840.00	330.00	880.00	337.50	1
7	880.00	337.50	905.00	335.00	1
8	905.00	335.00	940.00	325.00	1
9	940.00	325.00	993.00	300.00	1
10	623.00	175.00	1000.00	251.70	2

1 ISOTROPIC SOIL PARAMETERS

 2 Type(s) of Soil

Soil Type No.	Total Unit Wt. (pcf)	Saturated Unit Wt. (pcf)	Cohesion Intercept (psf)	Friction Angle (deg)	Pore Pressure Param.	Pressure Constant (psf)	Piez. Surface No.
1	120.0	120.0	1000.0	35.0	.00	.0	0
2	120.0	120.0	200.0	12.0	.00	.0	0

1 A Critical Failure Surface Searching Method, Using A Random
Technique For Generating Sliding Block Surfaces, Has Been
Specified.

The Active And Passive Portions Of The Sliding Surfaces
Are Generated According To The Rankine Theory.

 50 Trial Surfaces Have Been Generated.

 2 Boxes Specified For Generation Of Central Block Base

Length Of Line Segments For Active And Passive Portions Of
Sliding Block Is 62.0

Box No.	X-Left (ft)	Y-Left (ft)	X-Right (ft)	Y-Right (ft)	Width (ft)
1	623.00	174.00	723.00	194.30	.10
2	723.10	194.30	900.00	230.30	.10

1 Following Are Displayed The Ten Most Critical Of The Trial
Failure Surfaces Examined. They Are Ordered - Most Critical
First.

* * Safety Factors Are Calculated By The Modified Janbu Method * *

Failure Surface Specified By 8 Coordinate Points

*** .947 ***

Failure Surface Specified By 8 Coordinate Points

*** .952 ***

1

Failure Surface Specified By 7 Coordinate Points

*** .960 ***

Failure Surface Specified By 8 Coordinate Points

*** .963 ***

1

Failure Surface Specified By 8 Coordinate Points

*** .968 ***

Failure Surface Specified By 8 Coordinate Points

*** .972 ***

1

Failure Surface Specified By 8 Coordinate Points

*** .979 ***

Failure Surface Specified By 8 Coordinate Points

*** .989 ***

1

Failure Surface Specified By 7 Coordinate Points

*** .990 ***

Failure Surface Specified By 7 Coordinate Points

*** .991 ***

Note: Failure surface coordinates omitted from the original PCSTABL output.

CHAPTER 6.0 LIQUEFACTION POTENTIAL ANALYSIS

6.1 INTRODUCTION

6.1.1 Description of the Project

A highway project includes a channel crossing with an approach embankment and a major cable-stayed bridge structure. The embankment, which will reach a maximum height of 3.5 m near the abutment wall, is founded upon potentially liquefiable soil. The bridge will be supported on a large diameter concrete pier founded upon steel H-piles in the center of the channel. The tasks of the geotechnical engineer are to:

- evaluate the stability of the approach embankment, including the effects of seismic loading; and
- provide the structural engineer with response spectra for design of the bridge structure.

Of primary concern in this case is the evaluation of the liquefaction potential of the foundation soil for the approach embankment and the effect of local soil conditions upon the response spectra.

6.1.2 Source Materials Required

The source materials required to solve this problem include:

- Volume I of this document;
- geotechnical subsurface information;
- computer program SHAKE91 for seismic site response analysis (Schnabel, *et al.*, 1972, and Idriss and Sun, 1992); and
- computer program STABL4 for slope stability analyses (Lovell, *et al.*, 1984).

6.2 GEOLOGICAL SETTING

6.2.1 Regional Setting

The site is located along a broad coastal plain of limited relief surrounded by mountains to the north and east, and water to the south and west. The site lies in an area of high seismic exposure due to its proximity to three major fault zones. Figure 6-1 shows the site location relative to these known faults (Faults A, B, and C). Evaluation of the historical seismicity indicated that not all of the major earthquakes (magnitude > 5.0) in the region can be attributed to the three major faults. Recent studies indicated that the seismicity not attributable to these identified faults may be attributable to an unmapped buried thrust and fold belt that is capable of producing earthquakes up to magnitude 6.5 to 7.0. Therefore, in addition to the three recognized faults, the blind thrust and fold belt has been identified as a seismic source zone impacting the site. Figure 6-1 shows the location of the fold and thrust zone established on the basis of micro-seismicity studies and seismic reflection profiling.

6.2.2 Local Geology

Available data from previous subsurface investigations indicated that schist and basalt basement rocks can be found at a depth of approximately 40 to 60 m in the vicinity of the site. These basement rocks are

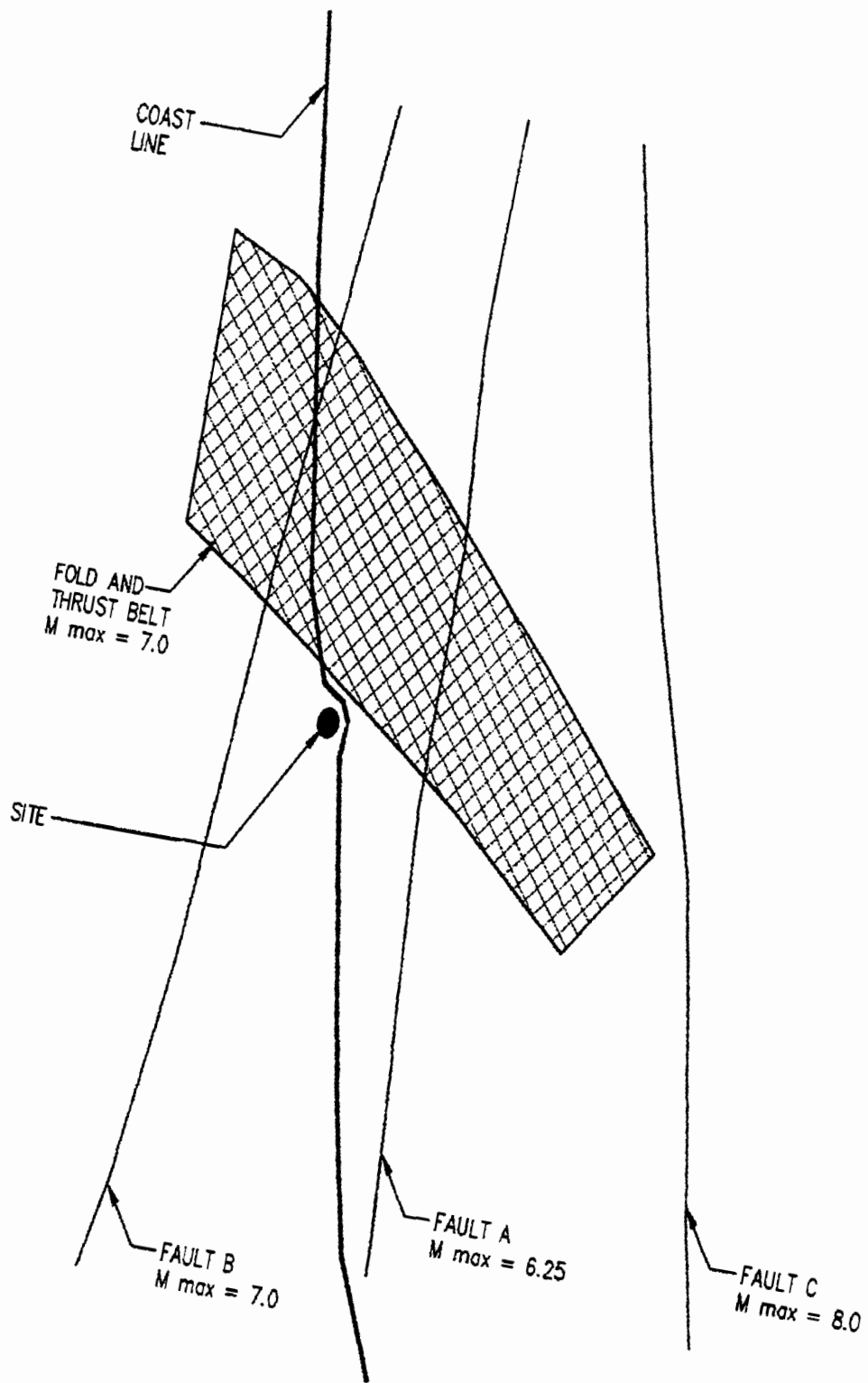


Figure 6-1: Example 5 Site Location and Seismic Source.

overlain by approximately 20 m of Miocene marine shale and sandstone deposits which are, in turn, overlain by Pleistocene and Holocene sediments. Borings indicate that, on shore, the top 30 m at the site consists of Pleistocene marine terrace deposits covered by 3 to 5 m of alluvium. The channel is filled with recent sediments, having been incised into the Pleistocene marine terrace and Miocene shale and sandstone deposits when sea level fell below its present elevation during the Late Pleistocene period and being subject to periodic dredging. At the project site, the channel is filled with approximately 30 m of recent deposits of silts, clays, and sand.

6.3 SEISMIC DESIGN CRITERIA

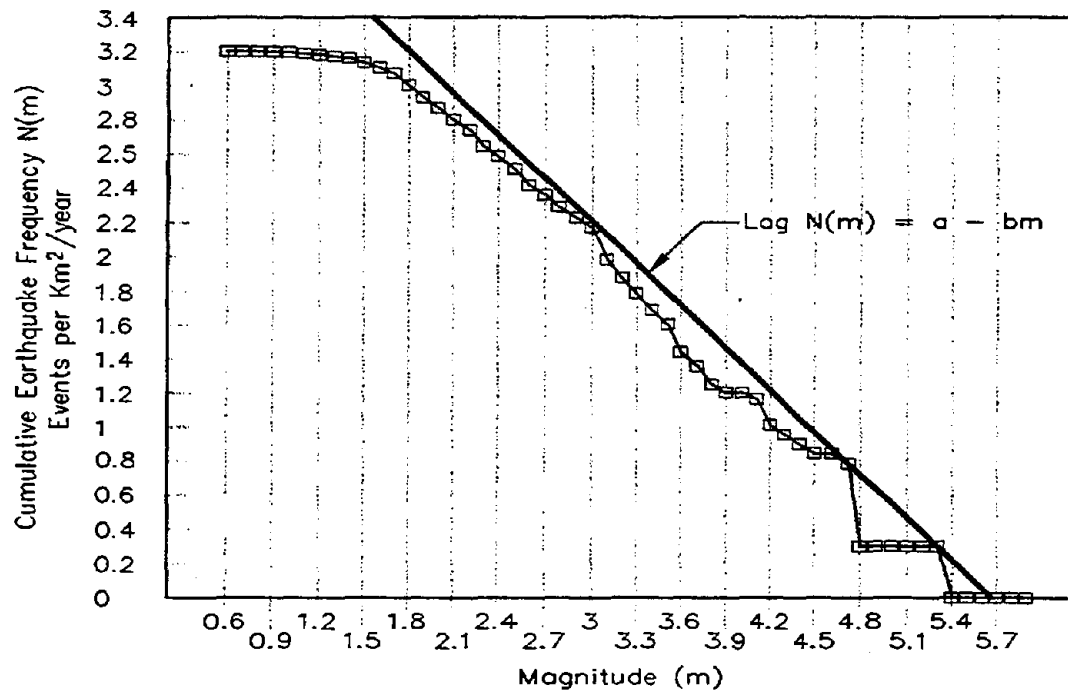
Two levels of ground motions were established by the owner in developing the seismic design criteria for the project: an "operational" level at which the structure is assumed to respond elastically with little to no damage and a "contingency" level at which some "acceptable" level of damage is expected. The amount of damage considered to be acceptable at the contingency level depends on the function of the facility, the ease of repair, and the availability of alternative transportation routes. For critical facilities defined as lifelines, the criteria for acceptable damage requires the structure to remain serviceable. For important facilities where loss of service for limited periods of time can be accommodated, the criteria is that the damage be easily repairable. For ordinary facilities, where alternative transportation routes are available, it is simply necessary to prevent collapse of the structure and loss of life. For this project, the approach embankment and bridge crossing were judged to be important, but not critical facilities, as they were important for moving freight but there were alternative routes that could accommodate emergency services. Due to the importance of the route as a freight corridor, acceptable "downtime" following a major earthquake was limited to 2 to 4 weeks.

The Operational Level Event (OLE) and Contingency Level Event (CLE) were defined by the owner on a probabilistic basis. The OLE is defined as the most damaging event with a peak horizontal ground acceleration (PHGA) that has 50 percent probability of not being exceeded in a 50 year period. The CLE is defined as the most damaging event with a PHGA that has 10 percent probability of not being exceeded in a 50 year period.

6.4 PROBABILISTIC SEISMIC HAZARD ANALYSIS

The firm ground intensity levels for the OLE and CLE design motions were evaluated on the basis of a conventional probabilistic strong shaking seismic hazard evaluation. The analyses followed the procedure originally suggested by Cornell (1968), as embodied in the computer program EQRISK (McGuire, 1976). Active faults within 100 km of the project site were identified, assigned earthquake magnitude recurrence rates on the basis of observed slip rates and historic seismicity, and assigned maximum magnitudes on the basis of the length of the fault segments. Historical seismicity and regional deformation not assigned to active faults were then assigned to either "random" seismicity or to buried blind fold and thrust belts. The three major known active faults were treated as line seismic sources while the blind thrust and fold belts and the sources of the "random" seismicity were treated as area sources. Figure 6-2 presents the Gutenberg-Richter recurrence plot developed for the blind thrust and fold belt on the basis of the historical seismicity. Once the magnitude-recurrence relationships were established for each source, the contribution of each source to the PHGA hazard at the site was calculated using the EQRISK computer program on the basis of the attenuation relationships developed by Campbell (1993). The sensitivity of the results to the choice of attenuation relationship and to assumptions regarding the "random" seismicity and the blind thrust and fold belt events was then investigated in subsequent analyses. The resulting seismic hazard curve adopted for the project is shown in Figure 6-3. On the basis of this curve, the PHGA on firm soil in the

FOLD AND THRUST ZONE



$$a = 4.50$$

$$b = 0.80$$

Data covers a 34 year period

Figure 6-2: Recurrence Relationship for Blind Thrust and Fold Belt.

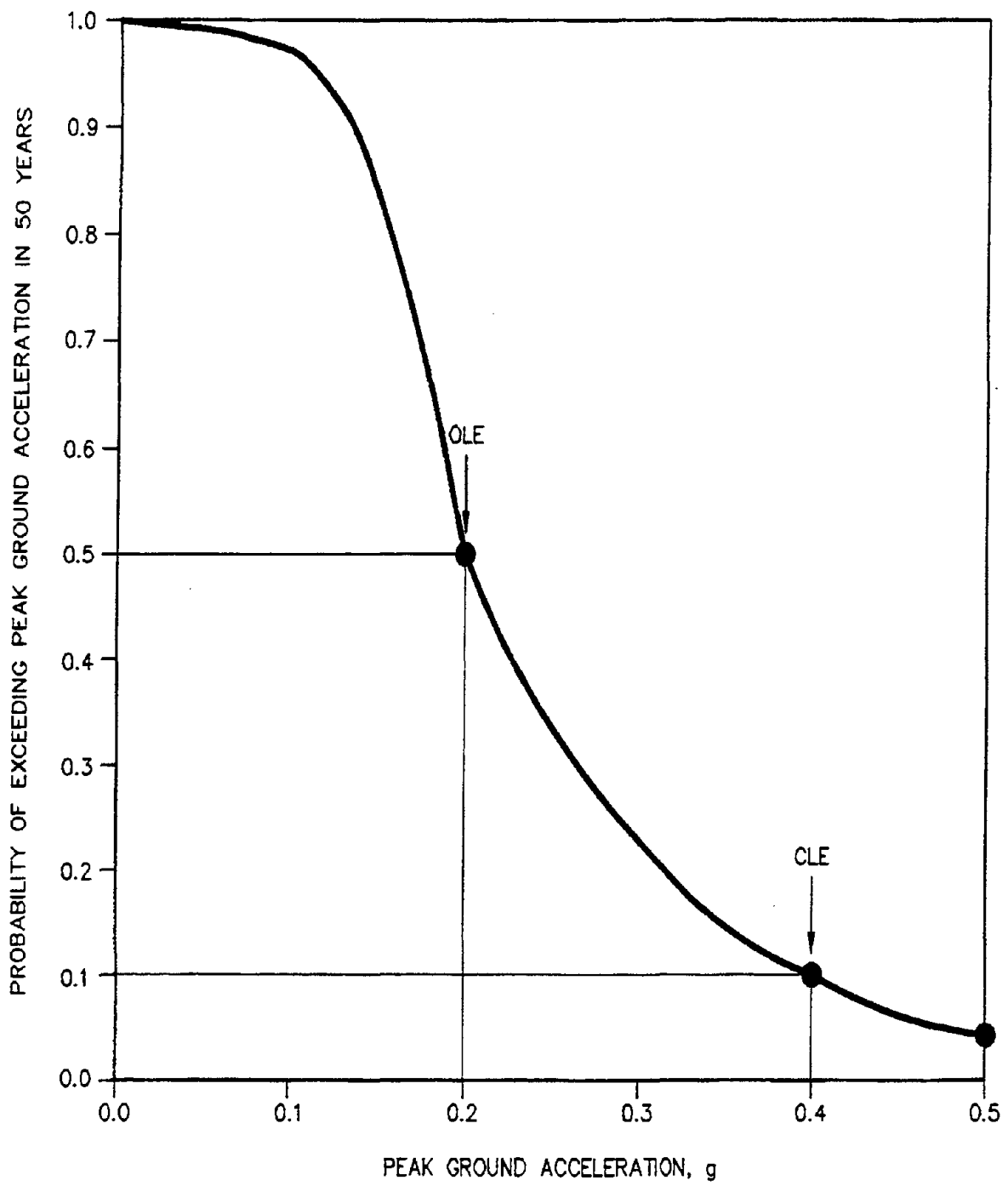


Figure 6-3: Seismic Hazard Curves.

OLE was established as 0.2 g. The PHGA on firm soil in the CLE was established as 0.4 g. Analysis of the results indicated that the most damaging source of the 0.2 g PHGA for the OLE would be a magnitude 8.0 event on Fault C (see Figure 28) at a distance of 52 km. The most damaging event associated with the 0.4 g PHGA for the CLE was determined to be a magnitude 7.0 event within the blind thrust and fold belt at a distance of 11.3 km from the site. Table 6-1 summarizes the parameters of the design earthquakes.

6.5 GEOTECHNICAL INFORMATION

A subsurface exploration program which consisted of 12 geotechnical borings, 6 cone penetrometer tests (CPT), and laboratory testing on samples recovered from the borings was conducted at the site. Four of the soil borings were drilled from a barge in the channel. Cross hole seismic profiling was conducted within three of these channel borings to develop a shear wave velocity profile for seismic response analyses. The soil borings were drilled using rotary wash drilling equipment. Relatively undisturbed samples of the silts and clays in the channel were obtained for laboratory testing using 75-mm-diameter Shelby tubes. In the land-side borings, Standard Penetration Tests were conducted in accordance with ASTM Standard D 1586-84 at 1.5 m intervals. The six CPT soundings were advanced on land to continuously log the resistance of soil strata at the site to identify weak layers that may go unnoticed in traditional borings. The SPT blow counts and equivalent blow counts from the CPT soundings were used in the liquefaction potential analysis.

Based on the results of the subsurface exploration program, characteristic stratigraphic profiles were developed for the site. For the purpose of geotechnical analyses, typical properties were assigned to each of the characteristic stratigraphic units. The stratigraphic profile beneath the approach embankment is shown in Figure 6-4. The log for Boring B-2 is shown in Figure 6-5. The idealized stratigraphic profile of sediments found beneath the embankment near the bridge abutment consists of 1.5 m of soft organic silt underlain by 7 m of medium-dense sand underlain by 5 m of medium dense to dense silty sands underlain by dense to very dense sand and gravel. The representative profile of uncorrected SPT blow counts beneath the approach embankment, developed from both the borings and the CPT soundings, is shown in Figure 6-6. The stratigraphic profile at the center of the channel consists of 18 m of silt, sand, and clay layers underlain by dense sand and gravel. Figure 6-7 shows the shear wave velocity profile within the channel developed from the cross hole soundings. Figure 6-7 also shows the shear wave design profile used in the SHAKE analyses.

6.6 DESIGN OF THE EMBANKMENT

6.6.1 Design Considerations

Preliminary design called for an approach embankment with an 18-m-wide crest and side slopes at an inclination of 1.5H:1V. The design called for excavation of the 1.5-m layer of organic silt, placement of a geotextile separation layer, and construction of the embankment. The embankment was compacted to 95 percent of the maximum dry density determined using ASTM D-1557, the Modified Proctor Compaction Test. The embankment is about 150 m long and varies in height to reach a maximum of 3.5 m over the last 100 m near the abutment wall of the bridge. Conventional geotechnical analyses performed for design of the embankment, including static slope stability and settlement analyses, were performed but are not described herein. Seismic performance analyses for the embankment that are described herein include:

- dynamic slope stability;
- liquefaction potential of the underlying soil; and
- the consequence of liquefaction.

TABLE 6-1
SUMMARY OF DESIGN EARTHQUAKE PARAMETERS

Design Event			Assumed Local Site Conditions	Estimated Site-To-Source Distance	Design Strong Motion Parameters		
Earthquake	Style of Faulting	MCE Magnitude ⁽¹⁾			Peak Ground Acceleration ⁽³⁾	Significant Duration ⁽⁴⁾	RMSA ⁽⁵⁾
CLE (Faults A and B and the Blind Thrust)	Reverse (Blind-Thrust)	$M_w = 7$	Weak Rock (Joyner and Boore Site Class B) ⁽²⁾	11.3 km	PGA = 0.4 g	$D_s \approx 14.2$ sec	0.09 g
OLE (Fault C)	Strike-Slip (Right Lateral)	$M_w = 8$	Weak Rock (Joyner and Boore Site Class B) ⁽²⁾	(52 km)	PGA = 0.2 g	$D_s \approx 38.3$ sec	0.03 g

- Notes: (1) Moment Magnitude (M_w) corresponding to the Maximum Credible Earthquake (MCE).
(2) Joyner and Boore Site Class B assumes that shear wave velocity (V_s) in the upper 30 m of profile is between 360 and 750 m/s.
(3) Estimated median Peak Horizontal Ground Acceleration (PHGA) in hypothetical bedrock outcrop at geometric center of the site.
(4) Significant duration of strong shaking (D_s) defined by Trifunac and Brady (1975) as the time needed for the Husid plot to build from 5 to 95 percent of its final value. In this study, D_s was estimated, according to Dobry, *et al.* (1978), as: $\log D_s = 0.432 M_w - 1.83$.
(5) Root Mean Square Acceleration (RMSA) over the significant duration of the record. In this study, RMSA was estimated using the Kavazanjian, *et al.* (1985) attenuation equation for RMSA [Model I (TB)].

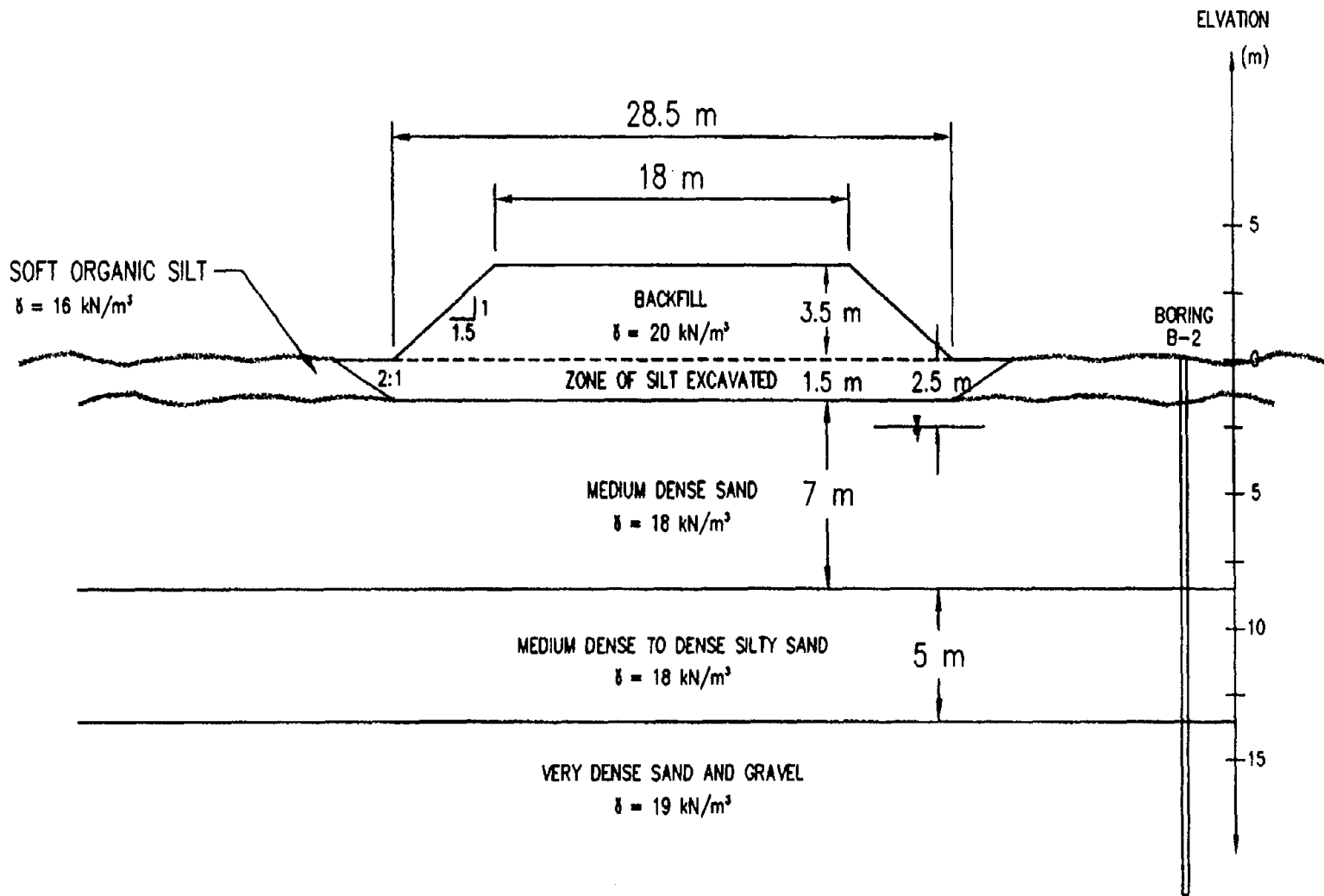


Figure 6-4: Stratigraphic Profile Under Embankment.

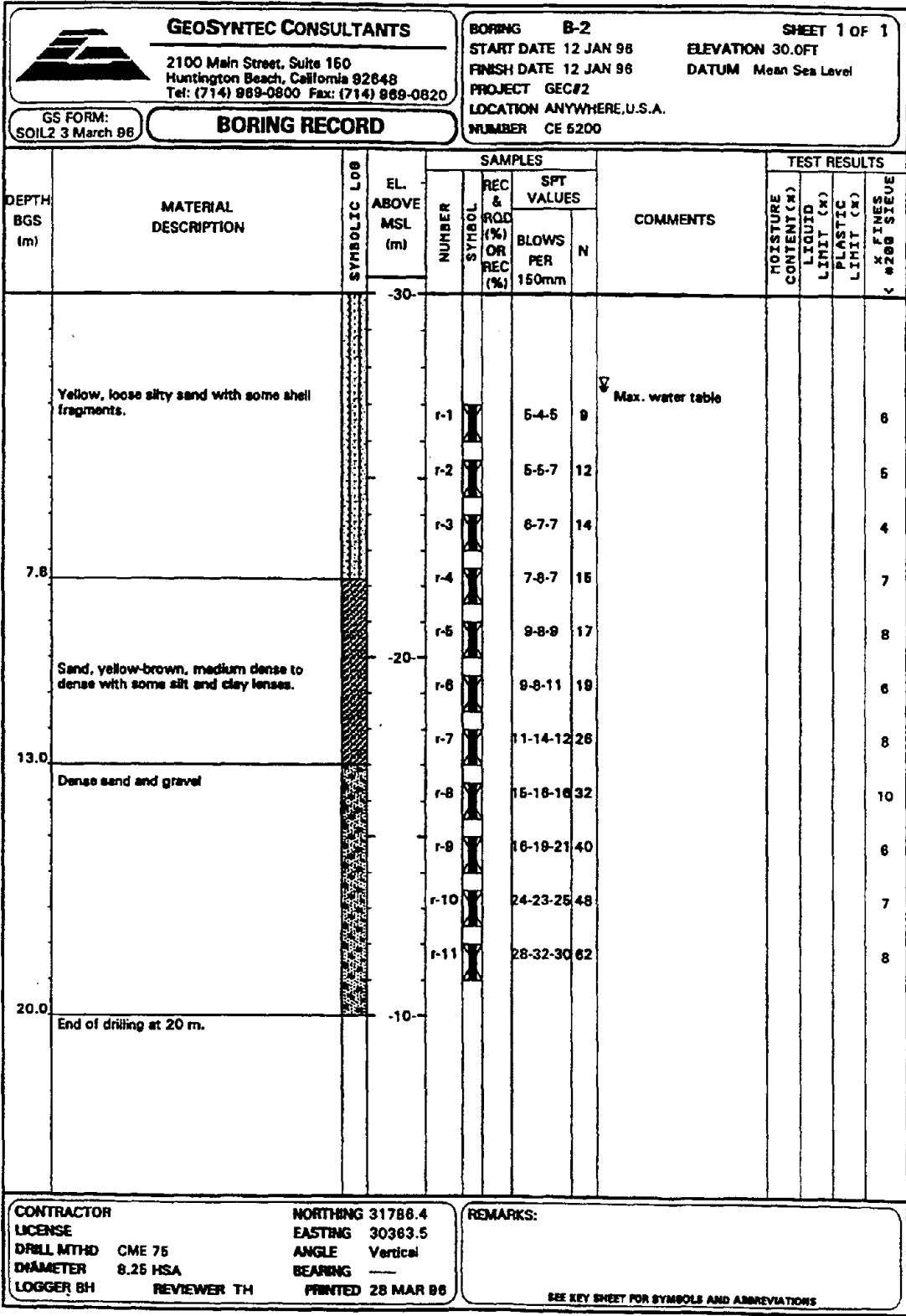


Figure 6-5: Example 5 Boring Log.

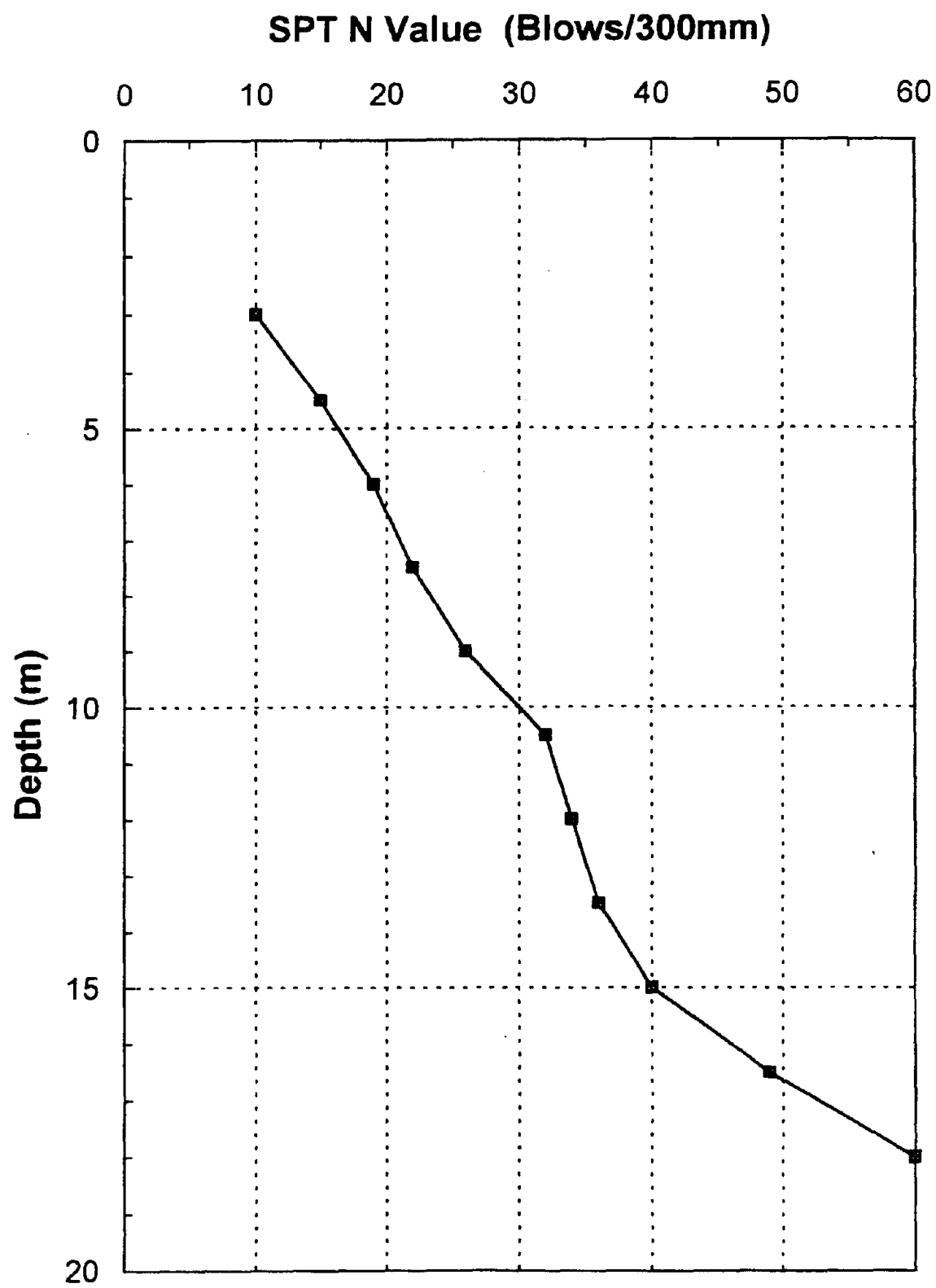


Figure 6-6: Field Uncorrected SPT N Value Distribution.

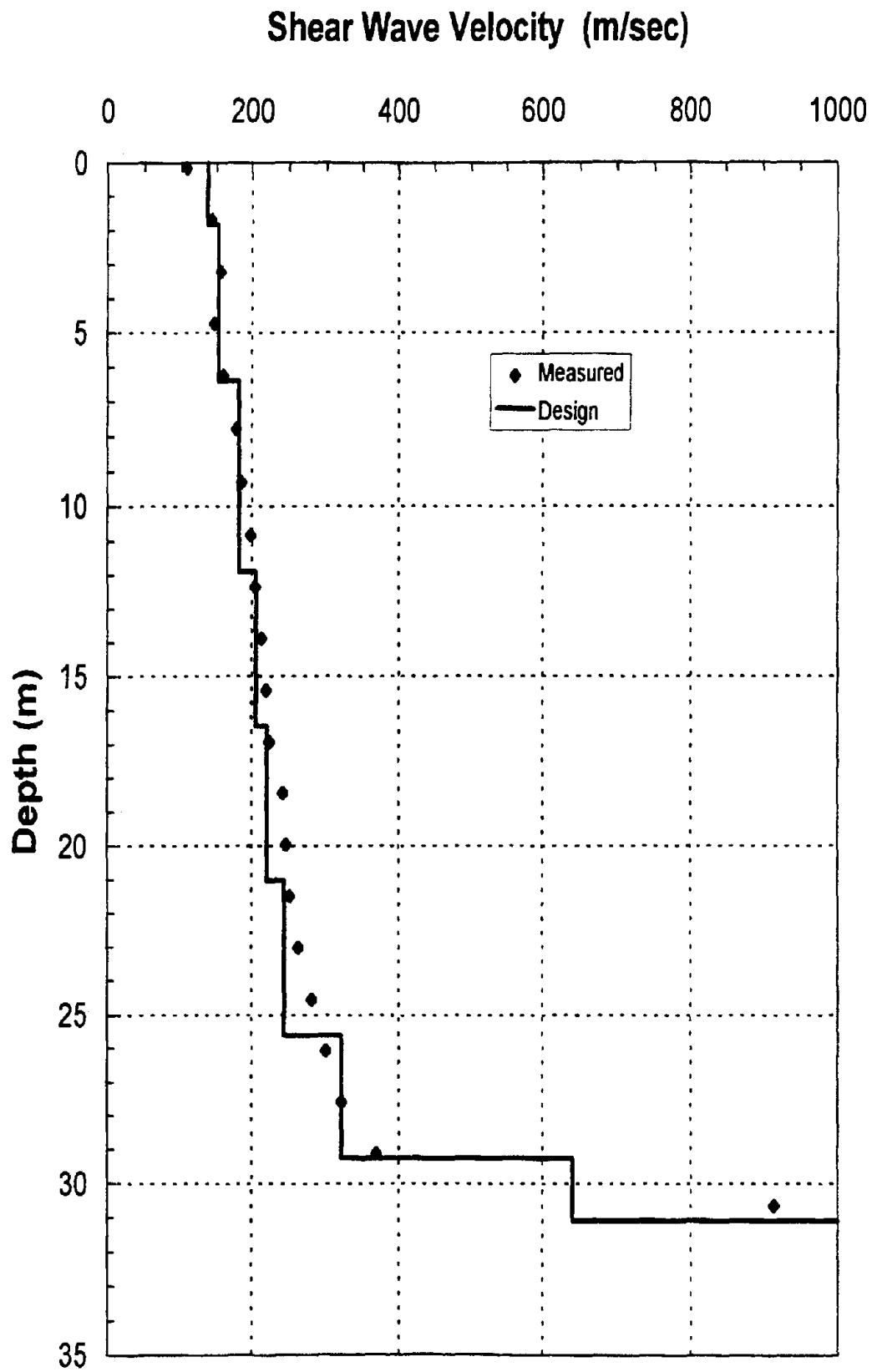


Figure 6-7: Shear Wave Velocity Profile in Channel.

6.6.2 Seismic Slope Stability

Pseudo-static slope stability analyses of the embankment were performed using the computer program STABL4 assuming that liquefaction would not occur. In the dynamic stability analyses, the seismic coefficient was set equal to one-half the PHGA divided by the acceleration of gravity, or 0.1 for the OLE and 0.2 for the CLE. Results of the analyses yielded a factor safety greater than 1.5 for both cases, indicating acceptable seismic performance in the absence of liquefaction. The critical failure surfaces are shown in Figure 6-8 for the OLE and Figure 6-9 for the CLE. Post-liquefaction stability analyses are described subsequently.

The input and output files for the STABL4 analyses using the OLE are provided in the attached calculation sheets.

6.6.3 Liquefaction Potential

Evaluation of liquefaction and seismic settlement potential is described in detail in Volume I. The step-by-step methodology developed in Section 8.3 of Volume I will be followed in this example.

First, the uncorrected blow counts were normalized to a confining pressure of 96 kPa and standardized for a hammer efficiency of 60 percent. As a safety hammer was used in the rotary wash borings, the standardization factor for hammer efficiency was 1.0 (see Section 8.3 of Volume I). The normalization procedure is illustrated in the calculations and summarized in Tables 6-4 through 6-6. Next, the factor of safety against liquefaction was calculated at each 1.5 m interval within the potentially liquefiable strata for both design earthquake loadings (the OLE and the CLE). Liquefaction potential was evaluated under the centerline of the embankment, beneath the toe of the embankment, and in the free-field beyond the embankment toe. Detailed calculations for liquefaction potential are provided in the attached calculation sheets.

Figure 6-10 shows the distribution of the factor of safety against liquefaction with depth for the free-field conditions. Under both the OLE and CLE conditions, liquefaction is expected to occur within approximately the top 10 m of the sand layer.

Figure 6-11 shows the distribution of the factor of safety against liquefaction with depth under the center of the embankment. Figure 6-11 shows that, due to the increase in confining stress imposed by the embankment, liquefaction is not anticipated under the embankment centerline in the OLE event but is expected to occur in the CLE event.

Figure 6-12 shows the distribution of the factor of safety under the toe of the embankment. At this location, liquefaction is also anticipated in the CLE but not in the OLE due to the beneficial influence of the initial static shear stress from the embankment on liquefaction potential. Note, however, that if the initial relative density of the surficial sand layer was less than 40 percent, the initial static shear stress from the embankment would increase the liquefaction potential. As indicated in Figure 8-8 of Volume I, the initial static shear stress correction factor k_a is larger than one for relative densities greater than 40 percent and less than one for relative densities less than 40 percent. The coefficient k_a appears in Tables 6-4 through 6-6 in the attached computations and, for this example, is always larger than one since the sand found at the site has estimated relative densities varying from 40 to 55 percent.

Figure 6-8: Critical Failure Surface for OLE.

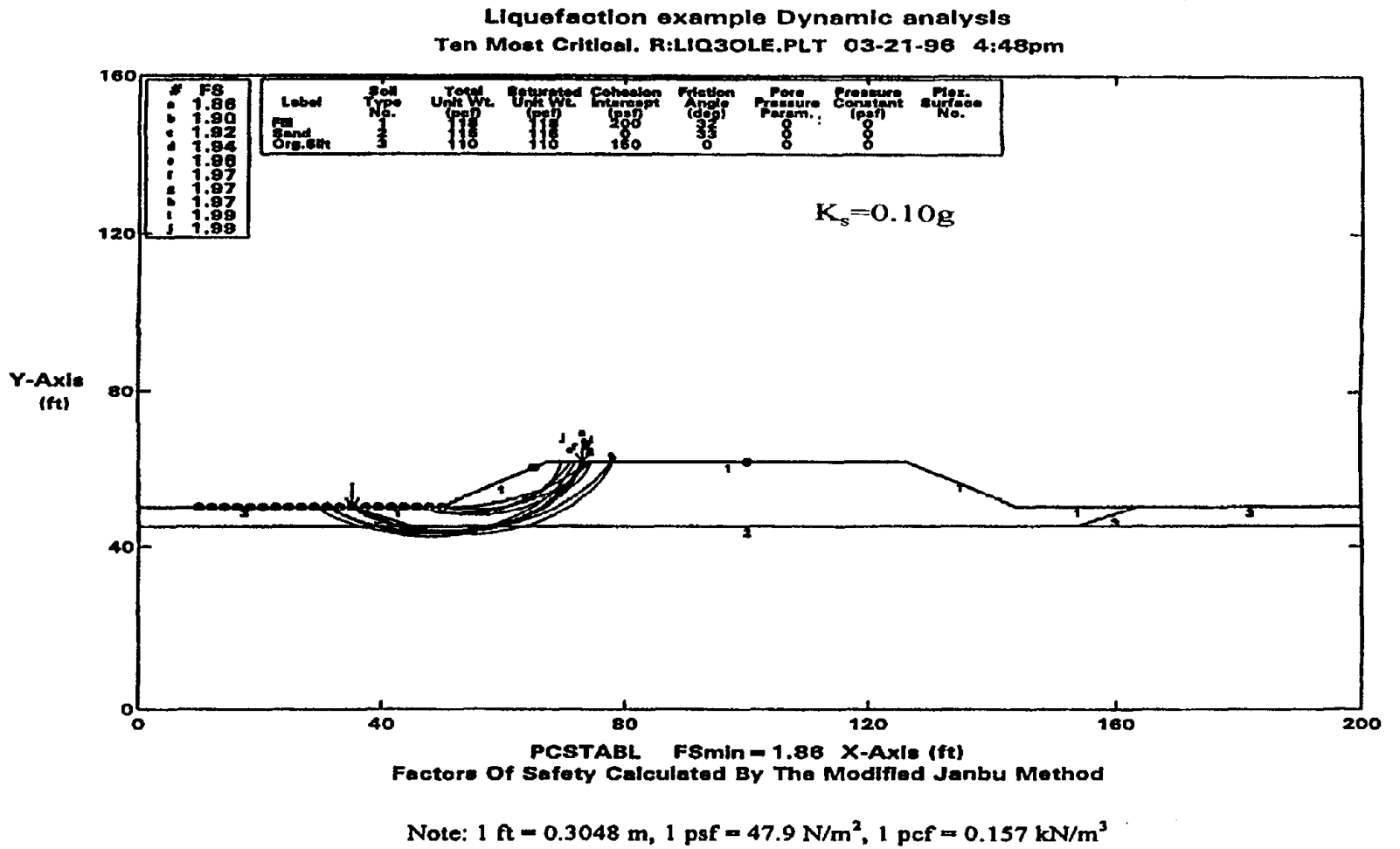
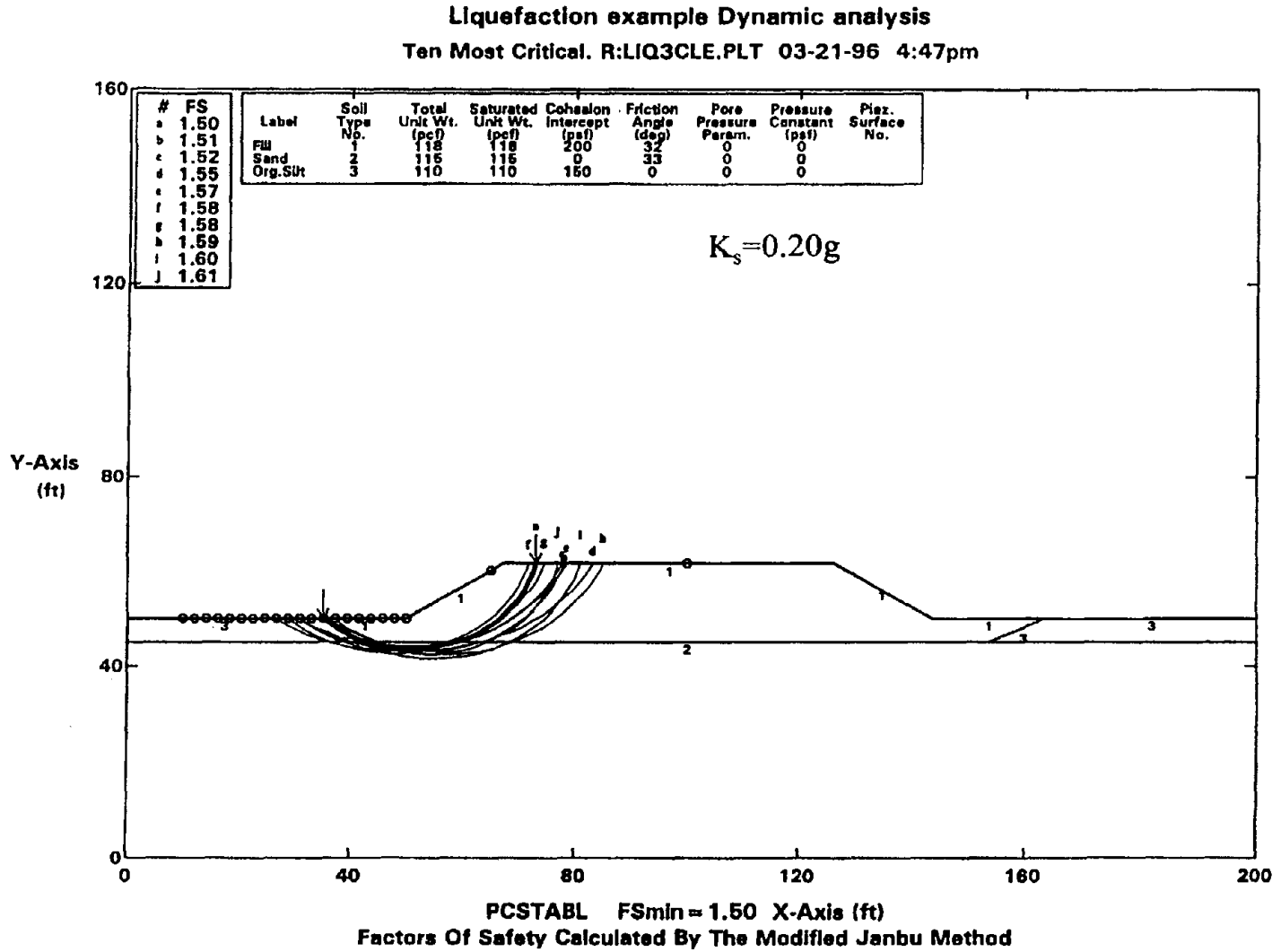


Figure 6-9: Critical Failure Surface for CLE.



Note: 1 ft = 0.3048 m, 1 psf = 47.9 N/m², 1 pcf = 0.157 kN/m³

6.6.4 Evaluation of the Consequences of Liquefaction

Since the analyses indicate that there is a potential for liquefaction in the free-field and under the embankment in both the OLE and CLE, the engineer must evaluate the consequences of liquefaction in these events. As discussed in Section 5.3, the design criteria are that in the OLE the embankment should remain usable and that in the CLE the damage will be repairable in 2 to 4 weeks.

The liquefaction analyses indicate that in the OLE liquefaction will occur in the free-field, as the factor of safety for the upper 10 m is in the range from 0.7 to 0.8. Due to the higher effective confining pressure the factor of safety against liquefaction in the OLE under the centerline of the embankment is improved to very near one from 5 m to 10 m, leaving about the upper 3.5 m of the sand layer vulnerable to liquefaction with factors of safety around 0.8. In the CLE, the factor of safety varies from about 0.5 in the free-field to about 0.7 under the embankment. Such low values indicate that extensive liquefaction may occur, resulting in large displacements (lateral spreading) and potential slope failure along the embankment.

To lower the risk of liquefaction, it was decided to densify the top 10 m of the sand layer. Target factors of safety of 1.1 under the embankment and 1.0 in the free-field during the CLE event were established. To achieve these factors of safety, it was determined that the cyclic shear ratio at which liquefaction will occur (the liquefaction resistance of the soil) must be greater than or equal to 0.3 over the top 10 m of sand layer. Based on Figure 8-3 of Part I, to achieve a liquefaction resistance of 0.3 for a soil with a fines content of 5 percent requires a value of $(N_1)_{60}$ of about 25. The remedial ground improvement program was designed on this basis to provide an $(N_1)_{60}$ of 25 or greater at the site. As the site was an open, undeveloped area with no structures or utilities nearby, dynamic compaction was selected as the most economical ground improvement method with which to achieve the required liquefaction resistance.

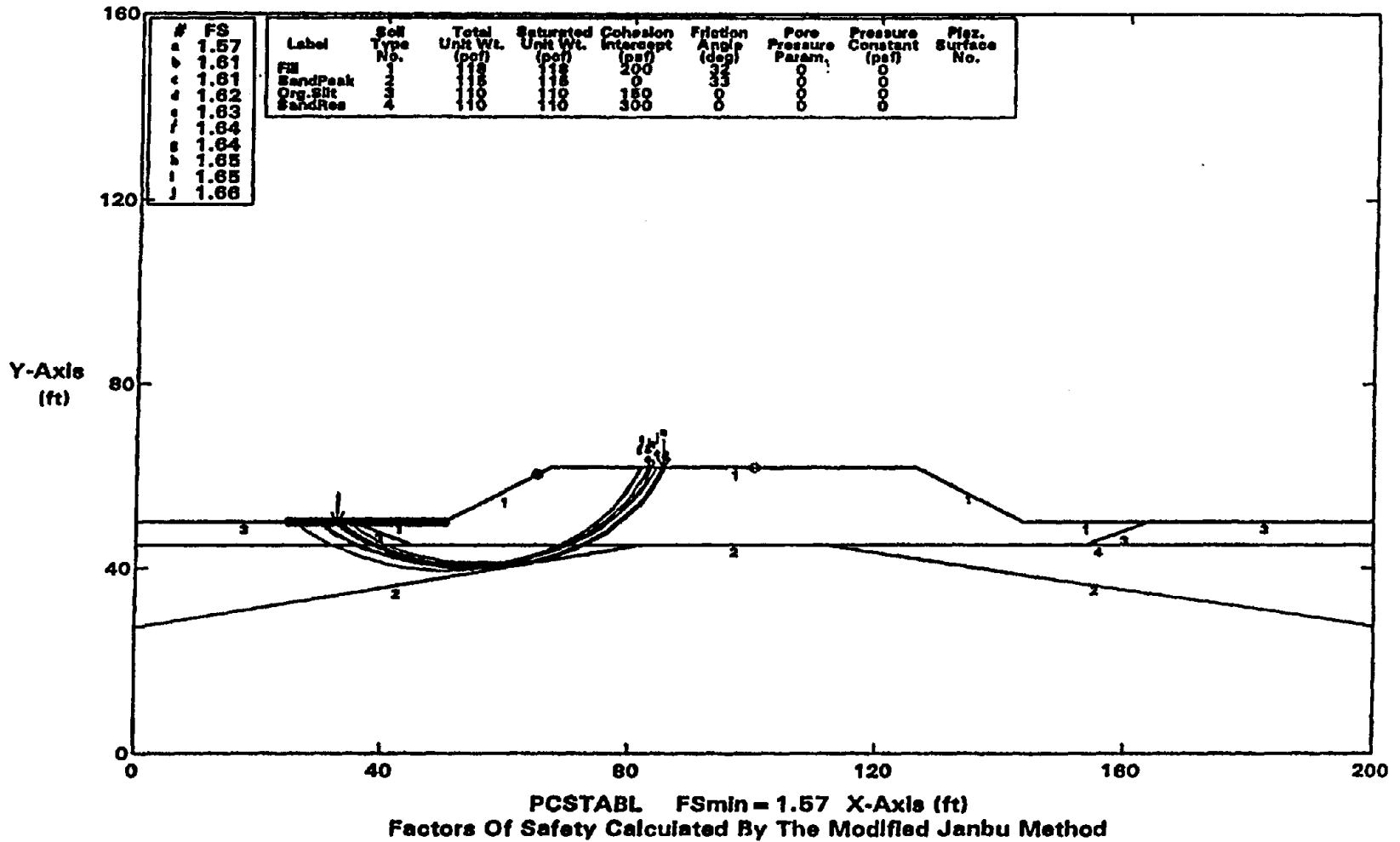
Even with a standardized and normalized blow count of 25, there is still a risk of liquefaction in the free-field in the OLE and CLE, as only the soil under the embankment footprint was designated for densification. The potential consequence of liquefaction in the free-field adjacent to the toe of the embankment is lateral spreading of the embankment. Lateral spreading can occur subsequent to liquefaction both during the earthquake (assuming liquefaction occurs prior to the cessation of strong shaking) and after the event. To evaluate the potential for lateral spreading in the CLE, a limit equilibrium analysis was performed using the residual shear strength for the potentially liquefiable soil beyond the toe of the embankment. The rationale for the use of residual shear strength in this analysis is discussed in Section 8.4 of Part I. The residual shear strength of the liquefied soil was evaluated using the correlation with SPT $(N_1)_{60-cs}$ values shown in Figure 5-15 of Part I.

Because the area outside the footprint of the embankment was not treated with dynamic compaction, the value of residual shear strength was obtained using the average initial SPT values over the top 10 m of the sand layer and the lower-bound curve on Figure 5-15 of Part I. On this basis, a value of 15 kPa was selected to characterize the residual shear strength of the sand.

Results of the residual strength stability analysis are presented in Figure 6-10. The figure indicates a static factor of safety of 1.57 for the embankment using residual shear strength parameters. This analysis indicates that, once the strong shaking stops, the embankment will be stable and lateral spreading will cease. The yield acceleration calculated using residual shear strength beyond the toe of the embankment is 0.14 g. Using this value in conjunction with the CLE PHGA of 0.4 g results in a value of 0.35 for the ratio of yield to peak acceleration. From the Hynes and Franklin (1984) chart presented in Figure 7-4 of Part I, this results in an upper bound permanent seismic deformation of 0.36 m, as shown in Figure 6-11. This is assumed to be the upper bound value for the lateral spreading anticipated during the CLE.

Figure 6-10: Post-Liquefaction Slope Stability Analysis.

Liquefaction example Post Liquefaction analysis
 Ten Most Critical. R:LIQ3PL.PLT 03-21-98 4:45pm



Note: 1 ft = 0.3048 m, 1 psf = 47.9 N/m², 1 pcf = 0.157 kN/m³

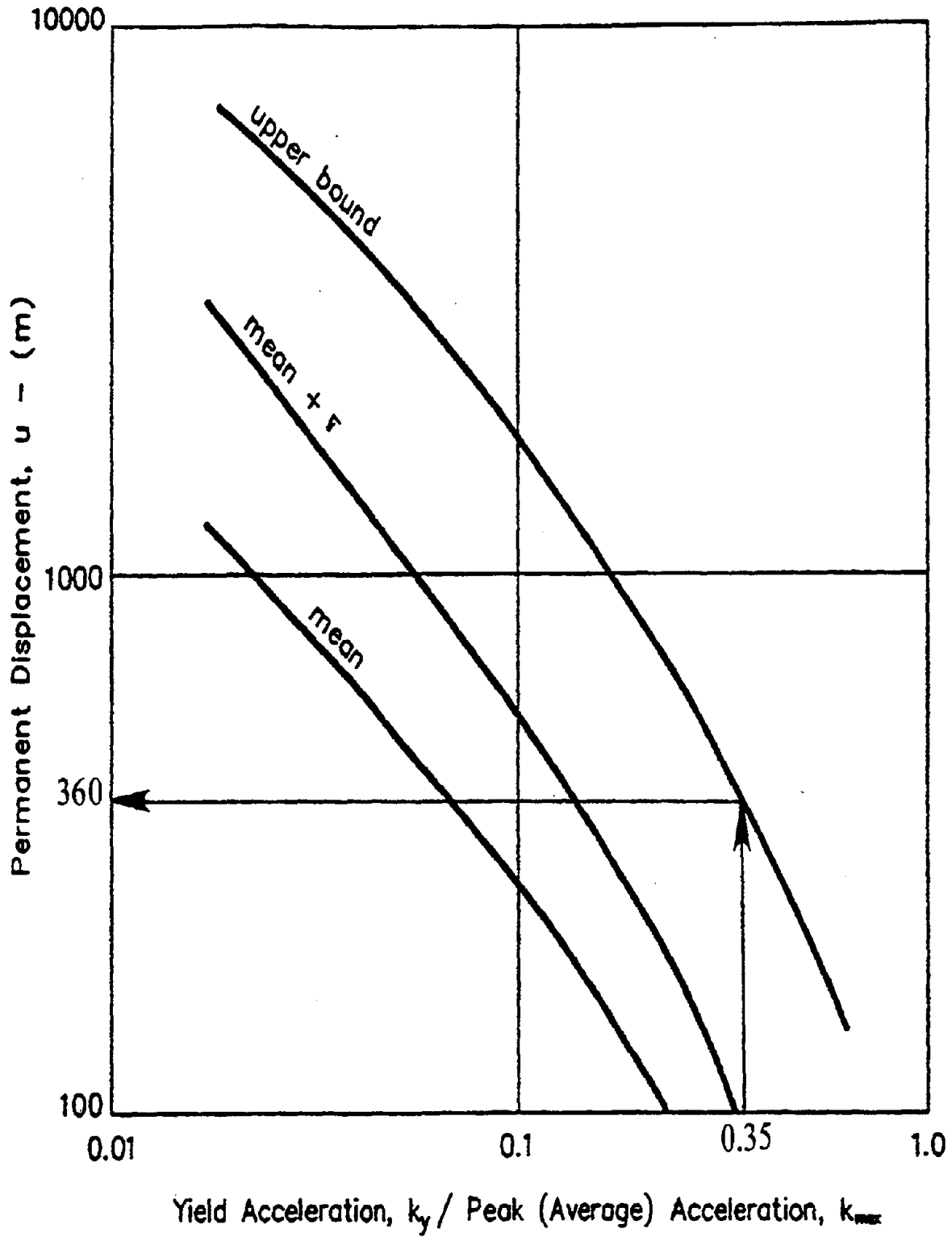


Figure 6-11: Permanent Seismic Deformation Chart (Modified from Hynes and Franklin, 1984, reprinted by permission of U.S. Army Engineer Waterways Experiment Station).

calculated assuming that the soil liquefies immediately following the start of strong ground motion. As this potential amount of lateral spreading at the toe of the embankment was considered to be repairable in the designated time period by the design engineers, no additional remedial action was considered necessary. Note that for the OLE, the ratio of yield to peak acceleration is 0.7 and the upper bound on the anticipated amount of lateral spreading is less than 0.15 m. This magnitude of lateral spreading is considered negligible.

6.7 SITE RESPONSE ANALYSES

A site specific response analysis was conducted to develop response spectra for the OLE and CLE for use in design of the bridge structure. The response analysis was conducted using the in-house modified computer program SHAKE91 (Schnabel et al., 1972; Idriss and Sun, 1992). Input time histories were selected using the methods described in Chapter 4 of Part I. Table 6-1 presents the target values for acceleration intensity, duration, and energy content for the two design events. Tables 6-2 and 6-3 show the time histories that were screened for use in the analyses and identify the selected time histories for the CLE and OLE, respectively.

The input time histories, scaled to the appropriate peak acceleration, were specified as outcrop motions in the SHAKE analyses. The soil profile for the SHAKE analyses were based upon the cross hole velocity profile shown in Figure 6-7, laboratory density and shear strength values for the silt and clay strata, and modulus reduction and damping curves from Vucetic and Dobry (1991). Results of the SHAKE analyses are presented in Figures 6-12 and 6-13. In Figure 6-12, response spectra at the top of the silty clay stratum in the channel are plotted for the three input OLE time histories. Also shown in this figure is the smoothed response spectra recommended for use in design. Figure 6-13 presents the same information for the CLE. In Figure 6-14, the smoothed response spectra for the OLE and CLE are plotted together for comparison. These results clearly demonstrate the focusing of seismic energy around the predominant period of the site, estimated to be approximately 0.3 seconds, and the influence of the long period motions of the CLE design event on site response.

6.8 DETAILED CALCULATIONS

EXAMPLE 5 - LIQUEFACTION POTENTIAL ANALYSIS (DEPTH = 4.5 m)

The calculation sheets for Example 5, "Liquefaction Potential Analysis" follow. Equation numbers that appear in the right margin of the calculation sheets refer back to Part I. Included are input and output files for a sample PCSTABL4 and SHAKE analysis.

The liquefaction potential at depth 4.5 m below the original ground surface is evaluated in this example. For other depths, a spreadsheet was developed and the calculations are shown in Tables 6-4, 6-5, and 6-6. The liquefaction potential analysis described in this example is found in Chapter 8 of Part I.

Free-Field

Step 1: Develop Subsurface Profile (see Figures 6-4 and 6-5)

Step 2: Evaluate Initial Stresses

$$\sigma_o = (1.5 \text{ m})(16 \text{ kN/m}^3) + (3 \text{ m})(18 \text{ kN/m}^3) = 78 \text{ kPa}$$

$$u_o = (2 \text{ m})(9.8 \text{ kN/m}^3) = 20 \text{ kPa}$$

$$\sigma'_o = \sigma_o - u_o = 78 - 20 = 58 \text{ kPa}$$

**TABLE 6-2
MAIN CHARACTERISTICS OF CANDIDATE CLE ACCELEROGRAMS**

Accelerogram	Earthquake	Recording Station		Strong Motion Characteristics		
		Epicentral Distance	Local Site Conditions	Uncorr. PHGA ⁽¹⁾	Significant Duration ⁽²⁾	RMSA ⁽³⁾
Los Angeles Dam-Right Abutment (S20W)	Northridge ($M_w = 6.7$)	11 km	Weak Rock (Non-marine deposit)	0.32 g	6.51 sec	0.113 g
Los Angeles Dam-Downhole (116 deg)	Northridge ($M_w = 6.7$)	11 km	Weak Rock (Non-marine deposit)	0.35 g	8.01 sec	0.088 g
Pacoima Dam-Downstream (265 deg)	Northridge ($M_w = 6.7$)	17.7 km	Hard Rock (Highly jointed Diorite gneiss)	0.446 g	4.11 sec	0.105 g
Pacoima-Kagel Canyon Fire Station (360 deg)	Northridge ($M_w = 6.7$)	17.7 km	Hard Rock (Sedimentary)	0.434 g	9.82 sec	0.104 g
Griffith Park (360 deg)	Northridge ($M_w = 6.7$)	24 km	Rock	0.166 g	11.4 sec	0.047 g
Castaic - Old Ridge Route (90 deg)	Northridge ($M_w = 6.7$)	41 km	Rock (Sedimentary)	0.58 g	9.06 sec	0.014 g
Corralitos-Eureka Canyon Road (0 deg)	Santa Cruz Mountains ($M_w = 6.9$)	14 km	Weak Rock (Pliocene Sediments)	0.643 g	6.86 sec	0.170 g
Saratoga-Aloha Avenue (0 deg)	Santa Cruz Mountains ($M_w = 6.9$)	11.7 km	Soft Rock (Plio-Pleistocene Sediment)	0.52 g	9.40 sec	0.099 g
Petrolia (90 deg)	Cape Mendocino/Petrolia ($M_w = 7.0$)	5 km	Weak Rock (Joyner & Boore Class B)	0.685 g	16.05 sec	0.122 g
Rio Dell (270 deg)	Cape Mendocino/Petrolia ($M_w = 7.0$)	15 km	Alluvium (50 ft or 15 m)	0.385 g	15.36 sec	0.076 g
C4 - Synthetic (Silva, 1995)	Synthesized for Northridge Earthquake ($M_w = 6.7$)	8.4 km	Weak Rock	0.417 g	6.70 sec	0.154 g
PEABP2TA - Synthetic (Chin, 1996)	Synthesized for Elysian Park Thrust ($M_w = 7.25$)	10-16 km	Weak Rock	0.85 g	8.33 sec	0.30 g

- Notes: (1) Uncorrected peak horizontal acceleration (PHGA) value of strong motion record before digital processing.
(2) Significant duration of strong shaking, D_s , as defined by Trifunac and Brady (1975).
(3) Root Mean Square Acceleration (RMSA) over the significant duration of the record scaled to PHGA.
Redlined Accelerograms eliminated from further consideration.

**TABLE 6-3
MAIN CHARACTERISTICS OF CANDIDATE OLE ACCELEROGRAMS**

Accelerogram	Earthquake	Recording Station		Strong Motion Characteristics		
		Epicentral Distance	Local Site Conditions	Uncorr. PHGA ⁽¹⁾	Significant Duration ⁽²⁾	RMSA ⁽³⁾
Indio-Coachella Canal (90 deg)	Landers ($M_w = 7.3$)	61 km	Deep alluvium	0.111 g	39.66 sec	0.023 g
Joshua Tree-Fire Station (90 deg)	Landers ($M_w = 7.2$)	14 km	Shallow alluvium over granite bedrock	0.287 g	28.22 sec	0.071 g
Taft-Lincoln School Tunnel (S69E)	Kern County ($M_w = 7.4$)	42 km	Weak Rock	0.187 g	28.87 sec	0.036 g
Olympia-Washington Highway Test Lab (N86E)	Western Washington ($M_w = 7.1$)	39 km	Deep Cohesionless Soil	0.275 g	18.08 sec	0.059 g
Tabas	Tabas-e-Golshan	3 km	Sedimentary and Conglomerated Rock	0.785 g	16.28 sec	0.176 g
Managua	Managua, Nicaragua ($M_w = 6.3$)	5 km	Soil (I-S)	0.382 g	6.50 sec	0.066 g
Lima	Lima, Peru ($M_w = 7.6$)	38 km	Soil	0.255 g	47.81 sec	0.041 g
Old Appleton (N340)	Cape Girardeau ($M_w = 4.8$)	46 km	-	0.175 g	34.90 sec	0.040 g
Sitka Observatory	Alaska ($M_w = 7.7$)	45 km	Soil	0.108 g	28.86 sec	0.016 g
University of Hawaii (344 deg)	Island of Hawaii ($M_w = 7.2$)	43 km	-	0.197 g	0.027 sec	0.027 g
A1 (Jennings et al., 1968)	Synthetic earthquake on San Andreas fault ($M_w = 8^+$)	General near-field	General stiff soil site	0.390 g	41.51 sec	0.120 g
MAG-8 (Seed and Idriss, 1969)	Synthetic earthquake on San Andreas fault ($M_w = 8.25$)	General near-field	General rock site	0.420 g	38.60 sec	0.102 g

Notes: (1) Uncorrected peak horizontal acceleration (PHGA) value of strong motion record before digital processing.
(2) Significant duration of strong shaking, D_s , as defined by Trifunac and Brady (1975).
(3) Root Mean Square Acceleration (RMSA) over the significant duration of the record scaled to PHGA.
Redlined Accelerograms eliminated from further consideration.

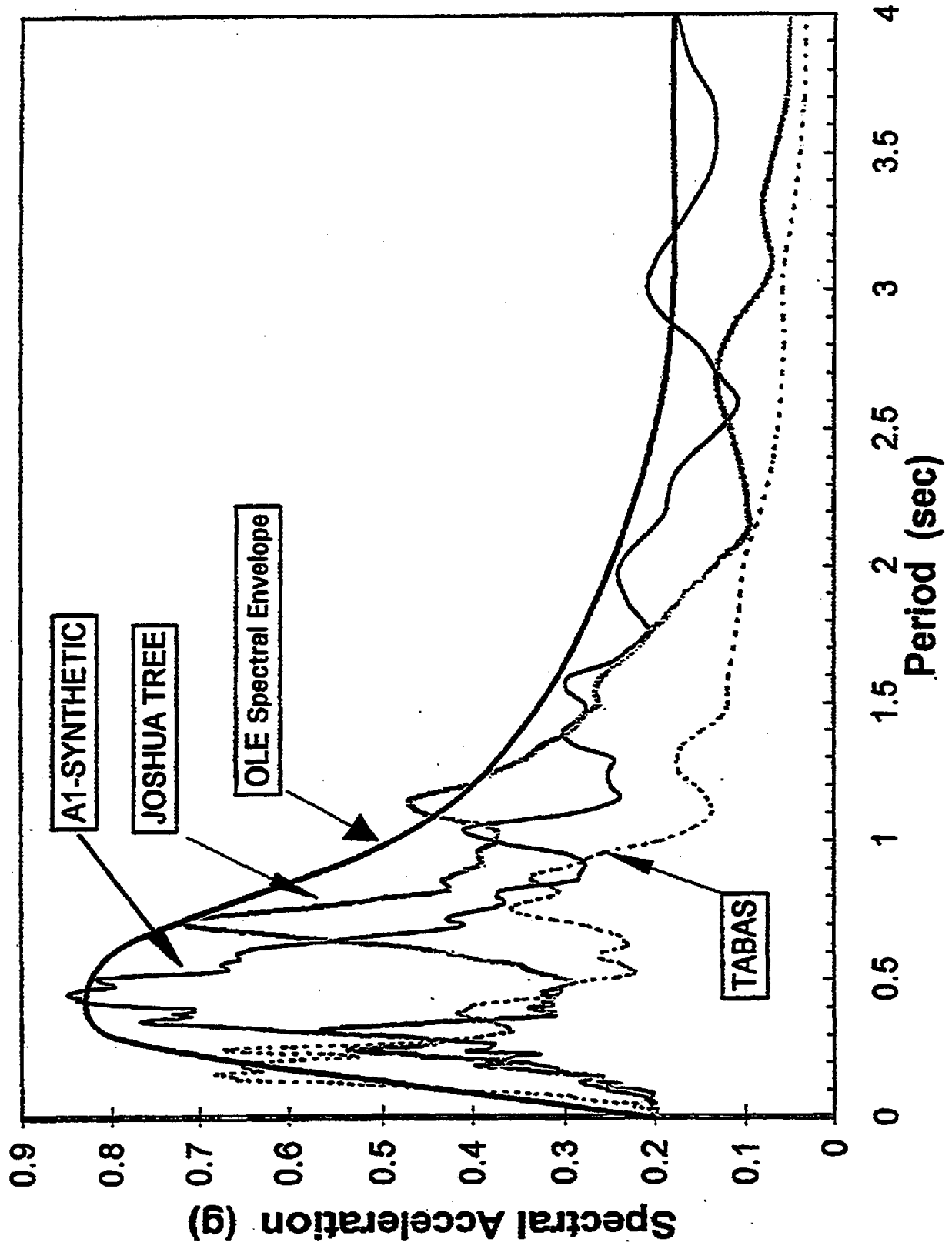


Figure 6-12: Response Spectra from SHAKE Analysis for OLE Events.

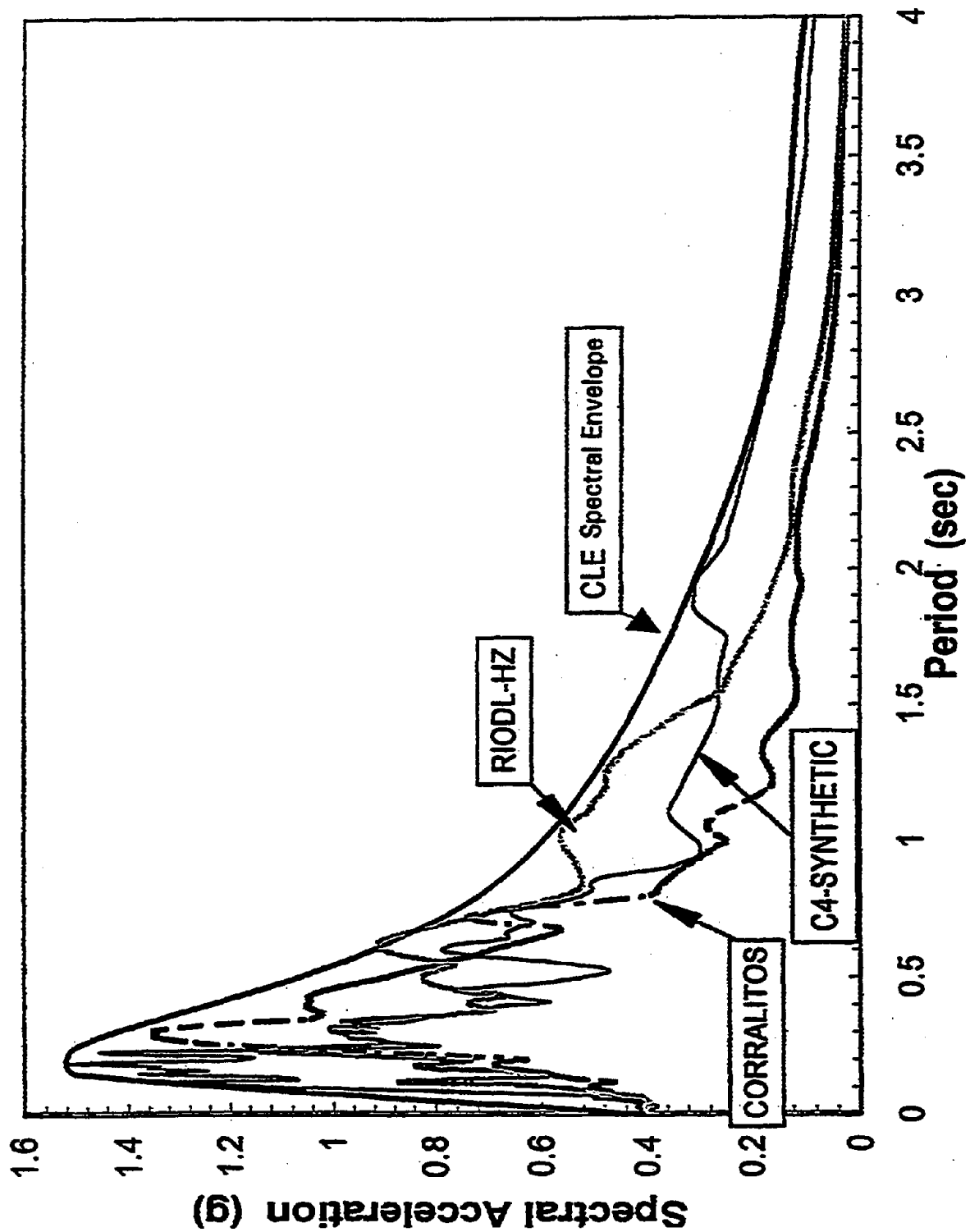


Figure 6-13: Response Spectra from SHAKE analysis for CLE Events.

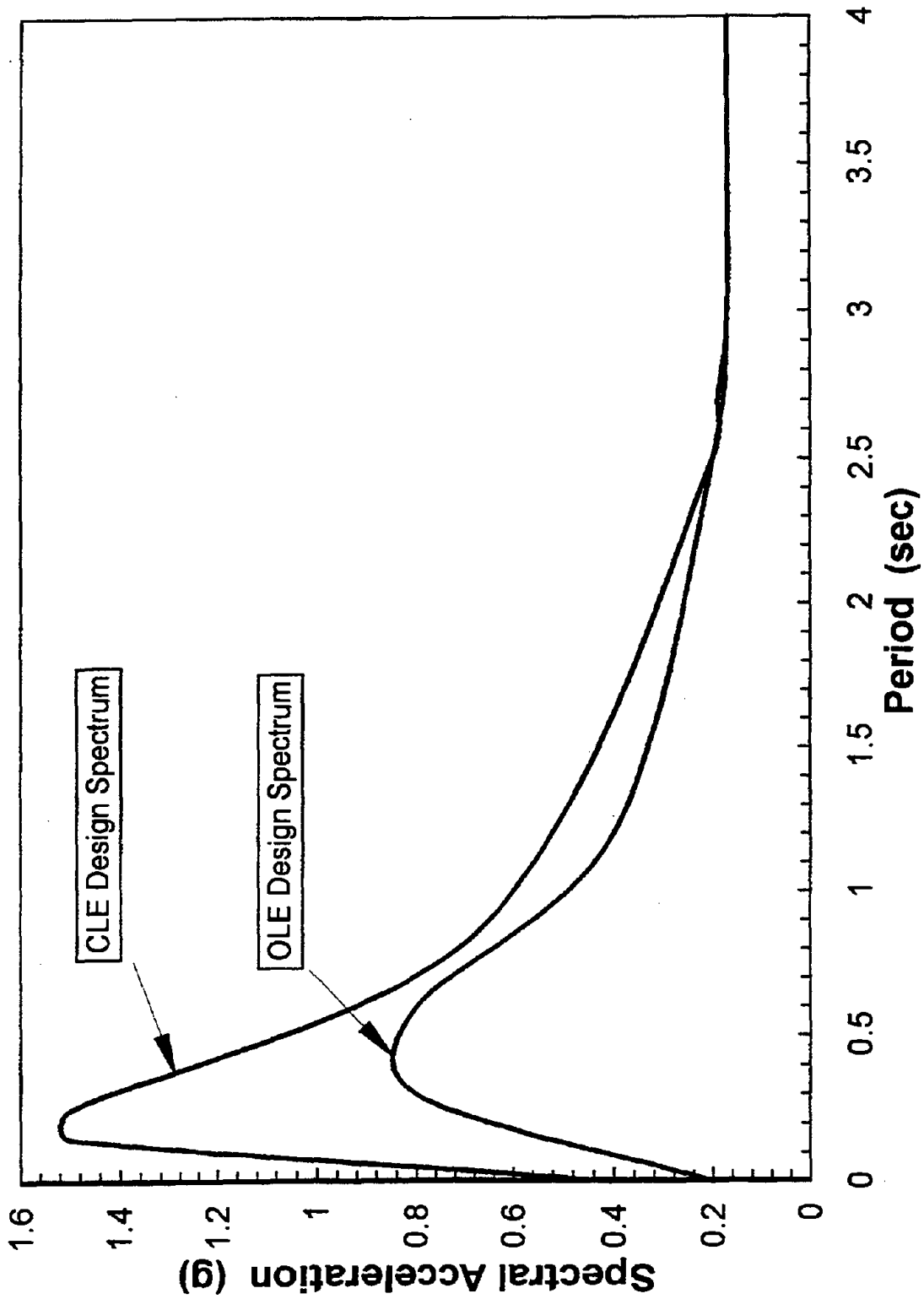


Figure 6-14: Design Response Spectra.

Step 3: Evaluate Stress Reduction Factor

$$r_d = 1 - 0.00765z = 0.00765(4.5) = 0.966 \quad (8-1)$$

Step 4: Evaluate the Critical Stress Ratio Induced by the Earthquake

$$CSR_{cq} = 0.65 (a_{max}/g) r_d \sigma_v/\sigma'_v \quad (8-3a)$$

Evaluate CSR_{cq} for two design events:

(1) OLE ($a_{max} = 0.2$ g; $M_w = 8.0$)

$$CSR_{cq} = (0.65)(0.2)(0.966) 78/58 = 0.169$$

(2) CLE ($a_{max} = 0.4$ g; $M_w = 7.0$)

$$CSR_{cq} = (0.65)(0.4)(0.966) 78/58 = 0.338$$

Step 5: Standardized Blow Count Value

Tables 5-2 and 5-3 in Part I are used to evaluate the standardized blow count. For this example, except for the rod length effect, C_{RL} , no corrections are necessary to apply since standard equipment was used for the SPT tests.

$$\text{Rod Length} \approx \text{Depth} + 1 \text{ m} = 4.5 + 1 \text{ m} = 5.5 \text{ m}$$

$$C_{RL} = 0.85 \text{ (from Table 8-3 in Part I)}$$

$$C_{60} = 0.85$$

$$N_{60} = N \cdot C_{60} = 11 \times 0.85 = 9.4 \quad (5-6)$$

Step 6: Correction for SPT N value for Overburden Pressure

$$C_N = 9.79 (1/\sigma'_o)^{1/2} = 9.79(1/58)^{1/2} = 1.29 \quad (5-10)$$

$$(N_1)_{60} = C_N N_{60} = (1.29)(9.4) = 12 \quad (5-11)$$

Step 7: Evaluate Critical Stress Ratio Resisting Liquefaction (Figure 8-3 in Part I)

$$\text{For } (N_1)_{60} = 12 \text{ and a fines content of } 5\%, CSR_{7.5} = 0.13$$

Step 8: Correct Critical Stress Ratio Resisting Liquefaction

$$CSR_L = CSR_{7.5} k_M k_x k_v \quad (8-4)$$

- k_M is read from Figure 8-4 in Part I

$$M_w = 8.0 \quad k_M = 0.84$$

$$M_w = 7.0 \quad k_M = 1.25$$

- $\sigma'_v = 58 \text{ kPa}$

$$\sigma'_m = [(1 + 2 K_\sigma) / 3] \sigma'_v = [(1 + 2 \times 0.5) / 3] 58 = 39 \text{ kPa} \quad (5-12)$$

$K_\sigma = 1.0$, read from Figure 8-5 in Part I

- $k_\alpha = 1.0$, no initial static shear

(1) OLE ($a_{\max} = 0.2 \text{ g}$; $M_w = 8.0$)

$$CSR_L = CSR_{7.5} k_M k_\alpha k_\sigma = (0.13)(1.0)(1.0)(0.84) = 0.11 \quad (8-4)$$

(2) CLE ($a_{\max} = 0.4 \text{ g}$; $M_w = 7.0$)

$$CSR_L = (0.13)(1.0)(1.0)(1.25) = 0.163$$

Step 9: Calculate Factor of Safety

(1) OLE ($a_{\max} = 0.2 \text{ g}$; $M_w = 8.0$)

$$FS_L = CSR_L / CSR_{eq} = 0.11 / 0.169 = 0.651$$

(2) CLE ($a_{\max} = 0.4 \text{ g}$; $M_w = 7.0$)

$$FS_L = CSR_L / CSR_{eq} = 0.163 / 0.338 = 0.482$$

The results of the calculation for other depths are presented in Table 6-4.

Under Centerline of Embankment (Depth = 8 m below top of embankment)

Step 1: Develop Subsurface Profile (see Figures 6-4 and 6-5)

Step 2: Evaluate Initial Stresses

$$\sigma_v = (5 \text{ m})(20 \text{ kN/m}^3) + (3 \text{ m})(18 \text{ kN/m}^3) = 154 \text{ kPa}$$

$$u_o = (2 \text{ m})(9.8 \text{ kN/m}^3) = 20 \text{ kPa}$$

$$\sigma'_v = \sigma_v - u_o = 154 - 20 = 134 \text{ kPa}$$

Step 3: Evaluate Stress Reduction Factor

$$r_d = 1 - 0.00765z = 1 - 0.00765(8) = 0.939 \quad (8-1)$$

Step 4: Evaluate the Critical Stress Ratio Induced by the Earthquake

$$CSR_{eq} = 0.65 (a_{\max}/g) r_d \sigma_v / \sigma'_v \quad (8-3a)$$

**TABLE 6-4
LIQUEFACTION POTENTIAL IN THE FREE-FIELD**

Depth (m)	N _{field}	σ _v	σ _v '	σ _m '	C _N	C ₆₀	(N ₁) ₆₀	r _d	CLE event: a _{max} = 0.4 g; M _w = 7						
									k _M	k _σ	k _σ	CSR _{eq}	CSR _{7.5}	CSR _L	FS
3	9	51.0	46	31	1.44	0.85	11	0.977	1.25	1.000	1.0	0.282	0.120	0.150	0.53
4.5	11	78.0	58	39	1.29	0.85	12	0.966	1.25	1.000	1.0	0.338	0.130	0.163	0.48
6	13	105.0	70	47	1.17	0.95	14.4	0.954	1.25	1.000	1.0	0.372	0.160	0.200	0.54
7.5	15	132.0	82	55	1.08	0.95	15.4	0.943	1.25	1.000	1.0	0.394	0.170	0.213	0.54
9	17	159.0	94	63	1.01	1	17.2	0.931	1.25	1.000	1.0	0.409	0.189	0.236	0.58
10.5	19	186.0	106	71	0.95	1	18.1	0.894	1.25	1.000	1.0	0.407	0.199	0.249	0.61
12	26	214.5	120	80	0.89	1	23.1	0.854	1.25	1.000	1.0	0.400	0.256	0.320	0.80
13.5	32	243.0	133	89	0.85	1	27.2	0.814	1.25	1.000	1.0	0.387	0.340	0.425	1.10
15	40	271.5	147	98	0.81	1	32.4	0.774	1.25	1.000	1.0	0.373	N/A	N/A	N/A
16.5	49	300.0	160	107	0.77	1	37.7	0.733	1.25	1.000	0.99	0.357	N/A	N/A	N/A
18	60	328.5	174	117	0.74	1	44.4	0.693	1.25	1.000	0.98	0.341	N/A	N/A	N/A
									OLE event: a _{max} = 0.2 g; M _w = 8						
3	9	51.0	46	31	1.44	0.85	11	0.977	0.84	1.000	1.0	0.141	0.120	0.101	0.72
4.5	11	78.0	58	39	1.29	0.85	12	0.966	0.84	1.000	1.0	0.169	0.130	0.109	0.64
6	13	105.0	70	47	1.17	0.95	14.4	0.954	0.84	1.000	1.0	0.186	0.160	0.134	0.72
7.5	15	132.0	82	55	1.08	0.95	15.4	0.943	0.84	1.000	1.0	0.197	0.170	0.143	0.73
9	17	159.0	94	63	1.01	1	17.2	0.931	0.84	1.000	1.0	0.205	0.189	0.159	0.78
10.5	19	186.0	106	71	0.95	1	18.1	0.894	0.84	1.000	1.0	0.204	0.199	0.167	0.82
12	26	214.5	120	80	0.89	1	23.1	0.854	0.84	1.000	1.0	0.200	0.256	0.215	1.08
13.5	32	243.0	133	89	0.85	1	27.2	0.814	0.84	1.000	1.0	0.194	0.340	0.286	1.47
15	40	271.5	147	98	0.81	1	32.4	0.774	0.84	1.000	1.0	0.187	N/A	N/A	N/A
16.5	49	300.0	160	107	0.77	1	37.7	0.733	0.84	1.000	0.99	0.179	N/A	N/A	N/A
18	60	328.5	174	117	0.74	1	44.4	0.693	0.84	1.000	0.98	0.171	N/A	N/A	N/A

*Fines Content = 5%

N _{field}	SPT blow-count from field investigations	σ _v	Total overburden stress
C _N	Correction factor for overburden pressure (Equation 5-10 of Part I)	σ _v '	Effective overburden stress
C ₆₀	Correction factor for equipment (Tables 5-2 and 5-3 of Part I)	σ _m '	Effective confining stress
(N ₁) ₆₀	SPT blow count corrected as per Equation 5-11 of Part I	FS _L	Factor of Safety against liquefaction
r _d	Stress reduction factor (Equation 8-1 of Part I)	a _{max}	Peak ground acceleration
k _M	Magnitude correction factor (Figure 8-4 of Part I)	M _w	Moment magnitude
k _σ	Initial static shear stress correction factor (Figure 8-6 of Part I)		CLE Contingency Level Event
k _σ	Stress level correction factor (Figure 8-5 of Part I)		OLE Operational Level Event
CSR _{eq}	Critical stress ratio imposed by the earthquake (Equation 8-3a of Part I)	N/A	Not Applicable (for (N ₁) ₆₀ > 30, CSR _{7.5} becomes very large as shown on Figure 8-3 of Part I)
CSR _{7.5}	Critical stress ratio read from Figure 8-3 of Part I		
CSR _L	Critical stress ratio from Figure 8-3 corrected as per Equation 8-4 of Part I		

Evaluate CSR_{cq} for two design events:

- (1) OLE ($a_{max} = 0.2$ g; $M_w = 8.0$)

$$CSR_{cq} = (0.65)(0.2)(0.939)154/134 = 0.140$$

- (2) CLE ($a_{max} = 0.4$ g; $M_w = 7.0$)

$$CSR_{cq} = (0.65)(0.4)(0.939)154/134 = 0.281$$

Step 5: Standardized Blow Count Value

Tables 5-2 and 5-3 in Part I are used to evaluate the standardized blow count. For this example, except for the rod length effect, C_{RL} , no corrections are necessary to apply since standard equipment was used for the SPT tests.

$$N_{60} = 9.4 \text{ (same as for the free-field analysis)}$$

Step 6: Correction for SPT N value for Overburden Pressure

The construction of the embankment has an effect on the overburden pressure but it is assumed that it will not affect the SPT values. Under the 3.5 meters of fill, the settlement of the sand layer will be negligible; consequently, the liquefaction resistance of the sand as measured by the SPT value is not affected by the increase in overburden pressure. Therefore the corrected SPT values to use in the analysis are the same as for the free-field analysis.

$$(N_1)_{60} = (N_1)_{60 \text{ free-field}} = 12$$

Step 7: Evaluate Critical Stress Ratio Resisting Liquefaction (Figure 8-5 in Volume I)

$$\text{For } (N_1)_{60} = 12 \text{ and a fines content of } 5\% \quad CSR_{7.5} = 0.13$$

Step 8: Correct Critical Stress Ratio Resisting Liquefaction

$$CSR_L = CSR_{7.5} k_M k_\alpha k_\sigma$$

- k_M is read from Figure 8-4 in Part I

$$M_w = 8.0 \quad k_M = 0.84$$

$$M_w = 7.0 \quad k_M = 1.25$$

$$\sigma'_v = 134 \text{ kPa}$$

$$\sigma'_m = [(1 + 2 K_0) / 3] \sigma'_v = [(1 + 2 \times 0.5) / 3] 134 = 89.3 \text{ kPa} < 96 \text{ kPa}$$

$$K_\sigma = 1.0 \text{ (see Figure 8-5 in Part I)}$$

- $k_\alpha = 1.0$, no initial static shear

(1) OLE ($a_{\max} = 0.2 \text{ g}$; $M_w = 8.0$)
 $CSR_L = (0.13)(1.0)(1.0)(0.84) \approx 0.11$

(2) CLE ($a_{\max} = 0.4 \text{ g}$; $M_w = 7.0$)
 $CSR_L = (0.13)(1.0)(1.0)(1.25) \approx 0.163$

Step 9: Calculate Factor of Safety Against Liquefaction

(1) OLE ($a_{\max} = 0.2 \text{ g}$; $M_w = 8.0$)
 $FS_L = CSR_L / CSR_{cq} = 0.11 / 0.14 = 0.786$

(2) CLE ($a_{\max} = 0.4 \text{ g}$; $M_w = 7.0$)
 $FS_L = CSR_L / CSR_{cq} = 0.163 / 0.281 = 0.58$

The results of the calculation for other depths are presented in Table 6-5.

TABLE 6-5
LIQUEFACTION POTENTIAL UNDER THE CENTERLINE OF THE EMBANKMENT.

Depth (m)	N_{field}	σ_v	σ_v'	σ_m'	C_N	C_{60}	$(N_1)_{60}$	r_d	CLE event: $a_{max} = 0.4 g$; $M_w = 7$						
									k_M	k_σ	k_τ	CSR_{eq}	$CSR_{7.5}$	CSR_L	FS_L
3	9	127	122	81	1.44	0.85	11	0.95	1.25	1.000	1.0	0.257	0.120	0.150	0.58
4.5	11	154	134	89	1.29	0.85	12	0.939	1.25	1.000	1.0	0.281	0.130	0.163	0.58
6	13	181	151	101	1.17	0.95	14.4	0.920	1.25	1.000	1.0	0.287	0.160	0.200	0.70
7.5	15	208	163	109	1.08	0.95	15.4	0.88	1.25	1.000	0.99	0.292	0.170	0.210	0.72
9	17	235	175	117	1.01	1	17.2	0.84	1.25	1.000	0.98	0.293	0.189	0.232	0.79
10.5	19	262	187	125	0.95	1	18.1	0.80	1.25	1.000	0.96	0.291	0.199	0.239	0.82
12	26	290.5	200.5	135	0.89	1	23.1	0.76	1.25	1.000	0.94	0.286	0.256	0.301	1.05
13.5	32	319	214	143	0.85	1	27.2	0.72	1.25	1.000	0.93	0.279	0.340	0.395	1.42
15	40	347.5	227.5	152	0.81	1	32.4	0.68	1.25	1.000	0.92	0.270	N/A	N/A	N/A
16.5	49	376	241	161	0.77	1	37.7	0.64	1.25	1.000	0.91	0.260	N/A	N/A	N/A
18	60	404.5	254.5	170	0.74	1	44.4	0.60	1.25	1.000	0.90	0.248	N/A	N/A	N/A
									OLE event: $a_{max} = 0.2 g$; $M_w = 8$						
3	9	127	122	81	1.44	0.85	11	0.95	0.84	1.000	1.0	0.129	0.120	0.101	0.78
4.5	11	154	134	89	1.29	0.85	12	0.939	0.84	1.000	1.0	0.141	0.130	0.109	0.77
6	13	181	151	101	1.17	0.95	14.4	0.920	0.84	1.000	1.0	0.144	0.160	0.134	0.93
7.5	15	208	163	109	1.08	0.95	15.4	0.88	0.84	1.000	0.99	0.146	0.170	0.142	0.97
9	17	235	175	117	1.01	1	17.2	0.84	0.84	1.000	0.98	0.147	0.189	0.156	1.06
10.5	19	262	187	125	0.95	1	18.1	0.80	0.84	1.000	0.96	0.146	0.199	0.160	1.10
12	26	290.5	200.5	135	0.89	1	23.1	0.76	0.84	1.000	0.94	0.143	0.256	0.202	1.41
13.5	32	319	214	143	0.85	1	27.2	0.72	0.84	1.000	0.93	0.140	0.340	0.266	1.90
15	40	347.5	227.5	152	0.81	1	32.4	0.68	0.84	1.000	0.92	0.135	N/A	N/A	N/A
16.5	49	376	241	161	0.77	1	37.7	0.64	0.84	1.000	0.91	0.130	N/A	N/A	N/A
18	60	404.5	254.5	170	0.74	1	44.4	0.60	0.84	1.000	0.90	0.124	N/A	N/A	N/A

Fines Content = 5%

N_{field}	SPT blow-count from field investigations	σ_v	Total overburden stress
C_N	Correction factor for overburden pressure (Equation 5-10 of Part I)	σ_v'	Effective overburden stress
C_{60}	Correction factor for equipment (Tables 5-2 and 5-3 of Part I)	σ_m'	Effective confining stress
$(N_1)_{60}$	SPT blow count corrected as per Equation 5-11 of Part I	FS_L	Factor of Safety against liquefaction
r_d	Stress reduction factor (Equation 8-1 of Part I)	a_{max}	Peak ground acceleration
k_M	Magnitude correction factor (Figure 8-4 of Part I)	M_w	Moment magnitude
k_σ	Initial static shear stress correction factor (Figure 8-6 of Part I)		CLE Contingency Level Event
k_τ	Stress level correction factor (Figure 8-5 of Part I)		OLE Operational Level Event
CSR_{eq}	Critical stress ratio imposed by the earthquake (Equation 8-3a of Part I)	N/A	Not Applicable (for $(N_1)_{60} > 30$, $CSR_{7.5}$ becomes very large as shown on Figure 8-3 of Part I)
$CSR_{7.5}$	Critical stress ratio read from Figure 8-3 of Part I		
CSR_L	Critical stress ratio from Figure 8-3 corrected as per Equation 8-4 of Part I		

EXAMPLE 5
PCSTABL Output File

** pcSTABL4 **

by
Purdue University

1 --Slope Stability Analysis--
 Simplified Janbu Method of Slices
 or Simplified Bishop Method

Run Date: 7-23-96
Time of Run: 10:33
Run By: THH
Input Data Filename: liq3ole
Output Filename: liq3ole.out

PROBLEM DESCRIPTION Liquefaction example
 Dynamic analysis

BOUNDARY COORDINATES

7 Top Boundaries
10 Total Boundaries

Boundary No.	X-Left (ft)	Y-Left (ft)	X-Right (ft)	Y-Right (ft)	Soil Type Below Bnd
1	.00	50.00	35.00	50.00	3
2	35.00	50.00	50.00	50.00	1
3	50.00	50.00	67.22	61.48	1
4	67.22	61.48	126.26	61.48	1
5	126.26	61.48	143.48	50.00	1
6	143.48	50.00	163.60	50.00	1
7	163.60	50.00	200.00	50.00	3
8	35.00	50.00	45.00	45.00	3
9	153.60	45.00	163.60	50.00	3
10	.00	45.00	200.00	45.00	2

1 ISOTROPIC SOIL PARAMETERS

3 Type(s) of Soil

Soil Type No.	Total Unit Wt. (pcf)	Saturated Unit Wt. (pcf)	Cohesion Intercept (psf)	Friction Angle (deg)	Pore Pressure Param.	Pressure Constant (psf)	Piez. Surface No.
1	118.0	118.0	200.0	32.0	.00	.0	0
2	115.0	115.0	.0	33.0	.00	.0	0
3	110.0	110.0	150.0	.0	.00	.0	0

A Horizontal Earthquake Loading Coefficient
Of .100 Has Been Assigned

A Vertical Earthquake Loading Coefficient
Of .000 Has Been Assigned

Cavitation Pressure = .0 psf

1 A Critical Failure Surface Searching Method, Using A Random

Technique For Generating Circular Surfaces, Has Been Specified.

400 Trial Surfaces Have Been Generated.

20 Surfaces Initiate From Each Of 20 Points Equally Spaced
Along The Ground Surface Between X = 10.00 ft.
and X = 50.00 ft.

Each Surface Terminates Between X = 65.00 ft.
and X = 100.00 ft.

Unless Further Limitations Were Imposed, The Minimum Elevation
At Which A Surface Extends Is Y = .00 ft.

2.00 ft. Line Segments Define Each Trial Failure Surface.

1 Following Are Displayed The Ten Most Critical Of The Trial
Failure Surfaces Examined. They Are Ordered - Most Critical
First.

* * Safety Factors Are Calculated By The Modified Janbu Method * *

Failure Surface Specified By 26 Coordinate Points

*** 1.856 ***

Failure Surface Specified By 28 Coordinate Points

*** 1.901 ***

1 Failure Surface Specified By 29 Coordinate Points

*** 1.919 ***

Failure Surface Specified By 16 Coordinate Points

*** 1.935 ***

1 Failure Surface Specified By 17 Coordinate Points

*** 1.962 ***

Failure Surface Specified By 27 Coordinate Points

*** 1.968 ***

1 Failure Surface Specified By 19 Coordinate Points

*** 1.968 ***

Failure Surface Specified By 15 Coordinate Points

*** 1.971 ***

1

Failure Surface Specified By 29 Coordinate Points

*** 1.986 ***

Failure Surface Specified By 17 Coordinate Points

*** 1.987 ***

Note: Failure surface coordinates omitted from the original PCSTABL output.

SHAKE Output File

```

*****
* SHAKE -- A COMPUTER PROGRAM FOR EARTHQUAKE RESPONSE *
* ANALYSIS OF HORIZONTALLY LAYERED SITES *
* by: Per B. Schnabel & John Lysmer -- 1970 *
* ----- *
* Shake85 : IBM-PC version of SHAKE *
* by: S.S. (Willie) Lai, January 1985 *
* ----- *
* Shake88 : New modulus reduction curves for clays *
* added using results from Sun et al. (1988) *
* by: J. I. Sun & Ramin Golesorkhi *
* February 26, 1988 *
* ----- *
* Shake90/91: Adjust last iteration; Input now is either *
* Gmax or max Vs; up to 13 material types can *
* be specified by user; up to 50 Layers can *
* be specified; object motion can be read in *
* from a separate file and can have user *
* specified format; Different periods for *
* response spectral calculations; options *
* are renumbered; and general cleanup *
* by: J. I. Sun, I. M. Idriss & P. Dirrim *
* June 1990 - February 1991 *
* ----- *
* Shake91 : General cleanup and finalization of input / *
* output format ... etc *
* by: I. M. Idriss *
* December 1991 *
* ----- *
* Shake94 : Routine for direct calculation of average *
* (á1) acceleration is added to the program. Out- *
* put format is modified to enable the two - *
* - page landscape printing. The following *
* modulus reduction and damping curves are *
* added: Kavazanjian & Matasovic (1995) for *
* municipal solid waste; Matasovic & Vucetic *
* (1993) for SMB sand; and Vucetic and Dobry *
* (1991) for clays of various plasticities. *
* by: Neven Matasovic *
* August 1993 - May 1994 *
*****

```

```

MAX. NUMBER OF TERMS IN FOURIER TRANSFORM = 4096
NECESSARY LENGTH OF BLANK COMMON X = 25619

```

***** OPTION 1 *** READ RELATION BETWEEN SOIL PROPERTIES AND STRAIN

MATERIAL TYPE NO. 2

CURVE NO. 3: #2 ATTENUATION OF ROCK AVERAGE
CURVE NO. 4: DAMPING IN ROCK

CURVE NO. 3		CURVE NO. 4	
STRAIN	G/Gmax	STRAIN	DAMPING
.0001	1.000	.0001	.40
.0003	1.000	.0010	.80
.0010	.988	.0100	1.50
.0030	.952	.1000	3.00
.0100	.900	1.0000	4.60
.0300	.810	.0000	.00
.1000	.725	.0000	.00
1.0000	.550	.0000	.00

MATERIAL TYPE NO. 6

CURVE NO. 11:
CURVE NO. 12:

CURVE NO.11		CURVE NO.12	
STRAIN	G/Gmax	STRAIN	DAMPING

MATERIAL TYPE NO. 3

CURVE NO. 5: #3 Modulus for Peat (TETC modification of Seed & Idriss
CURVE NO. 6: Damping for Clay used for Peat (Seed & Idriss, 1990)

CURVE NO. 5		CURVE NO. 6	
STRAIN	G/Gmax	STRAIN	DAMPING
.0001	1.000	.0001	1.98
.0003	.830	.0003	2.03
.0010	.680	.0010	2.69
.0030	.550	.0030	3.54
.0100	.450	.0100	4.59
.0300	.366	.0300	6.56
.1000	.293	.1000	9.18
.3000	.225	.3000	3.77
1.0000	.160	1.0000	19.48
3.0000	.099	3.1600	25.38
10.0000	.020	10.0000	28.00

***** OPTION 2 *** READ SOIL / WASTE PROFILE

SOIL PROFILE NO. 1 Channel deposit

NUMBER OF LAYERS 9
DEPTH TO BEDROCK 112.0

NO.	TYPE	THICKNESS (ft)	DEPTH (ft)	TOT. PRESS. (psf)	MODULUS (ksf)	DAMPING (%)	UNIT WT. (pcf)	SH. VEL. (fps)

1	3	6.00	3.00	300.00	629.	5.00	100.00	450.0
2	5	15.00	13.50	1425.00	854.	5.00	110.00	500.0
3	1	18.00	30.00	3285.00	1286.	5.00	115.00	600.0
4	4	15.00	46.50	5220.00	1698.	5.00	120.00	675.0
5	1	15.00	61.50	7057.50	2040.	5.00	125.00	725.0
6	1	15.00	76.50	8955.00	2544.	5.00	128.00	800.0
7	1	12.00	90.00	10695.00	4502.	5.00	130.00	1056.0
8	4	16.00	104.00	12435.00	16435.	5.00	120.00	2100.0
9	BASE				39130.	1.00	140.00	3000.0

PERIOD = .500 sec FROM AVERAGE SHEAR WAVE VELOCITY OF 895.3 ft/sec

FREQUENCY AMPLITUDE:
 MAXIMUM AMPLIFICATION = 14.13
 FOR FREQUENCY (f) = 2.02 c/sec
 FOR PERIOD (1 / f) = .50 sec

***** OPTION 3 *** READ INPUT MOTION

FILE NAME FOR INPUT MOTION = ri odl-hz.sar
 NO. OF INPUT ACCEL. POINTS = 1800
 NO. OF POINTS USED IN FFT = 4096
 NO. OF HEADING LINES = 5
 NO. OF POINTS PER LINE = 8
 TIME STEP FOR INPUT MOTION = .0200
 FORMAT FOR OF TIME HISTORY = (8F9.6)

***** ACCELEROGRAM HEADER *****

CAPE MENDOCINO, CA EQ.; Mw = 7.0; Ms = 7.1; H = 15 km; Thrust
 RIO DELL - 101/PAINTER ST. OVERPASS; CHAN 4: 270 Deg. (free-field)
 UNCOR MAX = -0.385 g @ 5.575 sec; MAX IN FILE = .385732 @ 5.58 sec
 RMS ACCEL OF (UNCOR) RECORD = .041 g; Mean sq. freq. = 3.01 Hz
 8*225 = 1800 POINTS OF ACCEL DATA EQUALLY SPACED AT .020 SEC. (UNITS: g)

** FIRST & LAST 5 LINES OF INPUT MOTION *****

1	-.002296	-.001777	.000569	.000731	-.003688	-.000583	.004051	.002788
2	.000964	-.002422	-.004550	-.004451	-.005423	-.008852	-.014746	-.015439
3	-.011380	-.006311	-.005492	-.008705	-.008035	-.006091	-.004255	-.001129
4	.002864	.006916	.010118	.005313	-.004705	-.003748	.003541	.005366
5	.000370	-.000956	.004816	.007193	.010419	.013203	.011285	.008016
..... INPUT MOTION READ NOT ECHOED.....								
221	-.005527	-.003620	-.002145	-.002337	-.002461	-.004595	-.007641	-.008303
222	-.007946	-.006056	-.005096	-.005324	-.005166	-.005233	-.004698	-.004398
223	-.002852	-.002130	-.002072	-.002438	-.002967	-.001687	.001139	.004567
224	.006282	.006832	.006628	.008013	.009033	.007818	.006191	.003176
225	.000796	-.001591	-.001767	.000490	.000460	-.001572	.000280	.001179

MAXIMUM ACCELERATION = .385732
 AT TIME = 5.58 sec

THE VALUES WILL BE MULTIPLIED BY A FACTOR = 1.03698900
 TO GIVE NEW MAXIMUM ACCELERATION = .40000000

MEAN SQUARE FREQUENCY = 3.02 c/sec

***** OPTION 4 *** READ WHERE OBJECT MOTION IS GIVEN

OBJECT MOTION IN LAYER NUMBER 9 OUTCROPPING

***** OPTION 5 *** OBTAIN STRAIN COMPATIBLE SOIL PROPERTIES

MAXIMUM NUMBER OF ITERATIONS = 8
 FACTOR FOR UNIFORM STRAIN IN TIME DOMAIN = .80

ACCELEROGRAM - ri odl-hz.sar
 P R O F I L E - Channel deposit

ITERATION NUMBER 1

VALUES IN TIME DOMAIN

NO	TYPE	DEPTH (ft)	UNIFRM. STRAIN	<---- DAMPING ---->			<---- SHEAR MODULUS ---->			G/Go RATIO
				NEW	USED	ERROR	NEW	USED	ERROR	
1	3	3.0	.02549	.063	.050	20.2	238.0	628.9	-164.2	1.000
2	5	13.5	.08523	.060	.050	16.7	594.5	854.0	-43.6	1.000
3	1	30.0	.11440	.105	.050	52.4	445.8	1285.7	-188.4	1.000
4	4	46.5	.12843	.126	.050	60.4	615.7	1698.0	-175.8	1.000
5	1	61.5	.13289	.113	.050	55.7	654.6	2040.5	-211.7	1.000
6	1	76.5	.12099	.108	.050	53.7	857.5	2544.1	-196.7	1.000
7	1	90.0	.07291	.086	.050	41.6	1984.8	4502.1	-126.8	1.000
8	4	104.0	.02222	.068	.050	26.6	11413.7	16434.8	-44.0	1.000

ACCELEROGRAM - ri odl-hz.sar
P R O F I L E - Channel deposit

ITERATION NUMBER 2

VALUES IN TIME DOMAIN

NO	TYPE	DEPTH (ft)	UNIFRM. STRAIN	<---- DAMPING ---->			<---- SHEAR MODULUS ---->			G/Go RATIO
				NEW	USED	ERROR	NEW	USED	ERROR	
1	3	3.0	.07669	.086	.063	27.1	194.4	238.0	-22.4	.378
2	5	13.5	.14287	.072	.060	17.1	518.0	594.5	-14.8	.696
3	1	30.0	.39431	.167	.105	37.3	202.2	445.8	-120.4	.347
4	4	46.5	.36728	.166	.126	24.0	331.1	615.7	-86.0	.363
5	1	61.5	.38060	.166	.113	32.0	327.0	654.6	-100.2	.321
6	1	76.5	.29116	.153	.108	29.7	471.1	857.5	-82.0	.337
7	1	90.0	.13044	.112	.086	23.4	1458.8	1984.8	-36.1	.441
8	4	104.0	.02521	.072	.068	4.8	11092.5	11413.7	-2.9	.694

ACCELEROGRAM - ri odl-hz.sar
P R O F I L E - Channel deposit

ITERATION NUMBER 3

VALUES IN TIME DOMAIN

NO	TYPE	DEPTH (ft)	UNIFRM. STRAIN	<---- DAMPING ---->			<---- SHEAR MODULUS ---->			G/Go RATIO
				NEW	USED	ERROR	NEW	USED	ERROR	
1	3	3.0	.06958	.084	.086	-2.5	198.1	194.4	1.9	.309
2	5	13.5	.12044	.068	.072	-6.9	544.8	518.0	4.9	.607
3	1	30.0	.60652	.187	.167	10.5	156.3	202.2	-29.4	.157
4	4	46.5	.43734	.172	.166	3.6	301.5	331.1	-9.8	.195
5	1	61.5	.48310	.177	.166	6.2	286.5	327.0	-14.1	.160
6	1	76.5	.38556	.166	.153	7.8	404.9	471.1	-16.3	.185
7	1	90.0	.12972	.112	.112	-.3	1463.2	1458.8	.3	.324
8	4	104.0	.01833	.063	.072	-13.8	11902.5	11092.5	6.8	.675

ACCELEROGRAM - ri odl-hz.sar
P R O F I L E - Channel deposit

ITERATION NUMBER 4

VALUES IN TIME DOMAIN

NO	TYPE	DEPTH (ft)	UNIFRM. STRAIN	<---- DAMPING ---->			<---- SHEAR MODULUS ---->			G/Go RATIO
				NEW	USED	ERROR	NEW	USED	ERROR	
1	3	3.0	.05954	.081	.084	-4.2	204.0	198.1	2.9	.315
2	5	13.5	.10029	.063	.068	-8.0	573.5	544.8	5.0	.638
3	1	30.0	.69363	.193	.187	3.2	141.9	156.3	-10.1	.122
4	4	46.5	.41420	.170	.172	-1.1	310.7	301.5	3.0	.178

5	1	61.5	.50639	.179	.177	1.2	278.6	286.5	-2.9	.140
6	1	76.5	.40123	.168	.166	1.1	396.5	404.9	-2.1	.159
7	1	90.0	.11523	.105	.112	-5.8	1555.4	1463.2	5.9	.325
8	4	104.0	.01550	.058	.063	-7.8	12328.8	11902.5	3.5	.724

ACCELEROGRAM - ri odl-hz.sar
 P R O F I L E - Channel deposit

ITERATION NUMBER 5

VALUES IN TIME DOMAIN

NO	TYPE	DEPTH (ft)	UNIFRM. STRAIN	<---- DAMPING ---->			<---- SHEAR MODULUS ---->			G/Go RATIO
				NEW	USED	ERROR	NEW	USED	ERROR	
1	3	3.0	.05622	.079	.081	-1.6	206.2	204.0	1.1	.324
2	5	13.5	.09239	.061	.063	-2.3	584.1	573.5	1.8	.671
3	1	30.0	.74033	.196	.193	1.5	135.0	141.9	-5.2	.110
4	4	46.5	.38865	.168	.170	-1.3	321.5	310.7	3.4	.183
5	1	61.5	.50932	.179	.179	.1	277.6	278.6	-.4	.137
6	1	76.5	.39803	.168	.168	-.2	398.2	396.5	.4	.156
7	1	90.0	.10570	.101	.105	-4.4	1622.6	1555.4	4.1	.345
8	4	104.0	.01470	.057	.058	-2.6	12464.9	12328.8	1.1	.750

ACCELEROGRAM - ri odl-hz.sar
 P R O F I L E - Channel deposit

ITERATION NUMBER 6

VALUES IN TIME DOMAIN

NO	TYPE	DEPTH (ft)	UNIFRM. STRAIN	<---- DAMPING ---->			<---- SHEAR MODULUS ---->			G/Go RATIO
				NEW	USED	ERROR	NEW	USED	ERROR	
1	3	3.0	.05531	.079	.079	-.5	206.8	206.2	.3	.328
2	5	13.5	.09023	.061	.061	-.6	587.2	584.1	.5	.684
3	1	30.0	.76916	.198	.196	.9	130.9	135.0	-3.1	.105
4	4	46.5	.37179	.167	.168	-.9	329.0	321.5	2.3	.189
5	1	61.5	.50659	.179	.179	-.1	278.5	277.6	.3	.136
6	1	76.5	.39215	.167	.168	-.4	401.3	398.2	.8	.157
7	1	90.0	.10045	.098	.101	-2.7	1662.3	1622.6	2.4	.360
8	4	104.0	.01446	.056	.057	-.8	12506.2	12464.9	.3	.758

ACCELEROGRAM - ri odl-hz.sar
 P R O F I L E - Channel deposit

ITERATION NUMBER 7

VALUES IN TIME DOMAIN

NO	TYPE	DEPTH (ft)	UNIFRM. STRAIN	<---- DAMPING ---->			<---- SHEAR MODULUS ---->			G/Go RATIO
				NEW	USED	ERROR	NEW	USED	ERROR	
1	3	3.0	.05511	.079	.079	-.1	207.0	206.8	.1	.329
2	5	13.5	.08976	.061	.061	-.1	587.8	587.2	.1	.688
3	1	30.0	.78798	.199	.198	.6	128.3	130.9	-2.0	.102
4	4	46.5	.36169	.166	.167	-.6	333.7	329.0	1.4	.194
5	1	61.5	.50253	.179	.179	-.2	279.9	278.5	.5	.136
6	1	76.5	.38679	.167	.167	-.4	404.2	401.3	.7	.158
7	1	90.0	.09757	.097	.098	-1.2	1690.6	1652.3	1.7	.369
8	4	104.0	.01437	.056	.056	-.3	12522.0	12506.2	.1	.761

ACCELEROGRAM - ri odl-hz.sar
 P R O F I L E - Channel deposit

ITERATION NUMBER 8

VALUES IN TIME DOMAIN

NO	TYPE	DEPTH (ft)	UNIFORM. STRAIN			DAMPING			SHEAR MODULUS			G/Go RATIO
			NEW	USED	ERROR	NEW	USED	ERROR	NEW	USED	ERROR	
1	3	3.0	.05511	.079	.079	.0	207.0	207.0	.0	.329		
2	5	13.5	.08973	.061	.061	.0	587.9	587.8	.0	.688		
3	1	30.0	.80060	.200	.199	.4	126.6	128.3	-1.3	.100		
4	4	46.5	.35575	.165	.166	-.4	336.5	333.7	.8	.197		
5	1	61.5	.49852	.178	.179	-.2	281.2	279.9	.5	.137		
6	1	76.5	.38247	.166	.167	-.3	406.6	404.2	.6	.159		
7	1	90.0	.09561	.096	.097	-.8	1711.1	1690.6	1.2	.376		
8	4	104.0	.01432	.056	.056	-.2	12530.8	12522.0	.1	.762		

VALUES IN TIME DOMAIN

LAYER	MAT. TYPE	THICKNESS (ft)	DEPTH (ft)	MAX. STRAIN (%)	MAX. STRESS (psf)	AVG. ACC. (g)	TIME (sec)
1	3	6.0	3.0	.06888	142.57	.47524	5.90
2	5	15.0	13.5	.11217	659.38	.46272	5.90
3	1	18.0	30.0	1.00075	1284.00	.39087	5.92
4	4	15.0	46.5	.44469	1483.86	.28427	5.90
5	1	15.0	61.5	.62315	1743.93	.24710	6.00
6	1	15.0	76.5	.47809	1932.67	.21582	5.94
7	1	12.0	90.0	.11951	2020.45	.18892	5.90
8	4	16.0	104.0	.01790	2241.34	.18024	5.88

PERIOD = .815 sec FROM AVERAGE SHEAR WAVE VELOCITY OF 549.8 ft/sec

FREQUENCY AMPLITUDE:

MAXIMUM AMPLIFICATION = 3.79
 FOR FREQUENCY (f) = .81 c/sec
 FOR PERIOD (1 / f) = 1.23 sec

***** OPTION 6 *** COMPUTE MOTION IN NEW SUBLAYERS

ACCELEROGRAM - ri0d1-hz.sar
 D E P O S I T - Channel deposit

LAYER	DEPTH (ft)	MAX. ACC. (g)	TIME (sec)	MN.SQ.FR. (c/sec)	ACC. RATIO QUIET ZONE	TH SAVED ACC.REC.
OUTCR.	.0	.47618	5.88	1.16	.001	512
WITHIN	6.0	.46614	5.88	1.09	.001	512

***** OPTION 9 *** COMPUTE RESPONSE SPECTRUM

RESPONSE SPECTRUM ANALYSIS FOR LAYER NUMBER 9
 CALCULATED FOR DAMPING .050

TIMES AT WHICH MAX. SPECTRAL VALUES OCCUR

TD = TIME FOR MAX. RELATIVE DISP.

TV = TIME FOR MAX. RELATIVE VEL.

TA = TIME FOR MAX. ABSOLUTE ACC.

DAMPING RATIO = .05

PER = .01	TIMES FOR MAX.	- TD = 5.5600	TV = 5.6400	TA = 5.5600
PER = .03	TIMES FOR MAX.	- TD = 5.5600	TV = 6.1200	TA = 5.5600
PER = .04	TIMES FOR MAX.	- TD = 5.5600	TV = 4.3600	TA = 5.5600
PER = .05	TIMES FOR MAX.	- TD = 5.5600	TV = 6.1200	TA = 5.5600
PER = .06	TIMES FOR MAX.	- TD = 5.5800	TV = 6.1200	TA = 5.5800
PER = .07	TIMES FOR MAX.	- TD = 5.5400	TV = 4.4400	TA = 5.5400
PER = .08	TIMES FOR MAX.	- TD = 5.5600	TV = 5.4600	TA = 5.5600
PER = .09	TIMES FOR MAX.	- TD = 5.5800	TV = 4.8000	TA = 5.5800
PER = .10	TIMES FOR MAX.	- TD = 5.5000	TV = 5.6200	TA = 5.5000
PER = .11	TIMES FOR MAX.	- TD = 5.5200	TV = 5.8800	TA = 6.1400
PER = .12	TIMES FOR MAX.	- TD = 6.1600	TV = 6.1400	TA = 6.1600

PER = .13	TIMES FOR MAX. -	TD = 6.1800	TV = 6.1400	TA = 6.1800
PER = .14	TIMES FOR MAX. -	TD = 6.8200	TV = 5.9000	TA = 6.8200
PER = .15	TIMES FOR MAX. -	TD = 5.5400	TV = 5.9200	TA = 5.5400
PER = .16	TIMES FOR MAX. -	TD = 5.5600	TV = 5.9200	TA = 5.5400
PER = .17	TIMES FOR MAX. -	TD = 5.5600	TV = 6.2200	TA = 5.5600
PER = .18	TIMES FOR MAX. -	TD = 6.2000	TV = 6.2400	TA = 6.2000
PER = .19	TIMES FOR MAX. -	TD = 5.6000	TV = 5.6600	TA = 5.6000
PER = .20	TIMES FOR MAX. -	TD = 7.6400	TV = 6.5800	TA = 7.6400
PER = .21	TIMES FOR MAX. -	TD = 6.4400	TV = 6.6000	TA = 6.5400
PER = .22	TIMES FOR MAX. -	TD = 6.5600	TV = 6.6200	TA = 6.5600
PER = .23	TIMES FOR MAX. -	TD = 6.4600	TV = 6.5200	TA = 6.4600
PER = .24	TIMES FOR MAX. -	TD = 6.4800	TV = 6.5400	TA = 6.4800
PER = .25	TIMES FOR MAX. -	TD = 6.8800	TV = 6.4400	TA = 6.8600
PER = .26	TIMES FOR MAX. -	TD = 5.4800	TV = 5.4000	TA = 5.0600
PER = .27	TIMES FOR MAX. -	TD = 5.5000	TV = 5.4200	TA = 5.5000
PER = .28	TIMES FOR MAX. -	TD = 5.5200	TV = 5.4400	TA = 5.5200
PER = .29	TIMES FOR MAX. -	TD = 5.5400	TV = 6.1000	TA = 5.5400
PER = .30	TIMES FOR MAX. -	TD = 5.5600	TV = 6.1000	TA = 5.5600
PER = .31	TIMES FOR MAX. -	TD = 6.0600	TV = 5.9800	TA = 6.0600
PER = .32	TIMES FOR MAX. -	TD = 5.6000	TV = 6.0000	TA = 5.6000
PER = .33	TIMES FOR MAX. -	TD = 8.7800	TV = 8.8600	TA = 8.7800
PER = .34	TIMES FOR MAX. -	TD = 8.8000	TV = 8.7200	TA = 8.8000
PER = .35	TIMES FOR MAX. -	TD = 8.8200	TV = 8.7400	TA = 8.8000
PER = .36	TIMES FOR MAX. -	TD = 8.8200	TV = 8.7400	TA = 8.8200
PER = .37	TIMES FOR MAX. -	TD = 8.8400	TV = 8.7400	TA = 8.8200
PER = .38	TIMES FOR MAX. -	TD = 8.8400	TV = 4.6600	TA = 8.8400
PER = .39	TIMES FOR MAX. -	TD = 4.5800	TV = 4.6600	TA = 4.5800
PER = .40	TIMES FOR MAX. -	TD = 5.6200	TV = 4.6800	TA = 5.6200
PER = .41	TIMES FOR MAX. -	TD = 5.6400	TV = 5.7400	TA = 5.6200
PER = .42	TIMES FOR MAX. -	TD = 5.6400	TV = 5.7600	TA = 5.6400
PER = .43	TIMES FOR MAX. -	TD = 4.6000	TV = 4.7000	TA = 4.6000
PER = .44	TIMES FOR MAX. -	TD = 5.1000	TV = 4.7000	TA = 5.1000
PER = .45	TIMES FOR MAX. -	TD = 5.1200	TV = 5.2200	TA = 5.1000
PER = .46	TIMES FOR MAX. -	TD = 5.1200	TV = 5.2200	TA = 5.1200
PER = .47	TIMES FOR MAX. -	TD = 5.1400	TV = 5.2400	TA = 5.1200
PER = .48	TIMES FOR MAX. -	TD = 5.1400	TV = 5.2400	TA = 5.1400
PER = .49	TIMES FOR MAX. -	TD = 5.1600	TV = 5.2600	TA = 5.1400
PER = .50	TIMES FOR MAX. -	TD = 5.1600	TV = 5.2800	TA = 5.1600
PER = .51	TIMES FOR MAX. -	TD = 5.1800	TV = 5.0600	TA = 5.1600
PER = .52	TIMES FOR MAX. -	TD = 5.1800	TV = 5.0600	TA = 5.1800
PER = .53	TIMES FOR MAX. -	TD = 5.1800	TV = 5.0800	TA = 5.1800
PER = .54	TIMES FOR MAX. -	TD = 5.2000	TV = 5.0800	TA = 5.1800
PER = .55	TIMES FOR MAX. -	TD = 5.5400	TV = 5.0800	TA = 5.5200
PER = .56	TIMES FOR MAX. -	TD = 5.5600	TV = 5.7200	TA = 5.5400
PER = .57	TIMES FOR MAX. -	TD = 5.5800	TV = 5.7400	TA = 5.5600
PER = .58	TIMES FOR MAX. -	TD = 5.6000	TV = 5.7600	TA = 5.5800
PER = .60	TIMES FOR MAX. -	TD = 5.6200	TV = 5.7800	TA = 5.6000
PER = .62	TIMES FOR MAX. -	TD = 5.6400	TV = 5.7800	TA = 5.6200
PER = .64	TIMES FOR MAX. -	TD = 5.6600	TV = 5.8000	TA = 5.6400
PER = .66	TIMES FOR MAX. -	TD = 5.6600	TV = 5.8000	TA = 5.6600
PER = .68	TIMES FOR MAX. -	TD = 5.6800	TV = 5.8200	TA = 5.6600
PER = .70	TIMES FOR MAX. -	TD = 5.6800	TV = 5.8200	TA = 5.6800
PER = .72	TIMES FOR MAX. -	TD = 5.7000	TV = 5.8400	TA = 5.6800
PER = .74	TIMES FOR MAX. -	TD = 5.7200	TV = 6.3200	TA = 5.7000
PER = .76	TIMES FOR MAX. -	TD = 5.7200	TV = 6.3400	TA = 5.7000
PER = .78	TIMES FOR MAX. -	TD = 5.7200	TV = 6.3400	TA = 5.7200
PER = .80	TIMES FOR MAX. -	TD = 5.7400	TV = 6.3400	TA = 5.7200
PER = .82	TIMES FOR MAX. -	TD = 6.1600	TV = 6.3600	TA = 6.1600
PER = .84	TIMES FOR MAX. -	TD = 6.1800	TV = 6.3600	TA = 6.1800
PER = .86	TIMES FOR MAX. -	TD = 6.2000	TV = 6.3800	TA = 6.1800
PER = .88	TIMES FOR MAX. -	TD = 6.2200	TV = 6.0000	TA = 6.2000
PER = .90	TIMES FOR MAX. -	TD = 6.2200	TV = 6.0200	TA = 6.2200
PER = .92	TIMES FOR MAX. -	TD = 6.2400	TV = 6.0200	TA = 6.2200
PER = .94	TIMES FOR MAX. -	TD = 6.2600	TV = 6.0200	TA = 6.2400
PER = .96	TIMES FOR MAX. -	TD = 6.2600	TV = 6.0200	TA = 6.2400
PER = .98	TIMES FOR MAX. -	TD = 6.2800	TV = 6.0200	TA = 6.2600
PER = 1.00	TIMES FOR MAX. -	TD = 6.2800	TV = 6.0200	TA = 6.2800
PER = 1.05	TIMES FOR MAX. -	TD = 6.3200	TV = 6.0400	TA = 6.3000

PER = 1.10	TIMES FOR MAX.	- TD = 6.3600	TV = 6.0600	TA = 6.3400
PER = 1.15	TIMES FOR MAX.	- TD = 7.0400	TV = 6.1800	TA = 7.0200
PER = 1.20	TIMES FOR MAX.	- TD = 8.3400	TV = 7.4000	TA = 8.3200
PER = 1.25	TIMES FOR MAX.	- TD = 9.0400	TV = 8.7600	TA = 9.0200
PER = 1.30	TIMES FOR MAX.	- TD = 9.1400	TV = 8.8200	TA = 9.1200
PER = 1.35	TIMES FOR MAX.	- TD = 9.2200	TV = 8.9000	TA = 9.2000
PER = 1.40	TIMES FOR MAX.	- TD = 8.6600	TV = 8.9600	TA = 8.6400
PER = 1.45	TIMES FOR MAX.	- TD = 8.7000	TV = 6.9600	TA = 8.6800
PER = 1.50	TIMES FOR MAX.	- TD = 9.5000	TV = 6.9800	TA = 9.4800
PER = 1.55	TIMES FOR MAX.	- TD = 9.5800	TV = 7.0600	TA = 9.5600
PER = 1.60	TIMES FOR MAX.	- TD = 6.7600	TV = 7.0800	TA = 6.7400
PER = 1.65	TIMES FOR MAX.	- TD = 6.8000	TV = 7.1000	TA = 6.7600
PER = 1.70	TIMES FOR MAX.	- TD = 6.8200	TV = 5.6400	TA = 6.7800
PER = 1.75	TIMES FOR MAX.	- TD = 6.8400	TV = 5.6400	TA = 6.8000
PER = 1.80	TIMES FOR MAX.	- TD = 6.0400	TV = 5.6400	TA = 6.0000
PER = 1.85	TIMES FOR MAX.	- TD = 6.1000	TV = 5.6400	TA = 6.0800
PER = 1.90	TIMES FOR MAX.	- TD = 6.1200	TV = 5.6400	TA = 6.1000
PER = 1.95	TIMES FOR MAX.	- TD = 6.1200	TV = 5.6400	TA = 6.1000
PER = 2.00	TIMES FOR MAX.	- TD = 6.1400	TV = 5.6400	TA = 6.1000
PER = 2.05	TIMES FOR MAX.	- TD = 6.1400	TV = 5.6400	TA = 6.1200
PER = 2.10	TIMES FOR MAX.	- TD = 6.1400	TV = 5.6400	TA = 6.1200
PER = 2.15	TIMES FOR MAX.	- TD = 6.1400	TV = 5.6400	TA = 6.1200
PER = 2.20	TIMES FOR MAX.	- TD = 9.6400	TV = 5.6400	TA = 9.6200
PER = 2.25	TIMES FOR MAX.	- TD = 9.6800	TV = 5.6400	TA = 9.6400
PER = 2.30	TIMES FOR MAX.	- TD = 9.7000	TV = 5.6400	TA = 9.6600
PER = 2.35	TIMES FOR MAX.	- TD = 9.7400	TV = 5.6400	TA = 9.7000
PER = 2.40	TIMES FOR MAX.	- TD = 9.7800	TV = 5.6400	TA = 9.7400
PER = 2.50	TIMES FOR MAX.	- TD = 9.8400	TV = 5.6400	TA = 9.8000
PER = 2.60	TIMES FOR MAX.	- TD = 12.6400	TV = 5.6400	TA = 12.6000
PER = 2.70	TIMES FOR MAX.	- TD = 12.7200	TV = 5.8800	TA = 12.6800
PER = 2.80	TIMES FOR MAX.	- TD = 6.2000	TV = 5.8800	TA = 6.1600
PER = 2.90	TIMES FOR MAX.	- TD = 6.2200	TV = 5.8800	TA = 6.1600
PER = 3.00	TIMES FOR MAX.	- TD = 6.3800	TV = 5.8800	TA = 6.3400
PER = 3.10	TIMES FOR MAX.	- TD = 6.4000	TV = 5.8800	TA = 6.3600
PER = 3.20	TIMES FOR MAX.	- TD = 6.4000	TV = 5.8800	TA = 6.3600
PER = 3.30	TIMES FOR MAX.	- TD = 5.5000	TV = 5.8800	TA = 5.4600
PER = 3.40	TIMES FOR MAX.	- TD = 5.5000	TV = 5.8800	TA = 5.4600
PER = 3.50	TIMES FOR MAX.	- TD = 5.5200	TV = 5.8800	TA = 5.4600
PER = 3.60	TIMES FOR MAX.	- TD = 5.5200	TV = 5.8800	TA = 5.4600
PER = 3.70	TIMES FOR MAX.	- TD = 5.5200	TV = 5.8800	TA = 5.4600
PER = 3.80	TIMES FOR MAX.	- TD = 5.5200	TV = 5.8800	TA = 5.4600
PER = 3.90	TIMES FOR MAX.	- TD = 5.5200	TV = 5.8800	TA = 5.4600
PER = 4.00	TIMES FOR MAX.	- TD = 5.5200	TV = 5.8800	TA = 5.4600
PER = 4.10	TIMES FOR MAX.	- TD = 11.9200	TV = 5.8800	TA = 11.8600
PER = 4.20	TIMES FOR MAX.	- TD = 11.9400	TV = 5.8800	TA = 11.8800
PER = 4.30	TIMES FOR MAX.	- TD = 11.9600	TV = 5.8800	TA = 11.9000
PER = 4.40	TIMES FOR MAX.	- TD = 11.9800	TV = 5.8800	TA = 11.9200
PER = 4.50	TIMES FOR MAX.	- TD = 9.8600	TV = 5.8800	TA = 9.7800
PER = 4.60	TIMES FOR MAX.	- TD = 9.8800	TV = 5.8800	TA = 9.7800
PER = 4.70	TIMES FOR MAX.	- TD = 9.9000	TV = 5.8800	TA = 9.8000
PER = 4.80	TIMES FOR MAX.	- TD = 9.9400	TV = 5.8800	TA = 9.8400
PER = 4.90	TIMES FOR MAX.	- TD = 10.2400	TV = 5.8800	TA = 10.2000
PER = 5.00	TIMES FOR MAX.	- TD = 10.2800	TV = 5.8800	TA = 10.2000
PER = 5.10	TIMES FOR MAX.	- TD = 10.5600	TV = 5.8800	TA = 10.5200
PER = 5.20	TIMES FOR MAX.	- TD = 10.6000	TV = 5.8800	TA = 10.5200
PER = 5.40	TIMES FOR MAX.	- TD = 10.7400	TV = 5.8800	TA = 10.7000
PER = 5.60	TIMES FOR MAX.	- TD = 10.7800	TV = 5.8800	TA = 10.7200
PER = 5.80	TIMES FOR MAX.	- TD = 10.8200	TV = 5.8800	TA = 10.7400
PER = 6.00	TIMES FOR MAX.	- TD = 10.8600	TV = 5.8800	TA = 10.7600
PER = 6.20	TIMES FOR MAX.	- TD = 11.0400	TV = 5.8800	TA = 10.8000
PER = 6.40	TIMES FOR MAX.	- TD = 11.0800	TV = 5.8800	TA = 11.0200
PER = 6.60	TIMES FOR MAX.	- TD = 11.1000	TV = 5.8800	TA = 11.0400
PER = 6.80	TIMES FOR MAX.	- TD = 11.1400	TV = 5.8800	TA = 11.0600
PER = 7.00	TIMES FOR MAX.	- TD = 11.3400	TV = 5.8800	TA = 11.0800
PER = 7.20	TIMES FOR MAX.	- TD = 18.8000	TV = 5.8800	TA = 18.7000
PER = 7.40	TIMES FOR MAX.	- TD = 15.8000	TV = 5.8800	TA = 15.6800
PER = 7.60	TIMES FOR MAX.	- TD = 16.0000	TV = 5.8800	TA = 15.9600
PER = 7.80	TIMES FOR MAX.	- TD = 16.0800	TV = 5.8800	TA = 15.9800

PER = 8.00 TIMES FOR MAX. - TD = 16.2800 TV = 5.3400 TA = 16.2200
 PER = 8.50 TIMES FOR MAX. - TD = 16.4800 TV = 5.3400 TA = 16.2800
 PER = 9.00 TIMES FOR MAX. - TD = 12.7600 TV = 5.3400 TA = 12.6400
 PER = 9.50 TIMES FOR MAX. - TD = 9.1200 TV = 5.3400 TA = 8.6800

SPECTRAL VALUES --

[Acceleration of gravity used = 32.20]

Channel deposit

DAMPING RATIO = .05

NO.	PERIOD	REL.DISP.	REL.VEL.	PSU.REL.VEL.	ABS.ACC.	PSU.ABS.ACC.	FREQ.
1	.01	.00003	.00046	.02044	.39908	.39887	100.00
2	.03	.00030	.01027	.06226	.40595	.40497	33.33
3	.04	.00052	.01847	.08173	.39917	.39870	25.00
4	.05	.00081	.02559	.10145	.39709	.39591	20.00
5	.06	.00120	.04522	.12598	.40882	.40971	16.67
6	.07	.00164	.05642	.14726	.41139	.41050	14.29
7	.08	.00262	.08950	.20611	.50323	.50273	12.50
8	.09	.00345	.10164	.24073	.52235	.52193	11.11
9	.10	.00462	.15772	.29010	.57207	.56606	10.00
10	.11	.00615	.26615	.35140	.63195	.62335	9.09
11	.12	.01010	.37763	.52891	.86651	.86006	8.33
12	.13	.01022	.36754	.49392	.73485	.74138	7.69
13	.14	.00928	.33240	.41653	.59344	.58055	7.14
14	.15	.01189	.36002	.49805	.65094	.64790	6.67
15	.16	.01425	.42591	.55954	.67738	.68240	6.25
16	.17	.01900	.54535	.70222	.81595	.80603	5.88
17	.18	.02209	.66672	.77122	.83500	.83605	5.56
18	.19	.02231	.63587	.73766	.75761	.75757	5.26
19	.20	.02384	.68937	.74906	.73279	.73082	5.00
20	.21	.03245	.97318	.97098	.89860	.90223	4.76
21	.22	.04016	1.12919	1.14696	1.01850	1.01730	4.55
22	.23	.04893	1.34189	1.33681	1.13829	1.13413	4.35
23	.24	.05327	1.41448	1.39473	1.13022	1.13398	4.17
24	.25	.04816	1.19123	1.21031	.94875	.94467	4.00
25	.26	.04833	1.09688	1.16788	.88725	.87650	3.85
26	.27	.05457	1.12735	1.26998	.91243	.91782	3.70
27	.28	.05998	1.08096	1.34589	.93576	.93794	3.57
28	.29	.06573	1.20591	1.42409	.95755	.95821	3.45
29	.30	.07248	1.43049	1.51806	.98905	.98740	3.33
30	.31	.07869	1.49902	1.59491	.99943	1.00392	3.23
31	.32	.07603	1.52572	1.49289	.91779	.91033	3.13
32	.33	.08573	1.45130	1.63239	.95937	.96524	3.03
33	.34	.09293	1.58596	1.71735	.97889	.98561	2.94
34	.35	.08897	1.52094	1.59727	.89869	.89050	2.86
35	.36	.08518	1.45384	1.48672	.81032	.80584	2.78
36	.37	.08256	1.38740	1.40207	.74136	.73942	2.70
37	.38	.08057	1.38080	1.33224	.69048	.68410	2.63
38	.39	.08685	1.42869	1.39917	.69829	.70005	2.56
39	.40	.09506	1.45615	1.49319	.73210	.72841	2.50
40	.41	.10146	1.48890	1.55482	.73676	.73998	2.44
41	.42	.10170	1.50159	1.52137	.71580	.70682	2.38
42	.43	.10021	1.44514	1.46428	.66709	.66448	2.33
43	.44	.10779	1.42713	1.53923	.68129	.68261	2.27
44	.45	.11979	1.52055	1.67259	.73130	.72527	2.22
45	.46	.13195	1.60292	1.80228	.76705	.76452	2.17
46	.47	.14191	1.68114	1.89711	.79097	.78763	2.13
47	.48	.15144	1.70611	1.98230	.80937	.80585	2.08
48	.49	.15917	1.72732	2.04102	.81806	.81279	2.04
49	.50	.16681	1.72178	2.09625	.82019	.81808	2.00
50	.51	.17161	1.76990	2.11423	.81758	.80892	1.96
51	.52	.17727	1.82332	2.14200	.80362	.80379	1.92
52	.53	.17975	1.85917	2.13098	.79282	.78456	1.89
53	.54	.18304	1.89959	2.12978	.76951	.76960	1.85
54	.55	.18863	1.91174	2.15485	.76509	.76450	1.82
55	.56	.20404	2.05439	2.28929	.79816	.79769	1.79
56	.57	.21975	2.23594	2.42237	.83059	.82926	1.75

57	.58	.23475	2.39955	2.54306	.86037	.85556	1.72
58	.60	.26313	2.67290	2.75548	.89874	.89613	1.67
59	.62	.28459	2.83653	2.88412	.91214	.90771	1.61
60	.64	.29750	2.86089	2.92067	.89898	.89049	1.56
61	.66	.30479	2.76251	2.90162	.86215	.85787	1.52
62	.68	.30702	2.62209	2.83684	.81677	.81405	1.47
63	.70	.30669	2.45482	2.75283	.77387	.76737	1.43
64	.72	.30781	2.29779	2.68618	.72966	.72799	1.39
65	.74	.30475	2.25480	2.58759	.68812	.68232	1.35
66	.76	.30093	2.33112	2.48786	.64081	.63876	1.32
67	.78	.29415	2.35489	2.36949	.59603	.59277	1.28
68	.80	.28899	2.31478	2.26971	.55799	.55361	1.25
69	.82	.29072	2.29165	2.22763	.53167	.53009	1.22
70	.84	.29991	2.27060	2.24331	.52229	.52112	1.19
71	.86	.31341	2.25612	2.28980	.52080	.51955	1.16
72	.88	.32937	2.28778	2.35169	.52390	.52146	1.14
73	.90	.34723	2.36514	2.42414	.52790	.52558	1.11
74	.92	.36710	2.45947	2.50710	.53394	.53175	1.09
75	.94	.38744	2.55702	2.58975	.54118	.53759	1.06
76	.96	.41062	2.65669	2.68751	.54843	.54626	1.04
77	.98	.43341	2.75190	2.77878	.55693	.55329	1.02
78	1.00	.45545	2.83103	2.86170	.56130	.55840	1.00
79	1.05	.49637	2.93984	2.97028	.55560	.55199	.95
80	1.10	.50641	2.79994	2.89258	.51546	.51312	.91
81	1.15	.53286	2.85465	2.91137	.49652	.49400	.87
82	1.20	.55783	2.99701	2.92080	.47734	.47495	.83
83	1.25	.60256	3.05147	3.02879	.47561	.47281	.80
84	1.30	.62708	3.17183	3.03080	.45676	.45492	.77
85	1.35	.63041	3.14471	2.93406	.42645	.42409	.74
86	1.40	.61428	2.97409	2.75690	.38654	.38425	.71
87	1.45	.59415	2.71080	2.57458	.34938	.34647	.69
88	1.50	.55837	2.56719	2.33889	.30599	.30426	.67
89	1.55	.50576	2.39877	2.05019	.25933	.25810	.65
90	1.60	.50700	2.30907	1.99098	.24426	.24281	.63
91	1.65	.51166	2.17438	1.94839	.23202	.23042	.61
92	1.70	.50999	2.13678	1.88492	.21821	.21636	.59
93	1.75	.50093	2.10896	1.79855	.20273	.20054	.57
94	1.80	.49143	2.07196	1.71542	.18751	.18596	.56
95	1.85	.48759	2.02636	1.65602	.17498	.17467	.54
96	1.90	.48361	1.97456	1.59927	.16503	.16425	.53
97	1.95	.47797	1.91994	1.54009	.15519	.15411	.51
98	2.00	.47086	1.86601	1.47926	.14555	.14432	.50
99	2.05	.46441	1.81579	1.42339	.13678	.13549	.49
100	2.10	.45839	1.77142	1.37150	.12889	.12744	.48
101	2.15	.45358	1.73412	1.32554	.12188	.12030	.47
102	2.20	.47526	1.70419	1.35733	.12115	.12039	.45
103	2.25	.49811	1.68116	1.39098	.12151	.12063	.44
104	2.30	.51470	1.66412	1.40606	.12006	.11929	.43
105	2.35	.52568	1.65180	1.40550	.11737	.11670	.43
106	2.40	.53012	1.64287	1.38784	.11365	.11284	.42
107	2.50	.51775	1.63002	1.30126	.10234	.10157	.40
108	2.60	.52509	1.61702	1.26894	.09573	.09523	.38
109	2.70	.49002	1.62714	1.14033	.08311	.08241	.37
110	2.80	.44091	1.63050	.98939	.07030	.06895	.36
111	2.90	.42646	1.62437	.92399	.06349	.06217	.34
112	3.00	.41493	1.60920	.86902	.05700	.05652	.33
113	3.10	.40391	1.58668	.81866	.05221	.05153	.32
114	3.20	.39115	1.55909	.76802	.04755	.04683	.31
115	3.30	.37886	1.52877	.72134	.04427	.04265	.30
116	3.40	.37878	1.49779	.69998	.04182	.04017	.29
117	3.50	.37704	1.46779	.67685	.03937	.03774	.29
118	3.60	.37414	1.43998	.65300	.03701	.03539	.28
119	3.70	.37037	1.41513	.62894	.03477	.03317	.27
120	3.80	.36620	1.39366	.60551	.03268	.03109	.26
121	3.90	.36207	1.37569	.58332	.03076	.02919	.26
122	4.00	.35830	1.36110	.56282	.02902	.02746	.25
123	4.10	.38420	1.34961	.58878	.02841	.02802	.24
124	4.20	.40691	1.34094	.60874	.02871	.02828	.24

125	4.30	.42513	1.33467	.62120	.02865	.02819	.23
126	4.40	.43841	1.33041	.62605	.02824	.02776	.23
127	4.50	.44777	1.32777	.62521	.02753	.02711	.22
128	4.60	.47135	1.32640	.64382	.02769	.02731	.22
129	4.70	.49334	1.32597	.65952	.02771	.02738	.21
130	4.80	.51388	1.32620	.67266	.02762	.02735	.21
131	4.90	.53276	1.32684	.68314	.02748	.02720	.20
132	5.00	.56267	1.32763	.70707	.02791	.02759	.20
133	5.10	.59540	1.32848	.73353	.02827	.02807	.20
134	5.20	.63441	1.32921	.76656	.02901	.02876	.19
135	5.40	.71325	1.32992	.82991	.03016	.02999	.19
136	5.60	.78412	1.32919	.87978	.03099	.03066	.18
137	5.80	.84196	1.32673	.91210	.03111	.03069	.17
138	6.00	.88577	1.32254	.92758	.03061	.03017	.17
139	6.20	.92380	1.31669	.93619	.02960	.02946	.16
140	6.40	.95385	1.30931	.93644	.02884	.02855	.16
141	6.60	.96846	1.30058	.92197	.02766	.02726	.15
142	6.80	.96842	1.29075	.89482	.02615	.02568	.15
143	7.00	.96416	1.28006	.86543	.02438	.02412	.14
144	7.20	.96031	1.26867	.83803	.02296	.02271	.14
145	7.40	1.00756	1.25675	.85550	.02273	.02256	.14
146	7.60	1.05649	1.24439	.87343	.02260	.02243	.13
147	7.80	1.08640	1.23191	.87513	.02220	.02189	.13
148	8.00	1.10868	1.23626	.87076	.02146	.02124	.13
149	8.50	1.06940	1.26059	.79050	.01843	.01815	.12
150	9.00	1.04769	1.28333	.73142	.01618	.01586	.11
151	9.50	1.02550	1.30422	.67825	.01450	.01393	.11
152	10.00	.00000	.00000	.00000	.00000	.00000	.10

VALUES IN PERIOD RANGE .1 TO 2.5 SEC.

AREA OF ACC. RESPONSE SPECTRUM	=	1.064
AREA OF VEL. RESPONSE SPECTRUM	=	5.052
MAX. ACCELERATION RESPONSE VALUE	=	1.138
MAX. VELOCITY RESPONSE VALUE	=	3.172

6.9 SUMMARY AND CONCLUSIONS

A cable-stayed bridge with an approach embankment that traverses liquefiable ground is to be constructed in a coastal city in the western United States. The project site is located in a broad coastal plain and lies in an area of high seismic exposure due to its proximity to three faults and a "blind" fold and thrust belt.

The soil stratigraphy beneath the embankment consists of 5 m of recent alluvium overlying up to 20 m of marine terrace deposits of silty sand, sandy silt, and silty clay. The channel is underlain by approximately 30 m of recent deposits of silts, clays, and sands.

The owner dictated that a two-level earthquake design criteria be used. The criteria called for design to resist the Operational Level Earthquake (OLE) (defined as the event with a PHGA that has a 50 percent probability of not being exceeded in a 50-year period) without loss of serviceability and to withstand the Contingency Level Earthquake (CLE) (defined as the event with a PHGA that has a 10 percent probability of not being exceeded in 50 years), with damage repairable in 2 to 4 weeks.

The probabilistic seismic hazard analysis resulted in a magnitude $M_w = 7$ event with a peak horizontal ground acceleration of 0.4 g for the CLE and a magnitude $M_w = 8$ event with a peak horizontal ground acceleration of 0.2 g for the OLE.

The liquefaction analyses indicated that liquefaction is likely to occur in the free-field during both the OLE and CLE events. The analyses showed that liquefaction is likely to occur under the embankment during both the OLE and CLE events, although the thickness of the liquefied zone in the OLE event will be limited to about 3.5 m also.

Consequently, to minimize the extent of lateral spreading in the design earthquakes, it was decided to densify the potentially liquefiable soil to reduce the risk of unacceptable performance. As the site was in an undeveloped area with no structures or utilities in the vicinity, dynamic compaction was recommended. The densification program was designed to provide normalized and standardized blow counts, $(N_1)_{60}$, equal to or greater than 25 at the site.

Post liquefaction stability analyses were carried out using residual shear strength parameters for the liquefied sand. Results of the analyses yielded a static factor of safety greater than 1.5, indicating the embankment would stabilize once the shaking stopped, even if the soil did liquefy. The estimated permanent seismic deformation of the embankment in the OLE was less than 0.15 m. The estimated permanent seismic deformation of the embankment in the CLE was calculated to be 0.36 m. These magnitudes of potential deformation were considered acceptable.

A site-specific response analysis was conducted to develop response spectra for the soil in the main channel for the OLE and CLE. Three time histories were selected for each level of loading. The response spectra were obtained using the computer program SHAKE (Schnabel et al., 1972; Idriss and Sun, 1992) and were provided to the structural engineer for use in design of the bridge structure.

CHAPTER 7.0 REFERENCES

- AASHTO (1992), "Standard Specifications for Highway Bridges," 15th Edition, American Association of State Highway and Transportation Officials, Washington, District of Columbia.
- Abrahamson, N.A. and Silva, W.J. (1996), "Preliminary Attenuation Relations for Horizontal Response Spectra Including Data from the 1994 Northridge Earthquake," Draft Report to Brookhaven National Laboratory, New York.
- Algermissen, S.T., Perkins, D.M. (1976), "A Probabilistic Estimate of Maximum Acceleration in Rock in the Contiguous United States," U.S. Geological Survey Open File Report 76-416.
- Algermissen, S.T., Perkins, D.M., Thenhaus, P.C., Hanson, S.L. and Bender, B.L. (1991), "Probabilistic Earthquake Acceleration and Velocity Maps for the United States and Puerto Rico," U.S. Geological Survey, Miscellaneous Field Studies Map MF-2120.
- ASTM (1994), "Annual Book of ASTM Standards, Section 4, Construction," American Society for Testing and Materials, Philadelphia, Pennsylvania, 978 p.
- Campbell, K.W. (1993), "Empirical Prediction of Near Source Ground Motion from Large Earthquakes," Proc. International Workshop on Earthquake Hazard and Large Dams in the Himalayas, sponsored by the Indian National Trust of Art and Cultural Heritage (INTACH), New Delhi, India.
- Cheney, R.S. (1988), "Permanent Ground Anchors," Report FHWA-DP-68-1R, Federal Highway Administration, 136 p.
- Cornell, C.A. (1968), "Engineering Seismic Risk Analysis", Bulletin, Seismological Society of America, Vol. 58, No. 5.
- Dobry, R., Idriss, I.M. and Ng, E. (1978), "Duration Characteristics of Horizontal Components of Strong-Motion Earthquake Records," Bulletin of the Seismological Society of America, Vol. 68, No. 5, pp. 1487-1520.
- Frankel, A., Mueller, C., Barnhard, T., Perkins, D., Leyendecker, E.V., Dickman, N., Hanson, S., and Hopper, M. (1996), "National Seismic Hazard Maps: Documentation." United States Geological Survey.
- Gray, H. (1936), "Stress Distribution in Elastic Solids," Proc. 1st International Conference on Soil Mechanics and Foundation Engineering, Vol. 2, p. 157.
- Hynes, M.E. and Franklin, A.G. (1984), "Rationalizing the Seismic Coefficient Method," Miscellaneous Paper GL-84-13, U.S. Army Engineer Waterways Experiment Station, Vicksburg, Mississippi, 34 p.
- Idriss, I.M. and Sun, J.I. (1992), "User's Manual for SHAKE 91," Center for Geotechnical Modeling, Department of Civil and Environmental Engineering, University of California, Davis, California, 13 p. (plus Appendices).

- Imai, T. and Tonouchi, K. (1982), "Correlation of N-Value with S-Wave Velocity and Shear Modulus," Proc. 2nd European Symposium on Penetration Testing, Amsterdam, The Netherlands, pp. 67-72.
- Johnston, A.C. and Nava, S.J. (1994), "Seismic Hazard Assessment in the Central United States," Proc. ATC-35 Seminar on New Developments in Earthquake Ground Motion Estimation and Implications for Engineering Design Practice, Applied Technology Council, ATC 35-1, Redwood City, California, pp. 2-1 - 2-12.
- Lam, I.P., and Martin, G.R. (1986), "Seismic Design of Highway Bridge Foundations - Vol. II. Design Procedures and Guidelines," Report No. FHWA/RD-86-102, U.S. Department of Transportation, Federal Highway Administration, McLean, Virginia, 167 p.
- Lovell, C.W., Sharma, S. and Carpenter, J.R. (1984), "Introduction to Slope Stability Analysis with STABL4," prepared for Federal Highway Administration, U.S. Department of Transportation 104 p.
- McGuire, R.K. (1976), "FORTRAN Computer Program for Seismic Risk Analysis", U.S. Geological Survey Open-File Report 76-67.
- NHI (1996), "Design and Construction of Driven Pile Foundations," National Highway Institute Workshop Manual, Volumes I and II, (Working Draft).
- Nuttl, O.W. (1981), "Similarities and Differences Between Western and Eastern United States Earthquakes, and their Consequences for Earthquake Engineering," Earthquakes and Earthquake Engineering: The Eastern United States, Vol. 1, Assessing the Hazard - Evaluating the Risk, J.E. Beavers, Ed., Ann Arbor Science Publishers, Inc., Ann Arbor, Michigan, pp. 25-51.
- Poe, K.M. (1992), "Seismic Mitigation of the Memphis Water System," Proc. Lifeline Earthquake Engineering in the Central and Eastern U.S., ASCE Monograph No. 5, pp. 16-28.
- Poulos, N.G. and Davis, E.M. (1974), Elastic Solutions for Soil and Rock Mechanics, John Wiley and Sons, Inc., New York, 410 p. (Reprinted in 1991 by Centre for Geotechnical Research, University of Sydney, Australia).
- Reese, L.C., Cooley, L.A., and Radhakrishnan, R. (1984), "Laterally Loaded Piles and Computer Program COM624G," Waterways Experiment Station, U.S. Army Engineers, Technical Report K-84-2.
- Richards, R., Jr. and Elms, D.G. (1979), "Seismic Behavior of Gravity Retaining Walls" Journal of the Geotechnical Engineering Division, ASCE, Vol. 105, No. GT4, pp. 449-464.
- Schnabel, P.B., Lysmer, J., and Seed, H.B. (1972), "SHAKE: A Computer Program for Earthquake Response Analysis of Horizontally Layered Sites," Report No. UCB/EERC-72-12, Earthquake Engineering Research Center, University of California, Berkeley, California, 102 p.
- Seed, H.B. and Idriss, I.M. (1982), "Ground Motions and Soil Liquefaction During Earthquakes," Monograph No. 5, Earthquake Engineering Research Institute, Berkeley, California, 134 p.

- Seed, H.B., Wong, R.T., Idriss, I.M. and Tokimatsu, K. (1984), "Moduli and Damping Factors for Dynamic Analyses of Cohesionless Soils," Report No. UCB/EERC-84/14, University of California, Berkeley, Earthquake Engineering Research Center, 37 p.
- Somerville, P., Anderson, D., Sun, J., Punyamurthula, S., and Smith, N. (1998), "Generation of Ground Motion Time Histories for Performance-Based Seismic Engineering," Proceedings of the Sixth U.S. National Conference on Earthquake Engineering, Paper No. 222 (on CD-ROM), Earthquake Engineering Research Institute, Oakland, California.
- Trifunac, M.D. and Brady, A.G. (1975), "A Study of the Duration of Strong Earthquake Ground Motion," Bulletin of the Seismological Society of America. Vol. 65, pp. 581-626.
- Vucetic, M. and Dobry, R. (1991), "Effect of Soil Plasticity on Cyclic Response," Journal of Geotechnical Engineering, ASCE Vol. 117, No. 1. pp. 89-107.
- Wang, S.T. and Reese, L.C., (1991), "COM624P, Laterally Loaded Pile Analysis Program for the Microcomputer," Version 2.0, Report No. FHWA-SA-91-048, U.S. Department of Transportation, Federal Highway Administration, Office of Technology Applications, Washington District of Columbia, 504 p.

